IN THE UNITED STATES PATENT AND TRADEMARK OFFICE

APPLICANT:	HICKE ET AL	
SERIAL NO.:	10/031,193	EXAMINER: FORMAN, B.J.
FILED:	JANUARY 31, 2002	ART UNIT: 1634
TITLE:	TENACIN-C NUCLEIC ACID LIGANDS	CONFIRMATION NO. 6209

Mail Stop Appeal Brief
Commissioner for Patents
P.O. Box 1450
Alexandria, VA 22313-1450

APPEAL BRIEF

Sir:

In regard to the referenced application, Appellant submits this Appeal Brief.

I. REAL PARTY IN INTEREST

The real party in interest is Gilead Sciences, Inc. The right of Gilead Sciences, Inc. to take action in the subject application was established by virtue of the following chain of title:

1. An assignment from the inventors to Gilead Sciences, Inc. is recorded at Reel 013120, Frame 0536.

II. RELATED APPEALS AND INTERFERENCES

The undersigned legal representative of Appellant hereby confirms that there are no known appeals or interferences relating to the present application, or any parent application, which will directly affect or be directly affected by or have a bearing on the Board's decision in the pending appeal.

---

37 CFR 1.8
CERTIFICATE OF MAILING

I hereby certify that this correspondence is being deposited with the United States Postal Service as first class mail in an envelope addressed to: Mail Stop Appeal Brief, Commissioner for Patents, P.O. Box 1450, Alexandria, VA 22313-1450 on June 6, 2005.

Signature: _____
Name: Denise S. Magee

III. STATUS OF THE CLAIMS

Claims 33 and 44-58 are pending in the application. Claims 1-32 and 34-43 have been cancelled. No claims have been allowed. Claims 33 and 44-58 stand rejected under a final Office Action mailed September 7, 2004. The rejection of each of claims 33 and 44-58 is being appealed.

IV. STATUS OF THE AMENDMENTS

In response to the Office Action of January 30, 2004, an amendment was filed on June 1, 2004. The claims set forth in section VIII reflect the claims pending as of the entry of the amendment of June 1, 2004.

V. SUMMARY OF CLAIMED SUBJECT MATTER

Claim 33 is drawn to a method for detecting the presence of a disease in a biological tissue, wherein the disease is characterized by the expression of tenascin-C in said tissue and wherein the disease is selected from the group consisting of cancer, psoriasis, and atherosclerosis. The method is comprised of attaching a marker that can be used in *in vivo* diagnostics to a tenascin-C nucleic acid ligand to form a marker-nucleic acid ligand complex; exposing the biological tissue which may contain the disease to the marker-nucleic acid ligand complex; and detecting the presence of the disease in the tissue by detecting the presence of the marker-nucleic acid ligand in the tissue. (Specification, page 7, lines 12-26).

Claims 44 and 56-58 further define the method of claim 33. Claim 44 is drawn to the method of claim 33 wherein the marker is selected from a radionuclide, fluorophore, magnetic compound or biotin (Specification, page 9, lines 26-32, page 14, lines 29-30). Claim 56 is drawn to method of claim 33 further comprising attaching a therapeutic or diagnostic agent to the complex (Specification, page 15, lines 13-19 and page 14, lines 21-27). Claim 57 is drawn to the method of claim 33 wherein the disease is cancer (Specification, page 14, line 32) and claim 58 is drawn to the method claim 33 wherein the tenascin-C nucleic acid ligand is identified using the SELEX method (Specification, page 14, lines 12-14).

Claim 45 further defines claim 44. Claim 45 is directed to the method of claim 44 wherein the radionuclide is selected from technetium-99m (Tc-99m), Re-188, Cu-64, Cu-67, F-18, ^{125}I, ^{131}I, ^{111}In, ^{32}P or ^{186}Re (Specification, page 9, lines 29-30) and claim 46 is directed to the method of claim 45 wherein the marker is technetium-99m (Specification, page 14, lines 28-29). Claim 47 is drawn to the method of claim 46 wherein the tenascin-C nucleic acid ligand comprises a linker (Specification, page 15, lines 6-7). Claims 48-50 further define claim 47. Claim 48 is drawn to the method of claim 47 wherein said linker is $(CH_2CH_2O)_6$ (Specification, page 10, lines 1-6 and Figure 2), claim 49 is drawn to the method of claim 47 wherein the linker is $NH_2(CH_2)_6OPO_3$ (Specification, page 10, lines 1-6, and Figure 2) and claim 50 is drawn to the method of 47 wherein the tenascin-C nucleic acid ligand is selected from the group consisting of SEQ ID NOS: 4-65 (Specification, Tables 3 and 4, pages 27-29).

Claim 51 is drawn to the method of claim 50 wherein said tenascin-C nucleic acid ligand is 5'-B-G667667CG-$(CH_2CH_2O)_6$-CGUCGCCGU77U667U6UUUU6CUCCCU65, wherein all pyrimidines are 2' F; 6 is 2'OMe G; 7 is 2' OMe A; 5 is 3'-3' dT and B is a linker. (Specification, page 22, lines 6-11). Claim 52 is drawn to the method of claim 51 wherein said technetium-99m is associated with a chelator (Specification, page 22, lines 22-24). Claim 53 is drawn to the method of claim 52, wherein the complex is:

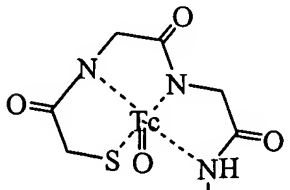

B–G667667CG-(CH2CH2O)6-CGUCGCCGU77U667U6UUUU6CUCCCU65

(Specification, page 22, lines 22-24) and claim 54 is drawn to the method of claim 53 wherein the complex is

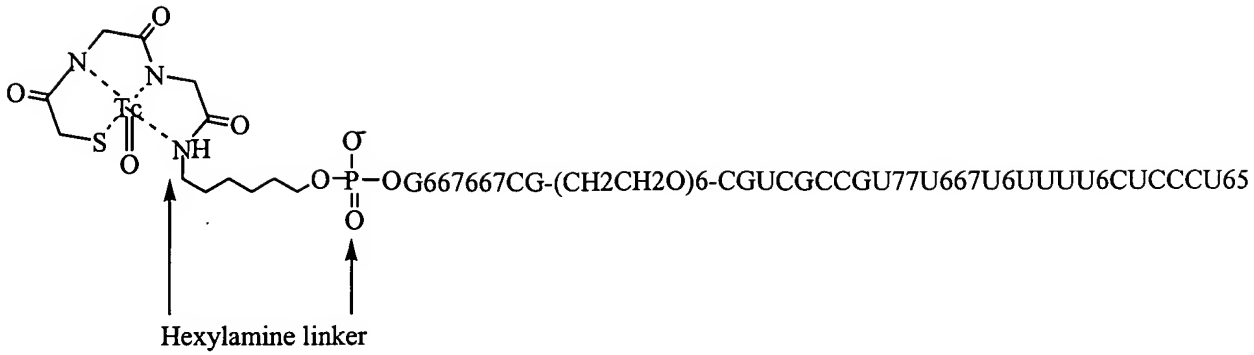

(Figure 10).

VI. GROUNDS OF REJECTION TO BE REVIEWED ON APPEAL

Claims 33 and 44-58 stand rejected under 35 U.S.C. § 112, first paragraph, as containing subject matter which was not described in the specification in such a way as to enable one skilled in the art to which it pertains, or with which it is most nearly connected, to make and/or use the invention.

VII. ARGUMENT

A. The Rejection of claims 33 and 44-58 under 35 U.S.C. § 112, first paragraph

1. Statement of the Relevant Law Pertaining to 35 U.S.C. § 112, first paragraph rejections.

The first paragraph of Section 112 requires that a patent application be written so as to "enable any person skilled in the art to which it pertains . . . to make and use the same." A specification is presumed to be enabling absent "a reason to doubt the objective truth of the statements contained therein." *In re Marzocchi*, 169 U.S.P.Q. 367, 369 (C.C.P.A 1971). A specification "may be enabling even though some experimentation is necessary," *United States v. Teletronics, Inc.*, 857 F.2d 778 (Fed. Cir. 1988), so long as the amount of experimentation required is not "undue experimentation." *In re Wands*, 858 F.2d 731, 737 (Fed. Cir. 1988). The test is whether the specification "provides a reasonable amount of guidance with respect to the direction in which the experimentation should proceed." *Id.*, 858 F.2d at 737. The fact that experimentation may be complex does not necessarily make it undue, if the art typically engages in such experimentation. *Id.* The *Wands* court set forth a number of non-exclusive factors,

which a court may consider in determining whether a disclosure would require undue experimentation. These factors were set forth as follows:

(1) the quantity of experimentation necessary,

(2) the amount of direction or guidance presented,

(3) the presence or absence of working examples,

(4) the nature of the invention,

(5) the state of the prior art,

(6) the relative skill of those in the art,

(7) the predictability or unpredictability of the art, and

(8) the breadth of the claims.

Id.

2. The Rejection of Claims 2-7 under 35 U.S.C. § 112, first paragraph is improper.

Claims 33 and 44-58 have been rejected under 35 U.S.C. § 112, first paragraph for failure to comply with the enablement requirement. Specifically, the Examiner has stated that the specification does not enable one skilled in the art to which it pertains to make or use the invention commensurate with the scope of the claims. In support of this rejection the Examiner analyzes the claims in light of the factors set forth by the court in *In re Wands*.

Breadth of the Claims

With respect to the breadth of the claims, the Examiner finds that the specification teaches that tenascin-C is expressed in a variety of non-diseased tissues. In support of this statement, the Examiner refers to Figure 7 of the instant specification and states that this figure illustrates tenascin-C expression in liver, lung, spleen, intestine, and kidney. The Examiner further finds that the specification teaches only the detection of three specific xenografted tumor cell lines in mice with a single tenascin-C nucleic acid ligand, whereas the claims are broadly drawn to detecting cancer. In light of these teachings, the Examiner finds that the claims are unduly broad.

Applicant first notes that courts have determined that the scope of enablement must only bear a "reasonable correlation" to the scope of the claims. *In re Fisher*, 427 F.2d 833, 839, 166 U.S.P.Q. 18, 24 (C.C.P.A. 1970).

Applicants respectfully disagree with the assertion that the specification teaches the expression of tenascin-C in non-diseased tissues. At that the time of filing the application, it was well known in the art that tenascin-C is expressed during embryogenesis. In adults, it expressed during wound healing, neoplasia, hyperproliferative skin disorders (such as psoriasis) and in atherosclerosis. See page 1, lines 17-32 where there is an extensive discussion of the prior art teaching that tenascin-C is expressed exclusively in such diseased tissue. In the case of tumors, tenascin-C expression is predictive of local tumor recurrence and is correlated with invasiveness and distant metastasis. See for example, Jahkola *et al.*, *Eur. J. Cancer* 34:1687-1692 (1998); Ishihara *et al.*, *Clin. Cancer Res.* 1:1035-1041 (1995); Jahkola *et al.*, *Br. J. Cancer* 78:1507-1513 (1998).

Figure 7, contrary to the Examiner's assertion, does not teach otherwise. Figure 7 illustrates the biodistribution of ^{111}In-DOTA or ^{111}In-DTPA radiolabeled tenascin-C aptamer. DOTA and DPTA are the chelators used to conjugate the ^{111}In radiolabel to the aptamer. It can be seen in Figure 7 that ^{111}In label is observed in liver, spleen, and kidney. It was well known in the art at the time the instant application was filed that the chelating agent used in the preparation of radiopharmaceuticals can affect the biodistribution of the radiopharmaceutical in a living animal. For example, different chelators can cause the non-specific uptake of radiopharmaceuticals to the kidneys, intestine, hepatobiliary system and lungs, even when the radiopharmaceutical comprises a specific targeting agent--such as a monoclonal antibody or aptamer--that would not be expected to bind in those regions. Such distributions are well known in the art as the inevitable consequence of administering an agent to living, metabolizing organism with a circulatory system. One skilled in the art realizes that after waiting an appropriate period to allow this normal tissue clearance of radioactivity to occur, the patient may then be imaged, and tumors are identified by defining regions of the body with increased tracer uptake. See, for example, Bast *et al.*, *Cancer Medicine*, 5th Edition, § 16, Part 65 (2000) (available online at << http://www.ncbi.nlm.nih.gov/entrez/query.fcgi?db=Books>>) where the authors state:

> In radioimmunoscintography, a tumor-specific antibody is labeled with a radionuclide that can be visualized outside the body by nuclear medicine imaging methods. After waiting an appropriate period for normal tissue clearance of radioactivity to occur, the patient is imaged, and tumors are identified by defining regions of the body with increased tracer uptake. ...

See also Hjelstuen, *Analyst.* 120: 863-866 (1995). Indeed, the instant specification teaches at page 23, lines 29-32:

> Tc-99m radioactivity also appears in other tissues, notably the small and large intestines. The hepatobiliary clearance pattern seen here can be readily altered by one skilled in the art, for example by altering the hydrophilicity of the Tc-99m chelator, changing the chelator, or changing the radiometal/chelator pair together.

Similarly, at page 25, lines 23-29 (referring to Figure 7):

> This experiment indicates that the chemical properties of the chelator have a large effect on the distribution of the radiolabel of TTA1/GS7641 within a living animal. Biodistribution patterns that are different from Hi15-TTA1/GS7641 may be useful for targeting tumors under certain conditions where hepatobiliary clearance is undesired. Such conditions include, but are not limited to radiotherapy applications as well as imaging of the intestines, prostate and other abdominal regions.

Thus, one skilled in the art at the time the application was filed would appreciate that the presence of the radiolabel in the normal tissues mentioned by the examiner does not indicate that those tissues express tenascin-C. Moreover, one skilled in the art, guided both by the prior art at the time of filing and the specific teachings of the instant specification quoted above, would be able to discriminate between tumor specific expression of tenascin-C and the non-specific presence of the label in certain tissues as a result of hepatobiliary clearance. For example, see Figure 3 of the instant specification where tumors are clearly visible despite the additional radioactivity in the gastrointestinal tract. Finally, the specification teaches that one may alter a hepatobiliary clearance pattern by altering the hydrophilicity of the chelator, changing the chelator, or changing the radiometal/chelator pair together. For example, the specification teaches that if one wants to perform abdominal imaging, then one selects a chelator that has a relatively low level of hepatobiliary clearance. See page 25, lines 23-39.

Turning now to the Examiner's finding that the specification teaches only detection of a few types of cancer using a single tenascin-C nucleic acid ligand whereas the claims are drawn broadly to the detection of cancer. Applicant respectfully submits that there is a reasonable

correlation between the scope of the claims and the enabling disclosure of the specification. Applicants have provided examples of the detection of widely varied types of human tumors xenografted into mice including (with reference to the cell types listed in Figure 6):

neural tumors	U87 glioblastoma-astrocytoma U251 glioma
breast tumors	MDA-MB-468 poorly metastatic breast cancer MDA-MB-435 highly metastatic breast cancer
colorectal tumors	SW620 colonic carcinoma
soft tissue sarcoma	A673 rhabdomyosarcoma

The prior art is replete with descriptions of the utility of the mouse xenograft model in the development of methods for the detection and treatment of human tumors, indicating that the mouse xenograft model is recognized in the art as an *in vivo* model that correlates well with human tumors. For example, see Rofstad & Lyng, *Mol Med Today*. 2:394-403 (1996) (xenograft model systems for human melanoma); Clarke, *Breast Cancer Res Treat.* 39:69-86 (1996) (xenograft model systems for breast cancer); Thompson *et al.*, *Biochim Biophys Acta.* 1400(1-3):301-19 (1998) (describing success of mouse xenograft model system in developing cancer therapeutics). In Bast *et al.*, *Cancer Medicine*, 5th Edition, § 13, Part 42 (2000), the authors state:

> The success of human tumor xenografting into the nude mice and the ability to maintain the histologic and biologic identity of tumors through successive passages in vivo revolutionized many aspects of cancer research, including drug development. Transplantation of tumor cell lines into nude mice can be accomplished via multiple routes: subcutaneous, intraperitoneal, intravenous, intracranial, intrasplenic, renal subcapsular, or through a new orthotopic model by site-specific organ inoculation. Each site has specific advantages and limitations.
>
> . . .
>
> Despite these changes in kinetics of invasive potential, the majority of the xenografted human tumors maintain the morphologic and biochemical characteristics of their original tumors. Therefore, it is expected that chemosensitivity would be similar in both the original and the xenografted human tumor, and that this correlation would predict for both active single agents and active drug combinations. In fact, excellent correlations can be made between

> average growth delay for human tumors in nude mice treated with the best available drug combinations and complete clinical response rates. ...

With respect to tenascin-C specifically, there are numerous reports of the use of the xenograft tumor model in combination with radiolabeled monoclonal antibodies. For example, Bourdon *et al.*, *Anticancer Res.* 4(3):133-140 (1984) describe the use of the anti-tenascin antibody 81C6 to image human tumor xenografts in mice. Indicating that such studies of the 81C6 antibody correlate well with studies in humans, Schold *et al.*, *Invest Radiol.* 28(6):488-496 (1993) and Zalutsky *et al.*, *Cancer Res.* 49(10):2807-2813 (May 1989) describe the use of radiolabeled 81C6 to image tumors in human patients; and Reardon *et al.*, *J Clin Oncol.* 20(5):1389-1397 (2002) describe the use of 81C6 to treat human tumors.

The prior art includes the descriptions of many types of tumors that express tenascin-C (including carcinomas of the lung, breast, prostate, colon, astrocytomas, glioblastomas, melanomas, and sarcomas), as well as other diseases such as hypoproliferative skin disorders (e.g., psoriasis). See page 1, line 17- page 2, line 1 of the instant specification where such descriptions are incorporated by reference. At the time the instant application was filed, tenascin-C had additionally been implicated in numerous other neoplasms, including: basal cell carcinoma (Stamp, *J Pathol.* 159(3):225-229 (Nov. 1989)), odontogenic tumors (Heikinheimo *et al.*, *Virchows Arch B Cell Pathol Incl Mol Pathol.* 61(2):101-109 (1991)), endometrial adenocarcinoma (Vollmer *et al.*, *Lab Invest.* 62(6):725-730 (Jun 1990)), hepatocellular carcinoma (Yamada *et al.*, *Liver* 12(1):10-16 (Feb. 1992)), salivary gland tumors (Soini *et al.*, *Virchows Arch A Pathol Anat Histopathol.* 421(3):217-222 (1992)), transitional cell carcinomas of the bladder (Tiitta *et al.*, *Virchows Arch B Cell Pathol Incl Mol Pathol.* 63(5):283-287 (1993)), and in rhabdomyosarcomas, fibromas and liposarcomas (Schnyder *et al.*, *Int J Cancer.* 72(2):217-224 (Jul 17,1997)).

In summary, the prior art recognizes that tenascin-C is expressed in a tremendous variety of human tumors, and in hyperproliferative skin disorders and atherosclerosis. As explained above, Figure 7 in the instant specification does not demonstrate extensive expression in normal tissue. The prior art also recognizes the general utility of the mouse xenograft model for the study of human tumors. Finally, the prior art recognizes that the specific utility of the mouse

xenograft model for the study of human tumors expressing tenascin-C. Thus, Applicants submit that by providing actual reduction to practice of the detection of xenografted human tumors of widely diverse origins, the scope of enablement reasonably correlates with the scope of the claims.

Nature of the Invention

The Examiner submits that the nature of the invention is such that detecting a disease using a ligand would require a teaching of a relationship between the ligand and the disease wherein the teaching would include an illustration or examples of the relationship between the ligand and the disease. As an example, the Examiner suggests a sample population study illustrating that tenascin-C expression detects cancer regardless of the amount, time, or pattern of expression.

As detailed in the foregoing section of this response, the state of the art at the time of filing of the invention was such that it was known that tenascin-C is expressed during embryogenesis, and during certain disease processes in adults, including cancer, proliferative skin disorders and atherosclerosis. See page 1, lines 17-32 of the instant specification where there is discussion of the types of diseased tissue where tenascin-C is expressed. The prior art also teaches that radiolabeled antibodies that bind tenascin-C are used for imaging and therapy of tumors in a clinical setting. See page 1, line 33-page 2, line 1. In addition, the specification provides examples in which tenascin-C aptamer recognizes a variety of morphologically distinct human tumors that have been xenografted into mice. Thus, the specification provides a teaching of the clear relationship between tenascin-C expression and disease.

As also explained in the foregoing section of this response, Figure 7 of the application does not depict the expression of tenascin-C in non-diseased tissues. Rather, Figure 7 depicts the inevitable hepatobiliary clearance pattern of a radiopharmaceutical in a living animal. Such hepatobiliary clearance patterns are well known in the radiopharmaceutical art. The specification teaches that one may alter a hepatobiliary clearance pattern by altering the hydrophilicity of the chelator, changing the chelator, or changing the radiometal/chelator pair together. See page 23, lines 29-32. For example, the specification teaches that if one wants to perform abdominal imaging, then one selects a chelator that has a relatively low level of hepatobiliary clearance. See page 25, lines 23-39.

For the foregoing reasons, Applicant respectfully submits there is a clear teaching of the relationship between tenascin-C expression and the diseases of cancer, psoriasis and atherosclerosis which would enable one skilled in the art to make and use the invention as claimed.

Level of Predictability in the Art

The Examiner states that the level of predictability in the art is very low with regard to detection of disease without a correlating relationship between the disease and the detecting molecule. The Examiner also states that the relationship between tenascin-C expression and cancer, psoriasis or atherosclerosis is unknown and that Figure 7 of the specification illustrates the expression of tenascin-C in normal tissue.

As discussed in detail above, the prior art clearly teaches a correlating relationship between expression of tenascin-C and cancer, psoriasis and atherosclerosis. See specification, page 1, lines 17-32. The prior art also teaches that radiolabeled antibodies that bind tenascin-C are used for imaging and therapy of tumors in a clinical setting. See page 1, line 33-page 2, line 1. Thus, the specification provides a teaching of the clear relationship between tenascin-C expression and disease.

In addition, Figure 7 of the application does not depict the expression of tenascin-C in non-diseased tissues. Rather, Figure 7 depicts the inevitable hepatobiliary clearance pattern of a radiopharmaceutical in a living animal. Such hepatobiliary clearance patterns are well known in the radiopharmaceutical art. The specification teaches that one may alter a hepatobiliary clearance pattern by altering the hydrophilicity of the chelator, changing the chelator, or changing the radiometal/chelator pair together. See page 23, lines 29-32. For example, the specification teaches that if one wants to perform abdominal imaging, then one selects a chelator that has a relatively low level of hepatobiliary clearance. See page 25, lines 23-39.

For these reasons, one skilled in the art would readily extrapolate the prior art teachings--that tenascin-C expression correlates with disease and that tenascin-C antibodies may be used for therapy and detection of those diseases--to the claimed invention. MPEP § 2164.03. Therefore, contrary to the Examiner's assertion the level of predictability in the art is high with regard to detecting tenascin-C in order to detect a disease.

Existence of Working Examples

The Examiner asserts that the specification does not provide working examples of the broadly claimed invention, stating that the specification teaches the expression of tenascin-C in a variety of non-diseased tissues. Applicants respectfully disagree.

It has been determined by the courts that no working examples are required to enable a patent application. *In re Borkowski*, 422 F.2d 904, 164 U.S.P.Q. 642 (C.C.P.A. 1970). Applicant, however, has provided a number of specific *in vivo* examples of the detection of widely varying types of human tumors using the art-recognized mouse xenograft model. The state of the art is such that the mouse xenograft model for tumor detection is accepted as reasonably correlating with the detection of human tumors *in vivo*. Note that a rigorous or invariable exact correlation is not required. *Cross v. Iizuka*, 753 F.2d 1040, 1050, 224 U.S.P.Q. 739, 747 (Fed. Cir. 1985). As discussed above in detail, the prior art recognizes both the general utility of the mouse xenograft model for the study of human tumors and the *specific* utility of the mouse xenograft model for the study of human tumors expressing tenascin-C. For example, Bourdon *et al.*, *Anticancer Res.* 4(3):133-140 (1984) describe the use of the anti-tenascin antibody 81C6 to image human tumor xenografts in mice. Indicating that such studies of the 81C6 antibody correlate well with studies in humans, Schold *et al.*, *Invest Radiol.* 28(6):488-496 (1993) and Zalutsky *et al.*, *Cancer Res.* 49(10):2807-2813 (May 1989) describe the use of radiolabeled 81C6 to image tumors in human patients; and Reardon *et al.*, *J Clin Oncol.* 20(5):1389-1397 (2002) describe the use of 81C6 to treat human tumors.

Contrary to the Examiner's assertion, Figure 7 of the application does not depict the expression of tenascin-C in non-diseased tissues. Rather, Figure 7 depicts the inevitable hepatobiliary clearance pattern of a radiopharmaceutical in a living animal. Such hepatobiliary clearance patterns are well known in the radiopharmaceutical art. The specification teaches that one may alter a hepatobiliary clearance pattern by altering the hydrophilicity of the chelator, changing the chelator, or changing the radiometal/chelator pair together. See page 23, lines 29-32 . For example, the specification teaches that if one wants to perform abdominal imaging, then one selects a chelator that has a relatively low level of hepatobiliary clearance. See page 25, lines 23-39.

In summary, the specification provides examples of the detection of widely varied human tumors using the art-recognized mouse xenograft model. Applicant submits that the Examiner's

focus on the difference between the working examples and the claimed methods is based on a standard of a rigorous or exact correlation, which is not the standard of enablement. The prior art recognizes that tenascin-C is an important marker for the detection of diseased tissue, including cancer, psoriasis and atherosclerosis (see page 1, lines 17-33 of the instant specification). Figure 7 of the application is not to the contrary. The prior art also recognizes that detection of tenascin-C in human tumors in xenografted mice correlates with the detection of tenascin-C expression in tumors in humans. For these reasons, Applicants respectfully submit that the specification provides working examples of the claimed invention, which would enable one skilled in the art to make and use the invention as claimed.

Quantity of Experimentation Required

The Examiner submits that it would require undue experimentation for one skilled in the art to make and use the invention as claimed in view of the breadth of the claims, the nature of the invention, the unpredictability in the art, and the lack of working examples. Applicants respectfully disagree. As detailed in the foregoing sections of the response, Applicants have demonstrated that the art recognizes the correlation between tenascin-C expression and cancer, psoriasis and atherosclerosis. Applicants have also demonstrated that the art recognizes the correlation between the detection and treatment of human tumors xenografted into mice with the detection and treatment of humans with the same tumors. In the specific case of tumors that express tenascin-C, Applicants have demonstrated that the art recognizes the correlation between the detection of tenascin-C expression in xenografted mice and the detection and therapy of the same tumors in humans. Applicants have demonstrated that a representative tenascin-C nucleic acid ligand detects a wide variety of human tumors in xenografted mice.

While development of a specific treatment or detection regimen may require a large quantity of experimentation, the amount of experimentation is not a controlling factor. It is a tenet of patent law that an applicant need not teach what the skilled artisan already knows. Instead, it is preferred that an applicant "omit what is known in the art." *Hybritech Inc. v. Monoclonal Antibodies*, 231 U.S.P.Q. 81, 94 (Fed. Cir. 1986). Certainly, much guidance and direction exists in the prior art with regard to administration routes and other details of treatment regimens. Antisense and other nucleic acid therapeutics have been used in the treatment of humans since at least as early as 1993. Additionally, the specification provides extensive

teaching of the preparation, administration, and analysis of treatment data in *in vivo* experiments. Applicants submit that such prior art treatments, together with the teachings of the specification, provide a reasonable amount of guidance with respect to the direction in which the experimentation should proceed and, and therefore satisfy the enablement requirement.

VIII. CLAIMS APPENDIX

1-32 (Canceled).

33 (Previously Presented). A method for detecting the presence of a disease in a biological tissue which may contain said disease, wherein said disease is characterized by the expression of tenascin-C in said tissue and wherein said disease is selected from the group consisting of cancer, psoriasis, and atherosclerosis, the method comprising:

a) attaching a marker that can be used in in vivo diagnostics to a tenascin-C nucleic acid ligand to form a marker-nucleic acid ligand complex;

b) exposing said biological tissue which may contain said disease to said marker-nucleic acid ligand complex; and

c) detecting the presence of said disease in said tissue by detecting the presence of said marker-nucleic acid ligand in said tissue.

34-43 (Canceled).

44 (Previously Presented). The method of 33 wherein said marker is selected from the group consisting of radionuclides, fluorophores, magnetic compounds, and biotin.

45 (Previously Presented). The method of 44 wherein said radionuclide is selected from the group consisting of technetium-99m (Tc-99m), Re-188, Cu-64, Cu-67, F-18, ^{125}I, ^{131}I, ^{111}In, ^{32}P, and ^{186}Re.

46 (Previously Presented). The method of 45 wherein said marker is technetium-99m.

47 (Previously Presented). The method of 46 wherein said tenascin-C nucleic acid ligand comprises a linker.

48 (Previously Presented). The method of 47 wherein said linker is $(CH_2CH_2O)_6$.

49 (Previously Presented). The method of 47, wherein said linker has the structure

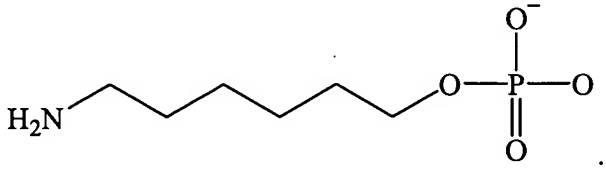

50 (Previously Presented). The method of 47 wherein said tenascin-C nucleic acid ligand is selected from the group consisting of SEQ ID NOS: 4-65.

51 (Previously Presented). The method of 50 wherein said tenascin-C nucleic acid ligand is

5'-B-G667667CG-$(CH_2CH_2O)_6$-CGUCGCCGU77U667U6UUUU6CUCCCU65

wherein:

all pyrimidines are 2' F;

6= 2'OMe G;

7= 2' OMe A;

5= 3'-3' dT; and

B= linker.

52 (Previously Presented). The method of 51 wherein said technetium-99m is associated with a chelator.

53 (Previously Presented). The method of 52, wherein said complex is

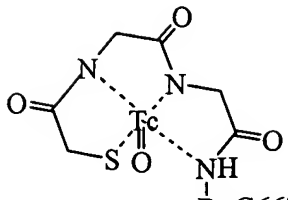

B–G667667CG-(CH2CH2O)6-CGUCGCCGU77U667U6UUUU6CUCCCU65

54 (Previously Presented). The method of 53 wherein said complex is

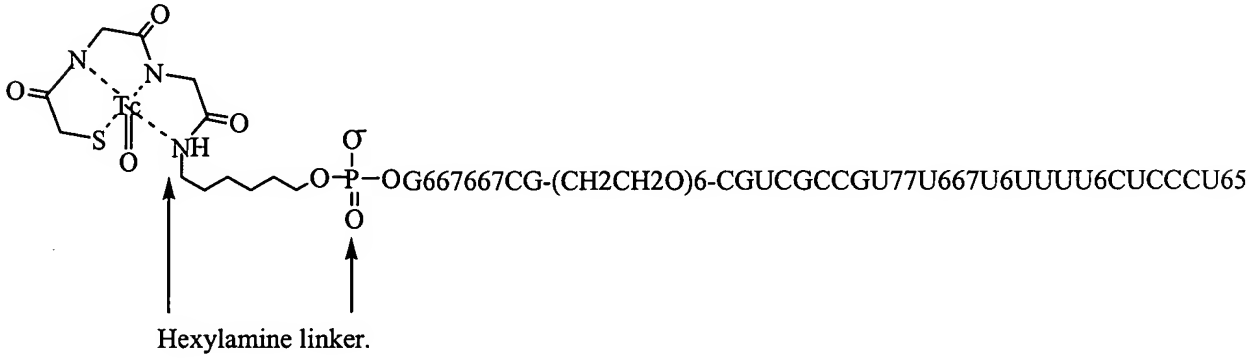

55 (Canceled).

56 (Previously Presented). The method of 33 further comprising attaching a therapeutic or diagnostic agent to said complex.

57 (Previously Presented). The method of 33 wherein said disease is cancer.

58 (Previously Presented). The method of 33 wherein said tenascin-C nucleic acid ligand is identified by:

i) contacting a candidate mixture of nucleic acids with tenascin-C wherein nucleic acids having an increased affinity to tenascin-C relative to the candidate mixture may be partitioned from the remainder of the candidate mixture;

ii) partitioning the increased affinity nucleic acids from the remainder of the candidate mixture;

iii) amplifying the increased affinity nucleic acids to yield a mixture of nucleic acids with relatively higher affinity and specificity for binding to tenascin-C, whereby a nucleic acid ligand of tenascin-C is identified.

IX. EVIDENCE APPENDIX

Enclosed please find copies of the following references of record in this appeal:

1. Jahkola *et al.*, Eur. J. Cancer 34:1687-1692 (1998)
2. Ishihara *et al.*, Clin. Cancer Res. 1:1035-1041 (1995)
3. Jahkola *et al.*, Br. J. Cancer 78:1507-1513 (1998)
4. Bast *et al.*, *Cancer Medicine*, 5th Edition, § 16, Part 65 (2000)
5. Hjelstuen, *Analyst.* 120: 863-866 (1995)
6. Rofstad & Lyng, *Mol Med Today.* 2:394-403 (1996)
7. Clarke, *Breast Cancer Res Treat.* 39:69-86 (1996)
8. Thompson *et al.*, *Biochim Biophys Acta.* 1400(1-3):301-319 (1998)
9. Bast *et al.*, *Cancer Medicine*, 5th Edition, § 13, Part 42 (2000)
10. Bourdon *et al.*, *Anticancer Res.* 4(3):133-140 (1984)
11. Schold *et al.*, *Invest Radiol.* 28(6):488-496 (1993)
12. Zalutsky *et al.*, *Cancer Res.* 49(10):2807-2813 (May 1989)
13. Reardon *et al.*, *J Clin Oncol.* 20(5):1389-1397 (2002)
14. Stamp, *J Pathol.* 159(3):225-229 (Nov. 1989)
15. Heikinheimo *et al.*, *Virchows Arch B Cell Pathol Incl Mol Pathol.* 61(2):101-109 (1991)
16. Vollmer *et al.*, *Lab Invest.* 62(6):725-730 (Jun 1990)
17. Yamada *et al.*, *Liver* 12(1):10-16 (Feb. 1992)
18. Soini *et al.*, *Virchows Arch A Pathol Anat Histopathol.* 421(3):217-222 (1992)
19. Tiitta *et al.*, *Virchows Arch B Cell Pathol Incl Mol Pathol.* 63(5):283-287 (1993)
20. Schnyder *et al.*, *Int J Cancer.* 72(2):217-224 (Jul 17,1997)

X. CLOSING REMARKS

For the foregoing reasons, Appellant submits that the lack of enablement of claims 33 and 44-58 has not been established, and that the claims are therefore patentable. Enclosed is a check in the amount of $500.00 to cover the cost of the fee for this Appeal Brief. It is believed that no other fees are due with this Appeal Brief. If this is in error, please charge any additional fees to Deposit Account No. 19-5117.

Respectfully submitted,

Date: June 6, 2005

Rosemary Kellogg, #39,726
Swanson & Bratschun, L.L.C.
1745 Shea Center Drive, Suite 330
Highlands Ranch, Colorado 80129
Telephone: (303) 268-0066
Facsimile: (303) 268-0065

Pergamon

European Journal of Cancer, Vol. 34, No. 11, pp. 1687–1692, 1998

Printed in Great Britain
0959-8049/98/$—see front matter

PII: S0959-8049(98)00215-9

Original Paper

Expression of Tenascin-C in Intraductal Carcinoma of Human Breast: Relationship to Invasion

T. Jahkola,[1] T. Toivonen,[2] S. Nordling ,[3] K. von Smitten[1] and I. Virtanen[4]

[1]Fourth Department of Surgery, Helsinki University Central Hospital, Kasarmikatu 11-13, FIN-00130 Helsinki; [2]Department of Pathology, Kymenlaakso Central Hospital, Kotka; [3]Department of Pathology, Haartman Institute; and [4]Department of Anatomy, Institute of Biomedicine, University of Helsinki, Helsinki, Finland

Tenascin-C (Tn-C) is an extracellular matrix glycoprotein that appears in areas of epithelial–mesenchymal interaction during fetal development and in neoplasia. The immunohistochemical expression of Tn-C and its relationship to histology, nuclear grade, microinvasion, oestrogen (ER) and progesterone receptors (PR), and to cell proliferation measured by Ki-67 expression were studied in 89 intraductal breast carcinomas (DCIS). Periductal Tn-C was noted in 87% and stromal Tn-C in 25% of the tumours. Stromal expression was associated with moderate to strong periductal expression and microinvasion. Periductal expression was associated with comedo-type, nuclear grade, microinvasion, Ki-67 expression, and lack of PR. The distribution of Tn-C was compared in DCIS and in the intraductal component from another series of small axillary node-negative invasive breast carcinomas ($n = 44$). Tn-C was present in the stroma of pure DCIS in 25% and in the intraductal component of the other series in 82%. Thus, stromal or moderate to strong periductal Tn-C expression in DCIS may relate to early invasion. DCIS with weak periductal or missing Tn-C expression may be a subgroup with benign behaviour. © 1998 Elsevier Science Ltd. All rights reserved.

Key words: tenascin, intraductal carcinoma, breast cancer, invasion
Eur J Cancer, Vol. 34, No. 11, pp. 1687–1692, 1998

INTRODUCTION

CARCINOMAS ARE composed of two discrete but interdependent compartments, malignant cells and the stroma [1]. The stroma differs from normal connective tissue and resembles the aggregations of mesenchyme observed during morphogenesis [2] or the granulation tissue that forms during wound healing [1]. Tenascin-C (Tn-C) is a large glycoprotein of the extracellular matrix, expressed transiently during fetal development, inflammation, wound healing and neoplasia. It is believed to have active functions in epithelial–mesenchymal interactions. Cell culture studies suggest that it has growth-promoting activity and anti-adhesive functions (for a review see [3]). Tn-C is produced by stromal fibroblasts, and also by epithelial cells of normal and malignant breast tissues, as shown by *in situ* hybridisation techniques [4, 5]. When expressed in normal adult breast tissue, Tn-C is located immunohistochemically as a continuous thin layer around the ducts. In intraductal carcinoma (ductal/carcinomas *in situ*, DCIS), Tn-C appears as broad bands and, in infiltrating ductal carcinomas, extensive immunostaining is noted in the stroma around clusters of carcinoma cells [6]. However, not all breast carcinomas express Tn-C [7, 8]. The reaction is most intense at the invasive edge of the tumour [6]. Tn-C may indicate the site of active cancer spread, since expression of Tn-C in the invasion border of small breast carcinomas is associated with an adverse patient outcome [9, 10].

DCIS is a precursor lesion of breast carcinoma. The epithelial cells are malignant, but growth is limited to the inside of the gland ducts by a basement membrane [11]. The comedo DCIS (which always presents with central necrosis) is known to be associated with occult foci of invasion more often than the other histological subtypes of DCIS [11] and the rate of local recurrences in the comedo type is also higher [12, 13]. Diagnostic classifications of DCIS, based on the nuclear grade and the presence or absence of central necrosis,

Correspondence to T. Jahkola.
Received 25 Mar. 1998; revised 16 Apr. 1998; accepted 12 May 1998.

have been proposed [12–14]. The search for treatment criteria for DCIS has started and in 1997 at least three prospective multicentre studies were under way to find out who should be treated with resection only, who needs postoperative radiotherapy and who should undergo mastectomy [15].

In the present study, the immunohistochemical distribution of Tn-C was analysed in tissue from 89 DCIS, with the aim of characterising the staining pattern and intensity of Tn-C and relating the results to subtype, nuclear grade and microinvasion. The level of Ki-67 antigen as a measure of proliferation activity and of oestrogen receptors (ER) and progesterone receptors (PR) had been determined previously in the majority of these tumours and the results are included in the study. The distribution of Tn-C expression was also compared in this group of pure DCIS and in the intraductal component areas of material from another 44 small invasive tumours.

PATIENTS AND METHODS

Patients

133 patients, were operated upon for primary DCIS during 1974–1996 at the Fourth Department of Surgery, Helsinki University Central Hospital (HUCH), Helsinki, Finland. For this study, the pathology reports and specimens of these 133 tumours were reviewed and the most representative sample of each case was selected for Tn-C immunohistochemistry. In 36 cases, either no tumour sample was available or no malignant tissue was left to investigate. A pre-operative core-needle biopsy had been taken of 16 tumours and these cases were excluded to avoid misinterpretation of possible stromal expression of Tn-C related to trauma [16]. The remaining 89 tumours were included in this study.

The median age of the patients was 52.5 years (range 28–82 years). 39 women (44%) had a breast-conserving operation and 28 of these (72%) received postoperative radiotherapy of 50 Gy to the breast area. No lymph node metastases were found in the 26 women (29%) who had an axillary dissection. The follow-up data were collected in November 1997 from the records of the Fourth Department of Surgery and the Department of Oncology, HUCH and the Finnish Cancer Registry.

Another group of 44 patients with small (1–25 mm) axillary node-negative tumours, comprised of both an invasive area and an intraductal component, has been characterised in detail previously [9].

Tumour samples

The tumours were re-examined and classified for histological subtype and nuclear grade. Nuclear grade was classified as low (1), intermediate (2) and high (3) [17]. The largest dimension of the tumours was obtained from the pathology reports. The mean size was 15 mm (range 2–40 mm). In 26 tumours (29%), the pathologist had not reported the size of the tumour, apparently because of widespread multifocality. The paraffin-embedded tumours were cut at 5 μm for Tn-C immunohistochemistry, and the sections were also stained with haematoxylin–eosin to verify histology.

Steroid receptors and Ki-67 were routinely determined in the laboratory, although in the earlier specimens these determinations were missing. No retrospective staining was carried out. ER was available in 64 (72%), PR in 63 (71%) and Ki-67 antigen in 61 (69%) of the tumours.

Tn-C immunohistochemistry

The monoclonal antibody 143BD7 against Tn-C has been previously characterised [18] and the immunohistochemical detection and evaluation of Tn-C has been described [9]. The extent and intensity of Tn-C expression was scored as −, +, ++ and +++ corresponding to negative, weak, moderate, and strong immunoreactivity. Tn-C staining was scored for periductal and stromal expression.

ER and PR immunohistochemistry

Until October 1995, the steroid receptors were assessed in frozen sections. Frozen sections were used for determinations of ER in 46 tumours and of PR in 45 tumours. Immunohistochemistry was performed using the ERICA and PRICA kits according to the instructions of the manufacturer (Abbott Laboratories, Chicago, Illinois, U.S.A.). The result was scored as weakly positive (+) when 10–40% of cells were stained, as moderately positive (++) when 40–70% were stained, and as strong (+++) when > 70% were stained. The staining intensity was not recorded. After October 1995 the staining was performed on paraffin-embedded sections. The tissue arrived fresh to the laboratory and the tumour specimen was immediately fixed in formaldehyde. Steroid receptors were determined from paraffin sections of 18 tumours using the monoclonal antihuman ER antibody (clone 1D5, Dako, Glostrup, Denmark) and PRICA kit for PR. The staining method for PR has been described previously [19]. ER was detected using the same microwave pretreatment as for PR, but the detection was carried out with a commercial ABC kit (Vectastain Elite, Vector Laboratories, Burlingame, California, U.S.A.). The scoring was the same as in frozen sections.

Ki-67 immunohistochemistry

Ki-67 immunohistochemistry was performed using monoclonal Ki-67 antiserum (Dakopatts) on frozen tissue in 21 tumours before February 1994 (for methods, see [20]) and thereafter, using the polyclonal Ki-67 antibody (Dako) on paraffin-embedded tissue in 40 tumours (for methods, see [21]). The level of immunoreactivity was expressed as the proportion of Ki-67 positive cells. The intensity of the staining was not recorded. The frozen sections were scored as weakly positive (+) when 1–2% of the nuclei were positive, as moderate (++) when 3–10% of the nuclei were positive and as strong (+++) when > 10% of the nuclei were positive. For the paraffin-embedded tumour material, the corresponding proportions of Ki-67-positive nuclei were 5–15% (+), 15–30% (++) and > 30% (+++).

Statistical methods

The statistical significance of differences in periductal and stromal Tn-C distribution between the intraductal component of invasive cancers and pure DCIS was tested with the chi-square test. The chi-square test was also used to test for an association between discrete variables and the Mann–Whitney U test for continuous variables. All tests were two-sided and P values below 0.05 were considered significant.

RESULTS

Expression of Tn-C in DCIS

Tn-C expression was observed periductally in 77 tumours (87%). It was weak in 23 (26%), moderate in 29 (33%) and strong in 25 tumours (28%). In some samples, Tn-C was not

present around all the affected ducts. In a few cases, periductal staining was also seen around benign hyperplastic ducts. When stromal Tn-C was encountered with microinvasion, it seemed to accompany the invading cells (Figure 1). Typically, the stromal Tn-C was focal, often forming bridges between the ducts of DCIS. In two cases, stromal Tn-C was expressed in areas of benign fibrotic stroma. Stromal expression was absent in 67 tumours (75%), but weak in nine (10%), moderate in nine (10%) and strong in four (5%). For analysis of associations with other factors, the stromal Tn-C-positive groups were combined ($n = 22$).

Expression of ER and PR in DCIS

In the 64 tumours studied, 20 (31%) were ER-negative tumours, four (6%) weakly positive, eight (13%) moderately positive and 32 (50%) strongly positive. For PR ($n = 63$) 32 (51%) were negative, five (8%) were weakly positive, 12 (19%) were moderately positive and 14 (22%) strongly positive. For analysis, the steroid receptors were dichotomised to positive and negative groups.

Expression of Ki-67 in DCIS

Of the 61 tumours studied, 18 (30%) were Ki-67 negative, 24 (39%) weakly positive, 13 (21%) moderately positive and six (10%) strongly positive. For analysis, the Ki-67-positive groups were combined ($n = 42$).

Relationship of Tn-C to other variables

Histological classification and Tn-C staining of the tumours are shown in Table 1. Only two of the tumours (2%) were of low grade, 29 (33%) of intermediate grade and 58 (65%) of high grade. In mixed types, the one with the worse

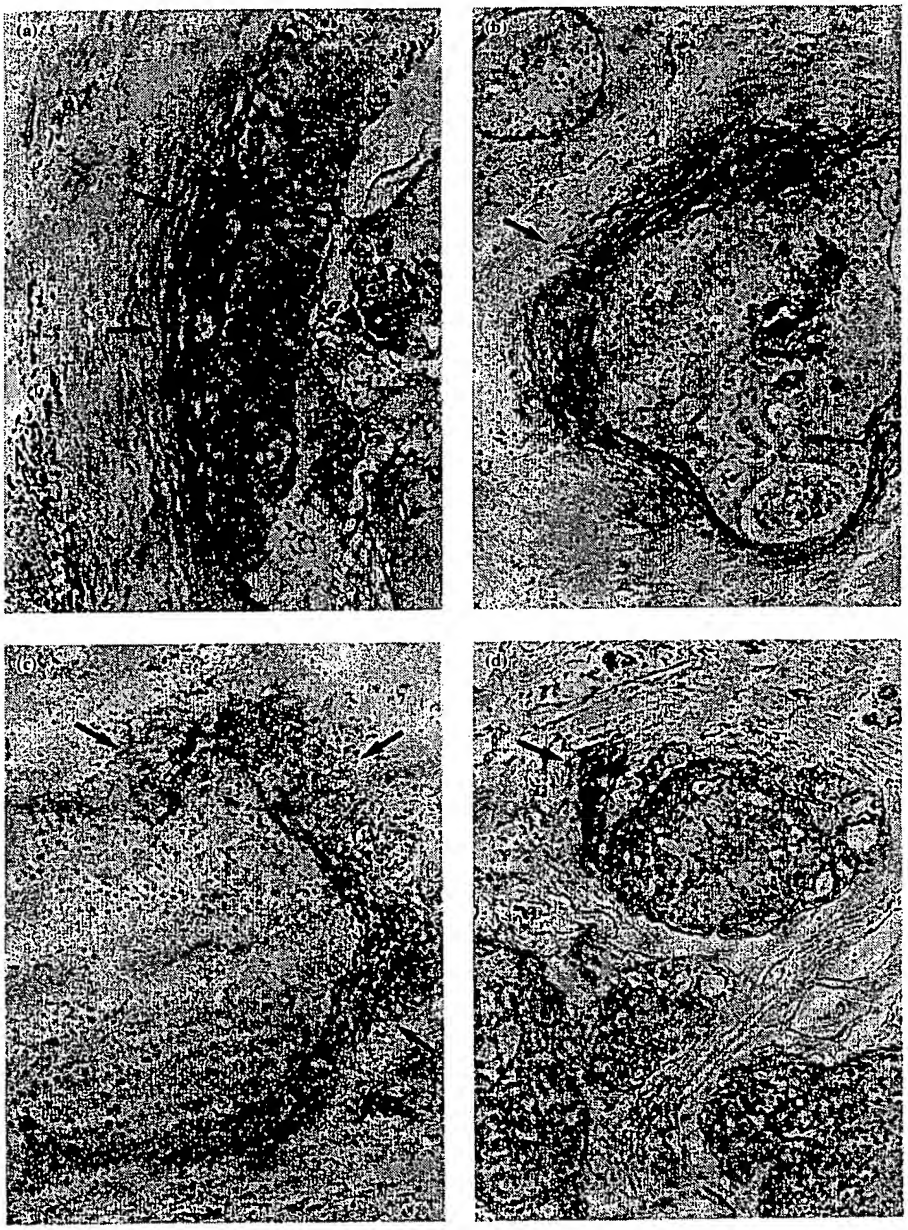

Figure 1. Periductal tenascin-C expression in four tumours of intraductal carcinomas (a–d). Note focally enhanced expression in microinvasive foci (arrows in a–d). (magnification×125).

Table 1. Distribution of periductal and stromal tenascin-C (Tn-C) immunoreactivity in intraductal carcinoma (DCIS) and subtypes

	Periductal				Stromal			
	– *n* (%)	+ *n* (%)	++ *n* (%)	+++ *n* (%)	– *n* (%)	+ *n* (%)	++ *n* (%)	+++ *n* (%)
All DCIS ($n=89$)	12 (13)	23 (26)	29 (33)	25 (28)	67 (75)	9 (10)	9 (10)	4 (5)
Comedo ($n=47$)	1 (2)	12 (26)	15 (32)	19 (40)	35 (74)	7 (15)	4 (9)	1 (2)
Non-comedo ($n=42$)	11 (26)	11 (26)	14 (33)	6 (14)	32 (76)	2 (5)	5 (12)	3 (7)
Cribriform ($n=12$)	2 (17)	1 (8)	6 (50)	3 (25)	6 (50)	2 (17)	3 (25	1 (8)
Micropapillary ($n=4$)	2 (50)	1 (25)	1 (25)	0	4 (100)	0	0	0
Not specified ($n=26$)	7 (27)	9 (35)	7 (27)	3 (12)	22 (84)	0	2 (8)	2 (8)

Table 2. Associations between periductal tenascin-C (Tn-C) expression and other variables of intraductal carcinoma (DCIS)

	Periductal Tn-C expression				
	– *n* (%)	+ *n* (%)	++ *n* (%)	+++ *n* (%)	Chi-square *P* value
All ($n=89$)	12 (13)	23 (26)	29 (33)	25 (28)	
Nuclear grade 1 ($n=2$)	0	1 (50)	1 (50)	0	
Nuclear grade 2 ($n=29$)	8 (28)	10 (34)	5 (17)	6 (21)	
Nuclear grade 3 ($n=58$)	4 (7)	12 (21)	23 (40)	19 (33)	0.04
Comedo ($n=47$)	1 (2)	12 (26)	15 (32)	19 (40)	
Non-comedo ($n=42$)	11 (26)	11 (26)	14 (34)	6 (14)	0.002
No microinvasion ($n=71$)	12 (17)	21 (30)	21 (30)	17 (24)	
Microinvasion ($n=18$)	0	2 (11)	8 (44)	8 (44)	0.04
ER- ($n=20$)	1 (5)	2 (10)	9 (45)	8 (40)	
ER+ ($n=44$)	8 (18)	12 (27)	14 (32)	10 (23)	0.13
PR- ($n=32$)	1 (3)	5 (16)	12 (37)	14 (44)	
PR+ ($n=31$)	8 (26)	8 (26)	11 (35)	4 (13)	0.008
Ki-67+ ($n=43$)	2 (5)	9 (21)	15 (35)	17 (39)	
Ki-67- ($n=18$)	5 (28)	3 (17)	7 (39)	3 (17)	0.04

ER, Oestrogen receptor; PR, Progesterone receptor.

known prognosis was chosen. Comedo or cribriform tumours were more frequently Tn-C-positive than other types (Table 1). Cribriform tumours were often positive for ER (8/9) and PR (6/9), and they expressed Tn-C periductally in 10/12 tumours (in 9/12 moderate to strong staining) and stromally in 6/12 tumours (Table 1).

The age of the patient was not related to Tn-C expression nor was the size of the tumour (data not shown). The tumours with a known size and the mainly multifocal tumours with no size definition were also compared and no difference was found in Tn-C distribution (data not shown).

The DCIS tumours that expressed (moderate to strong) periductal Tn-C were associated with microinvasion ($P=0.04$), comedo type ($P=0.002$), high nuclear grade ($P=0.04$), lack of PR ($P=0.008$) and positive Ki-67 expression ($P=0.04$) (Table 2). They tended to be ER-negative, but this association did not reach statistical significance. Stromal Tn-C expression was associated with periductal Tn-C expression ($P=0.05$) and microinvasion ($P=0.005$). A non-significant association with positive Ki-67-immunoreactivity was also noted ($P=0.07$; Table 3).

Microinvasion was considered to be present if it was mentioned in the original pathology report on paraffin samples or if it was noted in the sections made for this study. There was microinvasion in 18/89 tumours (20%). It was associated with periductal Tn-C expression ($P=0.04$), stromal Tn-C

Table 3. Association between tenascin-C (Tn-C) expression in the stroma and other variables of intraductal carcinoma (DCIS)

	Tn-C positive in stroma *n* (%)	Chi-square *P* value
All ($n=89$)	26 (29)	-
Tn-C periductal- ($n=12$)	1 (8)	
Tn-C periductal+ ($n=23$)	2 (9)	
Tn-C periductal++ ($n=29$)	8 (28)	
Tn-C periductal+++ ($n=25$)	11 (44)	0.02
Nuclear grade 1 ($n=2$)	1 (50)	
Nuclear grade 2 ($n=29$)	6 (21)	
Nuclear grade 3 ($n=58$)	15 (26)	0.6
Comedo ($n=47$)	12 (26)	
Non-comedo ($n=42$)	10 (24)	0.9
Microinvasion ($n=18$)	9 (50)	
No microinvasion ($n=71$)	13 (18)	0.005
ER- ($n=20$)	4 (20)	
ER+ ($n=44$)	13 (30)	0.4
PR- ($n=32$)	9 (28)	
PR+ ($n=31$)	8 (26)	0.8
Ki-67+ ($n=43$)	15 (35)	
Ki-67- ($n=18$)	2 (11)	0.07

ER, Oestrogen receptor; PR, Progesterone receptor.

Table 4. Distribution of periductal and stromal expression of tenascin-C (Tn-C) in purely intraductal carcinomas (DCIS) (n = 89) and in the intraductal component of small invasive ductal carcinomas (n = 44)

	Pure DCIS (%)	Intraductal component of invasive ductal carcinoma* (%)	*P* value
Tn-C periductal			
–	12 (13)	2 (5)	
+	23 (26)	6 (14)	
++	29 (33)	20 (45)	
+++	25 (28)	16 (36)	0.1
Tn-C stromal			
–	67 (75)	8 (18)	
+	9 (10)	11 (25)	
++	9 (10)	13 (30)	
+++	4 (5)	12 (27)	< 0.0001

*Detailed in [9].

expression ($P = 0.005$), comedo type ($P = 0.02$) and a Ki-67-positive immunoreaction ($P = 0.02$), but not with nuclear grade (data not shown).

Follow-up of the DCIS patients

None of the DCIS patients had metastases. The median follow-up for the local status of the patients treated with breast-conserving surgery was 2 years (range 5 months–9 years). Four local recurrences occurred 1.5–5.5 years, median 3.3 years, after the operation. All recurrences were DCIS and no invasive growth was encountered. In 2 patients the resection margin had not been tumour-free and in 1 patient the tumour was multifocal with an uncertain resection margin, the smallest distance from DCIS being 3 mm. 1 patient had not received postoperative radiotherapy and there was no reference to the resection margin in the pathology report. None of the histopathological variables were related to these local recurrences, but because of non-standardised surgical treatment, the series was not suitable for evaluation of local recurrence.

Tn-C in pure DCIS and in the intraductal component of invasive carcinomas

There was no significant difference in periductal Tn-C distribution in the pure DCIS group and the 44 small, invasive ductal carcinomas with an intraductal component [9] (Table 4). Stromal Tn-C expression was present in 25% of the pure DCIS and in 82% of the intraductal components ($P < 0.0001$; Table 4).

DISCUSSION

In this study of 89 DCIS tumours, an increased periductal expression of Tn-C was correlated with microinvasion and with comedo type. Comedo type is known to be associated with a higher risk of both invasion [11] and recurrence [12, 13]. Tn-C was also associated with lack of PR expression and with cell proliferation, measured by the Ki-67 antigen. Using *in situ* hybridisation, it has recently been shown that Tn-C is produced by the carcinoma cells of early invasive nests of DCIS and that these mRNA-positive cells are particularly frequent at the margins of the carcinoma cell nests [4, 5]. This is consistent with our observations of a connection between Tn-C and early invasion.

Tn-C expression in morphogenesis and in carcinogenesis have marked resemblances. Tn-C accumulates specifically in the dense mesenchyme around epithelial organ primordia [22] and in invasive nests of breast carcinoma [5, 6]. The source of Tn-C at these sites is predominantly or entirely the epithelial cells themselves [4, 5, 23]. After differentiation, this Tn-C production is downregulated [22–24]. An analogous downregulation may take place in infiltrating breast carcinomas, where the expression at the invading periphery is often intense, whereas the central parts of the tumour express less Tn-C [4, 6]. This downregulation of Tn-C expression within fully evolved advanced carcinomas may explain why Tn-C-negative tumours have a worse prognosis in breast cancer [25] and colorectal cancer [26]. The origin of the stromal Tn-C in infiltrating carcinomas may be different, produced by fibroblasts and related to desmoplasia, as shown in the scirrhotic type of breast carcinoma [5]. This type of tumour represents 'the wound that does not heal' [1] and Tn-C may reflect and participate in a process resembling wound healing or inflammation related to host-response and different from cancerous invasion. It seems as if carcinoma cells produce Tn-C at the invasion front in a manner similar to actively growing epithelia during fetal development.

The distribution of Tn-C in other benign, premalignant and malignant epithelial tissues resembles that of the breast. In colon adenomas, Tn-C expression in the basal lamina is increased as compared with the normal mucosa and in invasive adenocarcinomas Tn-C is found in the basal lamina and also in the stroma [27]. Analogous changes in expression have been reported in the prostate [28], the endometrium [29], the cervix uteri and the vulva [18], the urinary bladder [30], in salivary gland tumours [31], lung tumours [32], and premalignant oral lesions and squamous cell carcinoma [33]. It seems possible that measurement of Tn-C may be of clinical use and aid the identification of early stages of invasion in any carcinoma. Future studies are needed to show whether Tn-C can be used to help decisions on the extent of surgery and the need for radiotherapy and adjuvant medication in early carcinomas.

In vitro Tn-C participates in the control of cell proliferation and migration. According to both *in situ* hybridisation and immunohistochemical studies, Tn-C is produced by breast carcinoma cells at the site of early invasion and may, thus, have an active function in cancer invasion and metastasis. The expression of Tn-C in the invasion border of small infiltrating breast carcinomas predicts both local recurrence after breast-conserving surgery [10] and distant metastasis [9]. In the present study, moderate to strong periductal expression of Tn-C in DCIS was associated with comedo type, microinvasion, high nuclear grade, high Ki-67 expression and lack of PR. Expression in the stroma was associated with moderate to strong periductal staining and microinvasion. Enhanced periductal Tn-C expression may be a sign that DCIS is likely to progress into invasive breast cancer and it may aid in finding microinvasion. The stromal expression of Tn-C was considerably higher in the intraductal component of early infiltrating breast carcinomas than in pure DCIS. We suggest that Tn-C is related to invasion and it may be of value when measuring disease character and selecting treatments for carcinomas.

1. Dvorak HF. Tumors: wounds that do not heal. Similarities between tumor stroma generation and wound healing. Review. *N Engl J Med* 1986, 315(26), 1650–1659.

2. Birchmeier C, Birchmeier W. Molecular aspects of mesenchymal-epithelial interactions. *Ann Rev Cell Biol* 1993, **9**, 511–540.
3. Vollmer G. Biologic and oncologic implications of tenascin-C/hexabrachion proteins. *Crit Rev Oncol/Hematol* 1997, **25**, 187–210.
4. Lightner VA, Marks JR, McCachren SS. Epithelial cells are an important source of tenascin in normal and malignant human breast tissue. *Exp Cell Res* 1994, **210**(2), 177–184.
5. Yoshida T, Matsumoto E-I, Hanamura N, *et al.* Co-expression of tenascin and fibronectin in epithelial and stromal cells of benign lesions and ductal carcinomas in the human breast. *J Pathol* 1997, **182**, 421–428.
6. Howeedy AA, Virtanen I, Laitinen L, Gould NS, Koukoulis GK, Gould VE. Differential distribution of tenascin in the normal, hyperplastic, and neoplastic breast. *Lab Invest* 1990, **63**(6), 798–806.
7. Shoji T, Kamiya T, Tsubura A, *et al.* Immunohistochemical staining patterns of tenascin in invasive breast carcinomas. *Virchows Archiv A* 1992, **421**, 53–56.
8. Moch H, Torhorst J, Durmuller U, Feichter GE, Sauter G, Gudat F. Comparative analysis of the expression of tenascin and established prognostic factors in human breast cancer. *Pathol Res Practice* 1993, **189**, 510–514.
9. Jahkola T, Toivonen T, Smitten K von, Blomqvist C, Virtanen I. Expression of tenascin in invasion border of early breast cancer correlates with higher risk of distant metastasis. *Int J Cancer (Pred Oncol)* 1996, **69**, 445–447.
10. Jahkola T, Toivonen T, Virtanen, I. *et al.*, Tenascin-C expression in invasion border of early breast cancer—a predictor of local and distant recurrence. *Br J Cancer* (in press).
11. Rosai J. Breast. In Rosai J, ed. *Ackermann's Surgical Pathology*, vol. 2, 8th edn. Mosby, St Louis, Toronto, 1996, 1596.
12. Lagios MD, Margolin FR, Westdahl PR, Rose MR. Mammographically detected duct carcinoma *in situ*. Frequency of local recurrence following tylectomy and prognostic effect of nuclear grade on local recurrence. *Cancer* 1989, **63**, 618–624.
13. Fisher ER, Costantino J, Fisher B, *et al.* Pathologic findings from the National Surgical Adjuvant Breast Project (NSABP) Protocol B-17. Intraductal carcinoma (ductal carcinoma *in situ*). *Cancer* 1995, **75**, 1310–1319.
14. Silverstein MJ, Poller DN, Waisman JR, *et al.* Prognostic classification of breast ductal carcinoma-*in-situ*. *Lancet* 1995, **345**, 1154–1157.
15. Blume E. News: New clinical trials under way for DCIS. *J Natl Cancer Inst* 1997, **89**(15), 1094.
16. Mackie EJ, Halfter W, Liverani D. Induction of tenascin in healing wounds. *J Cell Biol* 1988, **107**, 2757–2767.
17. Holland R, Hendriks JHCL, Verbeek ALM, Mravunac M, Stekhoven JHS. Extent, distribution, and mammographic/histological correlations of breast ductal carcinoma *in situ*. *Lancet* 1990, **335**, 519–522.
18. Tiitta O, Wahlström T, Paavonen J, *et al.* Enhanced tenascin expression in cervical and vulvar koilocytotic lesions. *Am J Pathol* 1992, **141**(4), 907–913.
19. Boguslawski K von. Immunohistochemical detection of progesterone receptors in paraffin sections. A novel method using microwave oven pretreatment. *Apmis* 1994, **102**, 641–646.
20. Railo M, Nordling S, Boguslawski K von, Leivonen M, Kyllönen L, Smitten K von. Prognostic value of Ki-67 immunolabelling in primary operable breast cancer. *Br J Cancer* 1993, **68**, 579–583.
21. Railo M, Lundin J, Haglund C, Smitten K von, Boguslawski K von, Nordling S. Ki-67, p53, ER-receptors, ploidy and s-phase as prognostic factors in T1 node negative breast cancer. *Acta Oncol* 1997, **36**(4), 369–374.
22. Chiquet-Ehrismann R, Mackie EJ, Pearson CA, Sakakura T. An extracellular matrix protein involved in tissue interactions during fetal development and oncogenesis. *Cell* 1986, **47**, 131–139.
23. Koch M, Wehrle-Haller B, Baumgartner S, Spring J, Brubacher D, Chiquet M. Epithelial synthesis of tenascin at tips of growing bronchi and graded accumulation in basement membrane and mesenchyme. *Exp Cell Res* 1991, **194**, 297–300.
24. Sakakura T, Ishihara A, Yatani R. Tenascin in mammary gland development: from embryogenesis to carcinogenesis. In Lippman ME, ed. *Regulatory Mechanisms in Breast Cancer*. Boston; Kluwer Academic, 1991, 383–400.
25. Shoji T, Kamiya T, Tsubura A, *et al.* Tenascin staining positivity and the survival of patients with invasive breast carcinoma. *J Surg Res* 1993, **55**, 295–297.
26. Sugawara I, Hirakoshi J, Masunaga A, Itoyama S, Sakakura T. Reduced tenascin expression in colonic carcinoma with lymphogenous metastasis. *Invasion Metastasis* 1991, **11**, 325–331.
27. Riedl S, Faissner A, Schlag P, Herbay AV, Koretz K, Möller P. Altered content and distribution of tenascin in colitis, colon adenoma, and colorectal carcinoma. *Gastroenterology* 1992, **103**, 400–406.
28. Ibrahim SN, Lightner VA, Ventimiglia JB, *et al.* Tenascin expression in prostatic hyperplasia, intraepithelial neoplasia, and carcinoma. *Human Pathol* 1993, **24**, 982–989.
29. Sasano H, Nagura H, Watanabe K, *et al.* Tenascin expression in normal and abnormal human endometrium. *Modern Pathol* 1993, **6**(3), 323–326.
30. Tiitta O, Wahlström T, Virtanen I, Gould VE. Tenascin in inflammatory conditions and neoplasma of the urinary bladder. *Virchows Archiv B* 1993, **63**, 283–287.
31. Soini Y, Pääkkö P, Virtanen I, Lehto V-P. Tenascin in salivary gland tumours. *Virchows Archiv A* 1992, **421**, 217–222.
32. Soini Y, Pääkkö P, Nuorva K, *et al.* Tenascin immunoreactivity in lung tumors. *Am J Clin Pathol* 1993, **100**(2), 145–150.
33. Tiitta O, Happonen RP, Virtanen I, Luomanen M. Distribution of tenascin in oral premalignant lesions and squamous cell carcinoma. *J Oral Pathol Med* 1994, **23**, 446–450.

Acknowledgements—The technical assistance of Ms A. Takkinen, M.-L. Piironen and Mr R. Karppinen is acknowledged. This study was supported by a grant from The Finnish Cancer Organizations.

Tenascin Expression in Cancer Cells and Stroma of Human Breast Cancer and Its Prognostic Significance[1]

Akinori Ishihara, Toshimichi Yoshida, Hisao Tamaki, and Teruyo Sakakura[2]

Departments of Pathology [A. I.] and Surgery [H. T.], Matsusaka Chuo General Hospital, Matsusaka, Mie 515, and Department of Pathology, Mie University, School of Medicine, 2–174 Edobashi, Tsu, Mie 514 [A. I., T. Y., T. S.], Japan

ABSTRACT

Sections of formalin-fixed, paraffin-embedded tissues from 210 human breast cancers were immunohistochemically examined using the mAb against human tenascin (TN) RCB1. Immunoreactive TN was detected in the breast cancer stroma in 77 (36.7%) cases, whereas the remaining 133 (63.3%) were negative. Of the 77, 12 (5.7%) cases also showed positive staining in the carcinoma cell cytoplasm. The positive cells were often observed in the margin of the cancer nests at the site adjacent to the stroma. According to the staining pattern of TN, the breast cancer cases were classified into the three groups of cancer cell TN(+)/stromal TN(+), cancer cell(−)/stromal TN(+), and cancer cell(−)/stromal TN(−). Analysis of the relationship of these TN patterns with various clinicopathological characteristics of the tumors and the patient outcome revealed that, in comparison to the cancer cell(−)/stromal TN(−) group, the cancer cell TN(+)/stromal TN(+) group exhibited increased frequency of lymph node metastasis and exceptionally poor outcome, and the cancer cell(−)/stromal TN(+) group also showed more frequent metastasis and poorer outcome. Most of the cancer cell TN(+)/stromal TN(+) cases were c-*erb*B-2 positive and estrogen receptor negative. Furthermore, *in situ* hybridization of freshly obtained breast cancer tissues demonstrated that both cancer cells and stromal cells express TN mRNA. These results indicate that the TN in breast cancer is produced by cancer epithelial cells as well as by stromal mesenchymal cells, and that cancer cell TN might be involved in cancer spreading, resulting in unfavorable patient prognosis.

INTRODUCTION

TN[3] is an extracellular matrix glycoprotein with a unique six-armed macromolecular structure, which is known to be an essential factor for modulation of reciprocal interactions between the epithelium and mesenchyme during embryogenesis (1–3). A number of studies have demonstrated prominent TN expression in human cancers including those of brain (4), colon (5, 6), liver (7, 8), lung (9, 10), uterus (11), skin (12), prostate (13), and mammary gland (14–17). Because it was initially proposed as a stromal marker for epithelial malignancy (14), TN expression in cancers has usually been observed in the stroma. Examining human breast cancers by immunohistochemistry, investigators have found that TN is consistently present in the stroma of malignant tumors (14–16). Our previous examination also indicated intense staining in the connective tissue of invasive ductal carcinomas (17). Accordingly, it has been generally accepted that TN is produced by the mesenchyme and has an active function in cancer development, probably by promoting cancer cell proliferation and invasion.

Shoji *et al.* (18) proposed TN to be a marker useful in predicting the survival of breast cancer patients. They investigated immunoreactive TN in 82 patients with primary invasive breast carcinomas, and found a significantly superior outcome during the 5-year period after surgery in the TN-positive patients compared with the negative patients. Immunohistochemistry of primary colon carcinomas demonstrated no lymphogenous metastasis in patients in whom the cancer stroma showed strongly positive staining for TN (19). Taking these results into consideration, it is conceivable that TN may prevent rather than enhance the cancer cell outgrowth, probably by creating a barricade surrounding the cancer nests and inhibiting the movement of these cells. In fact, TN has been proposed as a boundary molecule in the somatosensory cortical barrel field during the development of mouse cerebral cortex (20). Thus, there are two different lines of speculation as to the role of TN in cancer development.

Ligthner *et al.* (21) have recently demonstrated that normal mammary epithelial cells express TN in culture and incorporate the protein into the underlying matrix. They have also examined human breast tissues by *in situ* hybridization and found that both normal and malignant mammary epithelial cells can express TN mRNA (21). Our previous findings have shown that A431 epidermal cancer cells which express no TN in culture can produce TN, with accumulation in the surrounding mesenchyme, when injected into the nude mouse subcutis (22). Thus, the TN in the breast cancer stroma is considered to be originated from both the epithelium and mesenchyme. We have proposed that TN in the tissue is heterogeneous in its structure and function (23). In breast cancer, the structure and function of epithelial TN are possibly different from those of the mesenchymal TN. Therefore, it is important to determine by which cells the TN in the cancer stroma was produced.

In this study, we used archival formalin-fixed and paraffin-embedded surgical materials of human breast cancers. In immunohistochemical studies of cancers using anti-TN antibody, we have found positive staining in the cytoplasm of cancer cells. Therefore, this study was designed to investigate the presence of both the cancer cell TN and stromal TN in breast cancer, and the implications regarding the relationship between the TN staining

Received 2/28/95; revised 4/14/95; accepted 5/1/95.
[1] This research was supported in part by Grants-In-Aid from the Ministry of Education, Science and Culture, Japan.
[2] To whom requests for reprints should be addressed.
[3] The abbreviations used are: TN, tenascin; ER, estrogen receptor; TBS, Tris-buffered saline; DIG, digoxygenin.

pattern and clinicopathological characteristics. TN staining was detected in cancer cells in the patients whose outcome was poor. The results were also compared with the c-*erb*B-2 and ER status. Furthermore, the cellular source of TN was identified in freshly obtained cancer tissues by *in situ* hybridization with human TN mRNA.

MATERIALS AND METHODS

Tissues. Primary breast cancers and axillary lymph nodes from 210 female patients who had undergone surgical resection at Matsusaka Chuo General Hospital between 1979 and 1987 were used in this study. The average age at the time of diagnosis was 54.4 (range, 28–89) years. The tumor diameter varied from 0.6 to 12 cm (mean diameter, 2.8 cm). Five years after the initial operation, 167 patients were still alive, 32 had died from relapsed breast cancer, and 11 had died of other causes.

The tumors were classified according to the WHO histological typing for breast cancer (24). The histological malignancy was categorized into three grades (I-III), based on the grades of architectural atypia and nuclear atypia, along with the number of mitotic figures as described initially by Bloom and Richardson (25). All cases were classified into the clinical TNM stages I, II, IIIa and b, and IV according to the size of the tumor, degree of lymph node metastasis, and distant metastasis status (26). The ER levels were determined at a commercial laboratory (Otsuka Assay Company, Tokushima, Japan).

Survival times were measured from the date of diagnosis using the multiple regression model developed by Cox (27) for censored survival data. The curves of the probability of survival were obtained using the product limit method of Kaplan and Meier (28). Differences among the groups for other prognostic parameters were analyzed using Student's *t* test with the Cochran-Cox method and χ^2 test.

Immunohistochemistry. The surgical specimens were fixed routinely in 10% phosphate-buffered formalin, embedded in paraffin, and cut at 4-μm thickness. Sections were examined by immunostaining for TN, c-*erb*B-2, and vimentin. After deparaffinization with xylene and hydration with downgraded ethanol, the sections were incubated in 0.3% H_2O_2 in methanol for 15 min to block endogenous peroxidase activity. For the staining of TN, the sections were treated in 10 mM TBS solution supplemented with 1% normal rabbit serum for 10 min to block nonspecific binding of rat immunoglobulins. Development and characterization of a rat mAb, RCB1, against human TN purified from conditioned medium of umbilical fibroblasts were previously described (29). Antibody RCB1 is commercially available from Cosmo Bio Japan, Ltd., as a clone name of 8C9. Sections were then incubated with RCB1 at a concentration of 1 μg/ml for 2 h, washed three times with TBS, incubated with biotinylated rabbit antirat IgG for 30 min, washed three times with TBS, and incubated with a complex of avidin and biotinylated horseradish peroxidase (Vector Laboratories, Burlingame, CA) for 30 min. After the sections were washed with TBS, the color reaction was developed with a freshly prepared solution of 0.1% diaminobenzidine tetrahydrochloride (Sigma, St. Louis, MO)/0.02% H_2O_2 in 50 mM Tris-HCl (pH 7.6). They were washed with TBS and counterstained with hematoxylin. All steps were performed at room temperature. In the staining for c-*erb*B-2 or vimentin, normal goat and horse serum was used, respectively, to block nonspecific binding of immunoglobulins, and polyclonal antibody against c-*erb*B-2 (Nichirei Co.) at a dilution of 1:100 and mAb against vimentin (DAKO-Japan, Kyoto, Japan) at 1:50, respectively, was used as the primary antibody. For the staining of controls, sections were treated in parallel fashion but incubated with normal sera instead of the primary antibodies. The TN-positive staining in the cancer stroma was evaluated, but the staining in the basement membrane and subbasement membrane zone was excluded, since it was observed around the normal ducts as well. The cytoplasmic staining of the cancer cells was also determined. The staining intensity was scored into three grades: strongly positive (++), positive (+), or negative (−).

Table 1 Expression of immunoreactive TN in human breast cancers

Histological classification	No. of cases	TN		
		−	+	++
Invasive ductal carcinoma	183	114	50 (4)[a]	19 (6)[a]
Noninvasive ductal carcinoma	9	7	2 (1)[a]	0
Lobular carcinoma	6	2	3	1
Other types	12	10	1	1 (1)[a]

[a] Numbers in parentheses, numbers of cases with TN-positive cancer cells.

***In Situ* Hybridization.** Freshly dissected breast cancer tissues were trimmed and fixed overnight with 4% paraformaldehyde in 0.1 M sodium phosphate buffer (pH 7.4) at 4°C. After being rinsed in the same buffer, they were dehydrated by a graded ethanol series and xylene, embedded in paraffin, cut at 3-μm thickness, and placed on glass slides coated with Biobond (British BioCell International, Cardiff, United Kingdom). TN mRNA expression was detected by *in situ* hybridization using a previously described method (30) with slight modifications. Briefly, antisense and sense cRNA probes were prepared by *in vitro* transcription of human TN cDNA (kindly given by Dr. L. Zardi, Genoa), using a DIG RNA labeling kit (SP6/T7; Boehringer Mannheim, Mannheim, Germany). Sections were deparaffinized with xylene, digested with 0.3 units/ml proteinase K (Boehringer Mannheim), postfixed with 4% paraformaldehyde, washed in PBS three times, then treated in 0.2 M HCl for 10 min. After being washed again in PBS, they were treated in 0.1 M triethanolamine (pH 8.0), washed in PBS, treated with 0.1 M triethanolamine/0.25% acetic anhydride, washed in PBS, dehydrated in upgraded ethanol, and air dried. The specimens were prehybridized with hybridization buffer composed of 50% formamide, 10 mM Tris-HCl (pH 7.6), 1 mM EDTA, 600 mM NaCl, 10 mM DTT, 1× Denhardt's solution (Sigma), 0.25% SDS, 10% dextran sulfate, and 200 μg/ml *Escherchia coli* tRNA (Boehringer Mannheim) for 2 h at 50°C, and incubated with 40 μl hybridization buffer containing alkaline-hydrolyzed DIG-labeled antisense or sense probes for 16 h at 50°C. After hybridization, sections were rinsed in 4× SSC followed by 50% formamide/2× SSC at 50°C for 15 min, and incubated in 1× STE (10 mM Tris-HCl, pH 7.5/500 mM NaCl/1 mM EDTA) at

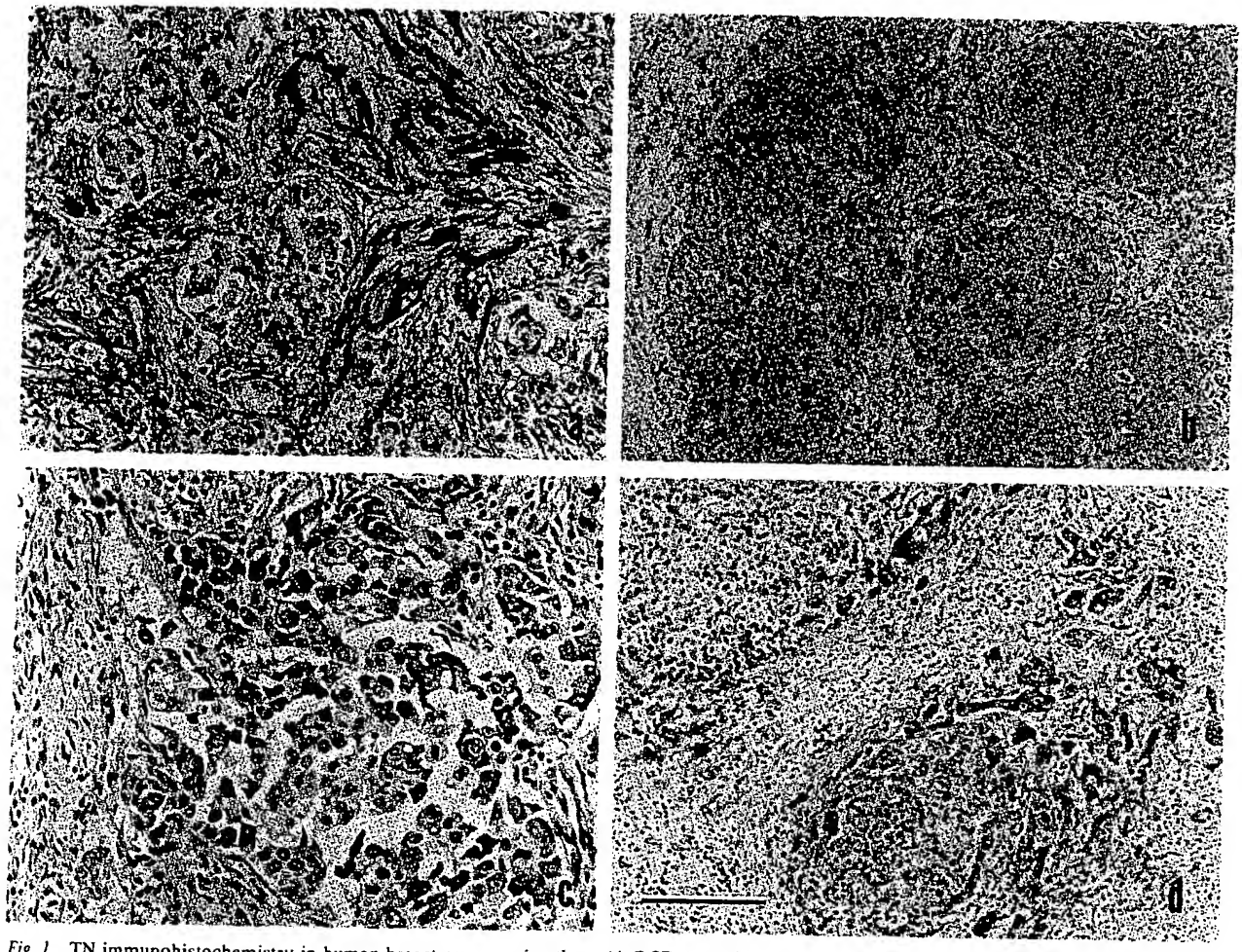

Fig. 1 TN immunohistochemistry in human breast cancer using the mAb RCB-1. Positive TN staining is widely distributed in the stroma of infiltrating ductal carcinoma (*a*). In another case, TN staining is not shown in the tissue (*b*). The cytoplasm of some cancer cells shows the intense positive reaction (*c*). TN-positive cancer cells are often located in the margin of cancer nests (*d*). *Bar in d*, 200 μm for *a*, *b*, and *d*, and 100 μm for *c*.

Table 2 Clinicopathological data in the 12 breast cancer cases with TN-positive cancer cells

No.	Age	Tumor size (cm)	Histology (grade)	Lymph node metastasis	Clinical stage	Outcome (mo)	Immunohistochemistry[a]			
							Stromal TN	c-*erb*B-2	Vimentin	ER
1	36	7.0	Inv.D.[b] (3)	16/25	IIIb	Died (27)	++	++	−	−
2	29	2.7	Inv.D. (3)	12/18	IIIa	Died (47)	++	++	−	−
3	75	3.0	Inv.D. (2)	0/18	II	Died (80)	+	−	−	+
4	54	10.0	Inv.D. (3)	3/10	IIIa	Died (5)	++	++	−	−
5	48	2.1	Inv.D. (3)	1/18	II	Died (55)	++	−	−	−
6	77	1.5	Inv.D. (3)	8/13	IIIa	Died (36)	++	++	−	−
7	31	4.0	Inv.D. (2)	0/11	II	Alive	+	++	−	−
8	63	1.5	NonI.D. (1)	0/11	I	Alive	+	−	+	+
9	69	2.5	Inv.D. (3)	0/19	II	Died (52)	+	+	−	−
10	52	7.0	Inv.D. (3)	4/19	IIIa	Died (10)	++	++	−	−
11	85	2.2	Ad-sq (3)	4/13	IIIa	Alive	++	−	−	−
12	34	4.0	Inv.D. (3)	9/19	IIIa	Died (58)	+	+	−	−

[a] Intensity of immunostaining: −, negative; +, positive, ++, strongly positive.
[b] Inv.D., invasive ductal carcinoma; NonI.D., noninvasive ductal carcinoma; Ad-sq, adenosquamous carcinoma.

Table 3 TN immunohistochemistry in relation to the clinicopathological characteristics of 210 breast cancer patients

Parameter	TN immunohistochemistry[a] CaC(+) St(+)	CaC(−) St(+)	CaC(−) St(−)	Total	*P* value[b]
No. of patients	12	65	133	210	
Mean age at diagnosis (yr)	54.4	53.9	55.1		
Mean tumor					>0.1
diameter (cm ± SD)	4.0 ± 2.7	2.9 ± 1.8	2.7 ± 1.8		>0.1
Lymph node metastasis					
+	8 (67%)	34 (52%)	49 (37%)	91	0.043
−	4 (33%)	31 (48%)	84 (63%)	119	0.038
Clinical stage					
I	1 (8%)	12 (18%)	42 (32%)	55	0.067
II	5 (42%)	33 (51%)	61 (46%)	99	0.111
III	6 (50%)	20 (31%)	30 (22%)	56	
c-*erb*B-2					
+	8 (67%)	19 (29%)	29 (22%)	56	0.001
−	4 (33%)	46 (71%)	104 (78%)	154	0.252
ER status[c]					
+	2 (17%)	30 (46%)	72 (54%)	104	0.007
−	10 (83%)	31 (48%)	53 (40%)	94	0.279

[a] The patients were divided into the following three groups according to the results of TN immunohistochemistry: CaC(cancer cell TN)(+)/St(stroma TN)(+), CaC(−)/St(+), and CaC(−)/St(−).

[b] The *P* value in the upper row for each parameter is that for the comparison between CaC(+)/St(+) and CaC(−)/St(−), and that in the lower row is that for the comparison between Ca(−)/St(+) and CaC(−)/St(−).

[c] ER levels were not available for 12 patients.

37°C for 15 min. To remove unhybridized RNA, the sections were incubated with 20 μg/ml RNase A in 1× STE at 37°C for 30 min, followed by one washing in 1× STE at 37°C for 10 min, twice in 2× SSC at 50°C for 10 min, and twice in 0.2× SSC for 10 min at 50°C. *In situ* hybridization signals were detected immunohistochemically with alkaline phosphatase-conjugated anti-DIG antibody used according to the manufacturer's instructions (DIG Nucleic Acid Detection kit; Boehringer Mannheim). When satisfactory signals were obtained, the sections were washed in 10 mM Tris-HCl/1 mM EDTA, soaked in distilled water, and counterstained with 0.1% nuclear fast red. The slides were air dried and mounted.

RESULTS

Histological Diagnosis. Of the 210 breast cancers, 183 cases were invasive ductal cancer, 9 were noninvasive intraductal cancer, 6 were lobular cancer, and 12 were other types of cancer. Microscopic metastasis in axillary lymph nodes had been found in 84 patients at surgery.

Immunohistochemistry. The results of immunostaining for TN are summarized in Table 1. Positive staining for TN in cancer stroma (Fig. 1*a*) was found in 77 of the 210 cases, while 143 cases were negative (Fig. 1*b*). Further examination of the 77 TN-positive breast cancers revealed that 12 showed intense staining for TN in the cytoplasm of the cancer cells (Fig. 1*c*). Histologically, TN-positive cancer cells were often located in the margin of cancer nests in contact with the underlying mesenchyme (Fig. 1*d*). Positive reactivity was also demonstrated in single cells or small groups of cells in a fibrous stroma. These cancers showed a high malignancy in terms of histological grading, and included 11 ductal carcinomas and 1 adenosquamous carcinoma (Table 2). Regional lymph node metastasis was found in eight of the 12 patients. Positive TN staining of cancer cells at a site of metastasis was found in only one case, and the other seven were negative. Among these 12 cases, positive staining for vimentin in cancer cells was found in 1, and the other 11 were negative. The epithelial cells in normal, hyperplastic, and benign neoplastic mammary lesions in the present samples showed no significant staining for TN.

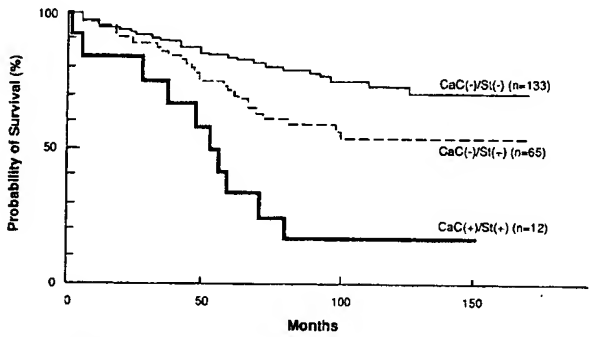

Fig. 2 Overall survival curves for different groups classified by TN staining patterns. The cancer cell TN-positive group [*CaC(+)/St(+)*], showed shorter survival than either of the cancer cell TN-negative groups with and without stromal TN [*CaC(−)/St(+)*, $P < 0.05$; *CaC(−)/St(−)*, $P < 0.001$]. The CaC(−)/St(+) group had a poorer outcome than the CaC(−)/St(−) group ($P < 0.05$).

Relationship of TN Immunohistochemistry with Clinicopathological Characteristics. The results of analysis of the relationship between TN immunohistochemistry and the clinicopathological characteristics of the patients are presented in Table 3. Compared with the patients with TN-negative breast cancers, those with positive staining of TN in the cancer cell cytoplasm showed greater frequency of lymph node involve-

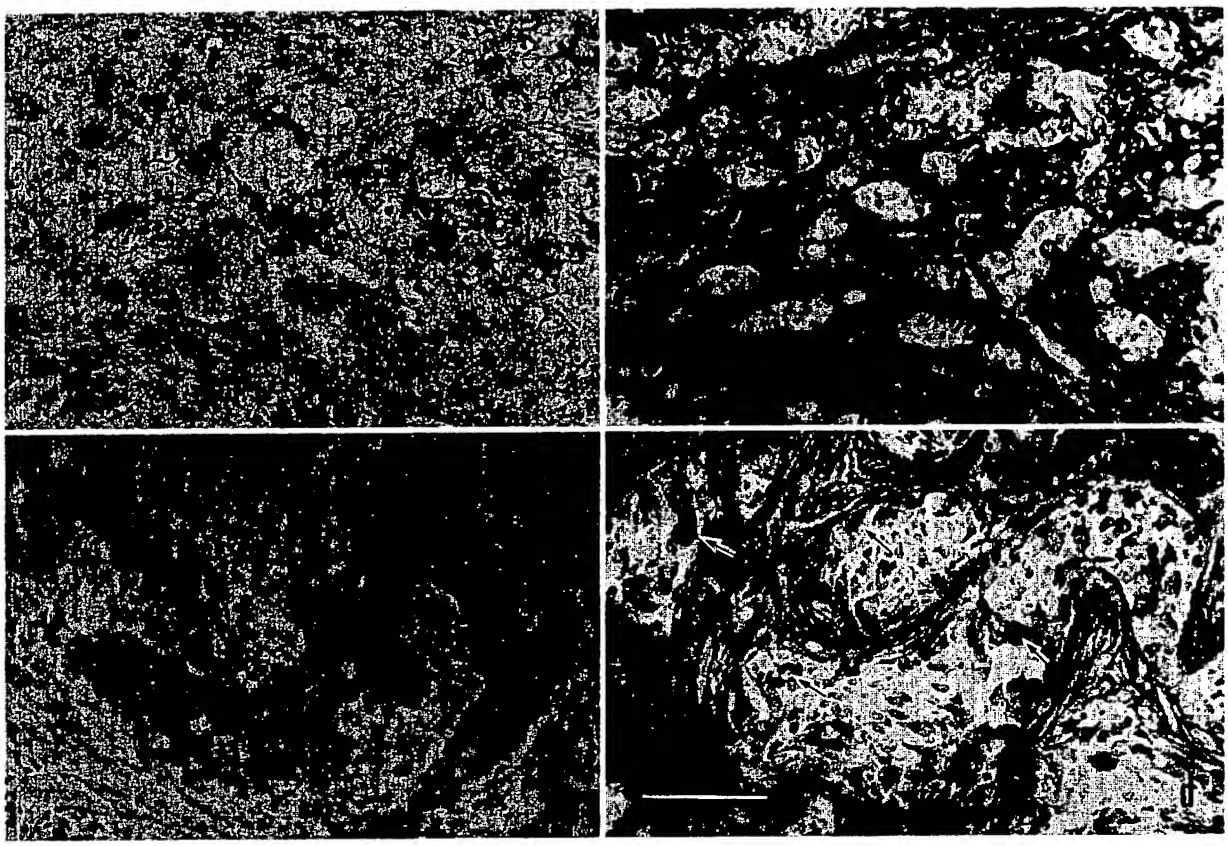

Fig. 3 *In situ* hybridization of human breast cancers using a DIG-labeled cRNA probe for TN mRNA. In an infiltrating ductal carcinoma, a large proportion of the stromal cells show positive signals for TN mRNA, but the cancer cells are not labeled (*a*). Immunoreactive TN is densely deposited in the stroma (*b*). Another carcinoma shows the cancer cells with positive signals for *in situ* hybridization (*c*), and the cells are also labeled by TN immunohistochemistry (*d, arrows*). *Bar in d*, 100 μm.

ment ($P = 0.043$), c-*erb*B-2 positivity ($P = 0.001$), and ER negativity ($P = 0.007$). The cancer cell TN-positive patients showed a tendency toward larger tumor diameter and later clinical stage ($P = 0.067$). Stromal TN was also correlated with lymph node metastasis ($P = 0.038$), but showed no significant correlation with other characteristics. Fig. 2 shows the survival curves for the 210 patients. The cancer cell TN(+) group showed shorter survival than the cancer cell TN(−) group having either stromal TN(+) status ($P < 0.05$) or stromal TN(−) status ($P < 0.001$). The stromal TN(+) group also showed a poorer outcome than the TN(−) group ($P < 0.05$).

***In Situ* Hybridization.** Nine fresh cancer tissues were examined for the expression of TN mRNA by *in situ* hybridization. In six cases, various amounts of mesenchymal cells expressing TN mRNA were seen in the cancer stroma (Fig. 3*a*). TN immunohistochemistry showed stromal staining in these specimens (Fig. 3*b*). In four of nine cases, TN mRNA was identified in cancer cells often located at the periphery of cancer nests adjacent to the mesenchyme (Fig. 3*c*). In two of these four cases, the cytoplasm of the cancer cells was positive for immunoreactive TN (Fig. 3*d*, *arrows*). This result confirmed that immunohistochemical TN staining of cancer cells denotes TN production by the cells themselves.

DISCUSSION

In breast cancers, an elevation of c-*erb*B-2 protein levels and this gene amplification have been found to be associated with increased tumor grade (31–34). The ER status of the breast cancer cells is correlated well with the response to hormonal treatment and to some extent with the risk of recurrence, and thus overall survival (35, 36). Each of these two factors is accepted as a possible prognostic marker in human breast cancer, but it is generally agreed that they do not correlate well with each other (31). Comparison of the results for these two parameters suggest that c-*erb*B-2 is much more effective than ER and a rather independent factor (37). In this study, the possible utility of TN as a prognostic marker of breast cancers was examined. Seventy-seven of 210 breast cancers showed stromal staining for TN; the survival of the patients was poorer than that in the other 133 stromal TN(−) patients. Among these 77 cases, we found 12 also showing TN(+) cancer cells; the 5-year survival of these patients was extremely poor. Thus, we identified TN to be a prognostic marker, especially when it is expressed in cancer cells, which permits the discrimination of a subgroup at a high risk of early relapse among breast cancer patients. However, we found that many of these cases were ER

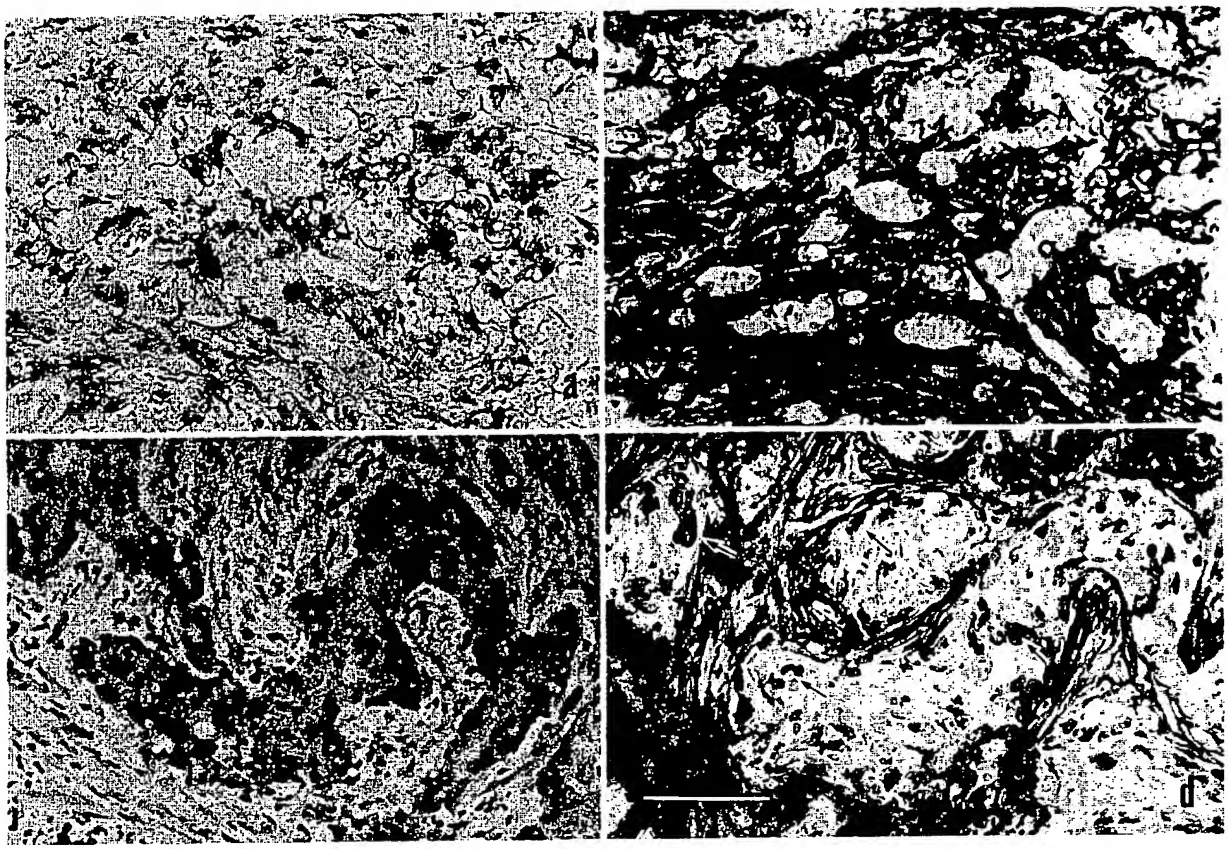

Fig. 3 *In situ* hybridization of human breast cancers using a DIG-labeled cRNA probe for TN mRNA. In an infiltrating ductal carcinoma, a large proportion of the stromal cells show positive signals for TN mRNA, but the cancer cells are not labeled (*a*). Immunoreactive TN is densely deposited in the stroma (*b*). Another carcinoma shows the cancer cells with positive signals for *in situ* hybridization (*c*), and the cells are also labeled by TN immunohistochemistry (*d*, *arrows*). *Bar in d*, 100 μm.

ment ($P = 0.043$), c-*erb*B-2 positivity ($P = 0.001$), and ER negativity ($P = 0.007$). The cancer cell TN-positive patients showed a tendency toward larger tumor diameter and later clinical stage ($P = 0.067$). Stromal TN was also correlated with lymph node metastasis ($P = 0.038$), but showed no significant correlation with other characteristics. Fig. 2 shows the survival curves for the 210 patients. The cancer cell TN(+) group showed shorter survival than the cancer cell TN(−) group having either stromal TN(+) status ($P < 0.05$) or stromal TN(−) status ($P < 0.001$). The stromal TN(+) group also showed a poorer outcome than the TN(−) group ($P < 0.05$).

***In Situ* Hybridization.** Nine fresh cancer tissues were examined for the expression of TN mRNA by *in situ* hybridization. In six cases, various amounts of mesenchymal cells expressing TN mRNA were seen in the cancer stroma (Fig. 3*a*). TN immunohistochemistry showed stromal staining in these specimens (Fig. 3*b*). In four of nine cases, TN mRNA was identified in cancer cells often located at the periphery of cancer nests adjacent to the mesenchyme (Fig. 3*c*). In two of these four cases, the cytoplasm of the cancer cells was positive for immunoreactive TN (Fig. 3*d*, *arrows*). This result confirmed that immunohistochemical TN staining of cancer cells denotes TN production by the cells themselves.

DISCUSSION

In breast cancers, an elevation of c-*erb*B-2 protein levels and this gene amplification have been found to be associated with increased tumor grade (31–34). The ER status of the breast cancer cells is correlated well with the response to hormonal treatment and to some extent with the risk of recurrence, and thus overall survival (35, 36). Each of these two factors is accepted as a possible prognostic marker in human breast cancer, but it is generally agreed that they do not correlate well with each other (31). Comparison of the results for these two parameters suggest that c-*erb*B-2 is much more effective than ER and a rather independent factor (37). In this study, the possible utility of TN as a prognostic marker of breast cancers was examined. Seventy-seven of 210 breast cancers showed stromal staining for TN; the survival of the patients was poorer than that in the other 133 stromal TN(−) patients. Among these 77 cases, we found 12 also showing TN(+) cancer cells; the 5-year survival of these patients was extremely poor. Thus, we identified TN to be a prognostic marker, especially when it is expressed in cancer cells, which permits the discrimination of a subgroup at a high risk of early relapse among breast cancer patients. However, we found that many of these cases were ER

negative and c-*erb*B-2 positive. There was also a significant relationship of cancer cell TN positivity to lymph node metastasis. Therefore, TN expression of cancer cells may not be an independent parameter.

It is generally accepted that the mesenchymal cells are the cellular source of TN (1, 14, 38, 39). Also, a few investigators have reported TN expression in the epithelium. In chick developing lung, *in situ* hybridization demonstrates TN mRNA in the most distal epithelial cells of the bronchi as well as the adjacent fibroblasts (40, 41). During chick feather morphogenesis, TN mRNA is detected initially in the overlying epithelia and then in the underlying mesenchyme (42). In these developing tissues, however, immunoreactive TN is positive in the basement membrane and/or the surrounding mesenchyme, but not in the epithelia. The results suggest that TN synthesized by the epithelium can be released promptly into the extracellular space and deposited there. Immunohistochemistry of cancer tissues, including comedo carcinomas of the breast (16), metastasized prostatic carcinoma in a lymph node (13), and squamous cell carcinomas and adenocarcinomas of the lung (9), has demonstrated cytoplasmic TN staining, suggesting that cancer cells also produce TN. The present results acquired by *in situ* hybridization clearly demonstrated TN synthesis by cancer cells as well as by the stromal cells. Four of the nine cases were positive for TN mRNA, but immunoreactive TN was found in cancer cells in only two of them. TN produced by cancer cells may be also released promptly into the extracellular space, but a small amount, probably caused by extreme overexpression or retardation of its release, is retained in the cancer cell cytoplasm.

Of the various proposed functions of TN, antiadhesion would seem to be the most probable (43, 44). Fibroblast attachment to fibronectin-coated plates is inhibited by TN addition to the culture medium in a concentration-dependent manner (45). TN released from cancer cells may loosen adhesions between the cells and adhesive extracellular matrix proteins, such as fibronectin, and may increase the mobility of cancer cells, with resulting increased invasive capacity. The TN function, at least partially, could account for the relationship between the TN positivity of the cancer cells and the clinicopathological characteristics, such as the tendency to larger tumor size and the significantly elevated incidence of lymph node metastasis. We also found that the outcome associated with TN(+) stroma was poor compared with TN(−) stroma, and that lymph node metastasis occurred more frequently in association with TN(+) stroma than with TN(−) stroma. According to this result, stromal TN in the cancer tissues may promote cancer spreading. Our study also indicates that the stromal TN detected by immunohistochemistry could have been secreted from both the cancer cells and the stromal cells, a state which may make it more complicated to determine TN functions in cancer stroma. Therefore, it is necessary to further clarify the TN-secreting cells and the timing of deposition during tumor progression.

ACKNOWLEDGMENTS

We are grateful to A. Kamimori of Matsusaka Chuo General Hospital for technological assistance.

REFERENCES

1. Chiquet-Ehrismann, R., Mackie, E. J., Pearson, A. C., and Sakakura, T. Tenascin: an extracellular matrix protein involved in tissue interactions during fetal development and oncogenesis. Cell, *47:* 131–139, 1986.

2. Ekblom, P., and Aufderheide, E. Stimulation of tenascin expression in mesenchyme by epithelial-mesenchymal interactions. Int. J. Dev. Biol., *33:* 771–779, 1989.

3. Erickson, H. P., and Bourdon, M. A. Tenascin: an extracellular matrix protein prominent in specialized embryonic tissues and tumors. Annu. Rev. Cell Biol., *5:* 71–92, 1989.

4. McComb, R. D., and Bigner, D. D. Immunolocalization of monoclonal antibody-defined extracellular matrix antigens in human brain tumors. J. Neurooncol., *3:* 181–186, 1985.

5. Riedl, S. E., Faissner, A., Schlag, P., Herbay, A. V., Koretz, K., and Moller, P. Altered content and distribution of tenascin in colitis, colon adenoma, and colorectal carcinoma. Gastroenterology, *103:* 400–406, 1992.

6. Sakai, T., Kawakatsu, H., Hirota, N., Yokoyama, T., Sakakura, T., and Saito, M. Specific expression of tenascin in colonic neoplasms. Br. J. Cancer, *67:* 1058–1064, 1993.

7. Van Eyken, P., Sciot, R., and Desmet, V. J. Expression of novel extracellular matrix component tenascin in normal and diseased human liver: an immunohistochemical study. J. Hepatol., *11:* 43–52, 1990.

8. Yamada, S., Ichida, T. Matsuda, Y, Miyazaki, Y., Hatano, T., Hata, K., Asakura, H., Hirota, N., Geerts, A., and Wisse, E. Tenascin expression in human chronic liver disease and in hepatocellular carcinoma. Liver, *12:* 10–16, 1992.

9. Soini, Y., Paakoo, P., Nourva, K., Kamel, D., Linnala, A., Virtanen, I., and Lehto, V-P. Tenascin immunoreactivity in lung tumors. Am. J. Clin. Pathol., *100:* 145–150, 1993.

10. Natali, P. G., Nicotra, M. R., Bigotti, A., Botti, C., Castellani, P., Risso, A. M., and Zardi, L. Comparative analysis of the expression of the extracellular matrix protein tenascin in normal human fetal, adult and tumor tissues. Int. J. Cancer, *47:* 811–816, 1991.

11. Vollmer, G., Siegal, G. P., Chiquet-Ehrismann, R., Lightner, V. A., Arnholdt, H., and Knuppen, R. Tenascin expression in the human endometrium and in endometrial adenocarcinoma. Lab. Invest., *62:* 725–730, 1990.

12. Anbazhagan, R., Sakakura, T., and Gusterson, B. A. The distribution of immuno-reactive tenascin in the epithelial-mesenchymal junctional areas of benign and malignant squamous epithelia. Virchows Arch. B Cell Pathol., *59:* 59–63, 1990.

13. Ibrahim, S. N., Lightner, V. A., Ventimiglia, J. B., Ibrahim, G. K., Walther, P. J., Bigner, D. D., and Humphrey, P. A. Tenascin expression in prostatic hyperplasia, intraepithelial neoplasia, and carcinoma. Hum. Pathol., *24:* 982–989, 1993.

14. Mackie, E. J., Chiquet-Ehrismann, R., Pearson, C. A., Inaguma, Y., Taya, K., Kawarada, Y., and Sakakura, T. Tenascin is a stromal marker of epithelial malignancy in the mammary gland. Proc. Natl. Acad. Sci. USA, *84:* 4621–4625, 1987.

15. Koukolis, G. K., Gould, V. E., Bhattacharyya, A., Gould, J. E., Howeedy, A. A., and Virtanen, I. Tenascin in normal, reactive, hyperplastic, and neoplastic tissues. Hum. Pathol., *22:* 636–643, 1991.

16. Howeedy, A. A., Virtanen, I., Laitinen, L., Gould, M. S., Koukolis, G. K., and Gould, V. E. Differential distribution of tenascin in the normal, hyperplastic, and neoplastic breast. Lab. Invest., *63:* 798–806, 1990.

17. Sakakura, T., Ishihara, A., and Yatani, R. Tenascin in mammary gland development: from embryogenesis to carcinogenesis. *In:* M. Lippman and R. Dickson (eds.), Regulatory Mechanisms in Breast Cancer, pp. 383–400. Dordrecht, the Netherlands: Kluwer Academic Publishers, 1991.

18. Shoji, T., Kamiya, T., Tsubura, A., Hamada, Y., Hatano, T., Hioki, K., and Morii, S. Tenascin staining positivity and the survival of patients with invasive breast carcinoma. J. Surg. Res., *55:* 295–297, 1993.

19. Sugawara, I., Hirakoshi, J., Masunaga, A., Itoyama, S., and Sakakura, T. Reduced tenascin expression in colonic carcinoma with lymphogenous metastasis. Invasion Metastasis, *11:* 325–331, 1991.

20. Steindler, D. A., Cooper, N. G. F., Faissner, F., and Schachner, M. Boundaries defined by adhesion molecules during development of the cerebral cortex: the J1/tenascin glycoprotein in the mouse somatosensory cortical barrel field. Dev. Biol., *131:* 243–260, 1989.

21. Lightner, V. A., Marks, J. R., and McCachren, S. M. Epithelial cells are an important source of tenascin in normal and malignant human breast tissue. Exp. Cell Res., *210:* 177–184, 1994.

22. Hiraiwa, N., Kida, H., Sakakura, T., and Kusakabe, M. Induction of tenascin in cancer cells by a diffusible factor. J. Cell Sci., *104:* 289–296, 1993.

23. Sakakura, T., and Kusakabe, M. Can tenascin be redundant in cancer development? Perspect. Dev. Neurobiol., *2:* 111–116, 1994.

24. Scarff, R. W., and Torloni, H. Histological Typing of Breast Tumors, pp. 15–25. Geneva: World Health Organization, 1982.

25. Bloom, H. J. G., and Richardson, W. W. Histological grading and prognosis in breast cancer. Br. J. Cancer, *11:* 359–377, 1957.

26. Eahrs, O. H., and Myers, M. H. Manual for Staging for Cancer, Ed. 2, pp. 127–133. Philadelphia: J. B. Lippincott Co., 1983.

27. Cox, D. R. Regression models and life tables. J. R. Stat. Soc. B., *34:* 187–202, 1972.

28. Kaplan, E., and Meier, P. Nonparametric estimation from incomplete observation. J. Am. Stat. Assoc., *53:* 457–481, 1958.

29. Oike, Y., Hiraiwa, S., Kawakatsu, H., Nishikai, M., Okinaka, T., Suzuki, T., Okada, A., Yatani, R., and Sakakura, T. Isolation and characterization of human fibroblast tenascin. An extracellular matrix glycoprotein of interest for developmental studies. Int. J. Dev. Biol., *34:* 309–317, 1990.

30. Tsukamoto, T., Kusakabe, M., and Saga, Y. *In situ* hybridization with non-radioactive digoxigenin-11-UTP-labeled cRNA probes: localization of developmentally regulated mouse tenascin mRNAs. Int. J. Dev. Biol., *35:* 25–32, 1991.

31. Slamon, D. J., Clark, G. M., Wong, S. G., Levin, W. J., Ullrich, A., and McGuire, W. L. Human breast cancer: correlation of relapse and survival with amplification of the HER-2/neu oncogene. Science (Washington DC), *235:* 177–182, 1987.

32. Van de Vijver, M., Van de Bersselaar, R., Devilee, P., Cornelisse, C., Peterse, J., and Nusse, R. Amplification of the neu (c-*erb*B-2) oncogene in human mammary tumours is relatively frequent and is often accompanied by amplification of the linked c-*erb*A oncogene. Mol. Cell. Biol., *7:* 2019–2023, 1987.

33. Varley, J. M., Swallow, J. E., Brammar, W. J., Whittaker, J. L., and Walker, R. A. Alterations to either c-*erb*B-2(neu) or c-*myc* proto-oncogenes in breast carcinomas correlate with poor short-term prognosis. Oncogene, *1:* 423–430, 1987.

34. Venter, D. J., Tuzi, N. L., Kukar, S., and Gullick, W. J. Overexpression of the c-erbB-2 oncoprotein in human breast carcinomas: Immunohistochemical assessment correlates with gene amplification. Lancet, *2:* 69–72, 1987.

35. Knight, W. A., Livingston, R. B., Gregory, E. J., and McGuire, W. L. Estrogen receptor as an independent prognostic factor for early recurrence in breast cancer. Cancer Res., *37:* 4669–4671, 1977.

36. Hahnel, A., Woodings, T., and Vivian, A. B. Prognostic value of estrogen receptors in primary breast cancer. Cancer (Phila.), *44:* 671–675, 1979.

37. McCann, A. H., Dervan, P. A., O'Regan, M., Codd, M. B., Gullick, W. J., Tobin, B. M. J., and Carney, D. N. Prognostic significance of c-*erb*B-2 and estrogen receptor status in human breast cancer. Cancer Res., *51:* 3296–3303, 1991.

38. Inaguma, Y., Kusakabe, M., Mackie, E. J., Pearson, C. A., Chiquet-Ehrismann, R., and Sakakura, T. Epithelial induction of stromal tenascin in the mouse mammary gland: from embryogenesis to carcinogenesis. Dev. Biol., *128:* 245–255, 1988.

39. Natali, P. G., Nicotra, M. R., Bortolazzi, A., Mottolese, M., Coscia, N., Bigotti, A., and Zardi, L. Expression and production of tenascin in benign and malignant lesions of melanocyte lineage. Int. J. Cancer, *46:* 586–590, 1990.

40. Koch, M., Wehrle-Haller, B., Baumgarten, S., Spring, J., Brubacher, D., and Chiquet, M. Epithelial synthesis of tenascin at tips of growing bronchi and graded accumulation in basement membrane and mesenchyme. Exp. Cell Res., *194:* 297–300, 1991.

41. Priet, A. L., Jones F. S., Cunningham, B. A., Crossin, K. L., and Edelman, G. M. Localization during development of alternatively spliced forms of cytotactin mRNA by in situ hybridization. J. Cell Biol., *111:* 685–698, 1990.

42. Tucker, R. P. The sequential expression of tenascin mRNA in epithelium and mesenchyme during feather morphogenesis. Rou'x Arch. Dev. Biol., 200, 108–112, 1991.

43. Sage, E. H., and Bornstein, P. Extracellular proteins that modulate cell-matrix interactions. J. Biol. Chem., *266:* 14831–14834, 1991.

44. Chiquet-Ehrismann, R. Anti-adhesive molecules of the extracellular matrix. Curr. Opin. Cell Biol., *3:* 800–804, 1991.

45. Chiquet-Ehrismann, R., Kalla, P., Pearson, C. A., Conrad, B., and Chiquet, M. Tenascin interferes with fibronectin action. Cell, *53:* 383–390, 1988.

British Journal of Cancer (1998) 78(11), 1507–1513

Tenascin-C expression in invasion border of early breast cancer: a predictor of local and distant recurrence

T Jahkola[1], T Toivonen[2], I Virtanen[3], K von Smitten[1], S Nordling[4], K von Boguslawski[4], C Haglund[5], H Nevanlinna[6], and C Blomqvist[7]

[1]Fourth Department of Surgery, University of Helsinki, Helsinki, Finland; [2]Department of Pathology, Kymenlaakso Central Hospital, FIN-48210 Kotka, Finland; Departments of [3]Anatomy, Institute of Biomedicine, and [4]Pathology, Haartman Institute, FIN-00014 University of Helsinki; [5]Second Department of Surgery, University of Helsinki, FIN-00290 Helsinki; Departments of [6]Obstetrics and Gynecology and [7]Oncology, Helsinki University Central Hospital, FIN-00290 Helsinki, Finland

Summary We have recently demonstrated an association between distant metastasis and the expression of the extracellular matrix glycoprotein tenascin-C (Tn-C) in the invasion border of small axillary node-negative breast carcinomas. Our purpose was to assess the relationship between the expression of Tn-C in the tumour invasion border and several histopathological and biological variables and to compare their usefulness in predicting local and distant disease recurrences. The original patient group consisted of 143 women with axillary node-negative breast cancer (one bilateral) treated with breast-conserving surgery and post-operative radiotherapy, and followed for a median of 8 years. Because of the small number of recurrences an additional group of 15 similarly treated women with recurrent breast cancer was also studied. The size of the tumour, its histology, including a possible intraductal component, and grade were re-evaluated. The expression of erbB-2, p53, Ki-67 and Tn-C was evaluated by immunohistochemistry. Ploidy and S-phase fraction (SPF) were assessed by flow cytometry. The only statistically significant prognostic factor for local recurrence was Tn-C expression in the invasion border. For metastasis Ki-67 positivity, tumour size and Tn-C expression in the invasion border were statistically significant, but Ki-67 positivity was the only independent prognostic factor. Tn-C expression in the invasion border was associated with a higher proliferation rate measured by Ki-67 and SPF, which is consistent with the suggested growth-promoting activity of Tn-C. Tn-C may be a useful marker in selecting patients for adjuvant therapies to reduce the rate of both local and distant cancer recurrences.

Keywords: tenascin-C; early breast cancer; metastasis; breast-conserving surgery; local recurrence

Tenascin-C (Tn-C) is an extracellular matrix glycoprotein expressed transiently during embryogenesis, inflammation and malignancy. It is variably present in the basement membrane region of some adult epithelia and enhanced periductally next to the basement membrane in intraductal carcinoma of the breast. In infiltrating breast carcinoma Tn-C is expressed deeper in the stroma (Ferguson et al, 1990; Howeedy et al, 1990). Cell culture experiments suggest that Tn-C promotes cell growth by augmenting the mitogenic effect of fibroblast growth factor and that it is a prerequisite for epidermal growth factor-induced proliferation (Sakakura et al, 1991; Jones et al, 1997). The most consistent function of Tn-C seems to be that it decreases cell adhesion, and therefore it has been speculated that Tn-C could promote cancer cell invasion and metastasis (Sakakura et al, 1991; Yoshida et al, 1995). In our recent study of axillary node-negative breast cancer none of the tumours that did not express Tn-C in the stroma (15/137) recurred. Eight out of the 11 tumours that developed distant metastases within 5 years expressed Tn-C in the invasion border (Jahkola et al, 1996). This association between the expression of Tn-C in the invasion area of small node-negative breast cancers and distant metastases suggests a role in tumour spread.

Received 21 October 1997
Revised 5 March 1998
Accepted 17 March 1998

Correspondence to: T Jahkola, Fourth Department of Surgery, Helsinki University Central Hospital, Kasarmikatu 11–13, FIN-00130 Helsinki, Finland

Breast cancer is a heterogeneous disease with different histological types and various biological features. Several parameters of malignancy have been proposed as prognostic markers. Theoretically, proliferation activity, genetic instability and markers of tumour invasion capacity indicate a more aggressive disease. In addition, rapid tumour growth also suggests a better response to chemotherapy. Tumour size and axillary nodal status are still important in predicting the outcome of breast cancer (Fisher et al, 1993). Metastatic tumour in axillary lymph nodes is the main criterion for adjuvant treatment. However, 10–30% of axillary node-negative patients develop distant metastases (EBCTCG, 1992). The value of prognostic markers in axillary node-negative patients is controversial and at present there is no agreement on any single prognostic factor strong enough to select patients with node-negative breast cancer for adjuvant therapies (Mansour et al, 1994).

Breast-saving surgery is the treatment of choice when the tumour is unifocal or confined to one quadrant, and a good aesthetic result can be achieved. Post-operative radiotherapy reduces the risk of local recurrence from 30% to 5% but does not improve survival (EBCTCG, 1995; Fisher et al, 1995). Adjuvant systemic treatment seems to prevent local recurrences (Haffty et al, 1991; Fisher et al, 1995). Patients with a local recurrence have an increased risk of distant metastases (Whelan et al, 1994; Veronesi et al, 1995). Moreover, it causes psychological morbidity and is usually treated with mastectomy. There is a need to investigate optional or additional treatment modalities such as more effective systemic therapies for women with a risk of local recurrence after limited surgery

and irradiation (Gelber and Goldhirsch, 1994). Attempts have also been made to find a subgroup of low-risk patients who do not need radiotherapy (Clark et al, 1992; Veronesi et al, 1993; Liljegren et al, 1994).

The aim of this work was to assess the relationship between the expression of Tn-C in the tumour invasion border and several histopathological and biological variables, and to compare their usefulness in predicting local and distant disease recurrences. All patients had undergone breast-conserving surgery and post-operative radiotherapy for node-negative breast cancer. Because the number of recurrences was low we extended the study to recurrent cases in another node-negative patient group treated in the same way. Other parameters studied were age, histology of the tumour, including a possible intraductal component, grade and size. An immunohistochemical analysis of erbB-2 oncoprotein, p53-protein and Ki-67 antigen, as well as ploidy and SPF determination by flow-cytometry, was also performed.

PATIENTS AND METHODS

Original group of patients with breast-saving treatment

The original group consisted of 143 women with 144 node-negative breast cancers (one bilateral) treated with breast-saving surgery and axillary dissection at the Maria Hospital of Helsinki (55 patients) and the Fourth Department of Surgery of the Helsinki University Central Hospital (HUCH) (88 patients) in 1985–89. Patients chosen for breast preservation presented preoperatively with a clinically unifocal T1N0 (2 cm or less in diameter) tumour without any cancer involvement at the resection margin found at surgery. A clear resection margin was defined as 5 mm or more of normal tissue measured histologically. Patients with narrower margins were referred to re-resection or mastectomy. Mastectomized patients were excluded from the study. All women received post-operative radiotherapy (25 times 2 Gy) at the Department of Oncology of HUCH but no adjuvant chemotherapy or hormonal therapy. The median follow-up time was 7.8 years, range 5.4–11.4 years.

Additional breast cancer patients with recurrent disease

In 1985–90 238 women with axillary node-negative breast cancer (not already included in the original study) were treated similarly and referred to the Department of Oncology of HUCH for radiotherapy. Twenty-six (11%) of these had had a disease recurrence. The rates of both local relapse (15/238, 6%) and distant metastasis (16/238, 7%) at 5-year follow-up were comparable with those in the original patient group, in which 4% had local recurrences and 8% distant metastases (Jahkola et al, 1996), suggesting an equal standard of treatment. Paraffin-embedded specimens were available from 15 out of 26 tumours that recurred: seven local recurrences and 11 distant metastases, three patients having both. These 15 patients formed the new patient material. A comparison between the patient groups with recurrent disease is presented in Table 1.

Table 1 Characteristics of the relapsed cases of the original and new patient groups

	Original patients	New patients	*P*-value
Number of patients	17	15	
Age of patients (years)			
Median	50.5	50.7	0.44[a]
Range	37.5–72.5	30.2–70.6	
Distant metastasis	14	11	0.68
Local relapse	7	7	>0.99
Breast	6	6	
Axilla	1	1	
Death of breast cancer	9	6	0.21
Histology			
Ductal	11	11	
Lobular	5	3	
Others	1	1	0.83[b]
Grade			
1	4	5	
2	2	3	
3	5	3	0.67[b]
Tumour size (mm)			
Median	15.0	13.5	0.23[a]
Range	1–25	7–23	
DCIS +	7	4	
DCIS –	10	11	0.47
EIC +	1	1	
EIC –	16	14	>0.99
Comedo-type DCIS	1	1	>0.99
erbB-2 +	2	Not performed	
erbB-2 –	13	Not performed	
p53 +	2	3	
p53 –	13	10	0.64
Ki-67 +	11	10	
Ki-67 –	3	4	0.69
SPF high	7	10	
SPF low	7	3	0.24
Aneuploid	3	4	
Diploid	11	11	>0.99
Expression of Tn-C in invasion border			
+	10	9	
–	2	2	>0.99

[a]Mann–Whitney *U*-test. [b]Chi-square test. Other associations assessed by Fisher's exact test.

Tumour samples and pathological parameters

Sections of paraffin-embedded tissue specimens of the primary tumours were reviewed and classified for histology, grade and size. The extent of the intraductal component (ductal carcinoma in situ; DCIS) was recorded. It was called extensive (EIC) if DCIS comprised 25% or more of the tumour area encompassed by the infiltrating tumour and DCIS was also present in the surrounding tissue (Schnitt et al, 1987). The grade of the ductal carcinomas was assessed according to Bloom and Richardson (1957). Tumour size was measured in the histological sections and varied from 1 to 26 mm. The whole cross-section of the tumour was examined in most cases. In prognostic studies with immunohistochemistry and flow cytometry 6–11% of the samples could not be interpreted because of technical failures or the fact that there was too little malignant tissue left. The assessment of histopathological and prognostic parameters was performed blinded to patient outcome.

Immunohistochemical analysis of Tn-C, p53 protein, Ki-67 antigen and erbB-2 protein

The monoclonal antibody 143BD7 against Tn-C was characterized previously (Tiitta et al, 1992) and the detection and evaluation of Tn-C in the invasion border of breast cancer by immunohistochemistry has been described (Jahkola et al, 1996). In short, tumours expressing Tn-C in the area of invasion with adjacent normal tissue clearly visible were called Tn-C positive (Figure 1). An invasion border of the tumour could be identified in 121 out of the 159 tumours. In the rest, the invasion border was not included in available specimens.

The monoclonal antibody to p53 protein (clone DO-7) and polyclonal anti-human Ki-67 were purchased from Dako (Glostrup, Denmark). The optimal working dilutions were determined by serial dilutions and was 1:300 for anti-p53 and 1:500 for anti-Ki-67. Mouse monoclonal antibody E2-4001 raised against the intracytoplasmic domain of the human erbB-2 antigen was obtained from Molecular Oncology, Gaithersburg, MD, USA. A final concentration of 6 μg ml^{-1} (dilution 1:20) in the working solution was used. p53 and Ki-67 primary antibodies were applied overnight and erbB-2 antibody for 2 h at room temperature in humidified chambers.

For immunostaining 4-μm-thick paraffin sections were cut and mounted on 3-aminopropyl-triethoxy-silane (APES) (Sigma, St Louis, MO, USA)-coated slides and treated in a microwave oven as described previously (Victorzon, 1996).

Immunohistochemistry was performed using the anti-alkaline phosphatase method as described (Jahkola et al, 1996) or the avidin–biotin complex (ABC) immunoperoxidase technique applying a commercial Elite ABC Kit (Vectastain, Vector Laboratories, Burlingame, CA, USA), also described previously (Victorzon, 1996).

The level of immunoreactivity of p53 and Ki-67 antigens was expressed as the percentage of positive cancer cell nuclei. Interpreting erbB-2 staining, all tumours with positive cell membranes were scored positive. The p53 staining could be interpreted in 143/159 (90%), the Ki-67 staining in 141/159 (89%) and the erbB-2 staining in 142/144 (99%) of the tumours. The anti-erbB-2 antibody E2-4001 was no longer available when the new material of 15 tumours was tested.

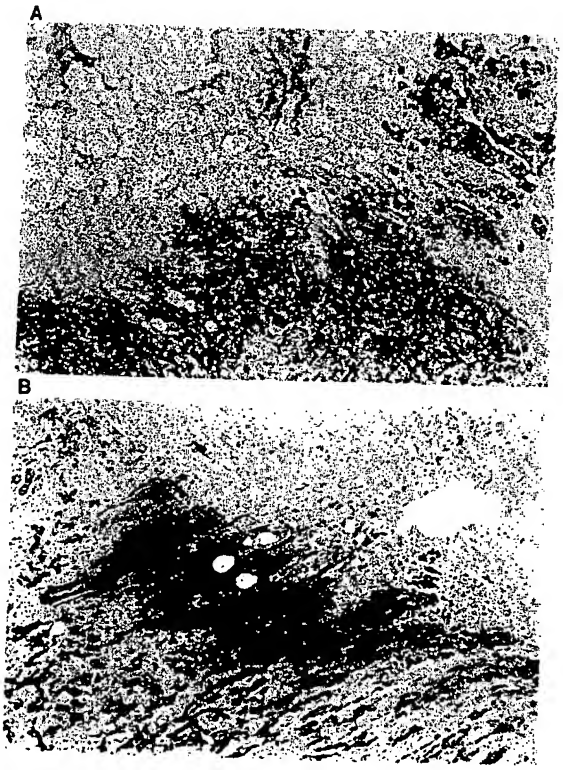

Figure 1 Expression of tenascin-C in the invasion border of infiltrating ductal (A) and lobular (B) carcinoma of the breast

Ploidy and S-phase fraction determined by flow cytometry

A modification of the method of Hedley et al (1983) was applied (Hedley et al, 1983). In brief, two 50-μm-thick sections were treated with 10 mg ml^{-1} proteinase K (Sigma) for 30 min at room temperature. After filtration, the nuclei were treated with RNAase (10 mg ml^{-1}) and stained with 25 μg ml^{-1} ethidium bromide (Sigma) for at least 1 h. The DNA was determined by flow cytometry (FACScan, Becton Dickinson, Mountain View, CA, USA) using 15-mW excitation at 488 nm, and the total emission above 560 nm was recorded. As the staining intensity of fixed nuclei varies from one sample to another, no internal standard was added. The lowest peak was assigned a DNA index (DI) value of 1.00 and the DI values of other peaks were calculated with this as a reference. Therefore, possible hypodiploid peaks were identified as diploid and the normal diploid peak as hyperdiploid. The S-phase fraction (SPF) was calculated either using the Cellfit program of the FACScan flow cytometer or manually by a modified rectilinear method. If the automatic and the manual methods gave different results, the lower SPF was chosen. Usually, the manual method gave a lower result, because it was only applied in those tumours in which it was felt that the automatic method gave too high a SPF, e.g. when there was a skewness to the right of the G_1 peak. If the sample contained less than 15% aneuploid cells, the SPF was not calculated. At least 10 000 nuclei from each specimen were analysed. DNA ploidy could be determined in 150/159 (94%) and SPF in 147/159 of the tumours (92%).

Statistical methods

Chi-square test, Fisher's exact test and Mann–Whitney *U*-test were used to test for association between variables and possible differences between patients with relapses in the original and in the new patient groups. Metastasis-free survival (MFS) in the original patient group according to each prognostic parameter was estimated with the Kaplan–Meier method. The statistical significance of differences in outcome between patients with or without a prognostic factor were calculated in the overall patient group (original and additional patients combined) using the Cox proportional hazard model to compute the hazard ratios of disease recurrence. The statistical significance of the effect of the continuous variables on disease recurrence was also tested with the Cox proportional hazard model with the variable to be tested as the only covariate. The multivariate analysis for metastasis was performed with the Cox proportional hazard model entering the variables significant in the univariate analysis. Two-sided *P*-values smaller than 0.05 were considered significant.

Assignment of cut-off values

The median size of 13 mm was chosen to dichotomize the study group. The median age at operation of all patients was 51.9 years. For analysis the patients were divided into two groups, 50 years or older or less than 50 years. The median SPF of diploid (2.4%) and the median SPF of aneuploid tumours (8.4%) were used as cut-off values. A cut-off value of 20% positive nuclei was used for p53. For Ki-67 5–15% positive expression in the nuclei was called weak (+), 16–29% moderate (++) and 30% or more strongly positive (+++). Because there was no difference in metastasis between Ki-67 +, ++ and +++ tumours, the classification was simplified by combining these classes into one Ki-67-positive category of 5% or more of positive nuclei. Five per cent was also the median of Ki-67 immunostaining. The cut-off values for prognostic factors presented here were also used when analysing local recurrences after breast-saving surgery.

RESULTS

Association of Tn-C in the invasion border with other variables

The expression of Tn-C at the site of invasion was correlated with a higher proliferation rate measured by the expression of Ki-67 antigen (≥ 5% positive nuclei) (P = 0.03) and a high SPF (P = 0.004). There was also an association with tumours not comprising an intraductal component (P = 0.04) (Table 2).

Rate and time of distant and local recurrences

The median follow-up of patients in the original study group was 7.8 years (range 5.7–11.4 years). Seven local relapses occurred (5%), six in the ipsilateral breast and one in the axilla. In addition, one patient had had an angiosarcoma in the treated breast. One mastectomy was performed because of a painful post-radiation mastitis, and one mastectomy with immediate reconstruction because of a poor cosmetic result. One cancer developed in the contralateral breast. Distant metastasis occurred in 14 women (10%), four of whom also had a local recurrence. The median time of local recurrence was 2.9 years (range 1.3–6.9 years) and that of distant metastasis 3.6 years (range 0.7–8.2 years) in the overall patient group.

Table 2 Association of Tn-C in invasion border with other prognostic factors in axillary node-negative breast cancers

	All tumours (%)	Tn-C-positive invasion border (%)	Chi-square P-value
All	121[a]	63 (52)	
DCIS +	43	17 (40)	
DCIS –	78	46 (59)	0.04
EIC +	6	4 (67)	
EIC –	115	59 (51)	0.46
erbB-2 +	7	3 (43)	
erbB-2 –	103	51 (50)	0.73
p53 +	19	11 (58)	
p53 –	92	47 (51)	0.59
Ki-67 +	65	40 (62)	
Ki-67 –	45	18 (40)	0.03
SPF high	62	40 (65)	
SPF low	51	19 (37)	0.004
Aneuploid	44	23 (52)	
Diploid	72	37 (51)	0.93

[a]An invasion border was present in 121 tumours out of the 159 in the archival specimens available.

Metastasis-free survival in the original patient group and prognostic factors

The 8-year metastasis-free survival (MFS) was 89% in the original patients. Age, histology, grade, erbB-2, p53, SPF and ploidy did not predict metastasis significantly in a univariate analysis. The MFS in tumours 13 mm or smaller was 94%, and 86% in those larger than 13 mm (P = 0.01). The MFS in Ki-67-positive tumours was 84% and 96% in Ki-67-negative ones (P = 0.04). When Tn-C was expressed in the invasion border the MFS was 84% compared with 98% when there was no such expression (P = 0.03).

Prognostic factors of distant and local recurrence in the overall patient group

In univariate analysis for metastasis, size (P = 0.05), SPF of diploid tumours (P = 0.0001) and Ki-67 (P = 0.03) were significant prognostic factors, whereas grade (P = 0.18), age (P = 0.51), SPF of aneuploid tumours (P = 0.77) or of all tumours as a group (P = 0.73) and p53 (P = 0.90) failed to show prognostic power as continuous variables. The prognostic comparison of the categorized variables is presented in Table 3. In addition, when the diploid tumours were dichotomized to low and high SPF, the relative risk for metastasis in the high group was 3.16 (P = 0.05), whereas there was no such difference in the aneuploid tumours. Tn-C in the invasion border was statistically significant in predicting metastasis, and for local recurrence it was the only statistically significant prognostic factor (Table 3) with a hazard ratio of 11.0, CI 1.4–85.1, P = 0.02.

The hazard ratio of metastasis in patients with a tumour larger than 13 mm was 2.6, CI 1.1–5.9, P = 0.02, in those with Ki-67-positive tumours 5.5, CI 1.6–18.7, P = 0.006, and in those with tumours with Tn-C expression in the invasion border 3.4, CI 1.1–10.4, P = 0.03 (Table 3). When these three variables were introduced in a multivariate analysis, Ki-67 remained the only independent prognostic factor for metastasis (Table 4).

DISCUSSION

Tn-C is produced by normal mesenchymal and epithelial cells as well as some carcinoma cells (Lightner et al, 1994; Ishihara et al, 1995). Tn-C produced by carcinoma cells has been suggested to facilitate the spreading of the carcinoma (Ishihara et al, 1995). Our recent observation suggests that the expression of Tn-C at the active site of epithelial–stromal invasion indicates a more aggressive disease (Jahkola et al, 1996). The present study shows that the expression of Tn-C at the site of invasion is correlated with a higher proliferation rate measured by flow cytometric analysis of SPF and the immunohistochemical detection of Ki-67 antigen, which gives further support to the active role of Tn-C in cancer dissemination.

Tumour size is a well-known risk factor in node-negative breast cancer for both distant and local recurrence. In a large study of

Table 3 Distributions of prognostic factors and hazard ratios (HRs) for local recurrence and metastasis in 158 women with 159 axillary node-negative breast cancers treated with breast-saving surgery and post-operative radiotherapy

	Number of tumours	HR for local recurrence	P-value	HR for metastasis	P-value
Age <50 years	56	1.0		1.0	
Age ≥50 years	103	0.95	0.93 (NS)	0.68	0.34 (NS)
Histology[a]					
Ductal	95	1.0		1.0	
Lobular	35	1.0		1.0	
Others	29	0.34	0.30 (NS)	0.37	0.18 (NS)
DCIS +	57	1.0		1.0	
DCIS –	102	0.77	0.63 (NS)	1.07	0.87 (NS)
EIC +	12	1.0		1.0	
EIC –	147	1.04	0.97 (NS)	0.97	0.96 (NS)
Grade[b]					
1	51	1.0		1.0	
2	34	1.0		0.66	
3	26	2.86	0.30 (NS)	1.72	0.35 (NS)
Size >13 mm	66	1.0		1.0	
Size ≤13 mm	91	0.80	0.69 (NS)	0.39	0.02
erbB-2 +[c]	11			1.0	
erbB-2 –	131		–	0.46	0.31 (NS)
p53 +[d]	22	1.0		1.0	
p53 –	121	0.88	0.87 (NS)	0.58	0.29 (NS)
Ki-67 +[e]	80	1.0		1.0	
Ki-67 –	61	0.69	0.55 (NS)	0.18	0.006
SPF high[f]	73	1.0		1.0	
SPF low	72	1.37	0.58 (NS)	0.47	0.10 (NS)
Aneuploid	55	1.0		1.0	
Diploid	95	1.82	0.37 (NS)	1.75	0.24 (NS)
Expression of Tn-C in invasion border					
+	63	1.0		1.0	
–	58	0.09	0.02	0.30	0.03

[a]Others: two papillary, one medullary, two mucinous, 14 tubular, ten tubulolobular. For comparison with 'others' ductal and lobular carcinomas were combined. [b]Grade of 111 ductal and tubular carcinomas. [c]erbB-2 was stained only of the original patient material. Hazard ratio could not be computed because of no local recurrences in the erbB-2 positive group. [d]p53 cut-off 20% of nuclei positive. [e]Ki-67 cut-off 5% of nuclei positive. [f]SPF cut-off: median SPF of diploid tumours 2.4% and median of aneuploid tumours 8.4%.

Table 4 Multivariate analysis (Cox proportional hazard model) of the three covariates statistically significant in univariate analysis of metastasis

Covariate	P	HR	CI (95%)
Ki-67 (±, 5% cut off)	0.03	10.0	1.3–77.2
Tumour size (continuous)	0.17	2.1	0.7–6.0
Tn-C in invasion border	0.34	1.8	0.56–5.8

1800 patients who received locoregional therapy and had an 8-year follow-up, tumour size was the strongest predictor for distant recurrence. A high proliferation activity measured by the [^{3}H]-thymidine labelling index provided additional prognostic information in intermediate size (1–2 cm) tumours. Cell proliferation was the most significant predictor for locoregional relapse (Silvestrini et al, 1995). As in our study, SPF has been found to be a significant prognostic factor of distant metastasis in diploid but not in aneuploid tumours (Clark et al, 1989). A similar observation has been made in soft-tissue sarcomas (Huuhtanen et al, 1996). The prognostic value of immunohistochemically detected erbB-2 and p53 protein in early node-negative breast cancer is controversial (Silvestrini et al, 1993; Ravdin and Chamness, 1995; Rosen et al, 1995). In this study those markers did not show prognostic power for either local or distant recurrence.

Young age, tumour size, presence of carcinoma at the resection margin and the presence of an extensive intraductal component (EIC) are associated with a higher risk of local recurrence after breast-conserving surgery (Boyages et al, 1990; Holland et al, 1990; Borger et al, 1994; Gage et al, 1996; Schnitt et al, 1987). In the present study EIC was present in only 8% of the tumours compared with 20% in many of the previous studies, probably because the selection criteria for breast conservation had been strict: only tumours up to 2 cm in diameter (measured clinically) and with histologically clear margins were accepted. In this selected material the expression of Tn-C in the invasion border was the only marker that predicted local recurrence. Our results suggest that patients with carcinomas that do not express Tn-C in the invasion border do not

need adjuvant treatments. On the other hand, patients with tumours expressing Tn-C in the area of invasion have an increased risk of developing both local and distant recurrences.

Small tumour size, low grade and old age have been proposed as selection criteria for patients who might not benefit from radiotherapy (Clark et al, 1992; Veronesi et al, 1993; Liljegren et al, 1994). However, in a highly selected group of 87 patients treated with breast-conserving surgery without radiotherapy, the rate of local recurrence rose to 16% when the median follow-up time was 56 months, therefore this prospective clinical trial was closed (Schnitt et al, 1996). Because of the lack of reliable exclusion criteria the importance of post-operative radiotherapy for all patients has been reappraised (Morrow et al, 1995). The expression of Tn-C in the invasion border seems to be a biological marker of a higher risk for local relapse, and the absence of Tn-C might be used as an adjunct to define a group that could be left without radiotherapy.

Our results suggest that more radical surgery should be considered, adjuvant treatment recommended and that follow-ups should be more frequent and continued longer when Tn-C is expressed in the tumour invasion border. Additional studies are needed to establish whether Tn-C expression in the invasion border can be used as a criterion to select conservatively treated axillary node-negative breast cancer patients for adjuvant chemotherapy or hormonal therapy to reduce the risk of both local and distant disease spread.

ACKNOWLEDGEMENTS

The skilful technical assistance of Ms L Pirjamo, A Takkinen, M-L Piironen, M Shoultz, P Peltokangas, A Mäki and Mr R Karppinen is acknowledged. Professor S Sarna has given valuable suggestions concerning the statistical presentation.

REFERENCES

Bloom HJG and Richardson WW (1957) Histological grading and prognosis in breast cancer. A study of 1409 cases of which 359 have been followed for 15 years. *Br J Cancer* **11**: 359–377

Borger J, Kemperman H, Hart A, Peterse H, van Dongen J and Bartelink H (1994) Risk factors in breast-conservation therapy. *J Clin Oncol* **12**: 653–660

Boyages J, Recht A, Connolly JL, Schnitt SJ, Gelman R, Kooy H, Love S, Osteen RT, Cady B, Silver B and Harris JR (1990) Early breast cancer: predictors of breast recurrence for patients treated with conservative surgery and radiation therapy. *Radiother Oncol* **19**: 29–41

Clark GM, Dressler LG, Owens MA, Pounds G, Oldaker T and McGuire WL (1989) Prediction of relapse or survival in patients with node-negative breast cancer by DNA flow cytometry. *N Engl J Med* **320**: 627–633

Clark RM, McCulloch PB, Levine MN, Lipa M, Wilkinson RH, Mahoney LJ, Basrur VR, Nair BD, McDermot RS, Wong CS and Corbett PJ (1992) Randomized clinical trial to assess the effectiveness of breast irradiation following lumpectomy and axillary dissection for node-negative breast cancer. *J Natl Cancer Inst* **84**: 683–689

EBCTCG (1992) Systemic treatment of early breast cancer by hormonal, cytotoxic, or immune therapy. 133 randomised trials involving 31,000 recurrences and 24,000 deaths among 75,000 women. Early Breast Cancer Trialists' Collaborative Group [see comments]. *Lancet* **339**: 1–15 and 71–85

EBCTCG (1995) Effects of radiotherapy and surgery in early breast cancer. *N Engl J Med* **333**: 1444–1455

Ferguson JE, Schor AM, Howell A and Ferguson MW (1990) Tn-C distribution in the normal human breast is altered during the menstrual cycle and in carcinoma. *Differentiation* **42**: 199–207

Fisher B, Anderson S, Redmond CK, Wolmark N, Wickerham DL and Cronin WM (1995) Renalysis and results after 12 years of follow-up in a randomized clinical trial comparing total mastectomy with lumpectomy with or without irradiation in the treatment of breast cancer. *N Engl J Med* **333**: 1456–1461

Fisher ER, Costantino J, Fisher B, Redmond C and CNSABaBP Investigators (1993). Pathologic findings from the National Surgical Adjuvant Breast Project (Protocol 4) – Discriminants for 15-year survival. *Cancer* **71**: 2141–2150

Gage I, Schnitt SJ, Nixon AJ, Silver B, Recht A, Troyan SL, Eberlein T, Love SM, Gelman R, Harris JR and Connolly JL (1996) Pathologic margin involvement and the risk of recurrence in patients treated with breast-conserving therapy. *Cancer* **78**: 1921–1928

Gelber RD and Goldhirsch A (1994) Radiotherapy to the conserved breast: is it avoidable if the cancer is small? *J Natl Cancer Inst* **86**: 652–654

Haffty BG, Fisher D, Rose M, Beinfield M and McKhann C (1991) Prognostic factors for local recurrence in the conservatively treated breast cancer patient: a cautious interpretation of the data. *J Clin Oncol* **9**: 997–1003

Hedley DW, Friedlander ML, Taylor IW, Rugg CA and Musgrove EA (1983) Method for analysis of cellular DNA content of paraffin-embedded pathological material using flow cytometry. *J Histochem Cytochem* **31**: 1333–1335

Holland R, Connolly JL, Gelman R, Mravunac M, Hendriks JHCL, Verbeek ALM, Schnitt SJ, Silver B, Boyages J and Harris JR (1990) The presence of an extensive intraductal component following a limited excision correlates with prominent residual disease in the remainder of the breast. *J Clin Oncol* **8**: 113–118

Howeedy AA, Virtanen I, Laitinen L, Gould NS, Koukoulis GK and Gould VE (1990) Differential distribution of tenascin in the normal, hyperplastic, and neoplastic breast. *Lab Invest* **63**: 798–806

Huuhtanen R, Wiklund T, Blomqvist C, Virolainen M, Yi P and Tribukait B (1996) High S-phase fraction is an adverse prognostic sign in diploid soft-tissue sarcomas. *Cancer* **77**: 1815–1822

Ishihara A, Yoshida T, Tamaki H and Sakakura T (1995) Tenascin expression in cancer cells and stroma of human breast cancer and its prognostic significance. *Clin Cancer Res* **1**: 1035–1041

Jahkola T, Toivonen T, Von Smitten K, Blomqvist C and Virtanen I (1996) Expression of tenascin in invasion border of early breast cancer correlates with higher risk of distant metastasis. *Int J Cancer (Pred Oncol)* **69**: 445–447

Jones PL, Cowan KN and Rabinovitch M (1997) Tenascin-C, proliferation and subendothelial fibronectin in progressive pulmonary vascular disease. *Am J Pathol* **150**: 1349–1360

Lightner VA, Marks JR and McCachren SS (1994) Epithelial cells are an important source of tenascin in normal and malignant human breast tissue. *Exp Cell Res* **210**: 177–184

Liljegren G, Holmberg L, Adami H-O, Westman G, Graffman S and Bergh J (1994) Sector resection with or without postoperative radiotherapy for stage I breast cancer. Five year results of a randomized trial. *J Natl Cancer Inst* **86**: 717–722

Mansour EG, Ravdin PM and Dressler L (1994) Prognostic factors in early breast carcinoma. *Cancer* **74**: 381–400

Morrow M, Harris JR and Schnitt SJ (1995) Local control following breast-conserving surgery for invasive cancer: results of clinical trials. *J Natl Cancer Inst* **87**: 1669–1673

Ravdin PM and Chamness GC (1995) The c-erbB-2 proto-oncogene as a prognostic and predictive marker in breast cancer: a paradigm for the development of other macromolecular markers – a review. *Gene* **159**: 19–27

Rosen PP, Lesser ML, Arroyo CD, Cranor M, Borgen P and Norton L (1995) p53 in node-negative breast carcinoma: an immunohistochemical study of epidemiologic risk factors, histologic features, and prognosis. *J Clin Oncol* **13**: 821–830

Sakakura T, Ishihara A and Yatani R (1991) Tn-C in mammary gland development: from embryogenesis to carcinogenesis. In *Regulatory Mechanisms in Breast Cancer*, Lippman ME (ed.) pp. 383–400. Advances in Cellular and Molecular Biology of Breast Cancer. Kluwer Academic Publishers: Boston

Schnitt SJ, Connolly JL, Khettry U, Mazoujian G, Brenner M, Silver B, Recht A, Beadle G and Harris JR (1987) Pathologic findings on re-excision of the primary site in breast cancer patients considered for treatment by primary radiation therapy. *Cancer* **59**: 675–681

Schnitt SJ, Hayman J, Gelman R, Eberlein TJ, Love SM, Mayzel K, Osteen, RT, Nixon AJ, Pierce S, Connolly JL, Cohen P, Schneider L, Silver, B, Recht A and Harris JR (1996) A prospective study of conservative surgery alone in the treatment of selected patients with stage I breast cancer. *Cancer* **77**: 1094–1100

Silvestrini R, Benini E, Daidone MG, Veneroni S, Boracchi P, Cappelletti V, Fronzo GD and Veronesi U (1993) p53 as an independent prognostic marker in lymph node-negative breast cancer patients. *J Natl Cancer Inst* **85**: 965–970

Silvestrini R, Daidone MG, Luisi A, Boracchi P, Mezzetti M, Fronzo GD, Andreola S, Salvadori B and Veronesi U (1995) Biologic and clinicopathological factors as indicators of specific relapse types in node-negative breast cancer. *J Clin Oncol* **13**: 697–704

Tiitta O, Wahlström T, Paavonen J, Linnala A, Sharma S, Gould VE and Virtanen I (1992) Enhanced tenascin expression in cervical and vulvar koilocytotic lesions. *Am J Pathol* **141**: 907–913

Veronesi U, Luini A, Vecchio MD, Greco M, Galimberti V, Merson M, Rilke R, Sacchini V, Saccozzi R, Savio T, Zucali R, Zurrida S and Salvadori B (1993) Radiotherapy after breast-preserving surgery in women with localized cancer of the breast. *N Engl J Med* **328**: 1587–1591

Veronesi U, Marubini E, Vecchio MD, Manzari A, Andreola S, Greco M, Luini A, Merson M, Saccozzi R, Rilke F and Salvadori B (1995) Local recurrences and distant metastasis after conservative breast cancer treatments: partly independent events. *J Natl Cancer Inst* **87**: 19–27

Victorzon M, Roberts PJ, Haglund C, von Boguslawski K and Nordling S (1996) Ki-67 immunoreactivity, ploidy and S-phase fraction as prognostic factors in patients with gastric carcinoma. *Oncology* **53**: 182–191

Whelan T, Clark R, Roberts R, Levine M, Foster G and IotOCO Group (1994) Ipsilateral breast tumour recurrence postlumpectomy is predictive of subsequent mortality: results from a randomized trial. *Int J Radiat Oncol* **30**: 11–6

Yoshida T, Ishihara A, Hirokawa Y, Kusakabe M and Sakakura T (1995) Tenascin in breast cancer development – is epithelial tenascin a marker for poor prognosis. *Cancer Lett* **90**: 65–73

AMERICAN CANCER SOCIETY
HOLLAND • FREI
Cancer Medicine 5e
Bast Kufe Pollock Weichselbaum Holland Frei
www.BCDecker.com

Radiolabeled Monoclonal Antibodies

Historical Perspective

Monoclonal antibodies directed against human cancer–associated antigens also have been used to selectively deliver radionuclides to malignant cell populations. The feasibility of antibody-mediated targeting of radioactivity to tumors was demonstrated more than 40 years ago.[120] Some years later, Spar and colleagues [121] reported that a variety of tumors could be visualized in patients by gamma camera imaging following injection with ^{131}I-labeled polyclonal antibodies reactive with fibrinogen. Although these studies confirmed the conceptual appeal of labeled antibodies for cancer diagnosis and therapy, progress in this area was impeded by methodologic limitations in the characterization and production of antibody, as well as in labeling and imaging.

Hybridoma technology, in concert with advances in the field of nuclear medicine, offered the prospect of utilizing monoclonal antibodies labeled with gamma-emitting radionuclides for the detection of tumor sites in a noninvasive fashion. These developments resulted in the investigation of radiolabeled antibodies reactive with nearly every type of malignancy as potential imaging and therapeutic agents. In general, these efforts were only marginally successful.

There is a broad range of factors that can profoundly alter the ability to achieve selective targeting in vivo and thereby influence the potential impact of labeled antibodies in clinical oncology. Tumor hemodynamic characteristics, such as blood flow, permeability, and interstitial pressure, can act as impediments to homogeneous uptake of an antibody in a tumor, [122] as can the "binding-site barrier." [123] Other considerations are specific for a given antibody–antigen system and include antibody specificity and affinity, the fraction of tumor cells which are antigen positive, the average number of antigen copies per cell, the presence or absence of circulating antigen, and the level of expression of the antigen on normal tissues. Finally, the physical

characteristics of the radionuclide and the nature of its attachment to the antibody also must be considered.

Unrealistic expectations for the application of radiolabeled monoclonal antibodies in clinical oncology were generated by the results of multiple investigations in athymic rodent models which demonstrated high uptake ratios between human tumor xenograft and normal rodent tissues, [124, 125] and the ability to achieve tumor regression, and even cures, in these model systems. [126, 127] Unfortunately, after intravenous injection of labeled antibodies into patients, only 0.001 to 0.01% of the injected dose was generally found per gram tumor,[128, 129] levels at least 10,000 times lower than those observed in rodent models.

Nonetheless, successful imaging and treatment of a variety of cancers have been accomplished in patients, despite the low degree of antibody accumulation in tumor after intravenous administration. As will be discussed in the following sections, the development of more specific antibodies, antibody fragments with improved pharmacokinetics, better labeling methods and radionuclides, as well as alternative routes of antibody administration, have enhanced the clinical potential of radiolabeled antibodies. TOP

Radioimmunoscintography

In radioimmunoscintography, a tumor-specific antibody is labeled with a radionuclide that can be visualized outside the body by nuclear medicine imaging methods. After waiting an appropriate period for normal tissue clearance of radioactivity to occur, the patient is imaged, and tumors are identified by defining regions of the body with increased tracer uptake. Although radioimmunoscintigraphy has yet to have the impact on diagnostic oncology that was originally anticipated, labeled antibody imaging, particularly with tomographic methods, has been shown to provide valuable information which complements that obtained using more anatomically rigorous modalities, such as computed tomography (CT) and magnetic resonance imaging (MRI).

An important application of radioimmunoscintigraphy is to study distribution of an antibody as a prelude to treatment with the same antibody that has been labeled with a more cytotoxic radionuclide. [130] Unlike conventional external beam radiotherapy, radioimmunotherapy offers the possibility of selectively targeting radiation to malignant cell populations, while minimizing destruction of neighboring normal cells which are antigen negative. Antibody imaging is an important component of this strategy because it provides the biokinetic data for calculating tumor and normal tissue dosimetry to determine whether an adequate therapeutic index would be achievable in a patient prior to initiation of therapy. In addition, antibody imaging can be utilized to perform dosimetry-based dose escalation, optimize parameters such as the amount of cold antibody, relate toxicity to normal tissue dose, and define tumor dose–response relationships. Tomographic imaging with positron emission tomography (PET) or single photon emission computed

tomography (SPECT) is particularly attractive for these types of studies because of their superior quantitative capabilities.

Radionuclide and Imaging Method.

^{131}I was the first radionuclide used for radiolabeled antibody imaging. Advantages of ^{131}I include its low cost, the ready availability of protein radioiodination methodology, and the fact that its γ-emissions allow its use for radioimmunotherapy as well as imaging. For this reason, ^{131}I is often utilized when imaging is performed as a prelude to or during therapy. Because the same radionuclide is administered for both purposes, acquiring meaningful estimates of tumor and normal tissue radiation dosimetry is greatly facilitated, particularly when monitoring the therapeutic dose itself is required. [130] For imaging alone, the fact that ^{131}I emits γ-particles is a disadvantage because they increase the radiation absorbed dose received by the patient. Furthermore, the 364-keV gamma ray of ^{131}I is not an ideal energy for imaging because it results in low count rate per unit dose, high scatter background, and collimator penetration. These characteristics all contribute to the suboptimal spacial resolution in images obtained with this radionuclide. A considerable effort has been directed at the development of monoclonal antibody–based imaging agents using radionuclides other than ^{131}I. Much of this work has focused on three radionuclides that emit gamma rays with energies that are better suited to planar gamma camera and SPECT imaging: Indium-111 (^{111}In) (2.8-day half-life, 171 and 245-keV gamma rays), ^{123}I (13-hour half life, 159 keV gamma rays), and Technetium-99m (^{99m}Tc) (6-hour half life, 140-keV gamma rays). ^{99m}Tc is the most widely used radionuclide in nuclear medicine, in part, due to its availability from a radionuclide generator system at low cost; ^{123}I is considerably more expensive. On the other hand, the longer half life of ^{123}I permits imaging at later times after injection, when contrast between tumor and surrounding normal tissues is generally more favorable.

The gamma rays emitted by ^{123}I and ^{99m}Tc are superior to those of ^{131}I (and to a lesser extent, ^{111}In) for both conventional gamma camera imaging and SPECT, particularly for applications where rigorous quantification of activity distribution is required. The tomographic nature of SPECT also is advantageous because it facilitates identification of tumor in the presence of background activity in overlying or underlying image planes. In addition, with the development of image registration techniques, the superior anatomic information obtainable from CT or MRI can be used in combination with SPECT antibody scans. [131] In this way, functional and anatomic data can be used together to better define both the location and nature of suspected abnormalities.

With the emergence of PET as a clinical imaging modality, a number of laboratories have been investigating the potential utility of antibodies and antibody fragments labeled with positron-emitting radionuclides. PET is the

modality of choice for quantification of tracer distribution in vivo, and is generally considered to be the best method for physiologic and metabolic imaging. Improved capabilities in the quantification of antibody distribution in patients could be valuable for radioimmunotherapy, not only for patient selection, but also to better define normal tissue maximum tolerated dose and tumor dose–response relationships.

The feasibility of immuno-PET has been demonstrated in a patient with neuroblastoma injected with ^{124}I-labeled 3F8 antibody. [132] Serial PET images were used to calculate the tumor-absorbed dose that the patient would have received from a therapeutic dose of ^{131}I-labeled 3F8. Thirty-six patients with suspected advanced primary or metastatic colorectal cancer have been imaged by PET scanning 4 to 36 hours after injection of (^{64}Cu)-labeled 1A3 antibody. [133] Immuno-PET was able to detect 11 new occult tumor sites including small abdominal foci (<2-cm diameter) that were not detected by CT or MRI. Unfortunately, further investigations of the feasibility of immuno-PET with ^{124}I- and ^{64}Cu-labeled antibodies have been hindered by the lack of availability of these radionuclides. Because (^{18}F) is the most widely used radionuclide in clinical PET, other investigators have pursued its use for immuno-PET; however, the 1.8-hour half-life of ^{18}F limits its use to smaller antibody fragments. In that regard, PET imaging of both primary and metastatic osteosarcoma in dogs with spontaneous tumors has been accomplished using a ^{18}F-labeled monoclonal antibody Fab fragment. [134] TOP

Imaging Studies with Radiolabeled Antibodies in Patients.

One of the first studies of the clinical utility of radioimmunoscintigraphy involved affinity-purified, polyclonal goat antibodies reactive with carcinoembryonic antigen (CEA) labeled with ^{131}I. In one series, a lesion detection rate of 91% was reported in patients with a variety of CEA-secreting tumors, [135] while in another study, a sensitivity of only 39% was observed. [136] The dissimilarity of these results likely reflects differences in variables that can influence lesion detection, such as circulating CEA levels, tumor size and location, and techniques to compensate for the blood pool background. TOP

Techniques.

Although these two series differed in terms of detection rate, both trials were critical, in that they demonstrated the feasibility of imaging tumors with radiolabeled antibodies.

The results obtained with ^{131}I-labeled polyclonal anti-CEA, in tandem with the development of hybridoma technology, provided motivation for numerous labeled antibody imaging trials. By 1993, nearly 200 clinical radioimmunodetection trials already had been performed, primarily with

intact murine monoclonal antibodies labeled with either ^{131}I or ^{111}In. [137] The feasibility of tumor imaging with labeled antibodies has now been investigated in many patient populations.[128, 129, 138] Although a wide range of sensitivities and specificities has been reported, lesion detection rates of greater than 70% are frequently observed. In general, tumor retention of radioactivity after injection of ^{111}In-labeled antibodies has been higher than those observed with radioiodine as a label. On the other hand, higher levels of accumulation in normal liver and spleen are seen with ^{111}In-labeled antibodies, which can complicate imaging of hepatic metastases. For example, only 53% of hepatic metastasises were detected in patients with colorectal cancer imaged with ^{111}In-labeled C110 monoclonal antibody. [139]

Radioimmunoscintigraphic agents are beginning to emerge from the commercial sector. The first antibody-based imaging product approved by the FDA was OncoScint which was developed by Cytogen Corporation (Princeton, NJ). This agent consists of a ^{111}In-labeled murine monoclonal antibody (CYT-103) reactive with TAG-72, a molecule found on more than 80% of colorectal adenocarcinomas and 95% of epithelial ovarian carcinomas. [140] OncoScint is approved for use in the detection of extrahepatic, intra-abdominal metastases from colorectal or ovarian carcinomas. The imaging approach used in tandem with OncoScint had a major impact on its utility; SPECT identified tumors that were not identified by planar imaging in 35% of patients. [141] OncoScint has been reported to be more sensitive than CT for identifying pelvic metastases and extra hepatic abdominal tumors, but CT is the preferred modality for detection of disease in the liver. [142] On a per-patient basis, the combined sensitivity of OncoScint and CT was 88%. However, when the value of OncoScint imaging was evaluated in terms of its impact on patient management, it had a beneficial effect in only 13% of patients. [143]

Efforts to improve sensitivity and specificity of tumor detection have been directed at multiple aspects of antibody imaging methodology. An important advance has been the use of enzymatically generated lower-molecular-weight Fab and $F(ab')_2$ monoclonal antibody fragments because they clear more rapidly from the blood pool and normal organs than does intact immunoglobulin,[128] achieving a more reasonable tumor-to-normal-tissue ratio. This greatly facilitates the use of ^{123}I and ^{99m}Tc, radionuclides with optimal imaging characteristics but with short half-lives. In a retrospective study of patients with colorectal cancer, 82% and 89% of tumor sites could be detected using SPECT imaging with ^{123}I-labeled $F(ab')_2$ and Fab fragments of an anti-CEA antibody, respectively. [144] In a subsequent prospective investigation, tumor sites were visualized that were either not observed or detected more than 1 month later by other imaging modalities. [145]

Prospective trials with ^{123}I-labeled antibody fragments, such as the one noted above, have been critical to the field of radioimmunoscintography because

they have demonstrated the potential role of this imaging method in the management of cancer patients. However, the cost and inconvenience of labeling antibodies and antibody fragments with ^{123}I have impeded the widespread application of this methodology. With the development of straightforward techniques for labeling monoclonal antibodies with ^{99m}Tc, radioimmunoscintography has become a practical imaging modality that could be applied at nearly every medical center.

Clinical investigation using ^{99m}Tc-labeled antibody fragments have now been performed in patients with many types of malignancies, and the results have generally been encouraging. In a multicenter study evaluating ^{99m}Tc-labeled antibody fragments in melanoma patients, 70% of lesions were visualized, including 92 that were previously occult but later confirmed. [146] A sensitivity of 94% and a specificity of 100% were observed in 15 patients with neck lymph node metastases from a squamous cell carcinoma of the head and neck. [147] Imaging with ^{99m}Tc-labeled Fab' fragments of LL2 antibody has been valuable in staging of B-cell NHL, resulting in an alteration of disease stage in 27% of patients. [148]

A ^{99m}Tc-labeled Fab' fragment of an anti-CEA murine antibody (CEA-Scan, arcitumomab; Immunomedics, Morris Plains, NJ) has been approved by the FDA for use in the detection of colorectal cancer. A multicenter phase III study was done with CEA-Scan in 210 presurgical patients with either recurrent or metastatic colorectal cancer. [149] Compared with conventional diagnostic modalities, the ^{99m}Tc-labeled anti-CEA Fab' fragment was significantly more sensitive in the pelvis (69% versus 48%) and extrahepatic abdomen (55% versus 32%). The positive predictive value in 122 patients with known disease was 98% for antibody plus conventional imaging. In a subsequent study in colorectal carcinoma patients, CEA-Scan imaging provided a more accurate indicator of resectability status than CT. [150] Recently, the diagnostic potential of CEA-Scan has been investigated in breast cancer patients. [151] In 89 patients with nonpalpable lesions, the specificity of CEA-Scan and mammography was 94% and 28%, respectively, and the positive predictive value of these two techniques was 76% and 31%, respectively.

Radioimmuno-guided surgery is a potentially useful imaging method that can assist the surgeon in identifying tumor sites during an operation. In this procedure, the patient is injected with the radiolabeled antibody prior to surgery, and sites of increased radioactivity are detected using a hand-held gamma probe. Using a ^{111}In-labeled anticolorectal cancer antibody, metastatic lymph nodes were detected, with 93% sensitivity and 97% specificity. [152] In a recent study with ^{125}I-labeled CC49 antibody, radioimmuno-guided surgery identified up to 90% of colorectal tumor sites and found additional lesions in more than half the patients that were later confirmed by histology. [153] Although the results obtained with this imaging approach have been promising, further refinements in methodology probably

will be needed before it can be used routinely. ↑ TOP

Radioimmunotherapy

In evaluating the clinical potential of radioimmunotherapy, it is important to bear in mind that this type of treatment generally is being applied in patients who have already failed standard treatment modalities, such as chemotherapy and external beam radiation therapy. It is anticipated that labeled antibody therapy ultimately will be most effective in a minimal disease setting because this will minimize the impact of nonuniformities in antigen expression, tumor hemodynamics, and the binding site barrier on tumor dose heterogeneity. An advantage of antibody-mediated radiotherapy that differentiates it from immunotoxin therapy is that a wide variation in range of action of cell kill can potentially be achieved through the use of different radionuclides. For example, irradiation of volumes with subcellular, cellular, and multicellular dimensions could be accomplished using radionuclides emitting Auger electrons, β-particles and α-particles, respectively. Thus, it should be possible to identify a radionuclide with physical properties compatible with the treatment of a tumor with a particular size, location, and radiosensitivity.

The first extensive investigation in patients of the feasibility of radioimmunotherapy was performed using polyclonal antiferritin antibodies labeled with the β-emitter ^{131}I, [154] and the vast majority of clinical radioimmunotherapeutic trials have involved antibodies labeled with ^{131}I or other β-emitting radionuclides. Because β-particles have an average tissue range of 1 to 10 mm, they are better suited for the treatment of larger tumors. From a theoretical perspective, the ideal β-emitter for labeling an antibody would depend on the size of the tumor, with shorter range β-emitters, such as ^{131}I and ^{67}Cu, preferred for micrometastatic disease because they would deposit a greater fraction of their decay energy within the tumor. [155] On the other hand, longer range β-emitters such as ^{90}Y facilitate the destruction of adjacent antigen-negative or poorly perfused tumor cells through radiative crossfire.

In some settings, such as the treatment of intracavitary disease, micrometastases, or tumors of the circulatory system, other types of radiation with shorter tissue range might be preferable to α-emitters. Alpha particles, such as those emitted by (^{211}At) or (^{213}Bi), have a range in tissue of only 55 to 80 μm and are radiation of high linear energy transfer (LET). As a result, their relative biologic effectiveness is much higher than that of β-emitters. In vitro studies have shown that only a few α-particle traversals are required per cell to achieve effective cell kill. [156] An additional advantage of high-LET radiation therapy is that cytotoxic effectiveness does not require the presence of oxygen nor is it dependent on dose rate. When localized in the cell nucleus, low-energy electron emitters, such as ^{125}I, also can act as high-LET radiation and these radionuclides have been explored for use in tandem with antibodies that become internalized into the tumor cell after binding. [157]

Clinical Radioimmunotherapy Trials.

Lymphoma.

Encouraging responses to several radioimmunotherapeutic agents have been observed in patients with B-cell lymphomas, a malignancy that is relatively sensitive to radiation. Because many of the antibodies that have been used also react with normal B-cell populations, it is critical to determine the optimal protein dose for maximizing tumor-to-normal organ dose ratios. This has been accomplished by imaging antibody distribution at several protein levels and selecting the radioimmunotherapy dose on the basis of projected patient-specific dosimetry. [158]

Many clinical radioimmunotherapy trials in lymphoma have involved the anti-CD20 antibody B1 provided from Coulter Corporation. In a phase II study, 21 patients received 345 to 785 mCi of ^{131}I-labeled B1 antibody, followed by autologous hematopoietic stem cell re-infusion. [159] Objective responses were seen in 86% of patients, and 16 complete remissions were observed. In a follow-up report, 14 of 29 patients were in unmaintained remission >27 to >87 months after labeled antibody therapy. [160] These promising responses were achieved with only minor toxicity. The ^{131}I-labeled B1 antibody also has been investigated in NHL patients at doses that did not require bone marrow transplantation; complete responses with a median duration of 471 days were reported. [161] Because of the lower ^{131}I activity levels that were administered, a recent study suggests that it may be possible to perform this treatment on an outpatient basis. [162]

Another labeled antibody that has been evaluated for the treatment of NHL is Lym-1, which targets malignant lymphocytes. In a recent study, ^{131}I-labeled Lym-1 was administered in a multidose protocol, with about a 4-week interval between doses. [163] Dose escalation was from 40 to 100 mCi/m^{2}body surface area, and the dose-limiting toxicity was grade 3 or 4 thrombocytopenia. Responses were reported in 10 of 14 patients who received 2 or more doses of ^{131}I-labeled Lym-1. A phase I trial in patients with lymphoma and leukemia of ^{90}Y-labeled T101, an antibody reactive with CD5-positive lymphocytes, also has reported partial responses in 5 of 10 patients, with the main toxicity being bone marrow suppression. [164] TOP

Colorectal Carcinoma.

Radioimmunotherapy has also been performed in patients with colorectal carcinoma using several different antibodies and radionuclides. Monoclonal antibody A33, which reacts with a high-molecular-weight glycoprotein that is rapidly internalized, has been labeled with ^{131}I and investigated in patients with colorectal carcinomas. [165] The maximum tolerated dose was 75 mCi/m^2, and no major clinical responses were observed in a heavily pretreated population of patients with advanced colon cancer. Because of the

internalization of this antibody, the use of a radionuclide emitting short-range radiation might increase the radiation dose received by tumor cells, while minimizing normal tissue toxicity. This provided the motivation for a second phase I/II trial of A33 labeled with ^{125}I, a radionuclide that emits low-energy electrons and gamma rays. [166] Doses of up to 350 mCi/m^2 were administered, without bowel or bone marrow toxicity, and prolonged tumor retention of ^{125}I activity was observed.

In another trial, 15 patients received 75 mCi/m^2 of ^{131}I-labeled CC49, an antibody reactive with the TAG72 antigen. [167] Tumor uptake could be demonstrated on gamma camera images; however, only limited therapeutic efficacy was seen. A phase I/II radioimmunotherapy study has been performed in 57 patients with CEA-expressing tumors, including 29 with colorectal carcinomas, with ^{131}I-labeled murine anti-CEA NP-4 antibody. [168] Activity levels of 44 to 268 mCi were administered on the basis of bone marrow dosimetry estimated from a prior imaging study. In 12 of 35 evaluable patients, some antitumor effect was observed, including one PR. Recently, 10 patients with nonresectable liver metastases were treated with the $F(ab')_2$ fragments of the anti-CEA antibody F6 labeled with 87 to 300 mCi ^{131}I. [169] Doses of 300 mCi were well tolerated with bone marrow re-infusion and doses of 200 mCi or less did not require bone marrow rescue. One partial response was observed. TOP

Other Cancer Types.

^{131}I-labeled murine monoclonal antibodies and F(ab')2 fragments also have been evaluated after intravenous administration to patients with other types of malignancies, including medullary thyroid carcinomas, [170] renal cell carcinomas, [171] and ovarian carcinomas. [172] In general, myelosuppression has been the dose-limiting toxicity, and responses have been modest at best.

One approach that has been investigated for improving the effectiveness of radioimmuno-therapy is to administer a biologic response modifier that can increase the expression of the target antigen. For example, recombinant IFN-α can enhance the expression of TAG-72, the tumor-associated glycoprotein to which the CC49 antibody reacts. A phase II trial was undertaken in 15 patients with breast cancer who received six daily doses of recombinant IFN-α and ^{131}I-labeled CC49. [173] Although the uptake of CC49 was increased, hematologic toxicity was also considerably higher. In 14 patients with prostate cancer, daily doses of IFN-γ were given for seven days followed by 75 mCi/m^2 of ^{131}I-labeled CC49. [174] Biopsies from three patients revealed a 2 to 6 times higher percentage of cells expressing TAG-72. Thrombocytopenia was the dose-limiting toxicity, and only minimal response was seen in 4 patients.

The lack of efficacy of ^{131}I-labeled antibodies in most patient populations can be attributed to multiple factors including the loss of the label from the

antibody as a result of dehalogenation, and the physical properties of this radionuclide. This has led to the clinical investigation of antibodies labeled with other β-emitters, most notably, ^{90}Y. Advantages of this radionuclide include its higher β-energy and longer retention on tumor, compared with antibodies radioiodinated using conventional methods. A disadvantage is the higher accumulation of ^{90}Y in normal tissues. Only limited data concerning clinical trials with ^{90}Y-labeled antibodies have been published. A preliminary study investigating the pharmacokinetics and toxicity of ^{90}Y-labeled HMFG1 given intraperitoneally to patients with ovarian cancer suggests that the appropriate dose for treatment will be 18.5 mCi/m^2, with bone marrow toxicity being the dose-limiting factor. [175] Radioimmunotherapy trials with ^{90}Y-labeled antibodies also are underway in patients with colorectal, [176] prostate, [177] and breast carcinoma [178] as well as lymphoma; [179] however, insufficient data are available at this time to realistically evaluate the clinical potential of these agents. TOP

Emerging Strategies for Radioimmunodiagnosis and Radioimmunotherapy

For radioimmunodiagnosis, it is important to maximize the ratio of radioactivity in tumor and neighboring normal tissues at a single point in time that is compatible with the physical half-life of the radionuclide. As described in the preceding sections, the use of enzymatically derived antibody fragments in tandem with ^{99m}Tc and ^{123}I has markedly improved the ability to image some types of tumors with excellent sensitivity and specificity. With radioimmunotherapy, the critical criterion is to maximize time-integrated tumor-to-normal-organ radiation dose ratios, while delivering sufficient activity to tumor to cause a significant therapeutic effect. Clinical radioimmunotherapy trials have provided encouraging results in lymphoma but not in other types of cancer. This has led to the investigation of a wide variety of strategies for increasing both tumor dose as well as tumor-to-normal-tissue radiation absorbed dose ratios. Clinical trials have commenced or are about to begin with several of these approaches—altering tumor hemodynamics, administration of antibody by nonintravenous routes, pretargeting regimens, utilization of molecular constructs designed via recombinant DNA technology, and labeling antibodies with α-particle emitting radionuclides. The current status of research in these areas is discussed in the sections which follow.

Alteration of Tumor Hemodynamics.

Heterogeneity in tumor blood flow, permeability, and interstitial pressure, all can have a major impact on both the homogeneity and level of accumulation of macromolecules in tumor. It is known that hyperthermia can alter tumor hemodynamics, and the potential for increasing the uptake of radiolabeled antibodies and fragments in tumor xenograft models with local hyperthermia has been investigated. Significant increases in tumor uptake with minimal alteration in normal tissue levels have been observed; [180–182] however, a

consensus has not been reached with regard to the temperature and duration of heating providing the optimal effects of hyperthermia on antibody pharmacokinetics. A phase I/II trial of ^{131}I-labeled anti-CEA antibody and hyperthermia has been performed in patients with advanced colorectal cancer. [183] Although 5 of 6 patients showed a decrease in serum CEA levels, only minimal therapeutic response was seen. Before further clinical evaluation of this combined modality approach is considered, it is recommended that experiments be performed in appropriate animal models, in order to determine the best conditions for combining hyperthermia and radioimmunotherapy.

Vasoactive compounds, such as norepinephrine, vasopressin, and histamine, can increase blood flow, and their effect on antibody uptake in tumor has been investigated. [184] Unfortunately, this tactic has not been very successful. A more fruitful approach has been to enhance tumor uptake through the use of antibodies coupled to vasoactive biologic response modifiers or other compounds. Administration of an antibody–IL-2 conjugate prior to the radiolabeled antibody resulted in a significantly higher tumor accumulation, with little alteration in normal tissue levels. [185] Antibody conjugates with TNF-α and IL-1 exerted similar effects albeit of a lower magnitude than seen with IL-2. [186] TOP

Nonintravenous Administration.

Another strategy for increasing the rate and magnitude of tumor uptake, applicable to some types of malignancies, is to administer the radiolabeled antibody by a nonintravenous route. This can be particularly effective for use with antibodies that also react with normal tissues because exposure of the labeled antibody to tumor occurs prior to interaction with high-capacity, normal-organ-binding sites. Intraperitoneal radioimmunotherapy has been investigated in patients with ovarian carcinomas. In a phase I/II trial, (^{177}Lu)-labeled CC49 was given to 27 ovarian cancer patients who had failed chemotherapy. [187] The maximum tolerated dose was 45 mCi/m^2, and marrow suppression was the dose-limiting toxicity. Prolonged disease-free survival (>6 to 35 months) was observed in 4 of 5 patients with microscopic or occult disease. The therapeutic potential of radioimmunotherapy with ^{90}Y-labeled HMFG1 antibody (18 mCi/m^2), given after chemotherapy, has been compared with that of chemotherapy alone. [188] Five-year survival was 80% for the combined modality therapy, significantly higher than the 55% obtained with chemotherapy alone.

Encouraging results have been reported for the treatment of tumors of the central nervous system by the nonintravenous administration of ^{131}I-labeled antibodies. Glioma patients with spontaneous recurrent cystic lesions and surgically created resection cavities have been treated with single or multiple doses of radioiodinated antibodies given directly into the cavity. [189] Prolonged retention of radioactivity in the cavity has been seen. ^{131}I anti-

tenascin 81C6 antibody has been given via an Ommaya reservoir to 34 patients with recurrent malignant glioma. [190] In this phase I study, groups of 3 to 6 patients were treated with 20 to 120 mCi of ^{131}I-labeled 81C6. Dose-limiting toxicity was neurologic or hematologic, and the maximum tolerated dose was 100 mCi. The median survival for all patients and those with glioblastoma multiforme (26 patients) was 56 and 60 weeks, respectively, which compares favorably with the median survival obtained with either conventional or other experimental treatment modalities.

^{131}I labeled monoclonal antibodies also have been administered intrathecally for the treatment of neoplastic meningitis. Significant clinical responses have been observed in patients with a variety of leptomeningeal tumors, including breast carcinoma, melanoma, lymphoma, and pineoblastoma. [191, 192] Thirty-one patients with leptomeningeal neoplasms have been treated with 40 to 100 mCi of ^{131}I-labeled 81C6. [193] The maximum tolerated dose in adults was 80 mCi with hematologic toxicity being the dose limiting factor. Five patients remained free of disease progression >409 days after radioimmunotherapy. ↑ TOP

Pretargeting.

An advantage of using intact antibodies for radioimmunotherapy is that their binding to tumor is both greater and more prolonged than that of antibody fragments, thereby resulting in higher tumor radiation dose. On the other hand, the larger molecular size of whole immunoglobulin decreases the rate of tumor accumulation and impedes diffusion within the tumor. Pretargeting approaches are attractive because they offer the possibility of obtaining the benefits of intact antibodies while minimizing the disadvantages. In pretargeting procedures, the antibody is administered first, and after a sufficient delay period to achieve sufficient uptake in the tumor, a radiolabeled lower-molecular-weight compound is injected. By shifting the label from the antibody to a smaller molecule, more rapid normal tissue clearance and tumor penetration can be achieved.

The most widely explored pretargeting strategy exploits the high affinity (~10^{13} to 10^{15} M^{-1}) binding of the ~60-kDa proteins avidin and streptavidin to the 244-Da water-soluble vitamin, biotin. A number of different regimens have been investigated, including injection of a radiolabeled biotin derivative after pretargeting of a streptavidin–antibody conjugate, and pretargeting of a biotinylated antibody, followed by streptavidin, followed by radiolabeled biotin. In some cases, a clearing agent is used before injection of the labeled biotin conjugate. Clinical investigations with streptavidin-biotin pretargeting in patients with lung, ovarian, and colorectal carcinomas have shown superior tumor-to-normal-tissue ratios, compared with directly labeled antibodies. [194] Recently, a three-step protocol that includes biotinylated anti-tenascin antibody, avidin and streptavidin, and finally, ^{90}Y-labeled biotin has been performed in 48 patients with recurrent grade 3 or 4 glioma. [195] The maximum tolerated dose of ^{90}Y-labeled biotin was 2.96 GBq/m^2, and median

survival was 11 and 19 months for grade 3 and 4 tumors, respectively. A randomized clinical trial of pretargeted ^{90}Y radioimmunotherapy is planned. ↑ TOP

Recombinant Antibody Constructs.

The development of an immune response frequently occurs in immunocompetent patients that have received murine monoclonal antibodies. These human antimurine antibodies, commonly referred to as HAMA, can alter the pharmacokinetics of subsequent doses of radiolabeled antibodies through the formation of labeled immune complexes that are rapidly removed from the circulation before they can be delivered to the tumor. Recombinant DNA technology has been used to generate molecules that can help minimize this problem by decreasing the fraction of the molecule that is of murine origin. Human/mouse chimeric antibodies, which consist of a murine variable region linked to a human constant region, and CDR-grafted, humanized antibodies, in which the murine component is limited to the hypervariable complementary determining regions, have been developed. A number of chimeric antibodies have been radiolabeled and their properties evaluated in clinical trials. By minimizing HAMA, these molecules should facilitate the use of multidose treatment radioimmunotherapy protocols; however, immune response to the antibody variable region may still be problematic.

Another class of recombinant molecules that has emerged as candidates for radiolabeled approaches are single-chain Fv (scFv) fragments. [196] These scFv molecules consist of a heavy-chain and a light-chain variable region amino acid sequence linked together by a peptide designed to maintain the immunoreactivity of the intact antibody parent. Several scFv molecules have been radiolabeled and evaluated as potential diagnostic and therapeutic agents. Although scFv offer superior tumor-to-normal-tissue ratios, the absolute magnitude uptake of scFv in a tumor is lower than that seen with intact IgG and large antibody fragments, suggesting that these monomeric scFv molecules probably will be more useful for diagnostic applications. The feasibility of imaging tumors in patients with radiolabeled scFv fragments has been demonstrated by Begent. [197] Using a ^{123}I-labeled scFv fragment of an anti-CEA antibody, all known tumor sites could be identified.

The rapid loss of radiolabeled scFv fragments from the tumor most likely reflects not only their small size but the monovalent nature of their binding. Recombinant DNA approaches have been utilized to generate a number of divalent constructs, and some of these have been evaluated in human tumor xenograft models. The construction of an scFv dimer that retained the specificity of its parent antibody, anti-c-*erb*B2 741F8, has been reported. [198] As predicted, the accumulation of the radioiodinated $(scFv)_2$ in the tumor was higher than that of the corresponding monomer. When a linker peptide of 14 amino acids was used to connect the heavy- and light-chain variable regions of an anti-CEA antibody, noncovalent dimers were formed. [199] In athymic mice with subcutaneous human tumor xenografts, tumor accumulation of this "diabody" was considerably higher than its monomer, reaching 10% of the

injected dose per gram at 1 hour, and maintaining that level until at least 6 hours after injection. Finally, a "minibody" derived from the same T84.66 anti-CEA antibody, and consisting of a spontaneously formed scFv-C_H3 dimer, has shown exceptional targeting ability, particularly when the linker between the C_H3 domain and the scFv used was the IgG_1 hinge region plus a 10-amino-acid spacer. [200] The tumor targeting capability of these recombinant constructs in patients remains to be ascertained. TOP

Alpha-Particle Radioimmunotherapy.

Alpha-particles are attractive for targeted radiotherapy because of their high cytotoxicity and short tissue range. Clinical radioimmunotherapy trials with α-particle emitters have awaited developments in isotope production, protein labeling chemistry, dosimetry, and determining the toxicity of these potential therapeutic agents in appropriate animal models. Recent advances in these areas have permitted the initiation of two clinical trials with antibodies labeled with α-particle-emitting radionuclides. These studies are important because they demonstrate that targeted radiotherapy with α-emitters is feasible in patients.

The Memorial Sloan-Kettering Cancer Center group has treated at least 10 patients with acute myelogenous leukemia (AML) using an antibody labeled with the 46-minute half-life α-particle emitter ^{213}Bi.[201] The antibody is a humanized recombinant form of M195, which reacts with the CD33 cell-surface glycoprotein present on most leukemias. Escalating activities of ^{213}Bi-labeled HuM195 in multiple fractions are being administered. At Duke University, a phase I trial is underway in recurrent malignant glioma patients to determine the maximum tolerated dose of human/mouse chimeric anti-tenascin antibody 81C6 labeled with the 7.2-hour half-life α-particle emitter ^{211}At administered into surgically created tumor resection cavities.[202] Retention of ^{211}At activity in the resection cavity has been excellent, and leakage into the blood pool has been less than 0.5% of the injected dose. Cavity interface–to–normal brain dose ratios were about 150 times higher than reported previously in a similar trial performed with ^{131}I-labeled murine 81C6. [190] Dose-limiting toxicity has yet to be observed in either targeted α-particle radioimmunotherapy trial. TOP

Technetium-99m Chelators in Nuclear Medicine*

A Review

Ole K. Hjelstuen

Isotope Laboratories, Institutt for Energiteknikk, 2007 Kjeller, Norway

Nuclear medicine is a branch of medical imaging that uses radioactive tracers to examine the function of body systems. The radionuclide used in about 90% of all examinations is ^{99m}Tc, which is available from $^{99}Mo/^{99m}Tc$ generators at most nuclear medicine departments. In aqueous medium, technetium is chemically stable as pertechnetate, $^{99m}TcO_4^-$. Injected into the human body, pertechnetate will be absorbed by the thyroid gland because of the similarity to iodide in its radius and charge. To reach targets in the human body other than glandula thyreoidea, ^{99m}Tc needs a carrier molecule, usually a chelating agent. Many chelators that form stable complexes with ^{99m}Tc have affinities for certain tissues in the human body. Other chelators can be manipulated by pharmaceutical formulation to be retained in certain body systems. In order to form bonds with technetium, the chelator must contain electron donors like nitrogen, oxygen and sulfur. Space between multiple electron donor atoms is required to allow several bonds to form with the central metal. The stability of the complex increases with increasing number of bonds. Today, chelators for the use with ^{99m}Tc exist for a number of highly sensitive scintigraphic studies of the brain, heart, skeleton, kidneys, hepatobiliary system and lungs. This includes chelators such as dimercaptosuccinic acid, 1,2-ethylenediylbis-L-cysteine diethyl ester, methylenediphosphonate, hexamethylpropyleneamineoxime and hexakis(methoxy isobutyl isonitrile).

Keywords: Technetium-99m, medical imaging, chelators

Introduction

The field of medical imaging comprises four main techniques: radiology [including computerized tomography (CT)], ultrasound (US), magnetic resonance imaging (MRI) and nuclear medicine [including single photon emission computerized tomography (SPECT) and positron emission tomography (PET)]. Used alone, or in conjunction with one of the other techniques, nuclear medicine offers valuable information about human health and disease.

In nuclear medicine, radioactive nuclides are injected in minute quantities into the human body and the distribution is detected by a gamma-ray camera. The gamma-ray camera used in SPECT comprises a photon absorption unit (sodium iodide crystal), a signal amplifier (photo-multiplier tubes) and a computerized image generator. The software of the image generator has undergone great progress recently, allowing detailed dynamic studies of various organs.

* Presented at The Fifth Nordic Symposium on Trace Elements in Human Health and Disease, Loen, Norway, June 19–22, 1994.

Technetium-99m

There are numerous radioactive nuclides that either have been, or potentially could be, used in nuclear medicine. However, at present ^{99m}Tc is used in about 90% of all scintigraphic examinations.

The easy and inexpensive access of ^{99m}Tc by a generator system makes it attractive for use in nuclear medicine.[1] The generator consists of a packed column with a quantity of radioactive molybdenum trioxide, $^{99}MoO_3$, applied on the top.[2] The radioactive molybdenum has a half-life of 66 h and decays with 87.5% yield to ^{99m}Tc, which is instantly oxidized to water soluble pertechnetate $^{99m}TcO_4^-$. The ^{99m}Tc activity can then be utilized on extraction by eluting the column with an aqueous saline solution.

Other main advantages of ^{99m}Tc are the physical properties of the radionuclide. (*i*) The 140 keV photon of this monoenergetic radionuclide is technically ideal for detection by a gamma-ray camera, owing to the absorption properties of the sodium iodide crystal.[1] (*ii*) The 6 h half-life means a rapid decay and a low total radiation dose to the patient. Usually, most of the radioactive substance is excreted from the body shortly after injection, and since the remaining activity decays to background levels within the next few days, the total dose to the patient will be low.

If the eluate is injected directly into a patient, pertechnetate will be absorbed by the thyroid gland.[3] The thyroid gland utilizes iodide in the production of the hormones triiodothyronin and thyroxin, and will absorb $^{99m}TcO_4^-$ because of its similarity to I^- in charge and radius. In order to reach other targets in the human body, carrier molecules for ^{99m}Tc are required. Many chelators are available that form stable complexes with ^{99m}Tc and which have affinities for certain tissues in the human body.

These chelators are prepared as freeze-dried kits for reconstitution with technetium eluate at the nuclear medicine department shortly before injection. In addition to the chelator, the kit must contain a reducing agent, usually stannous, to initiate the following reactions immediately after addition of technetium eluate:[4]

$$^{99m}TcO_4^- + Sn^{2+} + 8H^+ \leftrightarrow {}^{99m}Tc^{5+} + Sn^{4+} + 4H_2O \quad (1)$$

$$\text{Chelator} + {}^{99m}Tc^{5+} \leftrightarrow {}^{99m}Tc\text{-chelator} \quad (2)$$

It should be noted that the reduction of pertechnetate may continue to the charges 4+ and 3+. The final oxidation state is determined by multiple factors in the reaction solution. In general, complexation reactions as in reaction (2) are slow, but since ^{99m}Tc is present only in trace quantities compared to the chelator concentration, the complexation of technetium will take place rapidly. The quantity relations in the methylenediphosphonate (MDP) kit after addition of 800 MBq technetium eluate illustrate this statement [in approximate

values calculated from a kit from Ife (Kjeller, Norway)]: 0.05 nmol $^{99}Tc^{m}$; 1300 nmol Sn; and 56 800 nmol MDP.

This kit is ready for use 5 min after reconstitution, with a radiochemical purity of more than 99%.

The quantity of MDP is also very low compared to the molar amounts of active substances in regular drugs in human medicine. This is a characteristic of all kits in use in nuclear medicine. These drugs have no pharmacological effect, and the risk of toxic effects and saturation of receptor systems is very low.

Radiopharmaceuticals and Their Use

Bone/Skeleton

One of the most common examinations in nuclear medicine and oncology is the bone scan for metastases from cancer prostata and cancer mamma. The chelator used in bone scintigraphy is MDP.[6]

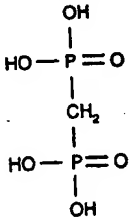

MDP

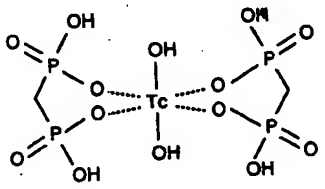

$^{99}Tc^{m}$–MDP

The proposed structure of the $^{99}Tc^{m}$–MDP complex is shown above.[6] Two MDP molecules bind to each $^{99}Tc^{m}$, and each MDP acts in a bidentate manner.

When injected into a normal patient, $^{99}Tc^{m}$–MDP will be distributed to the whole skeleton. The MDP is absorbed by all bone cells because of its phosphorus content, which is used as a building block for the bone substance hydroxyapatite.[7] When injected into a patient with bone metastases, the drug will be concentrated in areas of high metabolic activity, which is one of the characteristics of cancer cells. This technique gives the possibility for detection of metastases down to a few mm in size in all parts of the skeleton.

Brain

Scintigraphic examination of the brain is highly versatile in the case of diseases like cerebral infarction, strokes, abcessas and tumours.[8] The regional cerebral blood flow (rCBF) is measured and areas with increased or reduced blood flow can be found.

Brain scans are also proving useful in the difficult diagnosis of Alzheimer's disease. Alzheimer's disease is expressed physiologically as a bilateral temporoparietal hypoperfusion and can be detected by the use of a rCBF agent.[9]

One chelator for the measurement of rCBF is the dioxime HMPAO.

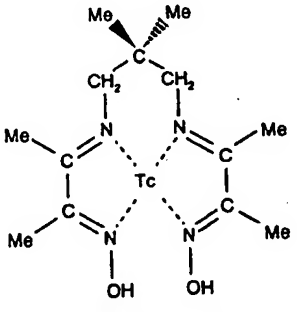

$^{99}Tc^{m}$–HMPAO

The $^{99}Tc^{m}$–dioxime HMPAO complex formed is lipophilic and able to cross the blood-brain barrier (BBB). About 5% of the total dose can be found in the brain, providing the opportunity for high-quality scintigraphy.

One limitation for the use of dioxime HMPAO has been that the complex is stable only for 30 min *in vitro*.

More stable complexes for brain scintigraphy have been developed recently. One of these is 1,2-ethylenediylbis-L-cysteine diethyl ester (ECD).

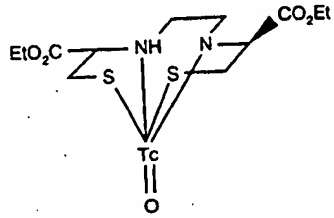

$^{99}Tc^{m}$–ECD

The compound is of a class of radiopharmaceuticals utilizing N and S as ligand moieties. It binds $^{99}Tc^{m}$ in a stable lipophilic complex, which is able to cross the BBB. The complex is trapped in the brain by metabolic transfer to a hydrophilic monoacid ester.[10] The complex concentrates in the cytosol of the brain cells. The indications for $^{99}Tc^{m}$-ECD are the same as for $^{99}Tc^{m}$-dioxime HMPAO, but, because of its better *in vitro* stability of >6 h, it is more useful to nuclear medicine departments.

Heart

One of the most important diagnostic uses of nuclear medicine is in cardiology for the examination of myocardal perfusion for diagnosis of infarction and ischemia.

Traditionaly, such studies were performed with the use of thallium-201 (Tl^{+}), which is absorbed intracellularly like K^{+}. But now technetium complexes for this use have been developed.

A compound for use in heart scintigraphy with $^{99}Tc^{m}$ is methoxyisobutyl isocyanide (MIBI).

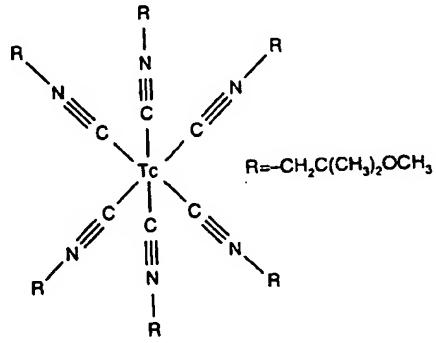

$^{99}Tc^{m}$–hexaMIBI

Each MIBI acts monodentally, so that six MIBI molecules are needed to form a hexa MIBI complex with single $^{99}Tc^{m}$ cations.[11] The complex will be cationic and be absorbed into the parenchymal cells of the heart myocardium.[12]

Note that, since MIBI is monodentate it is not really a chelator. The definition of a chelator is that it binds to a central metal with at least two bonds and MIBI is a monodentate ligand. However, MIBI is mentioned here because of its important place in nuclear medicine.

Valuable information can be obtained when several heart scans are combined to provide a dynamic view of the heart function by the sophisticated computer software in the gamma-ray camera.

Kidneys

Dynamic kidney scintigraphy, renography and determination of glomerular filtration rate (GFR) can be performed using $^{99}Tc^{m}$-diethylenetriaminepentaacetic acid (DTPA). This means that the physiological events in the kidneys can be studied.

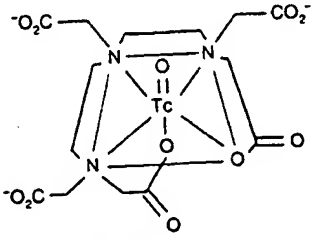

$^{99}Tc^{m}$–DTPA

DTPA (see structure[13]) is a familiar substance to most chemists and medical doctors because of its use as a complexing agent in laboratories and in the treatment of heavy metal poisoning in human medicine.

$^{99}Tc^{m}$-DTPA is a highly polar complex, and will be excreted exclusively by glomerular filtration shortly after injection. DTPA is used traditionally in nuclear medicine, but new drugs have been developed for use in kidney scintigraphy.

An example is mercaptoacetyltriglycine (MAG_3). $^{99}Tc^{m}$-MAG_3 is excreted by tubular excretion and can be used to determine effective renal plasma flow.[15]

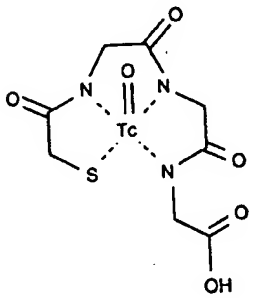

$^{99}Tc^{m}$-DTPA and $^{99}Tc^{m}$-MAG_3 are passed through the kidneys without any binding to kidney tissue. Kidney localization and conditions like infarction can be determined by the use of dimercaptosuccinic acid (DMSA).

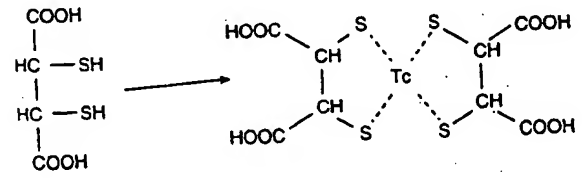

DMSA

$^{99}Tc^{m}$-DMSA concentrates in the kidney cortex, being retained in the proximal tubuli. About 50% of the dose is found in the cortex 2 h after injection, making $^{99}Tc^{m}$-DMSA well suited for cortex scintigraphy.

Liver/Hepatobiliary System

The hepatobiliary system can be visualised and its function examined by the use of an iminodiacetic (IDA) derivative.

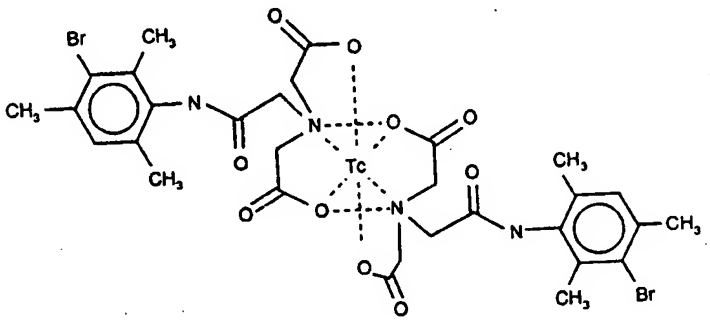

$^{99}Tc^{m}$–Mebrofenin

The diacetic acid derivative, mebrofenin, is an IDA derivative with a bromo substitution on the benzene ring. Two mebrofenin molecules bind to one technetium and each mebrofenin acts tridentally.[15] The complex will be concentrated in the hepatocytes of the liver. Maximum uptake is observed 12 min after injection. The half-life in the liver is 18 min and the complex appears in the gall bladder 14 min after injection.[16]

Lungs

Perfusion studies of the lungs can detect pulmonary embolies. In such studies, macroaggregated albumin (MAA) is labelled with $^{99}Tc_m$ and injected. In these protein particles technetium is complexed by sulfur-containing amino acids like cysteine and methionine. Several technetium atoms can, in theory, bind to one MAA sphere, but with the low molar quantities of technetium present, the probability is great for 1 : 1 binding.

The MAA kit consists of human serum albumins macroaggregated to particles with a size distribution of 10–90 μm.[17] Particles of this size will not be able to pass through the precapillaries and capillaries of the lungs.[3]

In this case, it is not the affinity of the carrier molecule for a certain target that serves as the basis for the scintigraphic examination, but rather the pharmaceutical formulation of particles of a certain size. The particles will be evenly distributed to all parts of the lungs with normal perfusion, leaving embonilic parts of the lungs as areas with no radioactivity.

Oncology

Detection of tumours by scintigraphy has traditionally been restricted to larger tumours, associated with one of the major human organs, by the use of one of the organ-specific complexes or the detection of bone metastases by the use of $^{99}Tc^{m}$-MDP.

The development of advanced biotechnology has given new methods to approach cancer for diagnostic purposes, especially by the labelling of tumour-specific antibodies. Within nuclear medicine, the approach is to label the antibodies with radionuclides primarily for diagnostic purposes. A second approach would be to label the antibodies with a radionuclide that damages the cancer cell, *i.e.*, an α- and β-emitting radionuclide.

Using technetium, antibodies can be labelled using two distinct approaches.

(*i*) Direct labelling to the sulfhydryl groups of the antibody is easy and useful, but has the risk of losing the tumour specificity of the antibody. In this technique the antibody itself is the chelator. First the sulfur bridges in the antibody have to be broken in order to attach technetium, and then the sulfur bridges must be reformed. There are several published

methods to accomplish this, though the Schwarz method is the best known[18] (Fig. 1).

(*ii*) The second approach uses the principle of bifunctional chelators.[20] In this case, a bifunctional chelator may be attached to the antibody Fc-chain by the organic chemist. This bifunctional chelator may for example be DTPA. Technetium may then be chelated by the DTPA moiety in a regular manner. Even though this technique leaves the antibody more tumour-specific and gives a better tumour uptake, the DTPA attachment procedure may be complicated and laborious, limiting the use of the technique (Fig. 2).

Experimental Chelators

The ongoing research on chelators for use with $^{99}Tc^{m}$ in nuclear medicine is, to a great extent, focusing on smaller biomolecules like proteins and peptides. The trend is to isolate the active site of larger biomolecules and synthesize the protein/peptide identical to the active site. Then a bifunctional chelator able to bind $^{99}Tc^{m}$ is attached, and if the targetting properties of the biomolecule can be left unaltered, the complex could potentially be used for imaging tumours, infection and inflammation.[21] The advantages of working with smaller biomolecules are that they can easily be synthesized and that the *in vivo* blood clearance is rapid, allowing tumour isolation in the obtained images.

Another exciting field within research for new radiopharmaceuticals is the development of antisense oligonucleotides. These are synthetic DNA analogues that can internalize in tumour cells and with a bifunctional chelator attached they could deliver the radionuclide intracellularly.[22] This approach can potentially provide a new and sensitive way of tumour detection.

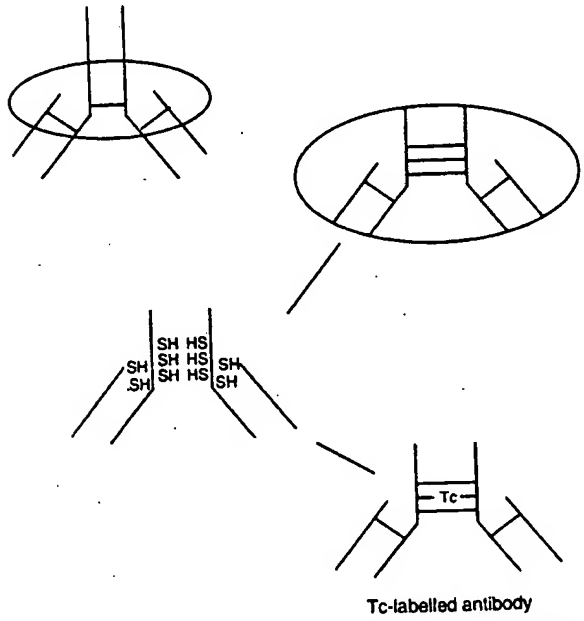

Fig. 1 Direct labelling of monoclonal antibodies with $^{99}Tc^{m}$.[19]

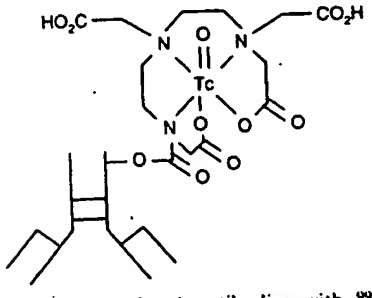

Fig. 2 Labelling of monoclonal antibodies with $^{99}Tc^{m}$ using a bifunctional chelator.

Conclusions

A number of chelators exist for routine use with $^{99}Tc^{m}$ for highly sensitive studies of the brain, heart, skeleton, kidneys, hepatobiliary system and lungs, and for detection of tumours and metastases. A common characteristic for technetium chelators is the presence of multiple electron-donor groups like nitrogen, oxygen and sulfur. The complexes formed with $^{99}Tc^{m}$ must be stable and, perhaps most importantly, they must be target-specific to the site of interest in the human body.

References

1 Jurisson, S., Berning, S., Jia, W., and Ma, D., *Chem. Rev.*, 1993, **93**, 1137.
2 Steigman, J., and Eckelman, W. C., *The Chemistry of Technetium in Medicine*, National Academy Press, Washington, DC, 1992, pp. 6–8.
3 Jurisson, S., Berning, S., Jia, W., and Ma, D., *Chem. Rev.*, 1993, **93**, 1145.
4 Saha, G. B., *Fundamentals of Nuclear Pharmacy*, Springer-Verlag, Berlin, 1992, 3rd edn., pp. 99–100.
5 Jurisson, S., Berning, S., Jia, W., and Ma, D., *Chem. Rev.*, 1993, **93**, 1144.
6 Hanson, R. N., *Radiopharmaceuticals Structure-Activity Relationships*, Grune and Stratton, New York, 1981, pp. 314–316.
7 Dewanjee, M. K., *Sem. Nucl. Med.*, 1990, **20**, 9.
8 Ell, P. J., Cullum, I., Costa, D. C., Jarrit, P. H., Hocknell, J. M. L., Lui, D., Jewkes, R. J., Steiner, T. J., Nowotnik, D. P., Pickett, R. D., and Neirinckx, R. D., *Lancet*, ii, 1985, 50.
9 Costagnoli, A., Borsato, N., Bruno, A., Ferlin, G., Gerundini, P., Masi, R., Vannucchi, L., Bigelow, R., and Walovitch, R. C., *Cerebral Ischemia and Dementia*, Springer-Verlag Berlin, 1991, pp. 327–333.
10 Walovitch, R. C., Cheesman, E. H., Maheu, L. J., and Hall, K. M., *J. Cereb. Blood Flow Metab.*, **14** (suppl. 1), 1994, S4–S11.
11 Lever, S. Z., and Wagner, Jr., H. N., *Technetium and Rhenium in Chemistry and Nuclear Medicine 3*, Cortina International, Verona, 1990, pp. 649–659.
12 Meerdink, D. J., and Leppo, J. A., *Am. J. Cardiol.*, 1990, **66**, 9E.
13 Chilton, H. M., and Thrall, J. H., *Pharmaceuticals in Medical Imaging*, Macmillan, New York, 1990, pp. 305–342.
14 Russell, C. D., Thorstad, B. L., and Yester, M. V., *J. Nucl. Med.*, 1988, **12**, 1931.
15 Pento, J. T., *Drugs of the Future*, 1987, **12**, 950.
16 Product specifications, Ife, Kjeller, Norway.
17 Specifications for MAA kit, Ife, Kjeller, Norway.
18 Schwarz, A., and Steinstrasser, A., *J. Nucl. Med.*, 1987, **28**, 721.
19 Mather, S. T., and Ellison, D., *J. Nucl. Med.*, 1990, **31**, 692.
20 Childs, R. L., and Hnatowich, D. J., *J. Nucl. Med.*, 1985, **26**, 293.
21 Babrich, J. W., Solomon, H., Pike, M. C., Kroon, D., Graham, W., Abrams, M. J., Tompkins, R. G., Rubin, R. H., and Fischman, A. J., *J. Nucl. Med.*, 1993, **34**, 1964.
22 Dewanjee, M. K., *J. Nucl. Biol. Med.*, 1994, **38**, 477.

Paper 4/04999C
Received August 15, 1994
Accepted November 15, 1994

Xenograft model systems for human melanoma

Einar K. Rofstad and Heidi Lyng

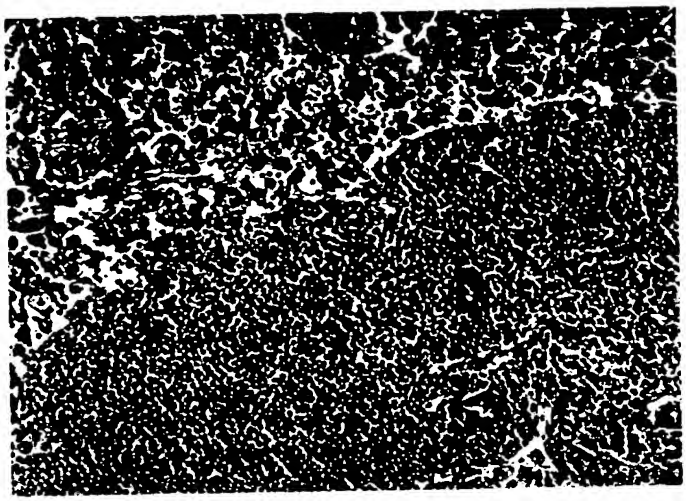

Human melanoma cells inoculated intradermally into congenitally immune-deficient mice initiate angiogenesis and give rise to tumors with a human parenchyma and a murine stroma. These tumors are similar to the donor patients' tumors with respect to histological appearance, karyotype and molecular pathology. The cellular treatment sensitivities and the organ-specific metastatic patterns of the donor patients' tumors are also retained after xenotransplantation. Consequently, human melanoma xenografts are exciting experimental models that show great promise for future studies of the molecular biology, angiogenesis, pathophysiology, treatment sensitivity and metastatic behavior of malignant melanoma.

Einar K. Rofstad PhD
Principal Scientific Officer

Heidi Lyng PhD
Postdoctoral Fellow

Department of Biophysics, Institute for Cancer Research,
The Norwegian Radium Hospital,
Montebello, 0310 Oslo, Norway.
Tel: +47 2293 4279
Fax: +47 2293 4270
e-mail: e.k.rofstad@labmed.uio.no

THE worldwide incidence of malignant melanoma is increasing substantially. In North America, a doubling of the incidence rate has occurred each decade for the past 40 years. The prognosis of advanced melanoma is poor owing to its general resistance to the various forms of therapy. Approximately three-quarters of all deaths from skin cancer result from melanoma[1].

Advances in the management of melanoma require experimental model systems for the exploration of basic mechanisms governing the clinical behavior of this disease and for the development and preclinical testing of novel diagnostic and therapeutic approaches. Ideally, experimental melanomas should show an identical behavior to melanomas in humans and, at the same time, be suitable for all types of experimental procedures. The ideal model system does not exist. However, several appropriate models for studying the progression, diagnosis and therapy of melanoma are available (Box 1). Animal models are considered to be more clinically relevant than *in vitro* models. However, *in vitro* models are less complex than animal models and are thus usually more suitable for mechanistic studies.

The most widely used *in vitro* models include established human melanoma cell lines grown in monolayer or suspension culture and human melanoma multicellular spheroids. Multicellular spheroids are particularly interesting because they are intermediate in complexity between monolayer cell cultures and solid tumors. They develop gradients of critical metabolites such as oxygen, glucose, lactate and

 1357 - 4310/96/$15.00 PII: S1357-4310(96)10035-

Box 1. Experimental model systems for human melanoma

***In vitro* models**

- Monolayer and suspension cultures of human melanoma cell lines
- Multicellular spheroids of human melanoma cells

Murine *in vivo* models

- Murine melanomas developing in transgenic mice
- Murine melanomas transplanted to syngeneic host mice

Human *in vivo* models

- Human melanomas transplanted to athymic nude (*nu/nu*) mice
- Human melanomas transplanted to beige–nude (*bg/bg nu/nu*) mice
- Human melanomas transplanted to nude–XID (*nu/nu xid/xid*) mice
- Human melanomas transplanted to beige–nude–XID (*bg/bg nu/nu xid/xid*) mice
- Human melanomas transplanted to SCID (*scid/scid*) mice
- Human melanomas transplanted to athymic nude (*rnu/rnu*) rats

H^+, and probably also of other nutrients, hormones and growth factors. Multicellular spheroids model avascular melanoma micrometastases and intervascular microregions of primary melanomas and larger metastatic deposits. A comprehensive review of the biology and treatment sensitivity of multicellular spheroids has been published by Sutherland[2].

Spontaneous melanomas in laboratory animals are extremely rare. A transgenic mouse developing ocular and cutaneous melanomas has therefore been created by Mintz[3,4] and co-workers. The transgene of this mouse consists of the tyrosinase promotor (expressed in melanocytes) fused to the coding regions of simian virus 40 early genes (Tyr–SV40E). The tumors of Tyr–SV40E transgenic mice are histopathologically similar to corresponding melanomas in humans: the ocular melanomas are aggressive, highly invasive and metastasize to local and distant sites; the cutaneous melanomas show a multistep tumor progression paralleling the sequence in human melanoma. Tyr–SV40E transgenic mice have a significant potential in studies of mechanisms underlying the development and metastasis of melanoma. Extensive utilization of this potential is expected when these mice become generally available.

The most frequently used animal models today are based on transplantation of tumor tissue. Two categories of transplantable melanomas are available: (1) melanomas derived from tumors that have arisen in rodents and have been transplanted to immunocompetent syngeneic animal recipients (rodent models); and (2) melanomas derived from tumors that have arisen in cancer patients and have been transplanted to immunologically incompetent animal recipients (human xenograft models). Human xenograft models are usually preferable to rodent models; transplantable rodent melanomas are, at best, nonspecific models for human melanoma, whereas transplantable human melanomas are considered to model 'adequately' the biology of the specific neoplastic disease of the donor patient[5].

Melanoma is a heterogeneous disease. No single human melanoma xenograft model is therefore appropriate for all types of questions related to this disease and research groups should endeavor to have available a panel of models. A panel is particularly useful if it is composed of melanoma xenograft lines that differ substantially in their biological characteristics, and, at the same time, reflect the biology of the donor patients' tumors[5]. The validity and usefulness of human melanoma xenografts as models for melanomas in humans are reviewed here. The advantages and disadvantages of melanoma xenograft models as a whole are summarized in Box 2.

Human melanoma xenografts

Recipient animals

Human melanomas xenotransplanted to immunologically competent rodents are usually rejected. The rejection of transplanted foreign malignant and normal tissues in immunologically competent animals is mediated by mature T cells, which develop in the thymus.

Before 1970, human melanomas were xenotransplanted to rodents in 'immunologically privileged' sites such as the anterior chamber of the eye, the cerebrum and the hamster cheek pouch. They were also transplanted to rodents made immunologically incompetent by thymectomy, whole-body irradiation and/or treatment with immunosuppressive chemical agents. These earliest xenotransplantation systems were of limited usefulness, mainly because of the low rates at which tumors became established and the difficulties in obtaining serially transplantable melanoma lines.

The use of xenotransplanted human melanomas as models for melanomas in humans entered a new era in 1966 with the discovery and characterization of the congenitally athymic nude (*nu/nu*) mouse[6]. This mouse mutant has no thymus at birth, reduced antibody production in response to a variety of antigen challenges, and almost no cell-mediated immune responses. Athymic mice accept xenotransplanted human tumor tissue readily without immunosuppressive treatment, and the first successful xenotransplantation of human tumor tissue was reported in 1969 by Rygaard and Povlsen[7]. Since the early 1980s, mice with other genetic immune-deficiencies have also been used as hosts for xenotransplanted human tumors: the beige–nude (*bg/bg nu/nu*) mouse, the nude–X-linked immune-deficient (XID) (*nu/nu xid/xid*) mouse, the beige–nude–XID (*bg/bg nu/nu xid/xid*) mouse and the severe combined immune-deficient

Box 2. Advantages and disadvantages of human melanoma xenografts

Advantages

- Human melanoma xenografts reflect the histological appearance, karyotype and molecular pathology of the donor patients' tumors.
- Cells isolated from human melanoma xenografts and donor patients' tumors show similar treatment sensitivities *in vitro*.
- Human melanoma xenografts show organ-specific metastatic patterns similar to those of the donor patients' tumors.

Disadvantages

- The volumetric growth rate in the recipient animal is faster for human melanoma xenografts than for the donor patients' tumors *in situ*.
- The hematological system and the vascular network of human melanoma xenografts originate from the recipient animal rather than from the patient.
- Immune reactions of the recipient animal are active against human melanoma xenografts.

Glossary

Bioluminescence imaging – A method for obtaining information on the distribution of metabolites (e.g. ATP, glucose, lactate) in tissues. The method is based on the detection of light emitted from cells as a result of oxidation of substrates in the presence of luciferase.

Cytokine – An extracellular signaling protein or peptide that acts as a local mediator in cell–cell communication.

Karyotype – The full chromosome set of the nucleus of a cell or the photomicrograph of chromosomes arranged according to a standard classification.

Killer cells – Differentiated T cells that can recognize and lyse target cells bearing specific antigens recognized by their antigen receptors.

Melanoma – A malignant tumor arising from the melanocytic system of the skin and other organs.

Metastasis – A secondary tumor growing in a site distant from the site of the primary tumor. A metastasis results from malignant cells released from the primary tumor and transferred to the distant site, usually via blood or lymph.

Natural killer (NK) cells – Lymphocytes without B- or T-cell surface markers that mediate cytotoxic reactions without prior sensitization against the target. NK cells can lyse a wide variety of tumor cells and are probably important in natural resistance to tumors.

Nuclear magnetic resonance (NMR) imaging and spectroscopy – Noninvasive methods for obtaining information on anatomical structures, physiological conditions and chemical compositions of tissues. The methods are based on interactions between radiofrequency fields and magnetic nuclei (for example, ^{1}H, ^{13}C, ^{15}N, ^{19}F, ^{31}P) in a magnetic field.

Oncogene – A gene whose activation is associated with the initial and continuing conversion of normal cells into cancer cells.

Organ-specific metastasis – The predilection of a tumor for developing metastases in a specific organ.

Orthotopic tumor cell inoculation – Inoculation of tumor cells into their 'normal' anatomical position corresponding to their origin.

Spin–lattice (T_1) and spin–spin (T_2) relaxation times – Time constants describing the rates at which an excited nucleus relaxes back to its normal state. Differences in proton T_1 and T_2 between tissues produce contrast in NMR images.

Tumor angiogenesis – The induction of the growth of blood vessels from surrounding tissue into a solid tumor by diffusible chemical factors released by the tumor cells.

Tumor differentiation – The extent to which the histological appearance of a tumor resembles that of its normal tissue counterpart.

Tumor hypoxia – Regions of oxygen deficiency in tumor tissue which, if prolonged, can lead to tumor cell death.

Tumor interstitial fluid pressure – The pressure of the interstitial fluid in tumor tissue, usually within the range 1–50 mmHg.

Tumor necrosis – Morphological changes in tumor tissue indicative of cell death, caused by the progressive degradative action of enzymes.

Tumor parenchyma – The functional element of a solid tumor (i.e. the malignant cells) as distinguished from its framework, or stroma.

Tumor stroma – The supporting tissue or matrix of a solid tumor, as distinguished from its functional element, or parenchyma.

Tumor suppressor gene – A gene whose deactivation is associated with the initial and continuing conversion of normal cells into cancer cells.

Xenograft – A graft of tissue transplanted between animals of different species.

(SCID) (*scid/scid*) mouse (Box 1). The beige (*bg/bg*) and XID (*xid/xid*) genes confer impaired natural killer (NK) and B-cell activity, respectively. The SCID mouse lacks both functional B and T cells because of nonfunctional rearrangements of the immunoglobulin and T-cell receptor genes. The athymic nude (*rnu/rnu*) rat, first described in 1978 (Ref. 8), has been used only to a limited extent in experiments involving xenotransplantation of human melanomas.

Comprehensive studies of the biological behavior and treatment sensitivity of a given melanoma require that the tumor is serially transplantable and can thus be subjected to different types of experiment over a long period of time. Several serially transplantable human melanoma xenograft lines have now been established and characterized, particularly in the *nu/nu* mouse and the SCID mouse. Either the *nu/nu* mouse or the SCID mouse was used as the recipient animal in all the studies described in this review unless otherwise stated. Experiments performed so far have suggested that there are no consistent differences in the biological characteristics of human melanoma xenografted tumors growing in either of these immune-deficient hosts.

Mouse anti-human immune reactions

Studies performed in immune-deficient mice have shown that recipient immune reactions are active against human tumor xenografts; although the cells responsible have not been identified conclusively, there is evidence of contributions from residual mouse T cells, NK cells and macrophages as well as other immune cells[9]. *bg/bg nu/nu xid/xid* mice and *nu/nu* mice show similar immune responses against xenotransplanted human tumor cells. Although the immune responses evoked in SCID mice are lower than those in *nu/nu* mice, they are still significant.

Immune reactions of the murine host would be expected to influence the transplantability, response to therapy and metastatic propensity of human tumor xenografts. Studies of human melanoma xenografts have also shown that the magnitude of the immune reactivity of the recipient differs significantly depending on the tumor line used[10]. The use of melanoma xenografts to explore the basic mechanisms underlying the clinical behavior and treatment sensitivity of melanomas in humans thus requires quantitative knowledge of the immune responses evoked by each xenograft line. Alternatively, immunosuppressive treatments to eliminate the immune reactivity in the recipient animal can be used if the immune responses are incompatible with the aims of the experiment.

Establishment and maintenance

Human melanoma xenograft lines can be established by several methods (Fig. 1). Immediately

after surgery to remove melanoma tissue, the surgical specimens are put into culture medium. Normal tissue, necrotic areas and blood clots are removed before the melanoma tissue is cut into small fragments. Single-cell suspensions are prepared by enzymatic disaggregation of the fragments. Both tumor fragments and aliquots of single-cell suspensions can be used to initiate melanoma xenografts. Tumor fragments are implanted subcutaneously whereas cell suspensions are usually inoculated intradermally. Transplantation to these sites facilitates inspection of the tumor and measurement of its growth. The procedure is then repeated using xenografted tumors as source tissue. Some melanomas show histopathological changes during the initial passages in mice, but stable xenograft lines are usually obtained within ten passages. Melanoma xenograft lines can be established from both primary tumors and metastatic lesions, but the rate of success is higher for metastases than for well-differentiated primary tumors.

Inoculation of tumor cells into their normal anatomical position (i.e. orthotopic inoculation) is a necessary prerequisite for xenografted tumors to retain the essential biological features of the donor tumor tissue[11,12]. If a tumor is heterogeneous, some of the tumor cells might possess a growth advantage at the transplantation site, depending on the concentrations of growth stimulatory and inhibitory factors and of angiogenic stimulatory and inhibitory factors[13,14]. The concentrations of organ-derived growth and angiogenic factors differ substantially among normal tissues, and the interaction of xenografted tumor cells with the relevant organ microenvironment seems to be particularly important for accurate reproduction of the metastatic behavior of human tumors[5,12–14].

The melanocyte, the normal-cell counterpart of the melanoma cell, is normally located at the dermal–epidermal junction of the skin. Intradermal inoculation of melanoma cells therefore results in orthotopic tumors within a short time as the tumor cells infiltrate the epidermis of the mouse and interact with the dermal–epidermal junction. Probably for this reason, there is substantial evidence that intradermal tumors are more relevant models for human melanoma than are subcutaneous tumors[5,12].

Growth and differentiation

Human melanoma xenograft lines frequently increase their volumetric growth rates during the first 3–5 passages *in vivo*, possibly as an adaptation to the new environment. Following subsequent transplantations, many lines retain relatively constant growth rates, even for several years. 'Permanent' melanoma xenograft lines studied in our laboratory have shown volume-doubling times ranging from 2 to 65 days at a tumor volume of 200 mm^3, which is considerably shorter than those reported for melanomas in humans. In a few lines, the increased volumetric growth rate was found to be a consequence of either an increased rate of cell proliferation or the selection of rapidly proliferating cell subpopulations. For most of the lines, it resulted from a reduction in cell loss by necrosis and also a reduced rate of removal of necrotic material.

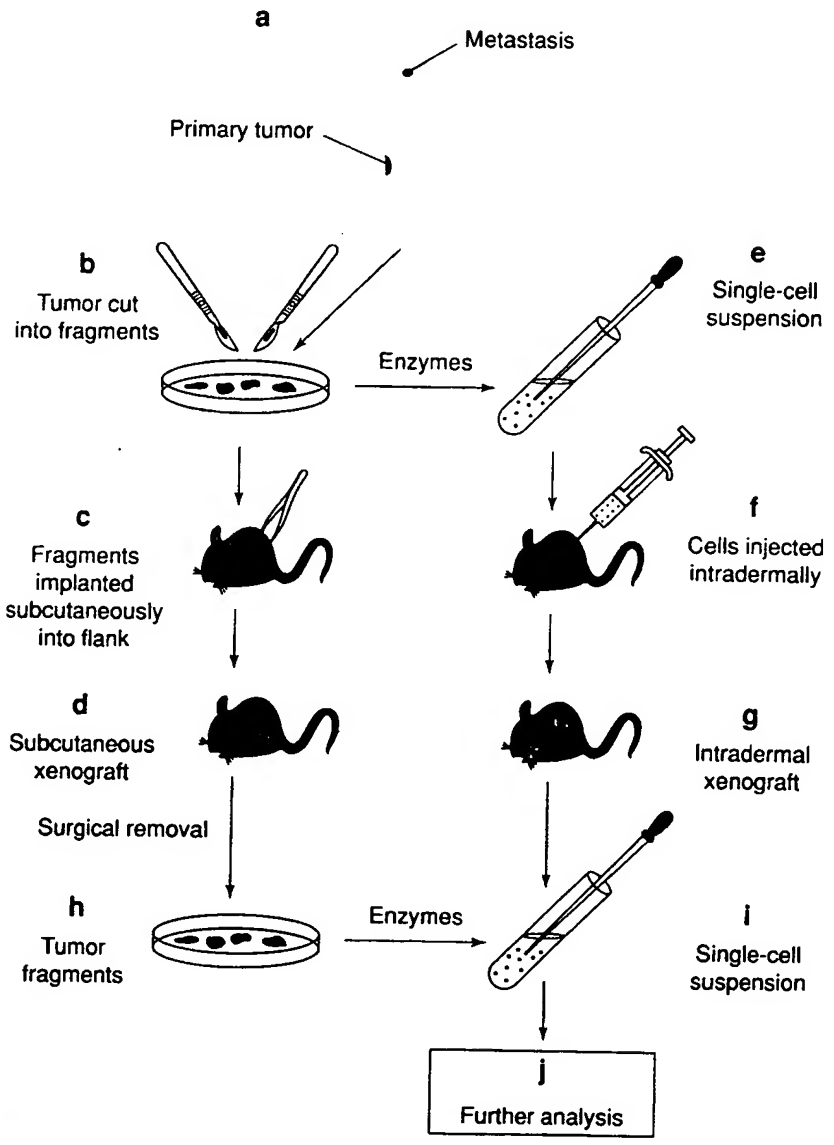

Figure 1. Establishment and maintenance of human melanoma xenograft lines. The primary tumor, or a metastasis, of a melanoma patient (**a**) is removed surgically and cut into small fragments using scalpels (**b**). A small incision is made in the skin in the flanks of recipient mice and tissue fragments are positioned subcutaneously using a pair of tweezers (**c**), resulting in the development of subcutaneous melanoma xenografts (**d**). Alternatively, a single-cell suspension is prepared by enzymatic treatment of tissue fragments (**e**) and aliquots are inoculated intradermally using a Hamilton syringe (**f**), resulting in the development of intradermal melanoma xenografts (**g**). The subcutaneous (**d**) and intradermal (**g**) melanoma xenografts are then removed surgically, and fragments (**h**) and single-cell suspensions (**i**) are prepared for transplantation to the second generation of recipient mice or for further analysis *in vitro* (**j**).

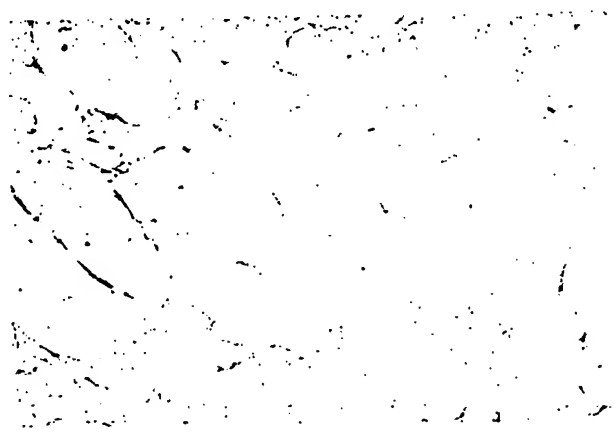

Figure 2. Immunohistochemical image of the human parenchyma and the murine stroma of a human melanoma xenograft grown intradermally in an athymic nude mouse. The stroma was stained brown using polyclonal rabbit anti-laminin and standard immunoperoxidase procedures. Hematoxylin was used for counterstaining.

Light- and electron-microscopic examinations have revealed a close correlation in histological appearance between the tumors of many 'permanent' human melanoma xenograft lines and the source tumors in the donor patients[5,12]; the extent of cellular pleomorphism and nuclear atypia is usually similar, and even the degree of differentiation is frequently well retained. This in itself is remarkable, because it means that human melanoma cells have the ability to stimulate connective tissue cells from the recipient mouse to provide a stroma whose structure resembles that of the source tumor.

Biological studies

Molecular pathology

Early xenotransplantation studies showed that the characteristic features of the karyotypes of donor patients' tumors were retained in xenografted melanomas. More recently, it has been shown that the activation, rearrangement and expression of oncogenes, as well as the expression and mutation pattern of tumor suppressor genes, are retained during xenotransplantation. These observations make it possible to use xenografted tumors to study, in detail, relationships between genetic characteristics of melanomas and their biology and response to therapeutics. As some oncogenes code for growth factor receptors, human melanoma xenografts are also useful models for studying the effects of growth factors and the identification of methods for blocking growth factor receptors.

Xenografted tumors of transfected human melanoma cells can be utilized to obtain information on the biological effects and therapeutic consequences of the expression of distinct genes. Some studies of this type can be performed using human melanoma monolayer cell cultures or multicellular spheroids as model systems, but many biological effects and therapeutic approaches can be more comprehensively studied by using *in vivo* model systems. Human melanoma xenografts are therefore very useful in these situations.

Antigen expression

The antigenic profile of donor patients' tumors is generally retained in human melanoma xenografts. They have therefore been useful models for the pre-clinical evaluation of the effectiveness of monoclonal antibody conjugates in the imaging and treatment of melanomas in humans[15,16]. Human melanoma xenografts have been particularly useful for comparing the effectiveness of F(ab')$_2$ fragments with that of whole immunoglobulins and for comparing the effectiveness of targeting intracellular antigens and membrane-associated antigens. The effects of varying antibody dose, of different radionuclide–antibody conjugates and of using interferons to enhance antigen expression have also been evaluated in human melanoma xenografts, and the effects were predictable for those in patients. However, the extent of tumor detection and the effectiveness of therapy with radiolabeled monoclonal antibodies have been overestimated using human melanoma xenografts when compared with melanomas in humans. The uptake of antibodies is 100–1000-fold higher in human melanoma xenografts than in melanomas in patients. This results, in part, from the fact that antibodies with a high specificity for an antigen on human melanoma cells will not usually cross-react with the equivalent antigen on normal mouse cells; thus there is less 'loss of antibody' *in vivo* in the mouse. Moreover, the use of mouse-derived

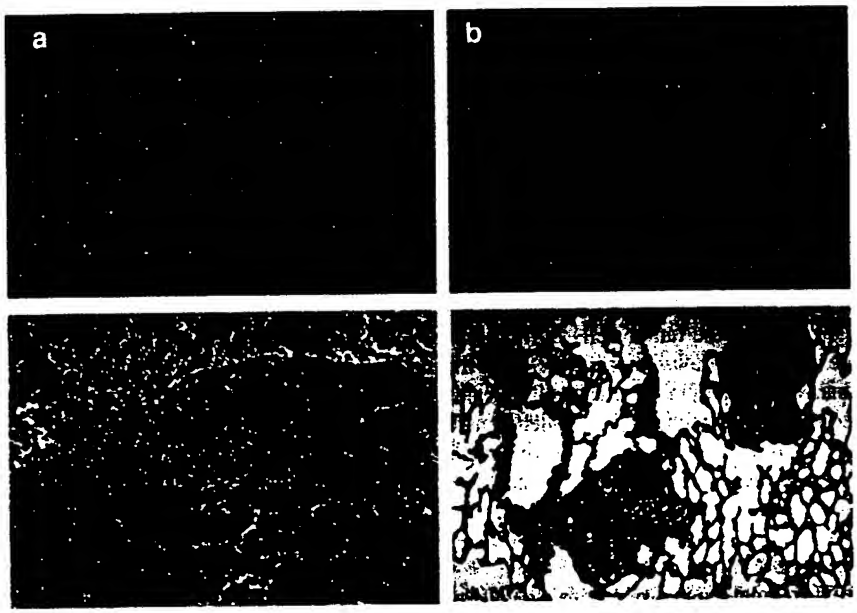

Figure 3. Human melanoma xenografts can develop metastases in athymic nude mice. The primary tumor was inoculated intradermally in the flank and removed surgically when a diameter of 10 mm was reached. (a) Athymic nude mice with lymph node metastases: one with a metastasis in the inguinal region, the other with a metastasis in the interscapular region. (b) Lungs of athymic nude mice with metastases: one pair with many small deposits, the other pair with a few large colonies. (c) Histopathological appearance of a lymph node metastasis. (d) Histopathological appearance of lung metastases.

antibodies in a recipient mouse cannot predict the behavior of the same antibodies in patients; this is particularly likely when multiple injections are implied therapeutically, which would be expected to elicit an immune response in patients, but are much less likely to in mice[17].

Pathophysiology

Xenotransplanted human melanomas promote neovascularization in the recipient mouse via endogenous tumor angiogenic factors. The vascular network and supporting stroma of human melanoma xenografts thus originate from the recipient, whereas only the tumor parenchyma is of human origin (Fig. 2). Moreover, the transport of oxygen to xenografted melanomas depends on the erythrocytes of the recipient mouse, which differ in several important respects from human erythrocytes; for example, the oxyhemoglobin dissociation curve for mouse blood is shifted to the right relative to that for human blood. The extent of the pathophysiological differences between melanomas in humans and in the xenografts, and possible implications for the validity of human melanoma xenografts as models for human melanoma, have yet to be elucidated.

Although the 'building blocks' of the vascular system of human melanoma xenografts originate from the recipient mouse, there is significant evidence that the 'architecture' of the capillary network and the rate of blood perfusion are determined, at least in part, by characteristics of the human parenchymal tumor cells. Thus, it has been shown that different human melanoma xenograft lines possess individual and characteristic microvascular structures, vessel densities and perfusion rates *in vivo*[5,18,19]. The 'patterns' of these characteristics in melanoma xenograft lines are also similar to those of the corresponding donor patients' tumors *in situ*[5].

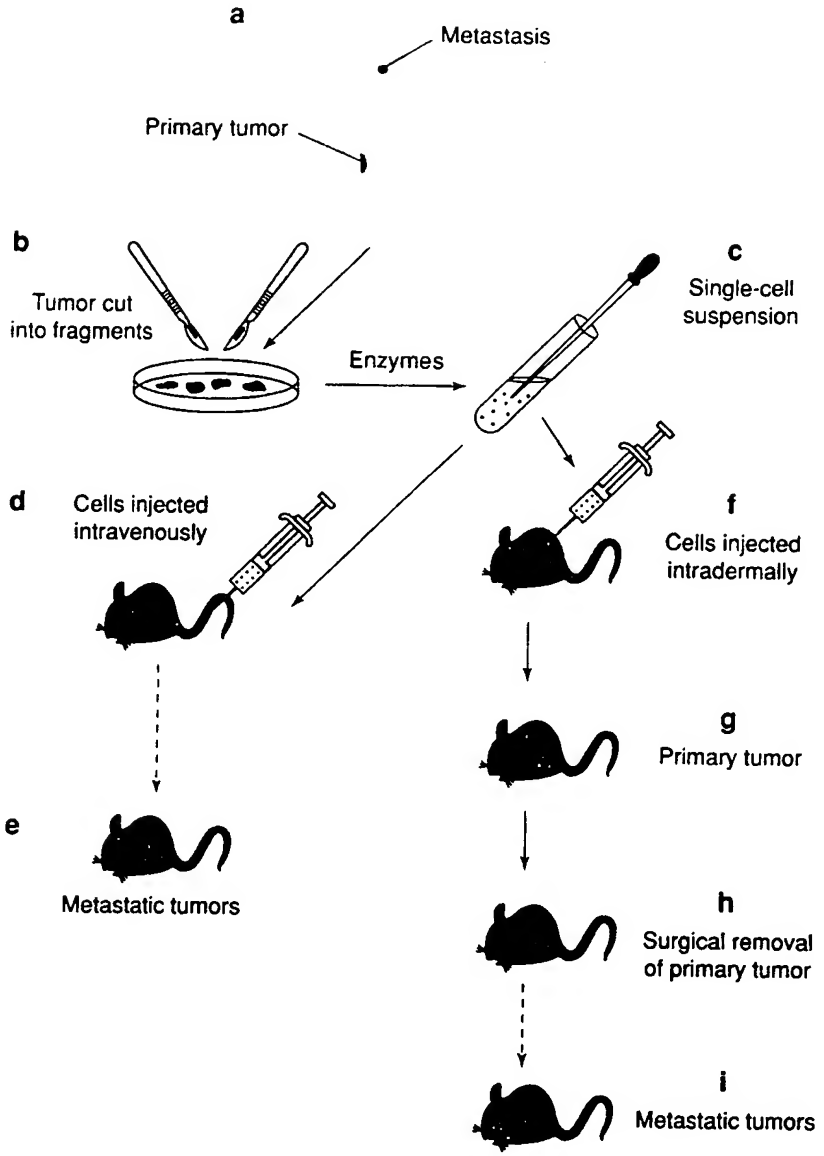

Figure 4. Studies of metastasis of human melanoma xenografts. The primary tumor or a metastasis of a melanoma patient (a) is removed surgically and cut into small fragments using scalpels (b). A single-cell suspension is prepared by enzymatic treatment of the tissue fragments (c) and aliquots are inoculated into the circulation of recipient mice (d). Some weeks later, metastases develop in distant organs (e). Alternatively, aliquots of the cell suspension are inoculated intradermally in recipient mice (f) and primary tumors develop (g). These are then removed surgically (h) and metastases develop in distant organs some weeks later (i).

The pathophysiological conditions of human melanoma xenografts are not just a consequence of the vascular supply, but also depend directly on distinct genetic and biochemical properties of the human parenchymal tumor cells; these affect the oxygen and glucose consumption and metabolic activity in the tumor, and the ability of the tumor cells to survive under hypoxic stress, acid pH and low glucose concentrations. The consequence of this is that melanoma xenograft lines derived from different patients differ significantly with respect to their rate of angiogenesis, interstitial fluid pressure, distribution of oxygen tension and bioenergetic status, parameters that can be visualized using ^{31}P nuclear magnetic resonance (^{31}P-NMR) spectroscopy and glucose, lactate and ATP bioluminescence imaging[20,21]. Comparative studies of these parameters in human melanomas *in situ* and in the xenografted tumors derived from them have yet to be performed, but would be very useful to evaluate the validity of human melanoma xenografts as models for human melanoma in studies of tumor pathophysiology.

Metastasis

Tumor metastasis, the spread of malignant cells from the primary neoplasm to regional and distant sites, is the major cause of death of patients with melanoma. Significant efforts have been made to

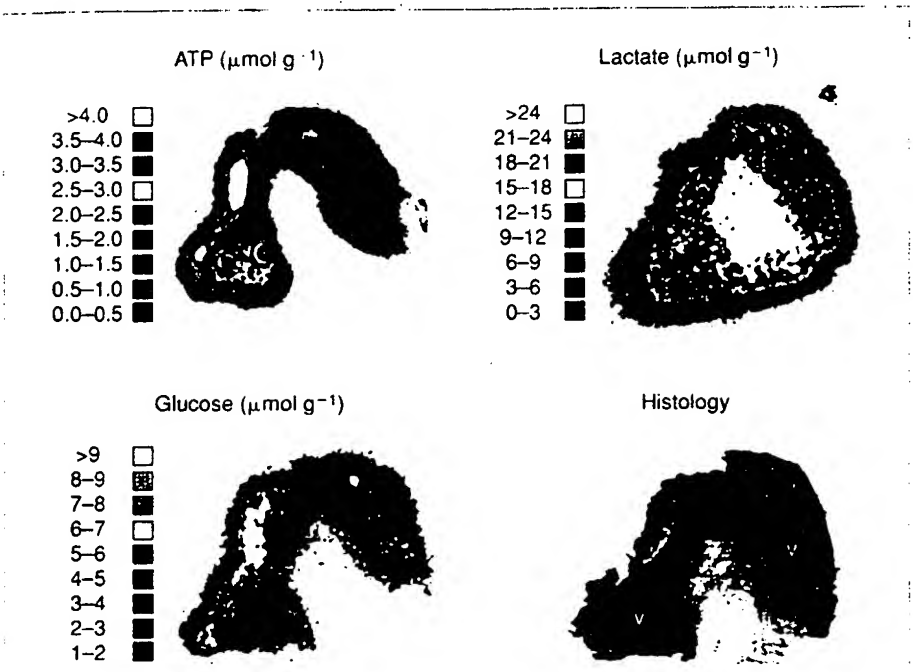

Figure 5. Bioluminescence images showing the regional distributions of ATP, glucose and lactate in relation to histology of a human melanoma xenograft. The ATP and glucose concentrations are higher in viable (v) than in necrotic (n) tissue, whereas the lactate concentrations are similar in these regions. Significant heterogeneities in the ATP, glucose and lactate concentrations are seen within the viable tissue. Reproduced by courtesy of Professor W. Müller-Klieser, Institute of Physiology and Pathophysiology, University of Mainz, Germany.

establish xenograft models for the study of the metastatic behavior of human melanoma. The earliest attempts used tissue fragments to initiate subcutaneous tumors, but met with no success as metastases developed extremely rarely. Some subcutaneous tumors initiated from single-cell suspensions did develop metastases, but the metastatic frequency was low[22]. Recent comparative studies have shown that orthotopic human melanoma xenografts develop distant metastases quite frequently, whereas subcutaneous tumors of the same melanoma xenograft lines never, or only rarely, develop metastases[5,12]. This difference might be related to the observation that subcutaneous transplantation gives rise to tumors surrounded by a dense fibrous capsule, whereas intradermal inoculation results in invasively growing tumors[11,12,14].

Melanoma xenograft lines developing metastases in the recipient mouse have now been established both from the primary tumor and from a metastatic lesion from several patients[23–26] (Fig. 3). Subpopulations of cells differing in metastatic propensity have been isolated from some of these lines by cloning cells *in vitro* or *in vivo*[25,26]. The subpopulations with the highest metastatic propensity have been isolated from metastatic foci in mice inoculated with the parent line. Although artificial melanoma metastasis, induced by wide dissemination of tumor cells, can be studied by inoculating tumor cells into the circulation of the mouse via the lateral tail vein, hepatic portal vein, internal carotid artery or left ventricle of the heart, spontaneous metastasis of melanoma can only be reliably induced after orthotopic inoculation of tumor cells into the dermis of the mouse. In these 'spontaneous metastasis' experiments, the rapidly growing primary tumors are usually removed surgically to allow time for the smaller metastases to develop before the recipient mouse has to be killed for humane reasons (Fig. 4).

Interestingly, melanoma xenografts show an organ-specific metastatic pattern that reflects the pattern of distant metastasis in the donor patient[5]. A given line develops the same organ specificity for metastasis after intravenous, intra-arterial or intradermal inoculation. The organs of preference for four lines established in our laboratory were the lungs for lines A-07 and D-12, lymph nodes for line R-18 and the brain for line U-25. The donor patients had all developed regional metastases at the time of initial diagnosis, and the patient from whom line R-18 was derived presented with extensive metastatic deposits in lymph nodes within the thorax and abdomen. The other patients developed distant metastases subsequent to the initial diagnosis, first in lymph nodes and then in the lungs in the patients from whom the lines A-07 and D-12 were derived, and in the brain for the patient from whom the U-25 line was derived. The deaths of the patients resulted from distant metastases involving the lungs ('A-07' and 'D-12' patients), the lymph nodes ('R-18' patient) and the brain ('U-25' patient). Human melanoma xenografts would thus appear to be interesting model systems for studying the molecular mechanisms governing organ specificity in the metastatic behavior of melanoma. However, it is not known whether the interactions between (1) melanoma cells and organ-derived growth-stimulatory and -inhibitory factors and (2) organ endothelium and melanoma-derived angiogenic-stimulatory and -inhibitory factors are similar in melanoma patients and immune-deficient murine hosts.

The metastatic frequency of human melanoma xenografts might, however, be a misleading quantitative measure of the intrinsic metastatic propensity of the melanoma cells owing to the cell-line-dependent immune reactivity of the host[10]. This can be illustrated by using the development of lung metastases from lines A-07 and D-12 as an example. The number of lung metastases developed by line D-12 is approximately eightfold higher than that developed by line A-07. However, the immune response evoked by line A-07 is approximately sixfold higher than that evoked by line D-12. These observations show that the intrinsic propensity for the development of lung metastases does not necessarily differ between the two cell lines A-07 and D-12; the lower number of lung metastases developed by line A-07 was probably mainly due to the higher immune response evoked in the recipient mice, rather than being caused by a lower intrinsic metastatic propensity. Consequently, if attempts to identify genes, membrane proteins or molecular mechanisms that elicit and augment organ-specific lung metastasis assumed that the cells in line D-12 were more metastatic than the cells in line A-07, this would be misleading. Quantitative assessment of the intrinsic metastatic propensity of human melanoma xenografts requires, in addition, detailed examination of the host immune reactivity against the melanoma cells.

Diagnostic and therapeutic studies

Diagnosis

In most hospitals, the routine diagnosis of melanoma aims to differentiate between benign and malignant melanoma-like lesions and to assess the invasion of primary malignant melanomas, and the nature and location of the dissemination of metastases. The physiological conditions in the tumor microenvironment differ substantially between individual melanomas, and there is significant clinical evidence that the prognosis of melanoma patients depends on the tumor physiology as well as on the stage of the disease. The diagnosis of melanoma might be improved if conventional diagnostic methods were supplemented with methods for assessing the physiological microenvironment.

Melanomas in some patients develop necrotic regions during their growth, mainly because of inadequate blood supply. The microenvironment of the cells of such tumors, particularly cells close to necrotic regions, is characterized by hypoxia, low extracellular pH, nutritional deprivation and elevated interstitial fluid pressure. This abnormal microenvironment promotes tumor progression and causes resistance to treatment. Hypoxia, acidity and low glucose levels alter the expression of several genes, such as those coding for p53, hemoxygenase, vascular endothelial growth factor and cathepsin L, which might lead to increased resistance to treatment with some chemotherapeutic agents, increased angiogenesis and increased metastatic frequency[27]. Hypoxic cells are more resistant to treatment with ionizing radiation and some chemotherapeutic agents than are aerobic cells because oxygen is necessary for some types of DNA damage to occur[28]. Moreover, tumors with an elevated interstitial fluid pressure are resistant to treatment modalities involving macromolecules because of the poor diffusion of macromolecules into the central regions of such tumors[29]. Human melanoma xenografts are currently being used as tumor models in an attempt to develop adequate methods for characterizing the physiological microenvironment of melanomas.

Metabolic imaging of cryosections of melanoma tissue, based on bioluminescence and single photon registration, is a promising technique that makes it feasible to study the inter-relationship between the histological image and the spatial distribution of metabolites[21] such as ATP, glucose and lactate (Fig. 5). Conventional diagnosis based on the examination of histological sections stained with Hematoxylin and Eosin might be improved if metabolic images were used as a supplement to histological images. Metabolic images appear to mirror blood supply rather than the fraction of hypoxic cells in human melanoma xenografts, indicating that metabolic imaging might be used to assess the supply rather than the consumption of oxygen and nutrients[30].

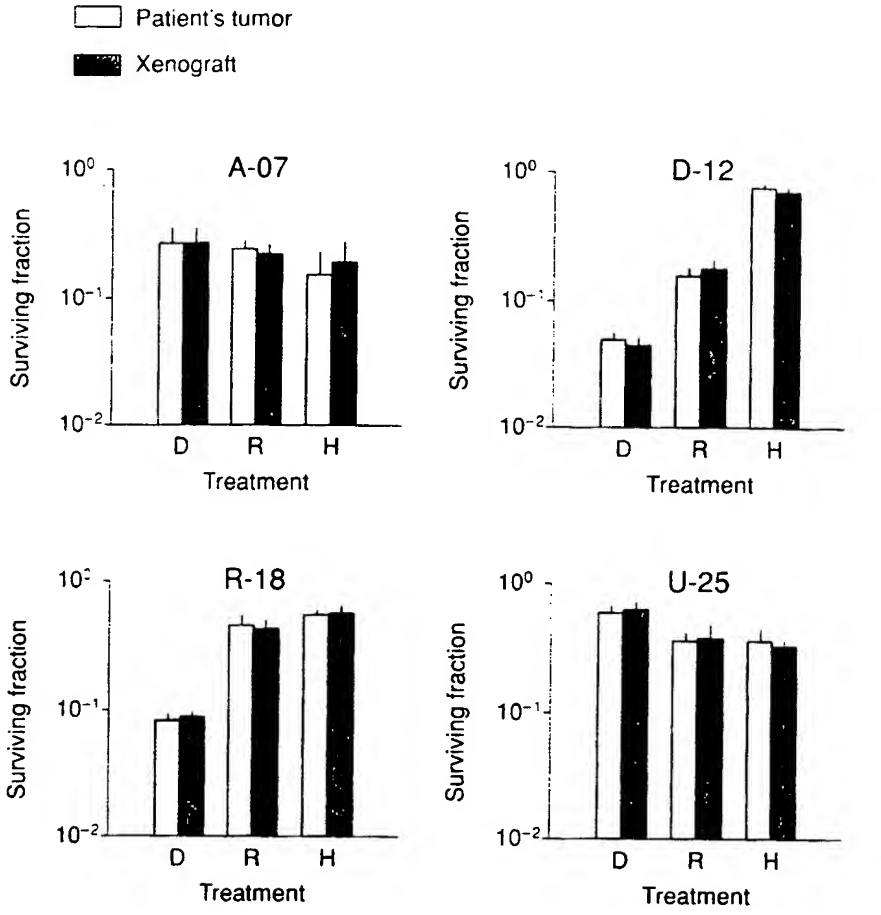

Figure 6. Comparison of sensitivity to treatment of cells isolated from donor patients' melanomas and melanoma xenograft lines derived from them (A-07, D-12, R-18 and U-25). The xenograft experiments were performed after stable melanoma lines had been established. The cells were treated *in vitro* with dacarbazine (D, 1×10^3 μg ml^{-1} for 60 min), radiation (R, 2.0 Gy) or hyperthermia (H, 43.5°C for 60 min). The surviving cell fraction following a given treatment, measured using a soft agar colony assay[32], differed substantially between the four melanomas. Cellular sensitivity to treatment was retained during xenotransplantation.

^{31}P-NMR spectroscopy is a potentially useful noninvasive method for characterizing the metabolic microenvironment of tumors *in situ*, and provides information related to lipid metabolism, energy metabolism and intracellular pH. Studies of human melanoma xenografts have shown that ^{31}P-NMR spectroscopy can be used to monitor changes in the blood supply and the proportion of hypoxic cells in individual tumors following treatment[20]. The pre-treatment ^{31}P-NMR spectrum of each tumor serves as a control in such studies. However, it has not been possible to demonstrate correlations between parameters derived from pre-treatment ^{31}P-NMR spectra and the blood supply or the proportion of hypoxic cells across different human melanoma xenograft lines. Although there are correlations between parameters derived from ^{31}P-NMR spectra and parameters describing the physiological microenvironment of human melanoma xenografts, different correlations exist for different lines. The clinical usefulness of ^{31}P-NMR spectroscopy has not been evaluated so far, although the response to treatment of melanoma patients has been shown to

depend on the physiological microenvironment of the tumor tissue. The xenograft studies suggest that ^{31}P-NMR spectroscopy has significant potential as a method for monitoring, but not for predicting, the response to treatment of individual melanoma patients[30].

^{1}H-NMR imaging is a well-established diagnostic method in clinical oncology that provides detailed information on macroscopic anatomical structures of tumors and surrounding normal tissues. Less attention has been paid to the technique as a potential method for providing information on metabolic and physiological conditions in tumors. This possibility has now been recognized, and rapid developments are expected in this field. Studies of human melanoma xenografts have shown that the spin–lattice (T_1) and spin–spin (T_2) relaxation times are shorter in necrotic regions than in regions of viable tissue[31]. These differences are sufficiently large that T_1, T_2 and synthetic spin–echo images show clear contrast between necrosis and viable tissue[31]. The possibility thus exists that ^{1}H-NMR imaging might in the future be used for the detection of necrotic regions in melanomas in humans and hence for predicting treatment resistance caused by hypoxia.

Therapy

The prognosis for patients with metastatic melanoma is poor because of the lack of efficient treatment modalities. Human melanoma xenografts are widely used as tumor models in attempts to develop new and improved treatment strategies, and adequate methods for measuring the treatment sensitivities of xenografted tumors have been established. The clonogenicity of single-cell suspensions prepared from human melanoma xenografts can be measured *in vitro* using a soft agar assay[32]. This assay is used to determine the proportion of surviving cells following treatment *in vivo* or *in vitro*. It can also be used to measure the sensitivity to treatment *in vitro* of single-cell suspensions isolated directly from the melanomas of some patients. The sensitivity of human melanoma xenografts treated *in vivo* can also be measured *in vivo* in the treated mice by using local tumor control or tumor regrowth delay as an endpoint[33].

A key question is whether melanoma xenografts show treatment sensitivities similar to those of the donor patients' tumors. Comparative studies of the sensitivity to chemotherapy, radiotherapy or hyperthermia *in vitro* of single-cell suspensions from donor patients' melanomas and melanoma xenograft lines derived from them have shown that the cellular sensitivity to a given treatment can differ substantially among melanomas in different patients and that the cellular treatment sensitivities are retained during serial xenotransplantation (Fig. 6). This conclusion is in agreement with the conclusions from similar studies using patients' tumors and xenograft lines derived from cervix, breast, colon and bladder carcinomas[34].

The response to treatment of human melanoma xenografts *in vivo* depends on the growth, and the pathophysiological and immunological characteristics of the tumor tissue, in addition to the cellular treatment sensitivity. As described above, melanoma xenografts most probably differ from the donor patients' tumors in these characteristics. Thus, although it has been demonstrated that the cellular treatment sensitivity *in vitro* of the donor patients' tumors is usually retained in 'permanent' melanoma xenograft lines, this does not necessarily mean that the treatment sensitivity *in vivo* of melanoma xenografts mirrors the clinical treatment sensitivity of the donor patients' tumors. Studies in this field are sparse. However, the response of human melanoma xenografts *in vivo* to treatment with chemotherapeutic agents has been compared with the general clinical sensitivity of melanomas to the same chemotherapeutic agents. These studies suggested that human melanoma xenografts and melanomas in humans have a similar response pattern to chemotherapy[35,36]. Detailed comparative studies of the treatment sensitivity *in vivo* of donor patients' tumors and melanoma xenograft lines derived from them have not so far been reported.

Future developments

Clinical studies have suggested that some melanomas respond well to various types of immunotherapy[37]. Experimental models to study the interaction between human immune cells and human melanomas *in vivo* are needed. Recent studies have shown that human hemopoietic tissues and immune cells can survive and remain functional in SCID mice for several months[38,39]. The so-called 'SCID–hu' mouse has been shown to support the growth and metastatic spread of human melanoma xenografts[20]. This tumor model should allow novel studies of the effects of human immunity on melanoma growth and dissemination. Moreover, it could be used for the pre-clinical evaluation of immunotherapies such as melanoma vaccines, antibodies for specific delivery of anti-melanoma agents and cultured human lymphoid cells such as tumor-infiltrating lymphocytes or lymphokine-activated killer cells.

Summary

Human melanoma xenografts have been shown to mirror the biology of the specific neoplastic disease of the donor patient and are therefore exciting experimental models for studies of the progression.

The outstanding questions

- How well do human melanoma xenografts in recipient mice mirror characteristics of the blood supply and the proportion of hypoxic cells in the donor patients' tumors?
- How well does the response to therapy of human melanoma xenografts *in vivo* in recipient mice reflect the treatment sensitivity of the donor patients' tumors? How useful are human melanoma xenografts as models to evaluate the likely clinical effectiveness of new treatment strategies for melanoma?
- To what extent do the interactions between (1) melanoma cells and organ-derived growth-stimulatory and -inhibitory factors and (2) organ endothelium and melanoma-derived angiogenic-stimulatory and -inhibitory factors differ between melanomas in patients and melanomas implanted in immune-deficient murine recipients?
- Can the immune reactions in murine recipients against human melanoma xenografts be eliminated by immunosuppressive treatment to avoid an 'artificially reduced' metastatic frequency and an 'artificially enhanced' treatment response?
- Can the SCID–hu model, where human hemopoietic cells are established in an immune-deficient mouse, be used for melanoma studies? Will this model allow studies of the human immune response to human tumors, but in an animal model that can be manipulated, and will this aid the development of clinical immunotherapy for melanoma?

diagnosis and therapy of malignant melanoma. The number of questions that can be answered by careful experimentation with this model system will no doubt increase when routine methods for replacing the murine hemopoietic tissue with a human hemopoietic tissue are established.

Acknowledgements. Financial support was received from The Norwegian Cancer Society. Fig. 5 was kindly supplied by Professor W. Müller-Klieser, Institute of Physiology and Pathophysiology, University of Mainz, Germany.

References

1 Lee, J.A.H. (1990) **Etiology, epidemiology, and prognosis of melanoma and skin neoplasms**, *Curr. Opin. Oncol.* 2, 388–393

2 Sutherland, R.M. (1988) **Cell and environment interactions in tumor microregions: the multicell spheroid model**. *Science* 240, 177–184

3 Bradl, M., Klein-Szanto, A., Porter, S. and Mintz, B. (1991) **Malignant melanoma in transgenic mice**. *Proc. Natl. Acad. Sci. U. S. A.* 88, 164–168

4 Mintz, B. and Silvers, W.K. (1993) **Transgenic mouse model of malignant skin melanoma**. *Proc. Natl. Acad. Sci. U. S. A.* 90, 8817–8821

5 Rofstad, E.K. (1994) **Orthotopic human melanoma xenograft model systems for studies of tumour angiogenesis, pathophysiology, treatment sensitivity and metastatic pattern**. *Br. J. Cancer* 70, 804–812

6 Flanagan, S.P. (1966) **'*Nude*', a new hairless gene with pleiotropic effects in the mouse**, *Genet. Res.* 8, 295–309

7 Rygaard, J. and Povlsen, C.O. (1969) **Heterotransplantation of a human malignant tumour to '*nude*' mice**, *Acta Pathol. Microbiol. Scand.* 77, 758–760

8 Festing, M.F.W. *et al.* (1978) **An athymic nude mutation in the rat**. *Nature* 274, 365–366

9 Silobrcic, V. *et al.* (1990) **Residual immunity of athymic NCr/Sed nude mice and the xenotransplantation of human tumors**, *Int. J. Cancer* 45, 325–333

10 Rofstad, E.K. (1995) **Metastatic behavior of human tumors in congenitally athymic nude mice: intrinsic properties of the tumor cells and host immune reactivity**, *Int. J. Cancer* 63, 744–749

11 Fidler, I.J. (1991) **Critical factors in the biology of human cancer metastasis: Twenty-eighth G.H.A. Clowes Memorial Award Lecture**, *Cancer Res.* 50, 6130–6138

12 Cornil, I., Man, S., Fernandez, B. and Kerbel, R.S. (1989) **Enhanced tumorigenicity, melanogenesis, and metastases of a human malignant melanoma after subdermal implantation in nude mice**, *J. Natl. Cancer Inst.* 81, 938–944

13 Fu, X., Besterman, J.M., Monosov, A. and Hoffman, R.M. (1991) **Models of human metastatic colon cancer in nude mice orthotopically constructed by using histologically intact patient specimens**, *Proc. Natl. Acad. Sci. U. S. A.* 88, 9345–9349

14 Fidler, I.J., Naito, S. and Pathak, S. (1990) **Orthotopic implantation is essential for the selection, growth and metastasis of human renal cell cancer in nude mice**, *Cancer Metastasis Rev.* 9, 149–165

15 Buchsbaum, D.J. (1995) **Experimental approaches to increase radiolabeled antibody localization in tumors**, *Cancer Res.* 55, 5729s–5732s

16 Knox, S.J. (1995) **Overview of studies on experimental radioimmunotherapy**, *Cancer Res.* 55, 5832s–5836s

17 Haisma, H.J. (1991) **Monoclonal antibodies**, in *The Nude Mouse in Oncology Research* (Boven, E. and Winograd, B., eds), pp. 231–245, CRC Press

18 Solesvik, O.V., Rofstad, E.K. and Brustad, T. (1982) **Vascular structure of five human malignant melanomas grown in athymic nude mice**, *Br. J. Cancer* 46, 557–567

19 Lyng, H., Skretting, A. and Rofstad, E.K. (1992) **Blood flow in six human melanoma xenograft lines with different growth characteristics**, *Cancer Res.* 52, 584–592

20 Lyng, H., Olsen, D.R., Southon, T.E. and Rofstad, E.K. (1993) **^{31}P-nuclear magnetic resonance spectroscopy *in vivo* of six human melanoma xenograft lines: tumour bioenergetic status and blood supply**. *Br. J. Cancer* 68, 1061–1070

21 Müller-Klieser, W., Kröger, M., Walenta, S. and Rofstad, E.K. (1991) **Comparative imaging of structure and metabolites in tumours**. *Int. J. Radiat. Biol.* 60, 147–159

22 Hill, L.L. *et al.* (1991) **Growth and metastasis of fresh human melanoma tissue in mice with severe combined immunodeficiency**. *Cancer Res.* 51, 4937–4941

23 Shoemaker, S.H. *et al.* (1991) **Practical spontaneous metastasis model for *in vivo* therapeutic studies using a human melanoma**, *Cancer Res.* 51, 2837–2841

24 Taylor, C.W. *et al.* (1992) **Growth and dissemination of human malignant melanoma cells in mice with severe combined immune deficiency**, *Lab. Invest.* 67, 130–137

25 Ishikawa, M., Fernandez, B. and Kerbel, R.S. (1988) **Highly pigmented human melanoma variant which metastasizes widely in nude mice, including to skin and brain**, *Cancer Res.* 48, 4897–4903

26 Ladanyi, A. *et al.* (1990) **Selection and characterization of human melanoma lines with different liver-colonizing capacity**. *Int. J. Cancer* 46, 456–461

27 Hill, R.P. (1990) **Tumor progression: potential role of unstable genomic changes**, *Cancer Metastasis Rev.* 9, 137–147

28 Coleman, C.N. (1988) **Hypoxia in tumors: a paradigm for the approach to biochemical and physiologic heterogeneity**, *J. Natl. Cancer Inst.* 80, 310–317

29 Jain, R.K. (1990) **Physiological barriers to delivery of monoclonal antibodies and other macromolecules in tumors**. *Cancer Res.* 50, 814s–819s

30 Kröger, M., Walenta, S., Rofstad, E.K. and Müller-Klieser, W. (1995) **Growth rates or radiobiological hypoxia are not correlated with local metabolite content in human melanoma xenografts with similar vascular network**, *Br. J. Cancer* 72, 912–916

31 Jakobsen, I., Kaalhus, O., Lyng, H. and Rofstad, E.K. (1995) **Detection of necrosis in human tumour xenografts by proton magnetic resonance imaging**, *Br. J. Cancer* 71, 456–461

32 Courtenay, V.D. and Mills, J. (1978) **An *in vitro* colony assay for human tumours grown in immune-suppressed mice and treated *in vivo* with cytotoxic agents**, *Br. J. Cancer* 37, 261–268

33 Rofstad, E.K. (1989) **Radiation biology of human tumour xenografts**, *Int. J. Radiat. Biol.* 56, 573–581

34 Rofstad, E.K. (1992) **Comparative sensitivity of cells from human tumors and derivative tumor xenografts to radiation and heat treatments**, *J. Natl. Cancer Inst.* 84, 1517–1524

35 Bellet, R.E., Danna, V., Mastrangelo, M.J. and Berd, D. (1979) **Evaluation of a '*nude*' mouse–human tumor panel as a predictive secondary screen for cancer chemotherapeutic agents**, *J. Natl. Cancer Inst.* 63, 1185–1188

36 Giovanella, B.C., Stehlin, J.S., Shepard, R.C. and Williams, L.J. (1983) **Correlation between response to chemotherapy of human tumors in patients and in nude mice**, *Cancer* 52, 1146–1152

37 Mastrangelo, M.J., Schultz, S., Kane, M. and Berd, D. (1988) **Newer immunologic approaches to the treatment of patients with melanoma**, *Semin. Oncol.* 15, 589–594

38 Mosier, D.E., Gulizia, R.J., Baird, S.M. and Wilson, D.B. (1988) **Transfer of a functional human immune system to mice with severe combined immunodeficiency**, *Nature* 335, 256–259

39 McCune, J.M. *et al.* (1988) **The SCID–hu mouse: murine model for the analysis of human hematolymphoid differentiation and function**, *Science* 241, 1632–1639

40 Müller, B.M. and Reisfeld R.A. (1991) **Potential of the scid mouse as a host for human tumors**, *Cancer Metastasis Rev.* 10, 193–200

Breast Cancer Research and Treatment 39: 69-86, 1996.

Human breast cancer cell line xenografts as models of breast cancer — The immunobiologies of recipient mice and the characteristics of several tumorigenic cell lines

Robert Clarke
Vincent T. Lombardi Cancer Center, Georgetown University Medical School, Washington, DC, USA

Key words: xenografts, breast cancer, cell lines, resistance

Summary

The ability to maintain and study human tissues in an *in vivo* environment has proved to be a valuable tool in breast cancer research for several decades. The most widely studied tissues have been xenografts of established human breast cancer cell lines into athymic nude mice. Human breast tumor xenografts provide the opportunity to study various important interactions between the tumor and host tissues, including endocrinologic, immunologic, and tumor-stroma interactions. The nude mouse is not the only immune-deficient recipient system in which to study xenografts. Additional single and combined mutant strains have been used successfully, including mice homozygous for the severe combined immune deficiency mutation (*scid*), both the beige (*bg*) and nude (*nu*) mutations in combination (*bg/nu*), and mice bearing the combined *bg/nu/xid* mutations. The differing immunobiologies are discussed, with particular reference to the immunobiology of breast cancer, as are the characteristics of several of the more frequently utilized breast cancer xenografts and cell lines. The ability of several endocrine treatments to modulate effectors of cell mediated immunity, *e.g.*, estrogens and antiestrogens, and the effect of site of inoculation on tumor take and metastasis, also are described.

Introduction

The incidence of breast cancer mortality has continued to rise over the past thirty years, despite the innovation of various cytotoxic and endocrine therapies. It is clearly important to generate new and innovative therapies based upon our developing knowledge of the cellular and molecular factors driving breast cancer growth and progression. In this regard, the application of human xenograft models has much to offer both for increasing our understanding of malignant progression, and for the development and screening of novel therapies.

While there are several classes of rodent models for breast cancer, human tumor xenografts provide the unique opportunity to study the regulation of human cell growth and metastasis in an *in vivo* environment. While breast tumor biopsies can be established directly in nude mice, the take rate is generally low [1]. However, it is clear that a significant proportion of the established human

Address for correspondence and offprints: Robert Clarke, PhD, Vincent T. Lombardi Cancer Center and Department of Physiology & Biophysics, W405A The Research Building, Georgetown University Medical School, 3970 Reservoir Road NW, Washington DC 20007, U.S.A.; *Tel:* (202) 687-3755; *Fax:* (202) 687-7505

breast cancer cell lines are tumorigenic in nude mice. Several have recently been determined to be metastatic in immune-compromised rodents. Human breast cancer xenografts have been widely used to study breast cancer progression, the effects of gene expression on tumorigenicity, and acquisition of antiestrogen resistance, and to screen new endocrine and cytotoxic agents. However, a major restriction has been the lack of a diverse panel of estrogen receptor (ER) positive and hormone-dependent cell lines. There are only three major hormone-dependent cell lines available, MCF-7 (the most widely used breast cancer cell line) [2], T47D [3], and ZR-75-1 [4]. The majority of breast cancer cell lines, and almost all of those with a significant inherent metastatic ability, as opposed to transfected cell line variants, are ER negative and hormone-unresponsive [5].

The development of additional breast cancer models is clearly of some importance. However, the nude mouse is not the only immune-compromised rodent available in which to establish xenografts. The additional immune-compromised systems will be briefly introduced in the following sections, and an indication of their diverse immunobiologies provided. The effects of endocrine manipulations on immunity and their importance for the use of breast cancer xenografts also will be addressed. Since the immunobiology of the rodent systems and the immunobiology of breast cancer are central to the use of xenografts, a brief discussion of these systems also is included. It is hoped that these discussions will encourage investigators to broaden the use of different immune-deficient systems, and to establish novel human breast cancer xenograft models.

Immunosurveillance of neoplastic cells: general comments

The precise role of immunosurveillance in breast and other cancers is unclear. In severely immune-compromised individuals, *e.g.*, patients with AIDS, there is evidence for an increased cancer risk. In normal women, both humoral and cell-mediated immunities likely contribute to the suppression of malignancy. The humoral aspects are difficult to study in experimental animal models, since almost all fully immune-competent animals reject xenografts. However, the role of cell-mediated immunity (CMI) can be modeled *in vivo*, at least partly, by using the diverse immune-compromised rodent models described below. While this is not the primary use of immune-compromised models, an understanding of the role of CMI in breast cancer, and of the immunobiologies of the different animal models, is important for the use of xenograft models of breast cancer.

Immunosurveillance of neoplastic cells: breast cancer

Cell-mediated immunity has been implicated in the pathogenesis of breast cancer, but its precise role remains to be established. For example, the skin window procedure, which provides an estimate of the extent of CMI, correlates inversely with metastatic disease [6,7]. Low levels of natural killer (NK) cell activity are associated with familial breast cancer [8], and with patients with stage III/IV disease [9-11]. NK cell activity is generally low or absent in the axillary lymph nodes of patients with demonstrable metastatic disease [12,13], although lymphokine-activated killer (LAK) precursor cells are often present [13]. There appears to be an inverse relationship between ER expression and NK activity [14,15]. ER-positive tumors have fewer T-cells when compared with ER positive tumors [9]. Aminoglutethimide reduces serum estrogens and increases NK activity in breast cancer patients [16].

The precise role of CMI and its effector cells in regulating the growth/tumorigenicity of breast cancer is unknown. The use of Matrigel (Collaborative Research Inc., Bedford MA) to increase xenograft take rate [17,18] also suggests that an effective barrier could protect cells from

locally infiltrating
from clinical studi
least to some de
cancer growth. Th
models currently
means to more ad
perimental animal
of some aspects c
plasia and metasta
in vivo.

**Immunosurveilla
Natural Killer (N
Activated Killer (**

Both cellular and
in the immunologi
of the immune-de
breast cancer rese
munity. T-cell in
e.g., aspects of cell
to consist of a nu
notably NK cell
macrophages [19]
distinct from cyt
cells lacking sign
genes. NK and
tumors and malig

NK cells mak
peripheral lymph
demonstrated to p
Since NK activity
of metastasis [1
potential of most
nude mice may
activities [19,22-2
able to suppress N

LAK cells are
a determination i
mice bearing diff
tions, *i.e.*, *nu* and
of killing neoplast
resistant to NK cy
duce material ca
ment of LAK cell

locally infiltrating CMI effectors. The evidence from clinical studies implicates CMI effectors, at least to some degree, in the control of breast cancer growth. The diversity of immune-deficient models currently available provides a potential means to more adequately determine, in an experimental animal model, the likely contribution of some aspects of CMI to the control of neoplasia and metastasis of human breast cancer cells *in vivo*.

Immunosurveillance of neoplastic cells: Natural Killer (NK) and Lymphokine-Activated Killer (LAK) cells

Both cellular and humoral immunities participate in the immunologic response to neoplasia. Most of the immune-deficient animal models used in breast cancer research lack T-cell-mediated immunity. T-cell independent immunosurveillance, *e.g.*, aspects of cell-mediated immunity, is thought to consist of a number of lymphoid cells, most notably NK cells, LAK precursor cells, and macrophages [19]. Both NK and LAK cells are distinct from cytotoxic T-lymphocytes, lysing cells lacking significant expression of the MHC genes. NK and LAK cells can infiltrate solid tumors and malignant effusions [20].

NK cells make up approximately 1-2.5% of peripheral lymphocytes and have been widely demonstrated to possess antitumor activity [19]. Since NK activity may also contribute to control of metastasis [19,21-23], the poor metastatic potential of most human xenografts growing in nude mice may reflect their elevated NK cell activities [19,22-24]. Some tumors appear to be able to suppress NK activity [25].

LAK cells are clearly distinct from NK cells, a determination initially derived from studies of mice bearing different immune-deficiency mutations, *i.e.*, *nu* and *bg* [26]. LAK cells are capable of killing neoplastic cells, and can kill tumor cells resistant to NK cytolysis [27]. Some tumors produce material capable of blocking the development of LAK cells from their precursors [28].

Immunosurveillance of neoplastic cells: macrophages

Macrophages are widely observed to infiltrate solid tumors [9,29,30] and can kill tumor cells by both phagocytic and non-phagocytic processes [30]. Non-phagocytic cytolysis may include the release of lysosomal enzymes by exocytosis. Macrophages may recognize some tumors on the basis of their abnormal growth [31] or by surface modifications [30] and can produce a non-specific cytolysis. The tumoricidal properties of macrophages are acquired following activation by contact with either the target cell and/or secreted products or by soluble lymphokines, *e.g.* interferon-γ [32].

The biology of macrophage-induced cytotoxicity is independent of the sensitivity of the target cells to lymphocyte or NK mediated cytolysis [33]. Tumor cells do not appear to acquire resistance to the cytotoxic effects of macrophages, in marked contrast to their ability to develop resistance to NK-mediated cytolysis [32-34]. The limiting factor in macrophage control of neoplasia appears to be effector:tumor cell ratio [32]. The sera from some cancer patients possess macrophage inhibitory activity [35], while some tumors secrete a macrophage colony-stimulating-like factor [30,36]. Macrophage infiltration is associated with tumor progression rather than inhibition, implying that some macrophages may secrete factors mitogenic for tumor cells [37].

Loss of immunosurveillance

Tumors proliferating successfully in the presence of cytotoxic host cells clearly indicate that the cells have evaded cytolytic effectors. The ability to become resistant to immunologic inhibition is thus a central problem in cancer biology and immunology. The precise mechanisms involved remain unknown, but modification or masking of surface antigens, the secretion of factors that inhibit NK, LAK, or macrophage activation/function, and an altered sensitivity to the direct cyto-

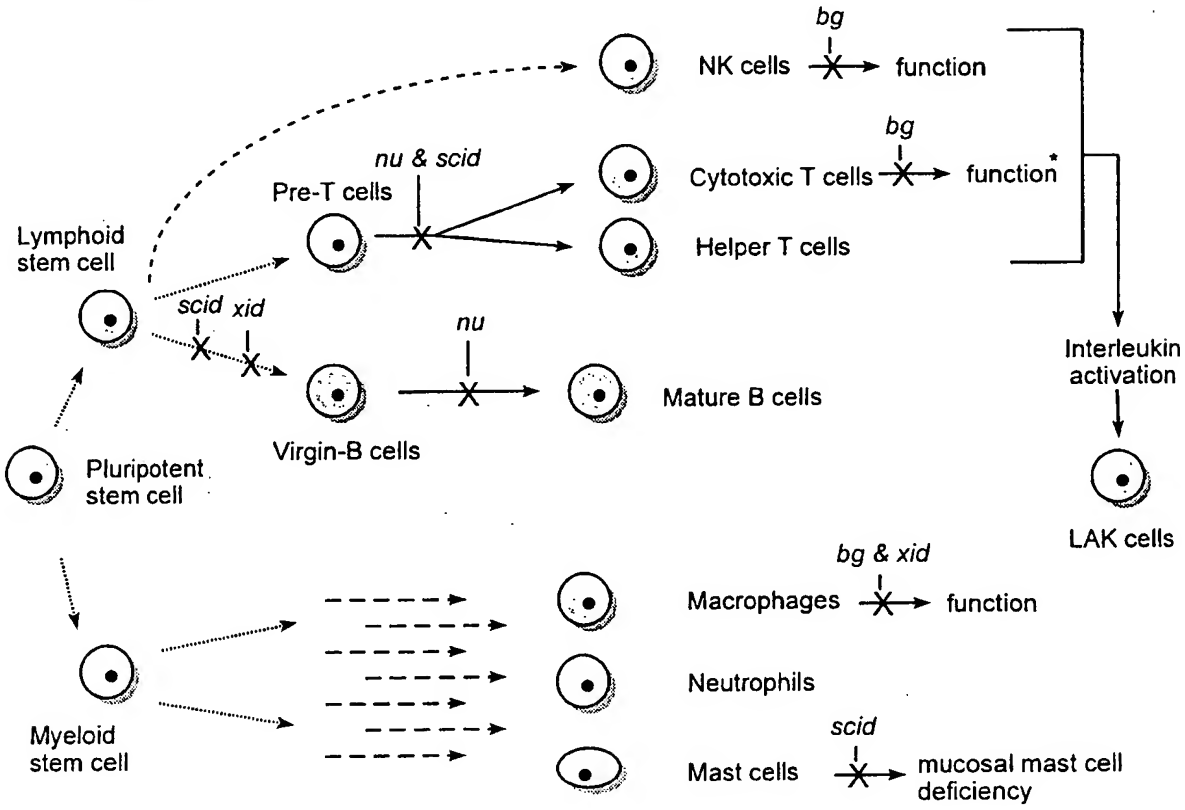

Figure 1. General representation of the likely defects in hematopoiesis associated with the different mutations. The figure is meant to be neither complete (*e.g.*, there are several myeloid lineages not shown) nor specific in terms of the precise/relative locations of the defects. For example, the precise origins of NK cells, and of the cells generating LAK activities, remain to be definitively established. The reader is referred to the text for more specific details. *The deficiencies should not necessarily be considered to represent a complete ablation of activity/function, *e.g.*, not all cytotoxic T cell functions are affected by the *bg* mutation.

lytic effects of effector cells, are probably involved [30]. The isolation of tumor cell variants that exhibit different biological properties in the presence of different immune effector systems should greatly facilitate the study of these complex tumor/immune interactions.

Immune-deficient rodent models

There are approximately 30 loci at which mutations can alter immune function in mice [38]. However, not all are amenable to human tumor xenograft studies. The most widely used immune-deficient rodent model is the nude mouse, mice homozygous for the *nu* mutation. In more recent years, other single and combined mutation bearing strains have become available and are gaining acceptance. These include mice bearing the beige (*bg*) and/or X-linked immunodeficiency (*xid*) mutations, also in combination with the *nu* mutation, and the single gene severe combined immunodeficiency (*scid*) mutation. The hematopoietic defects associated with these mutations are summarized in Figure 1.

Immunobiology of mice homozygous for the nude (*nu*) mutation

The nude phenotype (the mice have no hair; not to be confused with the hairless mutation) was

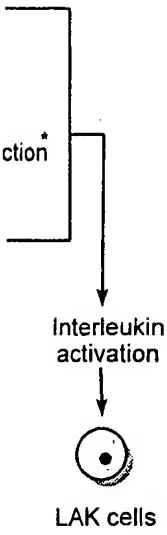

first described in Glasgow, Scotland, in 1962, with Pantelouris subsequently describing the predominating immune deficiency [39]. It was not long before Rygaard and Povlsen reported the ability to sustain human tumor xenografts in nude mice [40]. Since these early reports, the use of homozygous nude mice as recipients of tumor xenografts has become almost ubiquitous in cancer research. Breast cancer research is no exception, with a significant proportion of human breast cancer cell lines exhibiting tumorigenicity in nude mice [5]. While over 70 congenic strains of nude mice have been generated over the last 30 years, the respective immunologies and abilities to support xenografts appear strain dependent [41].

The nude mutation (*nu*) is located on mouse chromosome 11. Homozygous mice are essentially athymic [39], although a rudimentary thymus can be detected at necropsy in individual mice. The lack of a fully functional thymus is primarily responsible for the poor responses to T-dependent antigens [42], T-lymphocytes being generally at or below the limit of detection. These deficiencies may be reversed by reconstitution with T-cells [43-45]. B-cell maturation also is defective, at least that component dependent upon a fully functional thymus. The production of earlier forms of B-cells appears normal, since nude mice possess apparently normal virgin B-cells [46].

Despite the severe immunodeficiencies apparent in homozygous *nu/nu* mice, they are remarkably robust. This is almost certainly due to their remaining immune-competence. For example, *nu/nu* mice frequently exhibit an essentially normal response to T-cell-independent antigens [47]. Perhaps most notably, nude mice possess levels of NK cell activity that significantly exceed those present in normal and heterozygous *nu/+* mice of the same background [48,49]. The poor metastatic potential of most human xenografts growing in nude mice has been partly attributed to this elevated NK activity [19,22-24]. Splenocytes from *nu/nu* mice are capable of generating LAK cells at levels similar to normal mice [50]. The levels of tumoricidal macrophages are essentially equivalent in *nu/nu* and *nu/+* mice [51]. Serum IgM levels are similar to [47] or higher than [46] those in *nu/+* littermates, and while there is a significant decrease in the number of cells making IgG and IgA, both of these immunoglobulins can be detected in individual animals [44].

Clearly, nude mice are not totally immune-deficient. The elevated NK cell activity at least partly contributes to the relatively poor take rate of primary human breast tumors [1]. Of interest is the observation that tumor take rate in nude mice is frequently increased by encapsulating cells/biopsies in Matrigel [17,18]. This artificial basement membrane capsule could provide two important functions, (i) a protective barrier from the effects of tumoricidal macrophages, NK, and LAK precursor cells, and (ii) a more natural structural/dimensional environment for the tumor with access to several attachment and mitogenic molecules, *e.g.*, laminin, fibronectin, and type IV collagen.

The beige (*bg*) mutation

The *bg* mutation is located on mouse chromosome 13. Among several phenotypic modifications induced is a reduced synthesis of pigment granules in melanocytes which results in a light coat color. The general phenotype is considered analogous to Chédiak-Higashi syndrome in humans, a multisystem autosomal recessive disease, where afflicted individuals possess both structurally and functionally defective lysosomes. The main immune-deficiency exhibited by *bg/bg* mice is the direct result of a block in NK function [52,53]. However, there also are functional defects in T-cells, macrophages, and granulocytes [38]. For example, generation of cytotoxic T-cells is impaired in beige mice. A further complication in these mice is an apparent clotting disorder resulting from platelet dysfunction. Ovariectomies and hormone pellet supplementations are frequently performed with breast cancer xenografts, and the loss of animals during or shortly after surgery occurs

more frequently for mice with the *bg* mutation than for many of the other immune-deficient models.

The very low levels of NK activity in *bg* mice contrasts with the elevation in this activity in *nu* mice. The functional significance of the reduced NK cell and other immunologic activities is evidenced by the higher acceptance rate of low tumor cell inocula when compared with their heterozygous (*bg*/+) littermates [54].

Combined *bg/nu* mutations

Since the *bg* mutation essentially eliminates NK cell activity, it was hypothesized that combining the *bg* and *nu* mutations would eliminate the problems associated with the elevation of NK cell activity in nude mice. Double congenic *bg/nu* mice have now been available for several years [48,49]. Their phenotype is largely that predicted by the known effects of both single gene mutations. Thus, the defective B-cell maturation and impaired T-cell dependent responses are apparent., While the contribution of the *bg* mutation significantly reduces NK cell activity relative to homozygous *nu* and wild type (+/+) mice, the level remains higher than that in single mutant *bg/bg* mice [55-57]. Splenocytes from these mice cannot produce LAK activity, an observation that assisted in delineating NK cells from precursors of LAK cells [26]. Reduced IgA and IgM levels can be presumed as a result of the *nu* mutation, the levels being potentially dependent upon the mouse background. While more immune-deficient than mice bearing only the *nu* mutation, the *bg/nu* mice retain the clotting disorder produced by the *bg* mutation.

The X-linked immunodeficiency (*xid*) mutation

The *xid* mutation (X-chromosome) is associated with the X-linked lymphocyte regulated gene family [38]. Thus, males (*xid*/Y) and homozygous females are affected. While there are several impaired functions contributing to the immune-deficiencies in these mice, the major contributor is an impaired development of B-cells. Thus, B-cell colonies are not detected in *in vitro* assays [58]. A specific subset of mature B-cells is absent, and this appears to be the result of an inability of otherwise normal immature B-cells to respond to early activation signals.

The general response to thymus-independent type-II antigens is low in *xid* mice [38,59]. Macrophages are at least partially defective. In affected animals, macrophages produce low levels of IL-1 following stimulation with thymus-independent type-II antigens *in vitro* [38]. Immunoglobulin levels, particularly IgM and IgG_3, are low [60]. These mice, however, are not fully immune-compromised, producing essentially normal responses to thymus-independent type-I antigens [61].

Combined *bg/nu/xid* mutations

With the successful generation of homozygous *bg/nu* mice, it became apparent that a further reduction in immune-competence could potentially be achieved by also adding the *xid* mutation. Andriole *et al.* [26] generated a strain designated NIH III, which is homozygous for all three *bg/nu/xid* mutations. These mice have intermediate levels of NK cells and low levels of LAK precursor cells [26,62], and exhibit defects in the maturation of both B- and T-cells [63,64]. Macrophage activity/function may be partly defective, due to the contribution of the *xid* mutation [38]. The clotting disorder (*bg*) also remains.

The severe combined immune deficiency (*scid*) mutation

A relatively more recent addition to the single gene deficiency models is the severe combined immune deficiency (*scid*) mutation [65]. The locus occurs on mouse chromosome 16, the equi-

valent human mu
8q11 [66]. The *sc*
significantly sma
There is a clear
maturation of lyn
and B-cells are u
T-cells appear n
entire myeloid lin

The *scid* mutat
rearrangement of
receptors on both
scid models are '
bers of functional
majority of scid
i.e., by 10-14 mo
the precursor lym
ly join the cleave
catalyzed by the
binase [71]. In
are at or below t
2b, and 3a [38], I
detected. Howeve
deficient models,
some mice may p
or more IgG isot
phages, NK cells
cells [50] are es
However, the muc
perhaps due to a
required for their
[76].

In general, *scia*
more severely imr
the other viable
Nevertheless, the
usually considere
ance. It seems lik
more readily avai
will be more wide

Impact of the dif
xenografting

The different imr
rodent models p

valent human mutation occurring at chromosome 8q11 [66]. The *scid* mutation produces mice with significantly smaller lymphoid organs [65,67]. There is a clear defect in the differentiation/maturation of lymphocytes [68], and both pre-B and B-cells are undetectable. The few remaining T-cells appear non-functional. In contrast, the entire myeloid lineage appear normal [68,69].

The *scid* mutation produces a deficiency in the rearrangement of genes encoding antigen-specific receptors on both B- and T-cells [67]. Several *scid* models are "leaky", generating small numbers of functional B- and T-cells. However, the majority of scid mice become "leaky" with age, *i.e.*, by 10-14 months of age [70]. It appears that the precursor lymphocytes are unable to adequately join the cleaved variable region segments as catalyzed by the immunoglobulin V(D)J recombinase [71]. In general, immunoglobulin levels are at or below the limit of detection. IgGs 2a, 2b, and 3a [38], IgM, and IgA [65,69] are rarely detected. However, in common with all immune-deficient models, there is individual variation, and some mice may produce detectable levels of two or more IgG isotypes and/or IgM [65]. Macrophages, NK cells [72-75], and LAK precursor cells [50] are essentially normal in *scid* mice. However, the mucosal mast cells appear deficient, perhaps due to a lack of specific lymphokines required for their development from progenitors [76].

In general, *scid* mice bearing this mutation are more severely immune-compromised than any of the other viable single gene mutation models. Nevertheless, the standard SPF environment is usually considered sufficient for their maintenance. It seems likely that, as these mice become more readily available and less expensive, they will be more widely utilized.

Impact of the different immunobiologies on xenografting

The different immunobiologies of these other rodent models provide viable and important alternatives to the nude mouse, with several occasionally supporting the growth or metastasis of xenografts that are considered either "non-tumorigenic" or "non-metastatic" based on their lack of growth in nude mouse models. The issue of which immune-deficient model is most appropriate for maintaining xenografts is somewhat controversial [77]. There is no clear and compelling evidence that *scid* or *bg/nu/xid* mice have a reproducibly higher overall take rate than *nu/nu* mice, with most investigators finding these models essentially equivalent [77-81]. However, the overall take rate can be a misleading indicator when an investigator wishes to evaluate the tumorigenicity or metastatic potential of *specific* cell lines/biopsies. An individual cell line may be tumorigenic or metastatic in one immune-deficient model and not in another, an observation that may or may not be a direct reflection of the different immunobiologies of the recipient mice. While this seems most likely to occur when assessing metastatic potential [70,80,82], individual variability among cell lines for tumorigenicity also cannot be easily discounted. We have suggested that, particularly where *in vivo* growth is assessed as part of the characterization of a new cell line, more than one model be used [83]. While this may be less important for cell lines of mammary origin than for other cell lines, the designation of a cell line as "non-tumorigenic in the nude mouse" or "non-metastatic in the nude mouse" seems most appropriate, at least until its lack of tumorigenicity/metastatic potential is confirmed in other models [83].

Use of immune-deficient rodent models for endocrinologic studies

Endocrinologic studies of hormone-responsive xenografts are frequently performed with breast cancer xenografts. Mice can be purchased ovariectomized directly from each of the major vendors, including Taconic (Germantown NY), Charles River (Wilmington MA), Harlan Sprague Dawley (Frederick MD) and Jackson Laboratories

(Bar Harbor ME). Adrenalectomized and hypophysectomized mice can generally also be obtained in this manner, although viability of the mice requires supplementation with glucocorticoids/mineralocorticoids.

There are several relatively straightforward approaches for studying additive endocrine treatments. We have routinely used the sustained release pellets provided by Innovative Research of America (Toledo, OH). For hormone-dependent cells including MCF-7, we routinely use the 60-day release 0.72 mg 17β-estradiol pellets. These are easily placed *s.c.* between the shoulder blades using a sterile 10 or 12 gauge trocar. Many experimental agents also can be administered by implantation of silastic pellets or mini osmotic pumps. We have found the Alzet osmotic pumps from Alza Corp. (Palo Alto, CA) effective for administering growth factors and other agents. The smaller sizes (100 μl and 200 μl) can be introduced into a small *s.c.* pocket, although we also have introduced these *i.p.* into NCr *nu/nu* mice with no adverse effects. The larger pumps are for use only in rats, and can be used successfully in nude rats (*rnu/rnu*).

The hypogonadal/*scid* (*hpg/scid*) mouse as an ovarian-ablation model

Ovariectomies are frequently performed on nude mice to provide an endocrinologic environment equivalent to that of postmenopausal women [84]. This produces additional cost to the investigator and stress to the animal. The Jackson Laboratories have recently generated a novel model that could alleviate some of these concerns. Mice bearing the hypogonadal (*hpg*) mutation [85] express a non-functional (truncated) LHRH protein [86]. Thus, these mice are hypogonadic, with almost undetectable levels of LH and FSH, and have serum estrogen and progestin levels essentially equivalent to those detected in ovariectomized mice [87]. By combining the *hpg* and *scid* mutations, it has been possible to generate an immune-compromised strain with a postmenopausal endocrinologic environment [88]. It seems likely that this model may become more widely used in the future, both as a potential model of postmenopausal breast cancer, and to support the growth of breast tumor xenografts.

Effect of endocrine manipulations on the immune response in rodents

Estrogen and antiestrogen supplementation of rodents has been widely used to study the endocrine regulation of breast cancer xenografts. However, several endocrine agents are known to influence those effectors of CMI that remain in immune-compromised rodents. For example, pharmacological but not physiological concentrations of E2 can inhibit NK activity in athymic nude mice [89-92]. This has been invoked as a potential explanation for an apparent ability of E2 supplementation to increase the growth of estrogen receptor negative breast cancer xenografts. Clearly, it is important to consider the ability of endocrine agents to perturb several effectors of cell-mediated immunity in study design.

It could be argued that the apparent endocrine responsiveness of xenografts is actually an immunologic, rather than direct endocrinologic, phenomenon. This seems unlikely for several reasons. Firstly, it is widely acknowledged that estrogens tend to produce a biphasic effect on NK cell activity, where NK levels rise for the first 30 days with an overall reduction in NK activity not observed until later [89-92]. However, most MCF-7 xenografts produce palpable tumors, and can frequently be seen to grow, during this initial period when NK cell activity is rising above the already elevated levels in nude mice. Secondly, the concentrations of estrogens reported to suppress NK activity [89-92] appear higher than those required to support MCF-7 xenografts [84, 93-96]. Approximately 300 pg/ml/day of estradiol is released from the widely used 60-day release 0.72 mg estrogen pellets produced by Innovative Research of America, Toledo OH [97]. Finally, MCF-7 cells still require estrogen supplementation for growth in *bg/nu/xid* mice (R. Clarke, unpublished observations), despite the very low NK a
[52,53].

Also of rele
tamoxifen (TAM
[62]. Prolonged
produces a TAM
type [98,99], a
[100] despite the
on NK cell a
estrogens stimul
apparently stimu
xenografts in n
attributed to a re

Breast cancer c

Many of the br
available are tu
These cell lines
carcinomas *in vi*
differentiation ge
lines. As with m
characteristics o
generally faithfu
perimental syste
tive, PGR positi
independent, anti
and drug respo
cell lines observ
respective *in vivo*
teristics of many
have recently be

Breast cancer c
hormone-depen
hormone-indepe

The three most
human breast ca
[2], ZR-75-1 [4],
cell lines are rec
supplementation
The estrogen-ind
ed by an appropr
ER-positive tumc

very low NK activity apparent in these mice [52,53].

Also of relevance is the observed ability of tamoxifen (TAM) to stimulate NK activity *in vivo* [62]. Prolonged treatment of MCF-7 xenografts produces a TAM and estrogen dependent phenotype [98,99], as does transfection with FGF4 [100] despite the opposing effects of these agents on NK cell activity (estrogens inhibit, antiestrogens stimulate). An ability of estrogen to apparently stimulate MDA-MB-231 (ER-negative) xenografts in nude mice has been specifically attributed to a reduction in cell loss [101].

Breast cancer cell lines as xenografts

Many of the breast cancer cell lines currently available are tumorigenic in the nude mouse. These cell lines most frequently produce adenocarcinomas *in vivo*, with the degree of glandular differentiation generally greater in the ER-positive lines. As with many human tumor xenografts, the characteristics of the human breast tumors are generally faithfully reconstituted in *in vivo* experimental systems. Thus, the ER positive/negative, PGR positive/negative, hormone dependent/independent, antiestrogen responsive/unresponsive, and drug responsive/resistant characteristics of cell lines observed *in vitro* are reflected in their respective *in vivo* growth responses. The characteristics of many of the breast cancer cell lines have recently been reviewed in detail [5].

Breast cancer cell lines as xenografts: hormone-dependence and acquisition of hormone-independence

The three most widely used hormone-dependent human breast cancer xenografts are the MCF-7 [2], ZR-75-1 [4], and T47D cell lines [3]. These cell lines are require some degree of estrogenic supplementation for tumorigenesis in nude mice. The estrogen-induced growth of each is inhibited by an appropriate dose of antiestrogen. While ER-positive tumors frequently invade locally and metastasize in patients, these xenografts are poorly invasive and rarely, if ever, are metastatic in nude mice.

The requirement for estrogen is surprising, since all three cell lines were derived from malignant effusions in postmenopausal women. We wished to determine whether the application of appropriate selective pressures could generate variants that no longer require E2 for growth *in vivo*. This was readily achieved by selecting for growth in the mammary fat pads of ovariectomized nude mice [96,102]. These mice have steroid hormone levels approximately equivalent to those found in postmenopausal women [84, 103].

Cells selected by one passage (MCF7/MIII) [96] or two passages (MCF7/LCC1) [102] (Table 1), retain ER and PGR expression, sensitivity to antiestrogens [96,102], and sensitivity to LHRH analogues [104]. Both variants exhibit a significant increase in metastatic potential [105]. Since tumors with these characteristics arise frequently in women, we have suggested that the phenotypes exhibited by the MCF7/MIII and MCF7/LCC1 cells more closely reflect the major ER/PGR positive, antiestrogen responsive phenotype found in postmenopausal women with breast cancer [106].

Breast cancer cell lines as xenografts: acquisition of antiestrogen resistance

While >70% of ER/PGR positive tumors respond to antiestrogens, the great majority of these will ultimately acquire a resistant phenotype [107]. The modeling of this progression has generally taken two forms, *in vitro* selection either in a stepwise manner [108] or by treatment with a high dose of drug [109], or *in vivo* selection against a continuous drug exposure [98,99]. A prolonged *in vivo* selection almost exclusively generates cells that are TAM dependent, and at least initially E2 inhibited [98,99]. This endocrinologic phenotype may be similar to the occasional TAM-withdrawal responses observed in patients [110-112].

Table 1. Derivation of the MCF-7 variants.

	ER	PGR	Citation
MCF-7 → nude mouse → MCF7/MIII → nude mouse → MCF7/LCC1	116,600	29,300	[102]
MCF7/LCC1 → 4-hydroxytamoxifen *in vitro* → MCF7/LCC2	91,300	6,400	[108]
MCF7/LCC1 → ICI 182,780 → MCF7/LCC9	133,200	ND	[117]
MDA-MB-435 (ER negative) → nude mouse → MDA-435/LCC6	ND	ND	[120]

All nude mice were ovariectomized and did not receive E2-supplementation. Steroid hormone receptor data are presented as sites/cell and represent means of 3 or more determinations. ND = no data.

In vitro antiestrogen selection of hormone-dependent cells, *e.g.* MCF-7 cells, can produce resistant variants. However, these variants often are either unstable [113-116], or have lost tumorigenicity in nude mice [96]. We have taken a different approach, selecting hormone-independent cells first *in vivo*, followed by a stepwise *in vitro* selection against the antiestrogen of choice [108, 117] (Table 1). This procedure facilitates generation of stable resistant variants that retain tumorigenicity [108]. Thus, selection of the MCF7/LCC1 cells by 4-hydroxytamoxifen treatment produced MCF7/LCC2 cells (Table 1). These cells are resistant to triphenylethylenes but not to steroidal antiestrogens, an apparently clinically relevant phenotype [106,118]. Selection of MCF7/LCC1 cells against ICI 182,780 also appears to produce stable resistant cells that retain tumorigenicity [117].

Of interest is the observation that, whether selected *in vivo* or *in vitro*, antiestrogen resistant xenografts and cell lines retain ER expression, and often some degree of endocrine-responsiveness [95,102,108]. The majority of breast cancer patients also retain ER expression upon relapse on TAM therapy [119]. It seems likely that, based on these experimental models, there may be several mechanisms through which breast tumors can become antiestrogen resistant.

Breast cancer cell lines as xenografts: hormone-unresponsive models

The majority of breast cancer cell lines are ER-negative. Consequently, they are considered hormone-unresponsive both *in vitro* and *in vivo*. While this has been our general experience, and that of many others, recently Friedl & Jordan [101] have demonstrated an apparently estrogenic stimulation of the MDA-MB-231 (ER negative) cell line growing in nude mice. This response does not appear to be immunologic; rather, the authors reported an estrogen-induced decrease in cell loss. Clearly, investigators should be aware of the potential for host-treatment interactions that can influence tumor growth in a manner that may be independent of direct agent-tumor interactions.

Most of the ER-negative xenografts produce poorly differentiated adenocarcinomas, relative to the ER-positive xenografts. Several are highly locally invasive. We have recently generated an ascites variant of the MDA-MB-435 cell line [120]. These cells, designated MDA-435/LCC6, appear to have arisen from a locally invasive mammary fat pad tumor that invaded into the peritoneal cavity. The ascites can be maintained either *in vivo*, or as a monolayer culture *in vitro*, and have a highly reproducible duration of survival from cell inoculation to morbidity/death. These cells provide a novel model in which to study the pathogenesis of malignant ascites, and the effect of *in vitro* [120] or *in vivo* gene transfer by retroviral vectors [121]. The MDA-435/LCC6 ascites variants grow equally well in *nu/nu* mice and *rnu/rnu* rats [122].

Breast cancer cell lines as xenografts: drug resistance models

Probably the most widely used breast cancer model of drug resistance is the MCF-7^{ADR} cell line. These cells were stepwise selected against doxorubicin *in vitro* product (P-glycopr MDR1 gene. MCF- ER-negative and re: Despite its frequent agents, this cell l potential multiple MCF-7^{ADR}, but nc cells (CL 10.3), a Necrosis Factor indicates the prese anisms in addition include changes in mutase expression/a glutathione transfe spectively also are [127,128]. Of part tion that differenc of fluphenthixol f in MCF-7^{ADR} cell MDR1-transfected activities through n

To produce bre only major resista have transduced b 435/LCC6 cells [1 MDR1 cDNA. Th CL 10.3, retain ER antiestrogens [130] duced cells, *i.e.* MD negative, and retai rapidly proliferatin ascites [120].

Breast cancer metastatic models

Two ER-negative produce hematolog xenografts in nude MDA-MB-435 cel invasive tumors, found in the lung While the time to incidence is suffic

doxorubicin *in vitro*, and overexpress the gp170 product (P-glycoprotein, PGP) of the human MDR1 gene. MCF-7^{ADR} cells also have become ER-negative and resistant to antiestrogens [123]. Despite its frequent use to screen gp170-reversing agents, this cell line expresses several other potential multiple drug resistance mechanisms. MCF-7^{ADR}, but not MDR1-transduced MCF-7 cells (CL 10.3), are cross resistant to Tumor Necrosis Factor [124], an observation that indicates the presence of ADR resistance mechanisms in addition to gp170. While this would include changes in manganous superoxide dismutase expression/activity [124], the activities of glutathione transferase and topoisomerase II respectively also are altered in MCF-7^{ADR} cells [127,128]. Of particular concern is the observation that differences in the potency of isomers of fluphenthixol for reversing gp170 activity in MCF-7^{ADR} cells could not be confirmed in MDR1-transfected NIH 3T3 cells [129], implying activities through mechanisms other than gp170.

To produce breast cancer cell lines where the only major resistance mechanism is gp170, we have transduced both MCF-7 [130] and MDA-435/LCC6 cells [120] with the full length human MDR1 cDNA. The MCF-7 transduced cells, *e.g.* CL 10.3, retain ER expression and sensitivity to antiestrogens [130]. The MDA-435/LCC6 transduced cells, *i.e.* MDA-435/LCC6^{MDR1} remain ER-negative, and retain the ability to produce both rapidly proliferating solid tumors and malignant ascites [120].

Breast cancer cell lines as xenografts: metastatic models

Two ER-negative cell lines have been reported to produce hematologic metastases from solid tumor xenografts in nude mice. The MDA-MB-231 and MDA-MB-435 cell lines produce highly locally invasive tumors, with metastases reproducibly found in the lungs and other organs [131,132]. While the time to dissemination is often long, the incidence is sufficient to provide a reproducible metastatic model. The metastatic potential of the MDA-MB-435 cells appears amenable to modification by dietary factors [133].

While the ER-positive and hormone-independent MCF-7 variants (MCF7/MIII; MCF7/LCC1) exhibit increased metastatic potential [95,102], and can generate both lymphatic and hematologic metastases [105], the incidence and reproducibility are too low to provide viable models of metastasis [105]. In contrast, MCF-7 cells transfected with FGF-4 (kFGF) have a high and reproducible incidence of hematologic metastasis, probably the result of the significant increase in angiogenic potential. These xenografts have a significantly altered endocrine responsiveness, exhibiting a TAM-stimulated/E2-inhibited phenotype [100,134] similar to the *in vivo* TAM selected MCF-7 cells [98,99]. These cells are reviewed in detail in the accompanying article by McLeskey *et al.* [135].

Site of inoculation

There is now considerable evidence supporting the importance of the choice of site for implantation. Prior to the widespread availability of nude mice, the subrenal capsule was widely used. While there are other equally effect immune-privileged sites, these are becoming less frequently used since the ability of many cell lines to grow *s.c.* in immunocompromised rodents is now well established. While the *s.c.* site is convenient, it is likely that is not the optimal site for all xenografts.

While many breast cancer cell lines will grow *s.c.*, and frequently at other sites [136], it is not clear that this is the best approach. There is increasing evidence of the importance of tumor-host and tumor-stromal interactions in the progression of many cancers, including breast cancer [137]. The most appropriate site for breast tumor xenografts is the mammary fat pad (orthotopic site), a site we use routinely [95,102,105,108]. Orthotopic transplantation can significantly increase the take rate of tumors from several can-

cers, and occasionally facilitate metastatic spread that will not occur from a *s.c.* site [138-141]. When metastases in nude mice do occur, they tend to arise at sites representative of those observed in humans [105,132].

Concluding comments and future prospects

Human breast tumor xenografts have been of considerable value in studying several aspects of breast cancer biology. Their reproducibility, stability, and reflection of their human origin are clearly considerable strengths. However, the cell lines used to generate xenografts are not without limitations. For example, at some point in their genesis these cells have adapted to growth *in vitro*. Thus, the molecular, cellular, and metabolic changes in these cell lines may, or may not, fully reflect the human disease.

Despite the potential limitations, the similarities between these models and clinical breast cancer are substantial. The histology of these xenografts frequently closely reflects the variety of human adenocarcinomas. The inverse relationship between EGF-receptors and ER, and the association with a more aggressive and less well differentiated phenotype observed in cell lines and xenografts, holds true for the human disease [142-144]. The non-crossresistance of the TAM-resistant MCF7/LCC2 cells predicted the clinical responses to ICI,182780 in patients who responded and then failed TAM [106,118]. MCF-7 cells, when exposed to analogous selective pressures in mice, progress along a pathway apparently equivalent to the progression of many human breast cancers [95,106]. These observations suggest that the physiologic/endocrinologic environment of the rodent mammary fat pad may have significant similarity to the human mammary gland. The complex tumor/host interactions also may be similar for human xenografts in rodent mammary fat pads and the human disease.

There is a need for new xenograft models to facilitate research in at least two specific areas, endocrine responsiveness and metastasis. The majority of cell lines and xenografts are estrogen-unresponsive and ER-negative. Nevertheless, greater than 50% of all breast tumors express ER, and a significant proportion of these are endocrine responsive. It seems likely that there is considerable diversity in some of the cellular and molecular events driving the growth of these tumors. Thus, it is equally likely that the few endocrine-responsive models available inadequately reflect this potential diversity.

While metastasis may have several molecular events that occur independent of the cancer site, a number of the genes/proteins associated with this cascade are estrogen-regulated in breast cancer cells, *e.g.*, laminin receptor expression [145], chemoinvasion *in vitro* [96,146], and secretion of plasminogen activator [147]. Thus, some events may be regulated differently in breast cancer than in other cancers. There are relatively few endocrine responsive and metastatic cellular models in which to study the effect of hormones and antihormones on metastasis. While there are at least two endocrine unresponsive metastatic models, these also are likely to be too few to adequately reflect the diversity of the human disease.

The development of new breast cancer xenograft models, and variants of established models, will provide the opportunity to study host-tumor interactions in greater detail. This, and the emergence of novel immune-compromised and endocrine-compromised animal models, will further our ability to establish biologically relevant xenograft models of breast cancer.

Acknowledgments

This work was supported by Public Health Service grants R01-CA58022, P50-CA58185, and P30-CA51008 from the National Cancer Institute, and a research grant from the Cancer Research Foundation of America. The author thanks Dr. Boris Yankelevich for his critical reading of the text.

References

1. Steel GG, Cou response to che tumour xenograf
2. Soule HD, Vasq A human cell li from a human b 51:1409-1416, 1
3. Keydar I, Chen Radu M, Chaitci characterization origin. Eur J C
4. Engel LW, You O'Brien SJ, Joyc ization of three from human bre 3364, 1978
5. Clarke R: *In vi In:* Harris JR, H (eds) Diseases Philadelphia, 19
6. Black MM, Zac Skin window re An index of pro immunity. Canc
7. Humphrey LJ, S responsiveness c 46:893-898, 198
8. Strayer DR, Car rence of breast natural killer cyt 7:187-192, 1986
9. An T, Sood U, quantitation of ductal infiltratin 128:52-60, 1987
10. Contreras OO, S human breast ca 514, 1988
11. Akimoto M, Is Assessment of h patients. Cancer
12. Horst HA, Horny distribution of l lymph node met of the breast. C
13. Bonilla F, Alvar IL-2 induces cyt regional axillary Cancer 61:629-6
14. Levy SM, Herb Perceived social gesterone recept

References

1. Steel GG, Courtenay VD, Peckham MJ: The response to chemotherapy of a variety of human tumour xenografts. Br J Cancer 47:1-15, 1983
2. Soule HD, Vasquez J, Long A, Albert S, Brennan M: A human cell line from a pleural effusion derived from a human breast carcinoma. J Natl Cancer Inst 51:1409-1416, 1973
3. Keydar I, Chen L, Karby S, Weiss FR, Delarea J, Radu M, Chaitcik S, Brenner HJ: Establishment and characterization of a cell line of human carcinoma origin. Eur J Cancer 15:659-670, 1979
4. Engel LW, Young NA, Tralka TS, Lippman ME, O'Brien SJ, Joyce MJ: Establishment and characterization of three new continuous cell lines derived from human breast carcinomas. Cancer Res 38:3352-3364, 1978
5. Clarke R: *In vitro* models of human breast cancer. *In:* Harris JR, Hellman S, Lippman ME, Morrow M (eds) Diseases of the Breast. J.B. Lippincott, Philadelphia, 1995, pp 245-261
6. Black MM, Zachrau RE, Hankey BF, Wesley M: Skin window reactivity to autologous breast cancer. An index of prognostically significant cell-mediated immunity. Cancer 62:72-83, 1988
7. Humphrey LJ, Singla O, Volenec FJ: Immunologic responsiveness of the breast cancer patient. Cancer 46:893-898, 1980
8. Strayer DR, Carter WA, Brodsky I: Familial occurrence of breast cancer is associated with reduced natural killer cytotoxicity. Breast Cancer Res Treat 7:187-192, 1986
9. An T, Sood U, Pietruk T, Cummings G: In situ quantitation of inflammatory mononuclear cells in ductal infiltrating breast carcinoma. Am J Path 128:52-60, 1987
10. Contreras OO, Stoliar A: Immunologic changes in human breast cancer. Eur J Gynecol Oncol 9:502-514, 1988
11. Akimoto M, Ishii H, Nakajima Y, Iwasaki H: Assessment of host immune response in breast cancer patients. Cancer Detect Prev 9:311-317, 1986
12. Horst HA, Horny HP: Characterization and frequency distribution of lymphoreticular infiltrates in axillary lymph node metastases of invasive ductal carcinoma of the breast. Cancer 60:3001-3007, 1987
13. Bonilla F, Alvarez-Mon M, Merino F, de la Hera A: IL-2 induces cytotoxic activity in lymphocytes from regional axillary nodes of breast cancer patients. Cancer 61:629-634, 1988
14. Levy SM, Herberman RB, Whiteside T, Sanzo K: Perceived social support and tumor estrogen/progesterone receptor status as predictors of natural killer cell activity in breast cancer patients. Psychosom Med 52:73-85, 1990
15. Underwood JC, Giri DD, Rooney N, Lonsdale R: Immunophenotype of the lymphoid cell infiltrates in breast carcinomas of low oestrogen receptor content. Br J Cancer 56:744-746, 1987
16. Berry J, Green BJ, Matheson DS: Modulation of natural killer cell activity in stage I postmenopausal breast cancer patients on low-dose aminogluthemide. Cancer Immunol Immunother 24:72-75, 1987
17. Fridman R, Kibbey MC, Royce LS, Zain M, Sweeney TM, Jicha DL, Yannelli JR, Martin GR, Kleinman HK: Enhanced tumor growth of both primary and established human and murine tumor cells in athymic mice after coinjection with matrigel. J Natl Cancer Inst 83:769-774, 1991
18. Fridman R, Giaccone G, Kanemoto T, Martin GR, Gazdar AF, Mulshine JL: Reconstituted basement membrane (matrigel) and laminin can enhance the tumorigenicity and the drug resistance of small cell lung cancer cell lines. Proc Natl Acad Sci USA 87: 6698-6702, 1990
19. Wheelock EF, Robinson MK: Endogenous control of the neoplastic process. Lab Invest 48:120-139, 1983
20. Blanchard DK, Kavanagh JJ, Sinoviks JG, Cavanagh D: Infiltration of IL-2-inducible killer cells in ascitic fluid and pleural effusions of advanced cancer patients. Cancer Res 48:6321-6327, 1988
21. Talmadge JE, Meyers KM, Prieur DJ, Starkey JR: Role of NK cells in tumour growth and metastasis in beige mice. Nature 284:622-624, 1980
22. Gorelik E, Wiltrout RH, Okumura K, Habu S, Herberman RB: Role of NK cells in the control of metastatic spread and growth of tumor cells in mice. Int J Cancer 30:107-112, 1982
23. Richie JP: Abrogation of hematogenous metastases in a murine model by natural killer cells. Surgery 96:133-138, 1984
24. Vose BM, Moore M: Suppressor cell activity of lymphocytes infiltrating human lung and breast tumors. Int J Cancer 24:579-585, 1979
25. Mantovani A, Allavena P, Sessa C, Bolis G, Mangioni C: Natural killer activity of lymphoid cells isolated from human ascitic ovarian tumors. Int J Cancer 25:573-582, 1980
26. Andriole GL, Mule JJ, Hansen CT, Linehan WM, Rosenberg SA: Evidence that lymphokine-activated killer cells and natural killer cells are distinct based on an analysis of congenitally immunodeficient mice. J Immunol 135:2911-2913, 1985
27. Grimm EA, Mazumder A, Zhang HZ, Rosenberg SA: Lymphokine-activated killer cell phenomena. Lysis of natural killer resistant solid tumour cells by IL-2 activated autologous human peripheral blood lympho-

cytes. J Exp Med 155:1823-1827, 1982
28. Ebert EC, Roberts AI, Devereaux D, Nagase H: Selective immunosuppressive action of a factor produced by colon cancer cells. Cancer Res 50:6158-6161, 1990
29. Kelly PM, Davison RS, Bliss E, McGee JO: Macrophages in human breast disease: a quantitative immunohistochemical study. Br J Cancer 57:174-177, 1988
30. Key ME, Hoyer L, Bucana C, Hanna MG: Mechanisms of macrophage-mediated tumor cytolysis. Adv Exp Med Biol 146:265-311, 1982
31. Hibbs JB, Lambert LH, Remington JS: Control of carcinogenesis: a possible role for the activated macrophage. Science 177:9980-1000, 1972
32. Fidler IJ: Eradication of cancer metastasis by tumoricidal macrophages. Adv Exp Med Biol 233: 415-423, 1988
33. Fidler IJ, Schroit AJ: Recognition and destruction of neoplastic cells by activated macrophages: discrimination of altered self. Biochim Biophys Acta 948:151-173, 1988
34. Whitworth PM, Pak CC, Esgro J, Kleinerman ES, Fidler IJ: Macrophages and cancer. Cancer Metastasis Rev 8:319-351, 1990
35. Meredino RA, Arena A, Liberto MC, Iannello D: Influence of sera from patients affected by neoplasia on some human macrophage functions. Cancer Detect Prev 12:73-80, 1988
36. Ramakrishnan S, Xu FJ, Brandt SJ, Niedel JE: Constitutive production of macrophage colony-stimulating factor by human ovarian and breast cancer cell lines. J Clin Invest 83:921-926, 1989
37. Acero R, Polentarutti N, Bottazzi B, Alberti S, Ricci MR, Bizzi A, Mantovani A: Effect of hydrocortisone on the macrophage content, growth and metastasis of transplanted murine tumors. Int J Cancer 33:95-105, 1984
38. Shultz LD: Single gene models of immunodeficiency diseases. *In:* Wu B, Zheng J (eds) Immune-deficient Animals in Experimental Medicine. Karger, Basel, 1989, pp 19-26
39. Pantelouris EM: Absence of thymus in a mutant mouse. Nature 217:370-371, 1968
40. Rygaard J, Povlsen CO: Heterotransplantation of a human malignant tumour to "nude" mice. Acta Path Microbiol Scand 77:758-760, 1969
41. Maruo K, Ueyama Y, Hioki K, Saito M, Nomura T, Tamaoki N: Strain-dependent growth of a human carcinoma in nude mice with different genetic backgrounds: selection of nude mouse strains useful for anticancer agent screening system. Exp Cell Biol 50:115-119, 1982
42. Kindred B: The inception of the response to SRBC by nude mice injected with various doses of congenic or allogeneic thymus cells. Cell Immunol 17:277-284, 1975
43. Jacobson EB, Caporale LH, Thorbecke GJ: Effect of thymus cell injections on germinal center formation in lymphoid tissues of nude (thymusless) mice. Cell Immunol 13:416-430, 1974
44. Guy-Grand D, Griscelli C, Vassalli P: Peyer's patches, gut IgA, plasma cells and thymic function: study in nude mice bearing thymic grafts. J Immunol 115:361-364, 1975
45. De Sousa M, Pritchard H: The cellular basis of immunological recovery in nude mice after thymus grafting. Immunology 26:769-776, 1974
46. Weisz-Carrington P, Schrater AF, Lamm ME, Thorbecke GJ: Immunoglobulin isotypes in plasma cells of normal and athymic mice. Cell Immunol 44:343-351, 1979
47. Manning JK, Reed ND, Jutila JW: Antibody response to Escherichia coli lipopolysaccharide by congenitally thymusless (nude) mice. J Immunol 108:1470-1472, 1972
48. Herberman RB, Nunn ME, Holden HT, Staal S, Djeu JY: Augmentation of natural cytotoxic reactivity of mouse lymphoid cells against syngeneic and allogeneic tumors. Int J Cancer 19:555-564, 1977
49. Kiessling R, Klein E, Wagzell H: "Natural" killer cells in the mouse. I. Cytotoxic cells with specificity for mouse Moloney leukemia cells. Specificity and distribution according to phenotype. Eur J Immunol 72:2130-2134, 1975
50. Hasui M, Saikawa Y, Miura M, Takano N, Ueno Y, Yachie A, Miyawaki T, Taniguchi N: Effector and precursor phenotypes of lymphokine-activated killer cells in mice with severe combined immunodeficiency (Scid) and athymic (Nude) mice. Cell Immunol 120: 230-239, 1989
51. Johnson WJ, Balish E: Macrophage function in germ-free, athymic (nu/nu) mice and conventional flora (nu/+) mice. J Reticuloendothel Soc 28:55-66, 1980
52. Roder JC: The beige mutation in the mouse. I. A stem cell predetermined impairment in natural killer cell function. J Immunol 123:2168-2173, 1979
53. Roder JC, Duwe AK: The beige mutation in the mouse selectively impairs natural killer cell function. Nature 278:451-453, 1979
54. Karre K, Klein GO, Kiessling R, Klein G, Roder JC: Low natural in vivo resistance to syngeneic leukemias in natural killer-deficient mice. Nature 284:624-626, 1980
55. Karre K, Klein GO, Kiessling R, Klein G, Roder JC: In vitro NK-activity and in vivo resistance to leukemia: studies of beige, beige/nude and wild type hosts on C5
797, 1980
56. Clark EA, S
influence na
genetics 12:
57. Hioki K, Ma
Saito M, N
with low nat
the bg gene
beige-nude r
58. Kincade PW
lymphocytes
Med 145:24
59. Ahmed A, S
Sachs DH,
development
which disting
antigens. J I
60. Perlmutter R
I, Paul WE,
specific imm
B-lymphocyt
61. Scher I: Th
model illustr
on immunity
62. Gottardis MI
Differential
cancer cell
Cancer Res
63. Azar HA, H
mice with co
for human tu
Inst 65:421-
64. Karagogeos
arrest of B
immune-defi
1130, 1986
65. Bosma GC,
bined immu
Nature 301:5
66. Komatsu K,
MR: The sc
stores V(D)J
strand break
67. Schuler W,
Rosenberg N
Bosma MJ: I
is defective i
deficiency.
68. Dorshkind K
Bosma GC,
status of cell
mice with se
ease. J Immu

hosts on C57BL background. Int J Cancer 26:789-797, 1980
56. Clark EA, Shultz LD, Pollack SB: Mutations that influence natural killer (NK) cell activity. Immunogenetics 12:601-613, 1981
57. Hioki K, Maruo K, Suzuki S, Kato H, Shimamura K, Saito M, Nomura T: Studies on beige-nude mice with low natural killer cell activity. 1. Introduction of the bg gene into nude mice and the characteristics of beige-nude mice. Lab Animals 21:72-77, 1987
58. Kincade PW: Defective colony formation by B lymphocytes from CBA/N and C3H/HeJ mice. J Exp Med 145:249-263, 1977
59. Ahmed A, Scher I, Sharrow SO, Smith AH, Paul WE, Sachs DH, Sell KV: B-lymphocyte heterogeneity: development and characterization of an alloantiserum which distinguishes B-lymphocyte differentiation alloantigens. J Exp Med 145:101-110, 1977
60. Perlmutter RM, Nahm M, Stein KE, Slack J, Zitron I, Paul WE, Davie JM: Immunoglobulin subclass-specific immunodeficiency in mice with an X-linked B-lymphocyte defect. J Exp Med 149:993-998, 1979
61. Scher I: The CBA/N mouse strain: experimental model illustrating the influence of the X-chromosome on immunity. Adv Immunol 33:1-71, 1982
62. Gottardis MM, Wagner RJ, Borden EC, Jordan VC: Differential ability of antiestrogens to stimulate breast cancer cell (MCF-7) growth in vivo and in vitro. Cancer Res 49:4765-4769, 1989
63. Azar HA, Hansen CT, Costa J: N:NIH(S)II-nu/nu mice with combined immunodeficiency: a new model for human tumor heterotransplantation. J Natl Cancer Inst 65:421-430, 1980
64. Karagogeos D, Rosenberg N, Wortis HH: Early arrest of B cell development in nude, X-linked immune-deficient mice. Eur J Immunol 16:1125-1130, 1986
65. Bosma GC, Custer RP, Bosma MJ: A severe combined immunodeficiency mutation in the mouse. Nature 301:527-530, 1983
66. Komatsu K, Kubota N, Gallo M, Okumura Y, Lieber MR: The scid factor on human chromosome 8 restores V(D)J recombination in addition to double-strand break repair. Cancer Res 55:1774-1779, 1995
67. Schuler W, Weiler IJ, Schuler A, Phillips RA, Rosenberg N, Mak TW, Kearney JF, Perry RP, Bosma MJ: Rearrangement of antigen receptor genes is defective in mice with severe combined immune deficiency. Cell 46:963-972, 1986
68. Dorshkind K, Keller GM, Phillips RA, Miller RG, Bosma GC, O'Toole M, Bosma MJ: Functional status of cells from lymphoid and myeloid tissues in mice with severe combined immunodeficiency disease. J Immunol 132:1804-1808, 1984
69. Custer RP, Bosma GC, Bosma MJ: Severe combined immunodeficiency (scid) in the mouse. Pathology, reconstitution, neoplasms. Am J Path 120:464-477, 1985
70. Mueller BM, Reisfeld RA: Potential use of the scid mouse as a host for human tumors. Cancer Metastasis Rev 10:193-200, 1991
71. Malynn BA, Blackwell TK, Fulop GM, Rathbun GA, Furley AJW, Ferrier P, Heinke LB, Phillips RA, Yancopoulos GD, Alt FW: The *scid* defect affects the final step of the immunoglobulin VDJ recombinase mechanism. Cell 54:453-460, 1988
72. Quimby FW: Immunodeficient Rodents. A Guide to their Immunobiology, Husbandry, and Use. National Academy Press, Washington DC, 1989
73. Dorshkind K, Pollack SB, Bosma MJ: Natural killer (NK) cells are present in mice with severe combined immunodeficiency (SCID). J Immunol 134:2911-2913, 1985
74. Ikeda S, Neyts J, De Clercq E: Host defense mechanisms against murine cytomegalovirus infection induced by poly I:C in severe combined immune deficient (SCID) mice. Proc Soc Exp Biol Med 207: 191-196, 1994
75. Bancroft GJ, Kelly JP: Macrophage activation and innate resistance to infection in SCID mice. Immunobiology 191:424-431, 1994
76. Reed ND, Hall-Stoodley L, Shultz L: Mast cell production by *scid/scid* mice: *in vivo* and *in vitro* studies. *In:* Wu B, Zheng J (eds) Immune-deficient Animals in Experimental Medicine. Karger, Basel, 1989, pp 63-67
77. Fodstad O: Tumorigenicity and dissemination of human tumors in congenitally immune-deficient mice. J Natl Cancer Inst 83:1419-1420, 1991
78. Kubota N, Yamaguchi H, Watanabe M, Yamamoto T, Takahara T, Takeuchi T, Furukawa T, Kase S, Kodaira S, Ishibiki K: Growth of human tumor xenografts in nude mice and mice with severe combined immunodeficiency (SCID). Surg Today 23:375-377, 1993
79. Oakley CS, Welsch MA, Zhai YF, Chang CC, Gould MN, Welsch CW: Comparative abilities of nude mice and severe combined immune deficient (SCID) mice to accept transplants of induced rat mammary carcinomas: enhanced transplantation efficiency of those rat mammary carcinomas that have elevated expression of neu oncogene. Int J Cancer 53:1002-1007, 1993
80. Xie X, Brünner N, Jensen G, Albrectsen J, Gotthardsen B, Rygaard J: Comparative studies between nude and scid mice on the growth and metastatic behavior of xenografted human tumors. Clin Exp Metastasis 10:201-210, 1992

81. Fodstad O, Hansen CT, Cannon GB, Statham CN, Lichenstein GR, Boyd MR: Lack of correlation between natural killer cell activity and tumor growth control in nude mice with different immune defects. Cancer Res 44:4403-4408, 1984
82. Bosma MJ, Carroll AM: The SCID mouse mutant: definition, characterization, and potential uses. Annu Rev Immunol 9:323-350, 1991
83. Clarke R, Dickson RB: Animal models of tumor onset, growth and metastasis. *In:* Bertino JR (ed) Molecular Biology of Cancer, Vol. 1. Academic Press, San Diego (in press)
84. Seibert K, Shafie SM, Triche TJ, Whang-Peng JJ, O'Brien SJ, Toney JH, Huff KK, Lippman ME: Clonal variation of MCF-7 breast cancer cells in vitro and in athymic nude mice. Cancer Res 43:2223-2239, 1983
85. Cattanach B, Iddon A, Charlton H, Chiappa S, Fink G: Gonadotropin relcasing hormone deficiency in a mutant mouse with hypogonadism. Nature 269:338-340, 1977
86. Masom A, Hayflick J, Zoeller R, Young W, Philips H, Nickolics K, Seeberg PA: A deletion truncating the gonadotropin-releasing gene is responsible for hypogonadism in the *hpg* mouse. Science 234:1366-1371, 1986
87. Charlton H, Speight A, Halpin D, Bramwell A, Sheward W, Fink G: Prolactin measurements in normal and hypogonadal (*hpg*) mice: developmental and experimental studies. Endocrinology 113:545-548, 1983
88. Beamer WG, Shultz KL, Tennent B, Shultz LD: Granulosa cell tumorigenesis in genetically hypogonadal-immunodeficient mice grafted with ovaries from tumor-susceptible donors. Cancer Res 53:3741-3746, 1993
89. Screpanti I, Santoni A, Gulino A, Herberman RB, Frati L: Estrogen and antiestrogen modulation of mouse natural killer activity and large granular lymphocytes. Cell Immunol 106:191-202, 1987
90. Seaman WE, Blackman MA, Gindhart TD, Roubinian JR, Loeb JM, Talal N: β-estradiol reduces natural killer cells in mice. J Immunol 121:2193-2198, 1978
91. Hanna N, Schneider M: Enhancement of tumor metastases and suppression of natural killer cell activity by β-estradiol treatment. J Immunol 130:974-980, 1983
92. Seaman WE, Talal N: The effect of 17β-estradiol on natural killing in the mouse. *In:* Herberman RB (ed) Natural Cell-mediated Immunity Against Tumors. Academic Press, New York, 1980, pp 765-777
93. Shafie SM, Grantham FH: Role of hormones in the growth and regression of human breast cancer cells (MCF-7) transplanted into athymic nude mice. J Natl Cancer Inst 67:51-56, 1981
94. Welsch CW, Swim EL, McManus MJ, White AC, McGrath CM: Estrogen induced growth of human breast cancer cells (MCF-7) in athymic nude mice is enhanced by secretions from transplantable pituitary tumor. Cancer Lett 14:309-316, 1981
95. Clarke R, Brünner N, Katzenellenbogen BS, Thompson EW, Norman MJ, Koppi C, Paik S, Lippman ME, Dickson RB: Progression from hormone dependent to hormone independent growth in MCF-7 human breast cancer cells. Proc Natl Acad Sci USA 86: 3649-3653, 1989
96. Clarke R, Brünner N, Thompson EW, Glanz P, Katz D, Dickson RB, Lippman ME: The inter-relationships between ovarian-independent growth, anti-estrogen resistance and invasiveness in the malignant progression of human breast cancer. J Endocrinol 122:331-340, 1989
97. Blumenthal RD, Jordan JJ, McLaughlin WH, Bloomer WD: Animal modeling of human breast tumors: limitations in the use of estrogen pellet implants. Breast Cancer Res Treat 11:77-78, 1988
98. Gottardis MM, Jordan VC: Development of tamoxifen-stimulated growth of MCF-7 tumors in athymic mice after long-term antiestrogen administration. Cancer Res 48:5183-5187, 1988
99. Osborne CK, Coronado EB, Robinson JP: Human breast cancer in athymic nude mice: cytostatic effects of long-term antiestrogen therapy. Eur J Cancer Clin Oncol 23:1189-1196, 1987
100. McLeskey SW, Kurebayashi J, Honig SF, Zwiebel JA, Lippman ME, Dickson RB, Kern FG: Fibroblast growth factor 4 transfection of MCF-7 cells produces cell lines that are tumorigenic and metastatic in ovariectomized or tamoxifen-treated athymic nude mice. Cancer Res 53:2168-2177, 1993
101. Friedl A, Jordan VC: Oestradiol stimulates growth of oestrogen receptor-negative MDA-MB-231 breast cancer cells in immunodeficient mice by reducing cell loss. Eur J Cancer 30A:1559-1564, 1994
102. Brünner N, Boulay V, Fojo A, Freter C, Lippman ME, Clarke R: Acquisition of hormone-independent growth in MCF-7 cells is accompanied by increased expression of estrogen-regulated genes but without detectable DNA amplifications. Cancer Res 53:283-290, 1993
103. Brünner N, Svenstrup B, Spang-Thompsen M, Bennet P, Nielsen A, Nielsen JJ: Serum steroid levels in intact and endocrine ablated Balb/c nude mice and their intact litter mates. J Steroid Biochem 25:429-432, 1986
104. Jones DY, Schatzkin A, Green SB, Block G, Brinton LA, Ziegler RG, Hoover R, Taylor PR: Dietary fat and breast cancer in the National Health and Nutrition Examination Survey I epidemiologic follow-up study. J Natl Cancer Inst 7
105. Thompson EW, Br Boulay V, Wright A R: The invasive a mone-independent a MCF-7 human brea stasis 11:15-26, 199
106. Clarke R, Skaar T, MR, Lippman J, Th Hormonal carcinog and molecular stu Breast Cancer Res
107. Clarke R, Lippmar mechanisms and re Resistance in Oncol 1992, pp 501-536
108. Brünner N, Frands Thompson EW, Wa R: MCF7/LCC2: human breast cance to the steroidal antie 53:3229-3232, 1993
109. Bronzert DA, Gree and characterizatio resistant to the an crinology 117:1409-
110. Belani CP, Pearl P, fen withdrawal res Intern Med 149:449
111. Canney PA, Griffit Clinical significan response. Lancet i:
112. Stein W, Hortobag sponse of metastatic drawal: report of a 1983
113. Nawata H, Chong Estradiol independe human breast cance 256:6895-6902, 198
114. Nawata H, Bronzert characterization of derived from MCF- Biol Chem 256:501
115. van den Berg HW, (zation of a tamo oestrogen responsiv ZR-75-1. Br J Can
116. van den Berg HW, Dickson GR, Croc tamoxifen-resistant breast cancer cell lin resistant phenotype.
118. Clarke R, Brünner N

J Natl Cancer Inst 79:465-471, 1987

105. Thompson EW, Brünner N, Torri J, Johnson MD, Boulay V, Wright A, Lippman ME, Steeg PS, Clarke R: The invasive and metastatic properties of hormone-independent and hormone-responsive variants of MCF-7 human breast cancer cells. Clin Exp Metastasis 11:15-26, 1993
106. Clarke R, Skaar T, Baumann K, Leonessa K, James MR, Lippman J, Thompson EW, Freter C, Brünner N: Hormonal carcinogenesis in breast cancer: cellular and molecular studies of malignant progression. Breast Cancer Res Treat 31:237-248, 1994
107. Clarke R, Lippman ME: Antiestrogen resistance: mechanisms and reversal. *In:* Teicher BA (ed) Drug Resistance in Oncology. Marcel Dekker, New York, 1992, pp 501-536
108. Brünner N, Frandsen TL, Holst-Hansen C, Bei M, Thompson EW, Wakeling AE, Lippman ME, Clarke R: MCF7/LCC2: a 4-hydroxytamoxifen resistant human breast cancer variant which retains sensitivity to the steroidal antiestrogen ICI 182,780. Cancer Res 53:3229-3232, 1993
109. Bronzert DA, Greene GL, Lippman ME: Selection and characterization of a breast cancer cell line resistant to the antiestrogen LY 117018. Endocrinology 117:1409-1417, 1985
110. Belani CP, Pearl P, Whitley NO, Aisner J: Tamoxifen withdrawal response: report of a case. Arch Intern Med 149:449-450, 1989
111. Canney PA, Griffiths T, Latief TN, Priestman TJ: Clinical significance of tamoxifen withdrawal response. Lancet i:36, 1989
112. Stein W, Hortobagyi GN, Blumenschein GR: Response of metastatic breast cancer to tamoxifen withdrawal: report of a case. J Surg Oncol 22:45-46, 1983
113. Nawata H, Chong MT, Bronzert D, Lippman ME: Estradiol independent growth of a subline of MCF-7 human breast cancer cells in culture. J Biol Chem 256:6895-6902, 1981
114. Nawata H, Bronzert D, Lippman ME: Isolation and characterization of a tamoxifen resistant cell line derived from MCF-7 human breast cancer cells. J Biol Chem 256:5016-5021, 1981
115. van den Berg HW, Clarke R: Preliminary characterization of a tamoxifen resistant variant of the oestrogen responsive human breast cancer cell line ZR-75-1. Br J Cancer 52:421 1985
116. van den Berg HW, Lynch M, Martin J, Nelson J, Dickson GR, Crockard AD: Characterization of a tamoxifen-resistant variant of the ZR-75-1 human breast cancer cell line (ZR-75-9a1) and stability of the resistant phenotype. Br J Cancer 59:522-526, 1989
118. Clarke R, Brünner N: Cross resistance and molecular mechanisms in antiestrogen resistance. Endocr Related Cancer 2:59-72, 1995
119. Johnston SRD, Saccanti-Jotti G, Smith IE, Newby J, Dowsett M: Change in oestrogen receptor expression and function in tamoxifen-resistant breast cancer. Endocr Related Cancer 2:105-110, 1995
120. Leonessa F, Green D, Licht T, Wright A, Wingate-Legette K, Lippman J, Gottesman MM, Clarke R: MDA435/LCC6 and MDA435/LCC6^{MDR1}: ascites models of human breast cancer. Br J Cancer (in press)
121. Yee D, Kozelsky TW, Allred DC, Brünner N, Chen S-C, Woo SLC: Adenoviral *in vivo* gene transfer using a xenograft ascites model of human breast cancer. Breast Cancer Res Treat 32(suppl):77, 1994
122. Nicholson GL, Gallick GE, Sphon WH, Lembo TM, Tainsky MA: Transfection of activated c-HarasEJ/pSV2neo genes into rat mammary cells: rapid stimulation of clonal diversification of spontaneous metastatic and cell surface properties. Oncogene 7: 1127-1135, 1992
123. Vickers PJ, Dickson RB, Shoemaker R, Cowan KH: A multidrug-resistant MCF-7 human breast cancer cell line which exhibits cross-resistance to antiestrogens and hormone independent tumor growth. Mol Endocrinol 2:886-892, 1988
124. Zyad A, Bernard J, Clarke R, Tursz T, Brockhaus M, Chouaib S: Human breast cancer cross-resistance to TNF and adriamycin: relationship to MDR1, MnSOD and TNF gene expression. Cancer Res 54:825-831, 1994
125. Doroshow JH, Akman S, Esworthy S, Chu FF, Burke T: Doxorubicin resistance is conferred by selective enhancement of intracellular glutathione peroxidase or superoxide dismutase content in human MCF-7 breast cancer cells. Free Radic Res Commun 12-13 Pt 2:779-781, 1991
126. Iwamoto S, Takeda K: Possible cytotoxic mechanisms of TNF in vitro. Hum Cell 3:107-112, 1990
127. Batist G, Tuple A, Sinha BK, Katki AG, Myers CE, Cowan KH: Overexpression of a novel anionic glutathione transferase in multidrug-resistant human breast cancer cells. J Biol Chem 261:15544-15549, 1986
128. Sinha BK, Mimnaugh EG, Rajagopalan S, Myers CE: Adriamycin activation and oxygen free radical formation in human breast tumor cells: protective role of glutathione peroxidase in adriamycin resistance. Cancer Res 49:3844-3848, 1989
129. Ford JM, Bruggemann EP, Pastan I, Gottesman MM, Hait WN: Cellular and biochemical characterization of thioxanthenes for reversal of multidrug resistance in human and murine cell lines. Cancer Res 50:1748-1756, 1990
130. Clarke R, Currier SJ, Kaplan O, Boulay V, Lovelace

E, Pastan I, Gottesman MM, Dickson RB: Role of MDR-1 expression in the hormone responsiveness of MCF-7 human breast cancer cells. Proc Am Assoc Cancer Res 32:366, 1991
131. Brünner N, Thompson EW, Spang-Thomsen M, Rygaard J, Dano K, Zwiebel JA: *lac*Z transduced human breast cancer xenografts as an in vivo model for the study of invasion and metastasis. Eur J Cancer 28A:1989-1995, 1992
132. Price JE, Polyzos A, Zhang RD, Daniels LM: Tumorigenicity and metastasis of human breast carcinoma cell lines in nude mice. Cancer Res 50:717-721, 1990
133. Rose DP, Hatala MA, Connolly JM, Rayburn J: Effect of diets containing different levels of linoleic acid on human breast cancer growth and lung metastasis in nude mice. Cancer Res 53:4686-4690, 1993
134. Kurebayashi J, McLeskey SW, Johnson MD, Lippman ME, Dickson RB, Kern FG: Quantitative demonstration of spontaneous metastasis by MCF-7 human breast cancer cells cotransfected with fibroblast growth factor 4 and LacZ. Cancer Res 53:2178-2187, 1993
135. McLeskey SW, Zhang L, Kharbanda S, Kurebayashi J, Lippman ME, Dickson RB, Kern FG: Fibroblast growth factor overexpressing breast carcinoma cells as models of angiogenesis and metastasis. Breast Cancer Res Treat (this issue)
136. Schackert G, Price JE, Bucana CD, Fidler IJ: Unique patterns of brain metastasis produced by different human carcinomas in athymic nude mice. Int J Cancer 44:892-897, 1989
137. Clarke R, Dickson RB, Lippman ME: Hormonal aspects of breast cancer: growth factors, drugs and stromal interactions. Crit Rev Oncol Hematol 12:1-23, 1992
138. Meyvisch C: Influence of implantation site on formation of metastases. Cancer Metastasis Rev 2:295-306, 1983
139. Volpe JPG, Milas L: Influence of tumor transplantation methods on tumor growth rate and metastatic potential of solitary tumors derived from metastases. Clin Exp Metastasis 8:381-389, 1990
140. Morikawa K, Walker SM, Nakajima M, Pathak S, Jessup JM, Fidler IJ: Influence of organ environment on the growth, selection, and metastasis of human colon carcinoma cells in nude mice. Cancer Res 48: 6863-6871, 1988
141. Kozlowski JM, Fidler IJ, Campbell D, Xu Z-L, Kaighn ME, Hart IR: Metastatic behavior of human tumor cell lines grown in the nude mouse. Cancer Res 44:3522-3529, 1984
142. Davidson NE, Gelmann EP, Lippman ME, Dickson RB: Epidermal growth factor receptor gene expression in estrogen receptor-positive and negative human breast cancer cell lines. Mol Endocrinol 1:216-223, 1987
143. Sainsbury JRC, Nicholson JA, Angus B, Farndon JR, Malcolm AJ, Harris AL: Epidermal growth factor receptor status of histological sub-types of breast cancer. Br J Cancer 58:458-460, 1988
144. Sainsbury JRC, Farndon JR, Nedham GK, Malcolm AJ, Harris AL: Epidermal growth factor receptor status as predictor of early recurrence and death from breast cancer. Lancet i:1398-1402, 1987
145. Castronovo V, Taraboletti G, Liotta LA, Sobel ME: Modulation of laminin receptor expression by estrogen and progestins in human breast cancer cell lines. J Natl Cancer Inst 81:781-788, 1989
146. Thompson EW, Paik S, Brünner N, Sommers C, Zugmaier G, Clarke R, Shima TB, Torri J, Donahue S, Lippman ME, Martin GR, Dickson RB: Association of increased basement membrane-invasiveness with absence of estrogen receptor and expression of vimentin in human breast cancer cell lines. J Cell Physiol 150:534-544, 1992
147. Butler WB, Kirkland WL, Jorgensen TL: Induction of plasminogen activator by estrogen in a human breast cancer cell line (MCF-7). Biochem Biophys Res Commun 90:1328-1334, 1979

Breast Cancer R

The T61 I
An experi

Nils Brünner[1]
[1] *Finsen Labo*
sity of Copenh
DC, USA

Key words: e
IGF-I, IGF-II

Summary

Endocrine the
and in advanc
of the effects
was originall
transplanted x
both estrogen
are stimulated

Molecular
of peptide gro
factors I and I
is the only pep
with physiolo
and rapid regr
antibody whic
bound IGF-II

These resu
estrogen thera
(IGF-II) by en

Introduction

Endocrine ther
adjuvant thera
disease in bre
content of estr

Address for corre
Copenhagen, Den

ELSEVIER

Biochimica et Biophysica Acta 1400 (1998) 301–319

BIOCHIMICA ET BIOPHYSICA ACTA
BBA

Review

Animal models for studying the action of topoisomerase I targeted drugs

Joyce Thompson [a], Clinton F. Stewart [b], Peter J. Houghton [c,*]

[a] *Department of Hematology-Oncology, St. Jude Children's Research Hospital, 332 N. Lauderdale, Memphis, TN 38105-2794, USA*
[b] *Department of Pharmaceutical Science, St. Jude Children's Research Hospital, 332 N. Lauderdale, Memphis, TN 38105-2794, USA*
[c] *Department of Molecular Pharmacology, St. Jude Children's Research Hospital, 332 N. Lauderdale, Memphis, TN 38105-2794, USA*

Accepted 17 April 1998

Abstract

Almost 30 years after the unsuccessful clinical evaluation of camptothecin sodium, there has been a revival in interest in this class of agent that poisons topoisomerase I. Currently there are four camptothecin analogues in clinical trials each at different levels of advancement. Clinical data suggest that patterns of antitumor activity and toxicity profiles differ between analogues. In preclinical models antitumor activity appears to be highly schedule-dependent. Here we review rodent and human tumor models used in evaluation of efficacy, and models used to predict toxicities of these compounds. The major limitation of rodent models is that the mouse tolerates significantly greater systemic exposure to each camptothecin analogue than do patients. This leads to a false overprediction of potential clinical activity. However, responses of human tumor xenografts in mice are highly predictive of responses of clinical cancer when camptothecins are administered at dose levels achieving similar systemic exposure in mice. Development of assays that identify analogues that maintain therapeutic activity in mice, but have less species differential toxicity, particularly to the hematopoietic system, may provide an early screen to select compounds having greater clinical utility.

Keywords: Rodent tumor; Human tumor; Schedule dependence; Toxicity; Combination chemotherapy; Interspecies difference

Contents

* Corresponding author. Fax: (901) 5211668; E-mail: peter.houghton@stjude.org

PII: S0167-4781(98)00143-2

1. Introduction

Many of the chemotherapeutic drugs that have been active in the curative or palliative treatment of human malignant diseases are now known to mediate their effects through interaction with DNA topoisomerases stabilizing covalent DNA-protein intermediates. Thus, epipodophyllotoxins, anthracyclines, anthrapyrazoles and actinomycins appear to target topoisomerase II, whereas drugs of the camptothecin class work specifically through their interaction with topoisomerase I. Some, such as actinomycin D, may be dual topoisomerase inhibitors [1]. The clinical utility of the epipodophyllotoxin, etoposide (VP-16-213), the anthracyclines doxorubicin and daunorubicin, and actinomycin D have been well established [2]. Less clinical data are available to support the broad utility of drugs such as mitoxantrone or amsacrine. The utility of camptothecin drugs in treatment of human cancer also remains to be determined. However, preliminary results from early clinical trials suggest that drugs that target topoisomerase I may represent novel agents with considerable activity in a relatively broad spectrum of malignancies.

Each of the agents that target topoisomerases currently in clinical trials, or are approved for use in particular indications, has proceeded through preclinical stages of identifying cytotoxic potency, and confirmation of in vivo antitumor activity. Acceptable toxicity in both rodents and other species, as mandated by regulatory agencies, has been studied prior to evaluation in patients. However, for many drugs, their preclinical efficacy against rodent and human tumors heterografted into immune-incompetent rodents has not translated into similar dramatic activity in patients. This is particularly apparent for camptothecin analogues, such as 9-aminocamptothecin (e.g. in colon carcinoma), that have spectacular activity against human colon cancers grafted into mice [3]. The purpose of this review is to examine this preclinical-clinical interface with respect to understanding the value and limitations of preclinical models, and potential lessons that can be applied to future development of drugs that induce cytotoxicity through their interactions with topoisomerases. Because of the current intensive interest in developing new camptothecin analogues, this article will focus on preclinical models to assess antitumor activity and toxicity for this class of compounds.

2. Early studies

Camptothecin was studied extensively in the Cancer Chemotherapy National Service Center (CCNSC) of the National Cancer Institute during the 1960s. In early in vivo testing, camptothecin, as the base, was formulated in carboxymethylcellulose, and administered by intraperitoneal injection. DeWys et al. [4] reported the activity of 19 agents in preclinical development at that time using the Walker 256 carcinosarcoma model as the test system. Drug treatment (daily×4) was started 3 days after inoculation of cells into the hind limb. Of interest is the relatively

Table 1
Ranking of drugs by increase in median survival time

Drug	Maximum tumor weight inhibition[a] (%)	Maximum increase in median survival time		30 day survivors	
		%	Number of dose levels giving this increase	Maximum per test group	Number of dose levels giving 30 day survivors
Triethylenemelamine	98	> 100	4	6/6	4
Merphalan	97	> 100	4	6/6	4
Thiotepa	100	> 200	3	6/6	3
Cyclophosphamide	100	> 100	3	6/6	3
Dibromodulcitol	97	> 150	4	6/6	4
Dibromomannitol	100	> 150	3	4/6	4
Melphalan	100	> 200	2	6/6	2
DL-*meta*-Sarcolysin	100	> 200	2	4/6	3
Hydrazine, 1-acetyl-2-picolinoyl	88	125	1	3/6	1
Ethanol, 2,2'-[*p*-nitroso-phenyl)imino]di, dimethanesulfonate	100	100	1	2/6	1
Methacrylic acid, 2,3-epoxypropyl ester	85	96	1	1/6	2
6-Mercaptopurine	100	90	2	1/6	1
Busulfan	98	65	2	1/6	1
Colchicine	93	67	1	0/6	–
Camptothecin	99	62	1	0	–
Vinblastine	99	55	1	1/6	1
Methotrexate	100	50	1	0	–
Azaserine	100	50	1	0	–
Uracil, 5-diazo-, hydrate	92	29	1	0	–

[a]Value may be that determined at a dose other than the dose giving maximum increase in survival time. From DeWys et al. [4].

low therapeutic activity of camptothecin, relative to other drugs evaluated (Table 1). Further studies, using the sodium salt of camptothecin, demonstrated significant activity in increasing survival time in several lymphocytic leukemias [5], including L1210, L5178Y, K1964, and P388. Particular note was a high proportion of long-term survivors in mice bearing L5178Y and K1964 (Table 2). In addition, no

Table 2
Activity of camptothecin against various mouse tumors

Tumor	Optimal dose (mg/kg) and schedule[a]	Increase in median survival time over controls (%)	Long-term survivors (%)[b]
Leukemia L1210	40, q,4.d.	265	0
Leukemia L5178Y	40, 1,5,9	> 1000[c]	90
Leukemia K1964	40, 1,5,9	> 1000	70
Leukemia P388	40, q,4.d.	185	0
Plasma cell YPC-1	40, 1,5,9	136	0
Mast cell P815	30, 1,5,9	65	0
Reticulum cell sarcoma A-RCS	40, q,4.d.	50	0

From Gallo et al. [5].
[a]Mice were treated i.p. with 30, 40, or 50 mg/kg on days 1, 5 and 9 after tumor inoculation or with 40 mg/kg every 4 days for as long as 6 months.
[b]Survivors 6 months or longer after death of all controls.
[c]Where there were over 50% survivors, long-term survivors' increase in median survival time was not calculated beyond 1000%.

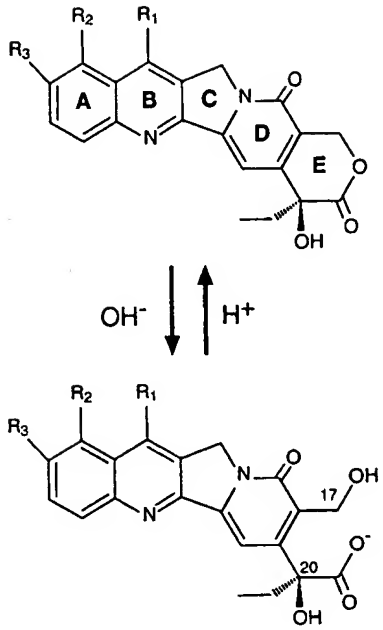

	R_1	R_2	R_3
Topotecan:	H	CH_3 CH_3 N CH_2	HO
9 Aminocamptothecin:	H	NH_2	H
9 Nitrocamptothecin:	H	NO_2	H
Irinotecan:	CH_2CH_3	H	O N N-C-O
SN-38:	CH_2CH_3	H	HO

Fig. 1. Chemical structures of camptothecin analogues in clinical trials. Each analogue exists in a pH-dependent equilibrium between lactone (active) and hydroxy acid (inactive) forms.

cross-resistance between dichloromethotrexate, 1,3-bis(2-chloroethyl)-1-nitrosourea (BCNU), cytosine arabinoside, or 6-mercaptopurine (in sublines of L1210), or L-asparaginase (L5178Y) or vincristine (P388) was found. Based on these studies it was proposed that camptothecin had a novel mechanism of action, and should be evaluated in patients with either solid tumors or lymphocytic leukemias. Camptothecin, evaluated as the sodium salt, was found to be ineffective in patients with advanced disseminated melanoma or gastrointestinal malignancies [6,7]. Other studies in China, however, demonstrated activity of 10-hydroxycamptothecin in treatment of head and neck and bladder cancers (reviewed in [8]). However, unpredictable and severe toxicities included myelosuppression, vomiting, diarrhea, and hemorrhagic cystitis that resulted in discontinuation of clinical trial of sodium camptothecin.

In retrospect, some of the toxicity manifest in clinical trials with sodium camptothecin can be understood, as under alkaline conditions the lactone ring opens to form the carboxylate (*cis*-hydroxy acid). The carboxylate has little activity as a topoisomerase I poison. However, elimination from the renal tubule into the acidic milieu of the urinary bladder would lead to ring closing (Fig. 1), and potential for toxic effects on that organ. Because of the insolubility of camptothecin in aqueous vehicles extensive studies have identified more soluble and active camptothecin analogues. The structures of camptothecin and analogues under clinical investigation are also shown in Fig. 1. Stimulus to develop these compounds also came from seminal studies that defined topoisomerase I as the target for camptothecin, and the observation that camptothecins caused trapping of topoisomerase I on DNA and induced single strand breaks [9,10]. Camptothecin traps topoisomerase I on DNA after a single strand nick has been made; in cells replicating DNA this could result in a collision between the complex and the advancing replication fork, leading to a double strand DNA break. It is considered that generation of this break initiates a cascade leading to apoptosis. Although outside the scope of this chapter, it is important to understand that camptothecins induce toxicity by converting a normal cellular enzyme into a cellular poison. Studies by Nitiss and Wang [11] showed that in yeast, camptothecin became toxic only in the presence of a functional topoisomerase I. Conceptually, therefore, increased levels of topoisomerase I would favor increased formation of DNA-topoisomerase I-drug complexes, which would increase the probability of

a collision with the advancing replication fork, and generation of a double strand DNA break. In the absence of DNA replication, the reversibly stabilized DNA-topoisomerase I-covalent complexes appear not to be toxic. This has significance in the design of therapeutic trials, as one would anticipate only S-phase cells would be sensitive to camptothecins [12]. Since many tumors have relatively low growth fractions, protracted infusions, or repeated exposures to drug over a long period should optimize cell killing.

3. Rodent tumor models

The primary in vivo screen for activity of camptothecin analogues has traditionally been in syngeneic transplanted rodent tumors. Most frequently, increase in lifespan (ILS) of mice bearing L1210 or P388 lymphocytic leukemias, inoculated intraperitoneally (i.p.), have been used where drug is also administered i.p. While such tests have been described as 'in vivo test tubes', it is pertinent to remember that a primary screen has as one of its objectives not to eliminate active compounds (i.e. false negatives). In the preclinical development of topotecan several in vivo criteria were established for selecting analogues for further development. These included (i) being as active as camptothecin in a panel of preclinical models and (ii) demonstration of potency in vivo (i.e. a maximally tolerated dose, MTD) at similar or lower levels than camptothecin in order to minimize the requirements for camptothecin as a starting material [8]. 9-Dimethylaminomethyl-10-hydroxycamptothecin (topotecan) met these criteria, demonstrating superior ILS in mice bearing L1210 leukemia compared to that achieved by camptothecin at their respective MTD (173 ± 16 vs. $118 \pm 6\%$ ILS). Because of the mechanism of action, and the potential to kill only cells during DNA replication, protracted therapy with topoisomerase I inhibitors theoretically should prove most efficacious. For this to be of practical value, analogues that are active after oral administration may prove to be most useful in therapy of human cancer. Secondary evaluation of topotecan compared the efficacy of oral and intravenously (i.v.) administered drug in syngeneic mice bearing (a) advanced systemic (i.v. inoculated) L1210, (b) advanced systemic (i.v. inoculated) Lewis lung carcinoma, (c) subcutaneously (s.c.) implanted Lewis lung carcinoma, (d) systemic (i.v.) B16 melanoma, and i.p. implanted M5076 reticulum cell sarcoma [13]. Topotecan was administered every 3 h four times per day at 4 or 7 day intervals. Interestingly, orally administered topotecan was comparable in efficacy to parenteral treatment in four of five tumor models tested. The M5076 sarcoma implanted i.p. responded to

Table 3
Evaluation of antitumor activity of CPT-11 against s.c. implanted tumors

Tumor	Drug	Total dose (mg/kg)[a]		Dose for cure[b] (mg/kg)	No. of cured mice/total (dose. mg/kg)
		ID_{58}	ID_{90}		
S180	i.v.	50	180	200	4/10 (200)
	p.o.	100	365	400	3/10 (400), 6/10 (800)
Meth A	i.v.	61	195	>400	6/10 (1000)
	p.o.	140	420	1000	7/7 (1600)
Lewis lung ca.	i.p.	72	118	200	5/6 (200), 6/6 (400)
	p.o.	215	410	400	1/6 (400), 4/6 (600), 5/6 (800), 6/6 (1600)
Ehrlich	i.p.	32	92	50	1/6 (50), 3/6 (100), 3/6 (200)
	p.o.	110	450	400	2/6 (400), 3/5 (800)
MH134	i.p.	66	200	200	1/6 (200); 1/6 (400)
	p.o.	215	620	600	1/6 (600), 4/6 (800)
Mammary ca.	i.p.	96	>400	200	1/6 (200)
	p.o.	600	>800	800	1/6 (800)

From Kunimoto et al. [14].
[a]Total dose for 58% or 90% inhibition of tumor growth. The values were obtained graphically on a probit scale. Tumor-free mice were excluded from the calculation of 90% inhibition.
[b]The minimum total dose for incidence of total regression of the tumor.

Table 4
Responsiveness of human tumor xenografts to treatment with camptothecin analogues

Drug	Xenograft tumor	Dose (mg/kg) and schedule	Comment		Ref.
9-AC	Colon HT-29	10–12.5 mg/kg ×2/week for 5–6 weeks s.c.	Highly effective	ADR, 5FU, MTX, nitrosoureas, ALK, less effective/ineffective	[3]
	Colon CASE				
	Colon SW48				
CPT-11	Mammary MX-1	200 mg (TD) i.v.	Very significant antitumor activity against all tumors	ADR, 5FU, CDDP less effective	[17]
	Gastric St-15	400–800 mg (TD) q (4d×3) p.o.	Curative against MX-1		
	Gastric SC-6		CPT-11 more effective as three injections than one single injection for same total dose		
	Lung QG56				
	Colon Co-4				
CAM, 9-AC, 9-NC	Melanoma BRO	4 mg ×2/week i.m.	Growth inhibition and tumor regression	BRO tumors unresponsive to ADR, 5FU, VCR, VBL, MTX, nitrosourea, ALK	[18]
Topotecan	6 rhabdomyosarcoma lines	1.5–2.0 mg (d×5)3 i.v./p.o.	Complete regressions in rhabdomyosarcomas		[19]
	7 colon lines	12.5 mg q (4d×4) i.p.	Significant activity in osteosarcomas		
	3 osteosarcoma lines		Growth inhibition in several colon lines		
			Results suggest significant schedule dependence		
9-AC, 9-NC, 9-CL-AM	Breast carcinoma		9-AC effective	Short infusions (72 h every 21 days) not effective	[20]
			9-NC effective	Long infusions (5 days every 7 days) very effective	
			9-CL-CAM not effective		
			Results were dose-, schedule- and route of administration-dependent		
CPT-11	6 rhabdomyosarcoma lines	10–40 mg (d×5)2 i.v. and [(d×5)2]3 i.v.	All tumors very sensitive	CPT-11 effective against 2 xenografts selected for resistance to topotecan and rhabdomyosarcoma lines resistant to VCR and melphalan	[21]
	7 colon lines		Complete and partial regressions in 5/8 colon lines		
			Complete responses in 5/6 Rhabdomyosarcoma lines		
CPT-11	TNB9	15–59 mg q (4d×3) i.p.	Growth inhibition	VCR, aclarubicin, VP-16 5FU, THP-ADR, ineffective	[22]
	Neuroblastoma				
CPT-11, topotecan	6 rhabdomyosarcoma lines	CPT-11: 2.5–10 mg [(d×5)2]3 i.v.	CPT-11 highly active (complete regressions) against colon lines	CPT-11 and topotecan active against tumors selected for resistance to VCR	[23]
	8 colon lines	Topotecan: 0.5–1.5 mg (d×5) 12 p.o.	Both drugs similar high activity against rhabdomyosarcomas and brain tumors	CPT-11 active against tumor selected for resistance to melphalan	
	3 brain tumor lines		Concluded: low dose protracted scheduling of daily administration is equi-efficacious as shorter more intense schedules		

Table 4 (*Continued*).

Drug	Xenograft tumor	Dose (mg/kg) and schedule	Comment		Ref.
Topotecan, G1147211, G1149893	Colon HT-79	MTD divided into 3 doses infused q 4 hourly in 24 h ×2/week for 5 weeks	G1147211 and G1149893: Regressions >50% in HT79 and SW-48		[24]
	Colon SW-48				
	Mammary MX-1		Complete regressions in MX-1, growth inhibition in PC3		
	Prostate PC-3		Topotecan: Growth inhibition only		
CPT-11	PNET SKNMC	27–40 mg (d×5) i.v. and q (4d×3) i.v.	Very effective, high complete response rates		[25]
	Neuroblastomas N835 NB8 NB3				
CPT-11	6 neuroblastoma lines	10–40 mg (d×5) i.v.	Highly efficacious		[26,27]
		5–10 mg [(d×5)2]3 i.v. 25–50 mg (d×5)12 p.o.	Complete regression of all tumors on the protracted i.v. schedule and all tumors using oral schedule		
CPT-11	9 brain tumor lines	40 mg (d×5)2 i.p.	Tumor regression in every treated tumor line	CPT-11 active against tumors resistant to busulfan, procarbazine, cyclophosphamide and melphalan	[28]
	Gliomas Medulloblastomas Ependymomas				
9-AC	Prostate PC3	2 mg ×2/week for 3 weeks s.c. 0.35–1 mg (d×5) 3 p.o.	Inhibition and regression of tumor growth	PC3 is a hormone refractory prostate line	[29]
Topotecan	6 neuroblastoma lines	0.36–2 mg [(d×5)2]3 i.v.	Highly effective	Minimum daily systemic exposure related to objective response	[30]
			Complete regressions in all tumors		

CAM, camptothecin; 9-AC, 9-aminocamptothecin; 9-NC, 9-nitrocamptothecin; 9-CL-CAM, 9-chlorocamptothecin.

topotecan administered i.p. or subcutaneously, but not when given orally.

The camptothecin prodrug CPT-11 (irinotecan; 7-ethyl-10-(4-[1-piperidino]-1-piperidino)carbonyloxy-20(*S*)-camptothecin) has been extensively studied in murine syngeneic tumors [14–16]. The activity of CPT-11 against a panel of tumors implanted subcutaneously is presented in Table 3. CPT-11 demonstrated significant activity by parenteral and oral routes against a broad spectrum of tumors, either as disseminated models following intravenous inoculation systemic (i.v. inoculated highly metastatic B16-F10 melanoma), or in control of spontaneous metastases from subcutaneous implants (murine colon-26). The most comprehensive study reported [16] evaluated CPT-11 in ten murine tumors and one human xenograft. All 11 tumors responded to CPT-11, eight of them being responsive at the Decision Network-2 level (DN-2, where treated/control volumes were $< 10\%$), which is the criteria used by the NCI to justify further development. Of note was that CPT-11 was curative against early stage pancreatic ductal carcinoma (PO3), a highly chemorefractory neoplasm. This work also showed no cross-resistance in vivo in P388/VCR leukemic cells resistant to vincristine or human breast carcinoma cells selected for resistance to docetaxel (taxotere). However, the limited pharmacokinetic data reported showed that sig-

nificantly higher levels of SN-38, the active metabolite of CPT-11, were achieved in the mouse compared to limited data available from clinical trials.

4. Human xenograft models

Data with human tumor xenografts suggest that these models may be of value in selecting new agents for clinical development. As a minimum requirement the model should identify those agents known to be clinically effective and should parallel the chemosensitivity-chemoresistance profile of the clinical disease. The approach most commonly taken is to heterograft surgical specimens of tumor into congenitally immune deficient (athymic nude mice), or mice that have been immune-deprived to prevent graft rejection. Alternatively, cells cultured from human tumors may be injected into the mice subcutaneously. In certain circumstances it may be important to assess the pre-clinical activity of a new drug under conditions that mimic the clinical situation (i.e. metastatic disease), in which case the development of orthotopic models can be attempted by injecting cells into the natural occurring site within the host, or intravenously. Of importance in using human cell lines to develop therapeutically useful models is the potential of the cell lines to retain their sensitivity to chemotherapeutic agents. Clearly, a line derived from a single patient is unlikely to simulate the clinical disease. Thus, a number of lines are generally required to accurately simulate the clinical spectrum of offering the potential to conduct 'preclinical phase II evaluation'. However, conditions for tumor growth in the mouse differ from patients, hence the contribution of the mouse will be important in determining chemosensitivity of these xenografts. Generally, human tumor xenografts retain the chemosensitivity characteristics of the original tumor.

Thus the original report [3] on the curative activity of 9-aminocamptothecin (9-AC) against chemorefractory colon cancers served to focus considerable attention on this class of anticancer agent. Interestingly, while administration of drug by the subcutaneous route was highly active, subsequent studies with i.v. administration were relatively disappointing. Activity of camptothecin analogues has been confirmed against an extensive panel of human tumor xenografts commonly used for pre-clinical evaluation and possessing a broad pattern of biological properties and chemosensitivities [17–30] (Table 4). The growth of all xenografts was significantly inhibited by camptothecin analogue administration with a high percentage of complete and partial tumor regressions. In contrast, where reported, standard agents used for clinical treatment of the respective tumor type showed considerably less activity. 9-Aminocamptothecin, the first analogue where results of preclinical evaluations were reported, was able to induce complete remissions in mice bearing xenografts of colon adenocarcinoma and malignant melanoma BRO xenografts. 9-Nitrocamptothecin, a compound currently under clinical investigation, is converted to 9-AC, and has shown superior therapeutic efficacy over 9-AC and parental camptothecin in a large number of human xenograft models [31]. Topotecan also demonstrated good antitumor activity when administered i.v., i.p. and orally, against a variety of childhood tumors, with a high percentage of complete regressions against rhabdomyosarcomas, neuroblastomas and some brain tumors. In contrast, much reduced activity was found against colon carcinoma xenografts.

CPT-11 (irinotecan) appears to be the most efficacious analogue in preclinical studies, and has been investigated most extensively. CPT-11 when given by i.v., i.p. or oral routes showed substantial activity against a broad spectrum of human tumor xenografts, including human cancer xenograft lines unresponsive to many cytotoxic agents. High cure rates were obtained against MX-1 mammary tumor, rhabdomyosarcomas, neuroblastomas, colon cancers and brain tumors. Activity was also retained against tumors selected for resistance to topotecan, VCR, melphalan, and also busulfan, procarbazine, and cyclophosphamide. However, as will be discussed later, mice tolerate far higher systemic exposure to this agent than humans. Thus, exposures to CPT-11 or its active metabolite (SN-38) associated with tumor regressions in mice, may be far in excess of exposures achievable in patients.

GI147211 and GI149893, 10,11-methylenedioxy, 7-substituted compounds, two water soluble analogues of camptothecin have been assessed in preclinical models of colon and mammary cancers. Their anti-

tumor effects were dose- and schedule-dependent with a greater reduction in tumor volume achieved by prolonged dosing. Concurrent experiments demonstrated that they were more effective than topotecan in suppressing tumor growth, although optimal schedules for topotecan were not compared in these studies [24].

For camptothecin analogues evaluation of the antitumor efficacy requires schedules in the mouse that produce drug exposures similar to those in patients. For many of the experiments reported in Table 4 systemic exposures in the mouse to lactone forms of the camptothecin used far exceed exposures that can be achieved in patients. The results demonstrate the relative sensitivity of a given tumor to a series of analogues administered to their maximally tolerated dose levels in the mouse; however, such data may overpredict activity in patients. Without knowing the relative toxicities in humans, such data may have limited predictive value for selecting analogues for further development.

5. Schedule-dependent antitumor activity

Animal models may also be useful for examining alternative schedules of drug administration. Indeed, obtaining information about the schedule dependence in relation to both the activity and toxicity of an anticancer agent is one of the objectives of preclinical studies. However, for camptothecins in particular, experimental designs to assess both endpoints may have to be different. Topoisomerase I inhibitors exert their activity potentially during the S-phase of the cell cycle. It is assumed therefore that once a cytotoxic threshold is achieved, exposure time, rather than further dose escalation, is the important parameter for determining the response to these cell cycle specific agents. Consequently, protracted drug administration could increase antitumor activity.

Scheduling was first noted to be of importance in the study by Kawato et al. [17] and confirmed subsequently in additional models [18–20]. These studies showed that for similar total dosages administered prolonged schedules were more effective than more intense treatments of shorter duration. Several groups have reported schedule-dependent activity of camptothecin analogues, although this finding does not appear to have been used in design of the initial clinical trials. Schedule dependence is illustrated in Fig. 2, where the responses of individual human colon tumor xenografts have been measured in mice receiving drug vehicle (control) or 9-AC treatment. Both treatment groups received the same total dose of drug, the difference being that drug was given over 5 days or 10 days. Clearly, 9-AC administered over 10 days was significantly more active

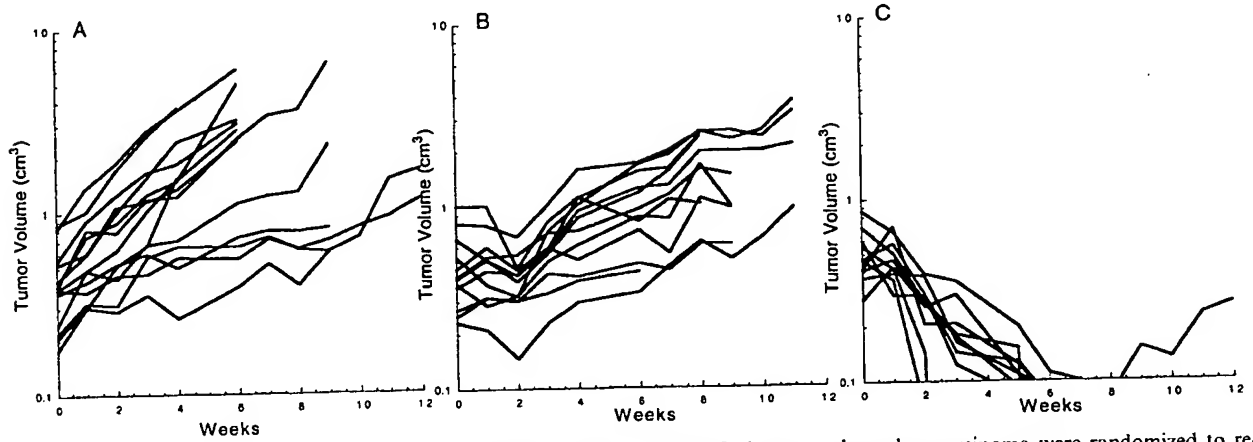

Fig. 2. Schedule-dependent activity of 9-aminocamptothecin. Mice bearing HC_1 human colon adenocarcinoma were randomized to receive no treatment (A), or 9-AC administered over an 8 week period (B,C). 9-AC was administered (B) at 1.5 mg/kg daily for 5 days repeated every 21 days for three cycles, or (C) 0.75 mg/kg daily for 5 days on 2 consecutive weeks with cycles repeated every 21 days (right panel). The total dose administered in each treatment group was 22.5 mg/kg. Each curve represents the growth of an individual tumor. (Unpublished data.)

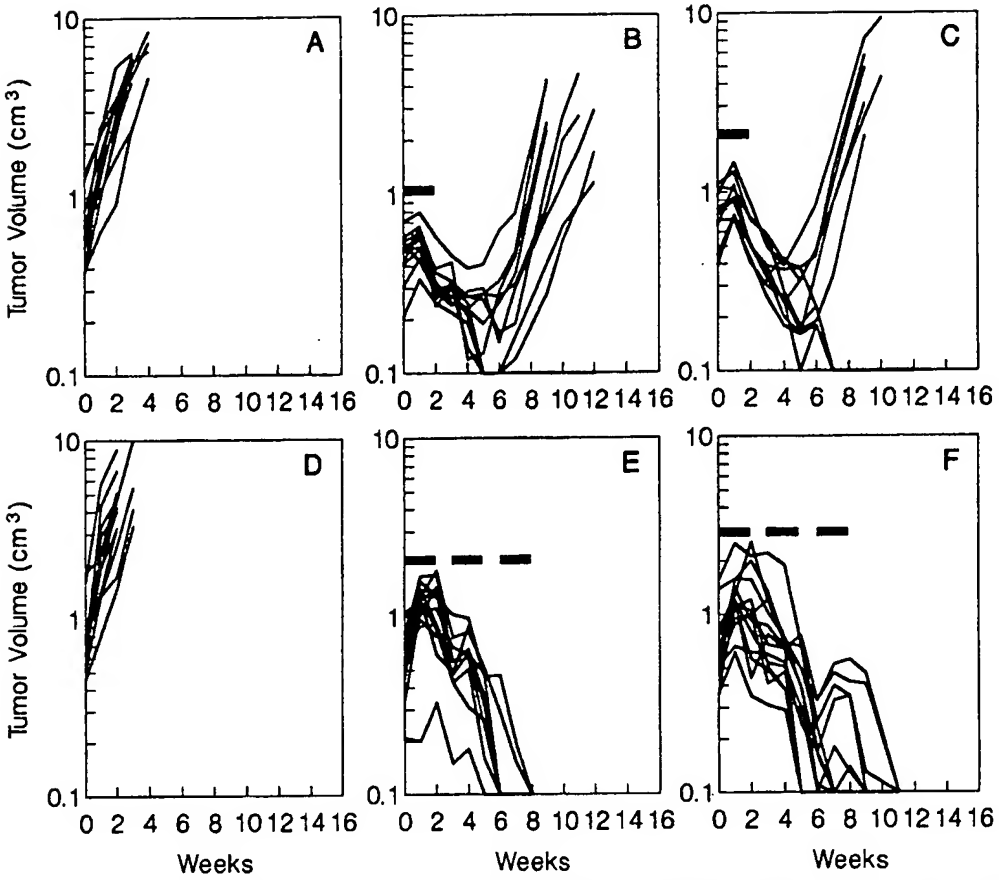

Fig. 3. Efficacy of repeated courses of therapy relative to more intense treatment schedules against VRC_5 colon xenografts. (A) Control; (B) CPT-11 40 mg/kg/dose; (C) 10 mg/kg/dose given (d×5)2 i.v.; (D) control; (E) CPT-11 10 mg/kg/dose; (F) 5 mg/kg/dose given (d×5)2 repeated every 21 days for three cycles (treatment periods marked by heavy horizontal bars). Each curve represents the growth of an individual tumor. Total doses administered were 400, 100, 300 and 150 mg/kg in groups B, C, E and F, respectively. (From Houghton et al. [21], with permission.)

than the same dose given over 5 days. In xenograft models, at least, drugs such as CPT-11 appear to be 'self-limiting', where increasing the dose per administration does not result in further antitumor activity. This is illustrated in Fig. 3, where mice received CPT-11 for two 5 day courses (d×5)2 for a single cycle, or where lower doses were administered for three cycles on the (d×5)2 schedule [21]. In this colon tumor, increasing the dose from 10 to 40 mg/kg per administration did not result in greater antitumor activity. In contrast, repeating the cycles of (d×5)2 therapy at 5 mg/kg over 8 weeks resulted in significantly greater activity compared to administration of a higher total dose of drug over 12 days (i.e. 150 mg/kg vs. 400 mg/kg total dose administered, respectively).

6. Combination therapy with topoisomerase I inhibitors

6.1. Irinotecan with inhibitors of topoisomerase II

Although a conceptual basis exists for anticipating synergistic activity between inhibitors of topoisomerases I and II, several studies have demonstrated antagonism in vitro in hamster ovary [32], human promyelocytic leukemia [33] and HT-29 human colon cancer cells [34]. Kim et al. [35] reported potentiation of cytotoxicity in several xenograft models when irinotecan was administered 24 h after doxorubicin, but antagonism when the agents were administered simultaneously. Houghton et al. [36] subsequently evaluated the combination of etoposide with CPT-

11 where both agents were administered i.v. using the (d×5)2 schedule. Using this schedule of administration where i.v. injection of agents was separated by 2 h, the combination was synergistically toxic. In combination, CPT-11 and etoposide could only be administered at 38% of their respective MTD when given as a single agent (toxicity index = 0.76). Hematopoietic toxicity of the combination was marked by significant myelosuppression and prolonged thrombocytopenia. Toxicity was similar whether CPT-11 was administered before or after etoposide. These results are in marked contrast to the antagonism between the topoisomerase inhibitors predicted from the combination studies using malignant cells in culture. The combination was compared to the activity of CPT-11 or etoposide given as single agents at the same dose levels used in the combination. Against the colon tumor models, the combination showed similar activity to that determined after CPT-11 as a single agent administered at the dose used in the combination. Thus, etoposide did not antagonize the activity of CPT-11, but also demonstrated no synergism, irrespective of the sequence of administration. Similar results were obtained in the rhabdomyosarcoma models when etoposide was administered before CPT-11. However, when etoposide was given 2 h after CPT-11, there was a significant antagonism in three of the tumor models tested. This was particularly marked in three rhabdomyosarcoma lines where CPT-11 as a single agent induced complete regression of all tumors. When CPT-11 was administered 2 h before etoposide there was a dramatic reduction in the rate of objective responses, as shown for Rh30 tumors in Fig. 4. If, as proposed by Bertrand et al.

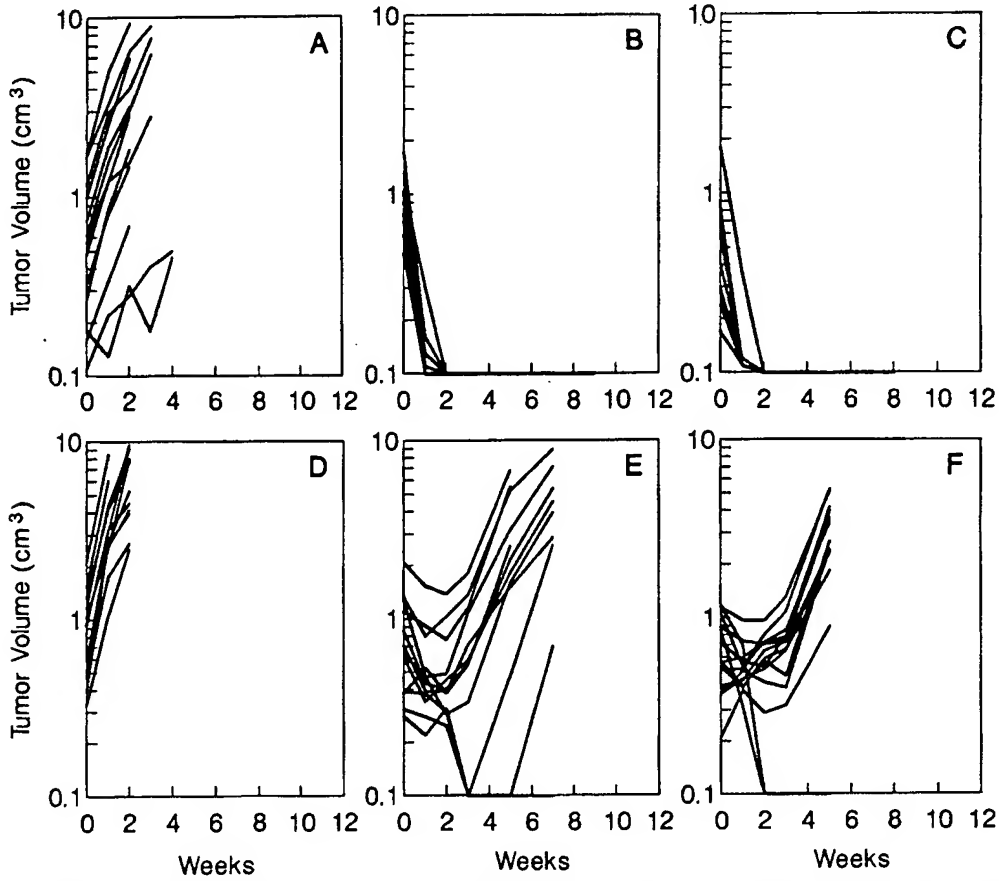

Fig. 4. Responses of Rh30 rhabdomyosarcoma xenografts to irinotecan or irinotecan administered 2 h prior to etoposide. (A,D) Controls; (B) irinotecan 15 mg/kg/dose; (C) irinotecan 10 mg/kg/dose; (E) irinotecan 15 followed by etoposide 4.7 mg/kg/dose; (F) irinotecan 10 followed by etoposide 3.1 mg/kg/dose. Mice received i.v. treatment on the (d×5)2 schedule. Each line demonstrates growth of an individual tumor. (From Houghton et al. [35], with permission.)

[34], the cellular response to inhibition of topoisomerase II by etoposide is to suppress replication, this would result in protection from generating potentially lethal double strand DNA breaks when the replication complex encounters the DNA-topoisomerase I-camptothecin complex. These results, particularly in the tumors reported, are of particular interest, as these xenografts are essentially unresponsive to etoposide. The data argue that despite their intrinsic resistance to etoposide, this agent is able to exert some action within cells that inhibits the cytotoxic activity of the topoisomerase I inhibitor. Consequently, resistance would appear not to be a consequence of poor drug penetration to the cells, but rather the cellular response to inhibition of topoisomerase II. In contrast, synergistic hematopoietic toxicity suggests that the response of murine hematopoietic cells to etoposide is different from rhabdomyosarcoma cells. Thus, in this normal tissue there is no antagonism to CPT-11 by etoposide.

Combinations of camptothecins with different cytotoxic agents have been extensively evaluated in vitro, although relatively few studies have been reported in animals. In part this is a consequence of the difficulty and expense of undertaking such studies. However, the importance of animal testing studies is that synergism between drug combinations is only valuable if it is tumor selective, and does not result in synergistic toxicity to limiting tissues of the host (i.e. net gain in therapeutic efficacy). Miki and Kotake [37] have reported significant activity when CPT-11 was combined with cisplatin rather than carboplatin. Several studies in vitro have suggested that treatment with topoisomerase I inhibitors after radiation may convert single strand DNA breaks to double strand breaks, potentially leading to cell death. Further, camptothecins have been reported to sensitize hypoxic cells to radiation treatment [38]. In the FSaIIC fibrosarcoma, the effect of topotecan and camptothecin on enhancement of daily fractionated radiation was found to result in a sensitizer enhancement ratio of 1.4 for topotecan and 1.2 for camptothecin. Using the MCa-4 mammary carcinoma, Kirichenko et al. [39] examined the dose dependence and schedule dependence of 9-AC combined with daily local radiation therapy (14 consecutive days of 2 Gy daily with a ^{137}Cs unit) to the tumor-bearing leg. Results are shown in Fig. 5, where tumor responses and host weight loss are presented. In these experiments 9-AC was administered 1 h before radiation. These results indicate that 9-AC potentiation of ionizing radiation is dose- and schedule-dependent. Maximum dose modifying factors of 2.4, 3.7 and 3.3 were obtained for groups of mice treated total doses of 2.0, 4.0 and 8 mg/kg 9-AC with 28 Gy ionizing radiation. Evaluation of the effect of 9-AC and radiation on normal tissue toxicity was examined in two tissues, jejunum and skin. It was found that jejunal crypt cell survival was decreased in mice receiving 9-AC plus 12.5 Gy total body radiation compared to those receiving radiation alone, suggesting that gastrointestinal tract could be a critical target tissue for the use of 9-AC combined with radiation.

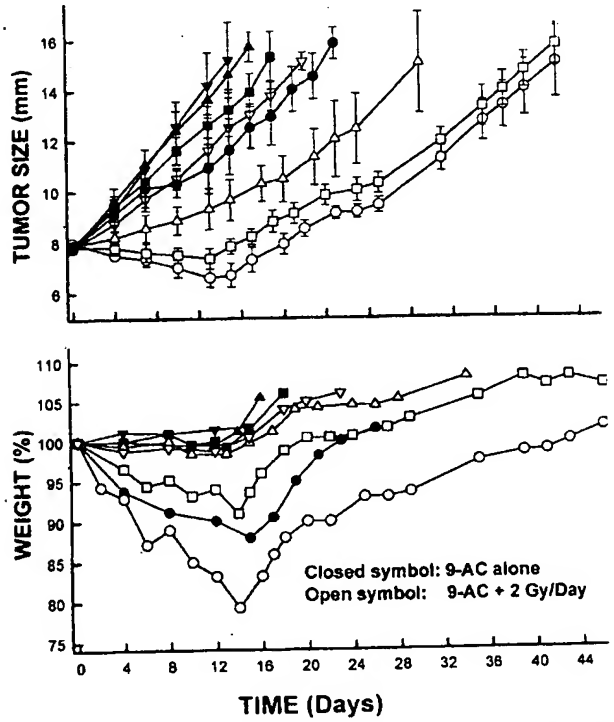

Fig. 5. Tumor regrowth delay (top panel) and percentage weight loss (bottom panel) as a function of treatment with various doses of 9-AC alone or in combination with a fractionated radiation schedule of 2 Gy daily for 14 days, for a total dose of 28 Gy. 9-AC was injected twice a week for 2 weeks, 1 h before radiation beginning the first day of treatment. ▼, no treatment; ▽, fractionated radiation alone; ▲, 9-AC alone (total dose, 2 mg/kg); △, 9-AC (2 mg/kg) + 28 Gy; ■, 9-AC alone (total dose 4 mg/kg); □, 9-AC (4 mg/kg) + 28 Gy; ●, 9-AC alone (total dose 8 mg/kg); ○, 9-AC (8 mg/kg) + 28 Gy. (From Kirichenko et al. [39], with permission.)

7. Toxicity

7.1. Hematopoietic toxicity

The impressive preclinical activity of the newer camptothecins in xenograft models derived from a variety of human tumors contrasts to the clinical activity observed in many phase II studies. The topoisomerase I inhibitors cause dose limiting toxicity to rapidly renewing tissues such as hematopoietic tissues in humans and animals. However, dose limiting toxicity occurs at tenfold lower doses in humans than in mice. Humans can only tolerate 11% as much topotecan per day as mice. This differential may be greater for CPT-11. From pharmacokinetic estimates of exposure to SN-38 at the maximum tolerated dose in patients receiving CPT-11 every 7 days, it was estimated that the systemic exposure represented only 6% of the MTD in mice [40]. The failure to achieve dosages in patients which are curative in the murine models might be due to greater sensitivity of human than mouse myeloid progenitors. Using in vitro clonogenic assays, Erickson-Miller et al. [41] have investigated whether hematopoietic progenitors of the myeloid lineage from humans, mice and dogs exhibit the differential sensitivity to these compounds that is evident in vivo. The toxicity of camptothecin analogues to human and animal myeloid progenitors was quantified from the inhibition of marrow CFU-GM colony formation as a result of continuous drug exposure. The camptothecins in clinical trials (camptothecin lactone, topotecan and 9-AC) inhibited colony formation in a concentration-dependent manner and the results suggest that humans cannot tolerate exposures to camptothecins which are curative in murine models because of the greater susceptibility of their myelopoietic tissue to the drug toxicity. Murine myeloid progenitors tolerated higher drug concentrations than did their human counterparts for all the compounds examined. The differences between mice and humans were large with topotecan and 9-AC (Table 5). The susceptibility of human CFU-GM to drug toxicity is more closely approximated by canine than by murine CFU-GM. This finding explains why even sub-curative doses of camptothecins are severely myelotoxic in patients. The greater sensitivity of human than of murine progenitors must be overcome to achieve in patients drug exposures that cure human tumor xenografts in mice.

7.2. Gastrointestinal toxicity

The clinical use of CPT-11, at higher dosages, has been associated with an unexpected and significant incidence of diarrhea, which is now recognized as a dose limiting toxicity of the compound [42]. However, this was not anticipated from studies in rodents, where diarrhea was not observed. Diarrhea may be caused by abnormalities of intestinal absorption or secretion, because of a change in intestinal flora, increased peristalsis, or drug induced epithelial damage. The considerable interpatient variability in the severity of the diarrhea has made it difficult to explain the mechanism of CPT-11-associated diarrhea. This toxicity, however, is not unique to CPT-11. The dose limiting toxicity of topotecan, when administered orally for 21 days was diarrhea in patients.

Table 5
The concentrations of drug (in nM) inhibiting CFU-GM colony formation from human, canine and murine femoral marrow by 50% (IC_{50}) and 90% (IC_{90})

Compound	IC_{50} (nM)			IC_{90} (nM)		
	Human	Murine	Canine	Human	Murine	Canine
CAM lactone	1.7	18	0.5	16	42	7.6
NA^+-CAM	n/a	17	n/a	29	67	6.9
TPT	2.8	128	1.7	39	381	7.6
s9-AC	0.6	20	0.3	6.2	66	7.6
ss9-AC	0.3	16	0.6	7.3	43	7.4
(*R,S*)-9-AC	0.7	75	0.6	16	331	6.9

The average percent inhibition of CFU-GM from 12, six, and three human, canine, and murine marrows, respectively.
(From Erickson-Miller et al. [41], with permission.)

The etiology of this side effect of camptothecins is not yet clear, although several animal models have been established that attempt to simulate CPT-11 induced diarrhea. However, whether any of these accurately recapitulate the human toxicity is unclear.

7.3. Mouse models

Ikuno et al. [43] recently reported on the mechanisms of CPT-11 induced diarrhea in mice. They observed characteristic changes in the intestinal mucosa of CPT-11 treated mice including marked shortening of the villi (villous atrophy), and epithelial vacuolation of the ileum, associated with increased apoptosis, and goblet cell hyperplasia in the cecum. These structural and functional effects were postulated as the main causes of CPT-11 induced diarrhea leading to malabsorption and hypersecretion of mucin. The malabsorption in CPT-11 treated mice was thought to be caused by villous atrophy following crypt damage and apoptosis of absorptive cells in the small intestine. The goblet cell hyperplasia with excessive production of mucin in the cecum could be another contributing factor to the cause of diarrhea with CPT-11.

7.4. Rat models

Recently, Sakai et al. [44] reported that relatively high concentrations of CPT-11 caused eicosanoid-mediated chloride secretion in isolated rat colon. Frequently, diarrhea is caused by the active secretion of electrolytes, especially chloride ions, suggesting this toxicity is independent of the action of CPT-11 or the active metabolite, SN-38, on topoisomerase I. CPT-11 diarrhea has also been characterized histologically and enzymologically in rats by assessing the relationship between intestinal toxicity and the activity of the enzymes involved in the major metabolic pathways of CPT-11 [45]. CPT-11 is converted to its active metabolite SN-38 by carboxylesterase, and one possible mechanism for the diarrhea might include the structural and functional injuries to the intestinal tract resulting from mitotic inhibitory activity of the SN-38. Following conjugation in the liver, SN-38 glucuronide (detoxified) is excreted into the bile and in the feces where it may be converted/processed to an active SN-38 by β-glucuronidase in the large intestinal microflora. In this study, histological damage was most severe in the cecum, with markedly decreased size and number of the crypts and superficial mucosal erosion. The segmental differences in the degree of damage showed good correlation with the β-glucuronidase activity in the contents of the lumen suggesting that this enzyme plays a key role in the exacerbation of intestinal toxicity induced by CPT-11. Intestinal tissue carboxylesterase activity, which also converts CPT-11 to its active form, showed poor correlation to the degree of tissue damage. Administration of antibiotics exerted a protective effect against the diarrhea by completely inhibiting the β-glucuronidase activity in intestinal flora and thus the formation of active SN-38.

7.5. Hamster models

Bacon et al. [46] have examined the hamster as a model for CPT-11 induced intestinal toxicity. Female Syrian hamsters were dosed i.p. with CPT-11 (50 mg/kg/day) for 10 days and observed through day 20. By day 5 all treated animals had developed diarrhea and deaths occurred starting on day 7. Histologically, a time-dependent loss of structural integrity of the jejunal and ileal mucosa was observed; the typical columnar morphology of the epithelial cells was lost and the villi appeared corrugated. In the colon, the epithelium was thinned and vacuolated within the first 5 days of treatment. Immunohistochemical techniques to detect proliferating cell nuclear antigen (PCNA), showed an increase in the number of labeled epithelial cells and labeling intensity in treated animals. The labeled cells were located further toward the tips of villi compared to control animals. Increased levels of PCNA and loss of differentiation in cell morphology suggested that CPT-11 induces a cell cycle block in S-G_2, with subsequent loss of physiologic function in hamster intestinal epithelium.

8. Interspecies differences that complicate translation of preclinical results

8.1. Interspecies differences in drug metabolism and disposition

Clearly, camptothecins have demonstrated consid-

erably greater activity against model tumors in rodents than against clinical cancer. In part, this appears a consequence of the tolerance of mice to these agents in contrast to that of humans. The plasma systemic exposure, expressed as an area under the concentration-time curve or AUC, for irinotecan and its active metabolite SN-38 in mice [16,47] and patients [48–50] is presented in Table 6. To facilitate comparison between schedules, systemic exposure has been expressed for each course of therapy, usually in a 21 day time frame at the highest non-toxic dose (HNTD) for mice and the MTD for humans. Because not all investigators report the lactone and total drug it is difficult to directly compare the systemic exposure of irinotecan and SN-38 between studies; however, when given as a single injection weekly in humans, the systemic exposure to irinotecan, and particularly SN-38, is significantly greater in mice than in humans.

This raises the concern that studies with syngeneic tumors or human xenografts grown in murine models may over-predict the potential clinical utility of this, as well as other classes of anticancer drugs. For camptothecins the reasons for the interspecies differences are not well understood. However, rather than use the mouse model to predict systemic drug exposures associated with toxicity, we have chosen to use it to determine the systemic exposure associated with antitumor effect against the human tumor xenograft. For example, we determined the daily systemic exposure to topotecan that caused objective regressions against neuroblastomas xenografts when the drug was administered 5 days per week for 2 consecutive weeks [30]. As shown in Fig. 6, partial responses were achieved in each of six independently derived neuroblastoma xenografts at a daily topotecan lactone systemic exposure of 100 ng/ml×h, whereas complete responses were achieved in four tumor lines. Thus, the results of these studies define the effective antitumor systemic exposure to the camptothecin analogue, and this may be directly extrapolated to the design of clinical trials of the agent.

8.2. Protein binding

Most studies of the systemic exposure to camptothecin analogues have measured total drug concentration which consists of both drug bound to plasma protein and unbound drug. For drugs extensively bound to plasma proteins, like SN-38, unbound drug concentrations correlate best with indices of pharmacologic effect. Thus, if significant interspecies variability exists in the plasma protein binding of anticancer drugs, comparisons between unbound drug concentrations and toxicity in humans and animals may be more appropriate. Interspecies differences in the serum or plasma protein binding of several drugs have been reported, including anticancer drugs.

The relevance of interspecies differences in drug protein binding is seen with camptothecin analogues. Camptothecin exists as a pentacyclic structure with a

Table 6
Comparison of irinotecan and SN-38 systemic exposure (AUC) between mice and humans

Ref.	Lactone irinotecan (ng/ml×h)	Lactone SN-38 (ng/ml×h)	Total irinotecan (ng/ml×h)	Total SN-38 (ng/ml×h)
Mice				
Irinotecan 52.5 mg/kg i.v. (Bissery et al. [16])	n/a	n/a	62.5	34.5
Irinotecan 10 mg/kg i.v. [(d×5)2]3 (Stewart et al. [47])	13.0	5.3	n/a	n/a
Humans				
Irinotecan 350 mg/m^2 i.v. once every 3 weeks (Abigerges et al. [48])	n/a	n/a	34.0	0.45
Irinotecan 100 mg/m^2 i.v. for 3 consecutive days every 3 weeks (Catimel et al. [49])	n/a	n/a	27.9	0.96
Irinotecan 150 mg/m^2/week i.v. for 4 of 6 weeks (Rothenberg et al. [50])	5.6	0.24	16.8	0.82
Irinotecan 20 mg/m^2 i.v. [(d×5)2]3 (Furman, Stewart, unpublished)	4.0	1.4	n/a	n/a

Total and lactone AUC have been calculated for the cumulative exposure for a 21 day cycle of therapy.

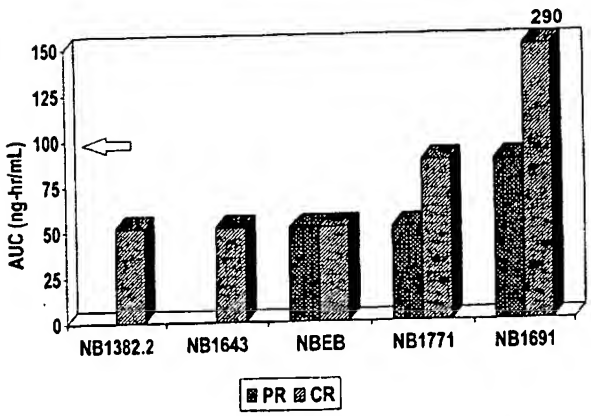

Fig. 6. Topotecan lactone AUC associated with response in neuroblastoma xenografts. Mice were treated with topotecan on an optimal i.v. schedule (daily×5) for 2 consecutive weeks, repeated every 21 days for three cycles over 8 weeks. Responses (PR, partial response; CR, complete response) were determined at decreasing daily dose levels of topotecan administered. Topotecan daily exposures associated with doses that caused PR or CR in each neuroblastoma line were determined. (Unpublished data.)

lactone moiety in the terminal E-ring. Studies have shown the presence of a lactone ring is a structural requirement for antitumor activity. Thus, factors influencing the lactone-carboxylate equilibrium are important determinants of drug activity (see Fig. 1). In addition to pH, presence of protein has been shown to be important to the stability of the lactone [51,52]. Investigators have shown that human serum albumin had a marked preference for the carboxylate form of camptothecin, greater than serum albumin from five other species. Thus, binding of the carboxylate to albumin drives the equilibrium away from the active lactone form of the drug. However, structural modifications to the camptothecin ring seen with CPT-11, SN-38, and topotecan diminished the interspecies differences in stabilization of the lactone. This is contrasted with 9-AC, where the marked interspecies difference in stabilization of the carboxylate form was similar to that observed with camptothecin. In mouse 4 h after intragastric administration, lactone forms of camptothecin or 9-nitrocamptothecin comprise 57–81% and 47–95% of the total drug, respectively. However, in plasma from humans treated orally with either drug, the lactone comprised only a minor component of total drug levels [53]. This interspecies variability in protein stabilization of the carboxylate form is important for translation of preclinical findings into clinical trials. These results also illustrate the importance of determining the systemic exposure to lactone forms of camptothecin analogues that induce objective regressions in xenograft models. This information could be valuable in understanding and designing phase II clinical trials. Attempts to encapsulate and stabilize lactone forms of camptothecins may also increase the therapeutic utility of drugs such as camptothecin or topotecan [54,55].

9. Future directions

Identifying camptothecin analogues, as well as other inhibitors of topoisomerase I, that will have greater therapeutic utility in clinical therapy remains a considerable challenge. Clearly the preclinical screens have selected several analogues of camptothecin that have more acceptable pharmaceutical properties (i.e. better water solubility). Topotecan and CPT-11 have demonstrated significant activity against ovarian, small cell lung cancer, and for CPT-11 activity in colon carcinoma. Against childhood cancers, topotecan is active in neuroblastoma and rhabdomyosarcoma, as predicted by the preclinical studies. Clinically there appear to be qualitative as well as quantitative differences between analogues that have been reported in xenograft models. However, response rates for these agents have been well below that anticipated from preclinical studies. As discussed above, this probably relates to differences in host (mouse vs. human) toxicity. More realistic response rates may be anticipated if exposure to camptothecins in the mouse were to simulate patient exposure. However, such information is not available when selecting between analogues at a relatively early stage in development. One way in which equi-efficacious analogues could be distinguished would be to introduce assays of differential species marrow toxicity at an early stage in development. This may allow identification analogues with good antitumor activity, but with little difference in species toxicity. Further development of models that are more predictive of the major toxicities of camptothecins would also assist in identifying agents with non-hematological toxicity, and assist in developing strategies for ameliorating diarrhea associated with CPT-11.

The full curative/therapeutic potential of these

drugs will not be realized without the development of approaches to compensate for the dose limiting neutropenia. Thus, approaches to reducing myelosuppression, through use of hematopoietic growth factors, reconstitution with peripheral blood cell progenitors, or protecting marrow through transduction of camptothecin-resistance genes, appear rational. Design of clinical protocols that more accurately recapitulate optimal schedules and drug exposures determined in xenograft models also seems appropriate with these agents that are highly schedule-dependent in their antitumor activity. Clearly an understanding of the biochemical/molecular events that determine such dramatic schedule dependence will help in more effective clinical utilization of these agents, alone, or in combination with other cytotoxic agents.

Acknowledgements

Work from these laboratories was supported by UPHS grants CA23099, CA 32613, CA21765 (Cancer Center Support CORE Grant), and by American Lebanese Syrian Associated Charities (ALSAC).

References

[1] D.K. Trask, M.T. Muller, Stabilization of type I topoisomerase-DNA covalent complexes by actinomycin D, Proc. Natl. Acad. Sci. USA 85 (1988) 1417–1421.

[2] J.F. Holland, E. Frei III, R.C. Bast Jr., D.W. Kufe, D.L. Morton, R.R. Weichselbaum (Eds.), Cancer Medicine, 4th edn., 1997.

[3] B.C. Giovanella, J.S. Stehlin, M.E. Wall, M.C. Wani, A.W. Nicholas, L.F. Liu, R. Silber, M. Pomesil, DNA topoisomerase I-targeted chemotherapy of human colon cancer xenografts, Science 246 (1989) 1046–1048.

[4] W.D. DeWys, S.R. Humphreys, A. Goldin, Studies on the therapeutic effectiveness of drugs with tumor weight and survival time indices of Walker 256 carcinosarcoma, Cancer Chemother. Rep. 52, (2) (1968) 229–242.

[5] R.C. Gallo, J. Whang-Peng, R.H. Adamson, Studies on the antitumor activity, mechanism of action, and cell cycle effects of camptothecin, J. Natl. Cancer Inst. 46 (1971) 789–795.

[6] J.A. Gottlieb, A.M. Guarino, J.B. Call, V.T. Oliverio, J.B. Block, Preliminary pharmacologic and clinical evaluation of camptothecin sodium (NSC 100880), Cancer Chemother. Rep. 54 (1970) 461–470.

[7] C.G. Moertel, A.J. Schutt, R.J. Reitemeier, R.G. Hahn, Phase II study of camptothecin (NSC-100880) in the treatment of advanced gastrointestinal cancer, Cancer Chemother. Rep. 56 (1972) 95–101.

[8] W.D. Kingsbury, J.C. Boehm, D.R. Jakas, K.G. Holden, S.M. Hecht, G. Gallagher, M.J. Caranfa, F.L. McCabe, L.F. Faucette, R.K. Johnson, R.P. Hertzberg, Synthesis of water soluble (aminoalkyl) camptothecin analogues: inhibition of topoisomerase I and antitumor activity, J. Med. Chem. 4 (1990) 98–107.

[9] Y.H. Hsiang, R. Hertzberg, S. Hecht, L.F. Liu, Camptothecin induces protein-linked DNA breaks via mammalian DNA topoisomerase I, J. Biol. Chem. 260 (1985) 14873–14878.

[10] A.Y. Chen, L.F. Liu, DNA topoisomerases: essential enzymes and lethal targets, Annu. Rev. Pharmacol. Toxicol. 34 (1994) 191–218.

[11] J. Nitiss, J.C. Wang, DNA topoisomerase-targeted drugs can be studied in yeast, Proc. Natl. Acad. Sci. USA 85 (1988) 7501–7505.

[12] L.F. Liu, Topoisomerase-I targeted drugs. Mechanism of inhibition and cytotoxicity, in: T. Taguchi, J.C. Wang (Eds.), Vth World Conference on Clinical Pharmacology and Therapeutics. Highlights of a Satellite Symposium: Approaches to Cancer Treatment by Topoisomerase-I Inhibitors, Biomedis, Tokyo, 1992, pp. 6–9.

[13] F.L. McCabe, R.K. Johnson, Comparative activity of oral and parenteral topotecan in murine tumor models: efficacy of oral topotecan, Cancer Invest. 12 (1994) 308–313.

[14] T. Kunimoto, K. Nitta, T. Tanaka, N. Uehara, H. Baba, M. Takeuchi, T. Yokokura, S. Sawada, T. Miyasaka, M. Mutai, Antitumor activity of 7-ethyl-10-[4-(1-piperidino)-1-piperidino]-1-carbonyloxy-camptothecin, a novel water soluble derivative of camptothecin, against murine tumors, Cancer Res. 47 (1987) 5944–5947.

[15] T. Matsuzaki, T. Yokokura, M. Mutai, T. Tsuruo, Inhibition of spontaneous and experimental metastasis by a new derivative of camptothecin, CPT-11, in mice, Cancer Chemother. Pharmacol. 21 (1988) 308–312.

[16] M.C. Bissery, P. Vrignaud, F. Lavelle, G.G. Chabot, Experimental antitumor activity and pharmacokinetics of the camptothecin analog irinotecan (CPT-11), Anti-Cancer Drugs 7 (1996) 437–460.

[17] Y. Kawato, T. Furuta, M. Aonuma, M. Yasuoka, T. Yokokura, K. Matsumoto, Antitumor activity of a camptothecin derivative, CPT-11, against human tumor xenografts in nude mice, Cancer Chemother. Pharmacol. 28 (1991) 192–198.

[18] P. Pantazis, H.R. Hinz, J.T. Mendoza, A.S. Kozielski, L.J. Williams, J.S. Stehlin Jr., B.C. Giovanella, Complete inhibition of growth followed by death of human malignant melanoma cells in vitro and regression of human melanoma xenografts in immunodeficient mice induced by camptothecins, Cancer Res. 52 (1992) 3980–3987.

[19] P.J. Houghton, P.J. Cheshire, L. Myers, C.F. Stewart, T.W. Synold, J.A. Houghton, Evaluation of 9-dimethylaminomethyl-10-hydroxycamptothecin against xenografts derived

from adult and childhood solid tumors, Cancer Chemother. Pharmacol. 31 (1992) 229–239.
[20] P. Pentazis, A.J. Kozielski, D.M. Vardeman, E.R. Petry, B.C. Giovanella, Efficacy of camptothecin congeners in the treatment of human breast carcinoma xenografts, Oncol. Res. 5 (1993) 273–281.
[21] P.J. Houghton, P.J. Cheshire, J.C. Hallman, M.C. Bissery, A. Mathieu-Boue, J.A. Houghton, Therapeutic efficacy of the topoisomerase I inhibitor 7-ethyl-10-(4-[1-piperidino]-1-piperidino)-carbonyloxy-camptothecin against human tumor xenografts: lack of cross resistance in vivo in tumors with acquired resistance to the topoisomerase inhibitor 9-dimethylaminomethyl-10-hydroxycamptothecin, Cancer Res. 53 (1993) 2823–2829.
[22] H. Komuro, P. Li, Y. Tsuchida, K. Yokomori, K. Nakajima, T. Aoyama, M. Kaneko, N. Kaneda, Effects of CPT11 (a unique DNA topoisomerase I inhibitor) on a highly malignant xeno-transplanted neuroblastoma, Med. Pediatr. Oncol. 23 (1994) 487–492.
[23] P.J. Houghton, P.J. Cheshire, J.D. Hallman, L. Lutz, H.S. Friedman, M.K. Danks, J.A. Houghton, Efficacy of topoisomerase I inhibitors, topotecan and irinotecan, administered at low dose levels in protracted schedules to mice bearing xenografts of human tumors, Cancer Chemother. Pharmacol. 36 (1995) 393–403.
[24] D.L. Emerson, J.M. Besterman, H.R. Brown, M.G. Evans, P.P. Leitner, M.J. Luzzio, J.E. Shaffer, D.D. Sternbach, D. Uehling, A. Vuong, In vivo antitumor activity of two seven-substituted water soluble camptothecin analogues, Cancer Res. 55 (1995) 603–609.
[25] G. Vassal, M.J. Terrier-Lacombe, M.C. Bissery, A.M. Venuat, F. Gyergyay, J. Benard, J. Morizet, I. Boland, P. Ardouin, B. Bressac-de-Paillerets, A. Gouyette, Therapeutic activity of CPT-11, a DNA-topoisomerase I inhibitor, against peripheral primitive neuroectodermal tumour and neuroblastoma xenografts, Br. J. Cancer 74 (1996) 537–545.
[26] J. Thompson, W.C. Zamboni, P.J. Cheshire, L. Lutz, X. Luo, Y. Li, J.A. Houghton, P.J. Houghton, Efficacy of systemic administration of irinotecan against neuroblastoma xenografts, Clin. Cancer Res. 3 (1997) 423–431.
[27] J. Thompson, W.C. Zamboni, P.J. Cheshire, L. Richmond, X. Luo, J.A. Houghton, C.F. Stewart, P.J. Houghton, Efficacy of oral administration of irinotecan against neuroblastoma xenografts, Anti-Cancer Drugs 8 (1997) 313–322.
[28] C.B. Hare, G.B. Elion, P.J. Houghton, J.A. Houghton, S. Keir, S.L. Marcelli, D.D. Bigner, H.S. Friedman, Therapeutic efficacy of the topoisomerase I inhibitor 7-ethyl-10- (4-[1-piperidino]-1-piperidino)-carbonyloxy-camptothecin against pediatric and adult central nervous system tumor xenografts, Cancer Chemother. Pharmacol. 393 (1997) 187–191.
[29] P.L. deSouza, M.R. Cooper, A.R. Imondi, C.E. Myers, 9-Aminocamptothecin: a topoisomerase I inhibitor with preclinical activity in prostate cancer, Clin. Cancer Res. 3 (1997) 287–294.
[30] W.C. Zamboni, C.F. Stewart, J. Thompson, V. Santana, P.J. Cheshire, L.B. Richmond, X. Liu, J.A. Houghton, P.J. Houghton, The relationship between topotecan systemic exposure and tumor response in human neuroblastoma xenografts, J. Natl. Cancer Inst. 90 (1998) 505–511.
[31] B.C. Giovanella, E. Natelson, N. Harris, D. Vardeman, J.S. Stehlin, Protocols for the treatment of human tumor xenografts with camptothecins, Ann. NY Acad. Sci. 803 (1996) 181–187.
[32] P. D'Arpa, C. Beardmore, L.F. Lui, Involvement of nucleic acid synthesis in killing mechanisms of topoisomerase poisons, Cancer Res. 50 (1990) 6919–6924.
[33] S.H. Kaufmann, Antagonism between camptothecin and topoisomerase II-directed chemotherapeutic agents in a human leukemia cell line, Cancer Res. 51 (1991) 1129–1136.
[34] R. Bertrand, P.M. O'Connor, D. Kerrigan. Y. Pommier, Sequential administration of camptothecin and etoposide circumvents the antagonistic cytotoxicity of simultaneous drug administration in slowly growing human colon carcinoma HT-29 cells, Eur. J. Cancer 28A (1992) 743–748.
[35] R. Kim, N. Hirabayashi, M. Nishiyama, K. Jinushi, T. Toge, K. Okada, Experimental studies on biochemical modulation targeting topoisomerase I and II in human tumor xenografts in nude mice, Int. J. Cancer 50 (1992) 760–766.
[36] J.A. Houghton, P.J. Cheshire, J.D. Hallman, L. Lutz, X. Luo, Y. Li, P.J. Houghton, Evaluation of irinotecan in combination with 5-fluorouracil or etoposide in xenograft models of colon adenocarcinoma and rhabdomyosarcoma, Clin. Cancer Res. 2 (1996) 107–118.
[37] T. Miki, T. Kotake, Advantages in combination chemotherapy using the camptothecin analogue CPT-11 and cisplatinum analogues for human testicular cancer xenografts, Hinyokika Kiyo (Acta Urol. Jpn.) 39 (1993) 1221–1225.
[38] R.E. Boscia, T. Korbut, S.A. Holden, G. Ara, B. Teicher, Interaction of topoisomerase I inhibitors with radiation in *cis*-diamminedichloroplatinum(II)-sensitive and -resistant cells in vitro and in the FSAIIC fibrosarcoma in vivo, Int. J. Cancer 53 (1993) 118–123.
[39] A.V. Kirichenko, T.A. Rich, R.A. Newman, E.L. Travis, Potentiation of murine Mca-4 carcinoma radioresponse by 9-amino-20(*S*)-camptothecin, Cancer Res. 57 (1997) 1929–1933.
[40] P.J. Houghton, C.F. Stewart, W.C. Zamboni, J. Thompson, X. Luo, M.K. Danks, J.A. Houghton, Schedule-dependent efficacy of camptothecins in models of human cancer, Ann. NY Acad. Sci. 803 (1996) 188–201.
[41] C.L. Erickson-Miller, R.D. May, J. Tomaszewski, B. Osborn, M.J. Murphy, J.C. Page, R.E. Parchment, Differential toxicity of camptothecin, topotecan and 9-aminocamptothecin to human, canine, and murine myeloid progenitors (CFU-GM) in vitro, Cancer Chemother. Pharmacol. 39 (1997) 467–472.
[42] L.R. Wiseman, A. Markham, Irinotecan, Drugs 52 (1996) 606–623.
[43] N. Ikuno, H. Soda, M. Watanabe, M. Oka, Irinotecan (CPT-11) and characteristic mucosal changes in the mouse ileum and cecum, J. Natl. Cancer Inst. 87 (1995) 1876–1883.
[44] H. Sakai, M. Diener, V. Gartmann, N. Takeguchi, Eicosa-

noid-mediated Cl^- secretion induced by the antitumor drug, irinotecan (CPT-11), in the rat, Naunyn-Schmiedeberg's Arch. Pharmacol. 351 (1995) 309–314.

[45] K. Takasuna, T. Hagiwara, M. Hirohashi, M. Kato, M. Nomura, E. Nagai, T. Yokoi, T. Kamataki, Involvement of beta-glucuronidase in intestinal microflora in the intestinal toxicity of the antitumor camptothecin derivative irinotecan hydrochloride (CPT-11), Cancer Res. 56 (1996) 3752–3757.

[46] J.A. Bacon, D.K. Petrella, C.T. Cramer, Y. Maruyama, C. Ford, D. Stapert, R.G. Ulrich, Intestinal toxicity and changes in proliferating cell nuclear antigen (PCNA) levels in hamsters induced by a camptothecin analogue, Toxicologist (1996) (abstr.).

[47] C.F. Stewart, W.C. Zamboni, W.R. Crom, P.J. Houghton, Disposition of irinotecan and SN-38 following oral and intravenous irinotecan dosing in mice, Cancer Chemother. Pharmacol. 40 (1997) 259–265.

[48] D. Abigerges, G.G. Chabot, J. Armand, P. Herait, A. Gouyette, D. Gandia, Phase I and pharmacologic studies of the camptothecin analog irinotecan administered every three weeks in cancer patients, J. Clin. Oncol. 13 (1995) 210–221.

[49] G. Catimel, G.G. Chabot, J.P. Guastalla, A. Dumortier, C. Cote, C. Engel, A. Gouyette, A. Mathieu-Boue, M. Mahjoubi, M. Clavel, Phase I and pharmacokinetic study of irinotecan (CPT-11) administered daily for three consecutive days every three weeks in patients with advanced solid tumors, Ann. Oncol. 6, (2) (1995) 133–140.

[50] M.L. Rothenberg, J.G. Kuhn, H.A. Burris et al., Phase I and pharmacokinetic trial of weekly CPT-11, J. Clin. Oncol. 11 (1993) 2194–2204.

[51] T.G. Burke, Z. Mi, The structural basis of camptothecin interactions with human serum albumin: impact on drug stability, J. Med. Chem. 37 (1994) 40–46.

[52] T.G. Burke, C.B. Munshi, Z. Mi, Y. Jiang, The important role of albumin in determining the relative human blood stabilities of the camptothecin anticancer drugs (letter) (published erratum appears), J. Pharm. Sci. 84 (1995) 518–519.

[53] J.G. Liehr, A.E. Ahmed, B.C. Giovanella, Pharmacokinetics of camptothecins administered orally, Ann. NY Acad. Sci. 803 (1996) 157–163.

[54] S.S. Daud, M.I. Fetouh, B.C. Giovanella, Antitumor effect of liposome-incorporated camptothecin in human malignant xenografts, Anti-Cancer Drugs 6 (1995) 83–93.

[55] T.G. Burke, X. Gao, Stabilization of topotecan in low pH liposomes composed of distearoylphosphatidylcholine, J. Pharm. Sci. 83 (1994) 967–969.

AMERICAN CANCER SOCIETY
HOLLAND • FREI
Cancer Medicine 5e
Bast Kufe Pollock Weichselbaum Holland Frei
www.BCDecker.com

Animal Tumor Models

The selection of the appropriate experimental model is critical to cancer drug discovery and development. The value of the model depends on its validity, selectivity, predictability, and reproducibility. [17–19] In cancer drug development, the animal model is selected to demonstrate the cytotoxic effect of the drug or biologic agent on the tumor passage in that model system.

There is no perfect tumor model for any human cancer. Nevertheless, in selecting the best model system, consideration should be given to the genetic stability and heterogeneity of the transplanted cell line, its immunogenicity within the host animal, and the appropriate biologic end point (local growth, metastasis, survival). For example, the KHT sarcoma is a tumor with high metastatic potential, making it a very suitable model for the evaluation of a combined-modality treatment[20] or inhibitor of metastasis.

In general, animal tumor models can be divided into either spontaneous or artificially transplanted systems. Solid tumors are usually transplanted by the inoculation of cell suspensions by the subcutaneous (SC), intradermal (ID), intramuscular (IM), intraperitoneal (IP), or intravenous (IV) routes. Leukemia models are transplanted only by the SC, IV, or IP routes.

The spontaneous tumor models that are idiopathic or that arise following carcinogenic [21, 22] or viral exposure mimic the clinical situation most closely. Spontaneous tumors are usually measurable only late in their course. Their metastatic pattern is not uniform, and their response to therapy is generally poor. They also resemble human cancers in kinetics and antigenicity. However, there are significant obstacles to the use of such model systems. For example, a relatively small percentage of animals may develop disease following exposure to carcinogen or virus, and the tumors may have a variable natural course. In addition, the inability to establish accurate staging makes these models quantitatively unsuitable for assessing therapeutic response to an agent given in a uniform fashion. Generally speaking, spontaneous tumor models have their greatest role in studying the biology of

human lung...
Figure 42.6. X-ray of a lung field...
Figure 42.7. Orthotopic in vivo human lung...
Figure 42.8. Human colon cancer cells grown...

Tables
Table 42.2. Orthotopic Models for Study of...

Search
Go
This book All books
PubMed

carcinogenesis. In the future, they may also be important in the development of chemopreventive or chemosuppressive drugs.

The models with the widest use in experimental therapeutics are the transplanted animal tumor models and the human tumor xenografts. These will be discussed in some detail below.

Transplantable Animal Tumor Models

Early passages of transplanted tumors resemble spontaneous cancer most closely. These early passages show significant heterogeneity in cell kinetics and histology. [23, 24] Despite these limitations, such models have been used in drug screening. Because established transplantable tumor models are well characterized and reproducible, they have traditionally been the foundation of cancer drug development. [25–27] How good are they in predicting clinical activity?

Multiple studies have been undertaken to assess the ability of preclinical animal activity to predict antitumor response in man. [9, 28, 29] Marsoni and co-workers evaluated the activity of all cytotoxic drugs introduced into phase II clinical trial by the NCI between 1970 and 1985. [30] Of the 75 drugs entered into clinical trial during this period, 24 showed some evidence for clinical activity. One interpretation of these data is that the screen is highly predictive for clinical activity. Approximately 30% of drugs taken to clinical trial showed some evidence of activity. However, 74% of the drugs were active against lymphoma, and 35% were active against leukemia. Only minimal activity was observed against solid tumors, including those represented in the phase II portion of the screen. Indeed, analysis showed a poor correlation between preclinical in vivo and clinical activity in the same tumors. One must conclude that either animal model systems using transplantable tumors do not predict for clinical activity or that the P388 prescreen effectively selected against compounds specifically active in human solid tumors. The new in vitro human cell–line screen will be important in answering these questions, since the initial identification of activity is in a human solid tumor rather than a murine leukemia-lymphoma model system.

A range of methods can be used to evaluate drug effect on tumors in animal models. Tumor size and tumor weight or volume changes are simple and easily reproducible parameters. Morphologic changes and alterations in tumor immunogenicity or invasiveness are other markers of response.[31]

In addition, many specific assays have been developed for the measurement of treatment effects on tumors. This section will discuss some assays that can be used to judge tumor response.

Excision Clonogenic Assay.

This assay has been used widely as a method to assess what fraction of cells in a tumor population retain proliferative capability after being exposed to a

chemotherapeutic agent. This assay is based on the assumption that the proliferative or clonogenic potential of tumor cells reflects the in vivo tumorigenicity of the tumor stem cell.[32] Thus, colony number is assumed to be proportionate to the number of viable cells.

The assay itself is straightforward. Tumor-bearing animals are tested with the drug under evaluation. At 24 hours, the tumors are excised from treated and untreated animals. A cell suspension is prepared from every tumor. The proliferative capacity of the cells in each suspension is evaluated either by in vivo inoculation intravenously into test animals of a selected cell suspension dilution[33,34] or by plating the cells in liquid or agar medium. [35,36] If an animal model is used, a colony count is then performed in specific tissues at necroscopy. The lung, liver, and spleen are commonly used for this purpose. If the cells were plated in agar, a colony count is performed in the dish. Colony-forming efficiency (CE) of the inoculated cells is calculated to assess the efficacy of treatment in terms of cell survival, as follows:

$$\text{CE} = \frac{\text{number of tumor colonies counted}}{\text{number of tumor cells plated}}$$

The ratio of the CE treated to the CE control is called *surviving fraction* (SF):

$$\text{SF} = \frac{\text{CE treated}}{\text{CE control}}$$

SF is the best parameter for expressing cell survival results from the excisional biopsy. [37, 38] This assay has the advantage of placing the treated and untreated tumors in identical environments. It is also able to select a resistant population of cells within the tumor at a low drug dose. In addition, excising the tumor 24 hours after exposing the animal to the cytotoxic agent allows giving doses up to the transplant range, which has important implications for the selection of agents for bone marrow transplantation. ↑ TOP

TD50 (End-Point Dilution Assay).

ZD50[39] is the tumor cell inoculum that produces tumor growth in 50% of inoculated animals or sites. It is a measurement of the number of cells required to produce tumors from inocula in vivo. The assay is based on the same principles as that of colony formation. A cell suspension is prepared from both treated and untreated animals, with ranges of dilutions for each tumor depending on the expected value of TD50. The suspension is inoculated into groups of test animals subcutaneously, intramuscularly, or intradermally for solid tumors and intraperitoneally or intravenously for leukemias. The percentage of tumor take versus cell number inoculated for each treatment is determined and compared to control animals to determine TD50. ↑ TOP

Tumor Growth Delay Assay.

Cytotoxic treatment can slow tumor growth and delay disease progression. These effects are measured by the tumor growth delay assay.[40] Tumor delay by definition is the time required for the treated tumor to reach a specific size minus the time for the untreated tumor to reach that certain size. This assay involves a very simple technique, little equipment, and can be completed for many types of tumors before animals are lost to metastasis or disease progression. Unlike the survival time assay discussed later, this evaluation does not require death as an end point.

The correlation between the growth delay and the amount of cell kill varies with the growth rate of the tumor.[40] Thus, when a treatment effect on tumors with different growth rates is assessed, a comparison of absolute growth delay between tumor models is misleading. Therefore, a specific growth delay (growth delay/doubling time of the tumor) reflects more accurately the differences in cell kill. Figure 42.3 illustrates the concept of specific growth delay. TOP

Survival Time Assay.

Another parameter that can be used to assess the effect of a drug on a tumor in the animal model is the survival time. Survival time is an obvious end point since it combines the sum total of interactions between tumor, drug, and host. Since drug toxicity and tumor growth both have independent effects on survival, a judgment can be made about therapeutic index. However, this approach cannot directly assess cell kill or time-dependent cytotoxicity.

The therapeutic efficacy can be assessed by determining the increase in survival as an effect of the escalating dose of the studied drug. As the dose of an active drug increases, the survival time increases because of increasing logarithmic tumor cell kill. Survival time reaches a maximum point as the toxic effect of the drug outweighs the therapeutic effect, and survival times diminish.[41] The maximum point of survival is called the optimal point (OP) or the maximum increase in lifespan (IL). The higher the OP, the better the given intervention's therapeutic efficacy. This model also helps in assessing the safety of certain drugs by measuring the therapeutic ratio (TR), i.e., the ratio between the optimal dose and the dose that leads to a specific increase in survival time (e.g., IL 20, IL 40, and so on). Therefore, in comparing drugs with the same maximum survival (optimal point), the higher the therapeutic ratio, the safer the drug.[41]

A common use of survival to assess drug efficacy or increase in lifespan is the *T/C* percent ratio. This is defined as the ratio of the survival time of treated animals to the survival time of control, expressed as a percentage. This parameter has been used by the NCI for decision making, setting specific criteria of activity before further development is undertaken. A *T/C* of .120 in the solid tumor panel has been used as the benchmark for clinical development (see Fig. 42.1). [42–44] TOP

Animal Tumor Xenografts

Before the availability of athymic or nude mice, human tumors were xenografted in mice immunocompromised by irradiation, thymectomy, or steroids. [45] The first nude mice arose spontaneously in a closed (but not inbred) colony of albino mice in a virus laboratory in Ruchill Hospital, Glasgow, Scotland,[46] and were described by Isaacson and Cattanach as lacking fur. The first xenograft in nude mice was performed by Rygaard and Povlsen in 1969 using a human colon adenocarcinoma. [47]

Flanagan initially described the genetic component of immunodeficiency in this important model. He found that the mutant gene (*nu*, for nude) is present on chromosome 11 as an autosomal recessive gene. [48] It is responsible for the absence of hair in addition to other abnormalities including retarded growth, low fertility, and short lifespan (100% mortality within 25 weeks of birth and 45% mortality within 2 weeks of birth).[46] It was not until 1968 that Pantelouris noted that some of the nude mice lacked a thymus gland. These mice were found to have a homozygous mutation *nu/nu*, while both the phenotypically normal 1/1 and the heterozygous *nu*/1 had a thymus. [49] Immunologically, the *nu/nu* athymic mice have a small number of T cells that are residual after transplacental passage from heterozygous mothers.

However, these T cells do not affect the rejection of tissue transplants (or other markers of T-cell function). [50] These animals preserve B-cell function [51] and exhibit a higher activity of natural killer cells.[52,53] These characteristics led to widespread use of nude mice in tissue transplantation and other areas of biomedical research, [48,54] including their use in human tumor transplantation.

The success of human tumor xenografting into the nude mice and the ability to maintain the histologic and biologic identity of tumors through successive passages in vivo revolutionized many aspects of cancer research, including drug development. [55–58] Transplantation of tumor cell lines into nude mice can be accomplished via multiple routes: subcutaneous, intraperitoneal,[59] intravenous, intracranial, [60] intrasplenic, renal subcapsular, or through a new orthotopic model by site-specific organ inoculation. Each site has specific advantages and limitations.

Subcutaneous implantation is the predominant site for transplantation of human tumor into the nude mouse because of its simplicity and easy access to tumor. Indeed, it provides the mainstay for in vivo testing of the drug discovery and screening program of the NCI.[61]

A tumor cell suspension is usually injected into the flank of the animal. Depending on the clonogenic potential of the tumor, between 106 and 107 cells are required for successful engraftment. Tumors usually require between a few days to a few months to grow, depending on the growth rate of the cell line used. Many human tumor xenografts have been established to date, including those from most of the solid tumors affecting adults. Human colon

cancer and melanoma have been passaged for the longest time in vivo. Brain tumors have proven the most difficult to maintain.[62,63] Approximately one-half of the brain tumor cell lines have been successfully xenografted into athymic mice.[62]

Of interest, subcutaneous xenografts metastasize infrequently and seldom invade adjacent tissues. This may be because of the retention of some host defenses, especially natural killer cell activity.[52,53] Thus, animal survival is not a feasible end point for assessing drug efficacy in nude mice, since large tumor burdens prior to death may be associated with discomfort. Instead, growth delay or clonogenic assay would be more appropriate in this model. However, it is possible to select primary tumors or to perturb the host defense mechanisms to develop models that are locally invasive or metastatic. Metastasis can be enhanced with the depletion of NK cells by pretreating the mice with cyclophosphamide, beta-estradiol, or other agents. [64, 65]

Human tumor cells undergo kinetic changes after transplantation and passage in the nude mice. Most frequently, the transplanted tumor adapted to growth in animals has a shorter doubling time than the original tumor isolated from a patient. Growth rates increase further during subsequent passages. [66] The vascularity of the primary and transplanted tumor also differ, with transplanted tumors showing better blood supply and less necrosis. This difference could be due to selection of the most rapidly growing cells from a heterogeneous primary animal, secretion of paracrine growth factors (which induce neovascularization), or simply tumor size.

Despite these changes in kinetics of invasive potential, the majority of the xenografted human tumors maintain the morphologic and biochemical characteristics of their original tumors. Therefore, it is expected that chemosensitivity would be similar in both the original and the xenografted human tumor, and that this correlation would predict for both active single agents and active drug combinations. In fact, excellent correlations can be made between average growth delay for human tumors in nude mice treated with the best available drug combinations and complete clinical response rates. [67] In increasing order of responsiveness, these correlations have been shown for human xenografts of non–small cell lung cancer, [55] colon cancer, [68] breast cancer,[69] and malignant melanoma. [11]

Renal Subcapsular Assay (RSC).

Unlike the subcutaneous xenograft assay, the renal subcapsular assay has a relatively short and constant period between tumor inoculation and the appearance of a grossly palpable mass. Tumors can usually be assessed in a period of 6 days. [70] Therefore, this model is particularly appropriate when a short-term in vivo assay is required. Cells are inoculated as a tumor fragment, usually 1 mm in size, under the kidney capsule of the nude mouse, as first described by Bogden and colleagues in 1978. [42] These tumors maintain true morphologic, functional, and growth characteristics of the original tumor

from which they were derived. [71] For example, they preserve cell-cell contact, maintain the spatial relationship of the tumor, and form a more representative model of human metastasis than the subcutaneous xenograft. Therefore, tumor response can be subsequently assessed by measuring tumor size (growth assay), colony formation by surviving cells (clonogenic assay), or simply animal survival. [72–74]

While appealing in many ways, the RSC has limitations. The subcapsular area of the kidney is not a totally immunoprivileged site. When sectioned and examined microscopically, variable amounts of tumor mass represent invading lymphocytes. [75,76] Thus, the immunogenicity of a given tumor in a given animal model is an important variable to control, and considerable controversy surrounds the use of this assay. [72] However, as will be discussed later, it might be an ideal orthotopic model for renal cell carcinoma (see below). [77] TOP

Intraperitoneal, Microencapsulated Tumor Assay

Because of the limitations of the RSC and its specific poor adaptability to slow-growing tumors, [71] alternative short-term in vivo assays have been developed. One of the more interesting is the microencapsulated tumor assay, which depends on microencapsulation technology. Tumor cells are encapsulated in semipermeable gels that can be formed into microcapsules of from 0.05 to 1 mm. [78] These microcapsules can be inoculated into the peritoneal space of experimental animals. Under typical assay conditions using mice, approximately 600 microcapsules are injected into the peritoneum. The semipermeability of the capsule protects the tumor cells from host cell–mediated immune cytotoxicity, so that athymic (nude) mice need not be used. At the same time, it allows nutrients and systemic cytotoxic agents to diffuse and reach the tumor cells. Anticancer effect is assessed by recovering microcapsules and counting viable tumor cells in treated versus control animals (Fig. 42.4). [79]

The microencapsulation assay is simple, rapid, and relatively inexpensive. For a given analysis, it requires fewer mice when compared to the subcutaneous transplanted tumor assay. [79] By definition, tumor cells are evaluated after exposure to drug concentrations that are obtainable in vivo. In addition, the system is adaptable to most solid tumors and, unlike the subcutaneous transplanted tumor assay, uses immunocompetent mice. For these reasons, the microencapsulated tumor assay is being evaluated by the NCI screening program as an in vivo second-line screen to follow initial drug leads that pass the in vitro screening system previously described.

Orthotopic Xenograft Model.

In 1889, after analyzing autopsies from patients with metastatic breast cancer, Paget concluded that metastasis is not a random phenomenon. Rather, he concluded, the malignant cells have special affinity for growth in the

environment of certain organs, the familiar seed-and-soil hypothesis.[80] Certainly, there exist organ site-specific interactions that are essential for optimal growth and progression of cancer in vivo. [81] The orthotopic xenograft model is a system in which tumor cells are implanted at the site of the organ of origin. This organ-specific site presumably provides the tumor cells with an optimal environment for growth and progression. Because of its relevant expense and novelty, this model has as yet not been used widely by the NCI drug-screening program. However, it is being used extensively to explore its role as an in vivo evaluation model for cytotoxic agents specific for organ sites such as the lungs in lung cancer.

Multiple tumor xenografts, including renal cell carcinoma, [64] pancreatic carcinoma, [47] certain brain tumors, [82] and prostate, colon, and (to a larger extent) lung cancer, have already been developed using nude mice (Table 42.2).[83] All of these models are potentially amenable to orthotopic development.

The lung tumor model is the predominant orthotopic model that has been explored by the NCI, [81] and application of other models is currently under way. In the case of lung cancer, tumor cells in suspension are inoculated through the right main stem bronchus into the right lung in a lightly anesthetized animal (Fig. 42.5). Tumor response can be evaluated by sacrificing the animal and histologically quantifying tumor growth, or, as shown in Figure 42.6, noninvasive chest x-rays may be sufficient to provide interim evaluation of tumor response.

Another approach toward establishing a lung tumor orthotopic model is through percutaneous intrathoracic implantation (Fig. 42.7).[83] A disadvantage to this model is the finding that as many as 30% of the inoculated tumor grows outside the lung parenchyma, either in the pleural space or the chest wall. Tumor-related mortality from the intrabronchial model is higher than that of intrathoracic implantation. Both orthotopic approaches have a much higher tumor mortality than the subcutaneous model of the same tumor cell line.[83] The far greater aggressiveness of identical inoculates of lung cancer injected into the bronchus compared with subcutaneous injection is a reflection of Paget's early observation on tumor cell tissue tropism and suggests that orthotopic models may reflect the clinical situation most closely. [84] TOP

Hollow Fiber Technology.

Recently, the NCI has incorporated semipermeable hollow-fiber assays into the in vivo phase of drug development. These hollow fibers allow tumor cells to grow in contact with each other, either in the log or stationary phases of cell growth (Plate 12, Fig. 42.8). The permeability of the fibers can be selected to limit the molecular weight of drug, which can penetrate into the tumor mass. A practical advantage of this system is that more than one tumor type can be implanted into a single animal, allowing more information to be

obtained from a single in vivo experiment. In addition, the system may be adaptable to epithelial cells, in an attempt to screen for compounds that interfere with angioneogenesis. Because this is an in vivo system, the agent must be bioavailable to show activity, correcting for the variables of serum protein binding and drug metabolism.

Another potential advantage of hollow-fiber technology is that it allows the successful maintenance of allogeneic and xenogeneic cells in immunocompetent hosts, thereby decreasing the costs associated with in vivo drug development considerably.

As currently used in the NCI program, malignant cells derived from patients with breast, kidney, lung, ovary, colon, central nervous system (CNS), hematologic, and melanoma cancers are encapsulated in polyvinylidene fluoride hollow fibers, which exclude molecules with a molecular weight of 500,000 or greater. The fibers are then implanted either subcutaneously or intraperitoneally, with each animal hosting six samples representing three tumor cell lines each, cultured both in the peritoneal and subcutaneous spaces. Already, this technique has shown promise with known active drugs, and hollow-fiber technology is increasingly being adapted to the in vivo phase of cancer drug development. TOP

ANTICANCER RESEARCH 4: 133-140 (1984)

Monoclonal Antibody Localization in Subcutaneous and Intracranial Human Glioma Xenografts: Paired-Label and Imaging Analysis

MARIO A. BOURDON[1], R. EDWARD COLEMAN[2], RONALD G. BLASBERG[3], DENNIS R. GROOTHUIS[4] and DARELL D. BIGNER[1]

[1]*Department of Pathology;* [2]*Department of Nuclear Medicine, Duke University Medical Center, Durham, NC 27710;* [3]*Department of Nuclear Medicine, Clinical Center, National Institutes of Health, Bethesda, MD 20205;* [4]*Department of Neurology, Evanston Hospital, Evanston, IL 60093, USA*

Abstract. *The murine antiglioma monoclonal antibody 81C6 has been shown to specifically localize in U-251 MG and D-54 MG human glioma subcutaneous and intracranial athymic mouse xenografts expressing the human glioma-mesenchymal extracellular matrix glycoprotein GMEM. In paired-label studies 81C6 reached peak levels of localization in subcutaneous and intracranial xenografts in 24 to 48 hours and persisted there for an additional 5 to 7 days before declining. The percent localized 81C6 in U-251 MG subcutaneous xenografts was tumor size dependent ranging from 2% in 200-300 mg tumors to 15% in 1 gram tumors. Subcutaneous xenografts of U-251 MG were readily radioimaged from 1 up to 6 days following administration of 131-I-81C6. The specificity of 81C6 localization has also been demonstrated by tissue autoradiography, elution of radiolabeled 81C6 from tumor xenografts, and in vivo inhibition of radiolabeled 81C6 localization by unlabeled 81C6. D-54 MG intracranial xenografts were permeable to 81C6 and control immunoglobulin but specific localization occurred only with 81C6. Radiolabeled 81C6 monoclonal antibody and U-251 MG and D-54 MG human glioma xenografts provide a useful operationally tumor specific monoclonal antibody tumor localization model for the examination of monoclonal antibody pharmacokinetics, radioimaging, radioimmunotherapy and combined modality therapy in intracranial human glioma xenografts.*

Human anaplastic gliomas have a very poor prognosis despite surgery and combined radiation and chemotherapy (1, 2). Immunologic approaches such as antibody mediated radioimaging and immunotherapy may offer the possibility of improvement in both diagnosis and treatment of human gliomas.

Key Words: Monoclonal antibody, human glioma, xenograft, radioimaging, tumor localization.

Correspondence: Prof. Darell D. Bigner, Department of Pathology, Box 3156, Duke University Medical Center, Durham, North Carolina 27710, USA.

Previous studies have demonstrated the potential of antibody radioimaging of human brain tumors (3, 4, 5, 6, 7). Nevertheless, major limitations of polyclonal and monoclonal antibodies in brain tumor radioimaging have been limited availability of specific antibody, low levels of radiolabeled antibody in the tumor, and the need for subtractive imaging techniques (8, 9).

In an effort to elucidate the pharmacokinetic and physiologic parameters involved in monoclonal antibody brain tumor localization we examined antiglioma monoclonal antibody 81C6 human glioma xenograft localization in U-251 MG and D-54 MG subcutaneous and intracranial human glioma xenografts in athymic mice. Monoclonal antibody 81C6 defines a distinctive human glioma associated extracellular matrix glycoprotein (GMEM) expressed by human anaplastic gliomas but not detected in normal human brain (10). Monoclonal antibody 81C6 was chosen for these studies on the basis of its well characterized reactivity with the target antigen; high levels of target antigen expression in U-251 MG and D-54 MG xenografts; and stable target antigen expression in the extracellular matrix of the glioma xenografts. Although not human tumor specific, the GMEM determinant with which 81C6 reacts is species specific. The expression of GMEM in human glioma xenografts provides an operationally tumor specific antigenic determinant model for the examination of 81C6 localization in human gliomas.

Since our ultimate goal is to evaluate radioimmunotherapy of human glioma xenografts with radiolabeled 81C6 either alone or in combination with chemotherapeutic agents, we chose to examine 81C6 localization in xenografts of the human glioma cell lines U-251 MG and D-54 MG. Both transplanted human glioma cell lines have stable growth characteristics in athymic mice (11) and have been used as sensitive human glioma treatment response models for radiation and chemotherapy studies (12). Radiolabeled 81C6 glioma xenograft localization was first examined in subcutaneous tumors which

are permeable to drugs and antibody and subsequently in intracranial tumors which may have limited and heterogeneous permeability characteristics (13).

We have demonstrated specific 81C6 localization in U-251 MG and D-54 MG human glioma subcutaneous xenografts in athymic mice and have successfully radioimaged U-251 MG subcutaneous xenografts. In addition we have shown that D-54 MG intracranial xenografts are permeable to monoclonal antibody and control immunoglobulin and that specific localization of radiolabeled 81C6 occurs in intracranial gliomas but not in other organs. Radiolabeled 81C6 administration to athymic mice bearing U-251 MG and D-54 MG gliomas should be useful for evaluation of radioimmunotherapy and combined modality therapy prior to human clinical investigation.

Materials and Methods

Cell Lines. Human and murine cell lines were cultured in Richter's zinc option minimal essential medium with 10% fetal calf serum as previously described (14). Human cell lines U-251MG, D-54MG and 2T have been described (14, 15).

Monoclonal Antibody. Monoclonal antibody 81C6 is an IgG_{2b} purified from hybridoma culture supernatant using protein A-Sepharose 4B (16). The IgG_{2b} myeloma immunoglobulin from 45.6TG1.7 was purified by the same procedure. Immunoglobulin radiolabeling with 131-iodine or 125-iodine (New England Nuclear) was performed by the chloramine T method (17). In paired-label experiments, both 81C6 and 45.6 control immunoglobulin were labeled to a specific activity of 2 to 4 μCi/μg protein. In radioimaging experiments 81C6 was labeled with ^{131}I to specific activities of 6.5 to 12.5 μCi/μg protein.

Radiolabeled immunoglubin was chromatographed on a 10 ml Sephadex G-25 fine column to separate labeled immunoglobulin from free iodine and injected i.v. into the tail vein of recipient mice within 4 hours of labeling. The radiolabel in these preparations was 97 to 99% trichloroacetic acid precipitable.

Human Tumor Xenografts. Human glioma cell lines U-251MG and D-54MG subcutaneous tumors were passaged in nude mice as described (11). An appropriate volume (30-50μl) of tumor homogenate was implanted subcutaneously in the right flank. The estimated tumor weight was determined twice weekly according to the formula [(short dimension)^2 × (long dimension)]/2 (11). Intracranial tumor xenografts were prepared as previously described (12). Tumor tissue homogenates from D-54MG subcutaneous tumor xenografts in athymic mice were prepared in an equal volume of 1% methyl cellulose (Fluka, Switzerland) in minimum essential medium and 5 μl injected into the cranium over the right cerebral hemisphere at a depth of 4 mm. using a Hamilton syringe fitted with a 26 gauge needle and plastic depth gauge. Intracranial tumor size was estimated from measurements of intracranial tumors in additional animals xenografted for this purpose.

Paired-Label Immunolocalization. 81C6 immunolocalization in human tumor bearing nude mice was determined by paired-label analysis (18). Mice bearing subcutaneous tumors between 200 to 300 mg were injected in the tail vein with a radiolabeled immunoglobulin preparation containing 10-20 μCi/5 μg ^{125}I-81C6 and 10-20 μCi/5 μg ^{131}I-45.6 or the reciprocal paired label combination. Athymic mice bearing 3 to 4 mm. diameter intracranial D-54MG tumors were injected in the tail vein with 10-20 μCi/5μg of both 125-I labeled 81C6 and 131-I labeled 45.6. Mice bearing intracranial xenografts were also injected via the tail vein with 200 μl Evan's blue (2%) one hour prior to being sacrificed. At each time point 3 subcutaneous and 3 intracranial tumor bearing mice were anesthetized with metaphan and blood samples were obtained by cardiac puncture using heparinized syringes. Following death by anesthesia and whole body perfusion with isotonic saline containing 5% dextrose, tumors and normal tissues (heart, lung, liver, kidney, spleen, muscle, brain) from both subcutaneous and intracranial tumor bearing mice were taken for weighing and gamma counting. Brains from intracranial tumor bearing mice were dissected into right and left cerebral hemisphere and cerebellum-brain stem. Evan's blue staining areas were dissected out and counted following gamma counting of each brain area. The Levels of 131-iodine and 125-iodine in tissue samples were corrected for isotope decay and cross-over of 131-iodine counts in the 125-iodine counts. Dose standards were prepared at the beginning of each experiment. The localization index (LI), and tumor/tissue ratio were calculated as described by Moshakis *et al* (19). Subcutaneous and intracranial tumor 81C6 LI time course data were curve fitted by quadratic and linear squares regression analysis respectively. Plasma half-life data for 81C6 and 45.6 were analyzed by linear regression analysis and analysis of covariance.

Radioimaging. Mice bearing U-251MG tumor on the right flank were injected with 130-250 μCi/20μg ^{131}I 81C6 and 10 to 20 μCi/20 μg ^{125}I 45.6 in the tail vein. Images were obtained daily for 3 to 6 days with a gamma camera using a pin hole collimator. The gamma camera imaged only the higher energy ^{131}I activity. All animals were positioned at the same distance from the collimator. In order to maintain the mice in position during image aquisition mice were anesthetized with metaphan. The image data was acquired on a dedicated computer in addition to the analog images. Subtraction techniques or other modification of the image were not employed to enhance the resulting localization image. Image data were used to compare the amount of radioactivity in the tumor to the amount in the whole body.

Immunohistochemistry and Autoradiography. Peroxidase-antiperoxidase immunohistochemical staining of tissues was carried out as previously described with cold acetone (-20° C) fixed frozen tissue sections (20). Tissue autoradiography was performed using Kodak autoradiographic emulsion. Slides were stored at -70° C for 1 to 3 weeks before developing.

Results

Radiolabeled IgG Characterization. Radiolabeled 81C6 and 45.6 were characterized by gel chromatography on sephacryl S-300 and by cell surface radioimmunoassay (CS-RIA). Radiolabeled 81C6 eluted as a single peak on sephacryl S-300 in the position of IgG (Fig. 1a). Aggregates and low molecular weight breakdown products were not observed, indicating little or no structural damage to either immunoglobulin. A small free iodine peak was detected at the included volume. Plasma samples from tumor bearing mice taken 4 hours and 3 days following injection with ^{125}I-labeled 81C6 (Fig. 1b, c) or 45.6 were also chromatographed on sephacryl S-300. The clution profile of radiolabeled protein in the plasma samples was indistinguishable from that of the freshly labeled immunoglobulin.

Radiolabeled 81C6 has also been shown to saturably bind target antigen, as determined in CS-RIA against the human glioma cell line U-251MG (Fig. 2).

Paired-Label Analysis of 81C6 Subcutaneous Tumor

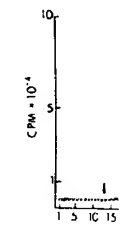

Fig. 1. *Sep preparation day plasma column usin Gel chroma monitored b cluded volu*

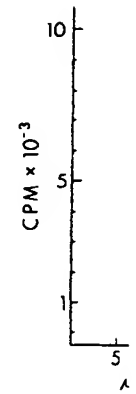

Fig. 2. *Bindi of U-251 MG 81C6 and 131I to washing a 125I counts a*

Fig. 3. *Plasm subcutaneous (B). Plasma va the mean ± st.*

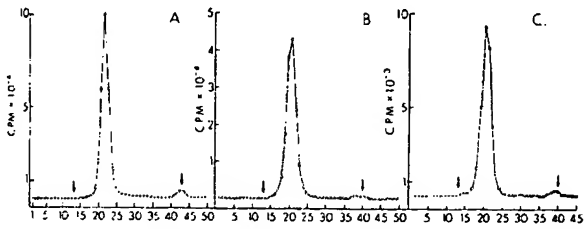

Fig. 1. *Sephacryl S-300 gel chromatography of (A) radiolabeled 81C6 preparation; (B) 4 hour plasma sample following i.v. injection and (C) 3 day plasma sample. Samples were chromatographed on a 0.9 cm × 56 cm column using 0.05M TRIS, 0.15M NaCl, 3mM EDTA pH 8.0 elution buffer. Gel chromatography of unlabeled 81C6 and normal mouse plasma was monitored by A280 absorption (not shown). Arrows mark void and included volume.*

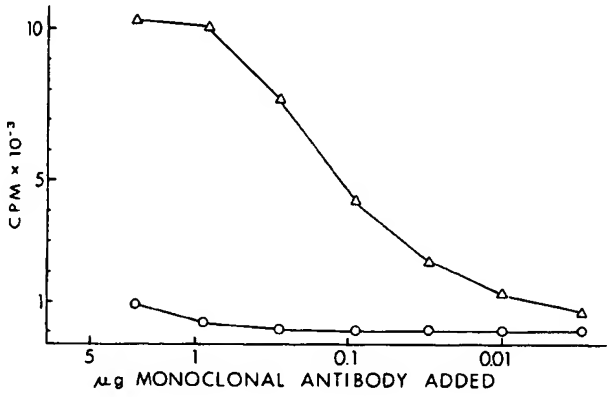

Fig. 2. *Binding of radiolabeled 81C6 (Δ) and 45.6 (O) to cell monolayers of U-251 MG in 96 well culture plates. Fifty μl samples containing ^{125}I-81C6 and ^{131}I-45.6 in HBSS, 0.5% BSA were incubated 1 hr at 37° C prior to washing and sample counting in a multichannel gamma counter. The ^{125}I counts are corrected for ^{131}I spill over.*

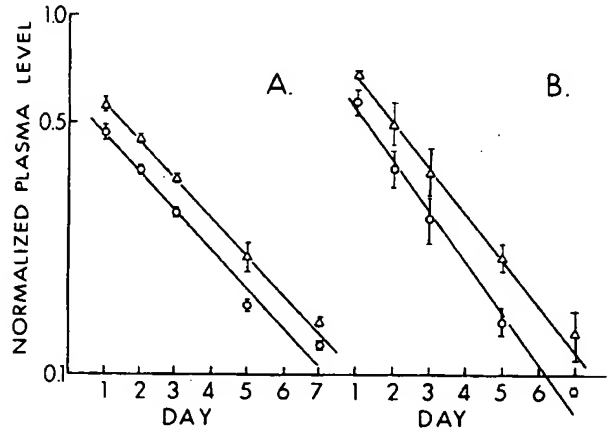

Fig. 3. *Plasma distribution of radiolabeled 81C6 (O) and 45.6 (Δ) in subcutaneous U-251MG tumor bearing (A) and non-tumor bearing mice (B). Plasma values are normalized to the 4 hour time point and represent the mean ± standard deviation for 3 animals in each group.*

Localization. The specificity and levels of 81C6 localization in glioma xenografts in athymic mice was determined by paired-label analysis. To determine the time course of 81C6 localization, mice bearing 150-200 mg U-251MG tumors were injected with ^{131}I-81C6 and ^{125}I-45.6 and blood and perfused tissue levels of each isotope analysed at 2 minutes, 4 hours, day 1 to day 8. In a second 15 day time course experiment ^{125}I-81C6 and ^{131}I-45.6 were injected into mice bearing 200-350 mg U-251MG xenografts. The plasma half life of both radiolabeled 81C6 and 45.6 in normal and subcutaneous tumor bearing mice was found to be approximately 2.5 days (Fig. 3). The plasma half-lifes of 81C6 and 45.6 were indistinguishable ($p < 0.001$) in sequential bleeds. However within the first 24 hours initial plasma levels of 81C6 declined more rapidly than 45.6 resulting in a small but significant difference ($p < 0.01$) in plasma levels for the two immunoglobulins (Fig. 3).

Tumor 81C6 LI increased over the first 5 to 6 days before beginning to decline on day 8 (Fig. 4). The peak tumor LI averaged 9 while tissue LI remained at approximately 1 at all time points (Fig. 4). Tumor/tissue ratios also increased over the first 4 to 6 days before declining in several tissues on day 8 (Table I). The percent injected 81C6 per gram tumor closely paralleled the LI and tumor/tissue ratio data. After rising over the first 4 days the percent injected 81C6 per gram tissue peaked at 3.6 ±0.8% before declining to 1.72 ±0.5% on day 8. Comparable results were obtained in the 15 day time course. At 15 days the percent 81C6 in tumor xenografts was still nearly half the peak levels of 81C6.

Utilizing the results of the paired-label time course experiment 81C6 localization was compared at a single time point (day 5) in nude mouse tumor xenografts (250-350 mg) of U-251 MG and D-54MG. Specific localization was seen in U-251MG and D-54MG glioma xenografts. Within the human glioma xenografts 81C6 LI averaged 7 and 9.5 in D-54MG and U-251MG tumors respectively (Table II). Normal tissue from mice bearing the U-251MG and D-54MG tumors had LI of 1.

The tumor to tissue ratio of 81C6 in the various normal organs of U-251MG and D-54MG tumor bearing mice ranged from 21 in heart to 235 in brain in U-251MG tumor bearing mice and from 15 in kidney to 107 in brain in D-54MG tumor bearing mice (Table II). In each group the tissue with the highest tumor to tissue ratio was brain. Nearly 5% of the initial injected dose localized in U-251MG tumors and 10% initial dose in D-54MG tumors. Control 45.6 immunoglobulin levels were 1.9% and 2.8% in U-251MG and D-54MG tumors respectively.

Tissue Autoradiography. Tissue autoradiography was carried out to determine the histologic localization of 81C6 in U-251MG subcutaneous xenografts. Radiolabeled 81C6 localized in the tumor extracellular stroma (Fig. 5a) but not in normal liver (Fig. 5b). The prominent 81C6 localization

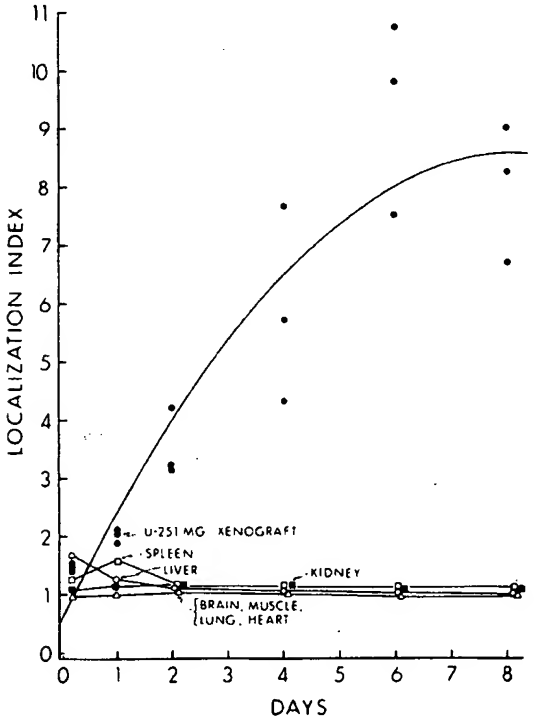

Fig. 4. *Paired-label analysis in U-251 MG glioma tumor bearing mice with ^{131}I-81C6 and ^{125}I-45.6.81C6 localization index (LI) was calculated as the tissue specific to nonspecific cpm ratio in the tissue divided by the specific to nonspecific cpm ratio in blood. The LI values are for 3 animals. The tumor LI curve is a quadratic least squares regression fit ($p < 0.04$) of LI values.*

in the extracellular stroma corresponds closely with the extracellular matrix distribution of antigen demonstrated by 81C6 PAP staining of frozen tissue sections of U-251MG tumors (10).

Elution of 81C6 from U-251MG Subcutaneous Tumors. The majority of tissue bound radiolabel in U-251MG tumors localizing ^{125}I-81C6 represents intact immunoglobulin. Pooled U-251MG tumor xenografts taken 5 days following injection of ^{125}I-81C6 in tumor bearing mice were repeatedly washed and tissue bound radiolabel eluted with 0.1M glycine buffer pH 3.0. The eluted counts were 98% trichloroacetic acid precipitable, and 89% of counts were precipitable in 50% saturated ammonium sulfate. The ammonium sulfate precipitate specifically bound to U-251MG cell monolayers but not negative control 2T monolayers and eluted as a single peak in the position of IgG on sephacryl S-200.

Inhibition of Radiolabeled 81C6 Localization. In vivo binding of radiolabeled 81C6 in U-251MG and D-54MG subcutaneous xenografts could be inhibited by excess unlabeled 81C6. In mice bearing moderately sized U-251MG tumors (640 mg) and receiving 20 μg 81C6, localization of radiolabeled 81C6 in the exenograft was inhibited 81% in animals receiving 1 mg unlabeled 81C6 2 hours prior to injection of radiolabeled antibody. Localization of 5μg radiolabeled 81C6 in 200 mg D-54MG xenografts *in vivo* was inhibited 76 % in animals receiving 1 mg 81C6 4 hours prior to injection of ^{125}I-81C6. No inhibition of radiolabeled 81C6 was noted in either U-251MG or D-54MG tumors in animals receiving 1 mg unlabeled 45.6.

Radioimaging of Human Glioma Xenografts. The potential of ^{131}I-81C6 in radioimaging human glioma xenografts in nude mice was assessed in U-251MG subcutaneous xenografts. In initial experiments mice bearing U-251MG tumors (1016 mg ± 11) were injected with 200 μCi/20 μg ^{131}I-81C6 and 10 μCi/20 μg ^{125}I-45.6. Images were obtained on days 1 to 3. Mice in groups of three were sacrificed on each succeeding day and analysed as in paired-label studies above. The U-251MG tumors were readily imaged beginning at 17 hours (Fig. 6). By 41 hours the blood pool levels had declined significantly while 81C6 levels remained constant as reflected in nearly constant radiolabel counts within the tumor. In the three animals imaged on each of 3 days total body image counts declined 70% in 3 days but tumor counts increased slightly over the same

TABLE I. *81C6 Tumor/Tissue Ratio[a] In U-251 MG Subcutaneous Xenografts.*

	4 hr	day 1	day 2	day 4	day 6	day 8
Heart	3[b]	7	8	10	11	12
Lung	5	5	8	13	8	11
Liver	2	7	16	20	19	17
Kidney	3	6	9	12	11	9
Spleen	1	2	4	7	8	6
Brain	27	22	48	37	52	30
Muscle	10	11	13	14	15	16
Tumor	1	1	1	1	1	1

a: Tumor/Tissue ratio is 81C6 tumor cpm/mg ÷ 81C6 Tissue cpm/mg.
b: Values are mean of 3 animals.

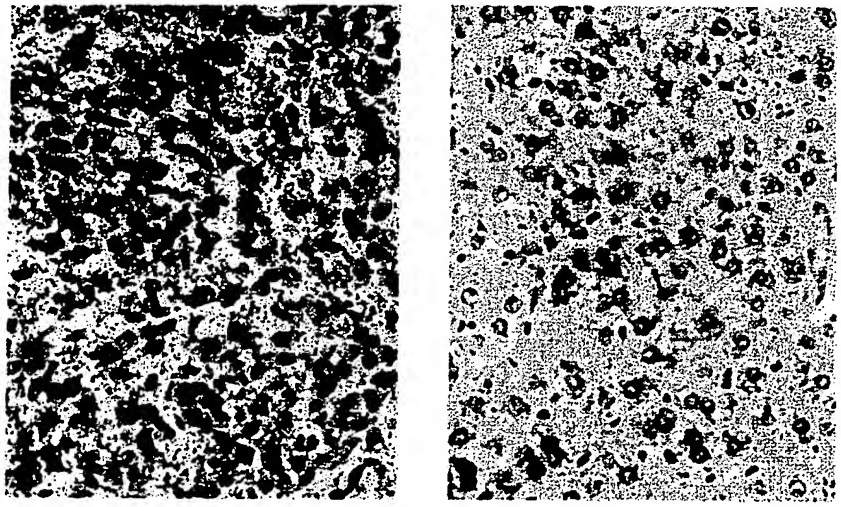

Fig. 5. *Tissue autoradiographic distribution of in vivo localized* ^{125}*I-81C6 in U-251MG subcutaneous xenografts (A) and liver tissues (B) processed five days following injection of* ^{125}*I-81C6. HE stain; 400X.*

time period in 2 of 3 animals and remained unchanged in one. The percent of total animal counts in the tumor rose from 22 ± 1% to 53 ± 3% over the 3 day time course while the percent of total counts within the tumor bearing mice exclusive of tumor declined from 78 ± 1% on day 1 to 46 ± 2% on day 3. To access the levels of 81C6 in the imaged tumors over the 3 day time course additional animals were sacrificed on day 1 and 2 following imaging to determine percent injected dose and localization index in the tumors. Imaging resolution and count levels were comparable to the group of three animals analysed for the entire 3 day time course. The percent injected dose for days 1 to 3 were 10.5 ± 6.4, 15.6 ± 1.8, and 15.5 ± 1% respectively. The localization index for days 1 to 3 averaged 5, 10, and 13.

In subsequent experiments tumors averaging 600 and 300 mg were successfully imaged over a 6 day time course following injection of 20 μg ^{131}I labeled 81C6 and 20 μg trace labeled ^{125}I-45.6. The levels of radiolabeled 81C6 were proportionally smaller in 600 and 300 mg tumors as determined by radioscintigraphy counts during the time course and by tissue gamma counting at the end of six days. The percent of total counts in the 600 mg group rose from 7.5 ± 1.5% to 32.3 ± 6.4% over 6 days while in the 300 mg tumor group the percent of daily total counts rose from 2.2 ± 0.5% to 12 ± 2.9% over the same time course. The percent injected 81C6 in 600 mg tumors after 6 days was 6.2% and in 300 mg tumors after 6 days, 2.4%.

Paired-Label Analysis of 81C6 Intracranial Tumor Localization. Levels of 81C6 and 45.6 in intracranial tumor were determined over a 6 day time course following excision of *in vivo* Evans'blue staining areas of the brain. The resulting

TABLE II. *81C6 Localization Index in Subcutaneous U-251 MG and D-54 MG Human Glioma Xenografts.*

	Localization Index[a]		Tumor/Tissue Ratio[a]	
	U-251 MG	D-54MG	U-251 MG	D-54 MG
Heart	0.97	1.0	21.5	15.7
Lung	0.91	1.1	23.2	28.5
Liver	0.79	0.6	98.0	27.6
Kidney	1.04	1.0	46.7	15.4
Spleen	0.86	0.5	25.2	19.2
Muscle	1.0	1.1	49.5	25.2
Brain	0.99	1.0	235.0	106.6
Tumor	9.47	7.05	1.0	1.0

[a] Mean of five animals sacrificed on day 5 following i.v. injection of radiolabeled 81C6 and 45.6.

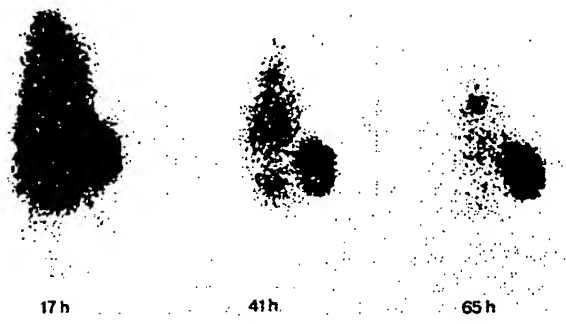

Fig. 6. *Radioimaging of U-251 MG xenografts in an athymic mouse was conducted on days 1 to 3 using a pin-hole collimator and computer image storage. Tumor bearing mice were injected with 200 μCi/20 μg* ^{131}*I-81C6. Images shown are from a single U-251MG tumor bearing animal.*

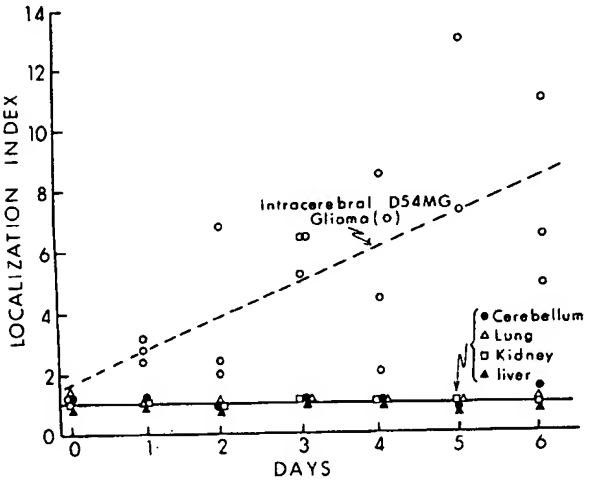

Fig. 7. *Localization index time-course in D-54MG intracranial xenografts and normal tissues of tumor bearing mice. Mice were injected with 7.5 μCi/5 μg ^{125}I-81C6 and 13 μCi/5 μg ^{131}I-45.6. Individual tumor localization index (O) and localization index linear regression curve ($p < 0.01$) (dashed line) are presented.*

localization indices show increased 81C6 localization in the excised tumor but not in remaining areas of left or right cerebral hemispheres (Fig. 7). Normal organs from tumor bearing mice did not localize 81C6.

Specific localization of 81C6 within the D-54MG intracranial xenografts was first observed on day 1. The localization index continued to rise over the next 4 to 5 days within the intracranial tumors. There was a linear increase in LI during the six day time course, similar to the rise in LI in subcutaneous xenografts; however, the range of LI in intracranial tumors (Fig. 7) was greater than observed in subcutaneous xenografts of D-54MG.

The relative specific activity of 81C6 in the glioma xenografts, compared to normal organs expressed as the cpm/mg tumor to tissue ratio, rose over the first 48 hours following injection of radiolabeled 81C6 and remained elevated throughout the 6 day experiment (Table III). The persistence of 81C6 in the intracranial tumors is indicated by the net percent injected 81C6 dose per gram of tumor above control 45.6 levels, which for day 1 to 6 were 2, 3.6, 3.1, 4.5, 8.1, and 5.4%, respectively. Normal organs had comparable levels of both 81C6 and 45.6 which declined in the same manner as the plasma levels.

TABLE III: *Tumor/Tissue Ratio of 81C6 in Athymic Mice Bearing D-54 MG Intracranial Tumors.*

	Day 1	Day 6
Heart	1.5	17.0
Lung	0.8	19.0
Liver	1.6	13.5
Kidney	1.4	7.5
Spleen	0.8	7.5
Muscle	2.7	16.0
Brain		
Left Hemisphere	14.4	12.5
Right Hemisphere	16.3	34.5
Cerebellum	12.9	122.5

Discussion

In this study we have demonstrated that radiolabeled antiglioma monoclonal antibody 81C6 specifically localizes in both subcutaneous and intracranial xenografts of the human glioma cell lines U-251 MG and D-54 MG in athymic mice; moreover, ^{131}I-81C6 can be used to image subcutaneous xenografts. In the well characterized human glioma xenograft model (2) we have been able to establish several of the pharmacokinetic parameters of 81C6 localization in an operationally tumor antigen specific system. Using paired-label analysis (18) in time-course experiments we have shown that both subcutaneous and intracranial D-54 MG xenografts are permeable to monoclonal antibody and have very similar localization kinetics. In both subcutaneous and intracranial xenografts 81C6 levels increase over the first 24 to 48 hours where they persist for 5 to 7 days before beginning to decline. This is reflected not only in the percent injected 81C6 localized but also in the linear increase in LI and tumor: tissue ratios during time-course experiments. We have also shown that the localization of 81C6 in tumor xenografts is the result of specific antigen binding. This has been demonstrated by the extracellular matrix distribution of radiolabeled 81C6 in xenograft autoradiographs following *in vivo* localization; this pattern corresponding to the extracellular matrix distribution of GMEM. In addition we have shown that a large majority of tissue bound radiolabel in subcutaneous xenografts has the properties of intact 81C6, and that radiolabeled 81C6 tumor localization can be specifically inhibited by unlabeled 81C6 but not control 45.6 IgG_{2b} immunoglobulin.

The results presented here are important for several reasons. First we have extended the analysis of antiglioma monoclonal antibody localization from subcutaneous glioma xenografts to intracerebral glioma xenografts, allowing the assessment of monoclonal antibody tumor localization within the special environment of the intracerebral tumor. The intracranial xenograft pharmacokinetic factors of particular interest in brain tumor imaging and immunotherapy include permeability to immunoglobulin (13) and levels of monoclonal antibody in the tumor and normal brain. In this study we have shown that D-54 MG intracranial xenografts are permeable to immunoglobulin and that 81C6 localizes in the tumor but not normal brain. Although the D-54 MG intracranial xenograft is permeable to immunoglobulin other human glioma

xenografts may be less permeable. Capillary permeability studies in five intracranial tumor models resulted in widely varying permeability in each model to the small molecular weight permeability probe α-aminoisobutyric acid (13). These results underscore the need to assess monoclonal antibody tumor localization in both subcutaneous and intracranial xenografts.

Second, the results demonstrate the potential of ^{131}I-labeled 81C6 for tumor imaging in subcutaneous glioma xenografts in athymic mice and point to the possibility of ^{131}I-81C6 radioimaging in intracranial glioma xenografts in larger animals. The large tumor: brain ratios in intracranial xenografts would likely result in enhanced radioimaging of intracranial xenografts and perhaps allow for radioimaging of tumors prior to the 24 hours necessary in subcutaneous xenografts. It may also be possible to enhance tumor radioimaging further by the use of radiolabeled F(ab′)$_2$ fragments of 81C6 as has been shown by Herlyn *et al.* (21) in the radioimaging of human colon carcinoma xenografts with monoclonal antibody.

Third, the results indicate that in both subcutaneous and intracranial xenografts 81C6 has the property of persisting over an extended period in the tumor xenograft, a characteristic relevant to its use in immunotherapy as a carrier of radiation or toxins (22).

Previous studies have demonstrated the potential of antibody radioimaging of human brain tumors. Immunolocalization and radioimaging of brain tumors was examined by DiChiro *et al.* (23) in human subjects using radiolabeled antifibrinogen antibodies prepared in rabbits. In this and subsequent studies (3, 4) about 80% of primary and metastatic brain tumors were detected. Day *et al.* (8) and Mahaley *et al.* (5) using radiolabeled affinity purified polyclonal antiglioma antibodies successfully localized antibody in 11 of 12 human gliomas. More recently Nelson *et al* (7) were able to image an adenocarcinoma brain metastasis using radiolabeled antibody to colon-specific-antigen-p. Major limitations of polyclonal antibodies in brain tumor radioimaging have been limited availability of specific antibody, low levels of radiolabeled antibody in the tumor, and the need for subtractive image techniques (8, 9). Modest results have also been obtained using a murine monoclonal antibody to image a colorectal carcinoma brain metastasis (6) and a human hybridoma immunoglobulin product to radioimage a recurrent glioma (24). The low monoclonal antibody to background ratios in the two studies make it unclear whether or not the radiolabeled immunoglobulins used specifically localized in the brain tumors, or offered any improvement over previous brain tumor radioimaging methods using radioiodinated serum albumin (RISA) or ^{203} Hg-Neohydrin (25) which accumulate, as a result of partial blood-brain barrier disruption, in brain tumors.

The use of human glioma xenografts for examining antiglioma monoclonal antibody tumor localization has provided a reproducible and reliable model for the examination of tumor localization and tumor imaging in a controlled manner not possible in human subjects. The localization studies reported here demonstrate the specific and persistent localization of 81C6 in both subcutaneous and intracranial human glioma xenografts over time. We have also demonstrated the potential of radiolabeled 81C6 for radioimaging glioma xenografts in an operationally antigen specific system. These studies have also provided a basis for analysis of regional 81C6 tumor localization pharmacokinetics (R.G.B.), future radioimaging, immunotherapy, and combined modality therapy studies.

Acknowledgements

The authors wish to thank Dr. Lawrence H. Muhlbaier for statistical analysis and Frances Slocum for her secretarial assistance in preparing the manuscript. This work was supported by NIH grants NS20023, CA11898 and CA32672 (D.D.B.), NIH RCDA grant and USPHS grant NS12745 (D.R.G.).

References

1 Walker MD, Alexander E, Hunt WE, MacCarty CS, Mahaley MS, Mealy J, Norell HA, Owens G, Ransahoff J, Wilson CB, Gehan EA, Strike TA: Evaluation of BCNU and/or radiotherapy in the treatment of anaplastic gliomas: a cooperative clinical trial. J Neurosurg *49*: 333-343, 1978.

2 Schold SC, Freidman HS: Human brain tumor xenografts. *In*: Rosenblum ML and Wilson CB (eds), Progress in Experimental Brain Tumor Research. Basel, S Karger. E983 (in press).

3 Marrack D, Kubala M, Corey P, Leavens M, Howze J, Dewey W, Bode WF, Spar IL: Localization of intracranial tumors: comparative study with 131-I-labeled antibody to human fibrinogen and neohydrin-203 Hg. Cancer *20*: 751-755, 1967.

4 McCardle RJ, Harper PV, Spar IL, Bale WF, Andros G, Jiminez F: Studies with iodine-131-labeled antibody to human fibrinogen for diagnosis and therapy of tumors. J Nucl Med *7*: 837-847, 1966.

5 Mahaley SM, Mahaley JL, Day ED: The localization of radioantibodies in human brain tumors II. Radioautography. Cancer Res *25*: 779-793, 1965.

6 Farrands PA, Pimm MV, Perkins AC, Hardy JD, Baldwin RW, Hardcastle JD: Radioimmunodetection of human colorectal cancers by an anti-tumor monoclonal antibody. Lancet *2*: 397-400, 1982.

7 Nelson DM, Deland FH, Shogat D, Bennett SJ, Goldenberg DM: External imaging of gastric-cancer metastases with radiolabeled CEA and CSAp antibodies. New England J Med *308*: 847, 1983.

8 Day ED, Lassiter S, Woodhall B, Mahaley JL, Mahaley MS: The localization of radioantibodies in human brain tumors I. preliminary exploration. Cancer Res *25*: 773-778, 1965.

9 Mach JP, Forni M, Ritchard J, Buchegger F, Carrel S, Widgren S, Donath A, Alberto P: Use and limitations of radiolabeled anti-CEA antibodies and their fragments for photoscanning detection of human colorectal carcinomas. Oncodev Biol Med *1*: 49-69, 1980.

10 Bourdon MA, Wikstrand CJ, Furtmayr H, Matthews TJ, Bigner DD: Human glioma-mesenchymal extracellular matrix antigen defined by monoclonal antibody. Cancer Res *43*: 2796-2805, 1983.

11 Schold SC, Bullard DE, Bigner SH, Jones TR, Bigner DD: Growth, morphology, and serial trasplantation of anaplastic human gliomas in athymic mice. J Neuro-Oncol *1*: 5-14, 1983.

12 Schold SC, Rawlings CE, Bigner SH, Bigner DD: Intracerebral

growth of a human glioma tumor line in athymic mice and treatment with procarbazine, BCNU, AZQ, *Cis*-platinum. Neurosurgery *12*: 672-677, 1983.

13 Groothuis DR, Molnar P, Blasberg RG: Regional blood flow and blood to tissue transport in five brain tumor models: implications for chemotherapy. *In*: Rosenblum ML and Wilson CB (eds), Progress in Experimental Brain Tumor Research, Basel, S. Karger, 1983 (in press).

14 Wikstrand CJ, Mahaley MS, Bigner DD: Surface antigenic characteristics of human glial brain tumor cells. Cancer Res *37*: 4267-4275, 1977.

15 Bigner DD, Bigner SH, Pontén J, Westermark B, Mahaley MS, Ruoslahti E, Herschman H, Eng LF, Wikstrand CJ: Heterogeneity of genotype and phenotypic characteristics of fifteen permanent cell lines derived from human gliomas. J Neuropath Exp. Neurol *40*: 201-229, 1981.

16 Ey PL, Prows SJ, Jenkin CR: Isolation of pure IgG_1, IgG_{2a}, and IgG_{2b} immunoglobulins from mouse serum using protein A-sepharose. Immunochem *15*: 429-436, 1978.

17 Greenwood FC, Hunter WM, Glover JS: The preparation of ^{131}I-labeled human growth hormone of high specific radioactivity. Biochem J *89*: 114-120, 1963.

18 Pressman D, Day ED, Blau M: The use of paired labeling in the determination of tumor-localizing antibodies. Cancer Res *17*: 845-850, 1957.

19 Moshakis V, McIlhinney RAJ, Raghaven D, Neville AM: Localization of human tumour xenografts after I.V. administration of radiolabeled monoclonal antibodies. British J Cancer *44*: 91-99, 1981.

20 Wikstrand CJ, Bourdon MA, Pegram CN, Bigner DD: Human fetal brain antigen expression common in tumors of neuroectodermal origin: Gliomas, neuroblastomas, and melanomas. J. Neuroimmunology *3*: 43-62 1982.

21 Herlyn D, Power J, Alavi A, Mattis JA, Herlyn M, Ernst C, Vaum R, Koprowski H: Radioimmunodetection of human xenografts by monoclonal antibodies. Cancer Res *43*: 2731-2735, 1983.

22 Bourdon MA, Coleman RE, Bigner DD: The potential of monoclonal antibodies as carriers of radiation and drugs for immunodetection and therapy of brain tumors. *In:* Rosenblum ML and Wilson CB, Progress in Experimental Brain Tumor Research, Basel S Karger, 1983 (in press).

23 DiChiro G, Spar IL, Bale WF, Loskowski EJ, Goodland RI, Matthews WB: "RIAF" radio-iodinated anti-fibrinogen encephalography. Acta Radiol Diagn *1*: 967-971, 1963.

24 Phillips J, Alderson T, Sikora K, Watson J: Localization of malignant glioma by a radioalabelled human monoclonal antibody. J Neurol Neurosurg Psychiatry *46*: 388-392, 1983.

25 Feindel W, Yamamoto YL, Rumin N: Comparison of radioactive iodinated serum albumin (RISA) and radioactive mercury^{203} for brain scanning. J Neurosurgery *21*: 1-6, 1964.

Received January 5, 1984

Evali

ANDREA

and [5]*Univ*

Abstract. *I*
stimulation
monal m
chemothera
attempt bee
perturbatio
schedules.
clinical tri
cancer usin
levels of t
(CEA) and
(GCDFP-1
monitoring
markers fa
trogens to p
men with
stimulation
exacerbatio
cancer, risk
and GCDF.
in tumor ce
tocols.

Preliminary
and breast
tion of tu
chemothera
prostate can
relatively r
is particular
current hyp

Correspondence
S. Hershey M

Key Words: C
breast cancer,

* This work w
tion Research

INVESTIGATIVE RADIOLOGY
Volume 28, Number 6, 488–496

Distribution and Dosimetry of I-123–Labeled Monoclonal Antibody 81C6 in Patients with Anaplastic Glioma

S. CLIFFORD SCHOLD, JR., MD,*¶ MICHAEL R. ZALUTSKY, PHD,†§ R. EDWARD COLEMAN, MD,† MICHAEL J. GLANTZ, MD,*‖ ALLAN H. FRIEDMAN, MD,‡ RONALD J. JASZCZAK, PHD,† SANDRA H. BIGNER, MD,§ AND DARELL D. BIGNER, MD, PHD§

Schold SC Jr, Zalutsky MR, Coleman RE, Glantz MJ, Friedman AH, Jaszczak RJ, Bigner SH, Bigner DD. Distribution and dosimetry of I-123–labeled monoclonal antibody 81C6 in patients with anaplastic glioma. Invest Radiol 1993;28:488–496.

RATIONALE AND OBJECTIVES. **Monoclonal antibody 81C6 reacts with the extracellular matrix antigen, tenascin, present on gliomas and other tumors, as well as several normal tissues, including spleen and liver tissue. Single photon emission computed tomography (SPECT) and I-123–labeled 81C6 at various protein doses were used to maximize tumor to normal tissue uptake ratios.**

METHODS. **The distribution of I-123–labeled monoclonal antibody 81C6 was determined in 16 patients with recurrent gliomas, using SPECT. Between 3.5 and 11.5 mCi of I-123 were administered to each patient, and the antibody doses were between 10.0 and 100.0 mg. Blood was obtained for pharmacokinetic studies, and patients were imaged 1 hour and 18 hours after antibody administration.**

RESULTS. **All tumors were visualized readily on the SPECT study in areas that corresponded to the contrast, enhancing abnormalities on anatomic neuroimaging studies. The half-life in blood of the I-123 81C6 ranged from 16 to 37 hours. Radiation dosimetry calculations suggest that it might be possible to administer more than 700 cGy to intracranial glioma with I-131 labeled 81C6 under optimal conditions with acceptable non-neurologic organ radiation exposure.**

CONCLUSIONS. **SPECT imaging with I-123 81C6 identified all tumors and suggests that, with this antibody, more favorable tumor-to-liver and tumor-to-spleen radiation dose ratios are obtained at higher protein doses.**

KEY WORDS. **Gliomas; monoclonal antibodies; radiation dosimetry.**

RADIOLABELED MONOCLONAL ANTIBODIES (MAbs) that have relative specificity for tumor tissue have been used to image and treat neoplasms in animals[1] and in people.[2,3] A variety of tumor types have been imaged and treated, including some gliomas.[4] Critical variables in the treatment of gliomas with radiolabeled MAbs include the specificity of the antibody and its access to the tumor. Because the specificity and kinetics of MAbs vary, each MAb must be evaluated individually regarding these factors.

81C6 is a murine MAb that reacts with an epitope of tenascin, an extracellular matrix antigen present on human glioma cell lines and primary human gliomas.[5] Preclinical studies with radiolabeled 81C6 have demonstrated selective accumulation[6] and therapeutic potential[1] in intracranial human glioma xenograft models. Specific localization of I-131 labeled 81C6 in brain tumors has been demonstrated in patients with gliomas and other intracranial malignancies.[7,8]

These results suggest that I-131 labeled 81C6 might be of potential use as a therapeutic agent in astrocytic neoplasms. However, a potential problem with using 81C6 MAb for radioimmunotherapy is that tenascin has been shown by immunohistochemistry also to be present on normal liver and spleen.[5] Planar imaging with I-131-labeled 81C6 in glioma patients demonstrated accumulation of activity in

From the *Department of Medicine, †Radiology, ‡Surgery, and §Pathology, Duke University Medical Center, Durham, North Carolina.

Current affiliation: the ‖Department of Clinical Neurosciences, Brown University School of Medicine, Memorial Hospital of Rhode Island, Pawtucket, Rhode Island, and the ¶Department of Neurology, The University of Texas Southwestern Medical Center at Dallas, Dallas, Texas.

Supported by NIH grants CA-33541, CA-32672, CA-42324, CA-11898 and NS-20023, training Grant T32-NS07304, DOE Grant DEFG0589ER60894, and Grant M01-RR-30 from the National Center for Research Resources (General Clinical Research Centers Program, NIH).

Reprint requests: Michael R. Zalutsky, PhD, Duke University Medical Center, Box 3808, Department of Radiology, Durham, NC 27710.

Received February 18, 1992, and accepted for publication, after revision, January 6, 1993.

these organs;[7] however, quantitation of uptake in liver and spleen was not possible from these images.

One approach for quantitating labeled MAb uptake in tissues of interest is single photon emission computed tomography (SPECT). Recently, Leichner et al.[9] have shown that SPECT could be used to quantitate In-111-labeled MAb uptake in the livers of dogs with an accuracy compared to autopsy data of approximately 5%. In the current study, we have used SPECT to quantitate the uptake of I-123–labeled 81C6 in liver, spleen, and tumor for a range of MAb protein dose levels. Our results suggest that at higher protein doses, more favorable tumor-to-liver and tumor-to-spleen uptake ratios are obtained.

Materials and Methods

Patients

Each patient enrolled in this study had clinical and radiographic evidence of recurrence of a previously biopsied and treated supratentorial anaplastic glioma. Each had received and failed radiotherapy and nitrosourea-based chemotherapy following surgery. Each patient signed an informed consent document that had been approved by the Institutional Review Board of Duke University. Patients received supersaturated potassium iodide (10 drops twice a day) and liothyronine sodium (Cytomel, SmithKline Beecham, Pittsburgh, PA) 75 to 100 mg per day for 3 days beginning at least 1 day before the labeled MAb injection to block uptake of I-123 iodide by the thyroid gland.

Monoclonal Antibody 81C6

Monoclonal antibody 81C6 is a murine IgG_{2b} antibody that is reactive with the extracellular matrix antigen tenascin, which is present in gliomas, but not in normal brain.[5] The MAb was harvested from ascitic fluid from athymic mice and was purified from hybridoma culture supernatant using Protein A Sepharose 4B chromatography (Pharmacia, Piscataway, NJ). The purified MAb was dialyzed against 50 mM phosphate buffered saline (pH 7.4), passed through a 22-μm filter, and stored at 4°C until needed. The MAb was documented to be free of bacterial and mycoplasma contamination by culture and assay in routine medium and free of murine viruses using guidelines suggested by the Food and Drug Administration.

Antibody Labeling

MAb 81C6 was labeled with I-123 using a variation of the original Iodogen method.[10] Iodine-123 was obtained from Nordion International (Kanata, Canada) in 0.1 M NaOH. To improve radioiodination efficiency, approximately 20 μl of 100 μg/ml sodium iodide carrier was added. The I-123–labeled MAb was purified by passage over a gas-sterilized, Sephadex G-25 column (Pharmacia, Psicataway, NJ). Protein-associated activity was determined by precipitation with trichloroacetic acid. The binding characteristics of each batch were determined in triplicate using a single-point homogenate assay at antigen excess. Approximately 100 ng of labeled MAb was diluted with phosphate buffer containing 1% human serum albumin and incubated at 37°C for 1 hour with D-54 MG human glioma[5], and normal rat liver homogenates. Specific binding was expressed as the percentage of I-123 bound to tumor minus the percentage bound to liver.

Blood Clearance Measurements

Blood samples were obtained at 5, 15, and 30 minutes, and at 1, 2, 4, 8, 18, 24, and 36 hours after MAb injection. Two-milliliter aliquots were counted for I-123 activity using an automated gamma counter and the percentage injected dose in the blood was calculated by comparison with standards prepared from the administered dose. In patients 10, 13, 14, and 16, the half-time of the fast component of blood clearance could not be calculated due to the lack of sufficient blood samples during the first hour after MAb injection.

Human Anti-Mouse Antibody (HAMA) Procedure

Monoclonal antibody 81C6 was diluted to a concentration of 2 μg/mL in 0.1 M sodium carbonate buffer, pH 9.0, and 50 μL was added per well to one half of a 96-well microliter plate. The other half of the plate was coated by adding 50 μL per well of a 2 μg/mL solution of human serum albumin (HSA) in 0.1 M sodium bicarbonate buffer. Plates were incubated overnight at 4°C. Plates were rinsed three times with 0.05% gelatin and 0.05% Brij 35 (Sigma, St. Louis, MO) in a 115-mM phosphate buffer (rinse buffer), pH 7.4, and then blocked by filling wells with 0.1% gelatin in 115-mM phosphate buffer, pH 7.4. Seven log-2 dilutions were made of human sera in rinse buffer, and 50 μL were added per well of undiluted serum and serum dilutions. Each serum dilution was run in triplicate on both the 81C6- and HSA-coated wells. As a positive control, eight log-2 dilutions were made in rinse buffer from a stock solution of goat anti-mouse IgG (20 μg/mL) (Sigma, St. Louis, MO). Triplicates of control dilutions were run on 81C6- and HSA-coated wells. Plates were incubated for 1 hour at room temperature and then rinsed eight times with rinse buffer. Fifty microliters of 2 μgs/mL biotinylated 81C6 diluted in rinse buffer were added per well, and plates were incubated for 1 hour at room temperature. Plates were again rinsed eight times with rinse buffer, and 50 μL of streptavidin-alkaline phosphatase (BRL cat. no. 9542SA, Gaithersburg, MD) diluted 1/2,000 in rinse buffer was added to each well. Plates were incubated for 1 hour at room temperature and then rinsed six times with rinse buffer and three times with 0.1 M Tris buffer, pH 8.0. After rinsing, 100 μL of substrate were added per well. The substrate was 4 mg/mL paranitrophenyl-phosphatase and 0.5 mM magnesium chloride in 10% diethanolamine buffer, pH 9.8. When color had developed the reaction was stopped by the addition of 50 μL of 25 mM L-cysteine. Plates were read in a model M-340 ELISA plate reader (Flow Laboratories, McLean, VA) at 405 nM. Binding ratios were calculated by the following formula:

$$\text{Binding Ratio} = \frac{\text{Mean 81C6-coated triplicates}}{\text{Mean HSA-coated triplicates}}$$

SPECT Imaging

Imaging of the brain and abdomen was performed 1 hour and 18 hours after radiolabeled antibody administration using either a dual-camera SPECT system (7 patients) or a triple-camera[11–14] (Triad-Trionix Research Laboratory, Twinsburg, Ohio) device (9 patients). The dual-camera SPECT system consisted of two large-field-of-view (LFOV) gamma cameras mounted on a rotatable gantry, a Concurrent Computer Corporation 3220 computer (Ocean Port, NJ), and a microprocessor-controlled display station. This research system was replaced during the course of this study with the Triad device, which consists of three rectangularly shaped scintillation cameras spaced at 120-degree intervals from each other. Digital corrections were provided for energy, linearity, flood uniformity, and X-Y offsets between the three heads. The data processing system used was a SUN 3/260 (Sun, Mountainview, CA) computer equipped with a 20 MFLOP Mercury

iting point array processor (Mercury, Lowell, MA). This ECT device is 50% more sensitive than the earlier dual-camera ice.

The acquisition and reconstruction protocols were similar for h SPECT systems. High resolution parallel-hole collimation s used for all patient studies. Reconstructed spatial resolution s approximately 12.0 mm for the brain images and approxitely 16.0 mm for images of the abdomen. Attenuation compenion was performed using a first-order Chang method.[11,15,16] To rease statistical noise, a generalized Hann filter having a cut- frequency equal to 0.75 times the Nyquist frequency and avging 2 or 3 slices in the axial direction was used. Compensation regional sensitivity variations (using an 80–100 million count age of a sheet source) and center-of-rotation calibration were formed before each study. Calibration images (in air and in a -cm-diameter water-filled cylinder) of a small syringe contain- a known concentration of I-123 were performed before the tient imaging studies. A multiplicative Chang attenuation cor- tion was applied to the scan of the syringe placed in the water- led cylinder using a value of 0.12 cm^{-1} for the effective attention coefficient. No additional compensation for scatter was rformed. Regions-of-interest (ROIs) were drawn around the ECT images of the syringe using an interactive thresholding chnique adjusted to accept 5% or greater of the peak counts. sed on the known activity in the syringe, these results were used convert ROI counts obtained from the SPECT patient images to tivity estimates.[17] Volumes were determined by summing the mber of pixels encompassing the organ of interest. For the pant studies, the ROIs also were determined using an interactive resholding method similar to that used for the in vitro calibration ans. Experimentally acquired phantom studies of known activity stribution were acquired throughout this investigation. These udies were used to validate the quantitative protocols further and ensure that the SPECT devices had not changed their imaging aracteristics.

nalysis of Tissue Samples

Patient 15 underwent a second resection of tumor approximately 8 hours after injection of 100.0 mg (10 mCi) of I-123–labeled 1C6. After adequate tissue was obtained for diagnosis, the remainder was divided into 20 samples of approximately equal size. The biopsy samples were blotted, placed in tared vials containing .0 ml of formalin, weighed, and then counted for I-123 activity. Comparison to injection standards permitted calculation of the ercent injected dose of I-123 per gram of tissue. After waiting 3 ays to allow the I-123 to decay, the biopsy samples were subected to conventional histologic analysis to estimate the fractional olume of tumor in each piece of tissue. Samples 1 through 3 ontained 98% to 100% normal brain tissue, so the average uptake n these tissues was used to correct for the presence of normal rain in some of the other samples.

Radiation Dosimetry

The absorbed radiation dose to tumor, liver, and spleen that would result from a hypothetical therapeutic dose of 100 mCi I-131-labeled 81C6 was estimated. It was assumed that the data obtained from these studies of patients who received diagnostic-level doses of I-123–labeled MAb were the same as the studies that would be obtained with the I-131 therapy dose. Using the methods described in the SPECT imaging section, average μCi/ml values were calculated for each tissue at each imaging time. After correcting for decay of I-123, the biologic clearance half-time was calculated. Blood clearance data were used to estimate whole body dose. Because the half-life of I-131 is 193 hours, the effective half-life for the hypothetical dose of I-131 labeled MAb was calculated as $1/T(\text{effective}) = 1/T(\text{biologic}) + 1/193\ \text{hour}^{-1}$. Using the "S" values tabulated for I-131, the standard MIRD approach was then used to estimate the radiation absorbed dose to these tissues.[18]

Results

Patients

Sixteen patients (10 men, 6 women) were enrolled in this protocol (Table 1). Their ages ranged from 36 to 71 years. The original histologic diagnoses were glioblastoma multiform in 9, gliosarcoma in 3, and anaplastic astrocytoma in 4.

Antibody Administration

The administered antibody dose was 10.0 mg in 2 patients, 20.0 mg in 7 patients, 50.0 mg in 5 patients, and 100.0 mg in 2 patients. The dose of I-123 ranged from 3.5 to 11.5 mCi; however, only 3 patients received less than 7.5 mCi, all of whom received 20.0 mg of 81C6. The specific binding ranged from 20% to 79%; however, only in 1 patient (patient 8) was the specific binding less than 50%. The protein-associated radioactivity of labeled antibody preparations exceeded 95% in all instances.

Blood Clearance

In 12 patients, a sufficient number of early blood samples was obtained to determine a first component T1/2; it ranged from 0.3 to 3.0 hours and represented 23% to 65% of the total dose (Table 2). There was a tendency for the first component T1/2 to lengthen with increasing dose of antibody with mean values of 0.5 hours with 10.0 mg 81C6 administered, 1.0 hour with 20.0 mg administered, and 1.9 hours with 50.0 mg administered. In all 16 patients, the

TABLE 1. Patient and Labeled Antibody Characteristics

Patient no. (age,sex)	Diagnosis	81C6 dose (mg)	I-123 dose (mCi)	Specific binding (%)*	TCA (%)†
1 (64,M)	GBM	10	9.8	74	99
2 (71,F)	GBM	10	10.0	59	98
3 (58,M)	GBM	20	4.0	58	98
4 (54,M)	GBM	20	7.5	65	99
5 (53,M)	GS	20	3.5	60	100
6 (45,F)	AA	20	4.4	70	100
7 (36,M)	AA	20	8.0	51	98
8 (61,F)	GBM	20	9.7	20	97
9 (33,M)	GS	20	9.3	75	98
10 (42,M)	GBM	50	8.0	70	99
11 (59,M)	GBM	50	9.0	57	98
12 (48,M)	GS	50	7.4	60	98
13 (44,F)	AA	50	7.5	74	96
14 (40,F)	GBM	50	10.0	79	99
15 (59,F)	GBM	100	11.5	67	99
16 (39,M)	AA	100	10.0	63	98

TCA: trichloroacetic acid. GBM: glioblastoma multiforme; GS: gliosarcoma; AA: anaplastic astrocytoma.

*Percentage bound to D-54 MG glioma homogenate minus percentage bound to rat liver in vitro (see methods).

†Protein-associated radioactivity determined by precipitation with TCA.

Patient number
1
2
3
4
5
6
7
8
9
10
11
12
13
14
15
16

*Insufficient data values.

T1/2 of the secor hours, which repr dose in those 12 points. Again, th second componer tibody. The mea hours in patients of 81C6, respecti

HAMA Analysis

HAMA titers serum and a posi on all 16 patien None of the 16 p than the control ered negative. F able for HAMA However, becau most near the en had available p administration o significant HA higher than bac administration. multiple occasic than backgroun

Imaging

The area of t and/or magnetic SPECT scannir

floating point array processor (Mercury, Lowell, MA). This SPECT device is 50% more sensitive than the earlier dual-camera device.

The acquisition and reconstruction protocols were similar for both SPECT systems. High resolution parallel-hole collimation was used for all patient studies. Reconstructed spatial resolution was approximately 12.0 mm for the brain images and approximately 16.0 mm for images of the abdomen. Attenuation compensation was performed using a first-order Chang method.[11,15,16] To decrease statistical noise, a generalized Hann filter having a cut-off frequency equal to 0.75 times the Nyquist frequency and averaging 2 or 3 slices in the axial direction was used. Compensation for regional sensitivity variations (using an 80–100 million count image of a sheet source) and center-of-rotation calibration were performed before each study. Calibration images (in air and in a 22-cm-diameter water-filled cylinder) of a small syringe containing a known concentration of I-123 were performed before the patient imaging studies. A multiplicative Chang attenuation correction was applied to the scan of the syringe placed in the water-filled cylinder using a value of 0.12 cm^{-1} for the effective attenuation coefficient. No additional compensation for scatter was performed. Regions-of-interest (ROIs) were drawn around the SPECT images of the syringe using an interactive thresholding technique adjusted to accept 5% or greater of the peak counts. Based on the known activity in the syringe, these results were used to convert ROI counts obtained from the SPECT patient images to activity estimates.[17] Volumes were determined by summing the number of pixels encompassing the organ of interest. For the patient studies, the ROIs also were determined using an interactive thresholding method similar to that used for the in vitro calibration scans. Experimentally acquired phantom studies of known activity distribution were acquired throughout this investigation. These studies were used to validate the quantitative protocols further and to ensure that the SPECT devices had not changed their imaging characteristics.

Analysis of Tissue Samples

Patient 15 underwent a second resection of tumor approximately 48 hours after injection of 100.0 mg (10 mCi) of I-123–labeled 81C6. After adequate tissue was obtained for diagnosis, the remainder was divided into 20 samples of approximately equal size. The biopsy samples were blotted, placed in tared vials containing 1.0 ml of formalin, weighed, and then counted for I-123 activity. Comparison to injection standards permitted calculation of the percent injected dose of I-123 per gram of tissue. After waiting 3 days to allow the I-123 to decay, the biopsy samples were subjected to conventional histologic analysis to estimate the fractional volume of tumor in each piece of tissue. Samples 1 through 3 contained 98% to 100% normal brain tissue, so the average uptake in these tissues was used to correct for the presence of normal brain in some of the other samples.

Radiation Dosimetry

The absorbed radiation dose to tumor, liver, and spleen that would result from a hypothetical therapeutic dose of 100 mCi I-131-labeled 81C6 was estimated. It was assumed that the data obtained from these studies of patients who received diagnostic-level doses of I-123–labeled MAb were the same as the studies that would be obtained with the I-131 therapy dose. Using the methods described in the SPECT imaging section, average μCi/ml values were calculated for each tissue at each imaging time. After correcting for decay of I-123, the biologic clearance half-time was calculated. Blood clearance data were used to estimate whole body dose. Because the half-life of I-131 is 193 hours, the effective half-life for the hypothetical dose of I-131 labeled MAb was calculated as $1/T(\text{effective}) = 1/T(\text{biologic}) + 1/193\ \text{hour}^{-1}$. Using the "S" values tabulated for I-131, the standard MIRD approach was then used to estimate the radiation absorbed dose to these tissues.[18]

Results

Patients

Sixteen patients (10 men, 6 women) were enrolled in this protocol (Table 1). Their ages ranged from 36 to 71 years. The original histologic diagnoses were glioblastoma multiform in 9, gliosarcoma in 3, and anaplastic astrocytoma in 4.

Antibody Administration

The administered antibody dose was 10.0 mg in 2 patients, 20.0 mg in 7 patients, 50.0 mg in 5 patients, and 100.0 mg in 2 patients. The dose of I-123 ranged from 3.5 to 11.5 mCi; however, only 3 patients received less than 7.5 mCi, all of whom received 20.0 mg of 81C6. The specific binding ranged from 20% to 79%; however, only in 1 patient (patient 8) was the specific binding less than 50%. The protein-associated radioactivity of labeled antibody preparations exceeded 95% in all instances.

Blood Clearance

In 12 patients, a sufficient number of early blood samples was obtained to determine a first component T1/2; it ranged from 0.3 to 3.0 hours and represented 23% to 65% of the total dose (Table 2). There was a tendency for the first component T1/2 to lengthen with increasing dose of antibody with mean values of 0.5 hours with 10.0 mg 81C6 administered, 1.0 hour with 20.0 mg administered, and 1.9 hours with 50.0 mg administered. In all 16 patients, the

TABLE 1. Patient and Labeled Antibody Characteristics

Patient no. (age,sex)	Diagnosis	81C6 dose (mg)	I-123 dose (mCi)	Specific binding (%)*	TCA (%)†
1 (64,M)	GBM	10	9.8	74	99
2 (71,F)	GBM	10	10.0	59	98
3 (58,M)	GBM	20	4.0	58	98
4 (54,M)	GBM	20	7.5	65	99
5 (53,M)	GS	20	3.5	60	100
6 (45,F)	AA	20	4.4	70	100
7 (36,M)	AA	20	8.0	51	98
8 (61,F)	GBM	20	9.7	20	97
9 (33,M)	GS	20	9.3	75	98
10 (42,M)	GBM	50	8.0	70	99
11 (59,M)	GBM	50	9.0	57	98
12 (48,M)	GS	50	7.4	60	98
13 (44,F)	AA	50	7.5	74	96
14 (40,F)	GBM	50	10.0	79	99
15 (59,F)	GBM	100	11.5	67	99
16 (39,M)	AA	100	10.0	63	98

TCA: trichloroacetic acid. GBM: glioblastoma multiforme; GS: gliosarcoma; AA: anaplastic astrocytoma.

*Percentage bound to D-54 MG glioma homogenate minus percentage bound to rat liver in vitro (see methods).

†Protein-associated radioactivity determined by precipitation with TCA.

TABLE 2. Blood Clearance of I-123 Activity in Patients Injected with I-123–Labeled 81C6

Patient number	Dose (mg)	First component		Second component	
		T1/2 (hr)	(%)	T1/2 (hr)	(%)
1	10	0.3	52	19.8	48
2	10	0.6	59	25.0	41
	Mean (range)	0.5 (0.3–0.6)	56 (52–59)	22.4 (19.8–25.0)	44 (41–48)
3	20	2.3	33	26.6	67
4	20	0.5	35	21.0	65
5	20	1.7	42	28.4	59
6	20	1.3	33	30.4	67
7	20	0.6	54	26.1	46
8	20	0.5	48	31.1	52
9	20	0.3	65	16.6	35
	Mean (range)	1.0 (0.3–2.3)	43 (33–65)	25.7 (16.6–31.1)	57 (35–67)
10	50	*	—	17.2	—
11	50	0.8	24	25.8	76
12	50	3.0	24	34.5	76
13	50	*	—	28.9	—
14	50	*	—	24.6	—
	Mean (range)	1.9 (0.8–3.0)	24	26.2 (17.2–34.5)	76
15	100	3.0	23	37.2	77
16	100	*	—	23.0	—
	Mean (range)	3.0	23	30.1 (23.0–37.2)	77

*Insufficient data at early time points to determine first component contribution; these patients were not used in calculating mean values.

T1/2 of the second component ranged from 16.6 to 37.2 hours, which represented between 41% and 77% of the total dose in those 12 patients who had sufficient early time points. Again, there was a tendency for the duration of the second component to increase with increasing dose of antibody. The mean values were 22.4, 25.7, 26.2, and 30.1 hours in patients receiving 10.0, 20.0, 50.0, and 100.0 mg of 81C6, respectively.

HAMA Analysis

HAMA titers with a normal volunteer negative control serum and a positive goat antibody control were performed on all 16 patients as a prerequisite for study eligibility. None of the 16 patients had pre-study HAMA titer greater than the control serum binding ratios, and all were considered negative. Fourteen of the 16 patients had serum available for HAMA analysis after antibody administration. However, because these were recurrent glioma patients, most near the end of their life span, only 4 of the 14 patients had available post-study serum more than 23 days after administration of 81C6. Two of the 4 patients developed significant HAMA titers, although one was only twofold higher than background and then only at 217 days after administration. Two patients, both of whom were tested on multiple occasions, did not develop HAMA titers greater than background control serum levels.

Imaging

The area of tumor as indicated by computed tomography and/or magnetic resonance imaging was well-visualized by SPECT scanning in the 16 patients injected with I-123–labeled 81C6 MAb. Contrast between tumor and normal brain regions was higher in the 18-hour images compared with the 1-hour images; however, all lesions were clearly delineated at both times. Transaxial SPECT images of the brain of patient 12, obtained 1 hour and 18 hours after the injection of 7.4 mCi and 50.0 mg of I-123–labeled 81C6, are shown in Figure 1. Uptake of I-123 activity in the liver and spleen was seen in all patients at 1 hour and 18 hours. Figure 2 illustrates anterior and posterior planar and SPECT images of patient 4 obtained 18 hours after the injection of 7.5 mCi and 20.0 mg of I-123 81C6 MAb.

Tumor Uptake by SPECT

Uptake of I-123 in the tumor (percent ID/g tissue) was determined at 1 hour and 18 hours after injection in all patients, except that 1- hour images were not obtained in the two patients who received 10.0 mg 81C6 and in one patient who received 50.0 mg 81C6 (Table 3). The mean tumor uptake increased between 1 hour and 18 hours at all antibody doses, although tumor uptake did not increase in all 13 patients scanned at both time points. There was a tendency for the percent ID/g to increase with increasing doses of antibody (3.0×10^{-3}% at 20.0 mg, 3.7×10^{-3}% at 50.0 mg, and 5.0×10^{-3}% at 100.0 mg) at the 1-hour image. The uptake was also higher at the 18-hour image in the two highest antibody doses (6.3×10^{-3}% at 50.0 mg and 5.3×10^{-3}% at 100.0 mg) than in the two lowest antibody doses (2.5×10^{-3}% at 10.0 mg and 3.4×10^{-3}% at 20.0 mg). However, there was considerable variability, and the numbers were small, so none of these differences was statistically significant. The tumor: brain ratio was also gen-

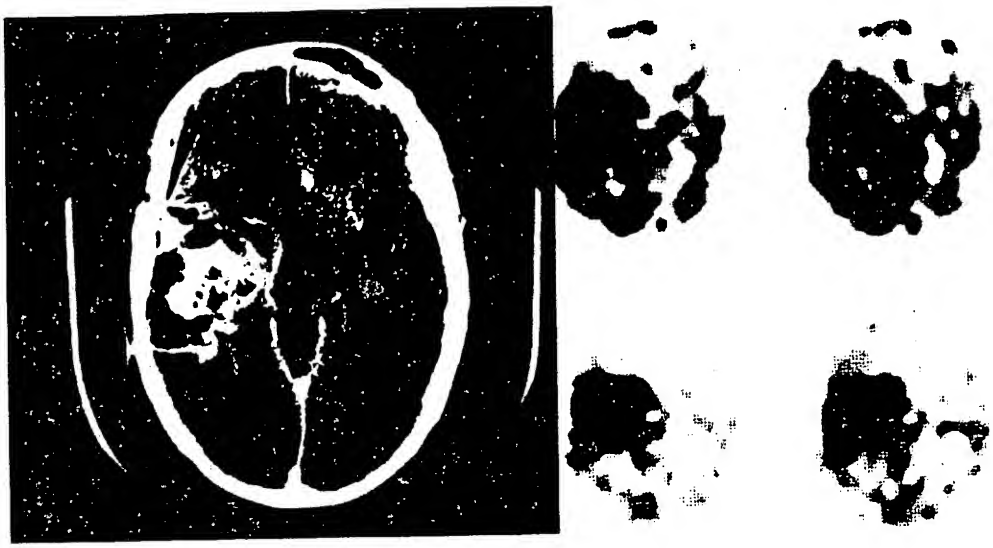

Fig. 1. Contrast-enhanced CT (left) and SPECT images (right) of patient 12 obtained 1 (upper) and 18 hours (lower) after intravenous administration of I-123 81C6.

erally higher at 18 hours than at 1 hour after antibody injection. Mean values ranged from 1.7 (50.0 mg and 100.0 mg at 1 hour) to 3.2 (50.0 mg at 18 hours).

Tumor Uptake by Tissue Analysis

In patient 15, who underwent surgery 48 hours after antibody administration, the resected tissue was separated into 20 samples. The percentage of tumor, normal brain, and necrosis was estimated microscopically in each of the samples (Table 4). Two samples contained no tumor, and one sample was estimated to contain 2% tumor. The amount of radioactivity in these samples was used to correct the other 17 samples for normal brain radioactivity levels, permitting an estimate of the tumor uptake (percent ID/g tissue) in these samples. The percent ID/g of "normal brain" (samples 1–3) ranged from 7.3 to 9.4 $\times$ 10^{-4}%, and in the 17 tumor samples it ranged from 1.2 $\times$ 10^{-3}% to 9.9 $\times$ 10^{-3}%. The highest uptake ($> 7.0 \times 10^{-3}$%) was found in those areas with at least 50% radionecrosis histologically. The tumor uptake determined by SPECT imaging in this patient was 5.1 $\times$ 10^{-3}% ID/g.

Dosimetry

From the I-123 SPECT imaging data, an estimate of the radiation dose that would be delivered to tumor, liver, and spleen from a hypothetical 100 mCi dose of I-131-labeled antibody was determined (Table 5). The mean estimated tumor dose ranged from 300 cGy in the 2 patients who received 10.0 mg 81C6 to 755 cGy in the 5 patients who received 50.0 mg. Whole body radiation absorbed dose, estimated from activity in the blood pool, also appeared to increase with increasing protein dose. In contrast, the dose to liver and spleen, normal organs known to contain tenascin, tended to decrease with increasing protein dose of MAb.

Discussion

Although anaplastic gliomas are highly refractory to current therapy, survival is prolonged with the use of external beam radiotherapy. Median survival was increased from 16 weeks to 37 weeks when 5,000 to 6,000 cGy was added to surgery in an early Brain Tumor Study Group (BTSG) randomized study.[19] There is also evidence of a dose-response relationship for external beam radiotherapy in the treatment of cerebral anaplastic gliomas in adults,[20] and brain stem tumors in children appear to be treated more effectively with higher total doses of radiation.[21] However, the efficacy of radiotherapy for anaplastic gliomas is limited by normal tissue tolerance, with the result that maximum tolerated doses of cranial radiotherapy generally do not cure anaplastic gliomas.

An antibody that is relatively specific for glioma tissue could be used as a carrier for therapeutic doses of radiation and could provide higher doses of radiation to tumor tissue with relative sparing of normal brain. The therapeutic use of radiolabeled MAbs has been demonstrated in other tumor types,[22,23] and more recently, in patients with malignant astrocytomas.[24] The therapeutic use of radiolabeled antibodies in gliomas is conceptually similar to the use of localized radiotherapy in the form of radioactive pellets or focused radiation, but the use of antibodies offers the potential advantages of greater specificity for glioma tissue and greater distribution into infiltrating tumor. Unlike conventional brachytherapy, antibody-delivered radiation therapy would be affected not only by the physical parameters of the therapeutic radionuclide, but also by the kinetics and heterogeneity of localization of the antibody.

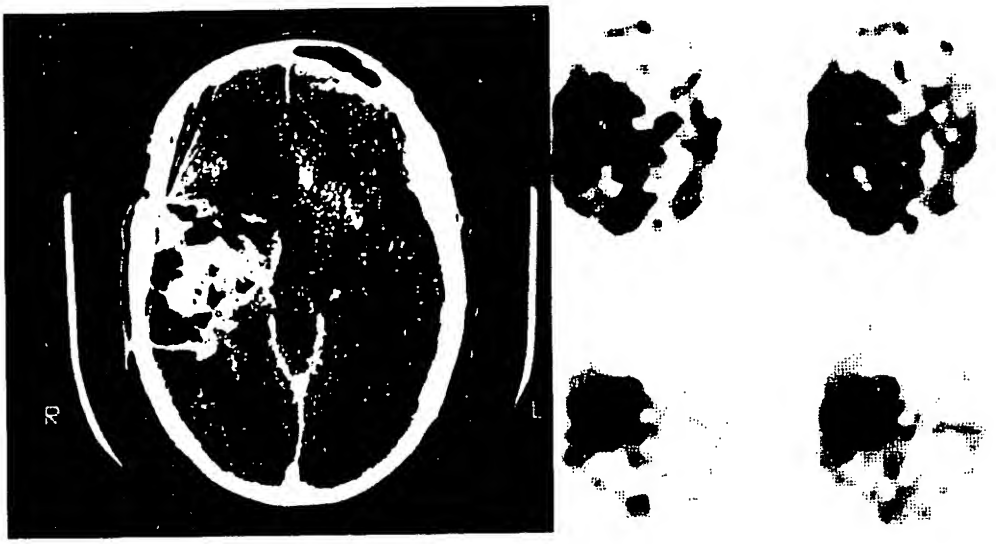

Fig. 1. Contrast-enhanced CT (left) and SPECT images (right) of patient 12 obtained 1 (upper) and 18 hours (lower) after intravenous administration of I-123 81C6.

erally higher at 18 hours than at 1 hour after antibody injection. Mean values ranged from 1.7 (50.0 mg and 100.0 mg at 1 hour) to 3.2 (50.0 mg at 18 hours).

Tumor Uptake by Tissue Analysis

In patient 15, who underwent surgery 48 hours after antibody administration, the resected tissue was separated into 20 samples. The percentage of tumor, normal brain, and necrosis was estimated microscopically in each of the samples (Table 4). Two samples contained no tumor, and one sample was estimated to contain 2% tumor. The amount of radioactivity in these samples was used to correct the other 17 samples for normal brain radioactivity levels, permitting an estimate of the tumor uptake (percent ID/g tissue) in these samples. The percent ID/g of "normal brain" (samples 1–3) ranged from 7.3 to 9.4 $\times 10^{-4}$%, and in the 17 tumor samples it ranged from 1.2 $\times 10^{-3}$% to 9.9 $\times 10^{-3}$%. The highest uptake ($> 7.0 \times 10^{-3}$%) was found in those areas with at least 50% radionecrosis histologically. The tumor uptake determined by SPECT imaging in this patient was 5.1 $\times 10^{-3}$% ID/g.

Dosimetry

From the I-123 SPECT imaging data, an estimate of the radiation dose that would be delivered to tumor, liver, and spleen from a hypothetical 100 mCi dose of I-131-labeled antibody was determined (Table 5). The mean estimated tumor dose ranged from 300 cGy in the 2 patients who received 10.0 mg 81C6 to 755 cGy in the 5 patients who received 50.0 mg. Whole body radiation absorbed dose, estimated from activity in the blood pool, also appeared to increase with increasing protein dose. In contrast, the dose to liver and spleen, normal organs known to contain tenascin, tended to decrease with increasing protein dose of MAb.

Discussion

Although anaplastic gliomas are highly refractory to current therapy, survival is prolonged with the use of external beam radiotherapy. Median survival was increased from 16 weeks to 37 weeks when 5,000 to 6,000 cGy was added to surgery in an early Brain Tumor Study Group (BTSG) randomized study.[19] There is also evidence of a dose-response relationship for external beam radiotherapy in the treatment of cerebral anaplastic gliomas in adults,[20] and brain stem tumors in children appear to be treated more effectively with higher total doses of radiation.[21] However, the efficacy of radiotherapy for anaplastic gliomas is limited by normal tissue tolerance, with the result that maximum tolerated doses of cranial radiotherapy generally do not cure anaplastic gliomas.

An antibody that is relatively specific for glioma tissue could be used as a carrier for therapeutic doses of radiation and could provide higher doses of radiation to tumor tissue with relative sparing of normal brain. The therapeutic use of radiolabeled MAbs has been demonstrated in other tumor types,[22,23] and more recently, in patients with malignant astrocytomas.[24] The therapeutic use of radiolabeled antibodies in gliomas is conceptually similar to the use of localized radiotherapy in the form of radioactive pellets or focused radiation, but the use of antibodies offers the potential advantages of greater specificity for glioma tissue and greater distribution into infiltrating tumor. Unlike conventional brachytherapy, antibody-delivered radiation therapy would be affected not only by the physical parameters of the therapeutic radionuclide, but also by the kinetics and heterogeneity of localization of the antibody.

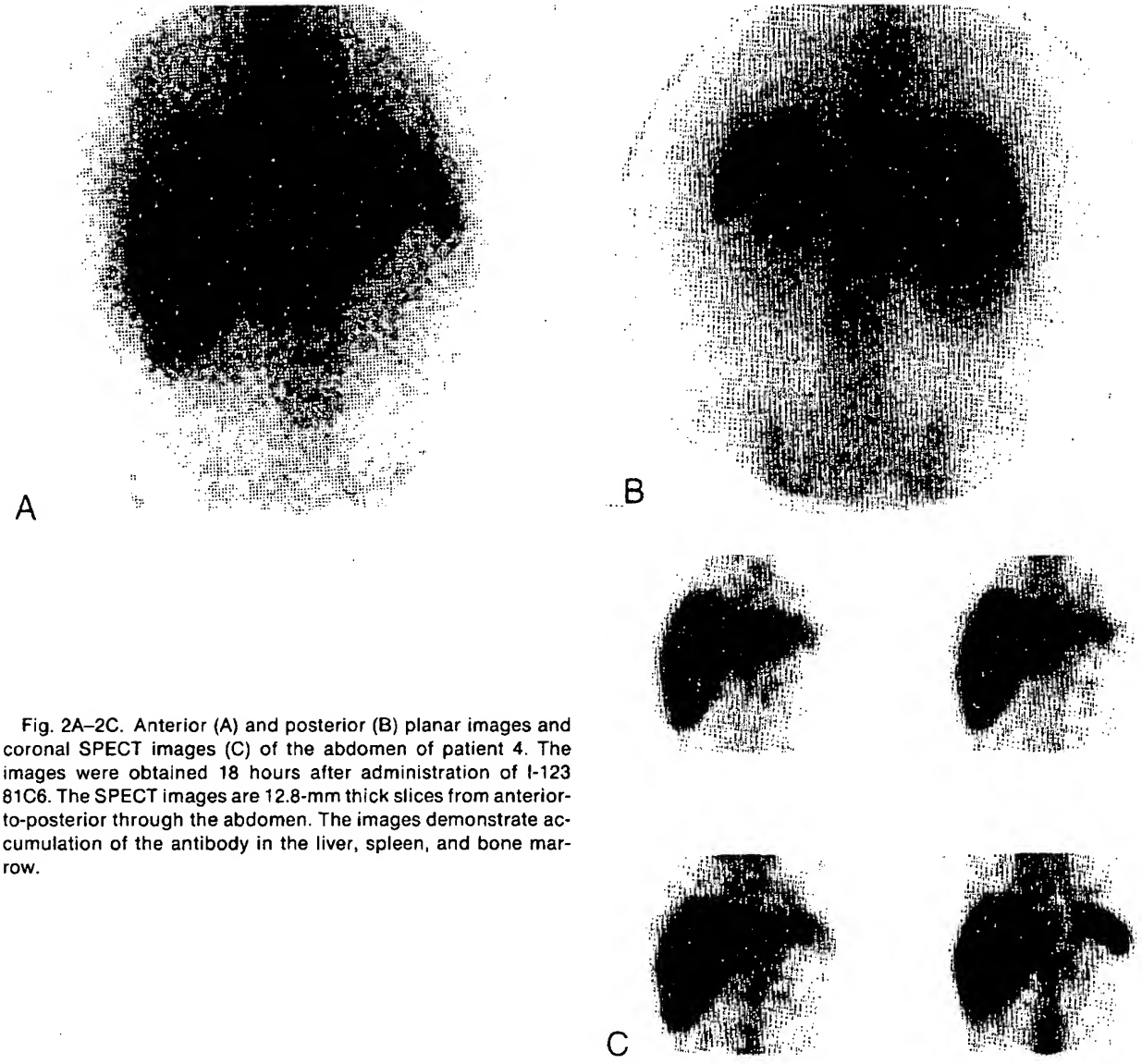

Fig. 2A–2C. Anterior (A) and posterior (B) planar images and coronal SPECT images (C) of the abdomen of patient 4. The images were obtained 18 hours after administration of I-123 81C6. The SPECT images are 12.8-mm thick slices from anterior-to-posterior through the abdomen. The images demonstrate accumulation of the antibody in the liver, spleen, and bone marrow.

81C6, a murine MAb derived from a human glioma cell line, reacts with tenascin, an extracellular matrix antigen. This antibody reacts with a high percentage of human anaplastic glioma tissue sections by immunoperoxidase staining with a predominantly extracellular localization.[5,25] When injected intravenously into athymic mice bearing a subcutaneous human glioma xenograft, peak localization of 81C6 radioiodinated using conventional methods occurred

TABLE 3. Tumor Uptake and Tumor to Normal Brain Ratios for I-123–Labeled 81C6 as Determined by SPECT Imaging

Dose of 81C6 (mg)	Tumor uptake* (%ID/g)		Tumor: brain ratio*	
	1 hour	18 hours	1 hour	18 hours
10 (n = 2)	†	2.5×10^{-3} (1.7–3.3)	†	2.1 (1.7–2.6)
20 (n = 7)	3.0×10^{-3} (2.2–5.9)	3.4×10^{-3} (1.8–5.7)	1.8 (1.0–2.3)	2.4 (1.0–4.7)
50 (n = 4 for 1 hour, n = 5 for 18 hours)	3.7×10^{-3} (2.5–5.4)	6.3×10^{-3} (3.8–10.4)	1.7 (1.4–2.3)	3.2 (2.3–4.6)
100 (n = 2)	5.0×10^{-3} (4.4–5.5)	5.3×10^{-3} (5.1–5.5)	1.7 (1.6–1.8)	2.7 (2.2–3.2)

*Reported as mean (range).
†Patients not scanned.

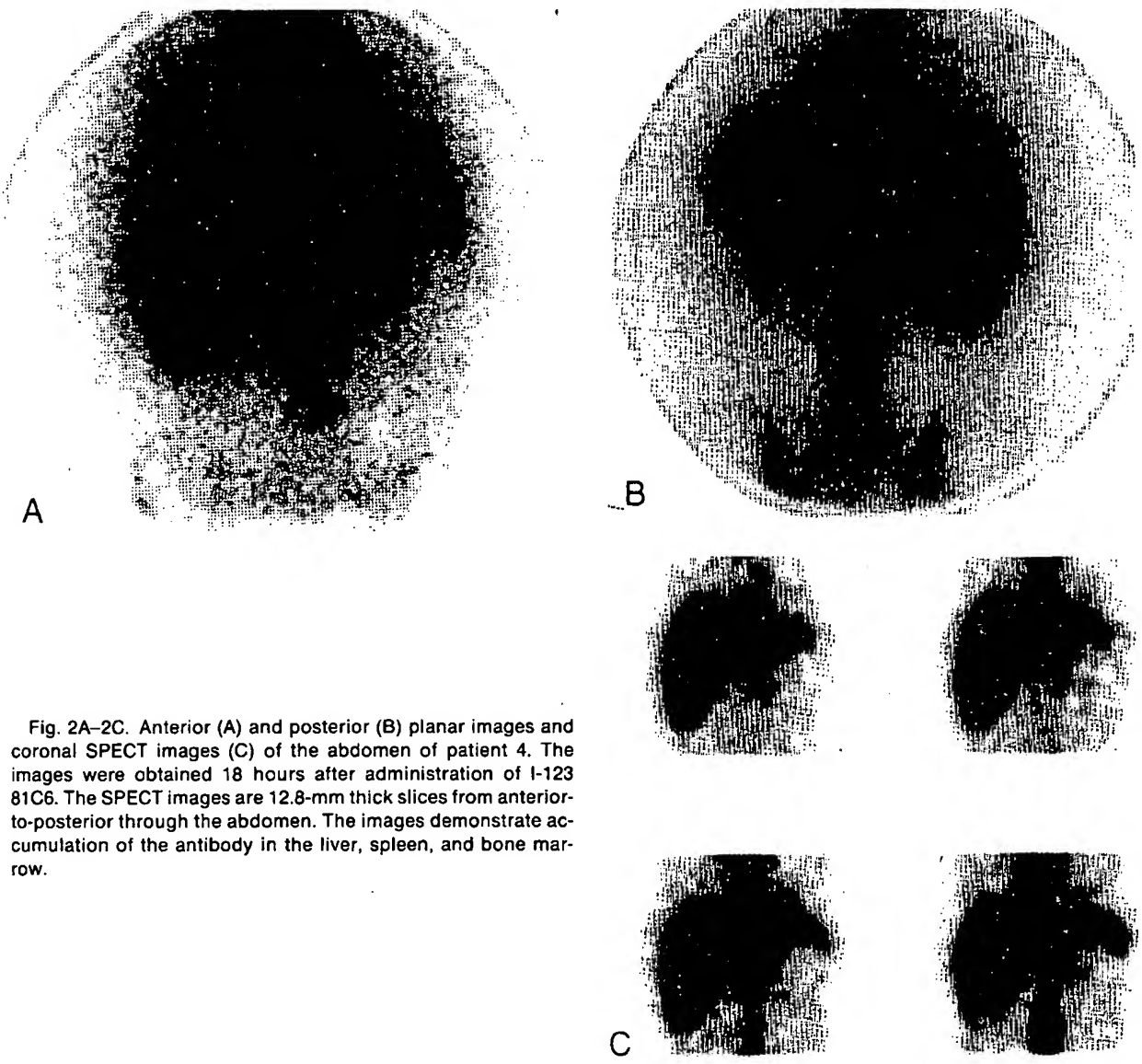

Fig. 2A–2C. Anterior (A) and posterior (B) planar images and coronal SPECT images (C) of the abdomen of patient 4. The images were obtained 18 hours after administration of I-123 81C6. The SPECT images are 12.8-mm thick slices from anterior-to-posterior through the abdomen. The images demonstrate accumulation of the antibody in the liver, spleen, and bone marrow.

81C6, a murine MAb derived from a human glioma cell line, reacts with tenascin, an extracellular matrix antigen. This antibody reacts with a high percentage of human anaplastic glioma tissue sections by immunoperoxidase staining with a predominantly extracellular localization.[5,25] When injected intravenously into athymic mice bearing a subcutaneous human glioma xenograft, peak localization of 81C6 radioiodinated using conventional methods occurred

TABLE 3. Tumor Uptake and Tumor to Normal Brain Ratios for I-123–Labeled 81C6 as Determined by SPECT Imaging

	Tumor uptake* (%ID/g)		Tumor: brain ratio*	
Dose of 81C6 (mg)	1 hour	18 hours	1 hour	18 hours
10 (n = 2)	†	2.5×10^{-3} (1.7–3.3)	†	2.1 (1.7–2.6)
20 (n = 7)	3.0×10^{-3} (2.2–5.9)	3.4×10^{-3} (1.8–5.7)	1.8 (1.0–2.3)	2.4 (1.0–4.7)
50 (n = 4 for 1 hour, n = 5 for 18 hours)	3.7×10^{-3} (2.5–5.4)	6.3×10^{-3} (3.8–10.4)	1.7 (1.4–2.3)	3.2 (2.3–4.6)
100 (n = 2)	5.0×10^{-3} (4.4–5.5)	5.3×10^{-3} (5.1–5.5)	1.7 (1.6–1.8)	2.7 (2.2–3.2)

*Reported as mean (range).
†Patients not scanned.

TABLE 4. Uptake of I-123 in Resected Tissue after Injection of 100 mg I-123–Labeled 81C6 (Patient 15)

Sample*	Microscopic evaluation: % tumor	% normal brain	% necrosis	Tissue uptake (%ID/g)
1	0	100	0	9.4×10^{-4}
2	0	100	0	9.0×10^{-4}
3	2	98	0	7.3×10^{-4}
4	20	80	0	2.6×10^{-3}
5	20	80	0	1.2×10^{-3}
6	30	70	0	3.0×10^{-3}
7	80	20	0	2.8×10^{-3}
8	85	15	0	2.1×10^{-3}
9	90	10	0	6.7×10^{-3}
10	90	10	0	1.6×10^{-3}
11	90	10	0	1.6×10^{-3}
12	95	5	0	2.9×10^{-3}
13	95	5	0	2.1×10^{-3}
14	95	5	0	2.0×10^{-3}
15	95	0	5	5.1×10^{-3}
16	50	0	50	9.9×10^{-3}
17	50	0	50	8.5×10^{-3}
18	50	0	50	7.4×10^{-3}
19	50	0	50	7.2×10^{-3}
20	10	0	90	5.7×10^{-3}

*Samples 4 through 20 reflect tumor uptake. Samples 4 through 14 are corrected for the presence of normal brain using the average value from samples 1 through 3 as normal brain uptake level.

at 48 to 72 hours and was as high as 15% of the injected dose per gram of tumor.[26] The localization index (ratio of specific to control 45.6 antibody in tumor, normalized to blood activity) ranged between 6 and 15, compared with a ratio of approximately 1 in normal tissues. With a more stable radioiodination method, a peak tumor accumulation of 25% injected dose per gram was observed at 24 hr with a localization index of approximately 30:1 at 5 days.[27] 81C6 labeled with I-131 has been used in athymic rats to image these tumors at sizes as small as 20.0 mg, long before I-131 labeled control antibody 45.6 localized sufficiently to allow successful imaging.[6] The epitopes to which 45.6 myeloma IgG_{2b} binds are undefined; however, there has been no evidence that 45.6 murine IgG_{2b} reacts specifically with any human or murine tissues.[1,5,6,28] The behavior of 45.6 MAb as an imaging agent would therefore be expected to be similar to that of albumin except for the difference in molecular size between the IgG molecule and albumin and any differences in plasma half-life. Thus, the higher localization of 81C6 compared with 45.6 indicates not only a relative specificity in vitro of 81C6 MAb for glioma tissue, but also the potential for achieving specific localization of this MAb in vivo.

TABLE 5. Projected Dosimetry of 300 mCi of I-131–Labeled 81C6 Monoclonal Antibody

81C6 dose (mg)	Radiation absorbed dose (cGy): Tumor	Liver	Spleen	Whole body
10	900	6,000	5,991	39
20	1,224	1,710	2,514	57
50	2,265	1,266	1,944	77
100	1,905	1,461	1,533	86

The kinetics of 81C6 in blood have been investigated in nonhuman primates after intravenous administration and in glioma patients after intravenous and intracarotid administration.[7,8] In macaque monkeys, intravenously administered I-123–labeled 81C6 had a serum half-life of 9.5 ± 0.7 hours (M. Zalutsky and D. Bigner, unpublished data, October 1987). In three patients with gliomas in whom I-131–labeled 81C6 (5.0–20.0 mg) was administered into the internal carotid artery, the half-time of the blood clearance ranged from 24 to 36 hours with similar half-times observed for I-125 labeled 81C6 co-administered intravenously.[8] No adverse reactions to the antibody administration were observed in either clinical study.

In this series of 16 patients with recurrent anaplastic gliomas, the amount of administered radioactivity was kept constant at approximately 10 mCi after using approximately 5 mCi in the first 3 patients, as requested by the Food and Drug Administration. The amount of antibody administered was increased from 10.0 to 100.0 mg during the study. There was a tendency for the blood clearance to decrease with increasing antibody dose, but no statistically significant differences were obtained. The first component T1/2 ranged from 0.3 to 3.0 hours in the 12 patients in whom it could be determined, and the second component T1/2 ranged from 16.6 to 37.2 hours in all 16 patients. These results are comparable to those observed previously in patients following intra-arterial or intravenous administration of 81C6 MAb.[7,8]

The number of postoperative sera available for testing for HAMA titers was not sufficient to draw general conclusions. Glioma patients in general, and especially those who have received chemotherapy and radiotherapy treatment, are often immunosuppressed. It is therefore not surprising that 2 of the 4 evaluated patients developed no HAMA response. Future studies will be necessary to address the capacity of glioma patients to form HAMA responses to murine MAbs such as 81C6.

The central objective of this study was to use SPECT to investigate whether varying the protein dose of 81C6 would result in more favorable tumor to normal tissue dose ratios. Previous studies using immunohistochemistry have documented reactivity of 81C6 with tenascin present in normal liver, spleen, and kidney.[5,28] However, accessibility of labeled 81C6 to antigen in these tissues in vivo would be required for specific, antigen-mediated uptake to occur. We hoped that if specific uptake of 81C6 in normal tissues was observed, that increasing the amount of protein administered could saturate this uptake without compromising tumor localization. The average tumor uptake (percent ID/g tissue) determined by SPECT was higher at 18 hours than at 1 hour for the 20.0-, 50.0-, and 100.0-mg antibody doses

(the two patients who received 10.0 mg were not scanned at 1 hour). The mean tumor uptake also increased with the 50.0- and 100.0-mg antibody dose administered compared with the 10.0-mg administered dose on both the 1-hour and the 18-hour images. The highest tumor uptake in an individual patient was 10.4×10^{-3}% in patient 13 at 18 hours. In the seven patients who received at least 50.0 mg of antibody I-123 activity levels, the uptake always exceeded 3.8×10^{-3}%. The tumor: normal brain ratio at 18 hours in these seven patients always exceeded 2.2. The accumulation of the antibody probably increases for 72 hours or more in humans, as it did in animals, but the half-life of the I-123 did not permit imaging at later time points. The tissue uptake in the patient who had surgery 48 hours after antibody administration demonstrated similar uptake compared with the quantitative SPECT imaging. All areas with at least 10% tumor histologically had at least 1.2×10^{-3}% ID/g tissue. In areas with at least 90% tumor, the range was 1.6 to 6.7×10^{-3}% ID/g.

In these patients, SPECT imaging was used to demonstrate MAb protein dose dependent uptake in liver of approximately 25% to 50% and in spleen of 2% to 8%. In contrast, in mice injected with radioiodinated 81C6, uptake in liver was only approximately 1% to 2% ID and in spleen, an order of magnitude less.[27] The presence of tenascin in the normal human liver and spleen, but absent in the mouse, is the likely cause of these observed differences and illustrates the limitations of using tissue distribution data obtained in the mouse to estimate dosimetry for patients.

Decreasing uptake in liver and spleen with increasing protein dose of 81C6 most likely reflects the saturation of available antigen in these tissues. As a consequence, a greater amount of 81C6 is expected to remain in circulation with increasing protein dose and the blood clearance data suggest that this is indeed the case. The increased uptake of 81C6 at higher protein doses presumably reflects decreased competition for antigen-mediated binding in normal tissues and the prolonged availability of antibody in the blood pool.

Using the SPECT data from these 16 patients, it was possible to estimate the radiation absorbed dose to tumor and various other organs assuming a treatment dose of 100 mCi of I-131–labeled 81C6 and various protein amounts (Table 5). The relative radiation absorbed dose to tumor compared with the liver and spleen increased with increasing antibody dose. At 100.0 mg of antibody, approximately 635 cGy would be delivered to tumor with 487 and 511 cGy to liver and spleen, respectively. Since these radiation doses are less than tolerance doses to liver and spleen, it may be possible to further increase the dose of antibody or isotope. Clearly, 635 cGy is not an adequate dose for therapeutic anti-tumor efficacy. Nevertheless, the higher doses that might be achieved with larger amounts of administered I-131 may supplement conventional external beam radiotherapy without the increased risk to normal brain that external beam doses would produce when increased beyond current levels. Because of the steep dose response curve of radiation relative to tumor cell kill, the ability to give a total tumor dose of approximately 8,000 cGy (6,000 cGy external beam plus 1,905 cGy from 300 mCi, I-131 81C6 for example), could be significant.

An additional observation from this study is the disagreement in the in vivo imaging results and predicted localization from the immunohistochemical analyses of normal organs. Immunohistochemistry was strongly positive for kidney and spleen;[5] and, in addition, kidney produces abundant tenascin mRNA of both tenascin isoforms.[28] Nevertheless, kidney uptake of I-123 was not observed in patients receiving 81C6 MAb, suggesting that immunohistochemistry is not always predictive of in vivo localization pattern.

These findings have led us to seek several alternate strategies for using radiolabeled anti-tenascin MAbs in the treatment of patients with gliomas. The first is to identify gene-spliced variants of tenascin present on tumor but not normal tissues. Further, the use of an unlabeled dose of 81C6 to block liver and spleen uptake before administration of a therapeutic dose of I-131–labeled 81C6 might improve tumor to liver and spleen radiation absorbed dose ratios. Liver and spleen uptake of 81C6 could also be minimized by restricting its use to tumors accessible by regional delivery. Clinical trials using I-131–labeled 81C6 administered directly into cystic gliomas and intrathecally to patients with neoplastic meningitis are underway at our institution and preliminary results have been encouraging.

Acknowledgment

We appreciate the contribution of Kim Greer, CNMT, for the acquisition and processing of the SPECT studies.

References

1. Lee Y, Bullard DE, Humphrey PA, et al. Treatment of intracranial human glioma xenografts with I-131-labeled anti-tenascin monoclonal antibody 81C6. Cancer Res 1988;48:2904–2910.
2. Larson SM. Lymphoma, melanoma, colon cancer: diagnosis and treatment with radiolabeled monoclonal antibodies. Radiology 1987;165:297–304.
3. Pizer B, Papanastassiou V, Hancock J, et al. A pilot study of monoclonal antibody targeted radiotherapy in the treatment of central nervous system leukaemia in children. Br J Hemat 1991;77:466–472.
4. Kalofonos HP, Pawlikowska TR, Hemingway A, et al. Antibody guided diagnosis and therapy of brain gliomas using radiolabeled monoclonal antibodies against epidermal growth factor receptor and placental alkaline phosphatase. J Nucl Med 1989;30:1636–1645.
5. Bourdon MA, Wikstrand CJ, Furthmayr H, et al. Human glioma-mesenchymal extracellular matrix antigen defined by monoclonal antibody. Cancer Res 1983;43:2796–2805.
6. Bullard DE, Adams CJ, Coleman RE, Bigner DD. In vivo imaging of intracranial human glioma xenografts comparing specific with non-specific radiolabeled monoclonal antibodies. J Neurosurg 1986;64: 257–262.
7. Zalutsky MR, Moseley RP, Coakham HB, Coleman RE, Bigner DD. Pharmacokinetics and tumor localization of I-131-labeled anti-

tenascin monoclonal antibody 81C6 in patients with gliomas and other intra-cranial malignancies. Cancer Res 1989;49:2807–2813.
8. Zalutsky MR, Moseley RP, Benjamin JC, Colapinto EV, Coakham HB, Bigner DD. Monoclonal antibody and $F(ab')_2$ fragment delivery to tumor in patients with glioma: comparison of intracarotid and intravenous administration. Cancer Res 1990;50:4105–4110.
9. Leichner PK, Vriesendorp HM, Hawkins WG, et al. Quantitative SPECT for Indium-111-labeled antibodies in the livers of beagle dogs. J Nucl Med 1991;32:1442–1444.
10. Franker PJ, Speck JC. Protein and cell membrane iodinations with sparingly soluble chloramide 1,3,4,6-tetrachloro-3α-6α-diphenylglycolouril. Biochem Biophys Res Commun 1978;80: 849–857.
11. Jaszczak RJ, Chang LT, Stein NA, Moore FE. Whole body single-photon emission computed tomography using dual, large field of view scintillation cameras. Phys Med Biol 1979;24:1123–1143.
12. Jaszczak RJ, Coleman RE. Instrumentation for single-photon emission computed tomographic studies of the brain. Am J Physiol Imag 1988;3:67–70.
13. Lim CB, Chang LT, Jaszczak RJ. Performance analysis of three camera configurations for single photon emission computed tomography. IEEE Trans Nucl Sci 1980;NS-27:559–568.
14. Lim CB, Gottschalk S, Walker R, Schreiner R, et al. Triangular SPECT system for 3-D total organ volume imaging: design concept and preliminary imaging results. IEEE Trans Nucl Sci 1985;NS-32:741–747.
15. Chang LT. A method for attenuation corrections in radionuclide computed tomography. IEEE Trans Nucl Sci 1978;25:638–643.
16. Jaszczak RJ, Coleman RE. Single photon emission computed tomography (SPECT). Principles and instrumentation. Invest Radiol 1985;20:897–910.
17. Jaszczak RJ, Coleman RE, Whitehead FR. Physical factors affecting quantitative measurements using camera-based single photon emission computed tomography (SPECT). IEEC Trans Nucl Sci 1981; 28:69–80.
18. Snyder WS, Ford MR, Watson SB. "S" absorbed dose per unit cumulated activity for selected radionuclides and organs (Medical Internal Radiation Dose Pamphlet, No. 11). New York, NY: Society of Nuclear Medicine, New York; 1975.
19. Walker MD, Alexander E Jr, Hunt WE, et al. Evaluation of BCNU and/or radiotherapy in the treatment of anaplastic gliomas: a cooperative clinical trial. J Neurosurg 1978;49:333–343.
20. Walker MD, Strike TA, Sheline GE. An analysis of the dose-effect relationship in the radiotherapy of malignant gliomas. Int J Radiat Oncol Biol Phys 1979;5:1725–1731.
21. Edwards MSB, Wara WM, Urtasun RC, et al. Hyperfractionated radiation therapy for brain-stem glioma: a phase I–II trial. Neurosurg 1989;70:691–700.
22. Dillman RO. Monoclonal antibodies for treating cancer. Ann Intern Med 1989;111:592–603.
23. Larson SM. Radioimmunology: imaging and therapy. Cancer 1991; 67:1253–1260.
24. Brady LW, Miyamoto C, Woo DV, et al. Malignant astrocytomas treated with iodine-125 labeled monoclonal antibody against epidermal growth factor receptor: a phase II trial. Int J Radiat Oncol Biol Phys 1992;22:225–230.
25. Bourdon MA, Matthews TJ, Pizzo SV, Bigner DD. Immunochemical and biochemical characterization of a glioma-associated extracellular matrix glycoprotein. J Cell Biochem 1985;28:183–195.
26. Wikstrand CJ, McLendon RE, Carrel S, Kemshead JT, Mach JP, Coakham HB, et al. Comparative localization of glioma-reactive monoclonal antibodies in vivo in an athymic mouse human glioma xenograft model. J Neuroimmunol 1987;15:37–56.
27. Zalutsky MR, Noska MA, Colapinto EV, Garg PK, Bigner DD. Enhanced tumor localization and in vivo stability of a monoclonal antibody radioiodinated using N-succinimidyl 3-(tri-n-butylstannyl)benzoate. Cancer Res 1989;49:5543–5549.
28. Ventimiglia JB, Wikstrand CJ, Ostrowski LE, Bourdon MA, Lightner VA, Bigner DD. Tenascin expression in human glioma cell lines and normal tissues. J Neuroimmunol 1992;36:41–55.

Announcements

7th Annual Symposium on Breast Disease: Diagnostic Imaging and Current Management, July 11–13, 1993, Grand Traverse Resort Village, Grand Traverse Resort, Michigan. Sponsored by the Department of Radiology, the University of Michigan Medical School. Credit 15: Category I AMA hours. Contact: Vivian Woods, Towsley Center for Continuing Medical Education, Department of Postgraduate Medicine and Health Care Professions, University of Michigan Medical School, P.O. Box 1157, Ann Arbor, MI 48106-1157. call 313-763-1400.

Contemporary Diagnostic Imaging, July 12–16, 1993, The Hilton Resort Hotel, Anchorage, Alaska. Sponsored by the Stanford University Medical Center, Department of Radiology. Credit: TBA. Fee: TBA. Contact: Dawne Ryals, Ryals and Associates, PO Box 1925, Roswell, GA 30077-1925; call 404-641-9773, or fax 404-552-9859.

Body Imaging in Alaska, July 12–14, 1993, The Anchorage Hilton, Anchorage, Alaska. Sponsored by the Stanford University Medical Center, Department of Radiology. Credit: 22.5 Category I AMA hours. Fee: Stanford Alumni $450; Physicians $500, (after June 28) $550; Resident, Fellow, and Technologist $300 (after June 28) $350. Contact: Dawne Ryals, Ryals and Associates, P.O. Box 1925, Roswell, GA 30077-1925; call 404-641-9773, fax 404-552-9859.

National Neuroradiology and Pediatric Radiology Review Course: 1993 A Comprehensive Tutorial, July 25–30, 1993, The Ritz-Carlton Resort Hotel Laguna Niguel, California. Sponsored by the Stanford University Medical Center, Department of Radiology. Credit: Combined Course—48.0, Pediatrics 24.0, Neuro 32.0 Category I AMA hours. Fee: Physician—Combined Course $895, Pediatric $495, Neuro $595; Resident, Fellow, and Technologist—Combined course $595, Pediatric $295, Neuro $395. Contact: Dawne Ryals, Ryals and Associates, P.O. Box 1925, Roswell, GA 30077-1925; call 404-641-9773, fax 404-552-9859.

Breast Imaging and Intervention Into the 21st Century, July 26–30, 1993, The Broadmoor Resort Hotel, Colorado Springs, Colorado. Sponsored by the Radiology Imaging Associates. Credit: Complete Course—Physicians, $30.75. Nurses, 31.00 Category I AMA hours. Fee: Physician—Complete Course $695, Morning Sessions $595; Resident, Fellow, and Technologist—Complete Course $500, Morning Sessions $400; Non-Physician Afternoon $200. Contact: Dawne Ryals, Ryals and Associates, P.O. Box 1925, Roswell, GA 30077-1925; call 404-641-9773, fax 404-552-9859.

[CANCER RESEARCH 49, 2807–2813, May 15, 1989]

Pharmacokinetics and Tumor Localization of ^{131}I-Labeled Anti-Tenascin Monoclonal Antibody 81C6 in Patients with Gliomas and Other Intracranial Malignancies[1]

Michael R. Zalutsky,[2] Robin P. Moseley, Hugh B. Coakham, R. Edward Coleman, and Darell D. Bigner

Departments of Radiology [M. R. Z., R. E. C.], Pathology [M. R. Z., D. D. B.], and the Preuss Laboratory for Brain Tumor Research [D. D. B.], Duke University Medical Center, Durham, North Carolina 27710; Brain Tumor Research Laboratory, Department of Neurosurgery, Frenchay Hospital, Bristol, England [R. P. M., H. B. C.]

ABSTRACT

We previously have reported that radioiodinated anti-tenascin monoclonal antibody 81C6 exhibits therapeutic potential against both s.c. and intracranial human glioma xenografts in athymic mice and rats. Herein we report the selective tumor localization of ^{131}I-labeled 81C6 in patients with gliomas and other intracranial malignancies. Nine patients were simultaneously administered 5–50 mg of ^{131}I-labeled 81C6 and 1–2 mg of ^{125}I-labeled 45.6, an isotype-matched control monoclonal antibody. The blood clearance half-time for 81C6, normalized to that of 45.6 in the same patient, appeared to decrease with 81C6 protein dose. Gamma camera images obtained at 1 to 3 days exhibited increased uptake of ^{131}I in regions corresponding to tumor with varying degrees of contrast to surrounding normal brain. Biopsy specimens of tumor and normal brain were obtained and analyzed histologically for tumor content. The average uptake of 81C6 in tumor ranged from 0.6 to 4.3 × 10^{-3}% of the injected dose per gram. In patients receiving 20–50 mg of 81C6, the average tumor-to-normal-brain ratio was 25:1 with ratios as high as 200:1 seen in some samples. Localization indices were calculated by normalizing the uptake of 81C6 per gram tumor to the uptake of 81C6 per gram blood and dividing by the same ratio for 45.6 control monoclonal antibody. Localization indices for muscle and brain were about 1, in contrast to up to five for tumor. These studies demonstrate that the tumor uptake of ^{131}I-labeled 81C6 in patients with gliomas and other intracranial malignancies is due to specific processes.

INTRODUCTION

The management of patients with gliomas and other intracranial malignancies is an extremely frustrating problem for the clinician. Current approaches to the treatment of these tumors are largely ineffective. Even multimodality regimens including surgery, external beam radiotherapy, and chemotherapy have extended the median survival of patients with malignant glioma by only a few weeks (1). While a multiplicity of factors contribute to the lack of effective therapeutic measures for primary and metastatic brain tumors, a central limiting factor is the nonspecific nature of these therapies which results in dose-limiting toxicity to normal brain tissue.

The potential for exploiting antibodies to deliver diagnostic and therapeutic radionuclides selectively to brain tumors was first explored by Day and coworkers (2) using polyclonal rabbit antisera. More recent studies have demonstrated that radiolabeled MAb[3] directed against human glioma-associated antigens can localize specifically in s.c. and intracranial human glioma xenografts in animals (3–6). The feasibility of utilizing radiolabeled MAbs for selectively delineating and treating gliomas has also been investigated in patients. Brain scans obtained after administration of ^{123}I-labeled F(ab)$_2$ fragments and ^{131}I-labeled intact antibodies have shown increased levels of radioactivity corresponding to regions of glioma as determined by computed tomography (7–11).

One MAb of interest for radioimmunodiagnosis and therapy is 81C6, an IgG$_{2b}$ immunoglobulin which reacts with an epitope of the extracellular matrix antigen tenascin, found in human glioma cell lines, glioma xenografts in athymic rodents, primary human gliomas, but not in normal adult or fetal brain (12). The potential utility of radioiodinated 81C6 MAb for the diagnosis and treatment of gliomas has been documented in several preclinical studies. Paired-label studies in intracranial and s.c. human glioma xenograft models have shown that tumor uptake of radioiodinated 81C6 is specific and permits the gamma camera imaging of intracranial xenografts as small as 20 mg (13, 14). In the intracranial model, paired-injection protocols were used to demonstrate that intracarotid administration increased tumor delivery of radioiodinated 81C6 by 20% over i.v.-injected MAb (15). With regard to its therapeutic potential, treatment with ^{131}I-labeled 81C6 has resulted in significant tumor growth delay and regression (16) in athymic mice bearing s.c. D-54 MG human glioma xenografts and in prolongation of median survival for athymic rats bearing intracranial tumors (17). Lack of response after treatment with ^{131}I-labeled control MAb demonstrated the specificity of these therapeutic effects.

The pharmacokinetics of ^{131}I-labeled MAb antibody 81C6 have been evaluated in patients with gliomas and other intracerebral malignancies. Using paired-label protocols (18), we have demonstrated that uptake of radioiodinated 81C6 in intracerebral tumors is significantly higher than coadministered isotype-matched control MAb. In addition, although the magnitude of tumor uptake of radioactivity is low, it does occur at levels comparable to those reported for other MAbs in extracranial lesions.

MATERIALS AND METHODS

Monoclonal Antibodies. Monoclonal antibody 81C6 and a control antibody of the same IgG$_{2b}$ isotype, 45.6 (produced by the myeloma cell line 45.6TG1.7), were harvested from the ascitic fluid of athymic mice carrying intraperitoneal 81C6 or 45.6 hybridoma. MAbs were purified from hybridoma culture supernatant using Protein A Sepharose 4B. Immunohistological analyses have shown that MAb 45.6 does not display specific antigen-mediated binding to normal human tissues (12). Purified MAbs were dialyzed against 0.05 M phosphate buffered saline (pH 7.4), passed through a 0.22-μm filter (Millipore) and stored at 4°C until used. The purity of each batch of MAb was examined by high-pressure liquid chromatography and sodium dodecyl sulfate-polyacrylamide gel electrophoresis. The MAbs were proven free of bacterial and viral contamination by culture in routine medium and murine antibody production testing in accordance with the guidelines suggested by the Food and Drug Administration.

Radioiodination of MAbs. MAbs 81C6 and 45.6 were labeled with ^{131}I and ^{125}I (Amersham), respectively, using the stationary-phase chloramide, Iodogen (Pierce Chemical Co.) (19). Radioiodinated MAbs were

Received 11/17/88; revised 2/14/89; accepted 2/21/89.

The costs of publication of this article were defrayed in part by the payment of page charges. This article must therefore be hereby marked *advertisement* in accordance with 18 U.S.C. Section 1734 solely to indicate this fact.

[1] Supported by grants CA 43638, CA 42324, CA 11898, NS 20023, and CA 14236 from the National Cancer Institute and by the Imperial Cancer Research Fund.

[2] To whom requests for reprints should be addressed.

[3] The abbreviations used are: MAb, monoclonal antibody; TCA, trichloroacetic acid.

separated from free ^{131}I and ^{125}I by passage through a gas-sterilized, 10-ml Sephadex G-25 column. The binding characteristics of radioiodinated 81C6 and 45.6 were analyzed in an immunoreactivity assay performed at antigen excess. Between 50 and 100 ng of each labeled MAb was incubated overnight in triplicate with 300 mg of both D-54 MG human glioma tumor homogenate and normal rat liver homogenate in 1 ml 0.15 M phosphate buffer containing 1% bovine serum albumin. The amount of 81C6 bound to rat liver after washing was considered to represent nonspecific binding and was subtracted from the percentage 81C6 bound to tumor in order to calculate the specific binding of ^{131}I-labeled 81C6. Specific binding also could be calculated by subtracting the percentage 45.6 bound to tumor from the percentage 81C6 bound to the same homogenate. For all the preparations of ^{131}I-labeled 81C6 and ^{125}I-labeled 45.6 used in these studies, greater than 97% of the radioiodine activity was precipitable in trichloroacetic acid. The absence of aggregates in the labeled MAb was demonstrated by chromatography over a 1.6 x 60 cm Sephacryl S300 gel (Pharmacia), which showed a single peak with a retention time corresponding to that of intact IgG.

Patients. Permission for this study was obtained from the Ethical Committee of Frenchay Hospital. Each patient, along with a close relative, gave informed written consent. Nine patients with clinically presumed, malignant glioma were entered into this study. As shown in Table 1, the histological diagnoses, based on the evaluation of tumor samples obtained at craniotomy, revealed that six patients had glioblastoma multiforme, and one each had an oligodendroglioma, an anaplastic astrocytoma, and a metastatic adenocarcinoma (but suspected initially of having an anaplastic astrocytoma). All patients were scheduled for treatment by surgical resection of tumor. Clinical evaluation included computerized tomography (CT) scan, performed with and without enhancement with Conray 420 (May and Baker, Dagenham, UK). One or two days prior to administration of radiolabeled MAbs, a radionuclide brain scan was obtained after i.v. injection of 20 mCi of [^{99m}Tc]glucoheptonate. All patients had been receiving dexamethasone prior to the investigation.

Administration of MAbs. During the week prior to the study, sera samples were obtained from each patient and tested for anti-murine antibodies. Absence of anti-mouse antibodies was confirmed in all patients. In order to minimize thyroid uptake of radioiodine, all patients received potassium iodide (100 mg) for 2 weeks, commencing 24 h before injection of labeled MAbs. Patients received 5–50 mg of 81C6 IgG labeled with 1.8–3.5 mCi of ^{131}I and 1–2 mg of 45.6 IgG labeled with 0.2–1.3 mCi of ^{125}I. The doses of 81C6 administered were 5 mg (two patients), 10 mg (one patient), 20 mg (three patients), and 50 mg (three patients). Both labeled MAb preparations were combined and diluted to 10–15 ml in sterile, phosphate buffered saline prior to administration. Since previous paired-injection studies in rats with intracranial human glioma xenografts demonstrated a 20% delivery advantage for the intracarotid administration of MAbs (15), this route was utilized for the first seven patients. The labeled MAb mixture was administered into the internal carotid artery ipsilateral to the tumor site. The appropriate carotid artery was cannulated following femoral puncture under local anesthetic. Prior to studying the eighth patient, enough evidence had been accrued to suggest that, in humans, intracarotid delivery offered no significant advantage (20). Therefore, because of the greater risk and discomfort associated with intracarotid administration, radiolabeled 81C6 and 45.6 were injected as an i.v. bolus to the remaining two patients.

Imaging. Scintigraphy was performed with a General Electric MaxiCamera 400T equipped with a high energy, parallel-hole collimator and linked to a DEC PDP 11/34 computer with Gamma 11 software. Ten-min images were accumulated at 10 min, 4 h, and 24 h after MAb injection, and daily thereafter. No subtraction techniques were used. Anterior and lateral views of the head, as well as anterior and posterior views of the thorax, abdomen, and pelvis, were obtained.

Pharmacokinetics. Blood samples were collected beginning at 5 min after administration of MAb and then periodically over the next 7 days. At least 17 samples were obtained from each patient. Aliquots (2 ml) were counted for ^{131}I and ^{125}I activity using a dual-channel automated gamma counter. A correction was applied for spillover of ^{131}I radiation in the ^{125}I counting window. The percentage injected dose remaining in the blood for both nuclides was calculated by comparison to ^{131}I-labeled 81C6 and ^{125}I-labeled 45.6 standards of appropriate count rate. Urine was also collected at daily intervals and 2-ml aliquots were counted in duplicate in order to calculate cumulative urinary excretion of ^{131}I and ^{125}I. Sera samples were obtained by centrifugation at 800 × *g* for 5 min. The protein bound ^{131}I and ^{125}I activity in sera and urine samples was evaluated by precipitation with 15% trichloroacetic acid, followed by centrifugation and gamma counting of the pellet and supernatant. Selected serum samples from each patient were also analyzed by chromatography over a Sephacryl S300 column as described above. For patients numbered 4, 5, and 6, the change in immunoreactivity of ^{131}I-labeled species in the sera as a function of time was determined using the homogenate assay described above. All assays were performed in triplicate. The volume of each serum sample used was selected such that the 81C6 content (estimated from the ^{131}I activity per milliliter) was about 50–100 ng. For these studies, specific binding was calculated by subtracting the percent ^{125}I-labeled 45.6 bound to the glioma homogenate from the percent ^{131}I-labeled 81C6 bound to the same homogenate.

Analysis of Tissue Samples. As part of their normal course of therapy, all patients underwent surgical resection of their tumors 29 to 77 h after injection of ^{131}I-labeled 81C6 and ^{125}I-labeled 45.6 MAbs (Table 3). Between four and 10 samples considered to be tumor at operation were analyzed from each patient. Separate tissue samples were sent for pathological evaluation for use in patient management. In addition, samples of temporalis muscle and normal brain were obtained whenever permitted by the operative approach (muscle, Patients 1, 2, 4–8; normal brain, Patients 1, 2, 4–9). All tissue samples were blotted, placed in tared plastic vials containing 1 ml of formalin, weighed and then counted for ^{131}I and ^{125}I activity. After waiting for 30–45 days to allow the ^{131}I levels to decay, the tissues were subjected to conventional histological analyses to confirm the nature of the malignancy and to estimate the relative amount of tumor and nontumor tissue in each sample.

RESULTS

Radiolabeled MAbs. The specific activities of the ^{131}I-labeled 81C6 preparations ranged between 0.06 and 0.4 μCi/μg. For ^{125}I-labeled 45.6, the specific activities were between 0.2 and 1.8 μCi/μg. In all cases, the trichloroacetic acid precipitability of the administered ^{131}I and ^{125}I activity was greater than 97%. No evidence for aggregate formation was found in the Sephracryl S300 chromatographic analyses of the labeled MAb used in these studies. The immunoreactivity of the ^{131}I-labeled 81C6 preparations was determined *in vitro* by measuring differential binding to antigen-positive D-54 MG human glioma tumor and antigen-negative normal rat liver homogenates. From the data presented in Table 1, one can calculate that the specific binding values ranged between 54 and 71%. When specific binding was calculated as the difference between the percentage 81C6 and

Table 1 *Patient studies with ^{131}I-labeled 81C6*

Tumor type, protein doses, and specific binding percentages of 81C6.

Patient number	Histological diagnosis	Dose 81C6 (mg)	81C6 binding *in vitro*		
			D-54 MG tumor (%)	Rat liver (%)	Specific (%)
1	GBM[a]	5	67	13	54
2	GBM	5	67	13	54
3	GBM	10	79	14	65
4	GBM	20	76	5	71
5	GBM	20	76	5	71
6	MA	20	75	12	63
7	GBM	50	75	12	63
8	Oligo	50	72	2	70
9	AA	50	72	2	70

[a] GBM, glioblastoma multiforme; MA, metastatic adenocarcinoma; Oligo, oligodendroglioma; AA, anaplastic astrocytoma.

nonspecific control MAb 45.6 binding to D-54 MG tumor, nearly identical specific binding percentages were obtained (data not shown).

Pharmacokinetics of ^{131}I-labeled 81C6 and ^{125}I-labeled 45.6. Nine patients received from 5 to 50 mg (1.8–3.5 mCi ^{131}I) of 81C6 and 1.0–1.7 mg (0.2–1.3 mCi ^{125}I) of isotype-matched control MAb 45.6 (Tables 1 and 2). Blood and urine samples were obtained serially over the next 7 days. Half-times for the disappearance of ^{131}I and ^{125}I activity from the blood pool are summarized in Table 2. Since Patient 6 died at 27 h after MAb administration, insufficient data were available for determination of blood clearance half-times. The clearance of 81C6 was better fit by least squares analysis to a biexponential equation; in contrast, the clearance of 45.6 was better fit to a monoexponential equation.

For 81C6, the mean first component half-time ($t_{½}$) ranged from 2.4 h at 5 mg to as short as 0.1 ± 0.05 h at the 50-mg dose. Although there appeared to be an inverse relationship between 81C6 protein dose and first component half-time, this correlation was significant ($r = -0.89$) only when Patient 7 was not included. The second component half-time ranged from about 35 h at 5 mg to as low as 22.4 ± 0.6 h at 50 mg. An inverse relationship between 81C6 protein dose and second component half-time again was apparent ($r = -0.81$) only when Patient 7 was excluded.

With the exception of Patient 7, the half-time for clearance of 45.6 control MAb ranged between 33.4 ± 0.8 and 46.0 ± 1.0 h with no correlation with either 45.6 or 81C6 protein dose observed. The clearance half-time for 45.6 in Patient 7 was 62.8 ± 1.9 h. If the second component half-time for 81C6 is normalized to the 45.6 blood clearance half-time, there is an excellent inverse correlation ($r = -0.93$) between this ratio and 81C6 protein dose administered (Fig. 1), even if the data from Patient 7 are included.

The cumulative urinary excretion of radioiodine following the injection of ^{131}I-labeled 81C6 and ^{125}I-labeled 45.6 is illustrated in Fig. 2. No significant differences between 81C6- and 45.6-associated radioiodine levels in the urine were observed at any time. When the data from all nine patients were combined, 18.3 ± 6.0% and 19.3 ± 3.6%, respectively, of the ^{131}I and ^{125}I were found in the urine 24 h after injection. Similarly, 37.2 ± 8.4% of the ^{131}I and 38.7 ± 4.7% of the ^{125}I administered were found in the urine at 48 h. The standard deviation for the variable protein dose 81C6 also was higher than that for the constant protein dose 45.6 on Days 3 through 7, suggesting the possibility that the rate of urinary excretion may be dose dependent. However, the correlation coefficients for the relationship between 81C6 dose and cumulative urinary excretion were less than 0.5 at all time points.

In addition, the protein-associated fraction of radioiodine activity in the blood and the urine was determined for both nuclides by TCA precipitability. In the blood, the TCA precipitable activity for both nuclides decreased from initial values of 97–99% to 93–96% at 4 to 7 days. No significant differences between 81C6- and 45.6-associated radioiodine TCA values were observed at any time point, nor were any dose-related effects seen. The fraction of both ^{131}I and ^{125}I in the urine that was TCA precipitable was less than 5% at all time points.

Sephacryl S300 gel permeation chromatography was performed on at least one sample from each patient obtained between 12 and 36 h after MAb administration. In all cases, greater than 90% of both the ^{131}I and the ^{125}I activity eluted with the anticipated retention time for unmodified IgG immunoglobulin. The remainder of the activity eluted as a low molecular weight species and was presumed to reflect free iodide.

Immunoreactivity in Serum. These studies were performed on

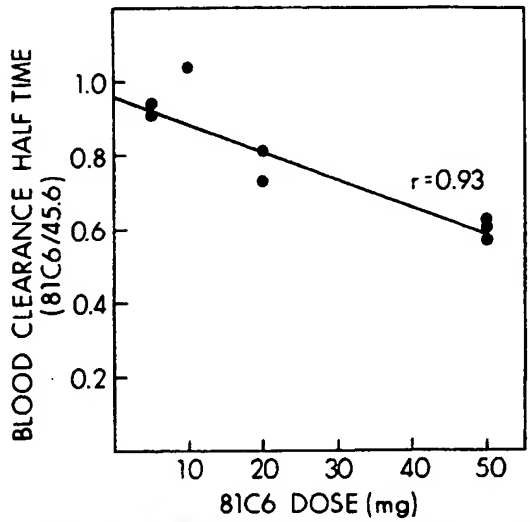

Fig. 1. Relationship between 81C6 protein dose and the ratio of the second component blood clearance half-time of 81C6 to the blood clearance half-time for 45.6 in each patient.

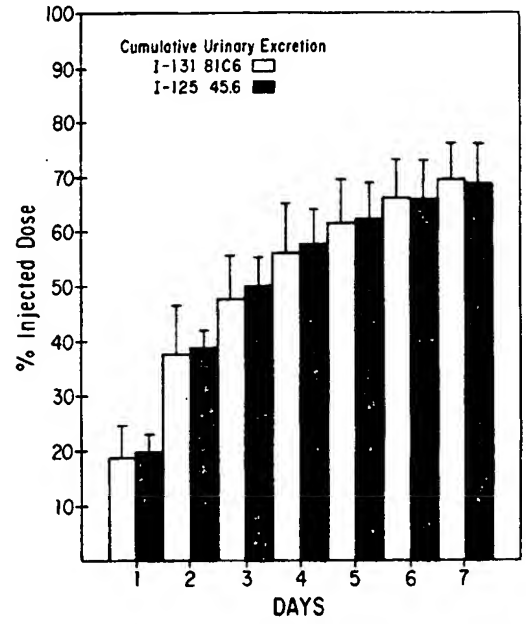

Fig. 2. Cumulative urinary excretion of ^{131}I and ^{125}I during the week following injection of ^{131}I-labeled 81C6 and ^{125}I-labeled 45.6 MAbs.

Table 2 *Blood clearance of ^{131}I and ^{125}I activity in patients injected with ^{131}I-labeled 81C6 and ^{125}I-labeled 45.6*

Patient number	^{131}I-labeled 81C6 Dose (mg)	First component $T_{½}$ (h)	Second component $T_{½}$ (h)	Second component (%)	^{125}I-labeled 45.6 Dose (mg)	^{125}I-labeled 45.6 $T_{½}$ (h)
1	5	2.3 ± 0.3	34.7 ± 1.0	68	1.0	36.8 ± 0.5
2	5	2.5 ± 0.3	36.0 ± 0.9	67	1.0	39.7 ± 0.7
3	10	1.4 ± 0.3	34.9 ± 2.1	59	1.7	33.4 ± 0.8
4	20	0.7 ± 0.2	28.6 ± 1.6	67	1.5	35.4 ± 0.8
5	20	1.1 ± 0.2	24.8 ± 1.4	67	1.5	34.1 ± 1.0
6	50	2.5 ± 0.8	36.1 ± 2.6	35	1.0	62.8 ± 1.9
7	50	0.5 ± 0.2	22.4 ± 0.6	67	1.0	36.9 ± 1.0
8	50	0.1 ± 0.05	27.6 ± 0.9	60	1.0	46.0 ± 1.0
9						

serum samples obtained from the three patients injected with 20 mg of 81C6. Specific binding was calculated by subtracting the percent ^{125}I-labeled 45.6 from the percent ^{131}I-labeled 81C6 bound *in vitro* to D-54 MG human glioma homogenates. As shown in Fig. 3, the immunoreactivity of ^{131}I activity in the serum decreased from pre-injection levels of about 70% to about 40% during the first 5 h and then declined at a more gradual rate thereafter.

Imaging. The nine patients were scanned at various intervals beginning 10 min after MAb administration with the last set of images obtained about 2–4 h prior to surgery. At 1 h, prominent blood pool activity and hepatic accumulation were seen. Activity in the liver, and in seven patients the spleen, was also observed in the later images. Uptake of ^{131}I in the liver and the spleen was more pronounced, relative to blood pool, in patients injected with lower protein doses (5–10 mg) of 81C6. Some evidence of bone marrow accumulation was observed on scans obtained after 24 h.

[^{99m}Tc]Glucoheptonate scanning performed prior to MAb administration revealed blood-brain barrier impairment in all nine patients. Known sites of tumor could not be identified on scans obtained earlier than 24 h after ^{131}I-labeled 81C6 MAb injection. In Patients 3, 4, 7, and 8, tumor could be identified on later images. Selective localization of ^{131}I-labeled 81C6 in tumor was more apparent in Patients 1, 2, 5, 6, and 9. Anterior and lateral planar images of Patient 5, which were obtained 24 h after injection of a 20-mg dose of ^{131}I-labeled 81C6, are shown in Fig. 4. In these scans, accumulation of ^{131}I in the region corresponding to tumor is clearly demonstrated.

Analyses of Tissue Specimens. Biopsy specimens removed at surgery were placed into coded, tared vials containing 1 ml of 20% formalin and assayed for ^{131}I and ^{125}I activity using an automated gamma counter. Between four and 10 samples of tumor were obtained from each patient (Table 3). Specimens of temporalis muscle were also analyzed from seven patients and normal brain from eight patients. The fraction of tumor in each biopsy sample was determined histopathologically for all tissue specimens obtained from Patients 4–9.

As shown in Table 3, the average tumor uptake, expressed as percentage injected dose per gram, ranged from 6.4×10^{-4} for Patient 9 (anaplastic astrocytoma, 50 mg 81C6) to 4.3×10^{-3} for Patient 6 (metastatic adenocarcinoma, 20 mg 81C6). The variation in tumor uptake for samples from an individual patient ranged from a 50% difference (Patient 7) to a 15-fold difference (Patient 6). The highest level of ^{131}I-labeled 81C6 observed in a tumor biopsy was 1.6×10^{-2} %ID/g.

With the exception of Patient 3, tumor-to-normal-brain uptake ratios also were calculated for ^{131}I-labeled 81C6. The average tumor:normal brain ratios ranged from 2.3:1 for Patient 9 to 76:1 for Patient 5 (Table 3). The highest tumor:normal brain ratio was 205:1 for one of the tumor specimens obtained from Patient 6.

By coadministering isotype-matched, ^{125}I-labeled 45.6 Mab, it was possible to determine the specificity of ^{131}I-labeled 81C6 uptake in brain tumors and other tissues. Using the formalism of Moshakis *et al.* (21), the localization index was expressed as the ratio of 81C6 ^{131}I to 45.6 ^{125}I activity in the tumor or other tissue of interest, divided by the same ratio in the blood. As shown in Table 4, the localization indices for muscle ranged between 1.00–1.17, and for normal brain ranged between 0.95–1.25. For the tumor samples, the average localization indices for patients receiving 5–10 mg of 81C6 varied between 1.3–1.5, and for patients injected with 20–50 mg ranged from 2.2 to 3.7. Four of the patients had tumor specimens in which the localization index was greater or equal to 4.0.

In evaluating these results, it is important to bear in mind that the three patients receiving the 5–10 mg doses of ^{131}I-labeled 81C6 did not have their uptake values corrected for the fraction of the biopsy determined to be tumor by histopathological analyses. Table 5 includes representative data from one patient (Patient 8) which illustrate the effect of incorrect identification of tissue composition on the percentage injected dose per gram tumor and normal brain as well as on the tumor-to-normal-brain tissue uptake ratio. In this patient, presence of tumor in the "normal brain" samples and presence of normal brain and/or necrosis in some of the "tumor" specimens decreased the apparent tumor:normal brain ratio by as much as 6-fold. Localization indices were also affected by heterogeneity in biopsy composition. For example, in this patient, correcting for the fact that one of the samples contained only 60% tumor increased the localization index from 2.0 to 2.7.

Toxicity. No toxicity was observed as a consequence of administration of radioiodinated 81C6 and 45.6 MAbs. In particular, results of liver function tests obtained 1–2 weeks after MAb injection were unchanged from baseline values determined immediately prior to the MAb study.

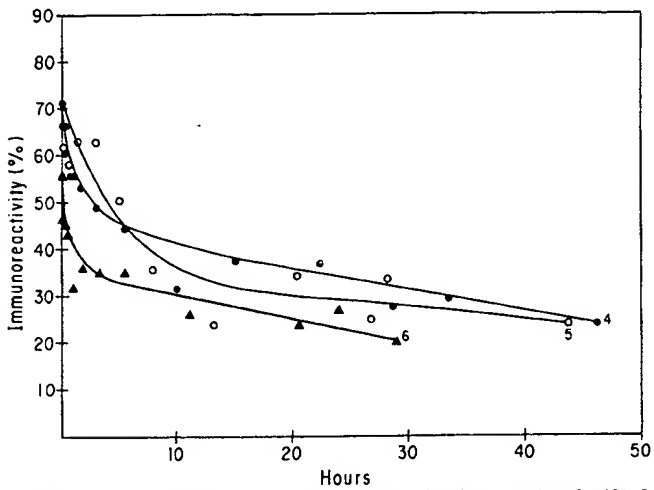

Fig. 3. Immunoreactivity of ^{131}I activity in sera of patients numbered 4 (●), 5 (○), and 6 (▲) injected with 20 mg of ^{131}I-labeled 81C6. Immunoreactivity defined as the percentage binding to D-54 MG human glioma homogenates *in vitro* of ^{131}I, derived from 81C6, minus the percentage binding of ^{125}I, derived from 45.6 control MAb.

DISCUSSION

Monoclonal antibody 81C6 was selected for pharmacokinetic evaluation in humans because of the wealth of preclinical information which suggests that this MAb may be useful for delivering radionuclides to gliomas and other neoplasms that express tenascin (3, 14, 16, 17). In these studies, both ^{131}I-labeled 81C6 and ^{125}I-labeled 45.6 control MAb were administered intracarotidly because a delivery advantage of approximately 20%, relative to i.v. injection, was observed in paired-injection studies in the D-54 MG glioma xenograft model (15). However, after studying the first seven patients, it was determined by paired-injection analysis, that intracarotid administration did not offer a delivery advantage for 81C6 in the human (20). Since there is a small, but finite risk associated with carotid angiography, the last two patients received MAbs via i.v. injection.

In this report, we have demonstrated that ^{131}I-labeled 81C6 was accumulated in brain tumors in concentrations sufficient to permit external imaging. Thus, disruption of the blood-brain

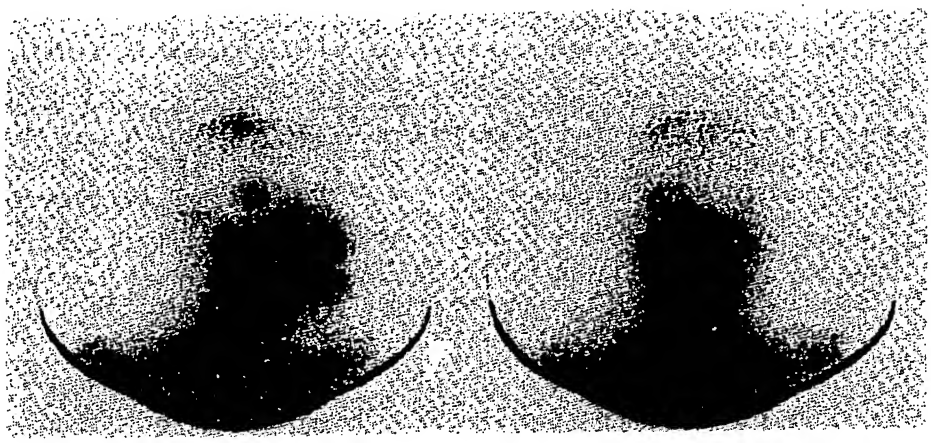

Fig. 4. Lateral and anterior planar images of the brain obtained 24 h after injection of a 20 mg (3.4 mCi) dose of ^{131}I-labeled 81C6. Patient 5, glioblastoma multiforme.

Table 3 *Tumor uptake and tumor to normal brain ratios of ^{131}I-labeled 81C6 determined from patient biopsy samples*

Patient number	Dose (mg)	Interval to surgery (h)	Tumor samples	Tumor uptake (% ID/g) Average	Range	Tumor:normal brain ratio Average	Range
1[a]	5	47	10	8.1×10^{-4}	$(0.4–1.4) \times 10^{-3}$	3.5	1.6–6.0
2[a]	5	68	8	1.3×10^{-3}	$(0.4–4.3) \times 10^{-3}$	2.6	1.1–8.6
3[a]	10	32	8	7.5×10^{-4}	$(0.5–1.2) \times 10^{-3}$	—[b]	—
4	20	73	8	6.8×10^{-4}	$(0.4–1.0) \times 10^{-3}$	4.3	2.4–6.6
5	20	77	4	4.1×10^{-3}	$(1.4–5.0) \times 10^{-3}$	76	26–93
6	20	29	7	4.3×10^{-3}	$(1.0–15.5) \times 10^{-3}$	56	10–205
7	50	74	5	1.2×10^{-3}	$(1.0–1.5) \times 10^{-3}$	14	11–17
8	50	70	4	1.0×10^{-3}	$(0.4–1.7) \times 10^{-3}$	15	6–26
9	50	70	8	6.4×10^{-4}	$(0.3–1.0) \times 10^{-3}$	2.3	1.0–3.6

[a] Composition of biopsy samples not determined by pathology.
[b] Normal brain sample not available.

Table 4 *Localization indices in tumor biopsy samples from patients injected with ^{131}I-labeled 81C6 and ^{125}I-labeled 45.6*

Patient number	Dose 81C6 (mg)	Localization index[a] Muscle	Normal brain	Tumor range (average)
1[b]	5	1.01	0.99	1.3–1.9 (1.5)
2[b]	5	1.00	1.25	1.1–2.4 (1.8)
3[b]	10	—[c]	—[c]	1.2–1.4 (1.3)
4	20	1.13	1.09	1.7–3.4 (2.3)
5	20	1.17	0.95	3.4–5.0 (3.7)
6	20	1.09	1.23	1.3–5.0 (3.2)
7	50	1.03	1.11	2.8–4.8 (3.7)
8	50	1.00	1.14	1.3–3.2 (2.2)
9	50	—[c]	1.12	1.3–4.0 (2.3)

[a] Localization index =

$$\frac{\text{81C6 in tissue/81C6 in blood}}{\text{45.6 in tissue/45.6 in blood}}$$

[b] Composition of biopsy samples not determined by pathology.
[c] Tissue samples not available.

Table 5 *Effect of correcting for histologically determined biopsy composition on tumor uptake and tumor to normal brain ratios*

Data from Patient 8.

Sample	% Tumor in biopsy	% ID/g Raw	Corrected	Tumor:brain ratio Raw	Corrected
Normal brain	70	3.0×10^{-4}	7.6×10^{-5}		
Normal brain	30	2.7×10^{-4}	5.5×10^{-5}		
Tumor	100	1.7×10^{-3}	1.7×10^{-3}	6.1	26
Tumor	100	7.3×10^{-4}	7.3×10^{-4}	2.6	11
Tumor	60	7.2×10^{-4}	1.2×10^{-3}	2.5	18
Tumor	70	3.3×10^{-4}	4.0×10^{-4}	1.2	6.0

barrier was sufficient to allow access of labeled immunoglobulin to intracerebral tumors. The contrast between tumor and surrounding normal brain seen on the scans increased with time, becoming optimal 24–48 h after MAb injection. In general, better tumor images were obtained in those patients with higher ^{131}I uptake levels as determined by gamma counting of their tumor biopsy specimens.

The amount of ^{131}I localizing in brain tumors after ^{131}I-labeled 81C6 injection was quite low, with average values ranging between 1 and 4×10^{-3} % per gram. The magnitude of 81C6 uptake in cerebral tumors was similar to that observed by Richardson *et al.* (10) following the injection of MAb UJ13A labeled with ^{131}I. While it is possible that an incompletely compromised blood-brain barrier might contribute to the low level of MAb uptake in brain tumors, it is important to point out that these values are comparable to those observed in tumor biopsies following i.v. MAb injection in patients with melanoma, breast, ovarian, and colorectal carcinoma (22–28).

One of the principal limitations of external beam radiotherapy for the treatment of primary brain tumors is radiation-induced toxicity to adjacent normal brain. When the biopsy data from the eight patients from which a specimen of adjacent normal brain are pooled, the average tumor:brain ratio for ^{131}I-labeled 81C6 was greater than 5:1. If only those specimens for which fractional tumor content was determined histologically are considered (Patients 4–9), then the average tumor:normal brain ratio for 81C6 increases to 25:1. MAb protein dose may be a pertinent factor since the average tumor:brain ratio for biopsies at 20 mg 81C6 was 38:1, in comparison to 9:1 for samples from patients receiving 50 mg of 81C6 MAb.

The tumor:normal brain uptake ratios seen in biopsies for 81C6 IgG are quite favorable when compared to those found in the literature for other MAb and fragments. After injection of radioiodinated UJ13A IgG into six patients with primary brain tumors, tumor:normal brain ratios at 3 to 16 days ranged from 3 to 13:1 in surgically resected tissues (10). Using the lower molecular weight F(ab')$_2$ fragment of Mel-14, Behnke *et al.* (7) observed tumor:brain ratios of 2 to 18:1 in four patients with gliomas.

Since nonspecific uptake of proteins in brain tumors is well known (29), it is essential to demonstrate that radiolabeled MAb accumulation in cerebral malignancies is related to specific processes. To address this concern, all patients receiving ^{131}I-labeled 81C6 also were injected with an ^{125}I-labeled, isotype-matched control MAb (45.6) so that specific and nonspecific immunoglobulin uptake in brain tumors could be differentiated. Unlike the results of a previous study in glioma patients in

which no difference between specific UJ13A and nonspecific HMFG2 uptake in tumor was seen (11), we have observed that the localization indices for 81C6 uptake in cerebral malignancies were as high as 5. For the patients whose biopsy composition was determined histopathologically, the average localization index for tumor was 2.83, compared to 1.07 and 1.11 for normal muscle and brain, respectively. These results indicate that the uptake of radioiodinated 81C6 in brain tumors is specific.

The uptake of 81C6 MAb in tumor specimens from individual patients was quite variable, ranging from a 15-fold difference for Patient 6 to a 50% difference for Patient 7. Patient 6, who had the greatest tumor uptake, was not known to have a metastatic adenocarcinoma until after histological evaluation of the biopsy. 81C6 reacts with tenascin, which is expressed in many tumor types, including fibrosarcoma, carcinoma of the breast and Wilms tumor (12); however, quantitation of differences in tenascin expression among tumor types or among different tumors of the same type has not yet been performed. Imaging of extracranial lesions could not be evaluated in Patient 6 since no evidence of primary or other sites of metastases was seen at autopsy. Studies to evaluate imaging of other tumor types with radiolabeled 81C6 are under consideration.

Heterogeneities in vascular permeability and antigenic expression may contribute to differences in 81C6 accumulation in a particular tumor. Since uptake of 45.6 MAb reflects nonspecific processes, regional variations in brain tumor uptake are related to heterogeneities in tumor blood flow and vascular permeability. In each patient's biopsy specimens, the variation in 45.6 uptake ranged from 25 to 500%; and, except for Patient 4, about a threefold lower variation in tumor accumulation of 45.6 compared to 81C6 was seen. These differences, in concert with the large variation in localization indices observed for 81C6 in most patients, suggest that regional variation in antigenic expression is an important factor influencing the heterogeneity of 81C6 accumulation in brain tumors. The importance of regional variations in antigen distribution in affecting 81C6 uptake has also been demonstrated in D-54 MG human glioma xenograft models using quantitative autoradiography (30). These studies suggest that it may be necessary to use mixtures of MAbs reactive with different glioma-associated antigens in order to obtain maximal and uniform uptake of radiolabeled MAbs in gliomas.

The influence of protein dose on MAb pharmacokinetics is not clear, partly because of intrinsic differences in the labeled MAb systems that have been investigated. In xenograft animal model studies, there is disagreement as to the effect of MAb dose on the magnitude of tumor uptake and tumor-to-normal-tissue ratios (31–37). Most clinical studies investigating the effect of MAb protein dose have been performed with ^{111}In-labeled MAbs (38–42). Lesion detectability appears to increase with increasing protein dose of ZME-018, 9.2.27, and 96.5 anti-melanoma MAbs (38–40, 42). However, higher protein doses of MAb also result in prolonged retention of ^{111}In activity in the blood pool with some MAbs (38, 39, 42), but not for others (39, 41). Since the catabolism of ^{111}In and ^{131}I-labeled MAbs is different, particularly with regard to the prolonged retention of ^{111}In-labeled catabolites (43), the relevance of these studies to the current investigation is questionable. In at least one study with an ^{131}I-labeled MAb (B72.3), immunoglobulin dose did not influence MAb pharmacokinetics and lesion detectability (23).

Although it is not possible to make a definitive statement concerning the effect of 81C6 dose on tumor uptake, it appears that expedited blood clearance is associated with higher protein doses of 81C6. This behavior is in marked contrast to that reported in the literature, particularly for ^{111}In-labeled MAbs. One possible explanation is that, at higher doses of 81C6, the rate of catabolism is increased. In contrast to ^{111}In-labeled MAb, radioiodinated MAb degradation products are excreted relatively rapidly via the urine and, thus, increased catabolism could lead to more rapid clearance. However, no dose-dependent effects were observed for the urinary excretion of 81C6 and, at all time points, the concentration of both 81C6 and 45.6 derived radioiodine in the urine was quite similar. It is worth noting that the cumulative urinary excretion observed for both 81C6 and 45.6 was about twice as high as that observed previously for ^{131}I-labeled B6.2 MAb (44). Since the tenascin antigen, which 81C6 recognizes, also is present in normal liver and spleen red pulp sinusoids (12), antigen-mediated binding to these tissues could also influence the pharmacokinetics of 81C6 associated radiolabel.

In summary, we have demonstrated that gliomas and an intracerebral metastatic adenocarcinoma can be detected in patients by gamma camera imaging after injection of ^{131}I-labeled 81C6. The magnitude of brain tumor uptake was small but comparable to that reported in the literature for other types of tumors. Analysis of biopsy specimens from patients injected with 20–50 mg of 81C6 revealed an average tumor-to-normal-brain ratio of about 25:1. By coadministering an ^{125}I-labeled control MAb, we were able to determine that the localization indices in tumor were as high as 5. In contrast, the localization indices in normal brain and muscle were approximately one, indicating that uptake of 81C6 in these cerebral malignancies was specific.

ACKNOWLEDGMENTS

The authors wish to thank Janet Wheeler for her assistance in performing the gamma camera imaging, Drs. John Bradshaw and Gordon Thompson for performing the angiographic administration of the MAbs, and Ann Tamariz for help in preparing the manuscript. Robin Moseley was supported as a research fellow by the Preuss Foundation.

REFERENCES

1. Green, S. B., Byar, D. P., Walker, M. D., Pistenman, D. A., Alexander, E., Jr., Batzdorf, U., Brooks, W. H., Hunt, W. E., Meaky, J., Jr., Odom, G. L., Paoletti, P., Ransohoff, J., II, Robertson, J. T., Seller, R. G., Shapiro, W. R., Smith, K., Jr., Wilson, C. B., and Strike, T. A. Comparisons of carmustine, procarbazine, and high-dose methylprednisolone as additions to surgery and radiotherapy for the treatment of malignant glioma. Cancer Treat. Rep., *67:* 121–132, 1983.
2. Day, E. D., Lassiter, S., Woodhall, B., Mahaley, J. L., and Mahaley, M. S. The localization of radioantibodies in human brain tumors. I. Preliminary exploration. Cancer Res., *25:* 773–778, 1965.
3. Bourdon, M. A., Coleman, R. E., Blasberg, R. G., Groothuis, D. R., and Bigner, D. D. Monoclonal antibody localization in subcutaneous and intracranial human xenografts: paired label and imaging analysis. Anticancer Res., *4:* 133–140, 1984.
4. Wikstrand, C. J., McLendon, R. E., Bullard, D. E., Fredman, P., Svennerholm, L., and Bigner, D. D. Production and characterization of two human glioma xenograft-localizing monoclonal antibodies (Mabs). Cancer Res., *46:* 5933–5940, 1986.
5. Takahashi, H., Herlyn, D., Atkinson, B., Powe, J., Rodeck, V., Alavi, A., Bruce, D. A., and Koprowski, H. Radioimmunodetection of human glioma xenografts by monoclonal antibody to epidermal growth factor receptor. Cancer Res., *47:* 3847–3850, 1987.
6. Wikstrand, C. J., McLendon, R. E., Carrel, S., Kemshead, J. T., Mach, J-P., Coakham, H. B., de Tribolet, N., Bullard, D. E., Zalutsky, M. R., and Bigner, D. D. Comparative localization of glioma-reactive monoclonal antibodies *in vivo* in an athymic mouse human glioma xenograft model. J. Neuroimmunol., *15:* 37–56, 1987.
7. Behnke, J., Mach, J-P., Buchegger, F., Carrel, S., Delaloye, B., and de Tribolet, N. *In vivo* localisation of radiolabelled monoclonal antibody in

human gliomas. Br. J. Neurosurg., *2:* 193–197, 1988.
8. Epenetos, A. A., Courtenay-Luck, N., Pickering, D., Hooker, G., Durbin, H., Lavender, J. P., and McKenzie, C. G. Antibody guided irradiation of brain glioma by arterial infusion of radioactive monoclonal antibody against epidermal growth factor receptor and blood group A antigen. Br. Med. J., *290:* 1463–1466, 1985.
9. Phillips, J., Alderson, T., Sikora, K., and Watson, J. Localisation of malignant glioma by a radiolabelled human monoclonal antibody. J. Neurol. Neurosurg. Psychiatry, *46:* 388–392, 1983.
10. Richardson, R. B., Davies, A. G., Bourne, S. P., Staddon, G. E., Kemshead, J. T., and Coakham, H. B. Radioimmunolocalization of brain tumours: Biodistribution of radiolabeled monoclonal antibody UJ13A. Eur. J. Nucl. Med., *12:* 313–320, 1986.
11. Davies, A. G., Richardson, R. B., Bourne, S. P., Kemshead, J. T., and Coakham, H. B. Immunolocalisation of human brain tumuors. *In:* N. Bleeham (ed.), Tumors of the Brain, pp. 83–99. Berlin: Springer-Verlag, 1986.
12. Bourdon, M. A., Wikstrand, C. J., Furthmayr, H., Matthews, T. J., and Bigner, D. D. Human glioma-mesenchymal extracellular matrix antigen defined by monoclonal antibody. Cancer Res., *43:* 2796–2805, 1983.
13. Bourdon, M. A., Coleman, R. E., Blasberg, R. G., Groothuis, D. R., and Bigner, D. D. Monoclonal antibody localization in subcutaneous and intracranial human xenografts: paired-label and imaging analysis. Anticancer Res., *4:* 133–140, 1984.
14. Bullard, D. E., Adams, C. J., Coleman, R. E., and Bigner, D. D. *In vivo* imaging of intracranial human glioma xenografts comparing specific with nonspecific radiolabeled monoclonal antibodies. J. Neurosurg., *64:* 257–262, 1986.
15. Lee, Y. S., Bullard, D. E., Wikstrand, C. J., Zalutsky, M. R., Mahlbaier, L. H., and Bigner, D. D. Comparison of monoclonal antibody delivery to intracranial glioma xenografts by intravenous and intracarotid administration. Cancer Res., *47:* 1941–1946, 1987.
16. Lee, Y. S., Bullard, D. E., Zalutsky, M. R., Coleman, R. E., Friedman, H. S., Colapinto, E. V., and Bigner, D. D. Therapeutic efficacy of murine monoclonal antibody 81C6 in a human glioma xenograft model. Cancer Res., *48:* 559–566, 1988.
17. Lee, Y., Bullard, D. E., Humphrey, P. A., Colapinto, D. V., Friedman, H. S., Zalutsky, M. R., Coleman, R. E., and Bigner, D. D. Treatment of intracranial human glioma xenografts with ^{131}I-labeled antitenascin monoclonal antibody 81C6. Cancer Res., *48:* 2904–2910, 1988.
18. Pressman, D., Day, E. D., and Blau, M. The use of paired labeling in the determination of tumor-localizing antibodies. Cancer Res., *17:* 845–850, 1957.
19. Fracker, P. J., and Speck, J. C. Protein and cell membrane iodinations with a sparingly soluble chloramide 1,3,4,6-tetrachloro-3α-6α-di-phenylglycouril. Biochem. Biophys. Res. Commun., *80:* 849–857, 1978.
20. Moseley, R., Zalutsky, M. R., Coakham, H. B., Coleman, R. E., and Bigner, D. D. Monoclonal antibody imaging of gliomas. Comparison of intracarotid and intravenous delivery in patients (Abstract). J. Nucl. Med., *29:* 847, 1988.
21. Moshakis, V., McIlhinney, R. A. J., Raghavan, D., and Neville, A. M. Monoclonal antibodies to detect human tumours: an experimental approach. J. Clin. Pathol., *34:* 314–319, 1981.
22. Colcher, D., Esteban, J., Carrasquillo, J. A., Sugarbaker, P., Reynolds, J. C., Bryant, G., Larson, S. M., and Schlom, J. Complementation of intracavitary and intravenous administration of a monoclonal antibody (B72.3) in patients with carcinoma. Cancer Res., *47:* 4218–4224, 1987.
23. Colcher, D., Esteban, J. M., Carrasquillo, J. A., Sugarbaker, P., Reynolds, J. C., Bryant, G., Larson, S. M., and Schlom, J. Quantitative analyses of selective radiolabeled monoclonal antibody localization in metastatic lesions of colorectal cancer patients. Cancer Res., *47:* 1185–1189, 1987.
24. Buraggi, G. L., Callegaro, L., Mariani, A., Turrin, A., Cascinelli, N., Attili, A., Bombardieri, E., Terno, G., Plassio, G., Dovis, M., Mazzuca, N., Natali, P. G., Scassellati, G. A., Rosa, U., and Ferrone, S. Imaging with ^{131}I-labeled monoclonal antibodies to a high molecular weight melanoma-associated antigen in patients with melanoma: efficacy of whole immunoglobulin and its F(ab')$_2$ fragments. Cancer Res., *45:* 3378–3387, 1985.
25. Epenetos, A. A., Snook, D., Durbin, H., Johnson, P. M., and Taylor-Papadimitriou, J. Limitations of radiolabeled monoclonal antibodies for localization of human neoplasms. Cancer Res., *46:* 3183–3191, 1986.
26. Mach, J-P., Carrel, S., Forni, M.. Ritschard, J., Donath, A., and Alberto, P. Tumor locationization of radiolabeled antibodies against carcinoembryonic antigen in patients with carcinoma. N. Engl. J. Med., *303:* 5–10, 1980.
27. Garrands, P. A., Perkins, A. C., Pimm, M. V., Hardy, J. D., Embleton, M. J., Baldwin, R. W., and Hardcastle, J. D. Radioimmunodetection of human colorectal cancers by an anti-tumor monoclonal antibody. Lancet, *2:* 397–400, 1982.
28. Halpern, S. E., Dillman, R. O., Witztum, K. F., Shega, J. F., Hagan, P. L., Burrows, W. M., Dillman, J. B., Clutter, M. L., Sobol, R. E., Frincke, J. M., Bartholomew, R. M., David, G. S., and Carlo, D. Radioimmunodetection of melanoma utilizing ^{111}In-96.5 monoclonal antibody: a preliminary report. Radiology, *155:* 493–499, 1985.
29. Chou, S. N., Aust, J. B., Moore, G. E., and Peyton, W. T. Radioactive iodinated human serum albumin as tracer agent for diagnosing and localizing intracranial lesions. Proc. Soc. Exp. Biol. Med., *77:* 193–195, 1951.
30. Blasberg, R. G., Nakagawa, H., Bourdon, M. A., Groothuis, D. R., Patlak, C. S., and Bigner, D. D. Regional localization of a glioma-associated antigen defined by monoclonal antibody 81C6 *in vivo*: kinetics and implications for diagnosis and therapy. Cancer Res., *47:* 4432–4443, 1987.
31. Badger, C. C., Krohn, K. A., Peterson, A. V., Shulman, H., and Bernstein, I. D. Experimental radiotherapy of murine lymphoma with ^{131}I-labeled anti-thy 1.1 monoclonal antibody. Cancer Res., *45:* 1536–1544, 1985.
32. Badger, C. C., Krohn, K. A., Shulman, H., Flournoy, N., and Bernstein, I. D. Experimental radioimmunotherapy of murine lymphoma with ^{131}I-labeled anti-T-cell antibodies. Cancer Res., *46:* 6223–6228, 1986.
33. Jakowatz, J. G., Beatty, B. G., Vlahos, W. G., Porudominsky, D., Philben, V. J., Williams, L. E., Paxton, R. J., Shively, J. E., and Beatty, J. D. High-specific-activity ^{111}In-labeled anticarcinoembryonic antigen monoclonal antibody: biodistribution and imaging in nude mice bearing human colon cancer xenografts. Cancer Res., *45:* 5700–5706, 1985.
34. Rogers, G. T., Harwood, P. J., Pedley, R. B., Boden, J., Rawlins, G., and Bagshawe, K. D. Dynamics of monoclonal antibody distribution and prolonged tumour localisation in nude mice bearing a human CEA-producing colon carcinoma xenograft. Tumor Biol., *6:* 453–463, 1985.
35. Rogers, G. T., Harwood, P. J., Pedley, R. B., Boden, J., and Bagshawe, K. D. Dose-dependent localisation and potential for therapy of F(ab')$_2$ fragments against CEA studies in a human tumour xenograft model. Br. J. Cancer, *54:* 341–344, 1986.
36. Wahl, R. L., Liebert, M., and Wilson, B. S. The influence of monoclonal antibody dose on tumor uptake of radiolabeled antibody. Cancer Drug Delivery, *3:* 243–249, 1986.
37. Zalutsky, M. R., Bast, R. C., Jr., and Knapp, R. C. Pharmacokinetics of a radioiodinated monoclonal antibody F(ab')$_2$ fragment in a xenograft model with circulating antigen. Nucl. Med. Biol., in press, 1989.
38. Murray, J. L., Rosenblum, M. G., Lamki, L., Glenn, H. J., Krizan, Z., Hersh, E. M., Plager, C. E., Bartholomew, R. M., Unger, M. W., and Carlo, D. J. Clinical parameters related to optimal tumor localization of Indium-111-labeled mouse antimelanoma monoclonal antibody ZME-018. J. Nucl. Med., *28:* 25–33, 1987.
39. Rosenblum, M. G., Murray, J. L., Lamki, L., David, G., and Carlo, D. Comparative clinical pharmacology of [^{111}In]-labeled murine monoclonal antibodies. Cancer Chemother. Pharmacol., *20:* 41–47, 1987.
40. Kirkwood, J. M., Neumann, R. D., Zoghbi, S. S., Ernstoff, M. S., Cornelius, E. A., Shaw, C., Ziyadeh, T., Fine, J. A., and Unger, M. W. Scintigraphic detection of metastatic melanoma using indium 111/DTPA conjugated anti-gp240 antibody (ZME-018). J. Clin. Oncol., *5:* 1247–1255, 1987.
41. Rosenblum, M. G., Murray, J. L., Haynie, T. P., Glenn, H. J., Jahns, M. F., Benjamin, R. S., Frincke, J. M., Carlo, D. J., Hersh, E. M. Pharmacokinetics of ^{111}In-labeled anti-p97 monoclonal antibody in patients with metastatic malignant melanoma. Cancer Res., *45:* 2382–2386, 1985.
42. Carrasquillo, J. A., Abrams, P. G., Schroff, R. W., Reynolds, J. C., Woodhouse, C. S., Morgan, A. C., Keenan, A. M.. Foon, K. A., Perentesis, P., Marshall, S., Horowitz, M., Szymendera, J., Englert, J., Oldham, R. K., and Larson, S. M. Effect of antibody dose on the imaging and biodistribution of indium-111 9.2.27 anti-melanoma monoclonal antibody. J. Nucl. Med., *29:* 39–47, 1988.
43. Carrasquillo, J. A., Mulshine, J. L., Bunn, P. A., Jr., Reynolds, J. C., Foon, K. A., Schroff, R. W., Perentesis, P., Steis, R. G., Keenan, A. M., Horowitz, M., and Larson, S. M. Indium-111 T101 monoclonal antibody is superior to iodine-131 T101 in imaging of cutaneous T-cell lymphoma. J. Nucl. Med., *28:* 281–287, 1987.
44. Hayes, D. F., Zalutsky, M. R., Kaplan, W., Noska, M., Thor, A., Colcher, D., and Kufe, D. W. Pharmacokinetics of radiolabeled monoclonal antibody B6.2 in patients with metastatic breast cancer. Cancer Res., *46:* 3157–3163, 1986.

Phase II Trial of Murine ^{131}I-Labeled Antitenascin Monoclonal Antibody 81C6 Administered Into Surgically Created Resection Cavities of Patients With Newly Diagnosed Malignant Gliomas

By David A. Reardon, Gamal Akabani, R. Edward Coleman, Allan H. Friedman, Henry S. Friedman, James E. Herndon II, Ilkcan Cokgor, Roger E. McLendon, Charles N. Pegram, James M. Provenzale, Jennifer A. Quinn, Jeremy N. Rich, Lorna V. Regalado, John H. Sampson, Timothy D. Shafman, Carol J. Wikstrand, Terence Z. Wong, Xiao-Guang Zhao, Michael R. Zalutsky, and Darell D. Bigner

Purpose: To assess the efficacy and toxicity of intraresection cavity ^{131}I-labeled murine antitenascin monoclonal antibody 81C6 and determine its true response rate among patients with newly diagnosed malignant glioma.

Patients and Methods: In this phase II trial, 120 mCi of ^{131}I-labeled murine 81C6 was injected directly into the surgically created resection cavity of 33 patients with previously untreated malignant glioma (glioblastoma multiforme [GBM], n = 27; anaplastic astrocytoma, n = 4; anaplastic oligodendroglioma, n = 2). Patients then received conventional external-beam radiotherapy followed by a year of alkylator-based chemotherapy.

Results: Median survival for all patients and those with GBM was 86.7 and 79.4 weeks, respectively. Eleven patients remain alive at a median follow-up of 93 weeks (range, 49 to 220 weeks). Nine patients (27%) developed reversible hematologic toxicity, and histologically confirmed, treatment-related neurologic toxicity occurred in five patients (15%). One patient (3%) required reoperation for radionecrosis.

Conclusion: Median survival achieved with ^{131}I-labeled 81C6 exceeds that of historical controls treated with conventional radiotherapy and chemotherapy, even after accounting for established prognostic factors including age and Karnofsky performance status. The median survival achieved with ^{131}I-labeled 81C6 compares favorably with either ^{125}I interstitial brachytherapy or stereotactic radiosurgery and is associated with a significantly lower rate of reoperation for radionecrosis. Our results confirm the efficacy of ^{131}I-labeled 81C6 for patients with newly diagnosed malignant glioma and suggest that a randomized phase III study is indicated.

J Clin Oncol 20:1389-1397.

IMPROVEMENT IN outcome for patients with the most common primary adult brain tumor, malignant glioma, has been elusive despite more than two decades of intensive clinical and laboratory research. In particular, outcome for patients with glioblastoma multiforme (GBM) remains unacceptable, with the median survival for patients with newly diagnosed GBM and recurrent GBM being only 40 to 60[1] and 16 to 24 weeks, respectively.[2] Failure to eradicate local tumor growth is a major factor contributing to poor outcome, as indicated by the development of 90% of GBM recurrences at or adjacent to the site of origin.[3] Therefore, adjuvant therapies designed to augment local control are critically needed. The delivery of chemotherapeutic agents, toxins, or radionuclides to tumor-associated antigens via monoclonal antibodies (mAbs) is one such approach. Our efforts have focused on administering tumor-associated radiolabeled mAbs directly into spontaneous tumor cysts, surgically created resection cavities (SCRCs), the intrathecal space, and solid tumors.[4-6]

Tenascin, an extracellular matrix hexabrachion glycoprotein, is expressed ubiquitously in high-grade gliomas and in breast, lung, and squamous cell carcinomas, but not in normal brain. mAb 81C6 is a murine immunoglobulin G_{2b} that binds an epitope within the alternatively spliced fibronectin Type III region of tenascin.[7,8] This tenascin isoform is abundantly expressed in gliomas.[9,10] Preclinical studies have confirmed the specificity of 81C6 for tenascin-expressing tumors in cell culture and xenograft model systems. Bourdon et al[11] first demonstrated preferential localization of radioiodinated antitenascin 81C6 mAb in subcutaneous and intracranial human xenografts in athymic mice and rats using paired-label analysis. Additional preclinical studies with ^{131}I-labeled 81C6 demonstrated signif-

From the Departments of Surgery, Medicine, Pathology, Radiology, and Biostatistics and Bioinformatics, Duke University Medical Center, Durham, NC; and Department of Medicine, University of California at Davis Medical Center, San Rafael, CA.

Submitted June 18, 2001; accepted November 13, 2001.

Supported by National Institutes of Health grant nos. NS20023 and CA11898 and by grant no. MO1 RR 30 through the General Clinical Research Centers Program, National Center for Research Resources, National Institutes of Health, Bethesda, MD.

Address reprint requests to David A. Reardon, MD, Department of Surgery, Division of Neurosurgery, Duke University Medical Center, Box 3624, Durham, NC, 27710; email: reard003@mc.duke.edu.

0732-183X/02/2005-1389/$20.00

icant tumor growth delay and regression in athymic mice bearing subcutaneous D-54/MG human glioma xenografts and prolongation of median survival for athymic rats bearing intracranial tumors.[12-14] These promising results in preclinical animal studies led to a paired-label study in humans with recurrent malignant glioma. In this study, biopsy specimens obtained after intravenous injection of ^{123}I-labeled 81C6 demonstrated tumor-to-normal brain ratios up to 25:1 and single photon emission computed tomography localization indices showed an up to five-fold higher tumor accumulation of 81C6 compared with control immunoglobulin G_{2b} murine immunoglobulin.[15]

We have performed a series of phase I clinical trials to establish the maximum-tolerated dose (MTD) of ^{131}I-labeled murine 81C6 (mu81C6) mAb injected directly into a patient's SCRC. The MTD for three subgroups of patients with CNS tumors was established by the following studies: (1) 80 mCi for adult patients with leptomeningeal neoplasms or brain tumor resection cavities that communicate with the subarachnoid space,[4] (2) 100 mCi for patients with recurrent malignant gliomas who received prior radiation therapy with or without chemotherapy,[5] and (3) 120 mCi for newly diagnosed and previously untreated adult patients with malignant gliomas.[6] In the latter group, delayed neurologic toxicity was dose-limiting and the median survival for all patients and those with GBM was 79 and 69 weeks, respectively. We now report the results of a phase II study using 120 mCi of ^{131}I-labeled mu81C6 mAb injected directly into the SCRCs of newly diagnosed and previously untreated adult patients with malignant gliomas.

PATIENTS AND METHODS

Patient Eligibility and Treatment

Eligible patients had a confirmed histologic diagnosis of a newly diagnosed, previously untreated, supratentorial primary malignant tumor and were candidates for surgical resection. Patients with tumors that were either infratentorial, diffusely infiltrating, or multifocal or that had intraventricular access or subependymal spread were not eligible. Histopathologic samples from initial surgery for all patients were centrally reviewed at Duke University Medical Center (R.E.M., Department of Pathology, Durham, NC), and we performed a test of immunoreactivity for tenascin using either fresh or paraffin-embedded tissue stained positively with 81C6 or affinity-purified polyclonal rabbit antitenascin serum, respectively. Patients were greater than 3 years of age and had a Karnofsky performance status (KPS) of at least 60% at study entry. Pregnant or lactating patients and those with iodine allergy were ineligible. Concurrent systemic chemotherapy was not allowed. Other requirements have been described previously.[4]

Patients underwent a gross total resection and placement of a Rickham reservoir and catheter into the SCRC. A magnetic resonance imaging (MRI) scan with contrast was obtained within 48 hours of resection to document any residual tumor and placement of the Rickham catheter. Residual tumor could not enhance measurably more than 1.0 cm beyond the margin of the SCRC. Patency of the Rickham catheter and intactness of the SCRC were confirmed by injecting technetium-99m (^{99m}Tc)-labeled albumin or diethylenetriamine pentaacetic acid into the Rickham reservoir and obtaining gamma camera images immediately, 4 hours, and 24 hours after injection. Patients with subgaleal leakage of ^{99m}Tc-labeled tracer from the SCRC or with a resection cavity that communicated with the subarachnoid space (ie, intrathecal communication) were not eligible for treatment on this protocol. A baseline [^{18}F]fluorodeoxyglucose positron emission tomography (^{18}FDG PET) scan was obtained after resection. Before and 30 to 120 days after treatment, patients were tested for circulating antibodies to mu81C6 antibody and human-mouse chimeric 81C6 (ch81C6) antibody constructs with a double antibody radioimmunoassay or an enzyme-linked immunoabsorbent assay.[4]

Eligible patients received four drops of a saturated solution of potassium iodine and 75 μg of liothyronine sodium (Cytomel; Smith-Kline Beecham, Pittsburgh, PA) daily from 48 hours before to 16 days after ^{131}I-labeled 81C6 mAb administration to decrease iodine accumulation to the thyroid. After a patient was admitted to the hospital, the Rickham reservoir was accessed with a 25-gauge butterfly needle using sterile technique. Cystic fluid up to a volume of 6 mL was removed when possible. Twenty milligrams of 81C6 mAb labeled with 120 mCi of ^{131}I was injected into the reservoir in a volume of 6 mL or less. The reservoir and catheter were flushed after the mAb injection. Patients were placed on radiation isolation until the whole-body retention of ^{131}I was less than 30 mCi, as determined with a cross-calibrated radiation survey meter. After this level was reached, radionuclide imaging with a gamma camera and serial blood sample measurements were performed to document the biodistribution of ^{131}I activity in the whole body. Patients were discharged after a posttreatment MRI was performed.

The Duke Investigational Review Board approved this investigation. Informed consent approved by the Duke Investigational Review Board was obtained from each subject or the subject's guardian.

Antibody Production and Labeling

The 81C6 mAb was grown in athymic mice in ascites form and purified over a Sepharose-staphylococcal protein-A column followed by polyethylenimine ion exchange chromatography. Food and Drug Administration guidelines for the manufacture and testing of mAb products were followed for each clinical batch.[16] Radiolabeling of 81C6 mAb was performed by a modified Iodo-Gen procedure (Pierce Chemical Company, Rockford, IL). All preparations had immunoreactivity of more than 75%, with more than 95% of the label eluting as immunoglobulin G on high-pressure liquid chromatography and precipitating with trichloroacetic acid.

Pharmacokinetics and Dosimetry

Absorbed dose calculations for the SCRC, whole body, and bone marrow were carried out as previously described.[17] Briefly, a serial, two-compartment system was used to model the pharmacokinetics of ^{131}I-labeled 81C6 mAb, where the SCRC and the whole body (not including the SCRC) were assumed to be the first and second compartments, respectively. We used gadolinium-enhanced T1-weighted axial MRI images (2 mm-thick slices, noninterleaved, zero-millimeter spacing) obtained after resection to generate a three-dimensional reconstruction of the head and SCRC using current image analysis software (VoxelView 2.5.4; Vital Images, St Paul, MN). The SCRC volume was then calculated and used to estimate the initial activity concentration in the SCRC at the time of administration, where

a uniform activity concentration was assumed. Depth-dose calculations of the SCRC interface, 2 cm-thick margin, and normal brain were then performed. Radiation-absorbed dose estimates for bone marrow were based on the activity in whole blood as a function of time after administration. A reduction factor of 0.3 was used to relate activity in blood to bone marrow.[18]

Toxicity and Response Determinations

Since treatment, patients have been monitored continually for toxicity. Initial follow-up occurred within the first month after treatment. Complete blood counts with differential were performed weekly for the first 8 weeks after ^{131}I-labeled 81C6 injection. Patients with GBM or anaplastic astrocytoma (AA) received conventional external-beam radiation therapy for 6 weeks starting 1 month after the mAb therapy. After radiation therapy, adjuvant alkylator-based chemotherapy was administered for approximately 1 year. Patients were re-evaluated before initiating chemotherapy and every 8 to 12 weeks during chemotherapy. Patients were then evaluated every 3 months for the first year, every 4 months for the second year, and biannually thereafter. In each follow-up appointment, a complete general and neurologic examination, KPS rating, ^{18}FDG PET scan, and MRI with contrast media were performed. Measurements of electrolytes and liver function tests were also repeated at each visit. A thyroid panel was obtained at 1 and 2 months after the treatment. Human antimouse antibody (HAMA) titers were obtained monthly for the first 6 months.

Common toxicity criteria, version 2.0 (Cancer Therapy Evaluation Program, National Cancer Institute, Bethesda, MD), was used to score toxicity. Although the occurrence of seizures was recorded, seizures were not included as an indication of neurologic toxicity because of their expected frequency in this disease setting. The precise etiology of nonseizure neurologic toxicity after ^{131}I-labeled 81C6 therapy was extremely difficult to define. Neither clinical features nor radiographic findings observed on either MRI or ^{18}FDG PET scan reliably distinguished between recurrent tumor and treatment-induced radiation necrosis. Although stereotactic needle biopsy is limited with regard to volume sampling, it remains the state of the art for diagnosis of focal brain lesions. Therefore, the etiology of observed neurologic toxicity was determined based on stereotactic needle biopsy result.

Progressive disease (PD) was defined by the presence of at least one of the following: (1) more than 25% increase in the enhancing tumor cross-sectional area or the appearance of radiographically new lesions that were also hypermetabolic on ^{18}FDG PET scan, (2) evidence of clinical deterioration and a more than 25% increase in enhancing tumor size or the appearance of radiographically new lesions on MRI, or (3) biopsy-proven recurrent tumor.

Statistical Analysis

A single-stage phase II study was conducted to determine the efficacy of ^{131}I-labeled 81C6 in the treatment of patients with newly diagnosed malignant gliomas. The primary end point of the study was the proportion of patients who survived for 1 year after initial treatment. The targeted accrual goal of 41 patients provided 90% power to differentiate between a success rate of 40% and 60%, where success is defined as living more than 1 year. If 21 or more patients lived more than 1 year, the treatment regimen was to be considered a success and worthy of further investigation in a phase III study.

The method of Kaplan and Meier[19] was used to estimate survival distributions, where survival was measured from the date of initial treatment to the date of death or last contact. Subgroup differences in survival were assessed with log-rank tests,[20] and the Cox Proportional Hazards Model[21] was also used to investigate for potential associations between variables and outcome. Logistic regression was used to examine the effect of cavity size as well as ^{131}I-labeled 81C6 absorbed and cumulative (^{131}I-labeled 81C6 plus external beam) radiation doses to the 2 cm-thick SCRC interface on toxicity. This analysis reflects patient follow-up through May 15, 2001.

Table 1. Characteristics of Newly Diagnosed Patients Treated With ^{131}I-Labeled 81C6 mAb

Characteristics	No. of Treated Patients (*N* = 33)	%
Age, years		
Median	50	
Range	19-68	
Sex		
Male	23	70
Female	10	30
Race		
White	32	97
Black	1	3
Karnofsky performance score		
100	28	85
90	1	3
80	3	9
70	1	3
Histology		
GBM	27	82
AA	4	12
AO	2	6
SCRC size, median = 10.45 cm		
<5 cm	7	21
5-9.9 cm	9	27
10-14.9 cm	10	33
>15 cm	7	21
Post ^{131}I-labeled 81C6 mAb treatment		
External-beam radiation therapy	29	88
Systemic chemotherapy	30	91

RESULTS

Patient Characteristics

The study population included 33 previously untreated patients with newly diagnosed high-grade glioma treated at Duke University Medical Center. Study accrual began in November 1996 and was discontinued in June 2000 once it became clear that the treatment regimen was worthy of further investigation in a phase III study (ie, 21 or more successes were observed) and ch81C6 became available for clinical use. Subsequent patients were enrolled onto a phase I clinical trial incorporating ch81C6 because it was shown to demonstrate superior tumor localization in paired label studies of human glioma xenografts and greater overall stability compared with mu81C6.[22] Characteristics of the patients enrolled onto the current study are listed in Table 1. Ten of the patients were women, and 23 were men. The

median age was 50 years (range, 19 to 68 years). Twenty-seven of the patients had GBM, four had AA, and two had anaplastic oligodendroglioma (AO). All patients had a KPS between 70% and 100%. The median time between diagnosis and ^{131}I-labeled 81C6 administration was 1.3 months (range, 1 to 3 months). Thirty-two patients received 120 mCi of ^{131}I conjugated to 20 mg of 81C6 mAb. One patient received 37 mCi of ^{131}I conjugated to 10 mg of 81C6 mAb because of a small SCRC. After ^{131}I-labeled 81C6 therapy, 29 patients underwent conventional external-beam radiation therapy, and 30 received systemic chemotherapy. There are 11 patients currently alive. Median follow-up among surviving patients is 93 weeks (range, 49 to 220 weeks). Twenty-two patients have died.

HAMA

Immunoassays were performed for HAMA to assess the patients' immune response to mu81C6 and ch81C6 antibody and to determine any HAMA-associated toxicity. Posttreatment blood samples were obtained from 31 patients within 1 to 6 months after treatment. When tested against the target immunoglobulin, 25 (86%) of 29 patients were positive for mu81C6, and 27 (90%) of 30 were positive for ch81C6. The maximum titer measured from each patient is presented in Table 2. No observed toxicity was related to HAMA reactivity.

Dosimetry Results

As demonstrated in previous studies, retention of the ^{131}I-labeled 81C6 in the SCRC and in the whole body differed significantly.[6] ^{131}I activity in the blood was characterized by exponential uptake followed by an exponential clearance. Overall, patients remained in radiation isolation for 3 to 8 days until adequate clearance was achieved. The average biologic half-life in the SCRC and in the whole body was 87 hours (range, 26 to 282 hours) and 39 hours (range, 8 to 66 hours), respectively. The average SCRC volume was 10.45 cm^3 (range, 0.5 to 30.5 cm^3). The average absorbed dose to the 2 cm-thick interface from ^{131}I-labeled 81C6 was 48 Gy (range, 24 to 116 Gy), with an average SCRC residence time of 78 hours (range, 34 to 169 hours). The average cumulative radiation dose to the 2 cm-thick interface (external-beam radiation therapy plus ^{131}I-labeled 81C6 absorbed dose) was 102 Gy (range, 51 to 137 Gy). The average whole-body dose was 0.58 Gy (range, 0.24 to 1.28 Gy), with an average whole-body residence time (excluding the SCRC) of 40 hours (range, 12 to 89 hours).

Toxicity

Toxicity was primarily hematologic and neurologic. Nine patients (27%) developed grade 4 hematologic toxicity within 8 weeks of ^{131}I-labeled 81C6 therapy and before the initiation of systemic chemotherapy. All hematologic toxicity was reversible. Five patients had thrombocytopenia (platelets < 20,000/mm^3) and grade 4 neutropenia, three had thrombocytopenia alone, and one had grade 4 neutropenia, anemia, and thrombocytopenia. There was no statistical correlation between whole-body radiation exposure and the development of hematologic toxicity (data not shown). Median duration to resolution of hematologic toxicity was 29 days (range, 4 to 56 days).

Three patients (3%) developed neurologic toxicity (grade ≥ 3), which resolved completely after the administration of corticosteroids. Five patients (15%) developed irreversible (> 6-month duration) neurologic toxicity and had stereotactic biopsies that revealed necrosis and reactive gliosis,

Table 2. Peak Human Antimouse Titers in Patients After ^{131}I 81C6 Therapy

Patient No.	Titer v ch81C6	Titer v mu81C6
1	6.25×10^{-2}	5.00×10^{-1}*
2	7.81×10^{-3}	7.81×10^{-3}
3	Neg	NT
4	7.81×10^{-3}	5.00×10^{-1}*
5	6.25×10^{-2}	5.00×10^{-1}*
6	2.50×10^{-1}	5.00×10^{-1}*
7	7.81×10^{-3}	Neg
8	2.50×10^{-1}	5.00×10^{-1}*
9	1.56×10^{-2}	5.00×10^{-1}*
10	Neg	Neg
11	7.81×10^{-3}	5.00×10^{-1}*
12	Neg	Neg
13	7.81×10^{-3}	7.81×10^{-3}
14	3.13×10^{-2}	3.91×10^{-3}
15	3.13×10^{-2}	5.00×10^{-1}*
16	6.25×10^{-2}	5.00×10^{-1}*
17	1.95×10^{-3}	3.91×10^{-3}
18	Neg	Neg
19	2.44×10^{-4}	9.77×10^{-4}
20	3.91×10^{-3}	3.91×10^{-3}
21	6.25×10^{-2}	NT
22	3.13×10^{-2}	5.00×10^{-1}*
23	1.56×10^{-2}	5.00×10^{-1}*
24	7.81×10^{-3}	1.95×10^{-3}
25	1.25×10^{-1}	5.00×10^{-1}*
26	3.13×10^{-2}	5.00×10^{-1}*
27	1.95×10^{-3}	9.77×10^{-4}
28	9.77×10^{-4}	1.95×10^{-3}
29	1.00×10^{-1}	3.13×10^{-3}
30	5.00×10^{-2}	6.25×10^{-3}
31	NT	Neg
32	NA	NA
33	NA	NA

Abbreviations: Neg, negative; NT, not tested; NA, no sample.

*Samples were tested only at 5.00×10^{-1} v mu81C6 to have enough sample to test v ch81C6.

without evidence of active tumor. Irreversible neurologic toxicity developed at a median of 8.5 months from treatment (range, 3 to 25 months). Specific neurologic deficits (grade ≥ 3) affected motor (n = 5), sensory (n = 1), and speech (n = 1) function. Of note, the SCRC of each of these five patients was immediately adjacent to the contralateral central sulcus, whereas that of the patient with additional speech toxicity also abutted the region of Broca's area in the left frontal lobe. The ^{131}I-labeled 81C6 absorbed and cumulative radiation doses determined for the 2 cm-thick SCRC interface, as well as the SCRC size, in the five patients with irreversible grade ≥ 3 neurologic toxicity were compared with the SCRC absorbed and cumulative doses and SCRC size in all other patients. None of these factors differed significantly between the two groups. In addition, there was no significant relationship between grade ≥ 3 neurologic toxicity and survival.

Two additional patients developed irreversible neurologic toxicity and refused stereotactic biopsy. However, clinical and radiographic findings clearly suggested that progressive tumor was responsible for their neurologic decline. The first patient developed grade 4 neuromotor and cognitive deficits 20 weeks after ^{131}I-labeled 81C6 therapy, at which point MRI examination revealed a new enhancing lesion separate from the original tumor that was also hypermetabolic on ^{18}FDG PET scan. This patient's course was remarkable for progressive worsening of neurologic and radiographic findings, and he died on hospice care 88 weeks after ^{131}I-labeled 81C6 therapy. The second patient developed grade 3 cognitive toxicity 5 weeks after ^{131}I-labeled 81C6 therapy. At that time, his MRI examination revealed enhancement extending into the corpus callosum. He also developed progressive neurologic deterioration and died 20 weeks after ^{131}I-labeled 81C6 therapy.

New onset, controllable seizures developed in four patients (12%) after ^{131}I-labeled mu81C6 therapy. One of the four patients had biopsy-proven PD at the onset of seizures, whereas biopsy samples were not obtained from the remaining three patients. Worsening of pre-existing seizures occurred primarily in the setting of tumor progression.

Other episodes of reversible grade ≥ 3 toxicity occurred primarily during the chemotherapy phase of treatment and, therefore, were most likely unrelated to 81C6 therapy. They included grade 3 thrombosis (n = 3), grade 3 infection (n = 2), grade 3 diarrhea (n = 1), grade 4 pulmonary toxicity (n = 1), and grade 4 hepatic (n = 1) toxicity. The grade 3 diarrhea, which developed in a patient receiving a course of irinotecan, is a well-established toxicity of this agent. The episode of hepatic toxicity resolved after an anticonvulsant dosage modification, and the episode of pulmonary toxicity developed in a patient after an aspiration pneumonia. Two additional patients died of infection while receiving systemic chemotherapy.

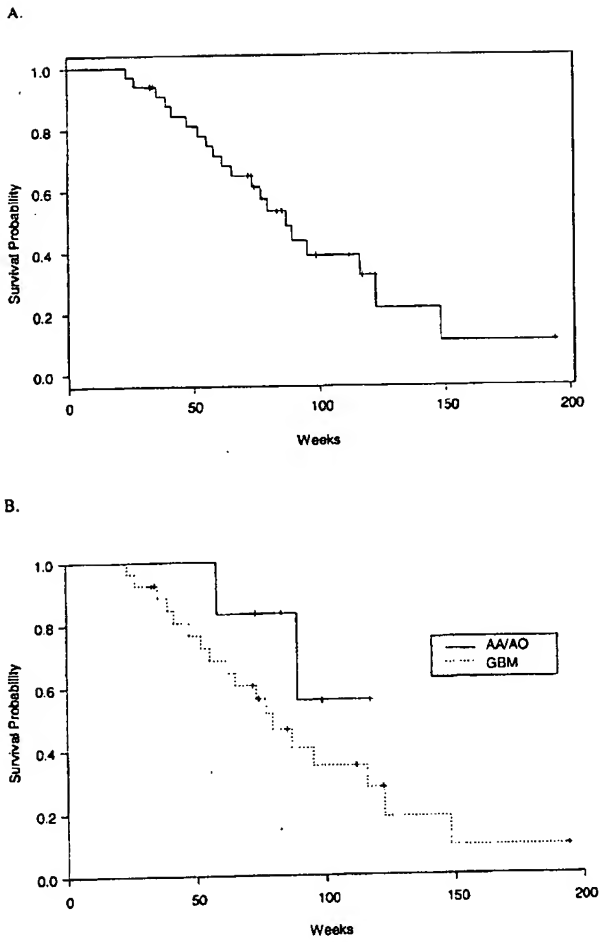

Fig 1. Kaplan-Meier overall survival estimates for (A) all patients and (B) after stratification by histology.

Biopsies and Reoperation

Sixteen patients (48%) underwent elective stereotactic biopsies for progressive clinical and/or radiographic changes. Nine biopsies showed gliosis and necrosis, and seven demonstrated recurrent tumor. Five of those with initial biopsies demonstrating gliosis and necrosis underwent additional elective stereotactic biopsies because they had progressive radiographic and/or clinical symptoms. Recurrent tumor was documented in three of these cases, whereas two again showed only gliosis and necrosis. Two patients underwent debulking resections to alleviate clinical deterioration and radiographically confirmed mass effect. A histopathologic sample from one of these patients revealed

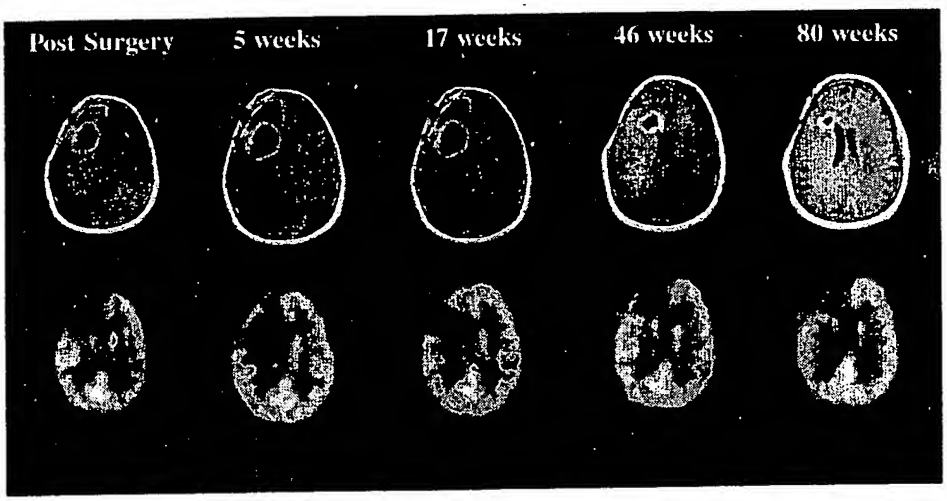

Fig 2. Serial MRI and ^{18}FDG PET scan results of a representative patient after ^{131}I 81C6 therapy. Over time, the SCRC gradually collapses as the rim develops more prominent enhancement. Corresponding ^{18}FDG PET scan images depicted below demonstrate a lack of increased metabolic activity in the region of the SCRC.

gliosis with a small focus of well-differentiated glioma. This patient is currently 93 weeks from diagnosis, has no evidence of recurrent tumor, and maintains a nearly full level of function, with only mild (grade 1) memory and speech deficits. The other debulking procedure was performed approximately 60 weeks from diagnosis and revealed evidence of recurrent tumor.

Response/Survival Data

Because all patients underwent total or near-total gross surgical resection, little or no residual tumor was detectable radiographically. Therefore, traditional radiographic interpretation of response was not feasible, and survival was the most important criterion for efficacy. Of the 33 patients treated on this protocol, 28 were clinically evaluated for at least 1 year. Two patients refused further treatment after ^{131}I-labeled 81C6 therapy and three patients died 5, 8, and 9 months after treatment. All patients showed some rim enhancement around and contiguous with the SCRC margin on the initial MRI after ^{131}I-labeled 81C6 therapy. From each follow-up MRI, the SCRC volume and that of the enhancing rim were calculated.

Eleven (33%) of the 33 patients are alive, including three of six with AA or AO and eight of 27 with GBM. The median survival after ^{131}I-labeled 81C6 therapy for all patients (Fig 1A) and the 27 patients with GBM (Fig 1B) was 86.7 weeks (95% confidence interval, 76.7 to ∞ weeks) and 79.4 weeks (95% confidence interval, 61.4 to ∞ weeks), respectively. Median follow-up among surviving patients is 93 weeks (range, 49 to 220 weeks). Cox's proportional hazards model was used to examine the effect of ^{131}I-labeled 81C6 absorbed and cumulative radiation doses to the 2 cm-thick SCRC interface on survival. Neither factor correlated with overall survival (P = .222 and P = .526, respectively). Biopsy-proven PD was local in all cases except one in which a biopsy-proven tumor recurrence developed in the contralateral hemisphere. Figure 2 demonstrates representative radiographic findings of a patient after ^{131}I-labeled 81C6 therapy.

DISCUSSION

The primary objective of the current phase II study was to assess the impact on survival of 120 mCi of ^{131}I-labeled mu81C6 administered directly into the SCRC of newly diagnosed and previously untreated patients with malignant glioma. Our secondary objective was to further assess the feasibility and toxicity associated with this therapy among such patients. Overall, 33 patients were treated, including 27 with GBM, four with AA, and two with AO. The most eligible patients were enrolled onto the study and received ^{131}I-81C6; however, a small percentage were ultimately excluded because of subgaleal leakage on the postoperative diethylenetriamine penta-acetic acid scan. A review of the last 36 consecutive patients meeting this study's eligibility criteria revealed that three (8%) were excluded for this reason. Of note, this development seemed to be related to the proximity of the SCRC to the CSF space rather than SCRC size. In fact, the SCRC of all three of these patients was less than 5 cm^3. After administration of ^{131}I-labeled 81C6 mAb, most patients received conventional external-beam radiotherapy followed by a year of alkylator-based chemotherapy. The average SCRC volume in this study was 10.45 cm^3 (range, 0.5 to 30.5 cm^3), and the average radiation absorbed dose to the 2 cm-thick region surrounding the cavity interface was 48 Gy (range, 24 to 116 Gy). Median survival was 86.7 weeks (range, 76.7 to ∞ weeks)

for all patients and 79.4 weeks (range, 61.4 to ∞ weeks) for those with GBM. Toxicity was primarily hematologic and neurologic, as predicted by our prior phase I study. Reversible grade 4 hematologic toxicity developed in nine patients (27%). Neurologic toxicity occurred primarily in the setting of PD documented by either biopsy or radiographic findings. However, five patients (15%) developed grade ≥ 3 irreversible neurologic toxicity without evidence of tumor recurrence on stereotactic biopsy.

The results of prior phase I clinical trials contributed to the design and implementation of the current study. In our initial phase I trial, 31 patients (18 with GBM) with either leptomeningeal neoplasms or brain tumor resection cavities with subarachnoid communication were treated with a single dose of intrathecal ^{131}I-labeled mu81C6.[23] Iodine-131 doses administered to patients ranged from 40 to 100 mCi. Hematologic dose-limiting toxicity correlated with ^{131}I dose and occurred at an absorbed dose to active bone marrow of approximately .20 Gy. No grade III or IV nonhematologic toxicity was encountered. One patient had a partial response, whereas 13 (42%) of 31 had disease stabilization. Twelve patients were alive (median follow-up > 320 days) and five were progression-free more than 409 days median after treatment. From this study, we concluded that 80 mCi of ^{131}I-labeled 81C6 was the MTD when administered as a single intrathecal administration in adults.

In a subsequent phase I study, 34 previously irradiated patients with recurrent or metastatic brain tumors (26 with GBM) received a single injection of ^{131}I-labeled mu81C6 through an Ommaya reservoir into the SCRC.[5] Administered doses of ^{131}I-labeled 81C6 ranged from 20 to 120 mCi. Dose-limiting toxicity was neurologic and defined the MTD to be 100 mCi for recurrent patients. The estimated median survival for those patients with recurrent GBM and for all patients was 56 and 60 weeks, respectively.

In a recently reported phase I study, 42 newly diagnosed, previously untreated patients with supratentorial primary malignant glioma (32 with GBM) received doses of ^{131}I-labeled mu81C6 directly into the SCRC via a Rickham catheter.[6] The average SCRC volume was 21 cm^3 (range, 2 to 81 cm^3). ^{131}I-labeled 81C6 doses ranged from 20 to 180 mCi and delivered an average 32 Gy (range, 2 to 59 Gy) to the 2 cm-thick region surrounding the cavity interface. Median survival for all patients and those with GBM was 79 and 69 weeks, respectively. Dose-limiting neurotoxicity was observed at the following administered activities: one of seven patients at 120 mCi, two of three patients at 140 mCi, two of seven patients at 160 mCi, and the sole patient treated with 180 mCi. The average absorbed dose to the 2-cm shell from radiolabeled mAb therapy for these six patients was 46 Gy (range, 37 to 55 Gy). Of note, only one of the 42 patients (2.5%) required debulking surgery for radionecrosis. Non–dose-limiting, reversible, hematologic toxicity was observed in seven patients (grade 3, n = 5; grade 4, n = 2). Based on these results, an MTD of 120 mCi was established for newly diagnosed, previously untreated patients. Presently, nine patients in that study remain alive, including all five with AO and four with GBM. Current posttreatment survivals range from 130 to 367 weeks.

Median survival in the current study exceeded that observed in our previous phase I trial, thereby further defining the efficacy of ^{131}I-labeled 81C6 administered into the SCRC of newly diagnosed malignant glioma patients. Irreversible treatment-related neurologic toxicity was associated with contiguity or immediate adjacency of the SCRC and respective functional CNS area. Specifically, each of the five patients with irreversible neuromotor toxicity in this study had an SCRC in direct proximity to the motor strip, whereas the anterior margin of the SCRC of the patient who also developed speech toxicity localized to the region of Broca's area. In addition, it is possible that the higher average radiation dose affecting the 2-cm SCRC shell (48 Gy) compared with that achieved in the prior phase I trial (32 Gy) may have contributed to the neurologic toxicity observed in the current study. A recently completed dosimetry analysis designed to evaluate the dose-response relationship observed in our previous phase I study suggested that a boost dose of 43 Gy to the 2-cm SCRC shell optimally maximized tumor control and minimized brain injury. Moreover, 2-cm SCRC shell doses greater than 43 Gy were more frequently associated with brain injury, and tumor recurrence occurred more frequently when 2-cm SCRC shell doses were less than 43 Gy.[24]

Curran et al[25] used recursive partitioning to assess the prognostic impact of 26 pretreatment characteristics and six treatment-related variables for 1,578 newly diagnosed malignant glioma patients entered onto three Radiation Therapy Oncology Group trials from 1974 to 1989. They confirmed age, histopathology, and performance status to be most predictive of survival. This analysis also determined survival rates for subsets of malignant glioma patients treated with conventional chemoradiotherapy, against which outcomes using novel therapeutic approaches could be compared. Such a comparison is limited by the sample size of our study and its exclusion of patients with tumors that are either diffusely infiltrating, multifocal, or accompanied by subependymal spread, but nonetheless suggests that the use of ^{131}I-labeled 81C6 provides a survival advantage for patients stratified by age, histology, and performance status. Median survival was 87 weeks for the 11 patients in the current study who were less than 50 years old at diagnosis and had GBM, compared with only 55 weeks for

a similar cohort in the Curran et al[25] analysis ($P < .05$). Similarly, median survival was 65 weeks for the 16 GBM patients over 50 years old with a KPS ≥ 70% in the current study compared with only 39 weeks for those reported by Curran et al ($P < .05$).

Other investigators have documented improved survival associated with the local application of radiolabeled mAbs for patients with malignant gliomas. Riva et al[26,27] injected ^{131}I-labeled antitenascin murine mAbs BC-2 and BC-4 into the resection sites of 74 newly diagnosed and recurrent glioblastoma patients in a phase II study. All patients received external-beam radiotherapy and systemic chemotherapy before mAb therapy. The mean administered activity was 2,035 MBq (approximately 55 mCi). Median survival was 76 weeks, and no neurologic toxicity was encountered. In a pilot study for patients with malignant gliomas, individual patient responses were documented after intracystic injection of ^{131}I-labeled erythropoietin-induced c-DNA-1 murine mAb.[28] Hopkins et al[29] reported a median survival of 24 weeks among 15 primary brain tumor patients treated with intratumoral ^{90}Y-labeled erythropoietin-induced c-DNA-1 murine mAb.

The 79.4-week median survival for patients with GBM in the current study compares favorably with that reported for either ^{125}I interstitial brachytherapy (IB) or stereotactic radiosurgery (SRS). Trials incorporating ^{125}I IB report a median survival of 48 to 88 weeks for newly diagnosed malignant glioma patients,[30-37] whereas those using SRS cite a 38- to 78-week median survival.[38-40] However, reoperation to alleviate increasing mass effect and radiation necrosis was required in 33% to 64% of ^{125}I IB cases and up to 33% of SRS patients. In contrast, only two (2.7%) of the 75 newly diagnosed patients combined from our phase I and II ^{131}I-labeled 81C6 trials required debulking resections for radionecrosis. In addition, median survival achieved in the current study with ^{131}I-labeled 81C6 exceeds the 56 weeks reported with interstitial chemotherapy using carmustine-loaded polymers (Gliadel; Guilford Pharmaceuticals Inc, Baltimore, MD) placed in the surgical resection cavity at the time of primary operation for patients with newly diagnosed malignant glioma.[41]

In summary, 120 mCi of ^{131}I-labeled mu81C6 mAb injected into the SCRC of newly diagnosed and previously untreated malignant glioma patients resulted in prolonged overall survival compared with that achieved with conventional therapy or interstitial chemotherapy. Our median survival compares favorably with that reported for SRS or ^{125}I IB, and significantly fewer patients in our study required reoperation for symptomatic radionecrosis than reported for either SRS or ^{125}I IB. Observed hematologic toxicity and neurologic toxicity in this trial were acceptable. The latter may be further reduced by limiting ^{131}I-labeled 81C6 mAb therapy to those patients in whom the SCRC is not immediately adjacent to critical CNS functional centers. In this regard, we have begun to routinely use intraoperative cortical mapping to further delineate such patients. Overall, these results suggest that a randomized phase III trial is warranted.

REFERENCES

1. Mahaley MS Jr: Neurooncology index and review (adult primary brain tumors): Radiotherapy, chemotherapy, immunotherapy, photodynamic therapy. J Neurooncol 11:85-147, 1991

2. Wong ET, Hess KR, Gleason MJ, et al: Outcomes and prognostic factors in recurrent glioma patients enrolled onto phase II clinical trials. J Clin Oncol 17:2572-2578, 1999

3. Gaspar LE, Fisher BJ, Macdonald DR, et al: Supratentorial malignant glioma: Patterns of recurrence and implications for external beam local treatment. Int J Radiat Oncol Biol Phys 24:55-57, 1992

4. Bigner DD, Brown M, Coleman RE, et al: Phase I studies of treatment of malignant gliomas and neoplastic meningitis with 131I-radiolabeled monoclonal antibodies anti-tenascin 81C6 and anti-chondroitin proteoglycan sulfate Me1-14 F (ab')2: A preliminary report. J Neurooncol 24:109-122, 1995

5. Bigner DD, Brown MT, Friedman AH, et al: Iodine-131-labeled antitenascin monoclonal antibody 81C6 treatment of patients with recurrent malignant gliomas: Phase I trial results. J Clin Oncol 16:2202-2212, 1998

6. Cokgor I, Akabani G, Kuan CT, et al: Phase I trial results of iodine-131-labeled antitenascin monoclonal antibody 81C6 treatment of patients with newly diagnosed malignant gliomas. J Clin Oncol 18:3862-3872, 2000

7. Bourdon MA, Wikstrand CJ, Furthmayr H, et al: Human glioma-mesenchymal extracellular matrix antigen defined by monoclonal antibody. Cancer Res 43:2796-2805, 1983

8. Bourdon MA, Matthews TJ, Pizzo SV, et al: Immunochemical and biochemical characterization of a glioma-associated extracellular matrix glycoprotein. J Cell Biochem 28:183-195, 1985

9. Ventimiglia JB, Wikstrand CJ, Ostrowski LE, et al: Tenascin expression in human glioma cell lines and normal tissues. J Neuroimmun 36:41-55, 1992

10. Zalutsky MR, Moseley RP, Coakham HB, et al: Pharmacokinetics and tumor localization of 131I-labeled anti-tenascin monoclonal antibody 81C6 in patients with gliomas and other intracranial malignancies. Cancer Res 49:2807-2813, 1989

11. Bourdon MA, Coleman RE, Blasberg RG, et al: Monoclonal antibody localization in subcutaneous and intracranial human glioma xenografts: Paired-label and imaging analysis. Anticancer Res 4:133-140, 1984

12. Colapinto EV, Lee YS, Humphrey PA, et al: The localisation of radiolabelled murine monoclonal antibody 81C6 and its Fab fragment in human glioma xenografts in athymic mice [published erratum appears in Br J Neurosurg 2:548, 1988]. Br J Neurosurg 2:179-191, 1988

13. Lee YS, Bullard DE, Wikstrand CJ, et al: Comparison of monoclonal antibody delivery to intracranial glioma xenografts by

intravenous and intracarotid administration. Cancer Res 47:1941-1946, 1987

14. Lee YS, Bullard DE, Zalutsky MR, et al: Therapeutic efficacy of antiglioma mesenchymal extracellular matrix 131I-radiolabeled murine monoclonal antibody in a human glioma xenograft model. Cancer Res 48:559-566, 1988

15. Schold SC Jr, Zalutsky MR, Coleman RE, et al: Distribution and dosimetry of I-123-labeled monoclonal antibody 81C6 in patients with anaplastic glioma. Invest Radiol 28:488-496, 1993

16. Food and Drug Administration: Director OoBRaR Center for Drugs and Biologics: Points to consider in the manufacture and testing of monoclonal antibody products for human use. Food and Drug Administration, Bethesda, MD, 1987

17. Akabani G, Reist CJ, Cokgor I, et al: Dosimetry of 131I-labeled 81C6 monoclonal antibody administered into surgically created resection cavities in patients with malignant brain tumors. J Nucl Med 40:631-638, 1999

18. Sgouros G: Bone marrow dosimetry for radioimmunotherapy: Theoretical considerations. J Nucl Med 34:689-694, 1993

19. Kaplan E, Meier P: Nonparametric estimation from incomplete observations. J Am Stat Assoc 53:457-481, 1958

20. Mantel N: Evaluation of survival data and two new rank order statistics arising in its consideration. Cancer Chemother Rep 50:163-170, 1966

21. Cox DR: Regression models and life tables. J R Stat Soc B 34:187-220, 1972

22. Zalutsky MR, Archer GE, Garg PK, et al: Chimeric anti-tenascin antibody 81C6: Increased tumor localization compared with its murine parent. Nucl Med Biol 23:449-458, 1996

23. Brown MT, Coleman RE, Friedman AH, et al: Intrathecal 131I-labeled antitenascin monoclonal antibody 81C6 treatment of patients with leptomeningeal neoplasms or primary brain tumor resection cavities with subarachnoid communication: Phase I trial results. Clin Cancer Res 2:963-972, 1996

24. Akabani G, Cokgor I, Coleman RE, et al: Dosimetry and dose-response relationships in newly diagnosed patients with malignant gliomas treated with iodine-131-labeled anti-tenascin monoclonal antibody 81C6 therapy. Int J Radiat Oncol Biol Phys 46:947-958, 2000

25. Curran WJ, Scott CB, Horton J, et al: Recursive partitioning analysis of prognostic factors in three Radiation Therapy Oncology Group malignant glioma trials. J Natl Cancer Inst 85:704-710, 1993

26. Riva P, Franceschi G, Arista A, et al: Local application of radiolabeled monoclonal antibodies in the treatment of high grade malignant gliomas: A six-year clinical experience. Cancer 80:2733-2742, 1997

27. Riva P, Franceschi G, Frattarelli M, et al: Loco-regional radioimmunotherapy of high-grade malignant gliomas using specific monoclonal antibodies labeled with 90Y: A phase I study. Clin Cancer Res 5:3275s-3280s, 1999

28. Papanastassiou V, Pizer BL, Coakham HB, et al: Treatment of recurrent and cystic malignant gliomas by a single intracavity injection of 131I monoclonal antibody: Feasibility, pharmacokinetics and dosimetry. Br J Cancer 67:144-151, 1993

29. Hopkins K, Chandler C, Bullimore J, et al: A pilot study of the treatment of patients with recurrent malignant gliomas with intratumoral yttrium-90 radioimmunoconjugates. Radioth Oncol 34:121-131, 1995

30. Gutin PH, Prados MD, Phillips TL, et al: External irradiation followed by an interstitial high activity iodine-125 "boost" in the initial treatment of malignant gliomas: NCOG Study 6G-82-2. Int J Radiat Oncol Biol Phys 21:601-606, 1991

31. Sneed PK, Lamborn KR, Larson DA, et al: Demonstration of brachytherapy boost dose-response relationships in glioblastoma multiforme. Int J Radiat Oncol Biol Phys 35:37-44, 1996

32. Videtic GMM, Gaspar LE, Zamorano L, et al: Use of the RTOG recursive partitioning analysis to validate the benefit of iodine-125 implants in the primary treatment of malignant gliomas. Int J Radiat Oncol Biol Phys 45:687-692, 1999

33. Laperriere NJ, Leung PMK, McKenzie S, et al: Randomized study of brachytherapy in the initial management of patients with malignant astrocytoma. Int J Radiat Oncol Biol Phys 41:1005-1011, 1998

34. Koot RW, Maarouf M, Hulshof MC, et al: Brachytherapy: Results of two different therapy strategies for patients with primary glioblastoma multiforme. Cancer 88:2796-2802, 2000

35. Scharfen CO, Sneed PK, Wara WM, et al: High activity iodine-125 interstitial implant for gliomas. Int J Radiat Oncol Biol Phys 24:583-591, 1992

36. Wen PY, Alexander E, III, Black PM, et al: Long term results of stereotactic brachytherapy used in the initial treatment of patients with glioblastomas. Cancer 73:3029-3036, 1994

37. Loeffler JS, Alexander EI, Wen PY, et al: Results of stereotactic brachytherapy used in initial management of patients with glioblastoma. J Natl Cancer Inst 82:1918-1921, 1990

38. Flickinger JC, Loeffler JS, Larson DA: Stereotactic radiosurgery for intracranial malignancies. Oncology (Huntingt) 8:81-86, 94-98, 1994

39. Masciopinto JE, Levin AB, Mehta MP, et al: Stereotactic radiosurgery for glioblastoma: A final report of 31 patients. J Neurosurg 82:530-535, 1995

40. Shrieve DC, Alexander E, III, Wen PY, et al: Comparison of stereotactic radiosurgery and brachytherapy in the treatment of recurrent glioblastoma multiforme. Neurosurg 36:275-282; discussion 282-284, 1995

41. Westphal MDP, Hilt D, Olivares R, et al: Placebo controlled multicenter double-blind randomized prospective phase III trial of carmustine implants (Gliadel) in 240 patients with malignant gliomas: Final results. Fifth Annual Meeting of the Society for Neuro-Oncology, Chicago, IL, November 9-12, 2000

JOURNAL OF PATHOLOGY, VOL. 159: 225–229 (1989)

TENASCIN DISTRIBUTION IN BASAL CELL CARCINOMAS

GORDON W. H. STAMP

ICRF/RCS Histopathology Unit, 35–43 Lincoln's Inn Fields, London WC2A 3PN, U.K.

Received 12 April 1989
Accepted 24 May 1989

SUMMARY

The distribution of tenascin, an extracellular matrix protein highly expressed in the stroma around sites of epithelial–mesenchymal interaction during morphogenesis and in malignant neoplasms, was assessed in cryostat sections of 17 basal cell carcinomas using a polyclonal antibody. There was marked staining of the vascularized stroma around neoplastic islands, usually as an intense, well-defined band, but being more widespread and diffuse in sclerosing, infiltrative areas. Apparently enhanced staining was seen in tumours showing retraction artefact, which may be related to the observation that tenascin interferes with the cell binding function of fibronectin. Reduced staining was seen in areas showing evidence of tumour regression. Tenascin is an important component of the epithelial–mesenchymal interactive process and further studies on its distribution in benign and malignant skin tumours are required.

KEY WORDS—Basal cell carcinoma, tenascin, extracellular matrix, epithelial–mesenchymal interactions, immunohistochemistry, morphogenesis and differentiation.

INTRODUCTION

Basal cell carcinomas (BCCs) have a prominent vascularized, fibroblastic stroma around the neoplastic cells, and it has been postulated that the characteristics and survival of the tumour are dependent on the presence and functional activity of this stroma.[1–3] Some major components of the extracellular matrix have been described in BCC, the neoplastic islands being surrounded by an intact and generally well-developed basement membrane containing immunoreactive fibronectin (FN), type IV collagen (CIV), and laminin (LM).[4] However, relatively few other components of the stroma have been studied which would account for the peculiar characteristics of this tumour.

Recently, another extracellular matrix protein—termed tenascin—has been described which appears to play a major role in normal morphogenesis. It is a glycoprotein found in induced mesenchyme in the early morphogenetic stages of development of lung, kidney, gut, teeth, muscle, bone, skin, and breast.[5–12] In the adult, it is located in more 'stable' sites such as peritendinous sheath, perichondrium, nerve sheath, and walls of blood vessels,[6,7] but is otherwise absent from most mature connective tissues.[5]

In neoplasia, tenascin is highly expressed in the stroma of breast carcinomas, but is apparently absent from benign lesions such as hyperplastic nodules or fibroadenomas,[12] both by immunohistochemical analysis and by inhibition ELISA.[12] Tenascin binds to FN[10] and proteoglycan[5] and interferes with the cell binding function of FN,[14] stimulating the growth of mammary tumour cells *in vitro*, possibly a function of the EGF-like repeats contained in the molecular structure.[15]

In view of the apparent association of tenascin with sites of active mesenchymal induction in embryogenesis and neoplasia, this paper reviews the distribution of tenascin in BCC, a tumour with morphological evidence of epithelial–mesenchymal interaction, proposed to recapitulate adnexal morphogenesis.[10]

MATERIALS AND METHODS

Seventeen BCCs were obtained immediately after excision, embedded in OCT compound, snap-frozen in liquid nitrogen-cooled isopentane, and stored at −70°C for a maximum of 7 months.

Addressee for correspondence: Dr G. W. H. Stamp, ICRF Histopathology Unit, 35–43 Lincoln's Inn Fields, London WC2A 3PN, U.K.

0022-3417/89/110225-05 $05.00

Immunological reagents

The antiserum to tenascin was a generous gift of Dr Ruth Chiquet-Ehrismann from the Friedrich Miescher-Institut, Basel and was raised in rabbits to tenascin purified from conditioned medium of chick embryo fibroblast cultures as previously described.[9] It has been shown to cross-react with rat, mouse, and human tenascin.[12] Other reagents were obtained from Dakopatts, U.K., apart from polyclonal antisera to laminin (BRL, U.S.A.) and type IV collagen (Eurodiagnostics, Holland).

Immunohistochemical staining

A standard peroxidase–antiperoxidase method was used. Briefly, 6 μm cryostat sections were mounted on poly-*l*-lysine coated slides, post-fixed in acetone for 10 min, and treated with normal swine serum diluted 1:5 in PBS to reduce non-specific background staining. The sections were incubated with rabbit primary antisera diluted in PBS overnight at 4°C: anti-tenascin (1:160); anti-laminin (1:250 after protease digestion); anti-fibronectin (1:100), anti-type IV collagen (1:320). Swine anti-rabbit antiserum (1:120) was applied, followed by rabbit PAP complex (1:120), with three washes in PBS for 5 min between each step. The reaction product was revealed using DAB at a concentration of 0·05 per cent in PBS.

Positive control sections included two invasive ductal carcinomas of the breast, and a developing tooth germ from a neonatal rat.[12] A fibroadenoma was used as a negative control. Two normal skin samples were also examined.

RESULTS

Non-neoplastic skin

Staining was absent or faint under the epidermis in normal skin and the uninvolved skin at the excision margin of BCC. One or more eccrine sweat glands were present in 12 specimens and invariably showed a small amount of band-like staining on the adjacent stroma, up to 20 μm in thickness, which was also seen around the duct.

Hair follicles showed intense staining around the hair bulb and lower isthmus in anagen and telogen hairs. It was also present in the dermal papilla with a delicate, pericellular pattern similar to that seen for CIV and LM. Sebaceous glands showed a weak and inconsistent border around the periphery, with slightly more staining of the duct where it merged with that around the isthmus of the hair.

Adipose tissue, dense collagen of the dermis, and actinically damaged collagen were all negative. The sheath of dermal nerves and muscular blood vessels also showed staining, and the smooth muscle of the arrector pili showed membrane positivity.

Basal cell carcinomas

All 17 BCCs showed enhanced staining of the peritumoural stroma compared with normal skin, but the level of intensity was highly variable, ranging from a thin, well-defined band under the peripheral basement membrane less than 20 μm (Fig. 1), to widespread rather diffuse staining of the tumour-associated stroma (Fig. 2).

Fig. 1—A fairly narrow, well-defined band of tenascin staining around a nodular BCC. Note the absence of staining around the sebaceous gland. Cryostat section (PAP)

In most cases, the staining appeared lamellated, following the direction of fine collagen fibres, but not on the fibroblastic cells in between. There was a sharply defined boundary between the unstained mature collagen in the adjacent dermis and the peritumoural stroma (Figs 1 and 2), except in three cases of fibrosing BCC where the staining gradually diminished, blending in with the more mature collagen.

Fig. 2—A rather wider
trating the sub-epitheli

although still relati
to the infiltrating r

The most strikir
in ten of the BCCs
'retraction artefac
very strong fibril
stromal collagen
example, there w
some of the tumo
iphery, but this wa
16 cases. In the n
showing focal ma
apparent accentu
with 'non-retracte
ducible, and did n
fact', as the quali
markedly from n
margins of the sec
Moreover, there w
that seen for CIV a
ment membrane
clefts, and FN, whi
membrane, less int
but also present o
the surrounding tis

igen of the dermis, and
ı were all negative. The
muscular blood vessels
e smooth muscle of the
ıne positivity.

ıanced staining of the
ıred with normal skin,
was highly variable,
efined band under the
ɔrane less than 20 μm
r diffuse staining of the
Fig. 2).

ıed band of tenascin staining
bsence of staining around the
PAP)

ıg appeared lamellated,
ine collagen fibres, but
in between. There was a
between the unstained
ent dermis and the peri-
l 2), except in three cases
staining gradually dim-
e more mature collagen,

Fig. 2—A rather wider band of staining around this BCC, illustrating the sub-epithelial accentuation. Cryostat section (PAP)

although still relatively intense immediately adjacent to the infiltrating nests.

The most striking and intense reactivity was seen in ten of the BCCs, which displayed a characteristic 'retraction artefact', and in two of these there was very strong fibrillar staining of the peritumour stromal collagen fibres (Fig. 3). In the illustrated example, there was also cytoplasmic staining of some of the tumour cells, most marked at the periphery, but this was not observed in any of the other 16 cases. In the more common situation of areas showing focal marginal retraction, there was an apparent accentuation of the staining compared with 'non-retracted' foci. This staining was reproducible, and did not appear to represent 'edge artefact', as the quality of the staining also differed markedly from non-specific uptake on tears and margins of the section elsewhere in the specimens. Moreover, there was a different distribution from that seen for CIV and LM, which labelled the basement membrane only on the stromal side of the clefts, and FN, which was maximal on the basement membrane, less intense on the peritumoural stroma, but also present on fibroblasts and endothelium in the surrounding tissues.

Fig. 3—A focus of BCC showing marked retraction artefact, with intense staining of the peritumoural collagen fibres. Some of the tumour cells, especially at the periphery, show marked cytoplasmic staining. Cryostat section (PAP)

Regressive areas were seen in two cases of nodular BCC, and were associated with a reduction in staining intensity in the areas of maximal lymphocytic infiltration, apart from a few collagenous strands.

DISCUSSION

Tenascin is clearly an important molecule in the chain of epithelial–mesenchymal interactions during development, morphogenesis, and neoplasia[5–14] although its exact functional role has yet to be established. In contrast to the adhesion and structural molecules of the extracellular matrix, such as LM and CIV (and to a lesser extent FN), its expression is variable and appears to be greatest at the time of maximal cellular interaction, gradually reducing as tissues become more stable.[6–8,10,11] One function of tenascin may be to oppose the cell binding function of FN, enhancing cellular mobility rather than adhesion.[14] In neoplasia, tenascin is observed to be highly expressed in the stroma of malignant tumours, but not in benign tumours or hyperplasias.[10,12,13] However, it remains to be seen

whether this distinction applies to a wider range of tumours.

In normal skin, the location of a narrow band of tenascin staining around blood vessels and nerves was consistent with the results of previous studies.[6] In addition, there was staining around eccrine sweat glands and ducts which contrasted with the paucity of expression around sebaceous glands (apart from the duct).

Tenascin has previously been noted around developing fetal rat vibrissae,[10] but its distribution of the adult has not been studied, to the author's knowledge. Its presence around the lower hair follicle and bulb is perhaps not surprising, especially within the dermal papilla, a site of intense morphogenetic activity even in the adult, where CIV and LM are also highly expressed.[17] It may be significant that tenascin appears to have a growth promoting effect on tumour cells *in vitro* and may be playing a similar role in hair growth, possibly a function of the EGF-like repeats within the molecule.[15]

Although tenascin was found around nearly all islands of BCC, the width of the stained mesenchyme did not appear to relate to any other morphological differences, even in the more invasive sclerotic forms where an increased level of fibroblastic activity might be expected, although the staining was much less defined in these areas. Tenascin was increased immediately adjacent to the epithelial elements, but only in one case did the neoplastic cells show consistent positive staining, in an area of prominent stromal retraction. Previous studies have indicated that tenascin is entirely mesenchymal in origin, but there is perhaps no reason to suppose that under certain circumstances epithelial cells may produce it, in a similar way that other extracellular matrix products such as LM, predominantly an epithelial product, can be elaborated by fibroblastic or other mesenchymal cells.[17,18]

Definite reduction in the overall staining intensity was seen in areas showing morphological evidence of regression.[19] There is other evidence that regressive foci in BCC show reduced proliferative activity and may account for this finding, but it could equally well be a consequence of degradative enzymes released by the inflammatory cells.

The most striking observation was the increased level of staining around the retraction spaces. These appear to result from separation of the peripheral tumour cells from the basement membrane, and may be related to a defect in the hemidesmosomes.[20] This may lead to a decreased level of adhesion in such areas and inability to interact with structural proteins of the extracellular matrix. Tenascin has previously been observed to provide a poor substrate for adhesion of tumour cells and has also been observed to be highly expressed in situations of increased cellular mobility and growth.[10] It may even actively interfere with the adhesive properties of FN.[14] These properties could therefore be connected with the increased level of staining around areas of retraction.

It is clear from this study that tenascin is abundant in the stroma around basal cell carcinomas and must be playing a significant role in the active epithelial–mesenchymal interaction associated with this tumour. It is doubtful whether this evidence could be used to refute the argument that BCC is not a truly malignant neoplasm on the grounds that it is expressed in malignant but not in benign tumours,[12,13] especially as few pathological situations have yet been studied. The significance of this important extracellular matrix component will be clarified once its structure and function are established.

ACKNOWLEDGEMENTS

The author wishes to thank Dr Ruth Chiquet-Ehrismann for her generous gift of antibody to tenascin. The Departments of Plastic Surgery at Queen Victoria Hospital, East Grinstead and St Thomas's Hospital, London kindly provided specimens for this study.

REFERENCES

1. Pinkus H. The borderline between cancer and non-cancer: interrelationships between stroma and epithelium. In: Andrade R, Gumport SL, Popkin GL, Rees TD, eds. Cancer of the Skin. Vol. I. Philadelphia: WB Saunders, 1976; 386–405.
2. Mehregan A. Basal cell epithelioma. In: Pinkus' Guide to Dermatohistopathology. 4th ed. Norwalk, CT: Appleton-Century-Crofts, 1986; 509–521.
3. Stamp GWH, Quaba A, Braithwaite A, Wright NA. Basal cell carcinoma xenografts in nude mice. Studies on epithelial differentiation and stromal relationships. *J Pathol* 1988; **156:** 213–225.
4. Nelson DL, Little CD, Balian G. Distribution of fibronectin and laminin in basal cell epitheliomas. *J Invest Dermatol* 1979; **80:** 446–452.
5. Chiquet M, Fambrough DM. Chick myotendinous antigen. I. A monoclonal antibody as a marker for tendon and muscle morphogenesis. *J Cell Biol* 1984; **98:** 1926–1936.
6. Maier A, Mayne R. Distribution of connective tissue proteins in chick muscle spindles as revealed by monoclonal antibodies: a unique distribution of brachionectin/tenascin. *Am J Anat* 1987; **180:** 226–236.
7. Mackie EJ, Thesleff I, Chiquet-Ehrismann R. Tanascin is associated with chondrogenic and osteogenic differentiation *in vivo* and promotes chondrogenesis *in vitro*. *J Cell Biol* 1987; **105:** 2569–2579.
8. Aufderheide E, Ekblom P. Tenascin during gut development: appearance in the mesenchyme, shift in molecular forms and dependence on epithelial–mesen 2341–2349.
9. Aufderheide E, Chic chymal interactions tenascin in the mese
10. Chiquet-Ehrismann cin: an extracellula during fetal develop
11. Thesleff I, Mackie E. distribution of tenas **101:** 289–296.
12. Inaguma Y, Kusal Ehrismann R, Sakak the mouse mammar *Dev Biol* 1988; **128:** 2
13. Mackie EJ, Chiquet stromal marker for e *Natl Acad Sci USA* 1

on epithelial–mesenchymal interactions. *J Cell Biol* 1988; **107:** 2341–2349.
9. Aufderheide E, Chiquet-Ehrismann R, Ekblom P. Epithelial–mesenchymal interactions in the developing kidney lead to expression of tenascin in the mesenchyme. *J Cell Biol* 1987; **105:** 599–608.
10. Chiquet-Ehrismann R, Machie EJ, Pearson CA, Sakakura T. Tenascin: an extracellular matrix protein involved in tissue interactions during fetal development and oncogenesis. *Cell* 1986; **47:** 131–139.
11. Thesleff I, Mackie E, Vainio S, Chiquet-Ehrismann R. Changes in the distribution of tenascin during tooth development. *Development* 1987; **101:** 289–296.
12. Inaguma Y, Kusakabe M, Mackie EJ, Pearson CA, Chiquet-Ehrismann R, Sakakura T. Epithelial induction of stromal tenascin in the mouse mammary gland: from embryogenesis to carcinogenesis. *Dev Biol* 1988; **128:** 245–255.
13. Mackie EJ, Chiquet-Ehrismann R, Pearson CA, *et al.* Tenascin is a stromal marker for epithelial malignancy in the mammary gland. *Proc Natl Acad Sci USA* 1987; **84:** 4621–4625.
14. Chiquet-Ehrismann R, Kalla P, Pearson CA, Beck K, Chiquet M. Tenascin interferes with fibronectin action. *Cell* 1988; **53:** 383–390.
15. Pearson CA, Pearson D, Shibahara S, Hofsteenge J, Chiquet-Ehrismann R. Tenascin: cDNA cloning and induction by TGF-β. *EMBO* 1988; **7:** 2977–2982.
16. Rosai J. Basal cell carcinoma with follicular differentiation (*Letter*). *Am J Dermatopathol* 1988; **10:** 457–458.
17. Couchman JR. Rat hair follicle dermal papillae have an extracellular matrix containing basement membrane components. *J Invest Dermatol* 1986; **87:** 762–767.
18. Woodley DT, Stanley JR, Rease MJ, O'Keefe EJ. Human dermal fibroblasts synthesize laminin. *J Invest Dermatol* 1988; **90:** 679–683.
19. Franchimont C, Pierard GE, van Cauwenberge D, Damseaux M, Lapiere ChM. Episodic progression and regression of basal cell carcinomas. *Br J Dermatol* 1982; **106:** 305–310.
20. Westgate GE, Weaver AC, Couchman JR. Bullous pemphigoid antigen localisation suggests an intracellular association with hemidesmosomes. *J Invest Dermatol* 1985; **84:** 218–224.

Virchows Archiv B Cell Pathol (1991) 61:101–109

Virchows Archiv B
Cell Pathology
Including Molecular Pathology

Distribution of extracellular matrix proteins in odontogenic tumours and developing teeth

Kristiina Heikinheimo[1,2], Peter R. Morgan[3], Risto-Pekka Happonen[1], Göran Stenman[4], and Ismo Virtanen[5]

[1] Department of Oral Pathology, University of Turku, Turku, Finland,
[2] Department of Pathology, University of Helsinki, Helsinki, Finland,
[3] Department of Oral Medicine and Pathology, UMDS (Guy's Campus), London, England,
[4] Department of Oral Pathology, University of Gothenburg, Gothenburg, Sweden and
[5] Department of Anatomy, University of Helsinki, Helsinki, Finland

Received October 10, 1990 / Accepted June 18, 1991

Summary. The distribution of two cellular fibronectins (cFn), tenascin, laminin, as well as type VII collagen was studied in 14 benign odontogenic tumours of epithelial (ameloblastoma) and epithelial-ectomesenchymal (ameloblastic fibroma) origins, as well as in developing human teeth by immunocytochemical means using monoclonal antibodies (Mabs). An extradomain sequence-A-containing form of cFn (EDA-cFn) was seen in the extracellular matrix (ECM) of all tumours studied and in the mesenchyme of the developing tooth germs, indicating that cFn in these tissues are predominantly produced locally. A form of cFn containing an oncofetal domain (Onc-cFn), hitherto found only in carcinomas, was detected focally in the stroma of most ameloblastomas but was absent from ameloblastic fibromas and tooth germs. Tenascin was strongly expressed in the basement membrane (BM) zone of all odontogenic tumours and in that of the early tooth germs. Focal absence of laminin and type VII collagen from the BM of some ameloblastomas and the presence of Onc-cFn in the ECM of most ameloblastomas may correlate with their aggressive behaviour. The results also suggest that EDA-cFn and tenascin are involved in epithelial-mesenchymal interactions during tooth development and in odontogenic tumours.

Key words: Cellular fibronectin – Extracellular matrix – Odontogenic epithelium – Tenascin – Tumour stroma

Introduction

Matrix components are known to influence normal processes of histodifferentiation and morphodifferentiation during tooth formation (Ruch et al. 1983). The tissue interactions proposed have provided a basis for the histological classification of odontogenic tumours (Pindborg et al. 1971; Reichart and Ries 1983). Odontogenic tumours are grouped, according to their putative origins, into epithelial, epithelial-ectomesenchymal, and ectomesenchymal neoplasms (Kramer et al. 1991). The roles of some extracellular matrix (ECM) proteins such as fibronectin, tenascin, and laminin in odontogenesis have recently been studied (Linde et al. 1982; Thesleff and Ekblom 1984; Thesleff et al. 1979, 1981, 1987; Chiquet-Ehrismann et al. 1986) but the distribution of these proteins in odontogenic tumours has not been widely explored (Thesleff and Ekblom 1984; Sauk 1985; Nadimi and Toto 1986).

Cellular fibronectins (cFn) are common in fetal tissues but absent from adult tissues. They are re-expressed in the stroma of malignant tumours (Matsuura and Hakomori 1985; Vartio et al. 1987; Carnemolla et al. 1989). Cellular Fn differ from plasma fibronectin (pFn) in that extradomain (ED) sequences are included in the protein. These sequences may contribute to functional differences between pFn and cFn (Hynes 1985; Kornblihtt and Gutman 1988). Differential glycosylation can also result in an oncofetal form of cFn (Onc-cFn). It has been suggested that Onc-cFn is strongly linked to human malignancy (Loridon-Rosa et al. 1990; Oyama et al. 1990).

Tenascin is an ECM glycoprotein which appears to participate in regulation of cell morphology (Chiquet-Ehrismann 1990). It has a more restricted tissue distribution than Fn and can interfere with the cell-binding function of Fn (Chiquet-Ehrismann et al. 1988). Tenascin has also been shown to be induced in vitro by transforming growth factor-β (TGF-β) (Pearson et al. 1988). Tenascin is most typically expressed in areas of epithelial-mesenchymal interaction during development (Chiquet-Ehrismann et al. 1986; Ekblom and Aufderheide 1989) and in the stroma of carcinomas (Mackie et al. 1987; Inaguma et al. 1988; Stamp 1989; Anbazhagan et al. 1990).

Laminin is an integral component of the basement membrane (BM) (Martin and Timpl 1978). Type VII

Offprint requests to: K. Heikinheimo, Institute of Dentistry, University of Turku, SF-20520 Turku, Finland

collagen is the major protein of the anchoring fibrils (Sakai et al. 1986). Both help bind BM to its underlying stroma (Sakai et al. 1986; Lunstrum et al. 1986). Studies indicate that BM constituents are altered in malignant tumours, according to their degree of differentiation (Liotta et al. 1980; Barsky et al. 1983), although in studies on odontogenic tumours (e.g. ameloblastoma) a continuous laminin-immunoreactive BM has generally been noted (Thesleff and Ekblom 1984; Sauk 1985).

ECM proteins have been shown to play important roles in cellular growth and differentiation by complex cell matrix interactions in normal organ development and tumour progression (Bruijn et al. 1988; Dvorak 1988; Nagy et al. 1989). We therefore undertook detailed comparison of the distribution of two cFns (EDA-cFn and Onc-cFn), tenascin, laminin and type VII collagen in a series of odontogenic tumours and in human tooth germs at different stages of formation.

Materials and methods

Tumours. A total of 14 odontogenic tumours, comprising 11 ameloblastomas and three ameloblastic fibromas, were studied (Table 1). Fresh tumour specimens were obtained during surgical removal. The samples were frozen promptly in liquid nitrogen and stored at −70° C until used. Cryostat sections (5 μm) from each tumour were cut and mounted on clean objective slides for indirect immunofluorescence staining, or on poly-L-lysine-coated slides for immunoperoxidase technique.

Table 1. Histopathological and clinical information relating to ameloblastomas and ameloblastic fibromas studied

Case	diagnosis	Age	Sex	Location
1.	Ameloblastoma, granular cell	37	F	Mandible, primary
2.	Ameloblastoma, plexiform	74	F	Maxilla, 1st rec.
3.	Ameloblastoma, granular cell	40	F	Mandible, 3rd rec.
4.	Ameloblastoma, plexiform	73	M	Mandible, 1st rec.
5.	Ameloblastoma, mixed	72	M	Mandible, primary
6.	Ameloblastoma, acanthomatous	73	M	Mandible, primary
7.	Ameloblastoma, plexiform	58	M	Maxilla, primary
8.	Ameloblastoma, plexiform	54	M	Mandible, 1st rec.
9.	Ameloblastoma, plexiform	39	M	Mandible, primary
10.	Ameloblastoma, mixed	49	M	Mandible, primary
11.	Ameloblastoma, plexiform	59	F	Mandible, 1st rec.
12.	Ameloblastic fibroma	14	F	Maxilla, primary
13.	Ameloblastic fibroma	9	M	Mandible, primary
14.	Ameloblastic fibroma	4	M	Maxilla, primary

Fetal tooth germs. Six mandibular specimens from 13–20 gestational-week-old human (gwh) fetuses were included in the study. These specimens were obtained in connection with legal abortions, after permission had been obtained from the Ethical Committee of the hospital. The samples were snap-frozen in freon cooled in liquid nitrogen, and were stored at −70° C until required. Cryostat sections were cut from each mandible as described above. The sections contained tooth germs at the cap, bell and appositional stages of development.

Immunocytochemistry. Monoclonal antibodies Mab 52DH1 against EDA-cFn (Vartio et al. 1987), Mab FDC6 against Onc-cFn (Matsuura and Hakomori 1985), Mab 100EB2 against tenascin (Howeedy et al. 1990) and rabbit antiserum against laminin (Liesi et al. 1983) have been characterized previously. These antibodies were applied to frozen sections, followed by a secondary antibody, fluorescein-isothiocyanate-coupled (FITC) goat antimouse IgG (Cappel Laboratories, Organon Teknika, West Chester, Pa, USA) or FITC-coupled goat antirabbit IgG (Cappel). By immunofluorescence microscopy, controls involved omission of the primary antibodies or their replacement with a Mab to a placental protein. After washing and embedding, the samples were examined in a Zeiss Axiophot microscope equipped for UV light and phase-contrast illumination.

The distribution of type VII collagen was demonstrated using Mab LH 7.2 (Leigh et al. 1987) and an immunoperoxidase technique. The sections were first exposed to Mab LH 7.2 followed by biotinylated antimouse IgG and streptavidin-peroxidase complex (Amersham International plc, Amersham, England). Diaminobenzidine with hydrogen peroxide was used as a chromogen and sections were counterstained with Harris's haematoxylin. In every case a negative control involved substitution of phosphate-buffered saline for the primary antibody and, in most cases, a section was

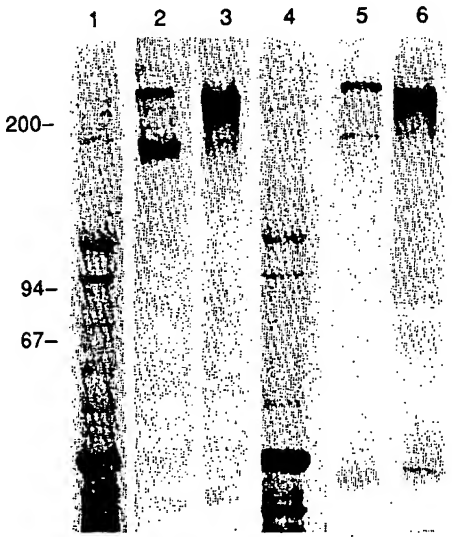

Fig. 1. Immunoblotting of the SDS-PAGE separated polypeptides of two ameloblastomas (lanes 1–3 and lanes 4–6) with Mabs against tenascin (100EB2) and EDA-cFn (52DH1). Mab 100EB2 reacts with two polypeptides of Mr 250000 and 180000 (lanes 2 and 5) while Mab 52DH1 reacts with a single polypeptide of Mr 240000 (lanes 3 and 6). Lanes 1 and 4 show the corresponding amido-black staining for proteins. The molecular weights of the marker proteins are indicated on the left side. Minor extra bands seen in the blots are due to degradation of ECM proteins

Fig. 2. EDA-cF
lastic fibroma
loblastic fibro
in the ectome
scope view of
ameloblastoma
contrast micro
lar immunorea

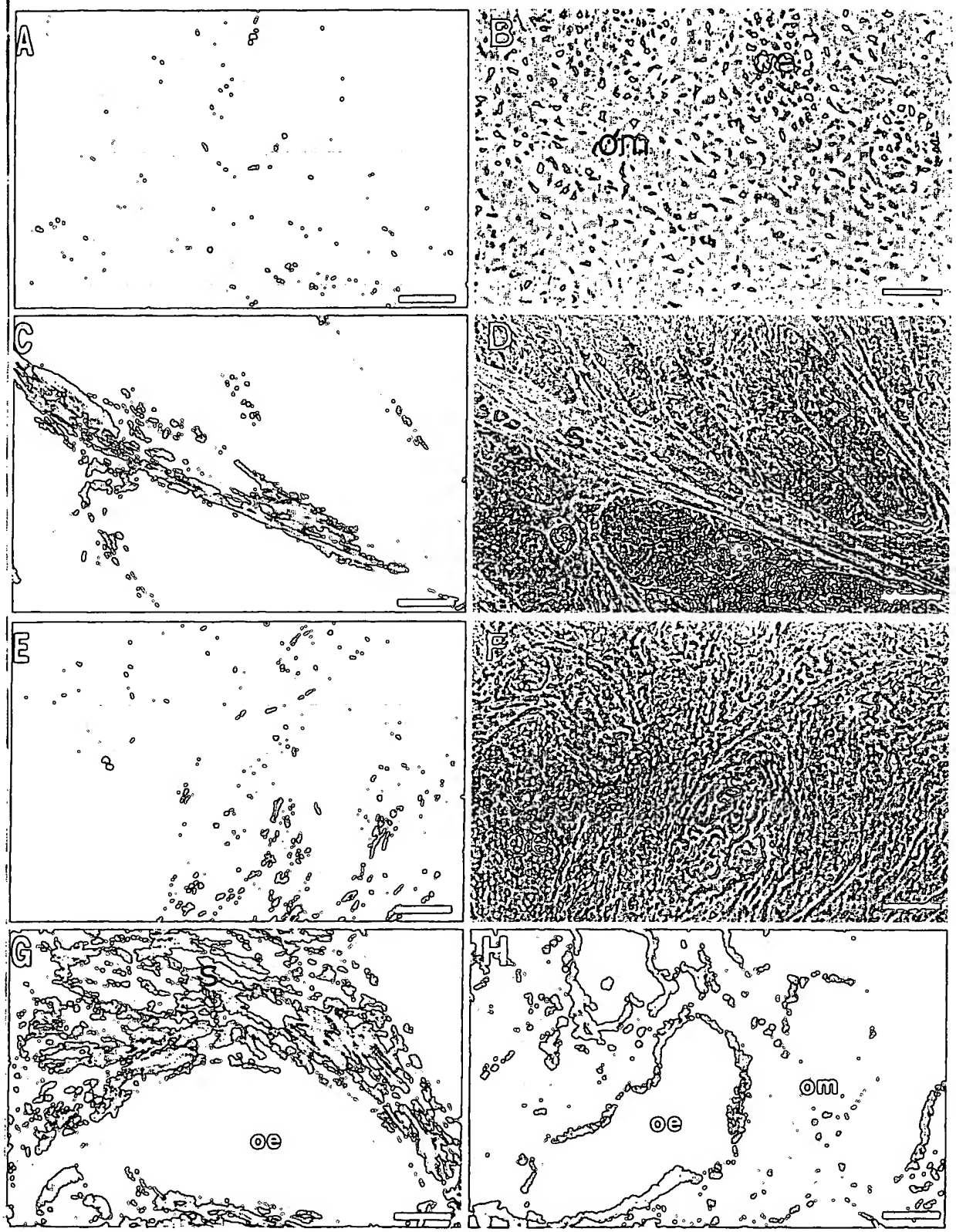

Fig. 2. EDA-cFn **A–D**, Onc-cFn **E–F** and tenascin **G–H** in ameloblastic fibroma **A**, **B**, **H** and ameloblastoma **C**, **D**, **E**, **F**, **G**. **A** Ameloblastic fibroma exhibits a weak immunoreaction for EDA-cFn in the ectomesenchymal tumour tissue. **B** Phase-contrast microscope view of the same field. **C** The stromal area of a plexiform ameloblastoma exhibits strong reactivity for EDA-cFn. **D** Phase contrast microscopy view of the same field. **E** Heterogenous fibrillar immunoreactivity for Onc-cFn is present focally in the tumour stroma of a recurrent plexiform ameloblastoma. **F** Phase contrast view of the same field. **G** The fibrous stroma of an ameloblastoma exhibits a uniformly bright reaction for tenascin. **G** Patchy immunoreaction for tenascin is seen in ectomesenchymal tissue component of ameloblastic fibroma. Note the positively outlined basement membranes in otherwise negative epithelial islands in H. *om* = odontogenic ectomesenchymal tumour tissue, *s* = stroma, *oe* = odontogenic tumour epithelium, *Bars:* **A–H** = 100 μm

incubated with an antikeratin antibody LP2K (Amersham), which was invariably positive in the odontogenic epithelium (Morgan et al. 1987). During each set of incubations with Mab LH 7.2 a section with oral mucosa was included to provide a positive tissue control.

Immunoblotting analysis. EDA-cFn and tenascin were detected in two ameloblastomas by dissolving small pieces of the tissue in the electrophoresis sample buffer (Laemmli 1970). The polypeptides were separated using sodium dodecylsulphate polyacrylamide gel electrophoresis (SDS-PAGE) using 6.5% slab gels under reducing conditions according to Laemmli (1970). The polypeptides were then transferred on to nitrocellulose sheets (Towbin et al. 1987) which were then exposed to the monoclonal antibodies and the appropriate peroxidase-coupled conjugate (Dakopatts, Glostrup, Denmark) or were stained for protein using amido black.

Immunoblotting of two of the ameloblastomas (Fig. 1, lanes 1–3, case 3; lanes 4–6, case 4) revealed distinct polypeptides of Mr 250000 and 180000, respectively, with Mab 100EB2 (Fig. 1, lanes 2, 5). Mab 52DH1 gave a prominent reaction with a polypeptide of Mr 240000 (Fig. 1, lanes 3, 6).

Results

Odontogenic tumours

Histological findings. The stroma of the odontogenic epithelial tumours (ameloblastoma) analysed was that associated with the epithelial components rather than the usually denser and more collagenous tissue near the periphery of the lesion. Both cellular and extracellular components of the ameloblastoma stroma exhibited considerable diversity. There were variations in the shapes and densities of the fibroblasts, in the consistencies of fibrous tissue, in the extents of the peri-epithelial hyalinization, and in the presence or absence and distribution of inflammatory infiltrate. Stromal degeneration, in some instances accompanied by early cyst formation, was present in half of the cases.

Ameloblastic fibromas consisted of dental papilla-like delicate tissue and cellular neoplastic ectomesenchymal

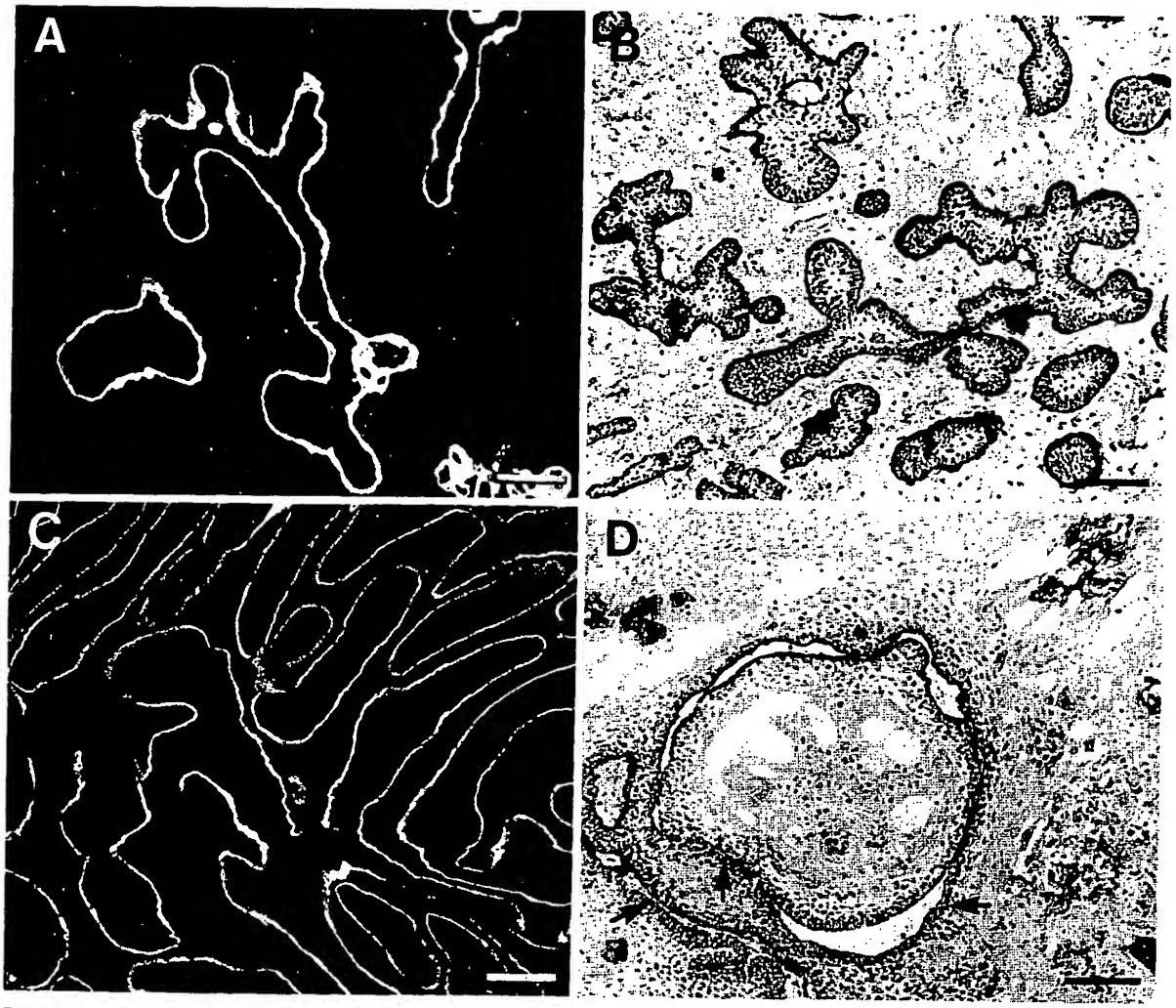

Fig. 3. Laminin A and C and type VII collagen B and D in ameloblastic fibroma A, B and ameloblastoma C, D. A Basement membrane (BM) of epithelial component of the ameloblastic fibroma exhibits a strong linear staining pattern for both laminin and type VII collagen B. C The BM of a plexiform ameloblastoma exhibits a generally continuous immunoreaction for laminin. D Marked type VII collagen-positive and negative (*arrows*) areas in the BM zone are present in a mixed acanthomatous, plexiform and follicular variant of ameloblastoma. *Bars:* A–D = 100 μm

Fig. 4. EDA-cFn
human tooth ger
intense reaction f
ectomesenchyme a
for EDA-cFn in
(*arrow* in A) and
in B). C There is
in the dental papi
that the follicle is

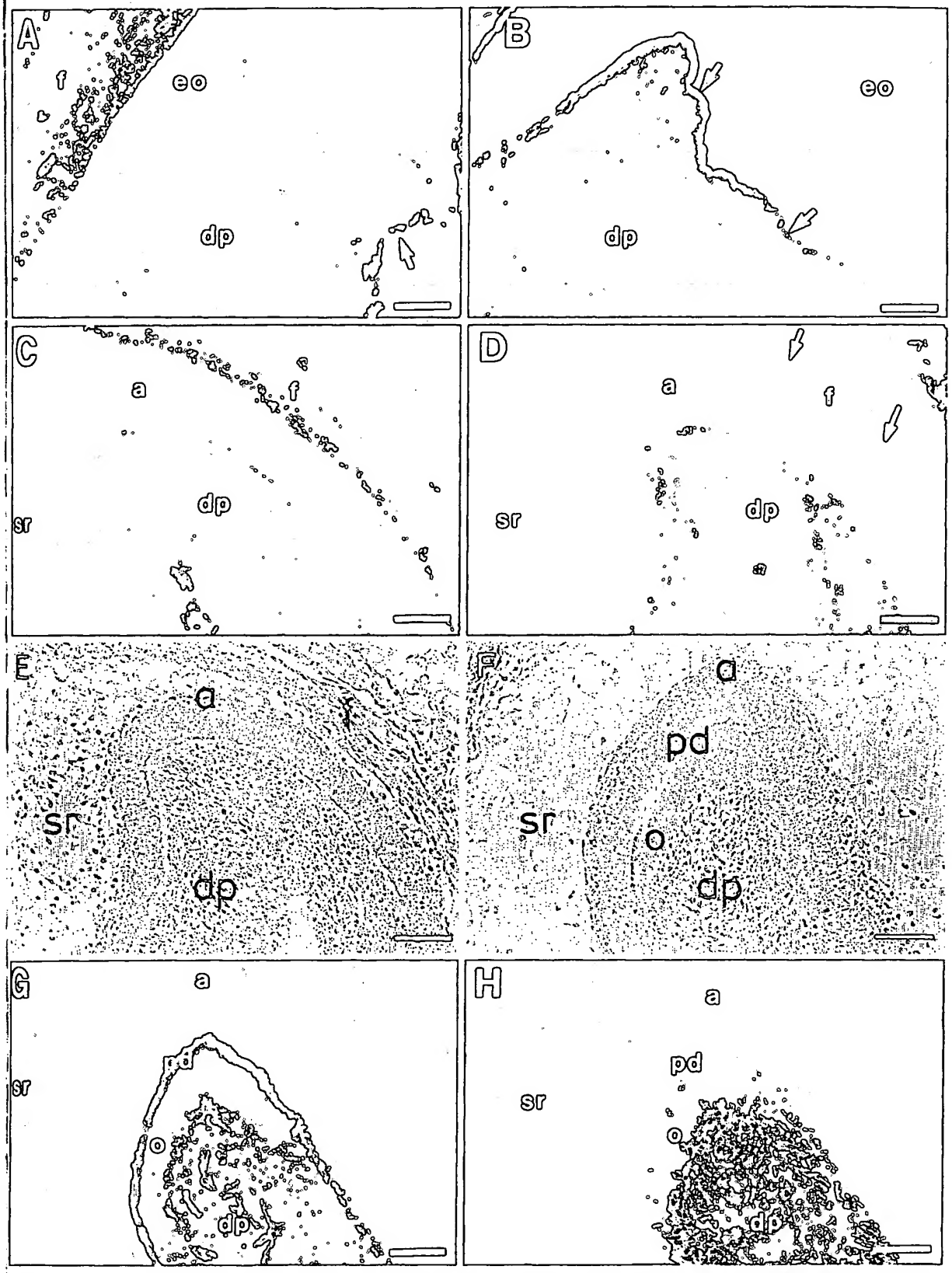

Fig. 4. EDA-cFn **A**, **C**, **G** and tenascin **B**, **D**, **H** in developing human tooth germs. **A** Faint staining for EDA-cFn and a more intense reaction for tenascin **B** are present in the dental papilla ectomesenchyme at the early bell-stage. Note the marked reactivity for EDA-cFn in the capillary endothelia of the developing pulp (*arrow* in **A**) and intense staining of the BM for tenascin (*arrows* in **B**). **C** There is positive staining for EDA-cFn and tenascin **D** in the dental papilla ectomesenchyme at the late bell-stage. Note that the follicle is positive for EDA-cFn but negative for tenascin (arrows in **D**). **E** Corresponding-phase contrast view for **C** and **D**. **G** Intense staining of the dental papilla at the stage of dental hard tissue formation is shown for EDA-cFn and tenascin **H**. Differentiated odontoblasts are devoid of both proteins but predentin is positive for EDA-cFn **G**. **F** Phase-contrast view for **G** and **H**. *f* = follicle, *eo* = enamel organ, *dp* = dental papilla, *sr* = stellate reticulum, *a* = ameloblasts, o = odontoblasts, *pd* = predentin, *Bars:* **A**, **B** = 100 μm, **C**–**H** = 200 μm

tissue with plump, prominent nuclei, and strands and islands of odontogenic epithelium. In some areas a zone of hyalinization surrounded epithelial nests. These neoplastic components formed discrete areas separated from each other by bands of less cellular, collagenous fibrous tissue. All three ameloblastic fibromas were free of inflammation.

EDA-cFn. Two ameloblastic fibromas (cases 13 and 14) revealed notably weak immunoreactivity in ectomesenchyme (Fig. 2A–B) for EDA-cFn. The third tumour (case 12) was brightly positive. All ameloblastomas studied, i.e. those with a stroma of dense cellular fibrous tissue (Fig. 2C–D, case 4) and those with looser, fibrous stroma exhibited immunoreactivity for EDA-cFn.

Onc-cFn. Focal immunoreactivity for Onc-cFn was seen in stromal areas of 10/11 ameloblastomas studied (Fig. 2E–F, case 4) but the ectomesenchymal and epithelial tumour components of all ameloblastic fibromas were negative.

Tenascin. Tenascin immunoreactivity was found in the stromal or ectomesenchymal components of all ameloblastomas (Fig. 2G, case 13) and ameloblastic fibromas (Fig. 2H, case 12) studied. Basement membranes (BM) surrounding epithelial tumour follicles were clearly outlined. All epithelial structures remained negative.

Laminin and type VII collagen. Laminin and type VII collagen immunoreactivities had almost identical distributions. The BM of the odontogenic epithelial cords and islands of all ameloblastic fibromas studied exhibited an intense, positive linear staining pattern with both antibodies (laminin, Fig. 3A, case 14; type VII collagen, Fig. 3B, case 12). The majority of the ameloblastomas showed staining of a continuous BM with both antibodies used (laminin, Fig. 3C, case 4). Focal loss of reactivity with antibodies to laminin and type VII collagen was detected in the BM zone of 6/11 ameloblastomas (Fig. 3D, case 5).

Developing tooth germs

EDA-cFn. In the cap stage of tooth development (13–14 gwh) the dental papilla ectomesenchyme was devoid of immunoreactivity. Faint staining was seen, however, in the condensed mesenchyme surrounding the tooth germ proper, and in the stroma surrounding the dental lamina and underlying the oral surface epithelium.

In the early bell stage, a faint immunoreaction was seen in the dental papilla ectomesenchyme. A very strong staining reaction was observed in the dental papilla capillary endothelia (Fig. 4A, 16 gwh). The dental follicle tissue and the mesenchyme next the dental lamina were more strongly reactive than in the cap stage. In the late bell stage the dental papilla ectomesenchyme had become more immunoreactive. The BM of the epithelial enamel organ was also faintly labeled. However, staining intensity remained relatively modest throughout the bell stage, except for the capillaries, which were brightly immunoreactive (Fig. 4C, 19 gwh). As tooth development reached the stage of early predentin secretion, the coronal portion of the dental papilla and the predentin became brightly immunoreactive. The differentiated odontoblasts remained negative (Fig. 4G, 19–20 gwh).

The dental follicle mesenchyme and the developing capillaries gave positive staining reactions throughout the period of tooth development studied. The intensity of staining was generally stronger than that of dental papilla ectomesenchyme. The epithelial tissue components, and dentin and enamel matrix remained unequivocally negative.

Onc-cFn. The Mab FDC-6 gave uniformly negative staining reactions in tooth germs and their adjacent tissues in all fetal mandibular specimens studied.

Tenascin. In the cap stage of tooth development the dental papilla ectomesenchyme was faintly immunoreactive. The BM surrounding the tooth germ and the oral surface epithelium were clearly outlined by a positive continuous staining reaction. The condensed mesenchyme surrounding the tooth germ was positive for tenascin.

In the early bell stage the dental papilla, follicle tissue and the BM were brightly immunoreactive (Fig. 4B, 16

Fig. 5. Immunoperoxidase staining for type VII collagen in the late bell stage tooth germ gives a strong reaction in the dental lamina basement membrane (BM) (*large arrows*), marked positive reaction in the outer enamel epithelium BM (*arrowheads*) and a weak immunoreaction in the inner enamel epithelium BM (*small arrows*). *dl* = dental lamina, *f* = follicle, *oe* = outer enamel epithelium, *sr* = stellate reticulum, *ie* = inner enamel epithelium and *dp* = dental papilla. *Bar:* 400 μm

development
n, the coron-
entin became
ed odontob-
h).
c developing
throughout
The intensity
iat of dental
ssue compo-
ied unequiv-

ily negative
adjacent tis-
d.

ient the den-
unoreactive.
oral surface
continuous
ie surround-

llicle tissue,
(Fig. 4B, 16

agen in the
the dental
ced positive
eads) and a
BM (*small*
iel epitheli-
n and *dp*=

gwh). By the late bell stage the dental papilla ectomesenchyme was less immunoreactive than at the earlier bell stage, and the follicle surrounding the tooth germ was devoid of tenascin reactivity. Nondental mesenchyme remained positive, however (Fig. 4D, 19 gwh). Intense staining was seen throughout the dental papilla ectomesenchyme at the apposition stage (Fig. 4H, 19–20 gwh). The odontoblasts and the follicle surrounding the developing tooth were devoid of tenascin. The predentin, dentin and enamel matrix were also negative.

Laminin and type VII collagen. All basement membranes of developing tooth germs studied exhibited continuous positive staining patterns with both antibodies. However, type VII collagen exhibited different intensities amongst BM of several enamel organ components. The BM surrounding dental lamina was strongly immunoreactive. That of the outer enamel organ displayed a weaker staining reaction. The reaction was weaker still in the BM of the inner enamel epithelium (Fig. 5, late bell stage, 17–18 gwh).

Discussion

Although there are many histological similarities between odontogenic tumours and normally developing teeth, it is important not to exaggerate their significance in attempting to assess tumour behaviour. The study reported here and previous studies indicate that some ECM proteins play major roles in developmental tissue interactions (Ruch et al. 1983; Kornblihtt and Gutman 1988; Ekblom and Aufderheide 1989). Other ECM proteins, e.g. Onc-cFn, may also influence, or be influenced by, neoplastic growth (Dvorak 1988; van den Hooff 1988; Loridon-Rosa et al. 1990; Oyama et al. 1990). In our immunocytochemical study we detected some consistent differences between ECM proteins in normal tooth germs and odontogenic tumours and also between the types of tumours studied.

Most odontogenic tumours are essentially benign, or at most locally aggressive (Lucas 1984; Regezi and Sciubba 1989). Ameloblastic fibroma is a rare epithelial-ectomesenchymal odontogenic tumour, occurring most commonly in childhood and adolescence. It is characterized by two components, including an immature ectomesenchymal tissue, resembling dental papilla, and odontogenic epithelial strands and islands. Ameloblastoma is usually a more infiltrative tumour, with a greater tendency to recur but not to metastasize. It is an epithelial neoplasm, possibly of ameloblastic origin. Ameloblastoma is characterized by odontogenic neoplastic epithelium with mature connective tissue stroma. It would have been helpful to have included some malignant odontogenic tumours in this study but, as they are so rare, fresh tissue is very rarely available. We also studied the ECM of human fetal tooth germs on the basis that they would contain the normal counterparts of the components of odontogenic tumours.

A previous study of Fn expression in ameloblastoma suggested that it would be a blood-borne product of their stroma (Nadimi and Toto 1986). In the study reported here, in which we used Mab 52DH1, which reacts with cFn but not with pFn, it was shown that Fn in the stroma of ameloblastoma and neoplastic ectomesenchyme of ameloblastic fibroma is predominantly of cellular type. EDA-cFn was seen equally in ameloblastomas with focal inflammation and in those free from it, suggesting that Fn is most likely produced locally by tumour cells or activated cells in their stroma. Studies by Peltonen et al. (1988) have shown that Fn in the stroma of basal cell carcinomas is of cellular type. These investigations also showed, using in situ hybridization, that Fn mRNA is synthesized predominantly by epithelial tumour cells (Peltonen et al. 1988). Individual cells responsible for Fn synthesis in odontogenic tumours remain to be identified.

Our results, showing that cFn in developing teeth is particularly concentrated in the blood vessel walls of dental papilla, and in BM and predentin zones, are in line with those in previous studies (Thesleff et al. 1979, 1981; Linde et al. 1982; Nadimi and Toto 1986). Because mature odontoblasts and mineralized dentine are negative for Fn, it has been suggested that Fn is not directly involved in dental mineralization but has an important role in the differentiation and maturation of odontoblasts. Two of the three ameloblastic fibromas exhibited faint positive reactions in their ectomesenchymal neoplastic tissue, with patterns similar to that of dental papilla in early tooth development. This is in keeping with the concept that the ectomesenchymal component of at least some ameloblastic fibromas has undergone some of inductive changes to form dental hard tissue and is thus developing towards ameloblastic fibro-odontoma (Regezi and Sciubba 1989).

It has been suggested that the presence of EDA-cFn (Vartio et al. 1987) and particularly that of Onc-cFn (Matsuura and Hakomori 1985; Carnemolla et al. 1989; Loridon-Rosa et al. 1990; Oyama et al. 1990), in the stroma indicate the presence of a malignant epithelial phenotype. As with tenascin, both Fns can be detected in embryonic tissues but are poorly expressed (in the case of EDA-cFn) or completely lacking (Onc-cFn) in normal adult tissues. It is interesting that EDA-cFn was found in both ameloblastoma and ameloblastic fibroma, generally considered as benign neoplasms. Onc-cFn was not found in ameloblastic fibroma but was focally present in ameloblastoma, which is a neoplasm with an aggressive behaviour, given to local infiltration and recurrence. In contrast, Onc-cFn was completely absent from the developing human tooth germ and is therefore presumably not involved in normal tooth development. Expression of Onc-cFn in some odontogenic tumours might therefore be associated with events in oncogenic transformation which activate regulation of altered splicing, leading to a functionally more aggressive neoplasm, as has been demonstrated with mammary tumours (Loridon-Rosa et al. 1990).

The results of studies of tenascin distribution in human solid epithelial neoplasms suggest that tenascin is expressed only in malignant tumours, such as mammary carcinoma (Mackie et al. 1987), basal cell carcinoma

(Stamp 1989) and squamous cell carcinoma (Anbazhagan et al. 1990) and is absent from benign tumours (Mackie et al. 1987; Imaguma et al. 1988). However, it is evident that too few neoplasms have been studied so far to allow tenascin expression to be unequivocally related to malignancy. Some recent publications have challenged such a black-and-white view (e.g. Howeedy et al. 1990). Tenascin expression has been strongly linked to epithelial-mesenchymal interactions in neoplastic transformation and to organogenesis of, for example, the kidney (Aufderheide et al. 1987), hair follicles and the mammary gland (Chiquet-Ehrismann et al. 1986) and teeth (Chiquet-Ehrismann et al. 1986; Thesleff et al. 1987). Both types of odontogenic tumours studied expressed tenascin indicating active epithelial-mesenchymal interactions.

In developing human tooth germs tenascin was found in the ectomesenchyme of dental papilla throughout the developmental span studied, and in dental BM prior to hard tissue formation. These results are essentially in line with findings of Thesleff et al. (1987) on mouse tooth development. The latter proposed that the presence of tenascin is necessary for the differentiation of dental papilla cells into odontoblasts. Ameloblastic fibromas exhibited an immunoreactivity for tenascin in their BM zones in a similar fashion as during early tooth development. Expression of tenascin in ameloblastoma was seen throughout the stromal tissue. This difference may be related to the capacity of some ameloblastic fibromas to form dental hard tissues. Ameloblastomas lack this capacity.

Tenascin appears to have a growth-promoting effect on tumour cells in vitro (Chiquet-Ehrismann et al. 1986; Stamp 1989). It is interesting, in this connection, that tenascin has been shown to share sequence homology with epidermal growth factor (EGF) (Pearson et al. 1988; Engel 1989). Tenascin expression in odontogenic tumours could therefore be related to its growth-promoting effect in an EGF-like fashion. Partanen et al. (1985) have shown that EGF inhibits cell differentiation in mouse embryo teeth in vitro, and stimulates the proliferation of undifferentiated mouse tooth-germ cells (Partanen and Thesleff 1987). It could therefore be hypothesized that tenascin expression in odontogenic neoplasms is related to growth regulation and the fetal phenotype of neoplastic cells. It would seem that in odontogenic tumours tenascin expression cannot be used as a marker of their clinical behaviour as may be the case with Onc-cFn.

During development, laminin is largely a soluble protein with a greater repertoire of functions than in adult BM, for instance, in the polarization of epithelial cells (Ekblom 1989). Very similar patterns of staining for laminin in the BM zones of developing tooth and ameloblastic fibroma suggest similarities in cellular functions. There has been a recent resurgence of interest in the integrity of BM components in carcinomas (D'Ardenne 1989). The general picture is that more aggressive or high grade neoplasms exhibit greater disruption of BM (Visser et al. 1986; Nakamura et al. 1987; Schmockel et al. 1989; Richards and Furness 1990). Farman et al. (1986) have reported marked interruptions in the basal lamina of an ameloblastic fibroma at ultrastructural level. However, the BM zone of all ameloblastic fibromas in the study reported here was found to be intact as revealed by laminin and collagen VII antibodies. In contrast to previous results relating to laminin (Thesleff and Ekblom 1984; Sauk 1985), some ameloblastomas in the tumours we studied exhibited focal loss of laminin and type VII collagen in the BM zone. No clear association could be observed between the presence of inflammatory infiltrate and the degree of loss of reactivity for these proteins. Disruption of BM may thus be related to the more aggressive nature of ameloblastoma, which is also supported by the expression of Onc-cFn in the stroma of most ameloblastomas studied.

Acknowledgements. The skilful technical assistance of Ms. Pipsa Kaipainen, Mr. Reijo Karppinen, Ms. Ritva Koskinen and Ms. Hanna Wennäkoski is gratefully acknowledged. We are grateful to Professor S. Hakomori, Dr. P. Liesi, and Dr. I.M. Leigh for the kind gifts of Mabs FDC6, laminin and LH 7.2, respectively. We also thank Ms. Marja-Leena Rissanen and Ms. Outi Rauanheimo for typing the manuscript. This study was supported by grants from the Finnish Cancer Research Fund, the Sigrid Juselius Foundation and by a research contract with the Finnish Medical Research Council.

References

Aufderheide E, Chiquet-Ehrismann R, Ekblom P (1987) Epithelial-mesenchymal interactions in the developing kidney lead to expression of tenascin in the mesenchyme. J Cell Biol 105:599–608

Anbazhagan R, Sakakura T, Gusterson BA (1990) The distribution of immunoreactive tenascin in the epithelial-mesenchymal junctional areas of benign and malignant squamous epithelia. Virchows Archiv [B] 59:59–63

Barsky SH, Siegal GP, Jannotta F, Liotta LA (1983) Loss of basement membrane components by invasive tumors but not their benign counterparts. Lab Invest 49:140–147

Bruijn JA, Hogendoorn PCW, Hoedemaeker PJ, Fleuren GJ (1988) The extracellular matrix in pathology. J Lab Clin Med 111:140–149

Carnemolla B, Balza E, Siri A, Zardi L, Nicotra MP, Bigotti A, Natali PG (1989) A tumor-associated fibronectin isoform generated by alternative splicing of messenger RNA precursors. J Cell Biol 108:1139–1148

Chiquet-Ehrismann R (1990) What distinguishes tenascin from fibronectin? FASEB J 4:2598–2604

Chiquet-Ehrismann R, Mackie EJ, Pearson CA, Sakakura T (1986) Tenascin: an extracellular matrix protein involved in tissue interaction during fetal development and oncogenesis. Cell 47:131–139

Chiquet-Ehrismann R, Kalla P, Pearson CA, Beck K, Chiquet M (1988) Tenascin interferes with fibronectin action. Cell 53:383–390

D'Ardenne AJ (1989) Use of basement membrane markers in tumor diagnosis. J Clin Pathol 42:449–457

Dvorak HF (1988) Tumor stroma. In: Colvin RB, Bhan AK, McCluskey RT (eds) Diagnostic immunopathology. Raven Press, New York, pp 401–419

Ekblom P (1989) Developmentally regulated conversion of mesenchyme to epithelium. FASEB J 3:2141–2150

Ekblom P, Aufderheide E (1989) Stimulation of tenascin expression in mesenchyme by epithelial-mesenchymal interactions. Int J Dev Biol 33:71–79

Engel J (1989) EGF-like domains in extracellular matrix proteins: localized signals for growth and differentiation. FEBS Lett 251:1–7

Farman AC
tissue ji
fibroma
15:176–
Van den Hc
Adv Ca
Howeedy A
Could V
hyperpl
Hynes R (1
Biol 1:6
Imaguna Y
ismann
tenascin
to carci
Kornblihtt
cellular
Kramer IR
of Odor
cation c
kyo (in
Laemmli U
assembl
Leigh IM, I
clonal a
sa zone
thelia 1:
Liesi P, Da
rat astro
Linde A, Jo
of fibro
Biol 27:
Liotta LA,
S (1980)
dation c
Loridon-Rc
Burtin F
mamma
sections.
Lucas RB (
chill Liv
Lunstrum (
(1986) L
contribu
261:904
Mackie EJ,
K, Kaw
marker
Natl Ac
Martin GR
branc cc
Matsuura H
nectin d
in fibro
in those
Sci USA
Morgan PR
Potentia
sis. J Or
Nadimi H,
mas: an
Nagy JA, B
ak AM,
eration:
tion. Bic
Nakamura
membra
munocyt

Farman AG, Gould AR, Merrell E (1986) Epithelium – connective tissue junction in follicular ameloblastoma and ameloblastic fibroma: an ultrastructural analysis. Int J Oral Maxillofac Surg 15:176–186

Van den Hooff A (1988) Stromal involvement in malignant growth. Adv Cancer Res 50:159–196

Howeedy AA, Virtanen I, Laitinen L, Gold NS, Koukoulis GK, Could VE (1990) Differential distribution of tenascin in normal, hyperplastic and neoplastic breast. Lab Invest 63:798–810

Hynes R (1985) Molecular biology of fibronectin. Annu Rev Cell Biol 1:67–90

Imaguna Y, Kusakabe M, Mackie EJ, Pearson CA, Chiquet-Ehrismann R, Sakakura T (1988) Epithelial induction of stromal tenascin in the mouse mammary gland: from embryogenesis to carcinogenesis. Dev Biol 128:245–255

Kornblihtt AR, Gutman A (1988) Molecular biology of the extracellular matrix proteins. Biol Rev 63:465–507

Kramer IRH, Pindborg JJ, Shear M (1991) Histological Typing of Odontogenic Tumours, 2nd ed. WHO International Classification of Tumours. Springer, Berlin Heidelberg New York Tokyo (in press)

Laemmli UK (1970) Cleavage of structural proteins during the assembly of the head of bacteriophage T4. Nature 227:680–685

Leigh IM, Purkis PE, Bruckner-Tuderman L (1987) LH 7.2 Monoclonal antibody detects type VII collagen in the sublamina densa zone of ectodermally-derived epithelia, including skin. Epithelia 1:17–29

Liesi P, Dahl D, Vaheri A (1983) Laminin is produced by early rat astrocytes in primary culture. J Cell Biol 96:920–924

Linde A, Johansson S, Jonsson R, Jonteil M (1982) Localization of fibronectin during dentinogenesis in rat incisor. Archs Oral Biol 27:1069–1073

Liotta LA, Tryggvason K, Garbisa S, Hart I, Foltz CM, Shafie S (1980) Metastatic potential correlates with enzymatic degradation of basement membrane collagen. Nature 284:67–68

Loridon-Rosa B, Vielh P, Matsuura H, Clausen H, Cuadrado C, Burtin P (1990) Distribution of oncofetal fibronectin in human mammary tumors: immunofluorescence study on histological sections. Cancer Res 50:1608–1612

Lucas RB (1984) Pathology of tumours of the oral tissues. Churchill Livingstone, London, pp 31–89

Lunstrum GP, Sakai LY, Keene DR, Morris NP, Burgeson RE (1986) Large complex globular domains of type VII procollagen contribute to the structure of anchoring fibrils. Biol Chem 261:9042–9048

Mackie EJ, Chiquet-Ehrismann R, Pearson CA, Inaguma Y, Taya K, Kawarada Y, Sakakura T (1987) Tenascin is a stromal marker for epithelial malignancy in the mammary gland. Proc Natl Acad Sci 84:4621–4625

Martin GR, Timpl R (1978) Laminin and other basement membrane components. Annu Rev Cell Biol 3:57–86

Matsuura H, Hakomori S (1985) The oncofetal domain of fibronectin defined by monoclonal antibody FDC-6: its presence in fibronectins from fetal and tumor tissues and its absence in those from normal adult tissues and plasma. Proc Natl Acad Sci USA 85:6517–6521

Morgan PR, Shirlaw PJ, Johnson NW, Leigh IM, Lane EB (1987) Potential applications of antikeratin antibodies in oral diagnosis. J Oral Pathol 16:212–222

Nadimi H, Toto PD (1986) Product identification of ameloblastomas: an immunohistochemical study. J Oral Pathol 15:439–444

Nagy JA, Brown LF, Senger DR, Lanir N, Van de Water L, Dvorak AM, Dvorak HF (1989) Pathogenesis of tumor stroma generation: a critical role for leaky blood vessels and fibrin deposition. Biochim Biophys Acta 948:305–326

Nakamura K, Mori M, Enjoji M (1987) Distribution of basement membrane antigens in clinical gastric adenocarcinomas: an immunocytochemical study. J Clin Pathol 40:1418–1423

Oyama F, Hirohashi S, Shimosato Y, Titani K, Sekiguchi K (1990) Oncodevelopmental regulation of the alternative splicing of fibronectin pre-messenger RNA in human lung tissues. Cancer Res 50:1075–1078

Partanen AM, Ekblom P, Thesleff I (1985) Epidermal growth factor inhibits morphogenesis and cell differentiation in cultured mouse embryonic teeth. Dev Biol 111:84–94

Partanen A-M, Thesleff I (1987) Localization and quantitation of 125I-epidermal growth factor binding in mouse embryo tooth and other embryonic tissues at different developmental stages. Dev Biol 120:186–197

Pearson CA, Pearson D, Shibahara S, Hofsteenge J, Chiquet-Ehrismann R (1988) Tenascin: cDNA cloning and induction by TGF-β. EMBO J 7:2977–2982

Peltonen J, Jaakkola S, Lask G, Virtanen I, Uitto J (1988) Fibronectin gene expression by epithelial tumor cells in basal cell carcinoma: an immunocytochemical and in situ hybridization study. J Invest Dermatol 91:289–293

Pindborg JJ, Kramer IRH, Torloni H. Histological typing of odontogenic tumours, jaw cysts, and allied lesions. International Histological Classification of Tumours No 5. WHO, Geneva 1971

Regezi J, Sciubba JJ (1989) Oral Pathology. Clinical-pathologic Correlations. MB Saunders, Philadelphia, pp 337–368

Reichart PA, Ries P (1983) Considerations on classification of odontogenic tumours. Int J Oral Surg 12:323–333

Richards CJ, Furness PN (1990) Basement membrane continuity in benign, premalignant and malignant epithelial conditions of the uterine cervix. Histopathology 16:47–52

Ruch JV, Lesot H, Karcher-Djuricic V, Meyer JM, Mark M (1983) Epithelial-mesenchymal interactions in tooth germs: mechanisms of differentiation. J Biol Buccale 11:173–193

Sakai LY, Keene DR, Morris NP, Burgeson RE (1986) Type VII collagen is a major structural component of anchoring fibrils. J Cell Biol 261:1577–1586

Stamp GWH (1989) Tenascin distribution in basal cell carcinomas. J Pathol 1103:225–229

Sauk JJ (1985) Basement membrane confinement of epithelial tumor islands in benign and malignant ameloblastomas. J Oral Pathol 14:307–314

Schmockel C, Stolz W, Sakai LY, Burgeson RE, Timpl R, Krieg T (1989) Structure of basement membranes in malignant melanoma and nevocytic nevi. J Invest Dermatol 92:663–668

Thesleff I, Ekblom P (1984) Distribution of keratin and laminin in ameloblastoma. Comparison with developing tooth and epidermoid carcinoma. J Oral Pathol 13:85–96

Thesleff I, Mackie E, Vainio S, Chiquet-Ehrismann R (1987) Changes in the distribution of tenascin during tooth development. Development 101:289–296

Thesleff I, Banach JH, Foidart JM, Vaheri A, Pratt RM, Martin GR (1981) Changes in distribution of type IV collagen, laminin, proteoglycan and fibronectin during mouse tooth development. Dev Biol 81:182–192

Thesleff I, Stenman S, Vaheri A, Timpl R (1979) Changes in the matrix proteins, fibronectin and collagen, during differentiation of mouse tooth germ. Dev Biol 70:116–126

Towbin H, Staehelin T, Gordon J (1979) Electrophoretic transfer of proteins from polyacrylamide gels to nitrocellulose sheets: procedure and some applications. Proc Natl Acad Sci 76:4350–4354

Vartio T, Laitinen L, Närvänen O, Cutolo M, Thornell L-E, Zardi L, Virtanen I (1987) Differential expression of the ED sequence-containing form of cellular fibronectin in embryonic and adult human tissues. J Cell Sci 88:419–430

Visser R, van der Beek JMH, Havenith MG, Cleutjens JPM, Bosman FT (1986) Immunocytochemical detection of basement membrane antigens in the histopathological evaluation of laryngeal dysplasia and neoplasia. Histopathology 10:171–180

0023-6837/90/6206-0725$02.00/0
LABORATORY INVESTIGATION

Vol. 62, No. 6, p. 725, 1990
Printed in U.S.A.

Tenascin Expression in the Human Endometrium and in Endometrial Adenocarcinomas

GÜNTER VOLLMER, GENE P. SIEGAL, RUTH CHIQUET-EHRISMANN, VIRGINIA A. LIGHTNER, HANS ARNHOLDT, AND RUDOLF KNUPPEN

Institut für Biochemische Endokrinologie, Medizinische Universität, Ratzeburger Allee 160, D-2400 Lübeck, Federal Republic of Germany; the Department of Pathology and Lineberger Cancer Research Center, School of Medicine, University of North Carolina at Chapel Hill, Chapel Hill, North Carolina; the Friedrich Miescher Institut, Postfach 2543, CH-4002 Basel, Switzerland; the Departments of Cell Biology and Medicine, Duke University Medical Center, Durham, North Carolina; and the Institut für Pathologie, Medizinische Universität, Ratzeburger Allee 160, D-2400 Lübeck, Federal Republic of Germany

To investigate the involvement of tenascin, an extracellular matrix glycoprotein, in epithelial growth and malignancy, its specific distribution pattern in the human uterus was examined immunohistochemically. During the proliferative phase of the menstrual cycle, this antigen was found as a sharp band around the endometrial glands. The immunoreactivity persisted until the early postovulatory phase of the menstrual cycle, but was not detectable in the glandular or stromal compartment during this later secretory stage, instead endometrial arterioles were immunostained. In marked contradistinction, when antibodies directed against tenascin were applied to sections of endometrial adenocarcinoma, almost the entire extracellular space stained, whereas the neoplastic cells themselves were nonreactive, whatever the degree of tumor differentiation. In precancerous proliferative lesions of the endometrium, tenascin's presence was variable. It was detectable around some superficial glands demonstrating cystic hyperplasia and around all deeply situated glands at the endometrial/myometrial interface. In cases of adenomatous hyperplasia, tenascin immunolocalized throughout the extracellular space of the stroma and the staining intensity was increased as the hyperplasia became more atypical. We therefore conclude that tenascin may be a stromal marker for epithelial proliferative states including those associated with malignancies of the endometrium.

Additional key words: Uterus, Epithelial/mesenchymal interaction, Extracellular matrix, Cell adhesion.

Tenascin, originally described as myotendinous antigen (3, 4) is a recently characterized extracellular matrix glycoprotein. It has been concomitantly described and characterized under a series of different names and by a variety of authors (for review, see Erickson and Lightner) (10). Its DNA sequence is now known (12). Tenascin is intimately involved in tissue interactions during fetal development and oncogenesis (5). Tenascin appears to mediate epithelial/mesenchymal interactions during kidney, tooth, and mammary gland development by inhibiting, in part, the binding of cells to fibronectin (6,13, 21). Such tissue interactions are equally as important for normal embryonic development as they are for altered growth seen in neoplastic states (20). Furthermore, tenascin has been described as a stromal marker for epithelial malignancies (17).

Human endometrial tissue, which is mainly composed of glandular epithelial cells and mesenchymal stromal cells, undergoes cyclic, hormonally-dependent changes of growth and development. This process is essentially proliferative during the first half and maturational (differentiative) during the second half of the menstrual cycle. It therefore can serve as an interesting and important model system to test whether tenascin is associated with any of these processes. Additionally, due to relative high incidence rates of endometrial carcinoma and its precursor lesions in western societies, the appearance of tenascin during neoplastic progression can be assessed. The aims of this study were therefore to investigate the involvement and possible functions of tenascin in both the hormonally regulated processes of growth and differentiation during the menstrual cycle, and during the

development of altered proliferative states in the endometrium up to and including endometrial carcinoma.

EXPERIMENTAL DESIGN

Human uteri were obtained immediately after surgical removal. These organs were removed for a number of different pathologic conditions ranging from descensus uteri to invasive endometrial carcinoma. Representative sections of 18 normal proliferative phase, 4 normal secretory phase, and 10 adenocarcinoma specimens of the endometrium were frozen at −80° C. These later 10 neoplastic cases often had associated hyperplastic foci in adjacent regions. An additional set of 9 proliferative, 5 secretory, and 12 other endometrial samples were embedded in paraffin after fixation in buffered 10% formalin. Specifically, these later cases were composed of 3 cases of cystic hyperplasia, 3 cases of (simple) adenomatous hyperplasia, 2 cases of atypical adenomatous hyperplasia and 3 cases of adenocarcinoma. In addition, 1 case showed progression from adenomatous hyperplasia, through atypical adenomatous hyperplasia to adenocarcinoma in juxtaposition on the histologic slides. Immunostaining with the polyclonal antibodies against tenascin was performed with an indirect immunohistochemical procedure on 8-μm thick frozen sections and by a number of standardized techniques on 5-μm thick paraffin sections.

RESULTS AND DISCUSSION

All tenascin stained cryostat sections could be evaluated. While some paraffin embedded uterine tissue samples did not react with the rabbit anti-chicken tenascin antibody, all showed immunoreactivity in the presence of the rabbit anti-human tenascin. The resolvable staining pattern did not differ significantly when comparing the two fixation methods and the two applied antibodies.

TENASCIN IN NORMAL ENDOMETRIUM

The human endometrium undergoes cyclic, hormonally-dependent changes of proliferation and differentiation. During the first half of the menstrual cycle, estrogens stimulate growth of the endometrium in a receptor-dependent process. During this phase, we found tenascin located as an intense fine band around the endometrial glands and as a rather diffuse and slight blush (minimally elevated above background) within stroma (Fig. 1*a*). This pattern was more prominent in the more superficial (functionalis) region of the endometrium as compared with the basalis portion. During the second half of the menstrual cycle, under the influence of progestins, endometrial tissue becomes transformed into its differentiated, secretory phenotype. During this period, tenascin stainability which at first persisted around the glands (Fig. 1*b*) completely disappeared from the endometrium (Fig. 1*c*). Endometrial arterioles in the functionalis layer, previously unrecognizable, now stained intensely (Fig. 1*d*). The visible number of vessels was increased significantly in tissue undergoing decidualization (figure not shown). Smooth muscle cells in the vascular wall of myometrial blood vessels were immunoreactive in all cases studied but varied in intensity (Fig. 1*e*). Whether or not tenascin can be used as marker for angiogenesis remains to be determined.

ENDOMETRIAL ADENOCARCINOMAS

In sharp contrast to the normal endometrium, in endometrial adenocarcinomas, the entire extracellular space of the tissue surrounding the tumor cells was stained by anti-tenascin antibodies (Fig. 1*f*, and Fig. 2*a*, *b*, and *c*). The malignant epithelial cells themselves were nonreactive. The pattern of tenascin staining and stromal localization was not dependent on the degree of tumor differentiation (Fig. 2) nor on whether the tumor was primary or metastatic, although admittedly the number of examined cases was small.

PROLIFERATIVE LESIONS OF THE ENDOMETRIUM

In atrophic endometrial tissue, no tenascin reactivity was detectable in the endometrial stroma. Rare glands with a scattered distribution within the endometrium retained their stainability at the epithelial/stromal interface. In an endometrium affected by glandular cystic hyperplasia, tenascin was again located around glandular structures with an irregular distribution. In comparison to the few glands recognized in atrophic states, the number of glands showing immunoreactivity at the epithelial/stromal interface in cystic hyperplasias had increased. In all cases of adenomatous hyperplasia, the staining intensity at the glandular/mesenchymal interface was enhanced with a gradient of increased intensity toward the surface. In tissue sections demonstrating progressive changes from the hyperplastic state toward carcinoma, larger regions of the extracellular space became covered by tenascin with an increased staining intensity (Fig. 3*a* and *b*).

DISCUSSION

In the present study, we describe patterns of tenascin immunoreactivity and its correlation with normal endometrial growth during the menstrual cycle. We further go on to document tenascin immunolocalization in cases of endometrial adenocarcinoma and precancerous proliferative states. In the normal endometrium, we were able to detect the presence of tenascin during the proliferative phase of the menstrual cycle, but not after secretory changes had occurred. As yet, we have no evidence to suggest that this is secondary to degradation of tenascin or if it reflects modifications of the carbohydrate moiety of the glycoprotein rendering it "invisible" to our immunohistochemical techniques. Our findings do suggest however, the involvement of tenascin in the processes of proliferation, rather than differentiation. This is strengthened by our observation of an increased mesenchymal reactivity in hyperplastic proliferative lesions of the endometrium. Indeed tenascin as a substrate has been shown to be growth stimulatory for mammary carcinoma cells *in vitro* (7), while tenascin itself can be stimulated by transforming growth factor-β (7, 19) a growth factor which is hormonally regulated in MCF-7 breast cancer cells (9, 14).

In endometrial adenocarcinomas, as in cancers of the breast (17), we find nearly all the extracellular space of

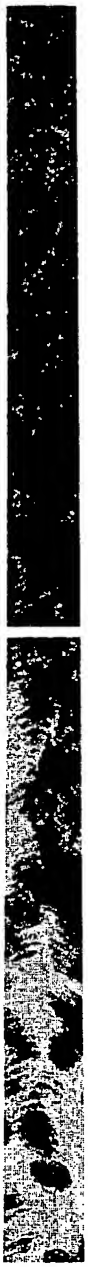

FIG. 1
tained w
During th
concentra
reactivity
least unt
absent ir

the stro
cin has
fibrone
functio
with th
tween t
already
(18). It

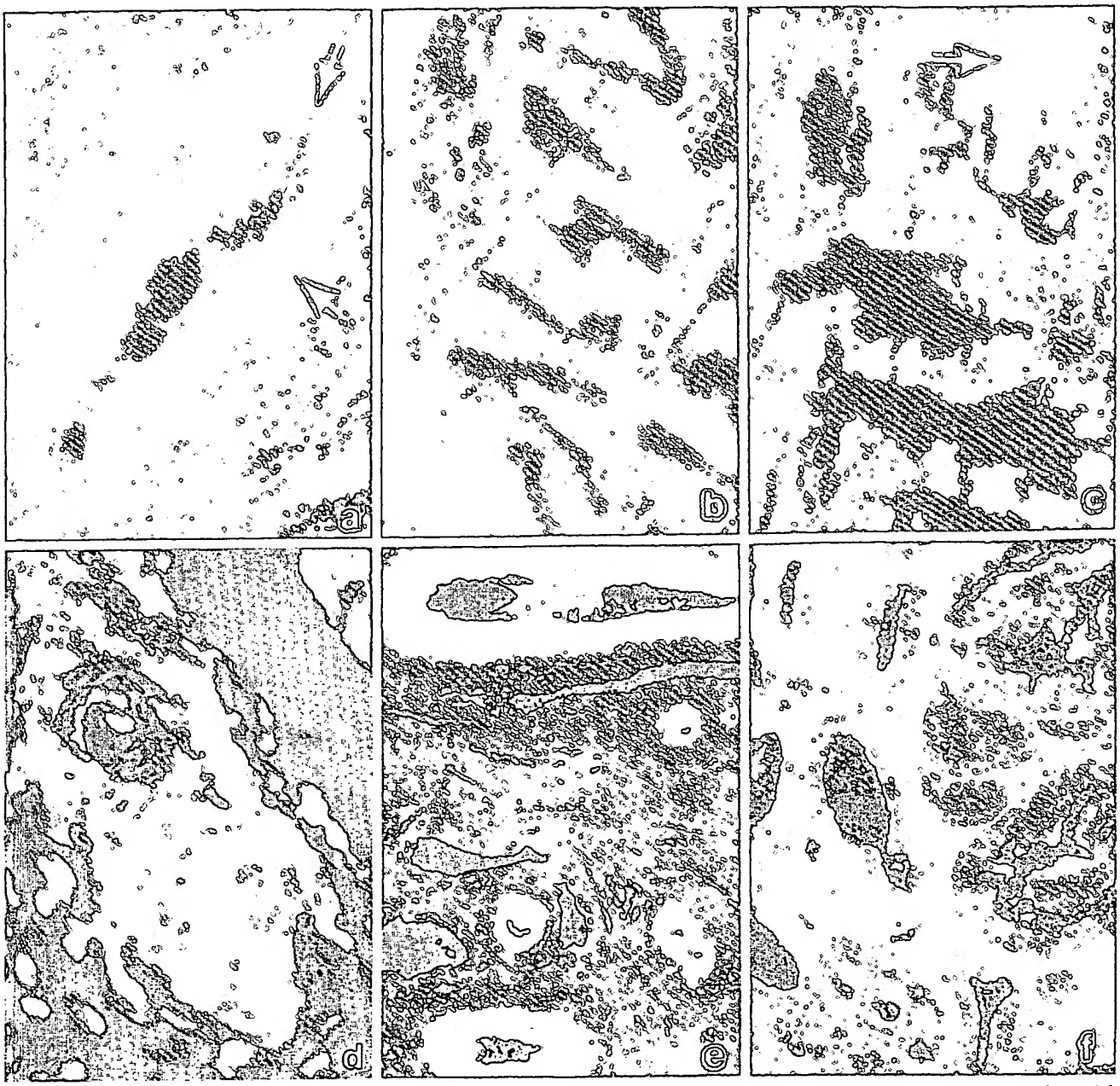

FIG. 1. Tenascin in the endometrium. The staining pattern obtained with the rabbit anti-chicken tenascin antibody is shown. *a*, During the proliferative phase of the menstrual cycle, tenascin is mainly concentrated around glands (*arrow* identifies a thin line of immunoreactivity near the basement membrane); *b*, the staining persists at least until the early secretory phase of the menstrual cycle and, *c*, is absent in the functionalis of the endometrium after the tissue has acquired its secretory phenotype, (*arrow*, immunostaining of arteriole is apparent). *d*, During the later phase, spiral arterioles are stained. *e*, Immunoreactivity of smooth muscle cells in the vascular wall of myometrial blood vessels. *f*, For comparison, the staining pattern of tenascin in a frozen section of an endometrial adenocarcinoma is shown. In this case the entire extracellular space of the stromal mesenchyme is intensely positive.

the stromal mesenchyme covered by tenascin. As tenascin has been described to inhibit cell attachment to fibronectin, in endometrial carcinomas tenascin may function as a substrate for tumor cells thereby interfering with their attachment to fibronectin. A correlation between the appearance of tenascin and cell migration has already been observed during neural crest development (18). It is therefore possible that tenascin may modulate tumor cell invasion at either the attachment or migration steps of the process.

It has been clearly shown for the developing mammary gland, the developing mouse kidney, and for mammary tumors, that it is the epithelium which induces the expression of tenascin in the stroma (1, 7, 13). Interestingly, this model of epithelial induction of tenascin in mesenchymal cells seems to be applicable to a variety of

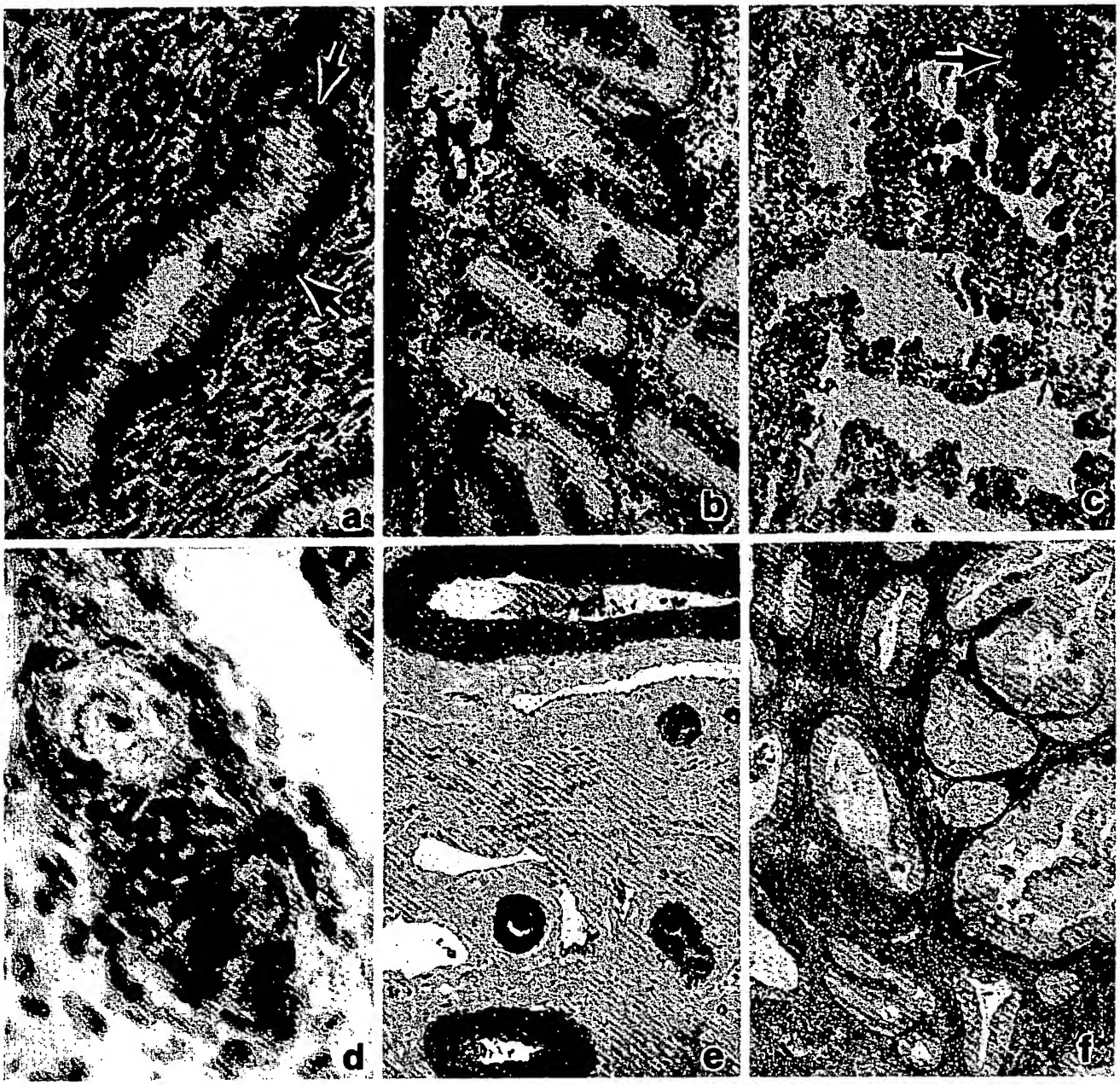

FIG. 1. Tenascin in the endometrium. The staining pattern obtained with the rabbit anti-chicken tenascin antibody is shown. *a*, During the proliferative phase of the menstrual cycle, tenascin is mainly concentrated around glands (*arrow* identifies a thin line of immunoreactivity near the basement membrane); *b*, the staining persists at least until the early secretory phase of the menstrual cycle and, *c*, is absent in the functionalis of the endometrium after the tissue has acquired its secretory phenotype, (*arrow*, immunostaining of arteriole is apparent). *d*, During the later phase, spiral arterioles are stained. *e*, Immunoreactivity of smooth muscle cells in the vascular wall of myometrial blood vessels. *f*, For comparison, the staining pattern of tenascin in a frozen section of an endometrial adenocarcinoma is shown. In this case the entire extracellular space of the stromal mesenchyme is intensely positive.

the stromal mesenchyme covered by tenascin. As tenascin has been described to inhibit cell attachment to fibronectin, in endometrial carcinomas tenascin may function as a substrate for tumor cells thereby interfering with their attachment to fibronectin. A correlation between the appearance of tenascin and cell migration has already been observed during neural crest development (18). It is therefore possible that tenascin may modulate tumor cell invasion at either the attachment or migration steps of the process.

It has been clearly shown for the developing mammary gland, the developing mouse kidney, and for mammary tumors, that it is the epithelium which induces the expression of tenascin in the stroma (1, 7, 13). Interestingly, this model of epithelial induction of tenascin in mesenchymal cells seems to be applicable to a variety of

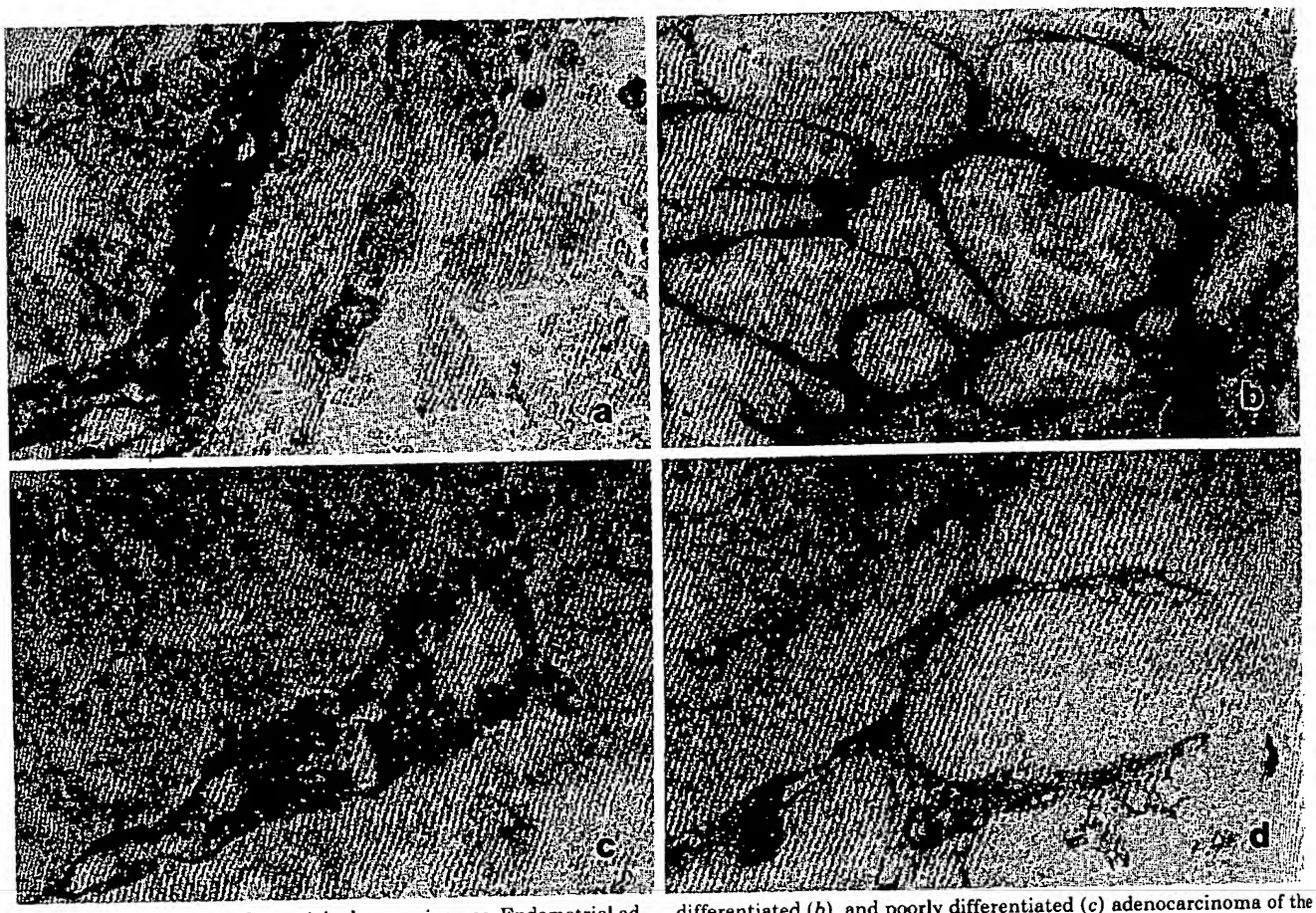

FIG. 2. Tenascin in endometrial adenocarcinomas. Endometrial adenocarcinomas were stained with the rabbit anti-human tenascin antibody. In all cases studied the entire extracellular space of the stromal mesenchyme was stained. In highly differentiated (*a*), moderately differentiated (*b*), and poorly differentiated (*c*) adenocarcinoma of the endometrium as well as in (*d*), a case of endometrial adenocarcinoma which had recurred in the vagina, the staining pattern and intensity were similar.

other epithelial-derived tumors. In these cases, tenascin immunoreactivity is absent or restricted to the basement membrane zone in the normal tissue whereas tenascin more or less completely covers the stromal mesenchyme in the malignant state. Preliminary results suggested that the uterine adenocarcinoma cell lines HEC 6 and the MCF-7 breast cancer cell line are not reactive when stained with anti-tenascin antibodies (G. Vollmer, unpublished data). Therefore, it seems that tenascin may be used to study the mechanisms of either induction or epithelial/mesenchymal interactions in normally growing human tissue *in vivo* and *in vitro*. Further, the uterus appears to be ideal for this purpose as it represents a steadily developing tissue in adults with a high incidence for malignant transformation.

METHODS

PREPARATION OF THE ANTISERUM

Two different antibody preparations were used in this study. The polyclonal antiserum initially used was prepared by Dr. R. Chiquet-Ehrismann and was raised to tenascin purified from conditioned medium of chicken fibroblast cultures as described elsewhere (5). A second polyclonal antiserum was prepared by Dr. V. A. Lightner and was raised in rabbits against tenascin purified from conditioned medium of the human glioma cell line U-251 MG (2, 15).

IMMUNOHISTOCHEMISTRY

Frozen sections of human endometrial tissue 8-μm thick, were fixed in acetone and air-dried overnight. Formalin-fixed, paraffin-embedded tissue obtained from the University of North Carolina Hospitals was prepared and processed as previously described (16). Additional tissues were treated as follows: The formalin-fixed, paraffin-embedded material (5-μm thick) was cut, deparaffinated, air-dried overnight, and pretreated with 1% pronase for 30 minutes to unmask the antigen. The slices were incubated for 1 hour at room temperature with anti-chicken tenascin antibody diluted 1:100 or 1:200 or the anti-human tenascin antibody diluted 1:2000 in RPMI 1640 medium containing 10% bovine serum and 0.1% azide, rinsed for 10 minutes with Tris-buffered saline. Thereafter, for detection of tenascin, sections were incubated with a goat anti-rabbit IgG antiserum which was either labeled by alkaline phosphatase diluted 1:500 with RPMI 1640 medium containing 10% human serum (cryostat sections; Dianova Hamburg or by strepavidin) biotinylated horseradish peroxidase (paraffin sections). Alkaline phosphatase was visualized by the New Fuchsin method (8), whereas peroxidase or streptavidin peroxidase was visualized by aminoethyl carbazol and hydrogen peroxide in an aqueous solution for 5 minutes. Subsequently, slides were counterstained with "hemalaun" and mounted. As a control, parallel

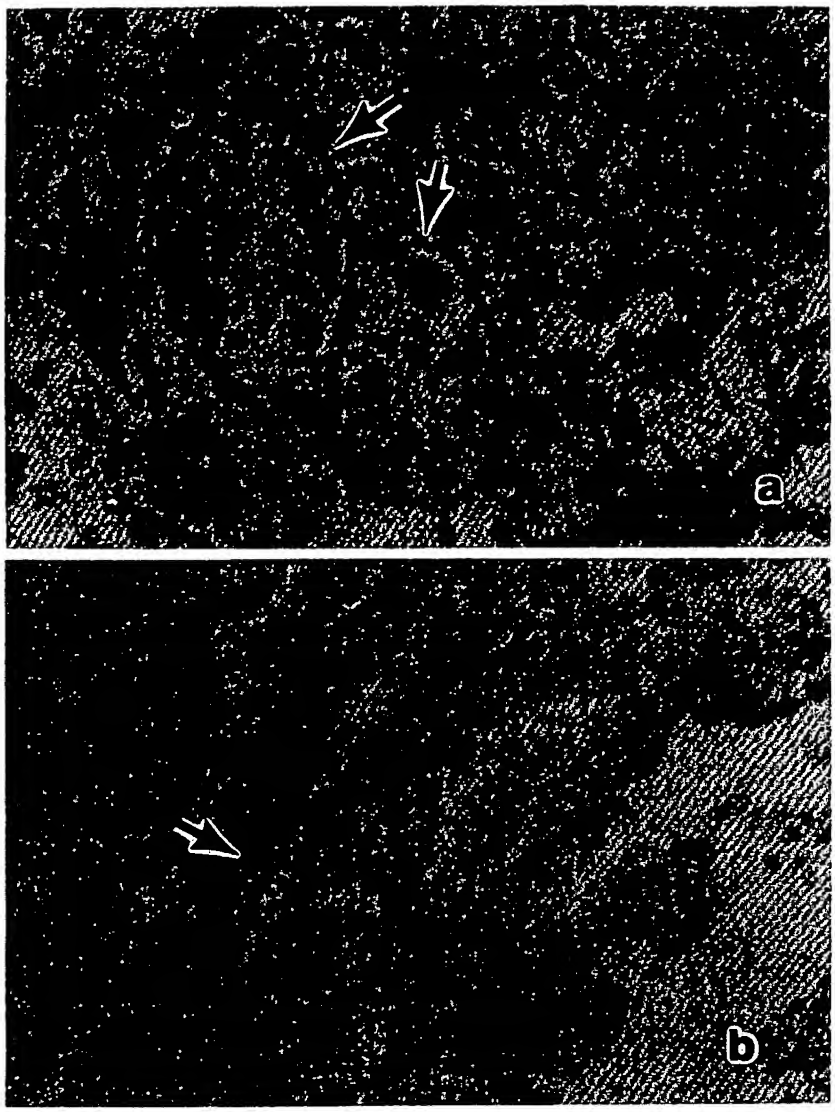

FIG. 3. Adenomatous hyperplasias. Adenomatous hyperplasias stain positively for tenascin (*arrows* highlight the zone of immunoreactivity at epithelial/mesenchymal interface). *a*, A case of focal adenomatous hyperplasia and (*b*) a case of diffuse adenomatous hyperplasia are shown (*arrow* highlights intense positivity of endometrial atroma compressed between nearly "back-to-back" endometrial glands). See text for details.

sections were treated with secondary reagent only to test for endogenous alkaline phosphatase or peroxidase activity or the primary antibody was replaced by a control IgG preparation and otherwise treated identically through all steps of the procedure.

Acknowledgments: We wish to thank M. Kniewe, U. Meyn, and D. Cowan for their expert technical assistance. We also wish to thank Prof. M. Dietel for his critical reading of the manuscript and Prof. H. P. Erickson for stimulating discussions.

Date of acceptance: January 22, 1990.

This work was supported by the Deutsche Forschungsgemeinschaft SFB 232A1. Additional work was performed at the University of North Carolina at Chapel Hill, Chapel HIll, NC. and was supported there by the Deutsche Forschungsgemeinschaft (travel Grant Vo 410/1-1) and National Institutes of Health Grants CA31733 and CA45727.

Professor Siegal is a Jefferson Pilot Fellow in Medicine at the University of North Carolina, at Chapel Hill, Chapel Hill, NC.

Address reprint requests to: Günter Vollmer, Ph.D., Institut für Biochemische Endokrinologie, Medizinische Universität, Ratzeburger Allee 160, D-2400 Lübeck, Federal Republic of Germany.

REFERENCES

1. Aufderheide E, Chiquet-Ehrismann R, Ekblom P: Epithelio-mesenchymal interactions in the developing kidney lead to expression of tenascin in the mesenchym. J Cell Biol. 105:599, 1987
2. Bourdon MA, Wikstrand CF, Furthmayer H, Matthews TF, Bigner DD: Human glioma-mesenchyman extracellular matrix antigen defined by monoclonal antibody. Cancer Res 43:2796, 1983
3. Chiquet M, Fambrough DM: Chick myotendinous antigen. I. A monoclonal antibody as marker for tendon and muscle morphogenesis. J Cell Biol 98:1926, 1984
4. Chiquet M, Fambrough DM: Chick myotendinous antigen. II. A novel extracellular glycoprotein complex consisting of large disulfide-linked subunits. J Cell Biol 98:1937, 1984
5. Chiquet-Ehrismann R, Mackie EJ, Pearson CA, Sakakura T: Tenascin: an extracellular matrix protein involved in tissue interactions during fetal development and oncogenesis. Cell 47:131, 1986
6. Chiquet-Ehrismann R, Kalla P, Pearson CA, Beck K, Chiquet M: Tenascin interferes with fibronectin action. Cell 53:383, 1988
7. Chiquet-Ehrismann R, Kalla P, Pearson CA: Participation of tenascin and TGF-beta in reciprocal epithelial-mesenchymal interactions of MCF 7 cells and fibroblasts. Cancer Res 49:4322, 1989
8. Cordell JL, Falini B, Erber WN, Ghosh AK, Abdulaziz Z, MacDonald S, Pulford KAF, Stein H, Mason DY: Immunoenzymatic labeling of monoclonal antibodies using immuno complexes of alkaline phosphatase and anti-alkaline phosphatase (APAAP)

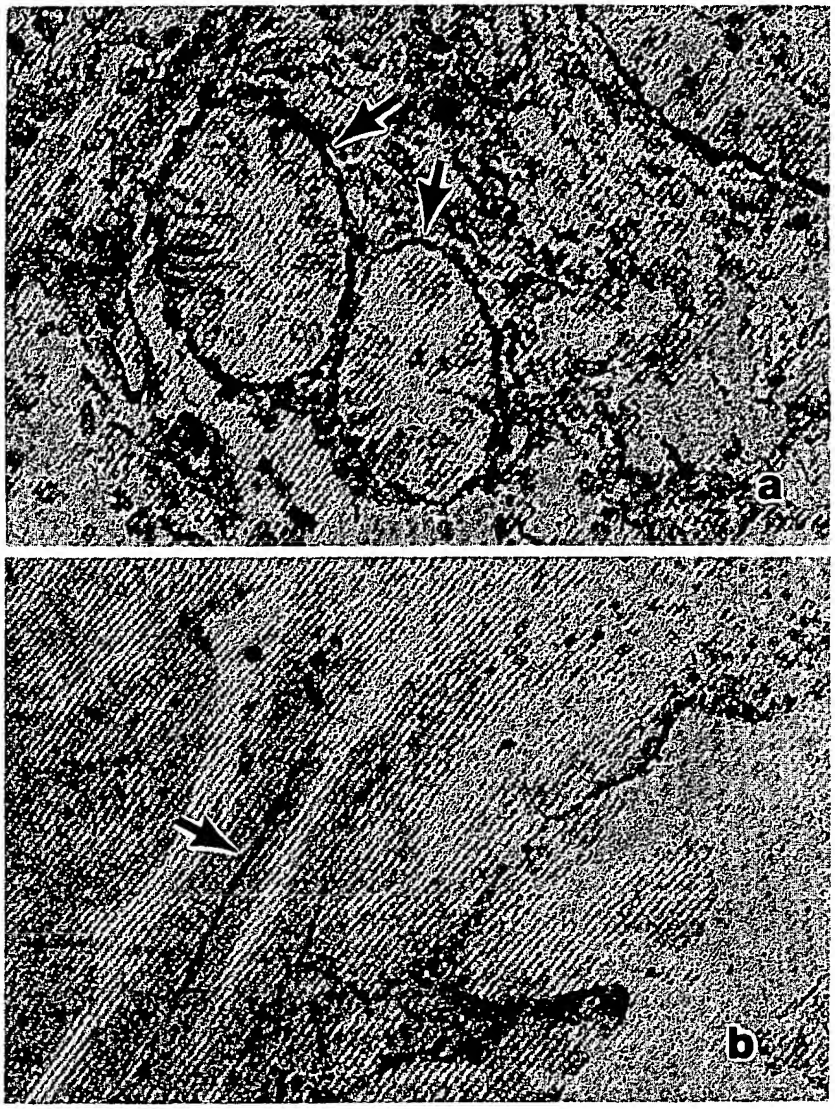

FIG. 3. Adenomatous hyperplasias. Adenomatous hyperplasias stain positively for tenascin (*arrows* highlight the zone of immunoreactivity at epithelial/mesenchymal interface). *a*, A case of focal adenomatous hyperplasia and (*b*) a case of diffuse adenomatous hyperplasia are shown (*arrow* highlights intense positivity of endometrial atroma compressed between nearly "back-to-back" endometrial glands). See text for details.

sections were treated with secondary reagent only to test for endogenous alkaline phosphatase or peroxidase activity or the primary antibody was replaced by a control IgG preparation and otherwise treated identically through all steps of the procedure.

Acknowledgments: We wish to thank M. Kniewe, U. Meyn, and D. Cowan for their expert technical assistance. We also wish to thank Prof. M. Dietel for his critical reading of the manuscript and Prof. H. P. Erickson for stimulating discussions.

Date of acceptance: January 22, 1990.

This work was supported by the Deutsche Forschungsgemeinschaft SFB 232A1. Additional work was performed at the University of North Carolina at Chapel Hill, Chapel HIll, NC. and was supported there by the Deutsche Forschungsgemeinschaft (travel Grant Vo 410/1-1) and National Institutes of Health Grants CA31733 and CA45727.

Professor Siegal is a Jefferson Pilot Fellow in Medicine at the University of North Carolina, at Chapel Hill, Chapel Hill, NC.

Address reprint requests to: Günter Vollmer, Ph.D., Institut für Biochemische Endokrinologie, Medizinische Universität, Ratzeburger Allee 160, D-2400 Lübeck, Federal Republic of Germany.

REFERENCES

1. Aufderheide E, Chiquet-Ehrismann R, Ekblom P: Epithelio-mesenchymal interactions in the developing kidney lead to expression of tenascin in the mesenchym. J Cell Biol. 105:599, 1987
2. Bourdon MA, Wikstrand CF, Furthmayer H, Matthews TF, Bigner DD: Human glioma-mesenchyman extracellular matrix antigen defined by monoclonal antibody. Cancer Res 43:2796, 1983
3. Chiquet M, Fambrough DM: Chick myotendinous antigen. I. A monoclonal antibody as marker for tendon and muscle morphogenesis. J Cell Biol 98:1926, 1984
4. Chiquet M, Fambrough DM: Chick myotendinous antigen. II. A novel extracellular glycoprotein complex consisting of large disulfide-linked subunits. J Cell Biol 98:1937, 1984
5. Chiquet-Ehrismann R, Mackie EJ, Pearson CA, Sakakura T: Tenascin: an extracellular matrix protein involved in tissue interactions during fetal development and oncogenesis. Cell 47:131, 1986
6. Chiquet-Ehrismann R, Kalla P, Pearson CA, Beck K, Chiquet M: Tenascin interferes with fibronectin action. Cell 53:383, 1988
7. Chiquet-Ehrismann R, Kalla P, Pearson CA: Participation of tenascin and TGF-beta in reciprocal epithelial-mesenchymal interactions of MCF 7 cells and fibroblasts. Cancer Res 49:4322, 1989
8. Cordell JL, Falini B, Erber WN, Ghosh AK, Abdulaziz Z, MacDonald S, Pulford KAF, Stein H, Mason DY: Immunoenzymatic labeling of monoclonal antibodies using immuno complexes of alkaline phosphatase and anti-alkaline phosphatase (APAAP)

complexes. J Histochem Cytochem 32:219, 1984
9. Dickson RB, Bates SE, McManaway ME, Lippman ME: Characterization of estrogen responsize transforming activity in human breast cancer cell lines. Cancer Res 46:1707, 1986
10. Erickson HP, Lightner VA: Hexabrachion protein (Tenascin, Cytotactin, Brachionectin) in connective tissues, embryonic brain, and tumors. Adv Cell Biol 2:1988
11. Graham RC, Karnovsky MJ: The early stages of absorption of injected horseradish peroxidase in the proximal tubules of mouse kidney: ultrastructural cytochemistry by a new technique. J Histochem Cytochem 14:291, 1966
12. Gulcher JR, Nies DE, Marton LS, Stefansson K: An alternatively spliced region of the human hexabrachion contains a repeat of potential N-glycosylation sites. Proc Natl Acad Sci USA 86:1588, 1989
13. Inaguma Y, Kusakabe M, Mackie EJ, Pearson CA, Chiquet-Ehrismann R, Sakakura T: Epithelial induction of stromal tenascin in the mouse mammary gland: From embryogenesis to carcinogenesis. Dev Biol 128:245, 1988
14. Knabbe C, Lippman ME, Wakefield LM, Flanders K, Kassid A, Derynck R, Dickson RB: Evidence that transforming growth factor-beta is a hormonally regulated negative growth factor in human breast cancer cells. Cell 48:417, 1987
15. Lightner VA, Gumkowski F, Bigner DD, Erickson HP: Tenascin/Hexabrachion in human skin: biochemical identification and localization by light and electron microscopy. J Cell Biol 108:2483, 1989
16. Loeffel SC, Gillespie GY, Miller EW, Mirmiran SA, Golden P, Askin FB, Siegal GP: Cellular immunolocalization of S-100 protein within fixed tissue sections by monoclonal antibodies. Arch Pathol Lab Med 109:117, 1985
17. Mackie EJ, Chiquet-Ehrismann R, Pearson CA, Inaguma Y, Taya K, Kawarada Y, Sakakura T: Tenascin is a stromal marker for epithelial malignancy in the mammary gland. Proc Natl Acad Sci USA 84:4621, 1987
18. Mackie EJ, Tuchler RP, Halfter W, Chiquet-Ehrismann R, Epperlein HH: The distribution of tenascin coincides with pathways of neural crest cell migration. Development 102:237, 1988
19. Pearson CA, Pearson D, Shibahara S, Hofsteenge J, Chiquet-Ehrismann R: Tenascin: cDNA cloning and induction by TGF-beta. EMBO J 7:2977, 1988
20. Sloan P, Lopes V, Scher SL, Chiquet-Ehrismann R: Anisotropic distribution of tenascin in the extracellular matrix of human oral mucosa in development, maintenance and oncogenesis (abstr). J Pathol 154:108, 1988
21. Thesleff I, Mackie EJ, Kaino S, Chiquet-Ehrismann R: Changes in the distribution of tenascin during tooth development. Development 101:289, 1987

Tenascin expression in human chronic liver disease and in hepatocellular carcinoma

Yamada S, Ichida T, Matsuda Y, Miyazaki Y, Hatano T, Hata K, Asakura H, Hirota N, Geerts A, Wisse E. Tenascin expression in human chronic liver disease and in hepatocellular carcinoma.
Liver 1992: 12: 10–16.

Abstract: Tenascin is an oligomeric glycoprotein of the extracellular matrix synthesized during embryonic development. It is prominently expressed in a variety of tumors. The role of tenascin in liver tissue is, however, unknown. We used immunocytochemistry to define the localization of tenascin and compare this with the localization of non-collagenous proteins, such as laminin and fibronectin, in normal human liver and pathological liver from patients with chronic hepatitis, liver cirrhosis and hepatocellular carcinoma. In normal liver, tenascin expression was localized along the sinusoidal and vascular wall. In fibrotic liver, tenascin was also observed in the region between the hepatic parenchyma and the fibrosing portal tracts, especially in areas of piecemeal necrosis in chronic hepatitis. Immuno-EM study of liver tissue in chronic hepatitis strongly suggested the synthesis and secretion of tenascin by fat-storing cells into the space of Disse. In hepatocellular carcinoma, tenascin was expressed in both the capsule and lobular septa, but not in the sinusoidal walls of the tumors. These results led us to postulate a close relationship between the occurrence of this protein and disease processes such as fibrosis and cancer invasion.

Shinji Yamada[1], Takafumi Ichida[1], Yasunobu Matsuda[1], Yutaka Miyazaki[1], Tohru Hatano[1], Koujirou Hata[1], Hitoshi Asakura[1], Norio Hirota[2], Albert Geerts[3] and Eddie Wisse[3]

[1]Third Department of Internal Medicine, Niigata University School of Medicine, Asahimachi-dori Ichibancho, Niigata City, Niigata, Japan, [2]Department of Pathology, Jichi Medical School, Kawachi-machi, Kawachi-gun, Tochigi, Japan and [3]Laboratory for Cell Biology and Histology, Faculty of Medicine and Pharmacy, Free University of Brussels, Brussel-Jette, Belgium

Key words: chronic liver diseases – extracellular matrix – fibronectin – hepatocellular carcinoma – immunohistochemistory – laminin – tenascin

Dr Takafumi Ichida, The Third Department of Internal Medicine, Niigata University School of Medicine, 754 Asahimachi-dori Ichibancho, Niigata Japan, 951

Received 3 May, accepted for publication 26 August 1991

Tenascin is an oligomeric glycoprotein complex of the extracellular matrix (1). It is a hexabrachion, consisting of two pairs of three arms connected to a central globule (2), and contains 13 epidermal growth factor-like repeats and segments that resemble the type III repeats found in fibronectin (3). The protein has been independently discovered in a number of laboratories and given several names including hexabrachion (4), myotendinous antigen (5), GP250 (6), glial mesenchymal extracellular matrix protein (7), cytotactin (8), J1 protein (9), and brachionectin (2). Tenascin occurs in both embryonic and adult tissues, and it has been reported to occur during the development of various organs such as mammary glands (10), teeth (11), neural crest (12), central nervous system (13), kidneys (14), and cartilage (15). The function of tenascin is largely unknown. However, *in vitro* studies suggest that tenascin promotes the growth of tumor cells (16), inhibits the spreading of cells, and antagonizes the attachment of some cells to fibronectin (17). In addition, it is reported that tenascin expression is found in the area of proliferating blood vessels in tumors (7), and is diffusely spread throughout the tumor stroma (18). These observations suggest that tenascin might be related to both fibrosis and malignant growth.

In general, it has been suggested that the extracellular matrix does not merely provide passive structural support, but also plays a role in maintaining the differentiated phenotype and normal function of liver parenchymal cells (19, 20). In both animal and human liver, several types of collagen and non-collagenous components were studied with monoclonal antibodies, suggesting that those components were actively deposited in fibrosing areas around portal tracts and central veins. Furthermore, both tenascin and fibronectin, as well as other extracellular matrix molecules, were parallel to increased collagen production in fibrosis and wound healing (20). In addition, Van Eyken et al. recently reported the appearance of tenascin in liver fibrosis (21). Liver cirrhosis can be the terminal state of fibrosis caused by viral infection of type B or type C hepatitis, and other chronic liver diseases. Liver cirrhosis is thought to be a risk factor for development of hepatocellular carcinoma. Clinically, more than 80% of hepatocellular carcinomas develop from liver cirrhosis caused by viral infection and other chronic liver diseases. We

/er

Ichida[1],
i Miyazaki[1],
ita[1], Hitoshi
bert

icine, Niigata
shimachi-dori
apan, [2]Depart-
School, Kawa-
apan and [3]Lab-
ogy, Faculty
niversity of

– extracellular
lar carcinoma
in – tenascin

artment of
ty School of
ibancho, Nii-

blication 26

be related

the extra-
le passive
: in main-
d normal
)). In both
f collagen
e studied
that those
fibrosing
eins. Fur-
as well as
re parallel
rosis and
yken et al.
enascin in
e the ter-
ifection of
ronic liver
be a risk
lar carci-
atocellular
caused by
seases. We

therefore investigated the distribution of tenascin in human liver in various fibrogenic diseases and in liver cancer.

Material and methods

Materials

Liver tissue was obtained from 10 normal livers, 20 cases of chronic hepatitis, 10 cases of liver cirrhosis, and 18 cases of hepatocellular carcinoma (HCC), which were classified as Edmondson-Steiner II or III. All tissues were obtained either by needle biopsy during peritoneoscopy or by hepatic resection.

Immunohistochemistry for light microscopy

The specimens were treated as follows. The formalin-fixed, paraffin-embedded material was cut, deparaffined, air-dried overnight, and pretreated with 0.4% pepsin for 120 min to unmask the antigen. The sections were immersed in 0.3% hydrogen peroxide in methanol to remove endogenous peroxidase staining, and then incubated overnight at 4°C with rabbit anti-human tenascin antibody (Telios Pharmaceut Inc., San Diego), rabbit anti-human fibronectin antibody and rabbit anti-human laminin antibody (kindly donated by Prof. Isemura M., Shizuoka Prefectural University, Japan). In addition, controls were performed utilizing normal rabbit serum instead of specific antiserum. Thereafter, the sections were incubated for 1 h with donkey anti-rabbit Ig labeled by horseradish peroxidase (Amersham, U.K.). After washing with phosphate-buffered saline (PBS), the bound antibody was visualized by cytochemical staining for peroxidase, using diaminobenzidine.

Immunocytochemistry for electron microscopy

Freshly obtained tissue samples were cut into 2-mm blocks and fixed with 4% periodate-lysin-

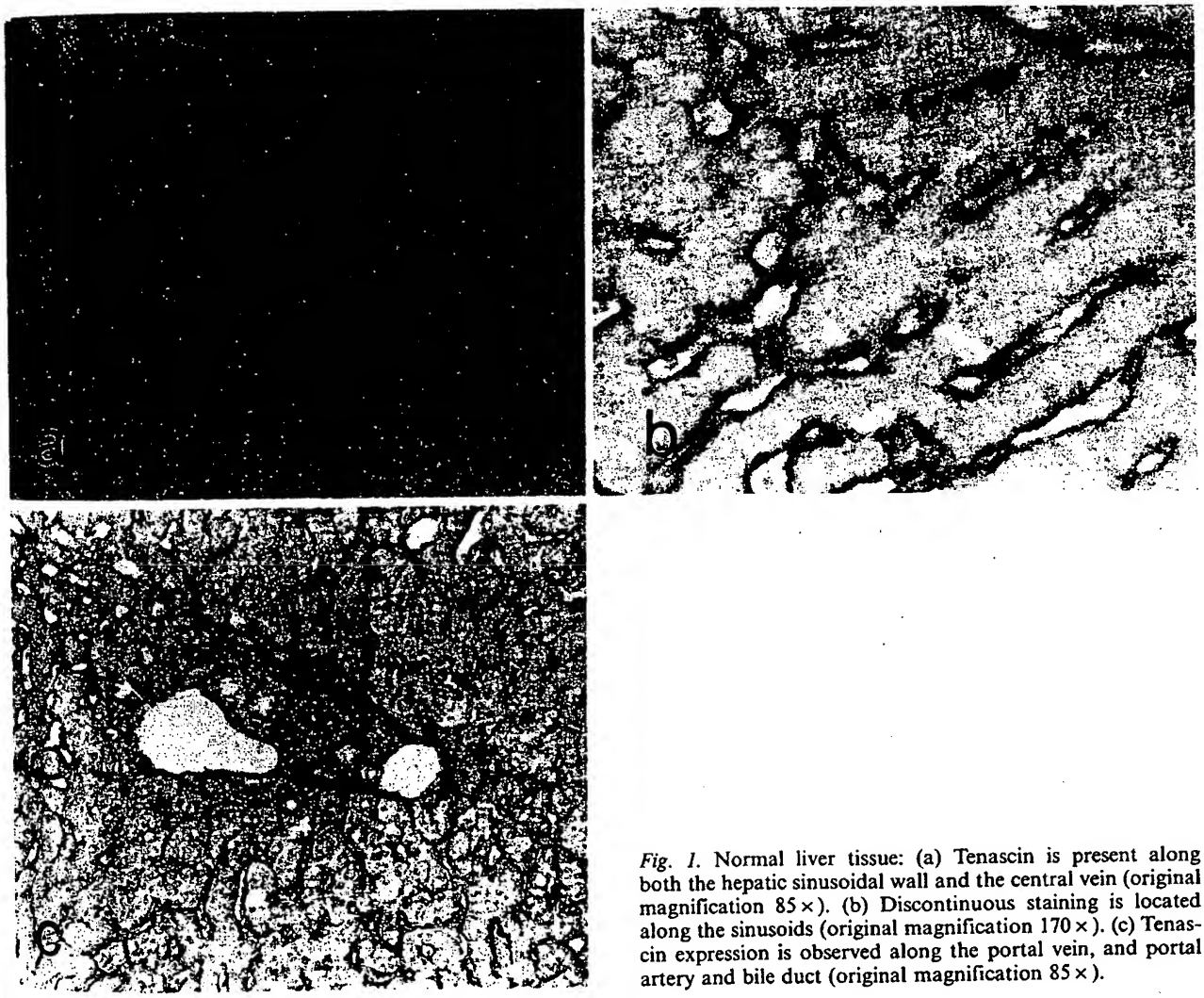

Fig. 1. Normal liver tissue: (a) Tenascin is present along both the hepatic sinusoidal wall and the central vein (original magnification 85×). (b) Discontinuous staining is located along the sinusoids (original magnification 170×). (c) Tenascin expression is observed along the portal vein, and portal artery and bile duct (original magnification 85×).

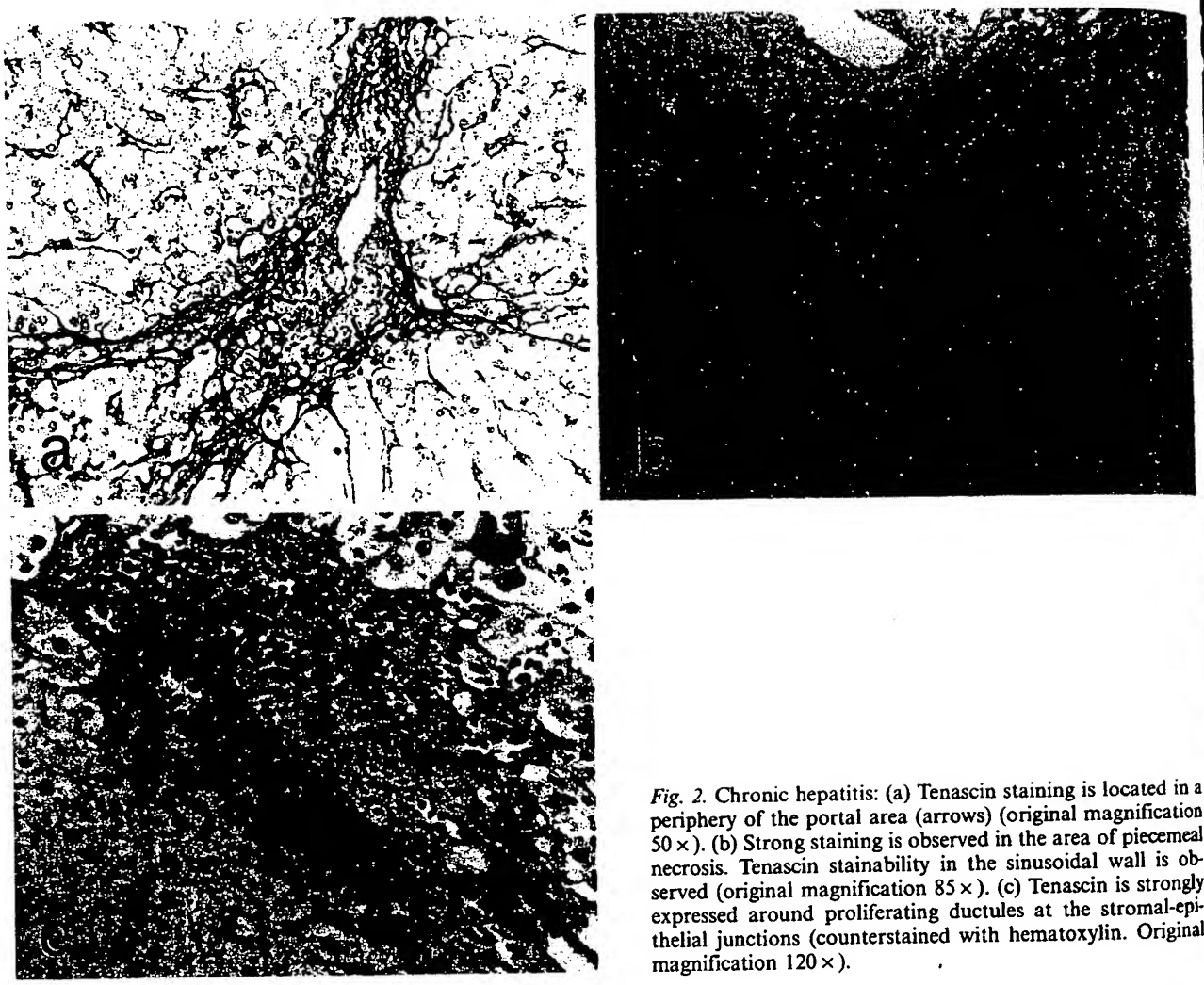

Fig. 2. Chronic hepatitis: (a) Tenascin staining is located in a periphery of the portal area (arrows) (original magnification 50×). (b) Strong staining is observed in the area of piecemeal necrosis. Tenascin stainability in the sinusoidal wall is observed (original magnification 85×). (c) Tenascin is strongly expressed around proliferating ductules at the stromal-epithelial junctions (counterstained with hematoxylin. Original magnification 120×).

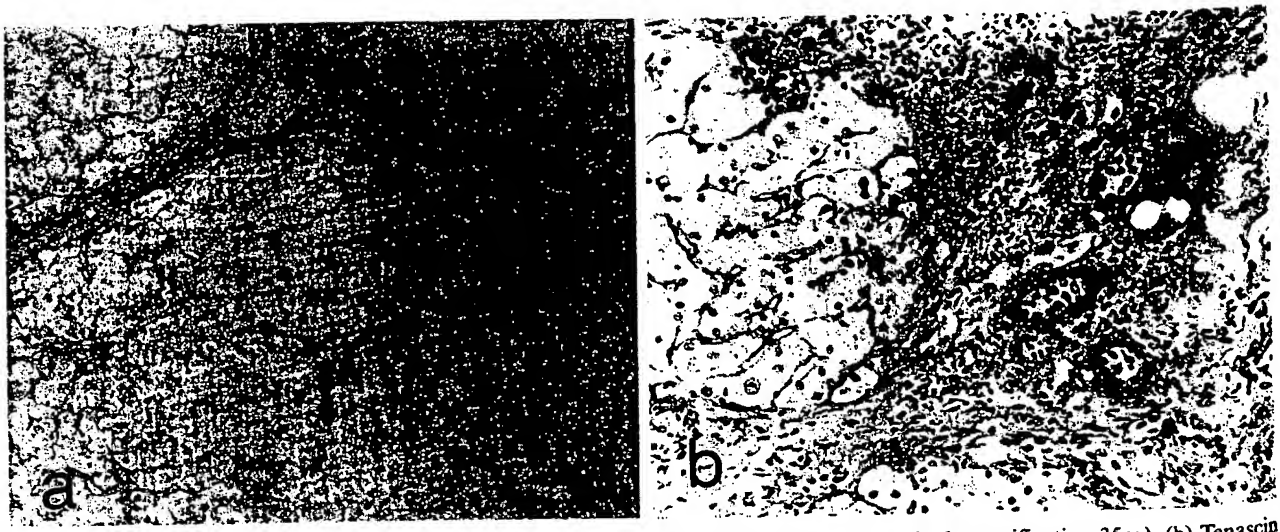

Fig. 3. Liver cirrhosis: (a) The stainability of tenascin is the same as in chronic hepatitis (original magnification 35×). (b) Tenascin is, also, strongly expressed around proliferating ductules in cases of liver cirrhosis. (counterstained with hematoxylin. Original magnification 85×).

paraformaldehyde (PLP). They were washed, embedded in Tissue-Tek O.C.T. compound (Miles Inc., USA), rapidly frozen, and stored at −70°C. The specimens were sectioned at 6 μm thickness using a cryostat. The sections were mounted on egg-albumin-coated slides, and air dried for 30 min. Suppression of endogenous peroxidase activity was carried out by Isobe's method (22). After being rinsed, they were incubated for 24 h at 4°C with the anti-human tenascin antibody. Thereafter, they were incubated for 12 h at 4°C with the same secondary antibody as above. The sections were washed, and the peroxidase activity was developed with diaminobenzidine. The stained sections were washed, post-fixed in 2% osmium tetroxide, and embedded in EPON. Ultrathin sections were examined in a Hitachi HS-9 electron microscope.

Results

Immunohistochemistry (light microscopy)

Normal liver (Fig. 1): The wall of central veins, portal veins and hepatic arteries was stained for tenascin. In the hepatic sinusoidal walls, stainability for tenascin was weak and discontinuous. No stainability for tenascin could be revealed in hepatocytes. Fibronectin was present along the sinusoidal wall and in portal tracts. Laminin expression was observed around portal veins, central veins, hepatic arteries and bile duct, but not in the sinusoidal wall.

Chronic hepatitis (Fig. 2): The sinusoidal wall and the vascular wall were stained for tenascin. Tenascin expression was observed in the tissue between the parenchyma and the fibrotic portal area, es-

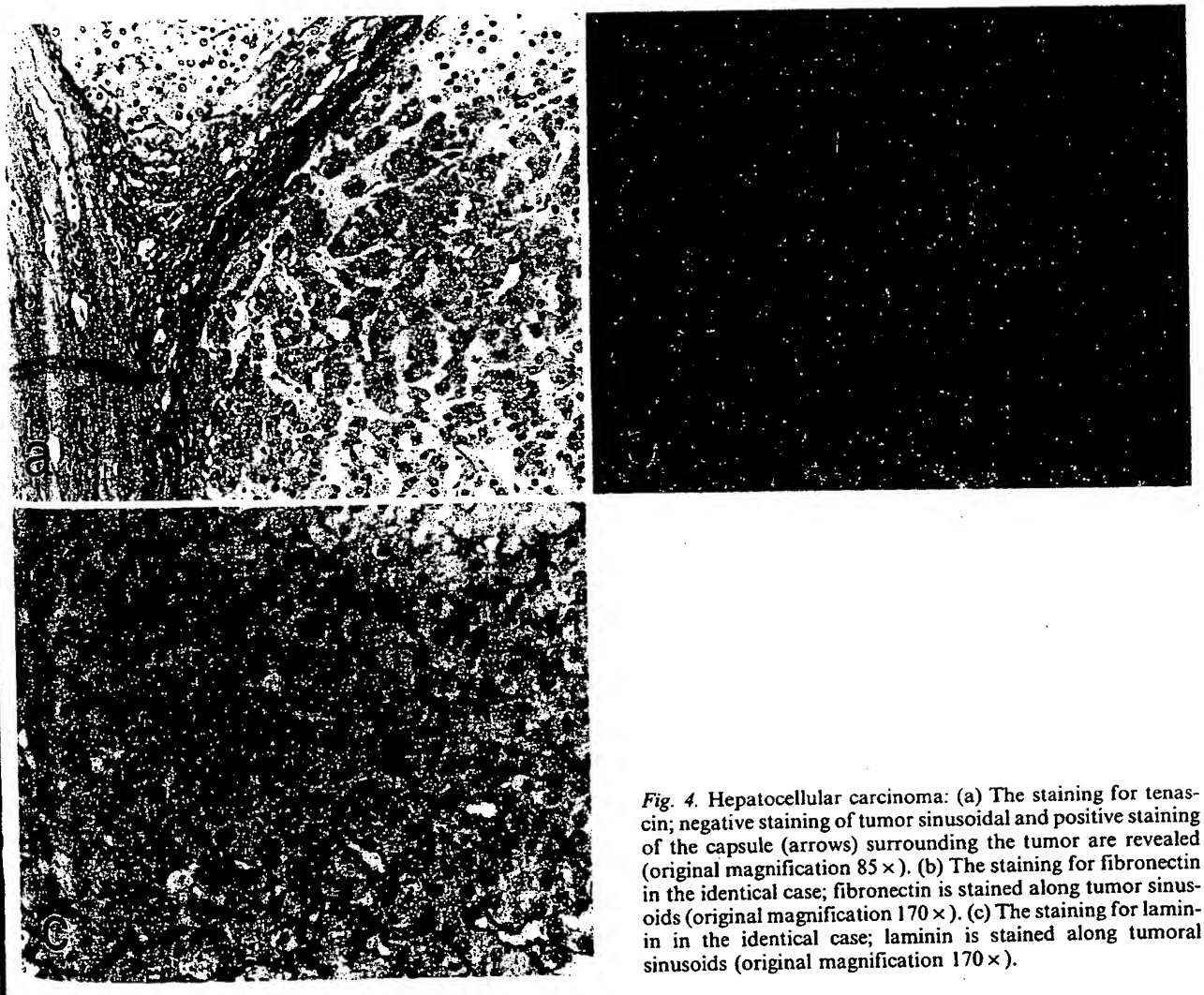

Fig. 4. Hepatocellular carcinoma: (a) The staining for tenascin; negative staining of tumor sinusoidal and positive staining of the capsule (arrows) surrounding the tumor are revealed (original magnification 85×). (b) The staining for fibronectin in the identical case; fibronectin is stained along tumor sinusoids (original magnification 170×). (c) The staining for laminin in the identical case; laminin is stained along tumoral sinusoids (original magnification 170×).

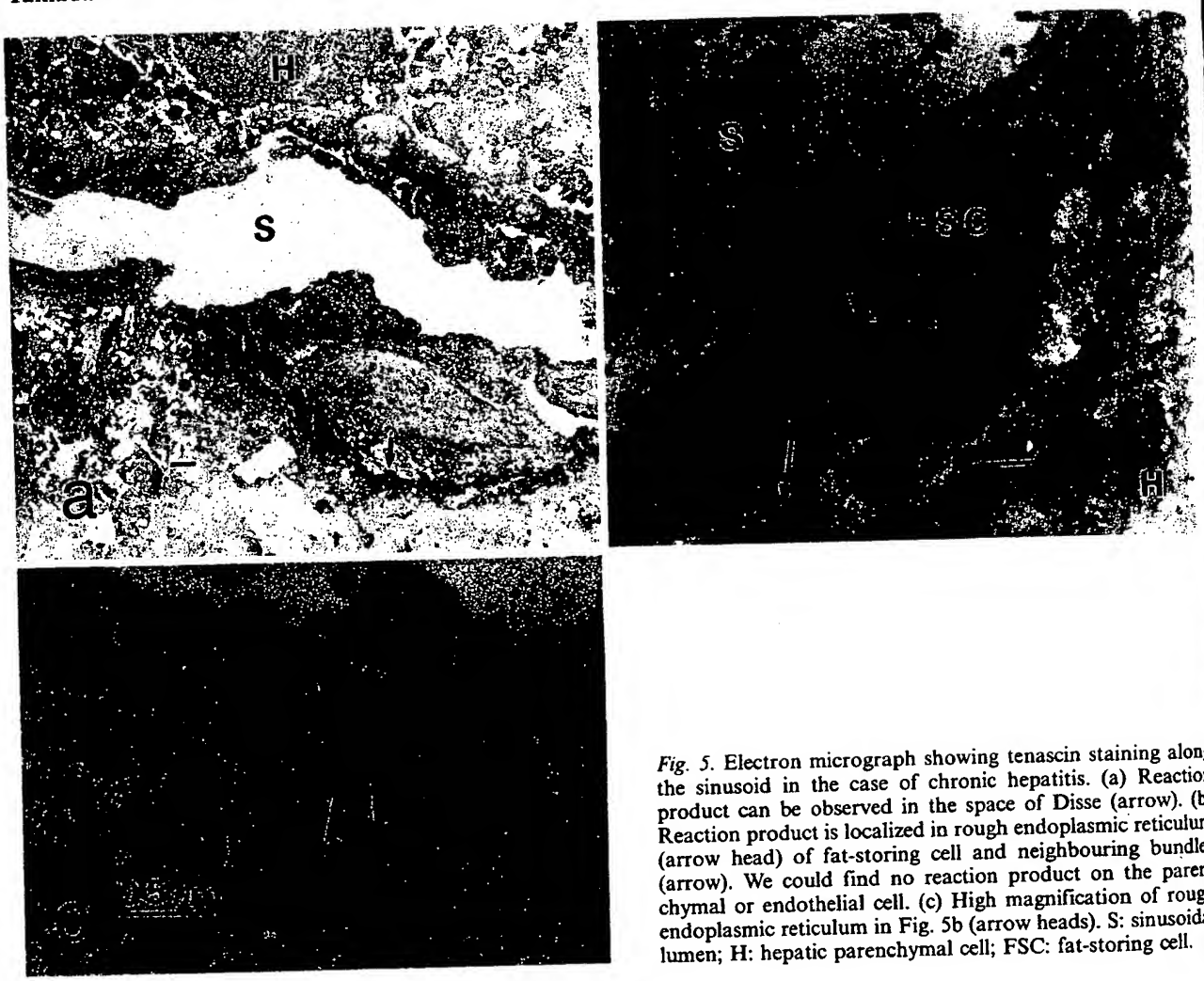

Fig. 5. Electron micrograph showing tenascin staining along the sinusoid in the case of chronic hepatitis. (a) Reaction product can be observed in the space of Disse (arrow). (b) Reaction product is localized in rough endoplasmic reticulum (arrow head) of fat-storing cell and neighbouring bundles (arrow). We could find no reaction product on the parenchymal or endothelial cell. (c) High magnification of rough endoplasmic reticulum in Fig. 5b (arrow heads). S: sinusoidal lumen; H: hepatic parenchymal cell; FSC: fat-storing cell.

pecially in piecemeal necrosis and around proliferating ductules. The central part of the portal area was not stained for tenascin. The staining for tenascin present in the sinusoidal wall was increased as compared to the sinusoidal wall in normal liver. On the other hand, fibronectin expression was observed diffusely in portal connective tissues. The distributions of tenascin and fibronectin were clearly different from each other. Laminin was expressed as in normal liver.

Liver cirrhosis (Fig. 3): Tenascin expression in liver cirrhosis was the same as in chronic hepatitis, both in the portal area and in the sinusoidal wall. In addition, strong staining for tenascin was observed around the proliferating ductules at the connective tissue-epithelial interface. Fibronectin was localized as in chronic hepatitis. Laminin was expressed in the sinusoids in the periphery of regenerative nodules, in addition to portal veins, hepatic arteries, central veins and around bile ducts.

HCC (Fig. 4): Fibronectin expression was observed in the sinusoids in 15 of 18 cases. In contrast, staining for tenascin was revealed in only 3 of these cases, whereas laminin was observed in 13 cases. The specimens which stained for tenascin also expressed laminin and fibronectin in the same location. No expression of tenascin could be revealed in tumor epithelia. On the other hand, in most of the HCC cases, tenascin was expressed at the stromal-epithelial junctions in the capsule and septa.

Table 1. Tenascin expression in human liver tissues

	Sinusoidal wall	Stroma
Normal liver	+	VW+ B.D.+
Chronic hepatitis	+/++	P.+/++ B.D.+ VW+
Liver cirrhosis	+/++	P.+/++ B.D.+/++ VW+
Hepatocellular carcinoma	−/+	C.+ VW+

VW: vascular wall, B.D.: bile duct, P.: epithelial-stromal interface in portal area, C.: capsule or septum of tumor.

Immunoelectron microscopy (Fig. 5): Tenascin staining could be observed as a diffuse, dense reaction product in the space of Disse. Positive reaction could also be seen in parts of the rough endoplasmic reticulum of fat-storing cells. However, we could not find reaction products in endothelial or parenchymal cells.

We can summarize the observations on the localization of tenascin in human liver tissue (Table 1) as follows: cancerous tissue did not express tenascin in sinusoids, whereas normal liver and fibrogenic liver presented positive tenascin staining on sinusoids and vascular walls. Tenascin was expressed in connective tissue in the stromal-epithelial junction, especially in areas of piecemeal necrosis.

Discussion

In this study, we were able to reveal a specific stainability for tenascin in both normal and pathological liver. In non-cancerous liver, tenascin could be observed in the vascular wall, sinusoidal wall and the interface between parenchymal areas and fibrotic portal areas, especially in areas of piecemeal necrosis in chronic hepatitis. The staining intensity was as strong as in the surrounding of proliferating ductules in the portal area. Van Eyken et al. did not find positivity in the vascular wall; however, our present study revealed that tenascin was expressed in the vascular wall. Therefore, endothelial cells of vessels might have an ability to induce production of tenascin. In livers with chronic viral infection, piecemeal necrosis and ductular proliferation are the apparent locations of fibrogenesis (24). The staining pattern of tenascin led us to assume a correlation between tenascin expression and fibrosis. In our study, laminin was not expressed in the sinusoidal walls of the normal liver. Laminin expression was the same as in the recent report (23).

In regions showing piecemeal necrosis, numerous collagen bundles and extracellular matrix components could be detected in the wall of the sinusoids (24, 25). Our immunoelectron microscopic observations suggest the production of tenascin by fat-storing cells. The reaction product of the staining for tenascin could be found in the cytoplasm of fat-storing cells and in the space of Disse in chronic active hepatitis. This observation supports the report from Desmet's group, indicating the production of tenascin by *in vitro* cultured rat liver fat-storing cells (Proceeding of Fifth International Symposium on Cells of the Hepatic Sinusoid, Tuscon, Arizona, U.S.A., August 26–30, 1990). Our results also suggest that the fat-storing cell is one of the candidates to produce tenascin in the space of Disse.

In hepatocellular carcinoma, tenascin was expressed in both the capsule and septa of the specimens studied, but was not expressed in the sinusoidal wall of tumorous tissue. However, both laminin and fibronectin were localized in the sinusoidal wall of the tumor in most cases of HCC. In our previous electron microscopic observation of human hepatocellular carcinoma, numerous basal laminae and excessive staining of extracellular matrix components such as type IV collagen, laminin and fibronectin were found (26–28). There are few fat-storing cells in tumoral sinusoids in hepatocellular carcinoma (28). Assuming that fat-storing cells produce tenascin, the lack of fat-storing cells might be one of the causes of tenascin not being demonstrated in the wall of tumoral sinusoids. In the present study, tenascin in tumorous tissue was localized in the capsule and septa, but not in basal laminae or the extracellular matrix. This observation might be related to tumor invasion. At the site of tumor invasion, synthesis and degradation of extracellular matrix components should occur. The tenascin deposits found at stromal-epithelial junctions in the tumor might not only stimulate tumor cell proliferation (16), but also decrease adhesiveness (17), and so facilitate detachment of tumor cells from epithelial sheets, enabling them to invade the stroma. We suppose that the staining pattern of tenascin has a functional implication, related to tumor spreading.

In conclusion, we studied the distribution and the cellular source of tenascin in normal, fibrotic and cancerous liver tissue. The function of tenascin is largely unknown. Our results, however, led us to postulate a relationship between the occurrence of this glycoprotein and the onset and development of fibrosis and malignant growth.

Acknowledgements

The authors thank Mr. N. Honda and Mr. T. Tsuchida for their expert technical assistance.

References

1. Erickson H P, Lightner V A. Hexabrachion protein in connective tissues, embryonic brain, and tumors. In: Advances in cell biology, Vol. 2. JAI Press Inc., 1988: 55–90.
2. Erickson H P, Inglesias J L. A six-armed oligomer isolated from cell surface fibronectin preparations. *Nature* 1984: **311**: 267–269.
3. Jones F S, Burgoon M P, Hoffmann S, Crossin K L, Cunningham B A, Edelman G M. A cDNA clone for cytotactin contains sequences similar to epidermal growth factor-like repeats and segments of fibronectin and fibrinogen. *Proc Natl Acad Sci USA* 1989: **85**: 2186–2190.
4. Erickson H P, Taylor H C. Hexabrachion proteins in embryonic chicken tissues and human tumors. *J Cell Biol* 1987: **105**: 1387–1394.

5. Chiquet M, Fambrough D M. Chick myotendinous antigen 1. *J Cell Biol* 1984: **98**: 1926–1936.
6. Carter W G, Hakomori S. A new cell surface, detergent insoluble glyco-protein matrix of human and hamster fibroblast. *J Biol Chem* 1981: **256**: 6953–6960.
7. Bourdon M A, Wilkstrand C J, Furthmayr H, Matthews T J, Bigner D D. Human glioma-mesenchymal extracellular matrix antigen defined by monoclonal antibody. *Cancer Res* 1983: **43**: 2796–2805.
8. Grumet M, Hoffman S, Crossin K L, Edelman G M. Cytotactin, an extracellular matrix protein of neural and non-neural issues that mediates glia-neuron interaction. *Proc Natl Acad Sci USA* 1985: **82**: 8075–8079.
9. Kruse J, Keilhauer G, Faissner A, Timpl R, Schner M. The J1 glycoprotein a novel nervous system cell adhesion molecule of the L2/HNK1 family. *Nature* 1985: **316**: 146–148.
10. Inaguma Y, Kusakabe M, Mackie E J, Pearson C A, Chiquet-Ehrismann R. Epithelial induction of stromal tenascin in the mammary gland. *Devel Biol* 1988: **128**: 245–255.
11. Thesleff I, Mackie E, Vainio S, Chiquet-Ehrismann R. Changes in the distribution of tenascin during tooth development. *Development* 1987: **101**: 281–296.
12. Epper H, Halfter W, Tucker R P. The distribution of fibronectin and tenascin along migratory pathways of the neural crest in the trunk of amphibian embryos. *Development* 1988: **103**: 743–756.
13. Stern C D, Norris W E, Bronner-Fraser M, et al. J1/tenascin-related molecules are not responsible for the segmented pattern of neural crest cells or motor axons in chick embryo. *Development* 1989: **107**: 309-319.
14. Aufderheide E, Chiquet-Ehrismann R, Ekblom P. Epithelial-mesenchymal interactions in the developing kidney lead to expression of tenascin in the mesenchyme. *J Cell Biol* 1987: **105**: 599–608.
15. Mackie E J, Thesleff I, Chiquet-Ehrismann R. Tenascin is associated with chondrogenic and osteogenic differentiation *in vivo* and promotes chondrogenesis *in vitro*. *J Cell Biol* 1987: **105**: 2569–2579.
16. Chiquet-Ehrismann R, Makie E J, Pearson C A, Sakakura T. Tenascin: an extracellular matrix protein involved in tissue interactions during fetal development and oncogenesis. *Cell* 1986: **47**: 131–139.
17. Chiquet-Ehrismann R, Kalla P, Pearson C A, Beck K, Chiquet M. Tenascin interferes with fibronectin action. *Cell* 1988: **53**: 383–390.
18. Anbazhagan R, Sakakura T, Guesterson B A. The distribution of immunoreactive tenascin in the epithelial-mesenchymal junctional areas of benign and malignant squamous epithelia. *Virchows Arch B Cell Pathol* 1990: **59**: 59–63.
19. Biagini G, Ballardini G. Liver fibrosis and extracellular matrix. *J Hepatol* 1989: **8**: 115–124.
20. Mackie E J, Halfter W, Liverani D. Induction of tenascin in healing wounds. *J Cell Biol* 1988: **107**: 2757–2767.
21. Van Eyken P, Sciot R, Desmet V J. Expression of the novel extracellular matrix component tenascin in normal and diseased human liver. *J Hepatol* 1990: **11**: 43–52.
22. Isobe Y, Chen S T, Nakane P K. Studies on translocation of immunoglobulins across intestinal epithelium. I. Improvements in the peroxidase-labeled antibody method for application to study of human intestinal mucosa. *Acta Histochem Cytochem* 1977: **10**: 161–171.
23. Martinez-Hernandez A, Delgado F M, Amenta P S. The extracellular matrix in hepatic regeneration: localization of collagen type I, III, IV, laminin, and fibronectin. *Lab Invest* 1991: **64**: 157–166.
24. Clement B, Grimaud J A, Campion J P, Deugnier Y, Guillouzo A. Cell types involved in collagen and fibronectin production in normal and fibrotic human liver. *Hepatology* 1986: **6**: 225–234.
25. Bianchi F B, Biagini G, Ballardini G et al. Basement membrane production by hepatocyte in chronic liver disease. *Hepatology* 1984: **4**: 1167–1172.
26. Hata K. Characteristics of the sinusoidal wall in human hepatocellular carcinoma. *Acta Hepatol Jpn* 1990: **10**: 1210–1217. (in Japanese)
27. Donato M F, Colombo M, Matarazzo M, Paronetto F. Distribution of basement membrane components in human hepatocellular carcinoma. *Cancer* 1989: **63**: 272–279.
28. Ichida T, Hata K, Yamada S et al. Subcellular abnormalities of liver sinusoidal lesions in human hepatocellular carcinoma. *J Submicrosc Cytol Pathol* 1990: **22**: 221–229.

therefore investigated the distribution of tenascin in human liver in various fibrogenic diseases and in liver cancer.

Material and methods

Materials

Liver tissue was obtained from 10 normal livers, 20 cases of chronic hepatitis, 10 cases of liver cirrhosis, and 18 cases of hepatocellular carcinoma (HCC), which were classified as Edmondson-Steiner II or III. All tissues were obtained either by needle biopsy during peritoneoscopy or by hepatic resection.

Immunohistochemistry for light microscopy

The specimens were treated as follows. The formalin-fixed, paraffin-embedded material was cut, deparaffined, air-dried overnight, and pretreated with 0.4% pepsin for 120 min to unmask the antigen. The sections were immersed in 0.3% hydrogen peroxide in methanol to remove endogenous peroxidase staining, and then incubated overnight at 4°C with rabbit anti-human tenascin antibody (Telios Pharmaceut Inc., San Diego), rabbit anti-human fibronectin antibody and rabbit anti-human laminin antibody (kindly donated by Prof. Isemura M., Shizuoka Prefectural University, Japan). In addition, controls were performed utilizing normal rabbit serum instead of specific antiserum. Thereafter, the sections were incubated for 1 h with donkey anti-rabbit Ig labeled by horseradish peroxidase (Amersham, U.K.). After washing with phosphate-buffered saline (PBS), the bound antibody was visualized by cytochemical staining for peroxidase, using diaminobenzidine.

Immunocytochemistry for electron microscopy

Freshly obtained tissue samples were cut into 2-mm blocks and fixed with 4% periodate-lysin-

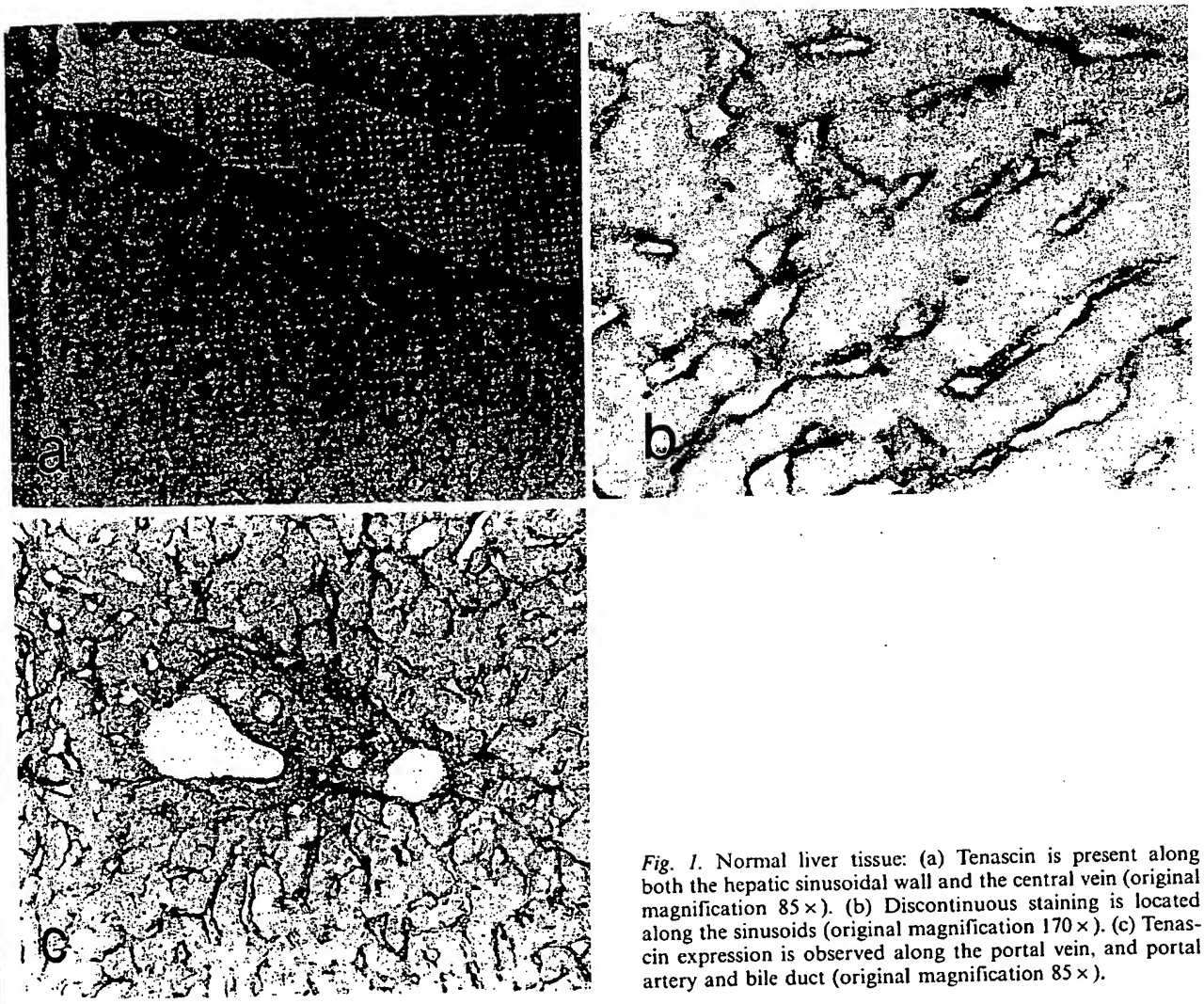

Fig. 1. Normal liver tissue: (a) Tenascin is present along both the hepatic sinusoidal wall and the central vein (original magnification 85×). (b) Discontinuous staining is located along the sinusoids (original magnification 170×). (c) Tenascin expression is observed along the portal vein, and portal artery and bile duct (original magnification 85×).

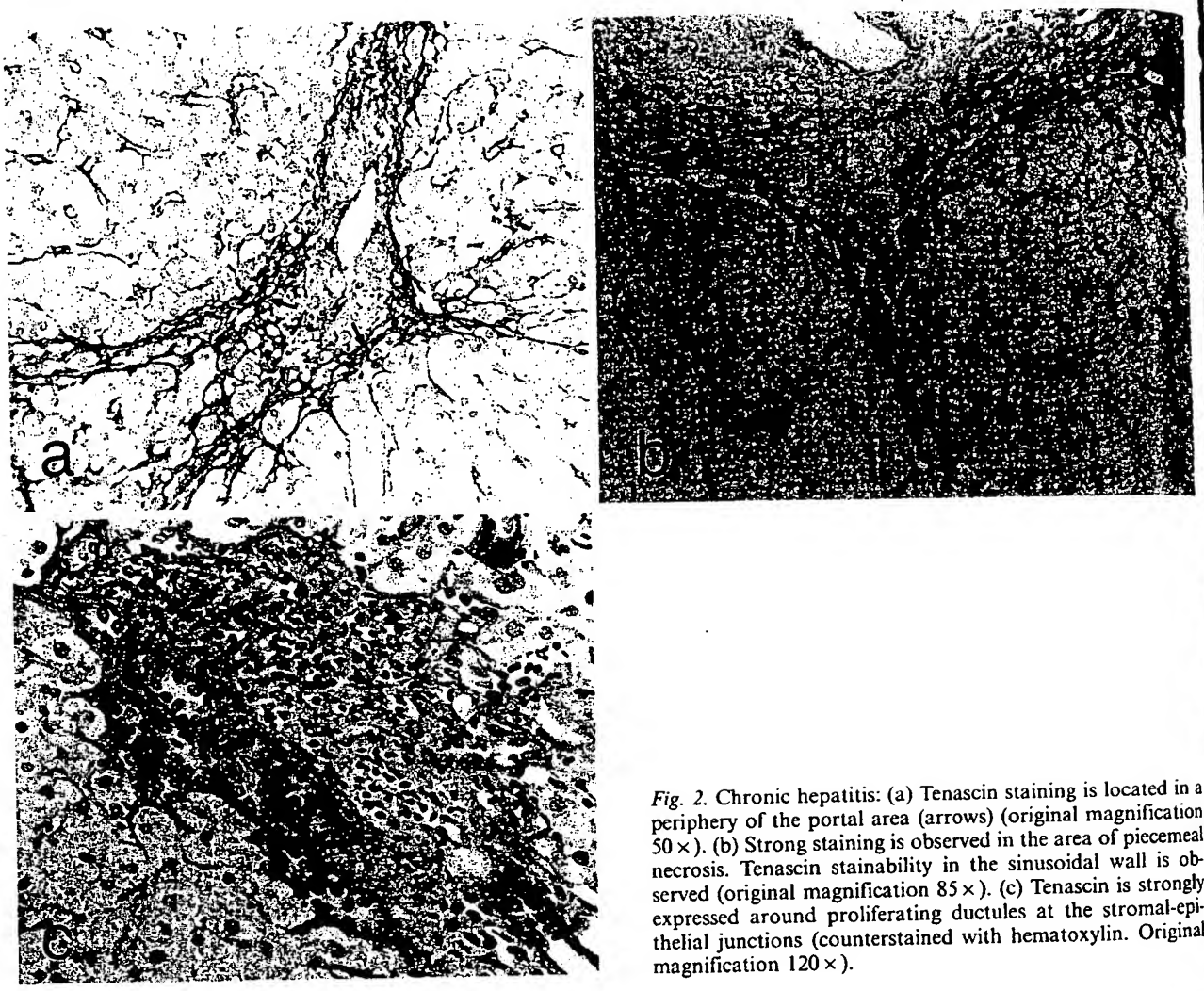

Fig. 2. Chronic hepatitis: (a) Tenascin staining is located in a periphery of the portal area (arrows) (original magnification 50×). (b) Strong staining is observed in the area of piecemeal necrosis. Tenascin stainability in the sinusoidal wall is observed (original magnification 85×). (c) Tenascin is strongly expressed around proliferating ductules at the stromal-epithelial junctions (counterstained with hematoxylin. Original magnification 120×).

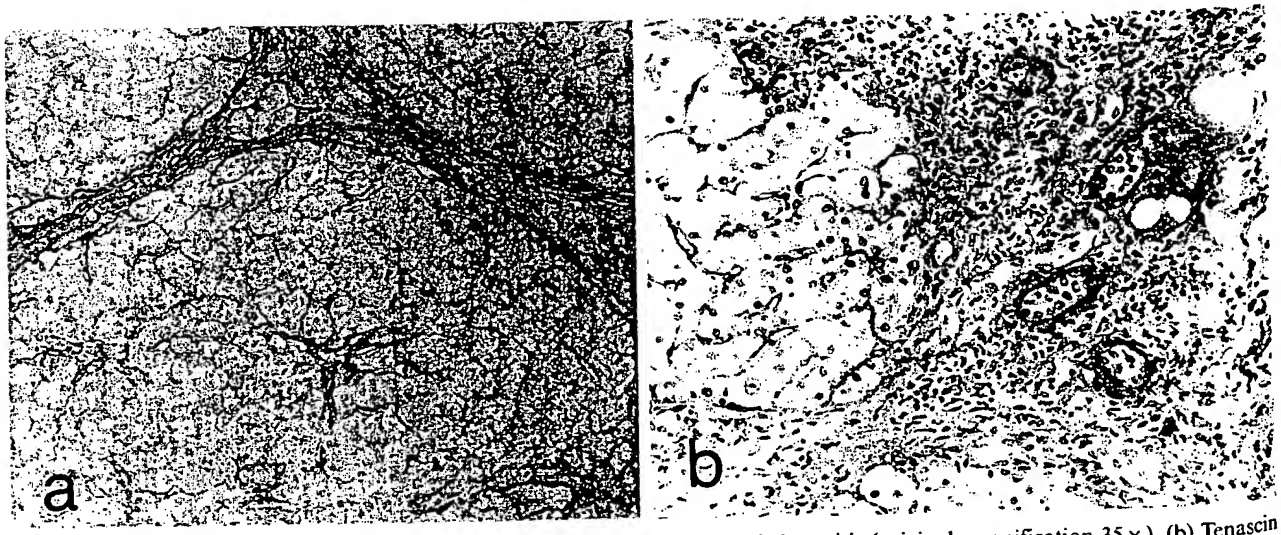

Fig. 3. Liver cirrhosis: (a) The stainability of tenascin is the same as in chronic hepatitis (original magnification 35×). (b) Tenascin is. also, strongly expressed around proliferating ductules in cases of liver cirrhosis. (counterstained with hematoxylin. Original magnification 85×).

paraformaldehyde (PLP). They were washed, embedded in Tissue-Tek O.C.T. compound (Miles Inc., USA), rapidly frozen, and stored at −70°C. The specimens were sectioned at 6 μm thickness using a cryostat. The sections were mounted on egg-albumin-coated slides, and air dried for 30 min. Suppression of endogenous peroxidase activity was carried out by Isobe's method (22). After being rinsed, they were incubated for 24 h at 4°C with the anti-human tenascin antibody. Thereafter, they were incubated for 12 h at 4°C with the same secondary antibody as above. The sections were washed, and the peroxidase activity was developed with diaminobenzidine. The stained sections were washed, post-fixed in 2% osmium tetroxide, and embedded in EPON. Ultrathin sections were examined in a Hitachi HS-9 electron microscope.

Results

Immunohistochemistry (light microscopy)

Normal liver (Fig. 1): The wall of central veins, portal veins and hepatic arteries was stained for tenascin. In the hepatic sinusoidal walls, stainability for tenascin was weak and discontinuous. No stainability for tenascin could be revealed in hepatocytes. Fibronectin was present along the sinusoidal wall and in portal tracts. Laminin expression was observed around portal veins, central veins, hepatic arteries and bile duct, but not in the sinusoidal wall.

Chronic hepatitis (Fig. 2): The sinusoidal wall and the vascular wall were stained for tenascin. Tenascin expression was observed in the tissue between the parenchyma and the fibrotic portal area, es-

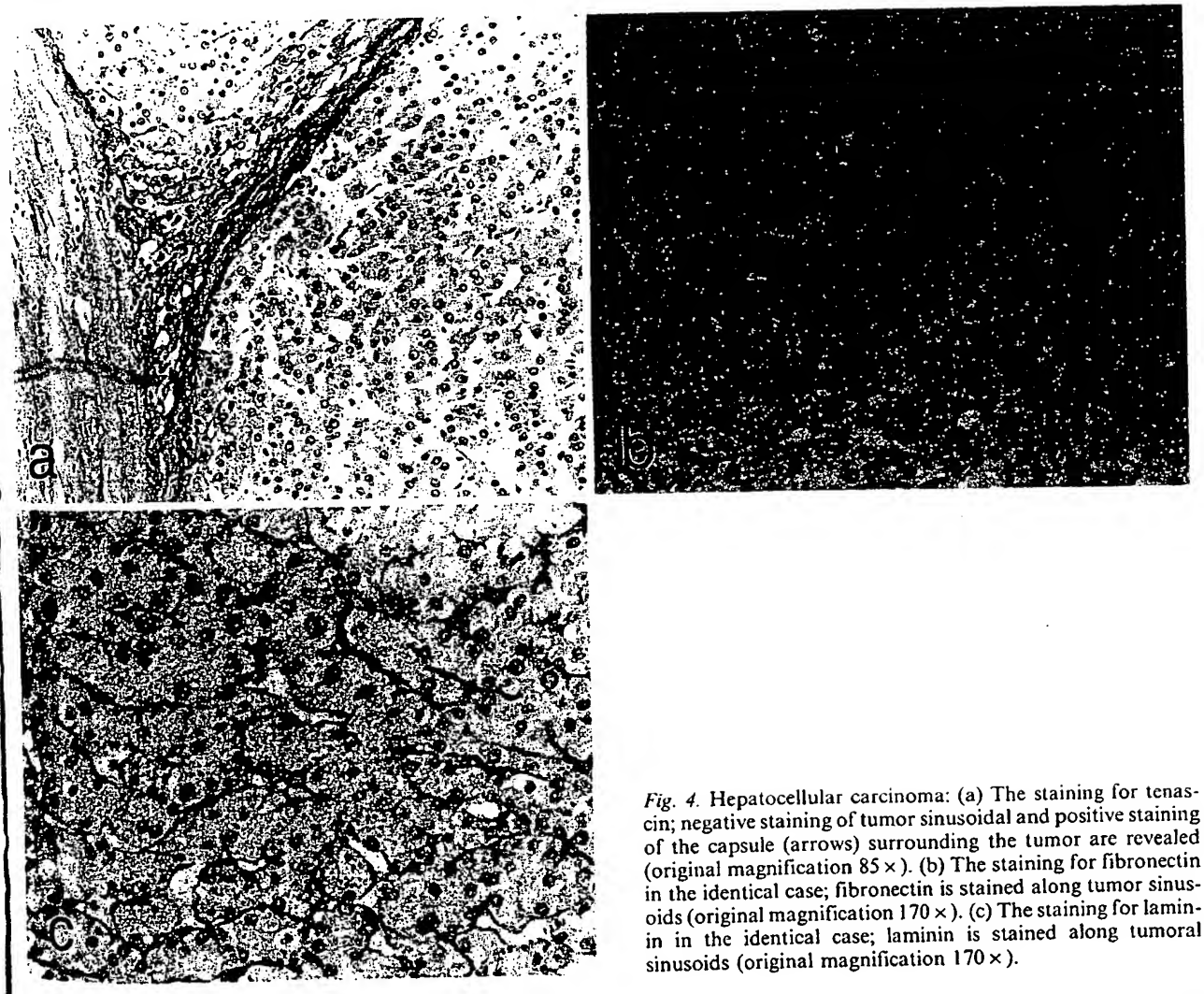

Fig. 4. Hepatocellular carcinoma: (a) The staining for tenascin; negative staining of tumor sinusoidal and positive staining of the capsule (arrows) surrounding the tumor are revealed (original magnification 85×). (b) The staining for fibronectin in the identical case; fibronectin is stained along tumor sinusoids (original magnification 170×). (c) The staining for laminin in the identical case; laminin is stained along tumoral sinusoids (original magnification 170×).

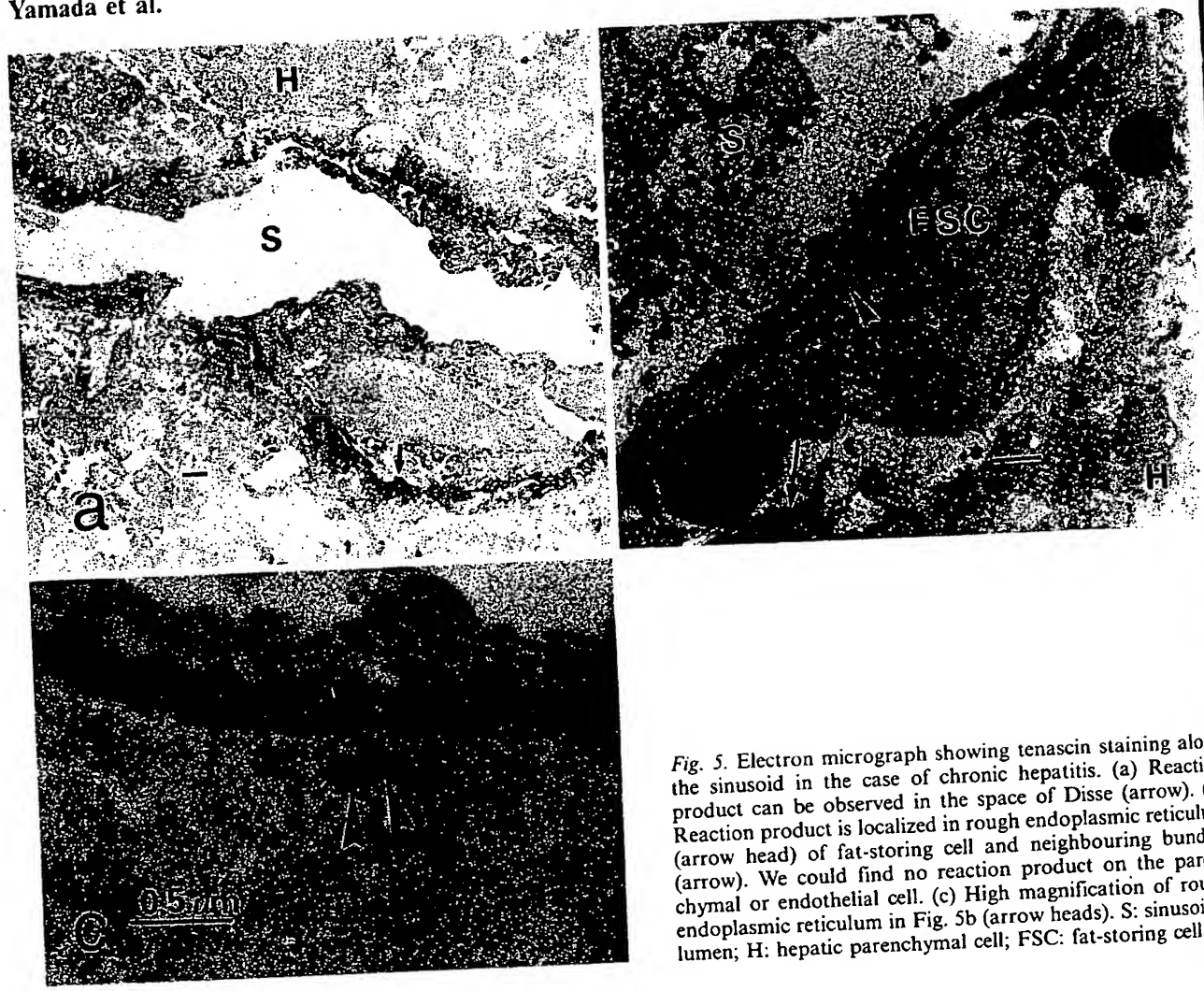

Fig. 5. Electron micrograph showing tenascin staining along the sinusoid in the case of chronic hepatitis. (a) Reaction product can be observed in the space of Disse (arrow). (b) Reaction product is localized in rough endoplasmic reticulum (arrow head) of fat-storing cell and neighbouring bundles (arrow). We could find no reaction product on the parenchymal or endothelial cell. (c) High magnification of rough endoplasmic reticulum in Fig. 5b (arrow heads). S: sinusoidal lumen; H: hepatic parenchymal cell; FSC: fat-storing cell.

pecially in piecemeal necrosis and around proliferating ductules. The central part of the portal area was not stained for tenascin. The staining for tenascin present in the sinusoidal wall was increased as compared to the sinusoidal wall in normal liver. On the other hand, fibronectin expression was observed diffusely in portal connective tissues. The distributions of tenascin and fibronectin were clearly different from each other. Laminin was expressed as in normal liver.

Liver cirrhosis (Fig. 3): Tenascin expression in liver cirrhosis was the same as in chronic hepatitis, both in the portal area and in the sinusoidal wall. In addition, strong staining for tenascin was observed around the proliferating ductules at the connective tissue-epithelial interface. Fibronectin was localized as in chronic hepatitis. Laminin was expressed in the sinusoids in the periphery of regenerative nodules, in addition to portal veins, hepatic arteries, central veins and around bile ducts.

HCC (Fig. 4): Fibronectin expression was observed in the sinusoids in 15 of 18 cases. In contrast, staining for tenascin was revealed in only 3 of these cases, whereas laminin was observed in 13 cases. The specimens which stained for tenascin also expressed laminin and fibronectin in the same location. No expression of tenascin could be revealed in tumor epithelia. On the other hand, in most of the HCC cases, tenascin was expressed at the stromal-epithelial junctions in the capsule and septa.

Table 1. Tenascin expression in human liver tissues

	Sinusoidal wall	Stroma
Normal liver	+	V.W.+ B.D.+
Chronic hepatitis	+/++	P.+/++ B.D.+ V.W.+
Liver cirrhosis	+/++	P.+/++ B.D.+/++ V.W.+
Hepatocellular carcinoma	−/+	C.+ V.W.+

V.W.: vascular wall, B.D.: bile duct, P.: epithelial-stromal interface in portal area, C.: capsule or septum of tumor.

Virchows Archiv A Pathol Anat (1992) 421:217–222

Virchows Archiv A
Pathological Anatomy and Histopathology

Tenascin in salivary gland tumours

Ylermi Soini[1], Paavo Pääkkö[1], Ismo Virtanen[2], and Veli-Pekka Lehto[1]

[1] Department of Pathology, University of Oulu, Oulu, Finland
[2] Department of Anatomy, University of Helsinki, Helsinki, Finland

Received November 10, 1991 / Received after revision March 14, 1992 / Accepted March 16, 1992

Summary. The distribution of tenascin immunoreactivity was analysed in salivary gland tissue and in various benign and malignant tumours of the salivary gland. In the non-neoplastic tissue, tenascin was seen in the areas of basement membranes of the ductal epithelium. No immunoreactivity could be observed in the serous or mucous glands. In pleomorphic adenomas, tenascin immunoreactivity could be seen in the stromal compartment. It was more pronounced in the dense stromal areas and chondroid elements than in the myxoid area. In Warthin's tumours, strong tenascin immunoreactivity could be observed in the basement membrane zone of the epithelial component. In the lymphatic component, faint reticular staining could be seen. In adenoid cystic carcinomas, acinic cell tumours and mucoepidermoid carcinomas, tenascin showed a linear stromal distribution. No intracytoplasmic immunoreactivity could be seen in any of the cases. The widespread tenascin positivity in salivary gland tumours suggests that tenascin may play a role in the induction and progression of salivary gland tumours, presumably by interfering with the normal parenchymal-mesenchymal interaction.

Key words: Tenascin – Salivary gland tumours – Immunohistochemistry

Introduction

Tenascin is a six-armed extracellular matrix glycoprotein with a molecular weight of 1,900 kDa (Erickson and Bourdon 1989; Chiquet-Ehrismann 1990). It was discovered independently in several laboratories and, consequently, is known by various names, such as hexabrachion, cytotactin, myotendineous antigen, GP250 and J-1 protein (Erickson and Lightner 1988). The subunits of tenascin show heterogeneity and, in SDS-polyacrylamide gel electrophoresis, three separate tenascin subunits can be found with molecular weights of 240 kDa, 200 kDa and 190 kDa (Chiquet-Ehrismann et al. 1986).

Tenascin is found in embryonic tissues (Chiquet and Famborough 1984; Crossin et al. 1986; Chuong et al. 1987), especially in areas of epithelial-mesenchymal junctions, and in developing brain tissue. It probably has a role in epithelial-mesenchymal induction and cell migration (Chiquet-Ehrismann et al. 1986; Crossin et al. 1986; Chuong et al. 1987; Erickson and Bourdon 1989; Chiquet-Ehrismann 1990). Tenascin is synthesized by glial cells and fibroblasts (Erickson and Bourdon 1989). By in situ hybridization, tenascin synthesis has also been shown in embryonic kidney and lung mesenchymal cells and in lung epithelial cells (Koch et al. 1991; Prieto et al. 1990).

In adult tissues tenascin can be found in healing wounds, in dense connective tissue, such as tendons and ligaments, in cartilaginous tissue and in smooth muscle (Erickson and Bourdon 1989; Chiquet-Ehrismann 1990; Chuong and Chen 1991). Tenascin has also been observed in the basement membranes of different epithelia of ectodermal and endodermal origin (Natali et al. 1991).

In malignant neoplasms, stromal tenascin immunoreactivity has been found in various tumours such as gliomas, sarcomas, melanomas and carcinomas (Bourdon et al. 1983; Erickson and Bourdon 1989; Natali et al. 1990, 1991; Vollmer et al. 1990; Howeedy et al. 1990). It is also been detected in some benign tumours such as naevocellular naevi and benign breast tumours (Howeedy et al. 1990; Natali et al. 1991).

In this study we used immunohistochemical techniques to investigate the distribution of tenascin in salivary gland tissue and neoplasms. We used two monoclonal antibodies, one of which detects tenascin also in formalin-fixed, paraffin-embedded specimens.

Materials and methods

Thirty-five cases of benign and malignant salivary gland tumours were selected from the files of the Department of Pathology, Oulu

Correspondence to: Y. Soini, Department of Pathology, University of Oulu, Kajaanintie 52 D, SF-90220 Oulu, Finland

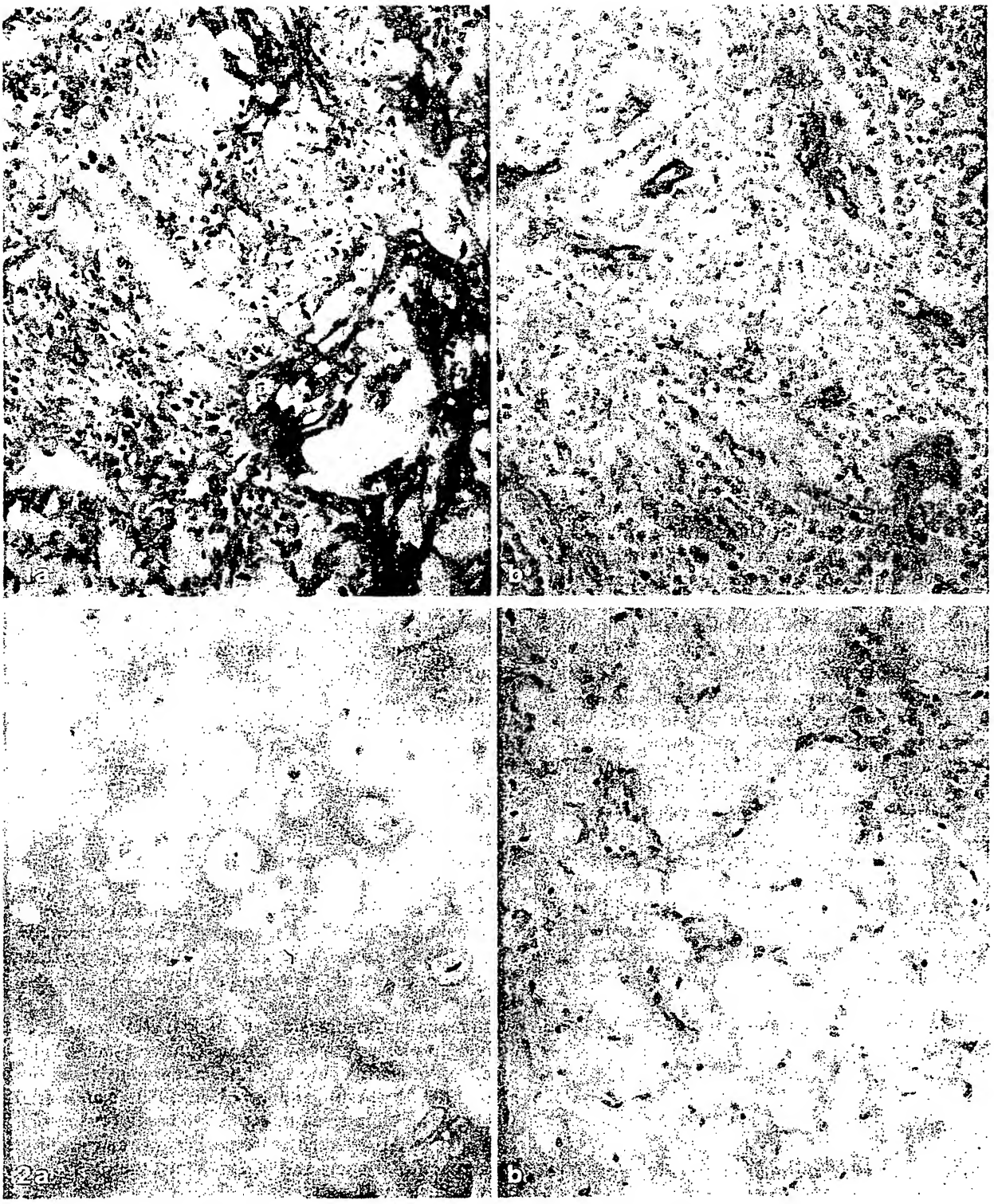

Fig. 1a, b. Immunoperoxidase staining for the demonstration of tenascin in pleomorphic adenoma. The stromal tissue stains positively for tenascin. The staining is more intense with the EB-100 antibody (**a**) than with 143DB7 (**b**). Immunoperoxidase stain, × 210

Fig. 2a, b. Immunoperoxidase staining for the demonstration of tenascin in pleomorphic adenoma. The cartilaginous component stains strongly for tenascin (**a**) while in the myxoid zones the staining is weak and delicate (**b**). Immunoperoxidase stain. × 210

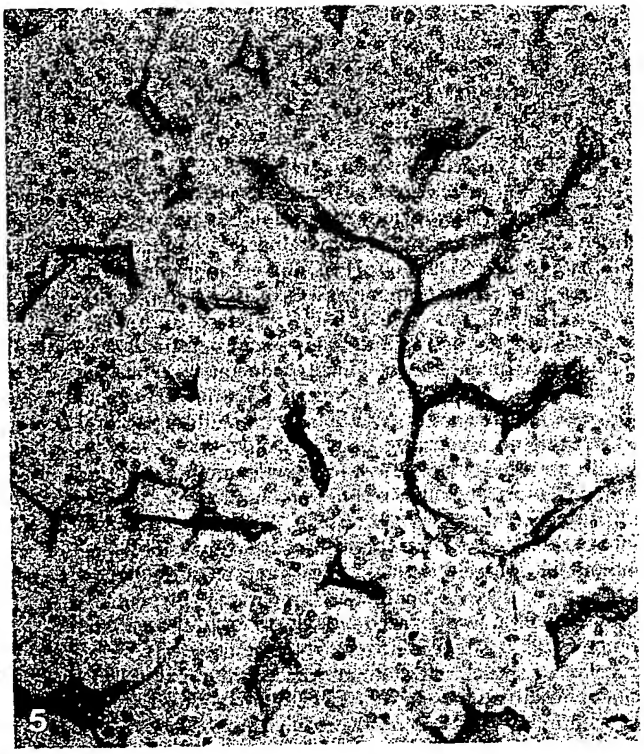

Fig. 3. Immunoperoxidase staining for the demonstration of tenascin in Warthin's tumour. The areas of the basement membranes stain positively. Delicate reticular staining can be observed in the lymphatic areas. Immunoperoxidase stain, ×210

Fig. 4. Immunoperoxidase staining for the demonstration of tenascin in mucoepidermoid carcinoma. The stromal tissue stains strongly for tenascin while the tumour cells are negative. Immunoperoxidase stain, ×155

Fig. 5. Immunoperoxidase staining for the demonstration of tenascin in acinic cell tumour. Delicate positive fibrous strands can be observed in the stroma. Immunoperoxidase stain, ×210

University Central Hospital. The cases were from the years 1985–1990 and the material was fixed in neutral formalin and embedded in paraffin. Some of the material (7 cases) was obtained fresh from the operating theatre and stored in liquid nitrogen. The tumours were classified according to the WHO International classification of salivary gland tumours (Seifert 1991). The diagnosis of all the cases was based on light microscopic examination using conventional haematoxylin and eosin stain.

The material consisted of 16 pleomorphic adenomas, 6 adenolymphomas, 6 mucoepidermoid carcinomas, 3 acinic cell tumours, 3 adenoid cystic carcinomas and 1 pleomorphic sarcoma of the salivary gland. Frequently, the specimens also contained non-neoplastic elements. Eight cases of non-neoplastic salivary gland tissue were also included (4 normal, 4 chronic inflammations of the salivary gland).

We aimed at producing a monoclonal antibody that also detects tenascin efficiently in formalin-fixed material. For that purpose, the mAb 143DB7 was raised as follows. First, tenascin was purified

from the culture medium of human embryonal fibroblasts by using affinity purification with a well-characterized anti-tenascin hybridoma clone 100EB2 (Howeedy et al. 1990). For that purpose, immunoglobulin fraction of 100EB2 was purified from the ascites fluid by using protein G column (Pharmacia, Uppsala, Sweden) in FPLC. It was then coupled to cyanogen bromide-activated Sepharose 4B (Pharmacia) according to the manufacturer's instructions. Culture medium of human embryonal fibroblasts was then passed over the column. After extensive washing, the bound tenascin was eluted with 3-[(Cholamidopropyl)-dimethyl ammonio]-1-propanesulfonate (CHAPS) buffer, pH 11, and used for immunization. Three days after the last immunization of BALB/c mice, the hybridoma production was initiated by standard techniques (Köhler and Milstein 1975). The hybridomas were screened, first, by using purified tenascin in enzyme-linked immunoassay, and then by immunohistochemistry on pepsin-treated paraffin sections of selected formalin-fixed tumours. The hybridoma culture 143BD7 was cloned by using standard techniques.

The specificity of mAb 143DB7 was shown by immunoblotting of whole human cultured fibroblasts. For immunoblotting, the cells were lysed in electrophoresis sample buffer, boiled and analysed in SDS-polyacrylamide gel electrophoresis, carried out according to Laemmli (1970), by using 6.5% stab gels and reducing conditions. The transfer of the electrophoretically separated polypeptides onto nitrocellulose paper was carried out according to the method of Towbin et al. (1979). To visualize the polypeptide bands, strips of the nitrocellulose sheets were cut and stained with amido black. The immunodetection was done by incubating the nitrocellulose sheets first with mAb 143DB7 and then with peroxidase-coupled rabbit anti-mouse IgG (Dakopatts, Copenhagen, Denmark). 3'-3' Diaminobenzidine was used as a chromogen. In immunoblotting, two distinct bands of 250,000 and 190,000 daltons were revealed. No polypeptide bands were revealed in experiments in which the primary antibody was either omitted or replaced by antibodies to proteins not produced by fibroblasts (not shown).

For paraffin sections, 5-µm-thick sections were deparaffinized in xylene and rehydrated in graded alcohol. The endogenous peroxidase was consumed by treating the sections with 0.3% hydrogen peroxidase in absolute methanol for 30 min. Prior to the immunostaining, the sections were treated with 0.4% pepsin (Merck, Darmstadt, FRG; 10 units/mg) for 30 min at 37° C. Monoclonal mouse antibody (143DB7) to human tenascin was used as the primary antibody. For the immunostaining, the avidin-biotin complex (ABC) method was used (Hsu et al. 1981). The sections were first incubated overnight with the primary antibody at 4° C, followed by biotinylated rabbit anti-mouse secondary antibody (1:200) and the ABC complex (Dakopatts). The colour was developed with diaminobenzidine, whereafter the sections were mounted in an aqueous medium. The sections were counterstained with a light haematoxylin stain. Negative control consisted of substituting PBS (140 ml sodium chloride, 0.01 M phosphate buffer, pH 7.2) for the primary antibody.

For frozen sections, 5-µm-thick sections were cut from the specimens. They were air-dried for 1 h and were then fixed in acetone for 10 min at −22° C. The endogenous peroxidase was consumed by treating the sections with 0.3% hydrogen peroxidase in methanol for 30 min. A monoclonal mouse antibody (EB-100) to human tenascin, with a dilution of 1:5, was used as the primary antibody (Howeedy et al. 1990). The sections were incubated with the primary antibody overnight at 4° C, followed by the biotinylated secondary rabbit anti-mouse antibody (1:200) and the ABC complex (Dakopatts).

The peroxidase reaction was developed with diaminobenzidine, whereafter the sections were mounted in an aqueous medium. The sections were counterstained lightly with haematoxylin. Negative controls were as described previously.

Results

In the normal salivary gland, tenascin immunoreactivity was seen in the basement membranes of the ducts and in the smooth muscle cells in the walls of the small arteries. The mucous and serous glands were negative. The finding was similar in the chronically inflamed salivary gland tissue.

In pleomorphic adenomas, linear immunoreactivity could be observed in the stromal tissue in all cases (Figs. 1, 2). Also the fibrotic capsule stained positive. In the dense, fibrotic areas, the immunoreactivity was stronger than in the myxoid areas (Fig. 2b). Some myxoid islands remained negative for the staining. Also the cartilaginous component stained positive for tenascin (Fig. 2a). Often, a uniform distribution of the staining was seen over the cartilaginous area. Occasionally, however, non-reactive stromal zones could be seen around individual chondrocytes. No intracellular tenascin was seen in tumour cells.

In Warthin's tumours (Fig. 3), tenascin immunoreactivity was seen in the areas of the basement membranes beneath the epithelial cell component. In some areas, positivity also occurred in the fibrous cores of the papillary projections. In the lymphatic component, immunoreactivity was confined to thin reticular fibres. Also the tumour capsule stained positive.

The stroma of all malignant salivary gland tumours was positive for tenascin. The staining was weaker in adenoid cystic carcinomas and in acinic cell tumour than in mucoepidermoid carcinomas. In adenoid cystic carcinomas and mucoepidermoid carcinomas, a linear tenascin immunoreactivity was observed, which sometimes concentrated around the tumour cell islands (Fig. 4). In acinic cell tumours, faintly positive linear strands could be observed (Fig. 5). No intracytoplasmic staining for tenascin was seen in tumour cells.

There was no difference between the results obtained with the two tenascin antibodies. The intensity of the immunostaining was stronger, however, in the EB-100 stained fresh frozen material. The control staining was negative in all cases.

Discussion

In this investigation we analysed the distribution of tenascin in benign and malignant salivary gland tumours and in non-neoplastic salivary gland. The immunostaining was carried out by using two different antibodies, EB-100 and 143DB7, both of which work well on fresh, frozen sections and the latter also on formalin-fixed, paraffin-embedded material. The staining results with the two antibodies were identical. However, the immunostaining of fresh frozen material with EB-100 yielded the most intense staining reaction. This probably depends not only on the difference in the reactivity between the antibodies, but also on the better preservation of the tenascin antigen in fresh frozen material and/or the fact that the antigenic determinants are partly hidden in formalin-fixed material.

In benign salivary gland tumours, stromal positivity was observed both in pleomorphic adenomas and in adenolymphomas. In pleomorphic adenomas, there was a strong stromal immunoreactivity in the dense, fibrotic stroma as well as in the cartilaginous component of the tumour. In the myxoid zones the staining was less intense, suggesting that there is a lower concentration of tenascin in the myxoid zones. Interestingly, pleomorphic adenomas contain fibronectin (Caselitz et al. 1988) and chondroitin sulphate proteoglycans (Harrison and Auger 1991), which both bind tenascin (Chiquet Ehrismann et al. 1991; Erickson and Lightner 1988). Thus the lower degree of staining for tenascin in the myxoid zone could also be a reflection of a lower concentration of these substances in this region.

A diffuse distribution of tenascin could also be seen in the chondroid compartment in pleomorphic adenomas. Tenascin is present in embryonic chrondroid tissue, where it is distributed throughout the tissue, while in adult tissue it is concentrated mainly in the perichondrium (Erickson and Lightner 1988). It may even by possible that the chondrogenic differentiation in pleomorphic adenomas is induced by tenascin. This is supported by the observation that tenascin is associated with chondrogenic differentiation in vivo (Chiquet-Ehrismann 1990).

In Warthin's tumours, as in normal salivary gland, a strong tenascin immunoreactivity was seen in the basement membrane areas beneath the epithelial component. This is in line with previous studies which have shown tenascin in the basement membranes of different epithelia of ectodermal and endodermal origin (Natali et al. 1991). Synthesis of tenascin has also been reported in the epithelial cells of developing lung buds (Koch et al. 1991). A receptor for tenascin has been described that belongs to a family of integrin molecules (Bourdon and Ruoslahti 1989). The epithelial cells of salivary gland ducts, as well as other epithelia, might harbour such surface receptors and tenascin might thus function as a structural protein in the ductal units to retain the integrity and orientation of the epithelial cells.

In malignant salivary gland tumours, stromal tenascin immunoreactivity could be seen in all cases. This is in accordance with previous results which indicate stromal tenascin immunoreactivity in various malignant neoplasms (Bourdon et al. 1983; Erickson and Bourdon 1989; Natali et al. 1990; Vollmer et al. 1990; Howeedy et al. 1990). In the present study, however, there were differences in the intensity of tenascin staining between different types of tumours.

The tissue distribution of tenascin is reminiscent of that of fibronectin, which is also found in the stromal areas, while laminin and type IV collagen are mainly found in the basement membrane areas of these tumours (Caselitz et al. 1988). This similarity in tissue distribution may be due to the fact that the 190 kDa isoform of tenascin is able to attach to fibronectin (Chiquet-Ehrismann et al. 1991).

In tumour tissue tenascin is considered to be synthesized by stromal fibroblasts which are stimulated by cytokines such as transforming growth factor-beta, which is produced by the tumour cells (Pearson et al. 1988; Chiquet-Ehrismann 1990). Tenascin contains epidermal growth factor-like repeats (Jones et al. 1988) and it has been suggested that tenascin might induce tumour growth by an autocrine mechanism (Engel 1989). The growth promotion induced by tenascin may also play a part in the maintenance and progression of both benign and malignant salivary gland tumours.

References

Bourdon MA, Ruoslahti E (1989) Tenascin mediates cell attachment through an RGD-dependent receptor. J Cell Biol 108:1149–1155

Bourdon MA, Wikstrand CJ, Furthmayr H, Matthews TJ, Bigner DD (1983) Human glioma-mesenchymal extracellular matrix antigen defined by monoclonal antibody. Cancer Res 43:2796–2805

Caselitz J, Schmitt P, Seifert G, Wustrow J, Schuppan D (1988) Basal membrane associated substances in human salivary glands and salivary gland tumours. Pathol Res Pract 183:386–394

Chiquet M, Fambrough DM (1984) Chick myotendineous antigen. I.A. Monoclonal antibody as a marker for tendon and muscle morphogenesis. J Cell Biol 98:1937–1946

Chiquet-Ehrismann R (1990) What distinguishes tenascin from fibronectin? FASEB J 4:2598–2604

Chiquet-Ehrismann R, Mackle EJ, Pearson CA, Sakakura T (1986) Tenascin: an extracellular matrix protein involved in tissue interactions during fetal development and oncogenesis. Cell 47:131–139

Chiquet-Ehrismann R, Matsuoko Y, Hofer U, Spring J, Bernasconi C, Chiquet M (1991) Tenascin variants: differential binding to fibronectin and distinct distribution in cell cultures and tissues. Cell Regulation 2:927–938

Chuong C-M, Chen H-M (1991) Enhanced expression of neural cell adhesion molecules and tenascin (cytotactin) during wound healing. Am J Pathol 138:427–440

Chuong C-M, Crossin KL, Edelman GM (1987) Sequential expression and differentiation function of multiple adhesion molecules during the formation of cerebellar cortical layers. J Cell Biol 104:331–342

Crossin KL, Hoffman S, Grumet M, Thiery J-P, Edelman GM (1986) Site-restricted expression of cytotactin during development of the chicken embryo. J Cell Biol 102:1917–1930

Engel (1989) EGF-like domains in extracellular matrix proteins: localized signals for growth and differentiation? FEBS Lett 251:1–7

Erickson HP, Bourdon MA (1989) Tenascin: an extracellular matrix protein prominent in specialized embryonic tissues and tumors. Annu Rev Cell Biol 5:71–92

Erickson HP, Lightner VA (1988) Hexabrachion protein (tenascin, cytotactin, brachionectin) in connective tissue, embryonic brain and tumors. Adv Cell Biol 2:55–90

Harrison JD, Auger DW (1991) Mucosubstance histochemistry of pleomorphic adenoma of parotid and submandibular salivary glands of man: light and electron microscopy. Histochem J 23:293–303

Howeedy AA, Virtanen I, Laitinen L, Gould NS, Koukoulis GK, Gould VE (1990) Differential distribution of tenascin in the normal, hyperplastic and neoplastic breast. Lab Invest 63:798–806

Hsu S-M, Raine L, Fanger H (1981) Use of avidin-biotin-peroxidase complex (ABC) in immunoperoxidase techniques: a comparison between ABC and unlabelled antibody (PAP) procedures. J Histochem Cytochem 29:577–580

Jones FS, Burgoon MP, Hoffman S, Crossin KL, Cunningham BA, Edelman GM (1988) A cDNA clone for cytotactin contains sequences similar to epidermal growth factor-like repeats and

segments of fibronectin and fibrinogen. Proc Natl Acad Sci USA 85:2186–2190

Koch M, Wehrle-Haller B, Baumgartner S, Spring J, Brubacher D, Chiquet M (1991) Epithelial synthesis of tenascin at tips of growing bronchi and graded accumulation in basement membrane and mesenchyme. Exp Cell Res 194:297–300

Köhler G, Milstein C (1975) Continuous cultures of fused cells secreting antibody of predefined specificity. Nature 256:495–497

Laemmli VK (1970) Cleavage of structural proteins during the assembly of the head of bacteriophage T4. Nature 227:680–685

Natali PG, Nicotra MR, Bartolazzi A, Mottolese M, Coscia N, Bigotti A, Zardi L (1990) Expression and production of tenascin in benign and malignant lesions of melanocytic lineage. Int J Cancer 46:586–590

Natali PG, Nicotra MR, Borri C, Castellani P, Risso AM, Zardi L (1991) Comparative analysis of the expression of the extracellular matrix protein tenascin in normal human fetal, adult and tumor tissues. Int J Cancer 37:811–816

Pearson CA, Pearson D, Shibahara S, Hofsteenge J, Chiquet Ehrismann R (1988) Tenascin: cDNA cloning and induction of TGF-beta. EMBO J 7:2977–2981

Prieto AL, Jones FS, Cunningham BA, Crossin KL, Edelman GM (1990) Localization during development of alternatively spliced forms of cytotactin mRNA by in situ hybridization. J Cell Biol 111:685–698

Seifert G (1991) World Health Organization (WHO) International histological classification of tumours. Histological typing of salivary gland tumours, 2nd edn. Springer, Berlin Heidelberg New York

Towbin H, Staehelin T, Gordon J (1979) Electrophoretic transfer of proteins from polyacrylamide gels to nitrocellulose sheets: procedure and some applications. Proc Natl Acad Sci USA 76:4350–4354

Vollmer G, Siegal GP, Chiquet-Ehrismann R, Lightner VA, Arnholdt H, Knuppen R (1990) Tenascin expression in the human endometrium and in endometrial adenocarcinomas. Lab Invest 2:725–730

Virchows Archiv B Cell Pathol (1993) 63:283–287

Virchows Archiv B
Cell Pathology
Including Molecular Pathology

Tenascin in inflammatory conditions and neoplasms of the urinary bladder

Outi Tiitta [1], Torsten Wahlström [2], Ismo Virtanen [1], and Victor E. Gould [3]

[1] Department of Anatomy, (Siltavuorenpenger 20 A) SF-00014 University of Helsinki, Finland
[2] Department of Pathology, P.O. Box 21 (Haartmaninkatu 3) SF-00014 University of Helsinki, Finland
[3] Department of Pathology, Rush Medical College, Chicago, IL 60612, USA

Received December 16, 1992 / Accepted January 28, 1993

Summary. Tenascin (Tn) is an extracellular matrix (ECM) glycoprotein strongly and widely expressed during embryogenesis. Tn is decreased in normal adult tissues but is reexpressed in numerous inflammatory, reparative and neoplastic processes. We immunostained samples of fetal and normal adult bladders and samples of bladder tissue from patients with chronic cystitis, detrusor hypertrophy, malakoplakia and transitional cell carcinomas (TCC) of all grades, with a monoclonal antibody (mAb) to Tn 143DB7. Sections of flat in situ carcinomas were also studied. In fetal bladders, strong and ragged Tn reactions were noted at the epithelial-stromal interface; in normal adult bladders, the reaction was delicate and less extensive. In chronic cystitis, Tn reactivity was enhanced particularly around prominent capillary blood vessels. In flat in situ carcinomas, Tn staining was stronger and more extensive than in normal mucosa but was often less extensive than in some examples of cystitis. In TCC I and II, Tn immunoreactivity was strong and predominated in the pericapillary stroma of the papillae; in infiltrating TCC II, comparatively limited Tn staining was noted. In deeply infiltrating grade III TCC with abundant stroma, Tn reaction was invariably strong and extensive, particularly around advancing tumor nests. The strongest Tn reactions were noted in invasive, high-grade TCC with abundant stroma. We conclude that in inflammatory-reactive processes, and in in situ carcinomas as well as in TCC, the extent and intensity of the Tn reaction correlates with the severity of the inflammatory infiltrate and with the extent of the stromal remodelling.

Key words: Tenascin – Urinary bladder – Inflammation – Malakoplakia – Carcinomas

Correspondence to: O. Tiitta

Introduction

Tenascin (Tn) is a large extracellular matrix (ECM) protein that has considerable structural homology with fibronectin, epidermal growth factor and fibrinogen (Jones et al. 1988; Siri et al. 1991). Early studies suggested that the distribution of Tn is temporally and topographically limited. It was shown to be a marker for muscle and tendon morphogenesis (Chiquet and Fambrough 1984) and to be involved in interactions during the development of tendon, muscle and bone (Mackie et al. 1987b), kidney (Aufderheide et al. 1987), teeth (Thesleff et al. 1987), gut (Aufderheide and Ekblom 1988) and neural tissues (Crossin et al. 1986). Strong Tn reactions were shown in the stroma of breast carcinomas while no reactions were noted in benign breast tumors or in the normal breast (Mackie et al. 1987b). Tn was shown to reemerge strongly during the healing of wounds in the epidermis and cornea (Chuong and Chen 1991; Mackie et al. 1988; Tervo et al. 1989). Enhanced Tn staining was also noted underlying growing and proliferating epithelial cells (Tiitta et al. 1992; Vollmer et al. 1990).

More recent studies have shown that the distribution of Tn is wider than originally envisaged, since it may be readily demonstrated, albeit at variable levels of expression, in a wide range of normal tissues and in inflammatory, reparative, immunorelated and neoplastic processes at many sites (for reviews, see Chiquet-Ehrismann 1990; Gould et al. 1990, 1992; Koukoulis et al. 1991).

Tn is readily detectable in the stroma of most carcinomas but the extent and intensity of the reaction varies considerably (Koukoulis et al. 1991). Tumors with conspicuous stroma, such as some carcinomas of the breast and lung, display rich Tn reactions while in most papillary carcinomas of the thyroid, ovary, kidney and ampulla of Vater, and in some low-grade carcinoids, Tn staining is intense but limited to the scanty stroma of the papillary cores often associated with small vessels (Koukoulis et al. 1991).

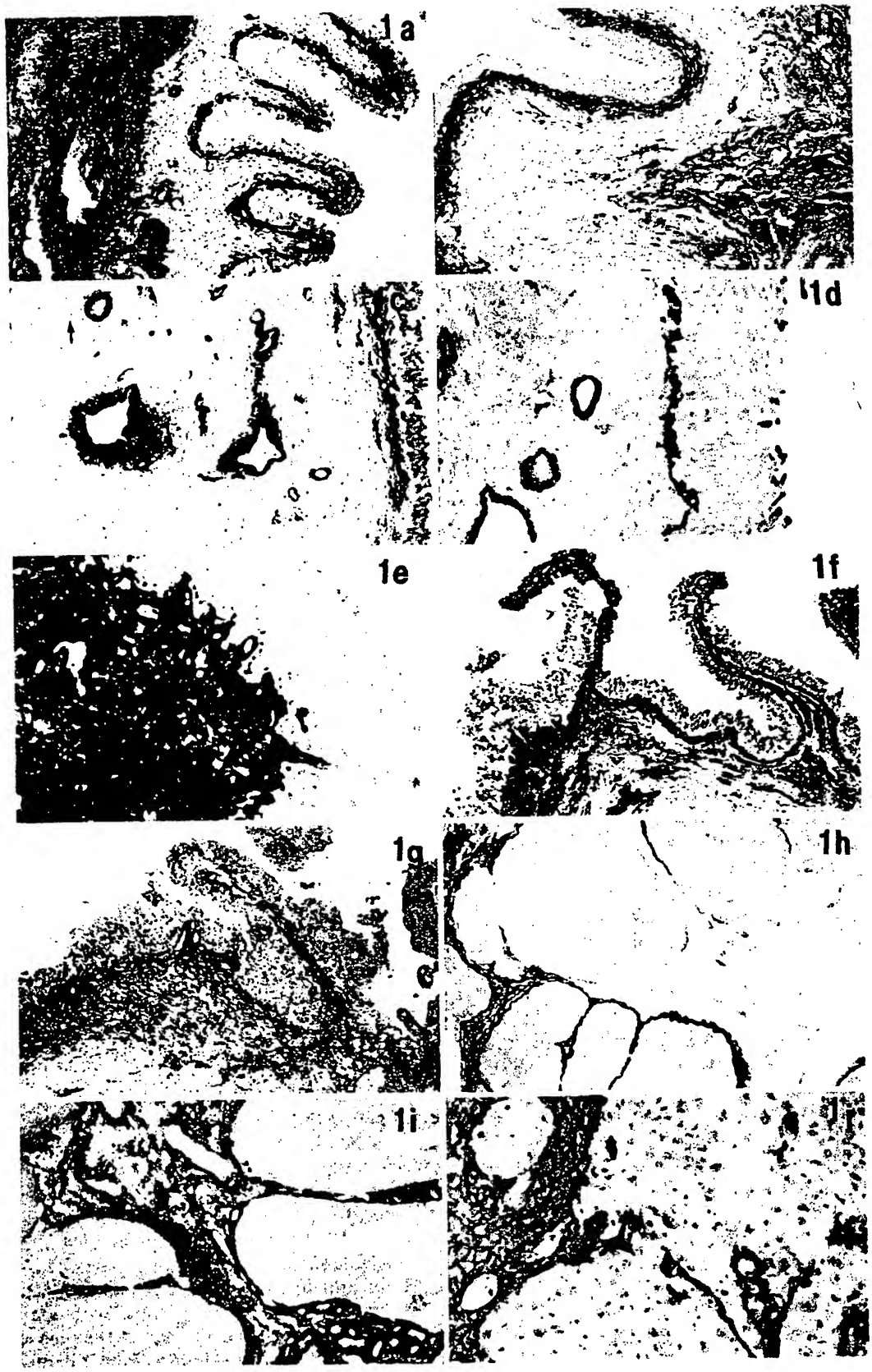

Fig. 1. a Fetal bladder; tenascin (Tn) immunoreactivity appears as a ragged band at the epithelial-stromal interface. Unstained submucosal mesenchyme is seen between the epithelial-stromal interface and the strongly reactive muscularis layer. Note brightly immunostained vessels in the mesenchyme. ×130. b Normal adult bladder showing convincing Tn reactivity at the epithelial-stromal interface. The lower portion of the submucosa is weakly reactive. ×130. c Chronic cystitis displaying ragged stromal immunoreactivity. Most vessels and perivascular stroma are prominently stained while others are negative (*arrow*). ×130. d Flat in situ carcinoma; note the focally discontinuous rim of Tn reaction . underlying the lesion; most of the vessels are strongly stained. ×130. e Flat in situ carcinoma; note strong and extensive Tn staining underneath the epithelium. ×130. f Transitional cell carcinoma (TCC) I displaying convincing stromal Tn staining not only in the delicate papillae but also in the submucosa. ×130. g TCC II revealing extensive stromal Tn reaction. ×130. h Invasive nests of TCC II showing delicate and incomplete Tn reactions around some neoplastic nests coexisting with more extensively stained areas. ×210. i Invasive TCC II displaying extensive stromal Tn immunoreactivity. ×210. j Deeply invasive TCC III showing intense and extensive stromal Tn staining also involving the stromal vessels. ×210

The urinary bladder offers an interesting model given that most of its carcinomas have papillary features although their grade of malignancy varies widely (Koss 1975). We immunostained samples of fetal and normal adult bladder, as well as bladder exhibiting chronic cystitis, detrusor hypertrophy, malakoplakia, flat in situ carcinoma, and papillary transitional cell carcinomas (TCC) grade I, II and III, with the monoclonal antibody (mAb) 143DB7 to Tn (Tiitta et al. 1992). We found that the extent and intensity of Tn expression correlated most closely with the cellular inflammatory response and the extent of stromal remodelling, and to a lesser extent with the degree of epithelial proliferation.

Materials and methods

Tissue samples. Blocks of paraffin-embedded tissue were retrieved from the files of the Departments of Pathology, University of Helsinki, Finland, and Rush Medical College, Chicago, Illinois, USA. Samples of normal fetal (gestational age 16 weeks, $n=3$) and normal adult bladder ($n=2$), and examples of cystitis ($n=4$), malakoplakia ($n=2$), flat in situ carcinomas ($n=4$) and papillary TCC grades I ($n=5$), II ($n=19$) and III ($n=16$) were obtained. Bladder samples showing detrusor hypertrophy ($n=2$) due to urethral atresia were obtained from mature stillborn babies. Sections were cut and stained with hematoxylin and eosin; the tumors were classified by widely accepted criteria (Koss 1975).

Immunohistochemistry. Sections were cut at 6 μm, deparaffinized, pretreated with pepsin (Tiitta et al. 1992), incubated with 3% hydrogen peroxide to block endogenous peroxidase activity and washed in phosphate-buffered saline (PBS). They were then incubated with normal swine serum (diluted 1:10) at room temperature for 20 min. After washing in PBS, immunostaining for Tn was performed with a modified ABC complex method (Hsu et al. 1981) applying the mAB 143DB7 (diluted 1:10) for 60 min at room temperature (Tiitta et al. 1992). To visualize the antibody binding sites 3-amino-9-ethylcarbazole (AEC) was used as a chromogen (Sigma, St. Louis, Mo.). Sections were briefly counterstained with Mayer's hematoxylin.

Results

In the fetal bladder, a continous, ragged and very intensely Tn immunoreactive band was noted at the epithelial-stromal interface; the muscle bundles of the muscularis also stained strongly while the loose submucosal mesenchyme was virtually negative (Fig. 1a). Submucosal vessels were also strongly reactive (Fig. 1a). Samples of hypertrophied bladder secondary to congenital urethral atresia showed a limited subepithelial reactivity, although the submucosal layer was significantly widened (not shown). The normal adult bladder displayed a convincing Tn reaction at the epithelial-stromal interface; the reaction was as extensive, but generally weaker than in the fetal samples (Fig. 1b). The upper portion of the submucosa was negative but the lower portion was weakly reactive for Tn. It was noted that a number of vessels displayed a focal Tn reaction while others were clearly negative (Fig. 1b).

Samples of bladder showing cystitis exhibited a continuous and strong Tn reactivity at the epithelial-stromal interface; the reactions were ragged even in examples with a sparse inflammatory reaction, whereas in those exhibiting a dense lymphocytic infiltrate, the Tn reactivity was far more extensive and also involved the prominent perivascular stroma (Fig. 1c). Similar features were noted in examples with a thin or distinctly hyperplastic epithelium. Chronic cystitis associated with prostatic hyperplasia and prostatitis showed strong Tn staining related predominantly to the inflammatory infiltrates (not shown). In malakoplakia, uneven but distinct rims of Tn positivity were noted between the epithelium and the underlying plaque. Notably, in other regions in which the plaques included or were surrounded by prominent inflammatory infiltrates, strong and extensive Tn reactions were evident (not shown).

Flat in situ carcinomas showed a wide range of subepithelial Tn reactions including weak, thin and discontinuous rims, and extremely thick, ragged bands that were at times continous with the normally stained muscularis (Fig. 1d, e). In these samples, the reactivity of the vessels varied considerably.

Predominantly exophytic papillary TCC I and II displayed consistent, albeit irregular, Tn reactions in the submucosa that extended into the stroma of the protruding papillae (Fig. 1f, g). Invasive TCC II showed variable rims of strong Tn reactivity ranging from delicate and incomplete to broad and extensive bands that sometimes included the stromal vessels (Fig. 1h, i). In clearly invasive TCC III, invariably there was rich stromal staining for Tn that seemed to include all the vessels (Fig. 1j).

Discussion

Initial investigations suggested that Tn was a significant ECM glycoprotein whose expression was chronologically and topographically restricted, since it was most readily, if not exclusively, found in certain sites during embryogenesis (Chiquet-Ehrismann et al. 1986; Erickson and Bourdon 1989), in some reparative processes (Mackie et al. 1988), and in certain malignant tumors (Chiquet-Ehrismann et al. 1986; Mackie et al. 1987b). In a recent study, no Tn was noted in the normal adult bladder (Natali et al. 1991). However, Tn has been reported recently, albeit at variable levels, in many normal adult tissues, inflammatory and hyperplastic processes, and in many benign as well as malignant neoplasms (for overviews see Howeedy et al. 1990; Koukoulis et al. 1991; Natali et al. 1991). Our findings in the normal adult bladder were of a thin, yet continuous Tn immunoreactive rim at the epithelial-stromal interface reminiscent of that found around normal mammary ducts and acini (Gould et al. 1990; Howeedy et al. 1990) and in the cervix (Tiitta et al. 1992). Not surprisingly, in samples of fetal bladder, the reactions were more extensive and stronger than in the adult, parallelling previous findings in the fetal breast (Howeedy et al. 1990).

In examples of chronic cystitis, subepithelial Tn reactions were decidedly enhanced, appearing as strongly stained bands with ragged edges extending into the submucosa. In examples showing a significant inflammatory

cell reaction, Tn staining was more extensive and intense than in those in which inflammation was sparse. These findings also parallel our recent observations in chronic cervicitis associated condylomatous lesions in which evidence of human papilloma virus infection was demonstrated (Tiitta et al. 1992). Erickson and Bourdon (1989) suggested that certain inflammatory cells may be responsible for activating Tn expression. Malakoplakia is a peculiar inflammatory lesion thought to be associated with chronic bacterial infection; it occurs in the urinary bladder but has also been described in other sites. It is of interest to note that the extent and intensity of Tn staining was more closely related to the inflammatory infiltrates within and around the plaques than with the plaques themselves. Strong Tn reactions have also been described in newly formed granulation tissue in experimentally induced skin wounds, but the reactions decreased in extent and intensity as the scar matured (Chuong and Chen 1991; Mackie et al. 1988); similar observations have been made in actively inflammed compared with sclerotic septa in liver cirrhosis (van Eyken et al. 1992), as well as in various forms of glomerulonephritis (Gould et al. 1990; Koukoulis et al. 1991). Thus, the apparently paradoxical weak Tn reactions noted in the wide and fibrotic submucosa of bladders showing detrusor hypertrophy associated with congenital urethral obstruction may simply reflect the presence of relatively mature fibrous tissue lacking inflammatory infiltrates.

Flat in situ bladder carcinomas displayed for the most part strong and extensive Tn reactions. In general, examples with severe dysplasia exhibited strong Tn reactions but rarely staining was delicate and comparatively weak. These findings contrast somewhat with our own descriptions of strong and consistent Tn staining in virtually all instances of in situ carcinoma of breast irrespective of the degree of dysplasia (Howeedy et al. 1990). On the other hand, in in situ cervical carcinoma, we did encounter examples with scanty Tn staining (Tiitta et al. 1992). Similarly, not all examples of endometrial hyperplasia showed uniform reactions (Vollmer et al. 1990). In this context, it should be noted that not all flat in situ carcinomas evolve into high grade invasive tumors (Koss 1975). Thus, it is possible that the various Tn distribution patterns observed in different proliferative and preneoplastic lesions may simply reflect uneven growth patterns. It should be mentioned that Tn sequencing has revealed regional homologies with epidermal growth factor (Jones et al. 1988; Siri et al. 1991), and that purified Tn stimulates the proliferation of mammary carcinoma cells in vitro (Chiquet-Ehrismann et al. 1989). Conversely, the production of Tn by mesenchymal cells appears to be regulated, partly at least, by transforming growth factor beta (Pearson et al. 1988).

In papillary, predominantly exophytic TCC grades I and II, the stroma of the protruding papillae displayed uniform and often strong Tn reactivity. However, in samples in which tumor invaded the underlying submucosa, Tn staining was comparatively limited and frequently weaker than that underlying flat in situ carcinomas. This apparently paradoxical finding may reflect that the aggressive biological potential and subsequent invasiveness of many initially in situ lesions exteeds that of some other already invasive grade I and II tumors (Koss 1975).

In all the samples of invasive TCC grade III, Tn reactions were intense and extensive. The distribution of the staining was somewhat difficult to assess as the samples consisted mostly of small fragments. However, it was evident that deeply invasive areas, inferred from the presence of adjacent smooth muscle, displayed the strongest staining whereas some superficial non-invasive foci retaining a papillary architecture, showed only weak reactions. These discrepancies probably reflect different growth rates and similar findings have been reported in carcinomas of the breast (Howeedy et al. 1990) and endometrium (Vollmer et al. 1990). However, weak and limited Tn reactions should not be equated with a low tumor cell proliferation rate or a limited invasiveness, since very limited Tn reactions have also been noted in highly aggressive neoplasms such as the small cell variant of neuroendocrine lung carcinoma (Koukoulis et al. 1991). In such tumors the weak Tn staining may be related to their poorly developed vascularity and scanty myofibroblast-poor stroma. These factors may be significant since, in epithelial neoplasms, endothelial cells and myofibroblasts appear to be the major site of Tn synthesis (Chiquet-Ehrismann et al. 1986; Ekblom and Aufderheide 1989), although under certain conditions, it has been suggested that embryonal, transformed and reactive, non-transformed epithelial cells may also produce Tn (Gould et al. 1992; Howeedy et al. 1990; Koch et al. 1991; Koukoulis et al. 1991; Prieto et al. 1990).

In the examples of TCC examined here it was noted that low grade carcinomas tended to have comparatively scanty connective tissue stroma, whilst that of high grade tumors was markedly increased; moreover, tumors with scanty stroma had abundant vessels. Since, endothelial, smooth muscle and myofibroblastic cells are capable of synthesizing Tn, it might be assumed that both low and high grade TCC would be associated with high levels of Tn expression. However, our findings in these and other tumors (Koukoulis et al. 1991; Tiitta et al. 1992) clearly indicate the opposite. It is also evident that neither abundant connective tissue nor all blood vessels are invariably Tn-immunoreactive. In healing wounds, Chuong et Chen (1991) and Luomanen and Virtanen (1993) noted that Tn was expressed in the walls of newly formed capillaries in granulation tissue. In this context, our finding of a variable vascular reactivity suggests that Tn might be a marker of injured and/or proliferating vessels reflecting dynamic reparative processes (Gould et al. 1992).

Dvorak (1986) has suggested that tumor stroma undergoes a sequence of maturation events that are reflected by variable cell populations and similarly variable ECM components. Our findings, like those of Koukoulis et al. (1991) suggest that in tumors with abundant stroma, Tn staining is strongest at the peripheral, expanding borders but is often less conspicuous in the center (Koukoulis et al. 1991). This concept is also illustrated by the consistently weak Tn reaction noted in mature

sclerotic septa in hepatic cirrhotic (van Eyken et al. 1992), and in sclerosed obsolete glomeruli in chronic renal disease (Gould et al. 1992; Koukoulis et al. 1991). Given that in the stroma of epithelial tumors and in the bladder submucosa, myofibroblasts may be responsible for most Tn synthesis, it can be suggested from our observations that prominent Tn staining accompanies comparatively abundant and active inflammatory infiltrates and/or myofibroblastic proliferations, but is not necessarily related to the degree of architectural distortion or to tumor grade.

Acknowledgements. The skilful technical assistance of Mrs. Tuula Halmesvaara, Mrs. Aili Takkinen and Mr. Reijo Karppinen is acknowledged. This study was supported by grants from the University of Helsinki, The Sigrid Juselius Foundation and the Finnish Medical Research Council.

References

Aufderheide E, Ekblom P (1988) Tenascin during gut development: appearance in the mesenchyme, shift in molecular forms, and dependance on epithelial-mesenchymal interactions. J Cell Biol 107:2341–2349

Aufderheide E, Chiquet-Ehrishmann R, Ekblom P (1987) Epithelial-mesenchymal interactions in the developing kidney lead to expression of tenascin in the mesenchyme. J Cell Biol 105:599–608

Chiquet-Ehrismann R (1990) What distinguishes tenascin from fibronectin. FASEB J 4:2598–2604

Chiquet M, Fambrough DM (1984) Chick myotenchinous antigen. I. A monoclonal antibody as marker for tendon and muscle morphogenesis. J Cell Biol 98:1926–1936

Chiquet-Ehrismann R, Mackie EJ, Pearson CA, Sakakura T (1986) Tenascin: an extracellular matrix protein involved in tissue interactions during fetal development and oncogenesis. Cell 47:131–139

Chiquet-Ehrismann R, Kalla P, Pearson CA (1989) Participation of tenascin and transforming growth factor-β in resiprocal epithelial-mesenchymal interactions of MCF7 cells and fibroblasts. Cancer Res 49:4322–4325

Chuong CM, Chen HM (1991) Enhanced expression of neural cell adhesion molecules and tenascin (cytotactin) during wound healing. Am J Pathol 138:427–440

Crossin KL, Hoffman S, Grumet M, Thiery JP, Edelman G (1986) Site-restricted expression of cytotactin during development of the chicken embryo. J Cell Biol 102:1917–1930

Dvorak HF (1986) Tumors: wounds that do not heal. N Engl J Med 25:1650–1655

Ekblom P, Aufderheide E (1989) Stimulation of tenascin expression in mesenchyme by epithelial-mesenchymal interactions. Int J Dev Biol 33:71–79

Erickson HP, Bourdon MA (1989) Tenascin: an extracellular matrix protein prominent in specialized embryonic tissues and tumors. Annu Rev Cell Biol 5:71–92

Eyken P van, Gearts A, Bleser P de, Jazon JM, Vrijsen R, Sciot R, Wisse E, Desmet VJ (1992) Localization and cellular source of the extracellular matrix protein tenascin in normal and fibrotic rat liver. Hepatology 15:909–916

Gould VE, Koukoulis K, Virtanen I (1990) Extracellular matrix proteins and their receptors in the normal, hyperplastic and neoplastic breast. Cell Differ Dev 32:409–416

Gould VE, Martinez-Lacabe V, Virtanen I, Sahlin KM, Schwartz MM (1992) Differential distribution of tenascin and cellular fibronectins in acute and chronic renal allograft rejection. Lab Invest 67:71–79

Howeedy AA, Virtanen I, Laitinen L, Gould NS, Koukoulis GK, Gould VE (1990) Differential distribution of tenascin in the normal, hyperplastic, and neoplastic breast. Lab Invest 63:798–806

Hsu SM, Raine L, Fanger H (1981) The use of avidin-biotin-peroxidase complex (ABC) in immunoperoxidase techniques: a comparison between ABC and unlabeled antibody (PAP) procedures. J Histochem Cytochem 29:553–560

Jones FJ, Burgoon MP, Hoffman S, Crossin KL, Cunningham BA, Edelman GM (1988) A cDNA clone for cytotactin contains sequences similar to epidermal growth factor-like repeats and segments of fibronectin and fibrinogen. Proc Natl Acad Sci USA 85:2186–2190

Koch M, Wehrle-Haller B, Baumgartner S, Spring J, Brubacher D, Chiquet M (1991) Epithelial synthesis of tenascin at tips of growing bronchi and graded accumulation in basement membrane and mesenchyme. Exp Cell Res 194:297–300

Koss LG (1975) Tumors of the urinary bladder. Atlas of tumor pathology. Armed Forces Institute of Pathology, Washington, DC

Koukoulis GK, Gould VE, Bhattacharyya A, Gould JE, Howeedy AA, Virtanen I (1991) Tenascin in normal, reactive, hyperplastic, and neoplastic tissues: biologic and pathologic implications. Hum Pathol 22:636–643

Luomanen M, Virtanen I (1992) Distribution of tenascin in healing incision, excision and laser wounds. J Oral Pathol Med (in press)

Mackie EJ, Thesleff I, Chiquet-Ehrismann R (1987a) Tenascin is associated with chondrogenic and osteogenic differentiation in vivo and promotes chondrogenesis in vitro. J Cell Biol 105:2569–2579

Mackie EJ, Chiquet-Ehrismann R, Pearson CA, Inaguma Y, Taya K, Kawarada Y, Sakakura T (1987b) Tenascin is a stromal marker for epithelial malignancy in the mammary gland. Proc Natl Acad Sci USA 84:4621–4625

Mackie EJ, Halfter W, Liverani D (1988) Induction of tenascin in healing wounds. J Cell Biol 107:2757–2767

Natali PG, Nicotra MR, Bigotti A, Botti C, Castellani P, Risso AM, Zardi L (1991) Comparative analysis of the expression of the extracellular matrix protein tenascin in normal human fetal, adult and tumor tissues. Int J Cancer 47:811–816

Pearson CA, Pearson D, Shibahara S, Hofsteenge J, Chiquet-Ehrismann R (1988) Tenascin: cDNA cloning and induction by TGF-β. EMBO J 7:2977–2981

Prieto AL, Jones FS, Cunningham BA, Crossin KL, Edelman GM (1990) Localization during development of alternatively spliced forms of cytotactin mRNA by in situ hybridization. J Cell Biol 111:685–698

Siri A, Carnemolla B, Saginati M, Leprini A, Casari G, Baralle F, Zardi L (1991) Human tenascin: primary structure, pre-mRNA splicing patterns and localization of the epitopes recoqnized by to monoclonal antibodies. Nucleic Acids Res 19:525–531

Tervo K, Tervo T, Setten GB van, Tarkkanen A, Virtanen I (1989) Demonstration of tenascin-like immunoreactivity in rabbit corneal wounds. Acta Ophtalmol 67:347–350

Thesleff I, Mackie E, Vainio S, Chiquet-Ehrismann R (1987) Changes in the distribution of tenascin during tooth development. Development 101:289–296

Tiitta O, Wahlström T, Paavonen J, Linnala A, Sharma S, Gould VE, Virtanen I (1992) Enhanced tenascin expression in cervical and vulvar koilocytotic lesions. Am J Pathol 141:907–915

Vollmer G, Siegal GP, Chiquet-Ehrismann R, Lightner VA, Arhholdt H, Knuppen R (1990) Tenascin expression in the human endometrium and in endometrial adenocarcinomas. Lab Invest 62:725–730

Int. J. Cancer: 72, 217–224 (1997)

Publication of the International Union Against Cancer
Publication de l'Union Internationale Contre le Cancer

DISTRIBUTION PATTERN OF TENASCIN-C IN NORMAL AND NEOPLASTIC MESENCHYMAL TISSUES

Bruno SCHNYDER[1,3,*], Reto O. SEMADENI[3], René W. FISCHER[1], Lloyd VAUGHAN[1], Bruce D. CAR[2], Philipp U. HEITZ[3], Kaspar H. WINTERHALTER[1] and Bernhard F. ODERMATT[3]

[1]*Laboratory of Biochemistry, Federal Institute of Technology-ETH, Zurich, Switzerland*
[2]*Institute of Toxicology, Federal Institute of Technology-ETH, Zurich, Switzerland*
[3]*Institute of Pathology, University Hospital, Zurich, Switzerland*

Descriptions for tenascin-C distribution are largely restricted to epithelial tumours. The present study utilized newly developed and characterized monoclonal (hT191) and polyclonal antibodies to investigate the distribution pattern of tenascin-C in a panel of mesenchymal tumours, which was contrasted with normal tissue. The specific antibodies recognized the distinctive star-like hexabrachion protein isolated from transformed cell-culture medium and serum from normal individuals. In normal tissues, a strong tenascin-C expression in the extracellular matrix was largely restricted to basement-membrane regions of epithelium and tonsilar sinusoids, pericellularly within smooth-muscle bundles, associated with perimysial, -chondrial, -neurial and -tendon surfaces, and diffusely within vascular adventitia. It was found in the corresponding tumours of the neural sheath (schwannoma) and smooth muscle (leiomyosarcoma), and was abundantly present around certain blood vessels of mesenchymal tumours. Although not detected in normal muscle, or in adipose or fibrous connective tissue, neo-expression of tenascin-C was shown in more than half of the rhabdomyosarcomas, fibromas and liposarcomas, with an increased positive percentage in variably malignant myxoid liposarcomas compared with lipoma-like sarcomas. Tenascin-C was typically found in the extracellular matrix of soft-tissue tumours, but was notably absent from the epithelial-cell components of mixed epithelial/mesenchymal tumours. Its apparently enhanced expression in soft-tissue tumours differs from that of most other large extracellular-matrix proteins, suggesting possible functional involvement of the cell-adhesion molecule, tenascin-C, in the neoplastic phenotype. *Int. J. Cancer* 72:217–224, 1997.
© *1997 Wiley-Liss, Inc.*

Tenascin-C (Tn) is an extracellular-matrix protein known to be expressed in the foetus, in regenerative adult tissues and in certain tumours. The various components of the extracellular matrix provide a substratum facilitating cellular adhesion and migration. This matrix is particularly prominent in mesenchymal tumours and is markedly altered in its composition when compared with non-neoplastic tissues. The matrix components fibronectin, collagens types I and II, certain proteoglycans, and the basement-membrane proteins collagen type IV and laminin tend to decrease during tumour development. It is not clear whether Tn is up- or down-regulated in mesenchymal tumour development. Sarcomas may exhibit high degrees of anaplasia and malignancy, and few useful immunohistochemical tumour markers of malignancy have been developed. Therefore, an objective of the present study was to contrast Tn-distribution in soft-tissue tumours with observations made in tumours of epithelial origin, for which Tn has been proposed as a marker (Mackie *et al.*, 1987).

Tenascin-C (Tn) was the first member of the tenascin family (tenascin-C, -R and -X) to be discovered. It is a prominent extracellular-matrix (ECM) component which is also present in body fluids but not on cell surfaces. Tn is a large (1.15 to 1.6×10^6) Da glycoprotein (Vaughan *et al.*, 1987), consisting of 6 identical sub-units connected amino-terminally by disulfide bridges. Each sub-unit of human Tn consists of repetitive epidermal-growth-factor-like (14 ½×), fibronectin-type-III homologous (8 to 16×) and fibrinogen-like (1×) domains; the number of respective domains characteristic for the individual sub-units (Gulcher *et al.*, 1989; Nies *et al.*, 1991). A single gene exists, which undergoes alternative splicing in the fibronectin-type-III homologous region, leading to the formation of at least 8 different human Tn-isoforms. Mechanisms regulating the splicing are based on development, pathological conditions and micro-environmental pH changes (Kaplony *et al.*, 1991; Borsi *et al.*, 1996). The smallest isoform consists of the conserved region common to all isoforms. The clear distinction between the large- and the small-molecular-weight isoforms allowed us to raise and screen antibodies recognizing the entire panel of the different forms of human Tn.

Abundant literature documents the anti-adhesive nature of Tn in cell-culture systems, which manifests as potent inhibition of the prototypic cell-adhesion molecule fibronectin (Spring *et al.*, 1989; Deryugina and Bourdon, 1996). Paradoxically, cell adhesion may also be promoted by Tn (Borsi *et al.*, 1992). The balance of cell adhesion and detachment together probably determine the migratory activity of cells. Mice with a disrupted non-functional Tn gene have been shown to develop normally (Saga *et al.*, 1992), so demonstrating apparent functional redundancy of Tn, although it is abundantly present during embryogenesis (Kaplony *et al.*, 1991). It is still unclear how Tn functions in adult tissues (Mackie *et al.*, 1987; Natali *et al.*, 1991) in particular with regard to pathophysiologic conditions. Since cell cultures of certain tumours were shown to secrete abundant Tn, particularly upon stimulation with tumour growth modifier TGFβ (Deryugina and Bourdon, 1996), the role *in vivo* was investigated by studying the expression in tissues from a representative selection of patients with mesenchymal tumours (n = 273). Tn immunostaining was found in all tumour types examined. Neo-expression was specifically shown in neoplasms derived from the normally immunonegative adipocytes, fibroblasts and skeletal myocytes.

MATERIAL AND METHODS

Materials

U251 MG is a permanent tumour cell line derived from a human glioblastoma. Murine monoclonal antibody (MAb) CIV22 to collagen type IV, and the anti-mouse immunoglobulin conjugated with alkaline phosphatase were from TAGO (Burlingame, CA). Peroxidase-, alkaline-phosphatase- and rhodamine-labelled immunoglobulins were obtained from Dakopatts (Glostrup, Denmark). Chromatography material was from Pharmacia (Uppsala, Sweden). Soft-tissue tumour material from patients was collected in 4% (v/v) formalin solution at the Pathology Institute of the University Hospital of Zurich, Switzerland, between 1977 and 1989. Normal human tissues were collected up to 10 hr post-mortem, and fresh normal marmoset (*Callithrix jacchus*) material was either fixed in 4% formalin or snap-frozen in liquid nitrogen. Serum and plasma were received from donors of the Swiss Red Cross, Zurich, Switzerland.

Contract grant sponsor: Swiss Cancer Society.

*Correspondence to: Dr. Bruno Schnyder, Institut de Physiologie, Université de Fribourg, rue du Musée 5, CH-1700 Fribourg, Switzerland.

Received 19 November 1996; revised 2 February 1997

Immunogen: isolation of tenascin-C by gel filtration and anion-exchange chromatography

Human tenascin-C was isolated from medium of U251 MG cell culture, a conditioned Dulbecco's modified Eagle's medium containing 1% FCS and the proteinase inhibitors 1 mM phenyl-methyl-sulfonyl-flouride (PMSF), 5 mM ethylene-diamino-tetraacetic acid (EDTA), 2 mM N ethyl maleimide (NEM), 1 mM pepstatin and 0.02% (w/v) sodium azide. Conditioned medium was freed from fibronectin by passage over a gelatin Sepharose 2B affinity column, which retains fibronectin, and was supplemented to 0.2 M ammonium bicarbonate at pH 8.3. This was concentrated 20-fold by ultrafiltration in an Amicon chamber using YW-100 filters with a cut-off of 100-kDa proteins (Licagon, Tagelswangen, Switzerland) or concentrated by precipitation in a 37% ammonium-sulfate solution (22.1 g/100 ml is 37% of a saturated solution) for 30 min at room temperature. After centrifugation for 20 min at 20,000 *g* at room temperature, the supernatant was dialysed against 0.2 M ammonium-bicarbonate, pH 8.3/0.02% Triton X-100. Up to 20 ml was loaded onto a 1.2 × 120 cm sephacryl S-500 gel filtration column and filtered at 17 to 20 ml/hr flow rate. The size-fractionated tenascin-C-enriched buffer was subsequently dialysed against 50 mM Tris-buffer, pH 8.3, and applied to a DEAE-Fractogel 650-M ion-exchange column (Merck, Darmstadt, Germany). The bound material was then eluted with a NaCl gradient from 0.05 to 2 M. Tenascin-C eluted at 0.25 M NaCl and its concentration was calculated using an extinction coefficient of A_{280nm} 1%, 1 cm = 0.97.

Production and purification of antibodies

BALB/c mice were immunized, each with 5 µg/500 µl human tenascin-C purified from conditioned medium of U251 MG cell culture. Harvested spleen cells were fused with the murine myeloma cell line X63-Ag.853 and cells producing tenascin-C antibodies were selected, using an enzyme-linked immunosorbent assay (ELISA), immunoblot technique, and the unique cryocut immunofluorescence pattern in tonsil. No cross-reactivity with the homologous proteins fibronectin, fibrinogen on epidermal growth factor was found (data not shown). Large-scale production of antibodies was performed in an "Opticell" bioreactor system (Charles River Digitana, Horgen, Switzerland) followed by precipitation in a 16% (w/v) sodium-sulphate solution and affinity purification by a Sepharose 6B column coupled with protein G.

Polyclonal antiserum was obtained from New Zealand white rabbits immunized with 20 µg/400 µl human tenascin-C per rabbit. Antibodies were affinity-purified over a column of human tenascin-C coupled to Sepharose 4B and selected as the MAbs.

Purification of tenascin-C from blood by immunoaffinity chromatography and electron-microscopic analysis

Plasma was obtained by anti-coagulation of blood with 0.129 M citrate or EDTA (0.5–2 mg/ml) and/or heparin (0.2 mg/ml). Large amounts of serum or plasma (>200 ml) were first concentrated up to 20-fold by salt precipitation in a 37% ammonium-sulfate solution (22.1 g/100 ml) for 30 min at room temperature, to remove albumin. After centrifugation for 20 min at 20,000 *g* at room temperature, the tenascin-C-containing supernatant was dialysed overnight against PBS, pH 7.4. Tenascin-C solution was applied to Sepharose 4B coupled with the hT191 MAb (2 mg/ml matrix material). Non-specifically bound retarded material was eluted with phosphate-buffered pH 7.4, 0.5 M NaCl solution PBS, pH 7.4, 0.2% (v/v) Triton X-100 solution. After a column wash with 0.5 M NaCl, the bound protein was eluted with 0.1 M triethylamine-HCl-buffered, pH 11.5, 150 mM NaCl solution. Purity was assessed by gel electrophoresis.

Rotary shadowing followed by electron microscopy analysis was carried out as described by Vaughan *et al.* (1987), using a shadowing angle of 6 to 8°. The curvilinear arm-lengths of tenascin-C on the micrographs were measured from the "T-junction" joining the 2 trimers to the center of the distal fibrinogen-homologous knob (n = 120), using a digitizer plate (IBAS system from Kontron, Zurich, Switzerland). For visualization of antigen-antibody complexes, tenascin-C and hT191 were incubated for 30 min at room temperature in an equimolar ratio in a 0.2 M ammonium-bicarbonate solution, pH 8.0, and the complexes were rotary-shadowed.

Immunofluorescence and immunohistochemistry

Sections (6 µm) of frozen human and marmoset tissue, were fixed in acetone for 10 min. A 10-min pre-incubation in 2% (w/v) milk powder/20 mM Tris-buffered 150 mM saline (TBS) blocking buffer, pH 7.4, was followed by incubation with 5 µg/ml monoclonal or polyclonal tenascin-C antibodies for 1 hr at room temperature. After washing in blocking buffer, goat anti-mouse IgG or pig anti-rabbit IgG, both conjugated with rhodamine and human IgG adsorbed, was overlaid on the tissue section for 30 min in a dark humidified chamber. Sections were embedded in Mowiol (Hoechst, Zurich, Switzerland). Identical staining was found for human and marmoset tissues, employing antibodies to human tenascin-C.

Formalin-fixed, paraffin-embedded tissue was cut at 5 µm, de-paraffinized in increasing ethanol series, air-dried and pre-treated with 0.1% (w/v) pronase for 15 min at 37°C to unmask antigens. The slices were then incubated for 1 hr at room temperature with 5 µg/ml polyclonal tenascin-C antibodies, followed by goat anti-rabbit IgG, labelled with alkaline phosphatase, and visualized by the New Fuchsin colour staining method.

Double immunostaining was performed on the same section, after initial neutralization of endogenous peroxidase in a 0.07% (v/v) hydrogen-peroxide solution. The MAb to collagen type IV (CIV22-hybridoma medium) and polyclonal tenascin-C antibodies were incubated simultaneously for 1 hr at room temperature. After washing, sections were first incubated with goat anti-mouse IgG labelled with alkaline phosphatase, followed by pig anti-rabbit IgG complexed with peroxidase according to the instructions of the manufacturer (ABC kit from DAKO). Colour reaction of phosphatase was executed as described above, and peroxidase staining was executed for 15 min in 0.05 M Tris-buffered/HCl solution, pH 7.5, with 0.06% (w/v) diamino-benzidine and 0.07% (v/v) hydrogen peroxide. Subsequently, slices were counterstained with filtered eosin-haematoxylin for 10 min in tepid water and embedded in aqueous Kaiser's gelatin solution.

RESULTS

Development of human-tenascin-C-specific antibodies

Monoclonal and polyclonal antibodies raised against tenascin-C (Tn) from glioma cells were prepared and selected for recognition of all Tn-antigenic forms. Antigen-binding was confirmed with rotary-shadowing electron microscopy and immunoblotting. The polyclonal and monoclonal antibodies hT191, hT58, hT63 exclusively recognized the typical human tenascin-C forms (195-265 kDa). Other members of the tenascin family, such as tenascin-R (160 kDa) and tenascin-X (500 kDa) were not recognized (data not shown). The rotary-shadowing technique demonstrated the hexameric structure of the purified antigen from glioma-cell-culture medium: 2 trimers joining to make up the star-like hexabrachion (Fig. 1*a*). An identical oligomeric hexabrachion structure for serum Tn isolated by immunoaffinity chromatography with the hT191 MAb was visualized ultrastructurally (Fig. 1*b*). A single trimer is shown on the projection to the right. No self-association of Tn-molecules was detected. Visualization of binding of the arrow-head-shaped hT191 MAb to glioma Tn revealed the epitope lying at a distance of 43 ± 3 nm from the central terminus of each arm, accounting for an entire length of 2 populations at 82.5 ± 4 or 96.5 ± 4 nm. According to an accepted structural model for human Tn (Nies *et al.*, 1991), the epitope of hT191 lies on all isoforms (in the conserved 4.—5. type-III fibronectin-like domains). This was confirmed by immunoblots (data not shown), using recombinant human Tn-fragments (provided by Dr. H. Erickson, Duke University Medical Center, Durham, NC). These monoclonal and polyclonal antibodies, which recognize and bind identical Tn-epitopes

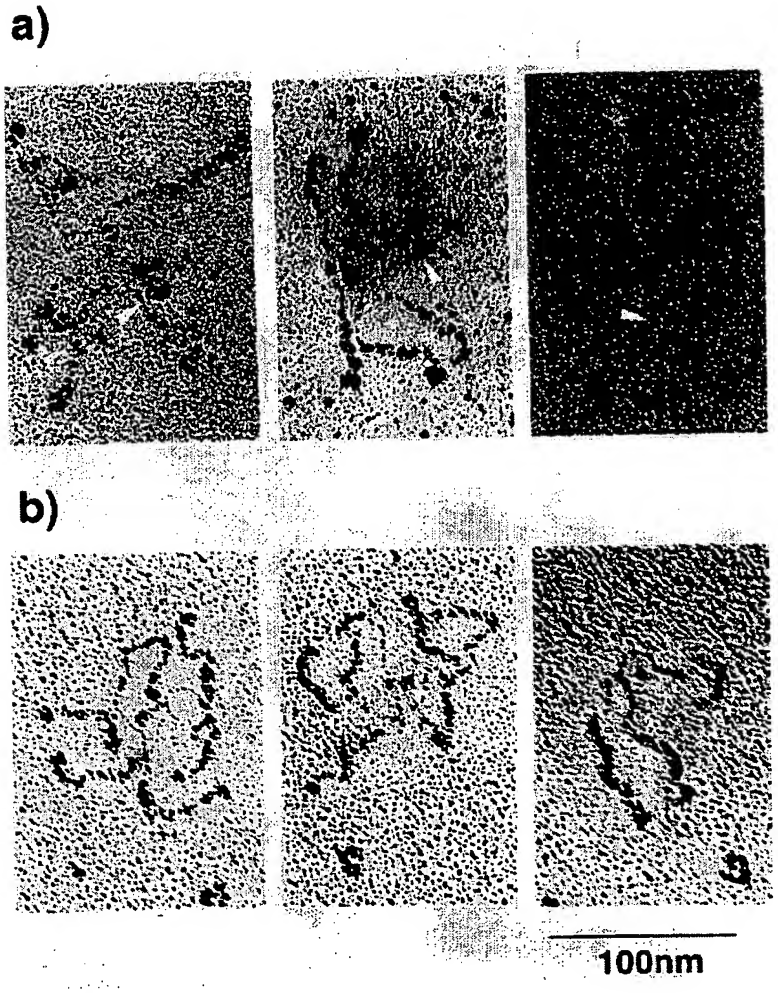

FIGURE 1 – Rotary-shadowed electron micrographs of the hexabrachionic human tenascin-C. *(a)* Isolation by gel filtration from conditioned medium of glioma-cell culture and *(b)* by immunoaffinity chromatography from serum, using monoclonal antibody hT191. hT191 bound glioma tenascin-C (indicated by arrowheads) in the thickened distal portion, the arm of the fibronectin-type-III region, which is flanked by the proximal thinner epidermal-growth-factor-like repeats and the distal-fibrinogen-homologous knob. Scale bar, 100 nm.

with high affinity, were subsequently used to demonstrate expression of Tn in normal and neoplastic tissues.

For control staining, incubation of the developed antibodies and a commercially available (purchased from Biokit Oy, Helsinki, Finland) in parallel showed an overlapping Tn-distribution pattern on normal tonsil (data not shown). Predominant stromal staining was also detected on human mammary-tumour sections (data not shown), consistent with Tn immunopositivity described in rat mammary tumours (Mackie *et al.*, 1987).

Tenascin-C distribution in normal and neoplastic tissues

Results shown in Table I were obtained from a wide variety of normal tissues by immunofluorescence microscopy for Tn. Tn-specific immunofluorescence in human and the marmoset (*C. jacchus*) tissues was found to be equivalent, therefore marmoset tissues were used to confirm staining in cases where tissue preservation rendered staining weak in human tissues. The marmoset distribution pattern is documented for bone marrow, spleen, lymph node and kidney. Thorough examination of the distribution pattern in normal tissues permitted an examination of the altered pattern of Tn distribution in corresponding tumour tissues. Statistics for Tn immunopositivity in various types of soft-tissue tumours are given in Table II. Polyclonal anti-Tn antibody was exclusively employed for tumours (collected between 1977–1989), since it provided more consistent reactivity with formalin-fixed, paraffin-embedded material.

A direct comparison of the staining pattern of Tn in normal adult tissues and soft-tissue tumours is shown in Figure 2 (*b–e*) in the left and right fields respectively. The 2 parts of Figure 2*a* compare normal epithelium in tonsil with the epithelial component in biphasic soft-tissue tumours. Figure 2*f* represents the comparison between a blood vessel in normal and tumour tissue in the left and right fields respectively.

The distribution pattern of Tn in tonsilar epithelium is broad, being more extensive than the basement membrane in the epithelial extracellular matrix (Fig. 2*a*). Tn is not an integral component of the basement membrane (currently marked by anticollagen-type-IV staining in red), confirming results of immunoelectron microscopy (Lightner *et al.*, 1989). Its staining extends into the mesenchymal tissue of the sub-epithelial region. Epithelia of normal adult tissue is consistently immunonegative for Tn. In tumours with co-existing

TABLE I - TENASCIN-C LOCALIZATION IN NORMAL TISSUES

Organs/tissues:	Epithelial basement-membrane region	Smooth muscle	Other positive structures
Vasculature			
thoracic aorta	+	+	adventitia
artery, vein	+	+	adventitia
capillary	+	●	
Bone marrow	●	●	stroma, blood sinusoids
Skin[1] and	+/−	●	(dermal adipose tissue is negative)
sweat, sebaceous glands	+/−	●	
hair follicle	+	●	
Other stratified epithelia[2]	+/−	●	
Parotid, salivary	+/−	●	
Thyroid	+/−	●	
Adrenal	+/− (cortex)	●	medulla, capsule
Lung	+	+	alveolar septa, bronchus
Intestine	+/−	+	
Colon	+/−	+	
Ileum	●	+	Peyer's patch
Kidney	●	●	glomerular mesangium, Bowman's capsule, (tubules are negative)
Prostate (urethra)	+	+	
Testis	+	●	
Uterus	+	+	
Tonsil	+	●	sinusoidal walls of T areas
Lymph node	●	●	sinusoidal walls of T areas
Spleen	●	●	sinusoidal walls of T areas, capsule, trabeculae,
Thymus	+	●	sinusoidal walls of T areas
Striated muscle	●	●	perimysium, (muscle cells are negative)
Tendon	●	●	tendon, myotendinous junction
Fascia	●	●	fibers
Cartilage	●	●	perichondrium
Nervous tissues	●	●	peripheral nerve: peri-, endoneurium spinal cord: glial cells

Summary of human tenascin-C distribution in adult human and marmoset tissues. + indicates that tenascin-C was immunologically detected in mesenchymal-derived locations such as smooth-muscle bundles or connective tissue and at the boundary structure (basement membrane) to the surrounding epithelium and to glands. +/− represents a discontinuous signal delineating epithelial basement membranes. MAbs hT191, hT58, hT63 were employed on frozen tissue sections, and polyclonal anti-tenascin-C antibodies on paraffin-embedded and frozen sections. [1]Keratinizing. [2]Non-keratinizing. The marmoset distribution pattern is documented for bone marrow, spleen, lymph node and kidney.

mesenchymal and epithelial components, such as the biphasic synovial sarcoma (Fig. 2*a*, right) and epithelioid sarcoma, the epithelial component is either negative or weakly positive when bordering immunopositive stroma. The sarcomatous (mesenchymal) areas of these tumours were frequently immunopositive. This pattern was also seen in mesothelioma. One third of Tn-positive mesothelioma also expressed a weak intracellular Tn immunopositivity. With the exception of the epithelial intracellular staining in mesothelioma, Tn was consistently shown to localize only to the extracellular matrix of the mixed epithelial-mesenchymal tumours.

Adipocytes in normal tissues did not stain with the Tn antibodies, whereas liposarcomas were immunopositive (Fig. 2*b*). The figure is representative for liposarcomas with a clear though moderate degree of immunopositivity in the extracellular matrix and a micropattern confined to blood vessels. Of the lipoma-like sarcomas, 25% were positive, and variably malignant myxoid tumours contained Tn in 60% of the examined cases.

Skeletal muscle myofibers contained no stainable Tn. Neoexpression of Tn was, however, evident in the extracellular matrix of rhabdomyosarcoma (Fig. 2*c*). Of the examined rhabdomyosarcomas, 50% were immunopositive for Tn.

Fibroblasts of the loose connective tissue of dermal corium only expressed Tn in dermal fibromas. Staining in such tumours was present focally along collagen fibers (Fig. 2*d*). As summarized in Table II, malignant transformation of the fibroblasts led to increased frequency of positive cases. Tn positivity was found in 50% (incidence) of examined fibroma, and in 100 and 93% of tested dermatofibrosarcoma and fibrosarcoma cases respectively

TABLE II - TENASCIN-C IMMUNOPOSITIVE CASES

Tumour type	Number	Positive (%)
Fibroma	20	50
Fibromatosis	35	60
Dermatofibrosarcoma	14	100
Fibrosarcoma	15	93
Malignant fibrous histiocytoma	22	50[1]
Melanoma	13	92
Neurinoma	19	94
Schwannoma	17	94
Leiomyoma	18	94
Leiomyosarcoma	16	80[1]
Synovial sarcoma	19	69[1]
Mesothelioma	20	70[1]
Epithelioid sarcoma	9	100
Liposarcoma	22	50[1]
lipoma-like	7	25
myxoid	11	60
Rhabdomyosarcoma	15	53

Summary of human tenascin-C expression in soft-tissue tumours. Tumours were from different patients. Numbers in body of table refer to percentage (%) of tumours with immunoreactivity using the polyclonal anti-tenascin-C antibody. Qualitative analysis of the staining, such as continous or focal patterns or degrees of staining intensity, are not shown in this table. Frequency data refer exclusively to the presence or absence of non-blood-vessel-associated tenascin-C immunopositivity. [1]Tumour types with reactivity in the cytoplasm of tumour cells.

(Table II). The relative increase from fibroma to malignant fibrous tumours was 100% for fibrosarcomas (Table II). Expression was also seen in 60% of fibromatosis cases. The distribution pattern in fibro- and dermato-fibrosarcoma (not shown) is similar to the Tn pattern shown for consistently positive regions of rhabdomyosarcoma and schwannoma in Fig. 2*b,c*.

A clear cell association of Tn was seen in normal perimysium (Fig. 2*c*) and in perineurium (Fig. 2*e*). As expected, 94% of the corresponding soft-tissue tumours, the nerve-sheath-derived neurinoma and the schwannoma, contained Tn. Immunopositivity was occasionally seen as fingerprint-like whorls, with sharp demarcation of Tn-positive and -negative tumour regions (Fig. 2*e*).

Blood vessels of all sizes in normal tissues exhibited peculiarly strong Tn expression. Although immunopositive areas completely surrounded vessels sectioned transversely, the vessel walls sectioned longitudinally were often stained in a discontinuous fashion (arrows in Fig. 2*f*). A vascular-associated micropattern of Tn expression was occasionally detected in soft-tissue tumours. In the schwannoma, Tn immunopositivity extended in an arboreal manner from blood vessel walls into surrounding tissue (Fig. 2*f*). In individual leiomyomas, leiomyosarcomas and rhabdomyosarcomas, the distribution was exclusively restricted to perivascular tissues. Focally more prominent perivascular labelling was seen in certain fibrosarcomas. The irregular, perivascularly located Tn does not appear to be associated with basement membranes surrounding the tumorous blood vessels (data not shown).

Apart from the blood vessels, the smooth muscle in the sub-mucosa of colon (Fig. 2*f*) shows strong Tn immunopositivity between and around single smooth-muscle cells, localized to the region where the cellular basement membrane is present. Smooth-muscle cells were confirmed as such by intracellular staining with alpha-smooth-muscle-actin antibody (not shown). Leiomyomas and leiomyosarcomas were Tn-immunopositive in 94% and 80% of cases respectively.

DISCUSSION

The presently developed antibodies raised to glioma-cell-culture-Tn enabled us to purify human tissue- and serum-Tn to homogeneity and therefore to project it on electron-microscopic pictures. These identified 2 brachion populations on ultrastructural analysis. The differences in length would account for a difference of at least 4 fibronectin-type-III extra domains, assuming 3.2 nm per domain (Kaplony *et al.*, 1991). These variations suggest alternative splicing of the 2 antigen sub-populations, reflected by separation on polyacrylamide gels (data not shown) and confirmed by Gulcher *et al.* (1989).

Consistent broad staining of epithelial basement-membrane regions was obtained utilizing antibodies able to identify the 2 populations of alternatively spliced Tn isoforms. Basement-membrane-associated Tn was found in all organs investigated. These results confirm earlier published work on human Tn distribution (Natali *et al.*, 1990, 1991; Lightner *et al.*, 1989). Tn was clearly stained in sebaceous-gland, ductus and acini and adrenal and thyroid-gland tissues, where conflicting results have been reported. In addition, Tn was found in uterus and testis. Natali *et al.* (1990, 1991) did not detect Tn in sebaceous glands, uterus, testis or in the sinusoids of the thymus. The anti-Tn MAb BC-2 used in their studies was specific for the extra domain consisting of at least 4 fibronectin-type-III-like motifs in the larger isoforms, and therefore failed to establish the presence or absence of the smaller isoforms in tissues. In the present study, the smaller Tn isoforms were isolated from the tonsil (195 kDa; data not shown) in order to confirm that the antibodies used in immunohistochemical analysis could detect epitopes both on larger and on smaller Tn molecules. The ability to recognize all isoforms led to the identification of Tn in the sinusoidal wall of the secondary lymphatic organs, thymus and tonsil. Tn was detected in all mesenchymal tissues of the normal adult in association with blood vessels, in contrast to the present assumption that expression is normally limited to certain organs in the adult and the foetus (Mackie *et al.*, 1987).

Tumour tissue and cell lines have been reported to contain predominantly the larger Tn isoforms (Borsi *et al.*, 1992, 1996; Hauptmann *et al.*, 1995), unlike many normal tissues. Published Tn staining with antibodies recognizing various Tn isoforms in solid tumours and glioma was therefore collectively compared with findings in the soft-tissue tumours.

Tn was shown to be particularly prominent around blood vessels of glioma; especially those staining negatively for fibronectin. Conversely, it was not found where blood-vessel-associated fibronectin was expressed (Higuchi *et al.*, 1993), where Tn probably replaced the function of fibronectin, possibly indicating a certain redundancy in function between the 2 proteins. We have found (Schnyder *et al.*, 1996; and data not shown) that Tn and fibronectin were optimal matrix sub-layers for vascular endothelial-cell adhesion and activation when compared with the structural protein, collagen type I. Expression of the fibronectin- and Tn-binding integrin, $\alpha_v\beta_3$, of vascular endothelial cells has been shown to correlate with neo-vascularization in tumours, and neutralizing antibodies to $\alpha_v\beta_3$ have been shown to inhibit metastasis formation *in vivo* (Friedlander *et al.*, 1995; Prieto *et al.*, 1993). A role for tenascin-facilitated tumour neo-vascularization may therefore exist, given the presently demonstrated marked up-regulation in mesenchymal tumours.

Tn provides a potentially useful tool for investigating the biology of soft-tissue tumours, since it was neo-expressed in fibroma, rhabdomyosarcoma and liposarcoma. Moreover, Tn expression was greater in variably malignant myxoid liposarcoma than in the lipoma-like liposarcoma and, similarly, demonstrated heightened expression in presently examined dermatofibrosarcoma and fibrosarcoma than in fibroma. Studies examining the role of Tn in neoplasia have hitherto been restricted to carcinomas. In the present study, only limited expression of Tn by malignant epithelial cells was seen, in contrast to that of mesenchymal cells. Tn expression was shown to be absent around single epithelial-tumour cells, being largely restricted to accompanying stroma (Mackie *et al.*, 1987). A related pattern was shown for the biphasic, epithelioid-mesenchymal mesothelioma in the present study. That epithelioid cells display a generally more matrix-degradative phenotype than their mesenchymal counterparts (Marshal *et al.*, 1993) is consistent with the occasional intracellular staining and absence of pericellular staining of epithelial cells for Tn in the epithelial component of mesothelioma examined in the present study. In contrast, *de novo* production and secretion of Tn by mesenchymal tumour cells was

FIGURE 2 – Immunofluorescence and histochemical staining of tenascin-C in normal human tissues (left fields) and in soft-tissue tumours (right fields). Distribution pattern is shown in *(a)* epithelium of tonsil and biphasic synovial sarcoma (epithelial/mesenchymal phases); *(b)* adipocytes in skin and liposarcoma; *(c)* skeletal muscle and rhabdomyosarcoma; *(d)* skin and fibroma; *(e)* perineurium of peripheral nerve and schwannoma; *(f)* sub-mucosa of colon, including blood vessel wall and blood vessel in a schwannoma. In normal tissues *(e, f)* immunofluorescence micrographs utilize MAb hT191. All other tissue-sections were formalin-fixed, paraffin-embedded and detected with the polyclonal anti-tenascin-C antibody, followed by alkaline-phosphatase staining. The normal tissue in *(a)* and *(d)* was double stained with tenascin-C (brown) and collagen type-IV using MAb CIV22 (red), followed by, respectively, peroxidase and phosphatase secondary steps. Abbreviations: ac, acini; bl v, blood vessel (or marked by arrow); co, corium; du, duct; ep, epithelium; ep t, epithelial tumour part; fat, adipose cells; fib, fibroma; lip, liposarcoma; pm, perimysium; pn, perineurium; rha, rhabdomyosarcoma; sarc, sarcomatous component; sk, skeletal muscle; sm, smooth muscle; sw, schwannoma; t, tendon. Original magnification ×250 (*a, d*, ×100). Figure appears on pages 222 and 223.

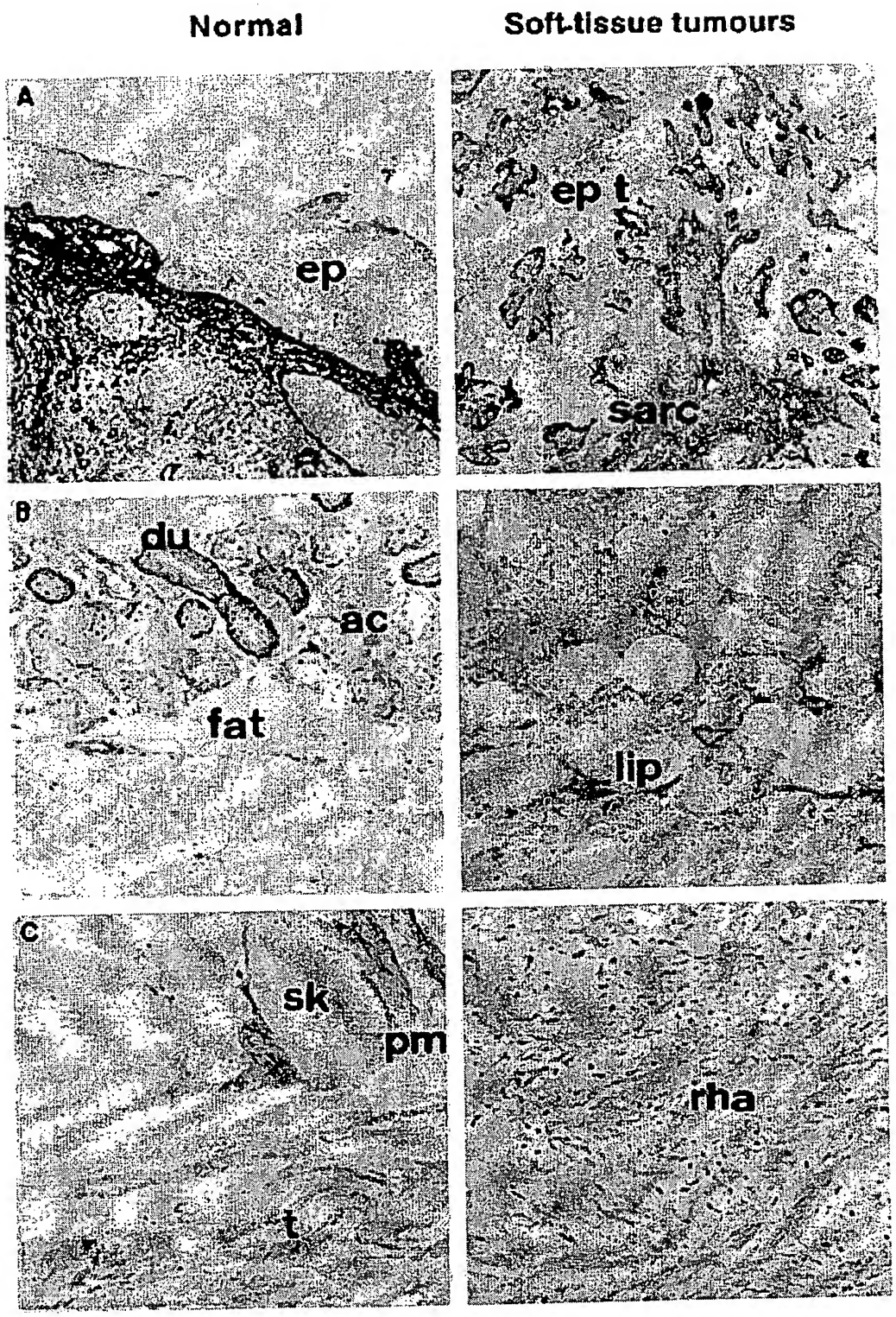
Normal
Soft-tissue tumours
A
ep
ep t
sarc
B
du
ac
fat
lip
C
sk
pm
t
rha

FIGURE 2

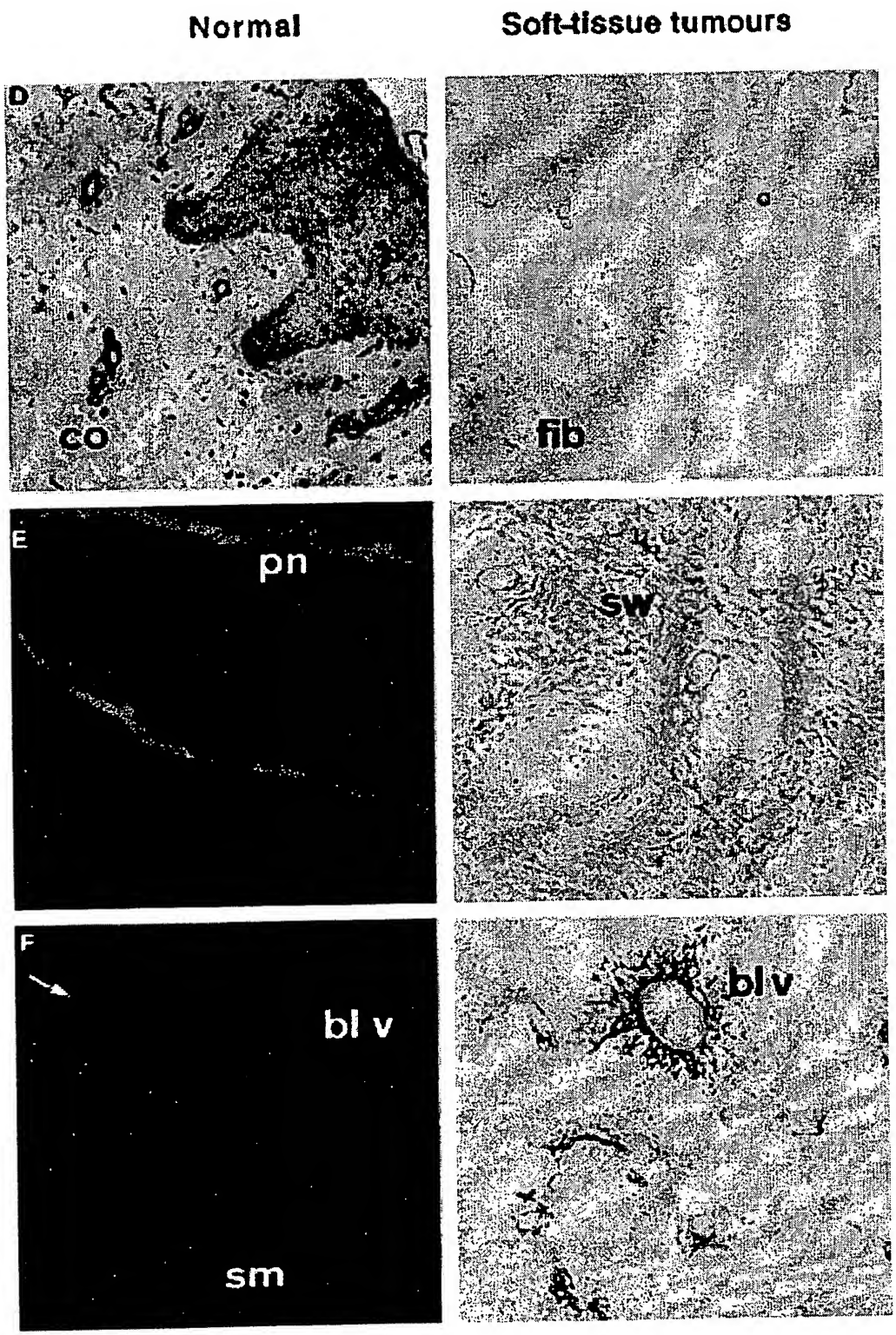

FIGURE 2

considered likely, due to its abundance within, around and in close association with mesenchymal-tumour cells.

In other studies, Tn was not associated with negative prognostic factors such as metastasis with invasion of blood vessels or tumour necrosis. Tn expression was, however, markedly increased in invasive carcinomas when compared with adenoma or fibrocystic diseases (Moch *et al.*, 1993; Sasano *et al.*, 1993). Involvement of the neo-expressed cell-adhesion protein in the expression of the malignant phenotype is also suggested in the present study, given the clear tendency to increased Tn expression in malignant tumours derived from adipocytes and skeletal-muscle cells. Consistent with a role for Tn in the malignant cell phenotype is the presence of elevated levels of Tn in the circulation of patients with neoplastic disease (Schenk *et al.*, 1995; Riedl *et al.*, 1995; and data not shown). Taking blood-level measurements as a screening tool, preliminary data showed coincidence of Tn-presence in implanted tumours with the elevated level in blood circulation in a nude-mouse model (data not shown). The diagnostic utility of Tn-expression after chemotherapeutical treatment of brain tumours was recently investigated with [^{131}I]-labelled anti-Tn MAbs (Brown *et al.*, 1996).

Our demonstration of high-level expression of Tn diffusely in the matrix and around the vasculature of mesenchymal tumours supports the hypothesis that increased expression of the cell-adhesion molecule Tn by tumour cells is associated with neo-vascularization and thus may facilitate tumour growth.

ACKNOWLEDGEMENTS

We thank Dr. M. Mueller for providing facilities for electron microscopy. We gratefully acknowledge the expert practical assistance and advice of Mr. P. Ferber, also of Drs. A. Kaplony, A. Zisch and M. Mendler, Dr. S. Schnyder-Candrian's critical comments are highly appreciated. B.S. was supported by a grant from the Swiss Cancer Society.

REFERENCES

BORSI, L., ALLEMANNI, G., GAGGERO, B. and ZARDI, L., Extracellular pH controls pre-mRNA alternative splicing of tenascin-C in normal, but not in malignantly transformed, cells. *Int. J. Cancer*, **66**, 632–635 (1996).

BORSI, L., CARNEMOLLA, B., NICOLO, G., SPINA, B., TANARA, G. and ZARDI, L., Expression of different tenascin isoforms in normal hyperplastic and neoplastic human breast tissues. *Int. J. Cancer*, **52**, 688–692 (1992).

BROWN, M.T. and 14 OTHERS, Intrathecal I-131-labeled anti-tenascin-monoclonal-antibody-81C6 treatment of patients with leptomeningeal neoplasms or primary brain-tumor resection cavities with sub-arachnoid communication-phase-I trial results. *Clin. Cancer Res.*, **2**, 963–972 (1996).

DERYUGINA, E.I. and BOURDON, M.A., Tenascin mediates human glioma-cell migration and modulates cell migration on fibronectin. *J. Cell Science*, **109**, 643–652 (1996).

FRIEDLANDER, M., BROOKS, P.C., SHAFFER, R.W., KINCAID, C.M., VARNER, J.A. and CHERESH, D.A., Definition of two angiogenic pathways by distinct α_v integrins. *Science*, **270**, 1500–1502 (1995).

GULCHER, J.R., NIES, D.E., MARTON, L.S. and STEFANSSON, K., An alternatively spliced region of the human hexabrachion contains a repeat of potential N-glycosylation sites. *Proc. nat. Acad. Sci. (Wash.)*, **86**, 1588–1592 (1989).

HAUPTMANN, S., ZARDI, L., SIRI, A., CARNEMOLLA, B., BORSI, L., CASTELUCCI, M., KLOSTERHALFEN, S., HARTUNG, P., WEIS, J., STOECKER, G., HAUBECK, H-S. and KIRKPATRICK, J.C., Extracellular matrix proteins in colorectal carcinomas. Expression of tenascin and fibronectin isoforms. *Lab. Invest.*, **73**, 172–182 (1995).

HIGUCHI, M., OHNISHI, T., ARITA, N., HIRAGA, S. and HAYAKAWA, T., Expression of tenascin in human gliomas: its relation to histological malignancy tumor de-differentiation and angiogenesis. *Acta Neuropathol. (Berl.)*, **85**, 481–487 (1993).

KAPLONY, A., ZIMMERMANN, D.R., FISCHER, R.W., IMHOF, B.A., ODERMATT, B.F., WINTERHALTER, K.H. and VAUGHAN, L., Tenascin Mr 220000 isoform expression correlates with corneal cell migration. *Development*, **112**, 605–614 (1991).

LIGHTNER, V.A., GUMKOWSKI, F., BIGNER, D.D. and ERICKSON, H.P., Tenascin/hexabrachion in human skin: biochemical identification and localization by light and electron microscopy. *J. Cell Biol.*, **108**, 2483–2493 (1989).

MACKIE, E.J., CHIQUET-EHRISMANN, R., PEARSON, C.A., INAGUMA, Y., TAYA, K., KAWARADA, Y. and SAKAKURA, T., Tenascin is a stromal marker for epithelial malignancy in the mammary gland. *Proc. nat. Acad. Sci. (Wash.)*, **84**, 4621–4625 (1987).

MARSHAL, B.C., SANTANA, A., XU, Q-P., PETERSEN, M.J., CAMPBELL, E.J., HOIDAL, J.R. and WELGUS, H.G., Metalloproteinases and tissue inhibitor of metalloproteinases in mesothelial cells. *J. clin. Invest.*, **91**, 1792–1799 (1993).

MOCH, H., TORHORST, J., DURMUELLER, U., FEICHTER, G.E., SAUTER, G. and GUDAT, F., Comparative analysis of the expression of tenascin and established prognostic factors in human breast cancer. *Pathol. Res. Pract.*, **189**, 510–514 (1993).

NATALI, P.G., NICOTRA, M.R., BARTOLAZZI, A., MOTTOLESE, M., COSCIA, N., BIGOTTI, A. and ZARDI, L., Expression and production of tenascin in benign and malignant lesions of melanocyte lineage. *Int. J. Cancer*, **46**, 586–590 (1990).

NATALI, P.G., NICOTRA, M.R., BIGOTTI, C., BOTTI, C., CASTELLANI, P., RISSO, A.M. and ZARDI, L., Comperative analysis of the expression of the extracellular matrix protein tenascin in normal human fetal adult and tumor tissues. *Int. J. Cancer*, **47**, 811–816 (1991).

NIES, D.E., HEMESATH, T.J., KIM, J.H., GULCHER, J.R. and STEFANSSON, K., The complete cDNA sequence of human hexabrachion. *J. biol. Chem.*, **266**, 2818–2823 (1991).

PRIETO, A.L., EDELMAN, G.M. and CROSSIN, K.L., Multiple integrins mediate cell attachment to cytotactin/tenascin. *Proc. nat. Acad. Sci. (Wash.)*, **90**, 10154–10158 (1993).

RIEDL, S., BODENMUELLER, H., HINZ, U., HOLLE, R., MOELLER, P., SCHLAG, P., HERFARTH, C. and FAISSNER, A., Significance of tenascin serum level as tumor marker in primary colorectal carcinoma. *Int. J. Cancer*, **64**, 65–69 (1995).

SAGA, Y., YAGI, T., IKAWA, Y., SAKAKURA, T. and AISAWA, S., Mice develop normally without tenascin. *Genes Develop.*, **6**, 1821–1831 (1992).

SASANO, H., NAGURA, H., WATANABE, K., ITO, K., TSUIKI, A., SATO, S., YAJIMA, A., KUSAKABE, M. and SAKAKURA, T., Tenascin expression in normal and abnormal human endometrium. *Mod. Pathol.*, **6**, 323–326 (1993).

SCHENK, S., MUSER, J., VOLLMER, G. and CHIQUET-EHRISMANN, R., Tenascin-C in serum: a questionable tumor marker. *Int. J. Cancer*, **61**, 443–449 (1995).

SCHNYDER, B., LUGLI, S.M., FENG, N.P., ETTER, H-U., LUTZ, R.L., RYFFEL, B., WUNDERLI-ALLENSPACH, H., SUGAMURA, K. and MOSER, R., IL-4 and IL-13 bind to a shared heterodimeric complex on endothelial cells mediating vascular-cell-adhesion-molecule-1 induction in the absence of the common gamma (γ_c). *Blood*, **87**, 4286–4295 (1996).

SPRING, J., BECK, K. and CHIQUET-EHRISMANN, R., Two contrary functions of tenascin: dissection of the active sites by recombinant tenascin fragments. *Cell*, **59**, 325–334 (1989).

VAUGHAN, L., HUBER, S., CHIQUET, M. and WINTERHALTER, K.H., A major, six-armed glycoprotein from embryonic cartilage. *EMBO J.*, **6**, 349–353 (1987).